Interim Final Report, Hydraulic Fracturing in the Upper Humboldt River Basin, Aquifer Quality Assessment Program

Greg Pohll
Jenny Chapman
Karl Pohlmann
Russell Plume
Rishi Parashar
Susan Rybarski
Ronald L. Hershey
Wyatt Fereday
Matt Reeves
James M. Thomas

October 2015

Publication No. 41263

Prepared by
Desert Research Institute, Reno, Nevada

Prepared for
Nevada Division of Environmental Protection
Nevada Division of Minerals
Noble Energy

THIS PAGE INTENTIONALLY LEFT BLANK

EXECUTIVE SUMMARY

Hydrocarbon resources are being explored in the upper Humboldt Basin of northeastern Nevada. The exploration area extends southwest from the Marys River Valley, along the west side of the Ruby Mountains, to the Huntington River Valley in the south. Modern drilling and completion techniques, including hydraulic fracturing, are being used to assess the economic viability of producing hydrocarbons from the low-permeability rock formations in the area. Given Nevada's statutory mandate to protect all waters of the state, the Nevada Division of Minerals (NDOM), the Nevada Division of Environmental Protection (NDEP), and the exploration company Noble Energy, Inc. (Noble), developed a memorandum of understanding (MOU) to develop, evaluate, and share data and information related to groundwater gathered during exploration activities, including before and after hydraulic fracturing. This MOU established the Aquifer Quality Assessment Program (AQUA) and identified the Desert Research Institute (DRI) as the entity that would collect data, develop hydrologic models, and prepare reports evaluating the fate and transport of chemicals used for hydraulic fracturing.

The MOU identifies three reports that will be prepared as part of the AQUA Program. The first two reports focus on water-quality monitoring and developing a baseline dataset of the chemical characteristics of groundwater, springs, and surface water in the exploration areas. The third report, which is this Interim Final Report, updates the water-quality monitoring data collected to date and interprets those data to characterize the flow systems and establish monitoring targets. Additionally, this report uses hydrogeologic data, provided by Noble and other sources, to develop hydrologic models that evaluate the potential fate and transport of chemicals used for hydraulic fracturing. The water-quality data, interpretations, and hydrogeologic conceptualizations and modeling are presented here to assess the potential effects of hydraulic fracturing stimulations in this region of the state of Nevada. As described in the MOU, additional data might be collected as future exploration occurs. This additional data would supplement the Interim Final Report and be incorporated in any future updates to this report.

Samples were collected for water-quality monitoring from three exploration areas and some wells, springs, and streams in the surrounding region. When possible, sampling occurred both prior to and after a hydraulic fracturing activity. The analytical suite included natural gas components associated with petroleum reservoirs, refined hydrocarbons, and related chemical compounds associated with ground-surface exploration activities, components associated with generic hydraulic fracturing fluids, and chemical, isotopic, and radiochemical constituents found in water. No systematic differences between pre- and post-hydraulic fracturing samples are evident.

There are numerous differences between groundwater from the reservoir horizon (hydrocarbon-producing zone) and shallow groundwater, springs, and surface water in the area. These differences can be used to monitor for incursion of reservoir-associated fluids into the near-surface environment. The recommended monitoring parameters are Total Dissolved Solids (or the surrogate field measurement of electrical conductivity), chloride, propane, methanol, ethanol, and 2-butoxyethanol. Methane is a poor choice as an indicator of the impact of production water on near-surface water because biogenic methane is present in numerous shallow groundwater and spring samples at concentrations similar to and greater than those observed in the production well groundwater. Any methane monitoring should include an isotopic analysis of carbon and hydrogen to distinguish biogenic and thermogenic sources. Compounds associated with refining and hydrofracturing are present in the production-zone water and rare in the near-

surface water. Nonetheless, the trace detection of toluene, TPH-DRO, TPH-GRO, ammonium persulfate, ethylene glycol, propylene glycol, and glycerol in pre-hydraulic-fracturing samples from some shallow well and spring locations show the difficulties of characterizing contaminants near analytical detection limits as indicators of drilling and fracturing activities. Benzene, ethylbenzene, the xylenes, methanol, ethanol, and 2-butoxethanol are uniquely observed in the production fluids and are better choices to identify drilling and hydraulic fracturing chemicals. The analyses reported here from the AQUA Program provide baseline water-quality data, prior to hydraulic fracturing, as comparisons for future monitoring results.

A conceptual model of the groundwater system in the upper Humboldt Basin was developed to evaluate the processes, pathways, and conditions that control the potential migration of hydraulic fracturing fluids from the Elko Formation oil reservoir to shallow groundwater. The first step in developing the model was to map and organize the geologic units into hydrogeologic units. The current target for hydrocarbon exploration in the three project areas is the Elko Formation, which is at an approximate depth of 8,000 ft in Exploration Area 2. Overlying the Elko Formation is the Indian Well Formation (which has a low to moderate permeability) and beneath the Elko Formation are carbonate rocks that are characterized as moderately to highly permeable. A groundwater budget was calculated that includes evapotranspiration, recharge from the mountains, streamflow accretions, spring flow, interbasin flow, and groundwater pumping. Generalized groundwater flow paths for the upper Humboldt Basin describe flow from the mountain ranges toward creeks and valleys, eventually leading to discharge along the Humboldt River.

The processes, pathways, and conditions that control the potential migration of hydraulic fracturing fluids from the Elko Formation are another important aspect of the conceptual model. Because there are unknowns about how a well will be hydraulically fractured and produced, and unknowns about the hydrogeologic conditions in the deep subsurface, there are many possible conceptualizations for contaminant transport. An event tree outlines many of these and allows identification of the scenarios that would allow greater transport. The initiating action in all scenarios is the drilling and completion of an exploration well. Once hydraulic fracturing and flowback testing are completed, the well might go into production or might be shut in. Because oil production is the primary incentive, oil production is the more likely outcome. Oil production will establish a hydraulic gradient toward the wellbore that will limit the potential for fluid migration in any other direction. If poor economic or operational conditions exist, the well could be shut in and natural hydraulic conditions will govern flow. Uncertainty exists in defining the natural hydraulic conditions because of the lack of data from these deep formations. If a well is not in production, the migration of the remaining hydraulic fracturing fluid to shallow aquifers is governed by the permeability of the Elko Formation, the stimulated fracture height, the sorption and degradation capacity of the chemicals of concern, matrix diffusion, the rate of flow through the carbonate unit (a function of recharge and permeability), and the existence and permeability of faults that connect the carbonate unit and the shallow aquifer. If hydraulic fracturing design conditions are achieved, stimulated fractures are limited to the Elko Formation, and because the permeability of oil shale formations is usually very low (10^{-7} m/day)—which is evidenced by the accumulation of oil and the need for fracturing—then hydraulic fracturing fluid will remain in the Elko Formation.

Several numerical models of groundwater flow were developed to quantify fate and transport of hydraulic fracturing chemicals in selected scenarios. A regional groundwater flow model of the upper Humboldt River Basin is used to estimate the distribution of hydraulic head, boundary conditions,

hydraulic gradients, and groundwater flow directions for local-scale groundwater flow and transport models. An important outcome from the regional model is that the hydraulic gradient is downward through the Elko Formation in Exploration Area 2.

One of the local models is a gas transport model to evaluate methane gas migration upward because of buoyancy effects after hydraulic fracturing in an exploration well. The methane gas migration model simulates migration from a hydraulically fractured zone in the Elko Formation. As gas-phase methane migrates buoyantly from the fractured zone of high concentration to regions of low concentration, methane enters the liquid phase and is effectively immobilized. It is estimated that methane gas migrates a vertical distance of 760 meters before this immobilization occurs, though greater distances are possible if a high conductivity fault is assumed to intersect the hydraulic fracture zone. None of the simulations (with or without a fault connection) predict that gaseous methane will approach the depth of the base of the shallow aquifer, meaning methane migration into shallow aquifers from hydraulic fracturing is unlikely in Exploration Area 2.

Another local model is designed to simulate groundwater flow and contaminant transport through the hydraulic fracturing zone to adjacent units. This hydraulic fracturing zone model computes transport in a dual-continua framework that considers the interaction between fractures and the surrounding matrix rock. Additional cross-sectional models couple the fracture-flow model to the overlying Indian Well Formation or underlying carbonate unit to evaluate the migration potential to shallow groundwater resources if contaminants move from the Elko Formation. The models and scenarios were built to represent specific conditions in Exploration Area 2. The dual-continua model of the Elko Formation evaluates the migration of hydraulic fracturing chemicals from a fracture zone. The expected "design" condition is based on hydraulic fractures being contained entirely within the Elko Formation and the Elko Formation having a very low permeability. Under these specific conditions, there is no migration of hydraulic fracturing fluid into either the carbonates or Indian Well Formation for at least 1,000 years (a timeframe used by the State of Nevada to evaluate contaminant migration in other settings, such as through the Federal Facility Agreement and Consent Order with the U.S. Department of Energy and Department of Defense).

Given that the fracture extent and Elko Formation permeability are uncertain, it is possible that the design conditions might not be realized and hydraulic fractures could extend to the boundary of the Elko Formation, allowing fracturing fluids to directly enter the over- or underlying formations. A comparison of simulated fracture lengths with typical hydraulic fracture lengths suggests there is at least a five percent probability that hydraulic fractures could extend to the boundary of the Elko Formation, allowing fracturing fluids to directly enter the over- or underlying formations. Additionally, limited drillstem tests in the Elko Formation indicate moderate rather than very low permeability that would allow migration into the underlying carbonate aquifer even if the fractures are restricted to the Elko Formation. To address these possibilities, the cross-sectional model takes the results of the dual-continua model for the moderate Elko Formation permeability condition and evaluates transport through the carbonate for that scenario, as well as for the low-probability condition in which hydraulically induced fractures either extend downward directly to the carbonate or extend upward to connect directly to a fault in the Indian Well Formation. A range of conditions are evaluated for recharge, hydraulic conductivity, fracture properties, and chemical sorption coefficients for each scenario. Simulated concentrations at a depth of 600 ft in the shallow aquifer are used as a metric of contaminant transport.

The simulation of hydraulic fractures extending upward to connect with faults in the Indian Well Formation did not result in breakthrough of hydraulic fracturing chemicals beyond the Indian Well Formation for at least 500 years. Vertical migration is confined to the hypothesized fault zone and the rate of lateral movement beyond that zone is so low that fracturing chemicals are not predicted to exit the Indian Well Formation for at least 1,000 years.

No migration to the shallow aquifer via the carbonate aquifer pathway is predicted to occur for at least 1,000 years when recharge to the carbonate aquifer is low, the hydraulic conductivity is low, the connection between the carbonate and shallow aquifer is limited, or sorption is high. Conversely, under conditions of moderate and high recharge and/or higher hydraulic conductivity of the carbonate, good fault connection to the shallow aquifer, and less sorption, breakthrough of fracture fluid to the shallow aquifer is simulated. This breakthrough does not occur for at least 400 years and is longer in many scenarios. The simulation of direct hydraulic fracture connection to the carbonate (in contrast to initial migration through a moderately permeable Elko Formation) results in faster breakthrough times, by 50 to 90 years, and concentrations approximately one-and-a-half times higher, though migration still requires adequate recharge, hydraulic conductivity, fault connection to the shallow aquifer, and low sorption. In all simulations, the normalized concentrations are low, with the highest simulated peak concentration on the order of three to four orders of magnitude lower than the initial concentrations. To place these normalized concentrations into context, migration of three different hydraulic fracturing chemicals are explicitly calculated and the predicted peak concentrations are all below EPA-approved analytical detection limits. The calculations did not consider the removal of fracturing chemicals from the subsurface during flowback testing, a process that would result in even lower concentrations in the aquifer.

The results of groundwater flow modeling indicate that, with the uncertainties about the deep subsurface, it is likely that conditions in the exploration area favor isolating hydraulic fracturing fluids from shallow aquifers for 1,000 years or more. A combination of specific conditions would be needed for carbonate rocks underlying the Elko Formation to function as a pathway for hydraulic fracturing fluids to migrate to shallow groundwater resources. These conditions include a lack of production at the exploration well, moderate permeability in the Elko Formation or hydraulic fractures that extend to the carbonate, at least moderate recharge to the carbonate aquifer, reasonably high carbonate permeability, a good hydraulic connection from the carbonate to the shallow aquifer through faults, and low sorption of contaminants. All of these events would have to occur to result in the migration of hydraulic fracturing fluid and even under these conditions, chemical concentrations in the shallow aquifer are calculated to be below EPA-approved analytical detection limits. Many other conditions would retain hydraulic fracturing fluids within the targeted Elko Formation. Data collection during oil exploration activities may be able to identify or document the presence or absence of conditions favoring migration at a particular exploration well.

CONTENTS

EXECUTIVE SUMMARY III
LIST OF PLATES IX
LIST OF FIGURES X
LIST OF ACRONYMS XIII
1.0 INTRODUCTION 1
1.1 AQUA Project Overview 1
1.2 Physiography 1
1.3 Climate 6
1.4 Overview of Hydraulic Fracturing 6
1.5 Literature Review 9
2.0 GEOLOGIC FRAMEWORK 15
2.1 Hydrogeologic Units 15
2.1.1 Cenozoic Basement 15
2.1.1.1 Crystalline Rocks 21
2.1.1.2 Older Carbonate Rocks 21
2.1.1.3 Thrusted Clastic Rocks 26
2.1.1.4 Clastic Rocks 26
2.1.1.5 Younger Carbonate Rocks 27
2.1.2 Cenozoic Units 27
2.1.2.1 Older Volcanic Rocks 27
2.1.2.2 Elko Formation 27
2.1.2.3 Indian Well Formation 28
2.1.2.4 Younger Volcanic Rocks 28
2.1.2.5 Humboldt Formation 29
2.1.2.6 Alluvium 29
2.2 Structural Features 30
2.3 Hydrogeologic sections 31
3.0 REGIONAL HYDROGEOLOGY 33
3.1 Groundwater Budget 33
3.1.1 Groundwater Recharge 33
3.1.2 Phreatophyte Evapotranspiration 37
3.1.3 Interbasin Flow 40

3.1.4 Streamflow Accretions/Depletions 40
3.1.5 Springs 42
3.1.6 Groundwater Pumping 45
3.1.7 System-wide Groundwater Budget 45
3.2 Generalized Groundwater Flow Directions 45
4.0 REGIONAL GROUNDWATER MODEL 52
4.1 Introduction 52
4.2 Assumptions 52
4.3 Model Construction 52
4.4 Hydrogeologic Units 55
4.5 Recharge, Discharge, and Boundary Flow 56
4.6 Results 60
4.7 Sensitivity Analysis 68
5.0 GEOCHEMISTRY AND WATER QUALITY 70
5.1 Role of Geochemistry in the Project 70
5.2 Parameter Selection 70
5.3 Sampling Procedures 74
5.4 QA Comparison of Tetra Tech and DRI Samples 81
5.4.1 Methane, Ethane, and Propane 81
5.4.2 TPH DRO and TPH GRO 82
5.4.3 Benzene, Ethylbenzene, Toluene, and Xylene 84
5.4.4 Cations, Anions, and Trace Elements 85
5.5 Hydrochemical and Isotopic Characterization 88
5.5.1 Characteristics of Shallow Groundwater, Springs, and Streams 88
5.5.1.1 Major-ion Composition 88
5.5.1.2 Stable Isotopic Composition of Water 91
5.5.1.3 Radionuclides 92
5.5.1.4 Methane 93
5.5.1.5 Noble Gases 97
5.5.1.6 Refined Hydrocarbons and Hydraulic Fracturing Components 99
5.5.2 Characteristics of Formation Water from the Oil Production Zone 99
5.5.2.1 Major-ion Composition of Water from the Oil Production Zone 99
5.5.2.2 Stable Isotopic Composition of Water from the Oil Production Zone 101

5.5.2.3 Radionuclides in Water from the Oil Production Zone 101
5.5.2.4 Methane Dissolved in Water from the Oil Production Zone 101
5.5.2.5 Noble Gases in Water from the Oil Production Zone 102
5.5.2.6 Refined Hydrocarbons and Hydraulic Fracturing Components in Water from the Oil Production Zone 102
5.5.3 Comparison of Pre- and Post-hydraulic-fracturing Samples 103
5.5.4 Parameter Recommendations for Monitoring 106
6.0 MIGRATION POTENTIAL FOR HYDRAULIC FRACTURING FLUIDS AND NATURAL GAS 110
6.1 Migration Potential under Oil Production 110
6.1.1 Methane Migration 110
6.2 Migration Potential under Shut-In Conditions 113
6.2.1 Fractures Contained in Elko Formation – Scenario NP1 117
6.2.2 Fractures Connect to Upward Fault in Indian Well Formation: Scenario NP2 124
6.2.3 Fractures Connect to Carbonate: Scenario NP3 124
7.0 CONCLUSIONS/RECOMMENDATIONS 130
8.0 REFERENCES 132
APPENDIX A: CHEMICAL AND ISOTOPIC PARAMETERS FOR UPPER HUMBOLDT RIVER BASIN WELLS, SPRINGS, AND STREAMS A-1
APPENDIX B: MIGRATION POTENTIAL TRANSPORT MODELING B-1
APPENDIX C: SUMMARY OF HYDRAULIC FRACTURING FLUID CHEMICALS AND PROPERTIES USED FOR HUNTINGTON K1L-1V, M10C-M10-11B, AND M2C-M2-21B C-1

LIST OF PLATES

Oversized plates located in the back of the report

1. Hydrogeologic map and oil well logs, upper Humboldt River basin, northeastern Nevada.
2. Hydrogeologic sections, upper Humboldt River Basin, northeastern Nevada.

LIST OF FIGURES

1-1. A Noble Energy drilling rig working in the upper Humboldt River basin. 2
1-2. Location of Noble Energy's upper Humboldt River Basin exploration areas. 3
1-3. Hydrographic basins within the study area. 4
1-4. Rivers and streams within the study area. 5
1-5. Distribution of mean annual precipitation (1981-2010) for upper Humboldt River Basin.. 7
2-1. Distribution of Cenozoic basement in the upper Humboldt River basin, northeastern Nevada. 16
3-1. Upper Humboldt groundwater system including the hydrographic areas. 34
3-2. Evapotranspiration units delineated using Landsat imagery from July 11, 2008. 38
3-3. Location of groundwater interbasin flow zones and hydrogeologic units. 41
3-4. Location of groundwater discharge to the South Fork Humboldt River. 43
3-5. Regional groundwater springs in the study area. 44
3-6. Groundwater pumping wells in the study area. 46
3-7. Groundwater levels and flow directions in the basin-fill deposits of the upper Humboldt River Basin, northeastern Nevada.. 50
4-1. Map view of the regional flow model domain showing perimeter boundary. 53
4-2. Configuration of layers in the regional flow model. 54
4-3. West-east profiles through the conceptual regional hydrogeologic framework of the upper Humboldt River basin. 57
4-4. Locations of recharge injection wells used to simulate mountain front recharge at the margins of basin-fill deposits and hydrogeologic classes. 58
4-5. Locations of pumping wells, streams, springs and hydrogeologic units that comprise greater than 95 percent of cell thickness in layer 1 of the flow model.. 59
4-6. Distribution of groundwater evapotranspiration simulated in the regional flow model. 60
4-7. Location of hydraulic conductivity zones. 62
4-8. Plot of simulated heads against observed heads in the shallow aquifer. 63
4-9. Heads simulated in layer 1 of the regional model. 65
4-10. Contours of simulated heads in layer 1 and layer 20 in the vicinity of Exploration Area 2.. 66
4-11. Vertical profiles of simulated head at three locations in Exploration Area 2.. 67
4-12. Plots of the variation of simulated head in Exploration Area 2 against a range of hydraulic conductivity values assigned to the Elko Formation in the regional flow model.. 69
5-1. Noble Energy exploration areas in the upper Humboldt River Basin and sample locations outside the vicinity of the exploration areas. 71
5-2. Noble Energy Exploration Area 1 (Huntington): pre-hydraulic-fracturing, water-quality sample locations. 75
5-3. Noble Energy Exploration Area 2 (Humboldt): pre-hydraulic-fracturing, water-quality sample locations. 76
5-4. Noble Energy Exploration Area 3 (Marys River): pre-hydraulic-fracturing, water-quality sample locations. 77
5-5. Noble Energy Exploration Area 2 (Humboldt): post-hydraulic-fracturing, water-quality sample locations. 78

5-6. Comparison of methane concentrations between Alpha Analytical and TestAmerica..... 83
5-7. Comparison of ethane concentrations between Alpha Analytical and TestAmerica..... 83
5-8. Comparison of Ca ion concentration between DRI labs and TestAmerica.. 86
5-9. Comparison of Na ion concentration between DRI labs and TestAmerica.. 86
5-10. Comparison of Li ion concentration between DRI labs and TestAmerica.. 88
5-11. Comparison of B ion concentration between DRI labs and TestAmerica.. 89
5-12. Total dissolved solids content of springs, streams, and groundwater sampled from the three study areas. 89
5-13. Piper diagram plotting the relative major-ion percentages for water sampled from Areas 1, 2, and 3 and the production well..... 90
5-14a. Oxygen ($\delta^{18}O$) and hydrogen ($\delta^{2}H$) stable isotope compositions of the area samples shown with the Global Meteoric Water Line and an estimate of local meteoric water.. 92
5-14b. Oxygen ($\delta^{18}O$) and hydrogen ($\delta^{2}H$) stable isotope compositions of the area samples shown with the Global Meteoric Water Line and an estimate of local meteoric water.. 93
5-15. Dissolved methane measured in area water samples. 94
5-16. Relationship between methane concentration (log scale) and $\delta^{13}C$ composition of the methane..... 95
5-17. Classification of methane origin based on $\delta^{13}C$ CH_4 and $\delta^{2}H$ CH_4 from Whiticar (1999).. 96
5-18. Relationship between $\delta^{13}C$ CH_4 and $\delta^{13}C$ DIC-H_2O used by Clark and Fritz (1997) to identify the pathway for methanogenesis. 97
5-19. ^{4}He versus Ne for samples from exploration areas 1, 2, and 3.. 98
5-20. Dissolved chloride distribution in area waters..... 100
5-21. Methane concentrations for the samples with reported results..... 102
5-22. ^{4}He versus Ne for samples from exploration areas 1, 2, and 3 and exploration well M2C. 103
5-23. Comparison of pre- and post-hydraulic-fracturing analyses of Area 2 waters for Na and HCO^{3}..... 104
5-24. Comparison of pre- and post-hydraulic-fracturing analyses of Area 2 waters for the ions Cl and SO_4 (units of mg/L) and radioactivity as gross alpha and gross beta (units of pCi/L)..... 104
5-25. Comparison of pre- and post-hydraulic-fracturing analyses of electrical conductivity in Area 2 waters..... 105
5-26. Pre- and post-hydraulic-fracturing sample temperatures for Area 2 waters.. 105
5-27. Pre- and post-hydraulic-fracturing methane concentrations in waters from Area 2.. 106
6-1. Event-tree diagram used for the evaluation of hydraulic fracturing fluid migration.. 111
6-2. Methane degassing scenario (OP4).. 112
6-3. Conceptual model of the regional groundwater flow system in the upper Humboldt River Valley. 114
6-4. Geologic cross section within exploration area 2. 115
6-5. Retardation factors for selected chemicals within the carbonate system..... 120
6-6. Conceptual model for the NP1 scenario in which fractures are contained in the Elko Formation.. 123
6-7. Scenario NP2: Fractures connect to an upward fault to the Indian Well Formation. 125
6-8. Probability of nonexceedance against downward propagating stimulated fracture height (ft).. ... 126
6-9. Observed upward fracture heights versus hydraulic fracture fluid volume injection.. 127

LIST OF TABLES

2-1. Lithology, thickness, extent and water-bearing characteristics of hydrogeologic units in the upper Humboldt River Basin, Nevada.. ... 17
2-2. Depth and thickness of hydrogeologic units penetrated by oil wells, upper Humboldt River Basin, Nevada. ... 22
3-1. Estimated mountain-block recharge for hydrographic basins within the upper Humboldt region. ... 35
3-2. MSAVI thresholds used in the evapotranspiration analysis. ... 39
3-3. Phreatophyte evapotranspiration area and annual discharge volume for each of the vegetation units. ... 39
3-4. Estimated gains/losses for streams by hydrographic area segment. ... 40
3-5. Estimated spring discharge by hydrographic basin. ... 42
3-6. Estimated well pumping for municipal, agricultural, and golf course wells. ... 47
3-7. Estimated groundwater budget. ... 48
4-1. Horizontal coordinates of the regional flow model mesh.. ... 52
4-2. Layer thicknesses in the regional flow model. ... 55
4-3. Values of calibrated model parameters. ... 61
4-4. Calculated groundwater budget and budget simulated by the regional model. ... 64
5-1. Chemical and isotopic parameters and the purpose these parameters were selected for the aquifer quality assessment program. ... 72
5-2. Chemical and isotopic parameters, units, analytical methods, and laboratories for water samples collected by Tetra Tech, Inc. ... 79
5-3. Chemical and isotopic parameters, units, analytical methods, and laboratories for water samples collected by DRI. ... 80
5-4. Comparison between duplicate TestAmerica (TestA) and Alpha Analytical (Alpha) results for methane and ethane.. ... 82
5-5. Comparison between duplicate TestAmerica (TestA) and Alpha Analytical (Alpha) results for TPH DRO and TPH GRO.. ... 84
5-6. Comparison between duplicate TestAmerica (TestA) and Alpha Analytical (Alpha) results for benzene, ethylbenzene, toluene, and xylene. ... 85
5-7. Comparison between duplicate DRI labs and TestAmerica results for Ca, Na, Li, and B. ... 87
5-8. Pre- and post-hydraulic-fracturing chemical and isotopic parameter analytical results for Exploration Area 2, Humboldt. ... 107
6-1. Shale permeability pummary. ... 117
6-2. Summary of flow and transport simulations performed for Scenario NP1 (Fractures contained in Elko Formation) and associated hydraulic and transport parameters and breakthrough results to the shallow aquifer. ... 122
6-3. Summary of flow and transport simulations performed for Scenario NP3 (Fractures connect to carbonate) and associated hydraulic and transport parameters and breakthrough results to the shallow aquifer. ... 128

LIST OF ACRONYMS

AMSTRAT	American Stratigraphic Company
AQUA Program	Aquifer Quality Assessment Program
BLM	U.S. Bureau of Land Management
BCM	Basin Characterization Model
CAS #	Chemical Abstract Service Number
DEM	Digital Elevation Model
DIC	Dissolved Inorganic Carbon
DRI	Desert Research Institute
EC	Electrical Conductivity
EPA	U.S. Environmental Protection Agency
ET	Evapotranspiration
HAs	Hydrographic Areas
HGU	Hydrogeologic Units
HUF	Hydrogeologic-Unit Flow
K_{ow}	octanol-water partition coefficients
K_{oc}	organic carbon sorption coefficients
MCL	Maximum Contaminant Level
MSDS	Material Safety Data Sheet
MOU	Memorandum of Understanding
MSAVI	Modified-Soil Adjusted Vegetation Index
MTBE	Methyl Tert-Butyl Ether
NAIP	National Agricultural Imagery Program
NDEP	Nevada Division of Environmental Protection
NDOM	Nevada's Division of Minerals
NIWR	Net Irrigation Water Requirement
NUFT	Non-isothermal Unsaturated-Saturated Flow and Transport
PCG	Preconditioned Conjugate-Gradient
RBC	Risk Based Concentrations
RMSE	Root Mean Squared Error
RSL	Regional Screening Levels
RWHet	Random Walk in Heterogeneous
STP	Standard Temperature and Pressure
TDS	Total Dissolved Solids
Tetra Tech	Tetra Tech, Inc.
TPH	Total Petroleum Hydrocarbons
TPH-DRO	Total Petroleum Hydrocarbons - Diesel Range Organics
TPH-GRO	Total Petroleum Hydrocarbons - Gasoline Range Organics
USGS	U.S. Geological Survey
UTM	Universal Transverse Mercator

THIS PAGE INTENTIONALLY LEFT BLANK

1.0 INTRODUCTION

1.1 AQUA PROJECT OVERVIEW

Noble Energy is actively engaged in the exploration of hydrocarbon resources (Figure 1-1) on 370,000 leased acres in Elko County, Nevada. The exploration wells are or will be drilled on a combination of private lands and lands managed by the United States Bureau of Land Management located in the upper Humboldt River Basin that stretch southwest from the Marys River Valley along the west side of the Ruby Mountains to the Huntington River Valley to the south. Figure 1-2 shows that the region is separated into three exploration areas.

This report represents the third of three reports by the Desert Research Institute (DRI) as part of the Aquifer Quality Assessment (AQUA) Program. The AQUA Program is the result of an agreement between the Nevada Division of Minerals (NDOM), the Nevada Division of Environmental Protection (NDEP), and Noble Energy to share and evaluate groundwater data and information gathered during exploration activities. The AQUA Program establishes a process by which Noble Energy, with assistance from DRI, will gather and share data and information on groundwater and geological conditions based on Noble's exploratory drilling. Data collection by groundwater monitoring and sampling, use of chemical and/or isotopic tracers, petrophysical logging, and microseismic monitoring are included in the program. Through the agreement, DRI is charged with using these data to develop a hydrologic model and prepare reports evaluating the fate and transport of chemicals used for hydraulic fracturing. These reports are expected to assist NDOM and NDEP in the development of a program to assess the effects of hydraulic fracturing stimulations in the state of Nevada.

Water quality monitoring and establishing baseline data prior to hydrocarbon resource development is an important part of the AQUA Program. The first two program reports focus on monitoring and the development of a baseline dataset of the chemical characteristics of groundwater, springs, and surface water in the exploration areas. The water quality data are updated here as a result of more recent sampling and analysis, and additional sampling is planned in conjunction with future exploration activities.

The Program requirement for development of a hydrologic model and evaluation of the fate and transport of chemicals used for hydraulic fracturing is the focus of this third report. It builds on interpretation of the water quality monitoring data and hydrogeologic data provided by Noble Energy and from other sources. It is presented as an interim report because the analyses and conclusions may require updating as additional data are obtained during future exploration activities and shared through the AQUA Program.

1.2 PHYSIOGRAPHY

The study area consists of nine hydrographic basins within the upper Humboldt River system (Figure 1-3). The hydrographic basins include Marys River (042), Starr Valley (043), North Fork (044), Lamoille Valley (045), South Fork (046), Huntington Valley (047), Tenmile Creek (048), Elko Segment (049), and Susie Creek (050). The study area is located in the headwaters of the Humboldt River, which originates in the Ruby, Jarbidge, and Independence Mountains and East Humboldt Range (Figure 1-4). The main stem of the Humboldt River receives flow from numerous tributaries including the North Fork Humboldt River, Marys River, Lamoille Creek, Huntington Creek, Tenmile Creek, Dixie Creek, and Susie Creek.

Figure 1-1. A Noble Energy drilling rig working in the upper Humboldt River basin (upper photo) and a pump jack installed at the completion of drilling (lower photo).

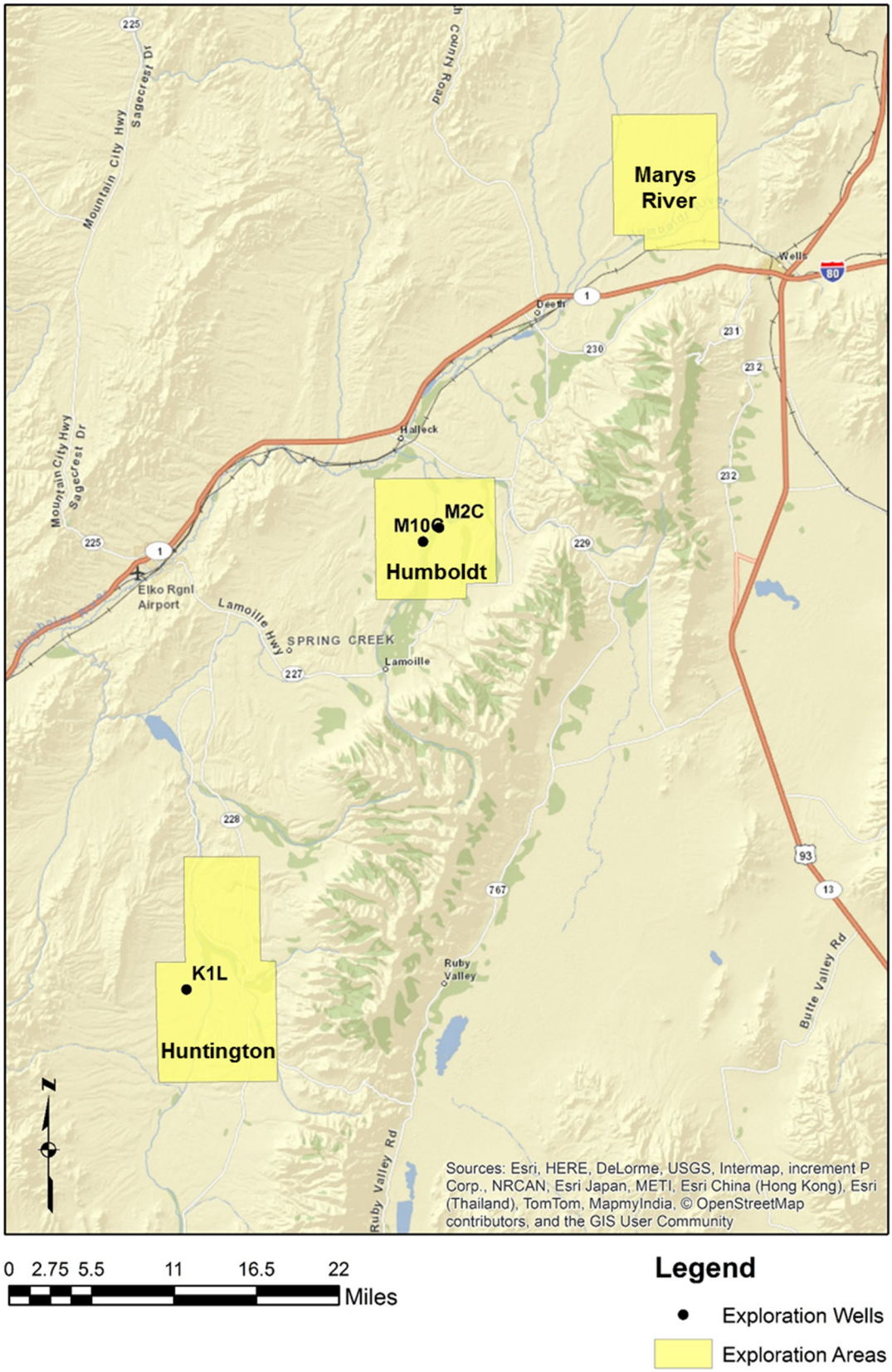

0 2.75 5.5 11 16.5 22 Miles

Legend

- Exploration Wells
- Exploration Areas

Figure 1-2. Location of Noble Energy's upper Humboldt River Basin exploration areas.

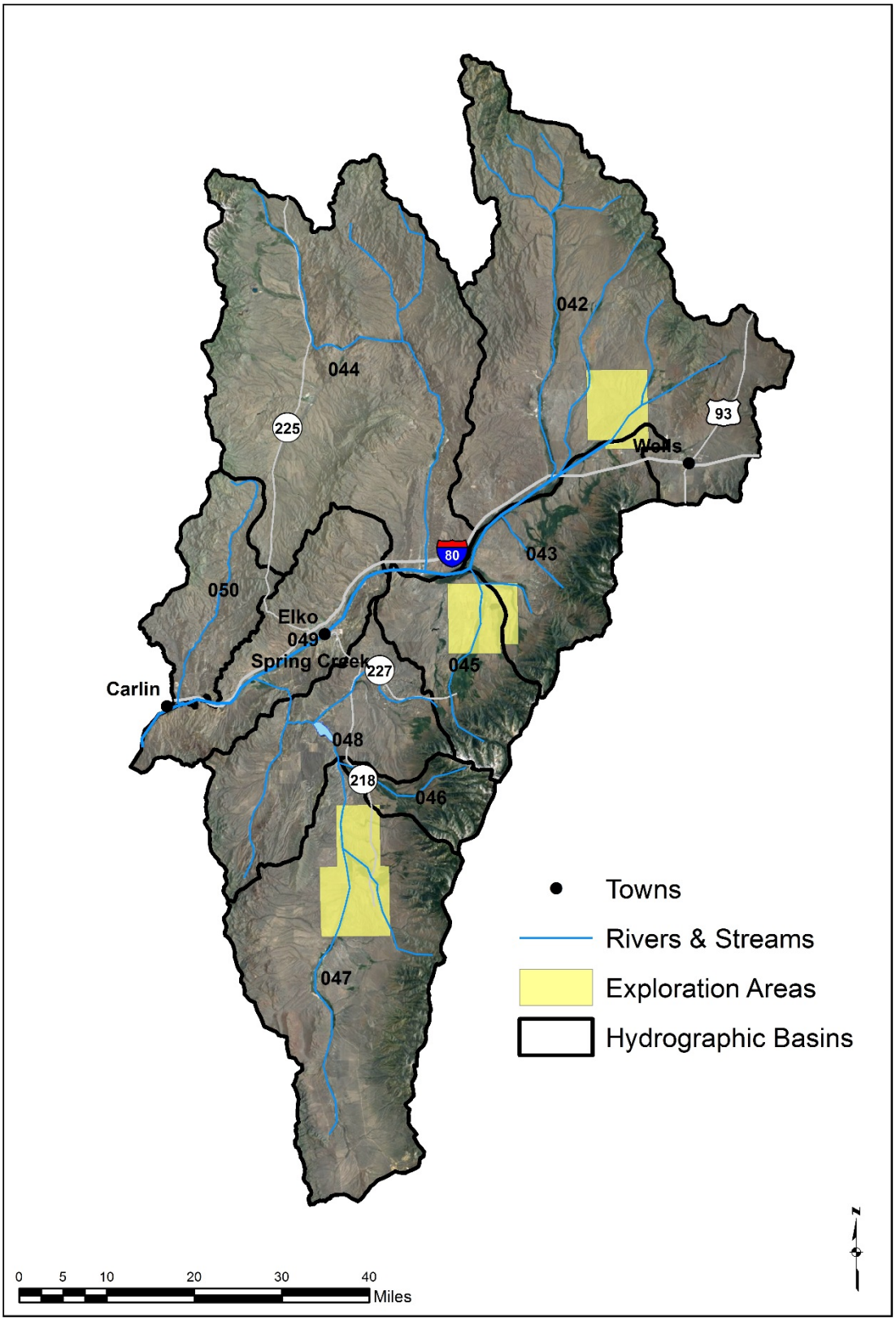

Figure 1-3. Hydrographic basins within the study area.

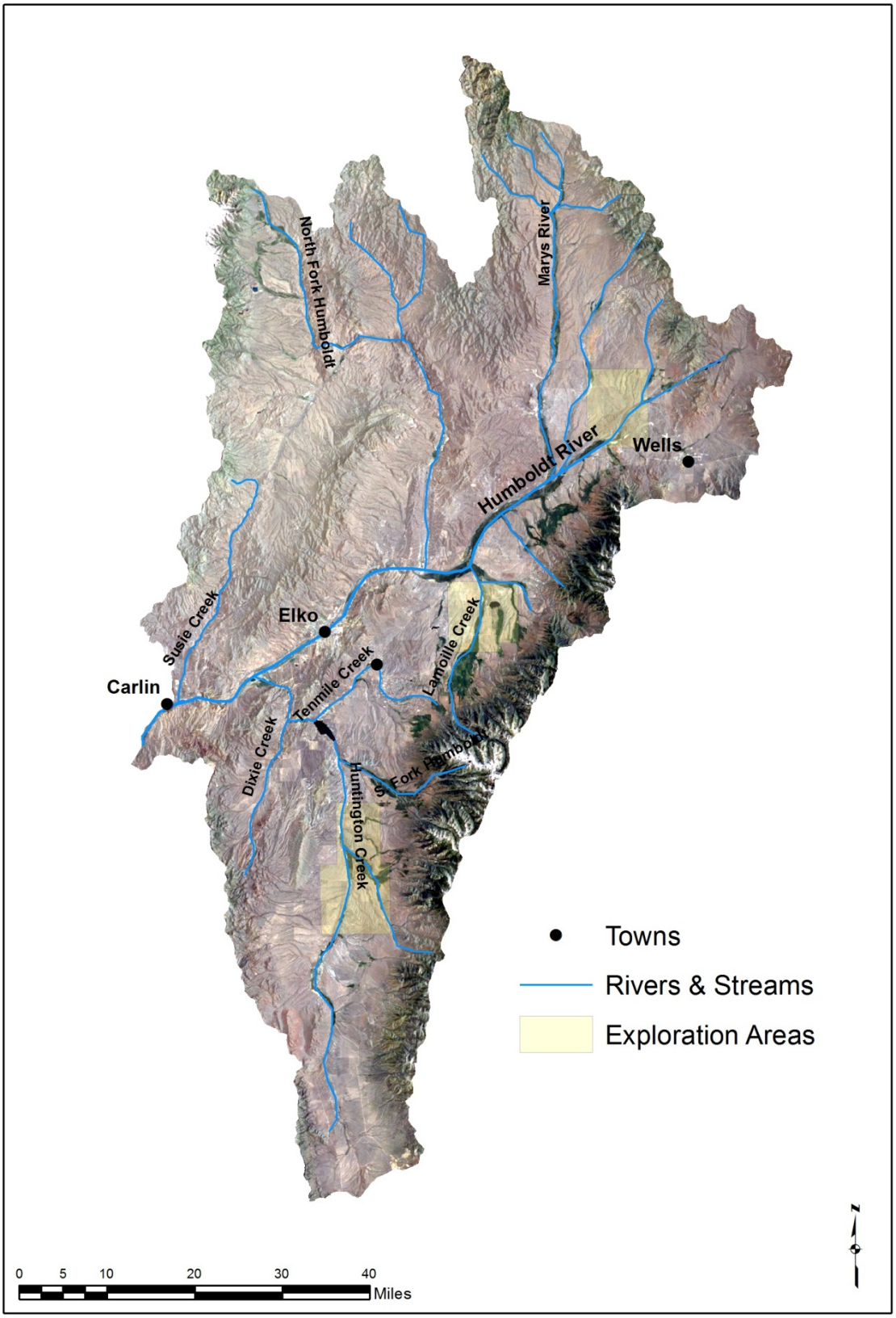

Figure 1-4. Rivers and streams within the study area.

North-south oriented mountain ranges dominate the landscape. North of the Humboldt River, Marys River drains a broad valley that is at an elevation of approximately 5,500 ft. The Jarbidge Mountains extend to elevations above 10,500 feet at the northern end of Marys River Valley. The Independence Mountains are the boundary of the northwestern portion of the study area and land-surface altitudes are near 10,000 ft. South of the Humboldt River, land-surface altitudes are more than 11,000 ft in parts of the Ruby Mountains and East Humboldt Range. Huntington Valley is another north-south-trending valley and it is at an elevation of 5,500 ft in the southern portion of the study area.

The study area covers nearly 4,600 square miles and is located primarily in Elko County, which has population of just over 50,000. The southern region extends into White Pine County. The main population centers include Wells, Elko, Carlin, and Spring Creek.

1.3 CLIMATE

The upper Humboldt River Basin is characterized by two climatic types (Houghton *et al.*, 1975, p. 3) that can be described as (1) mid-latitude steppe with cold winters, hot summers, and semiarid conditions and (2) subhumid continental with cold winters and moderate precipitation. The mid-latitude steppe climate type generally corresponds to lowlands and the subhumid continental climate type generally corresponds to mountain ranges. Average low temperatures in the winter months are near 10 °F and high temperatures in the summer exceed 90 °F (Western Regional Climate Center, Elko Airport). Precipitation in the area is derived primarily from snow in the upper elevations. Figure 1-5 shows that mean annual precipitation ranges from approximately 10 inches in the valleys to more than 36 inches in the Ruby, Jarbidge, and Independence Mountains and East Humboldt Range (PRISM Climate Group, 2012).

1.4 OVERVIEW OF HYDRAULIC FRACTURING

Hydraulic fracturing is a well completion technique in which the reservoir rock is altered to increase the flow of oil or natural gas to the wellbore by fracturing the formation surrounding the wellbore and placing sand or other granular materials in those fractures to prop them open. The purpose of hydraulic fracturing is to increase the permeability of the formation so that oil or gas can be extracted economically. Permeability is the parameter that describes the ability of fluid to flow through the subsurface. Shale units have permeabilities on the order of 10^{-8} to 10^{-4} darcies (Freeze and Cherry, 1979). For comparison, a productive groundwater aquifer has a permeability of 10^{0} to 10^{2} darcies.

The hydraulic fracturing process occurs after a well has been drilled, cased, and cemented. Often, the hydraulic fracturing treatments are performed in multiple stages. To provide isolation between the fracture intervals, a plug or packer is set above and below the specified interval. The next step involves perforating the well casing in the target zone by setting a small charge. To hydraulically fracture the formation, an engineered fluid is injected under pressure in a controlled process. Fluid pressures are increased to counteract the least compressive stress in the rock, which causes the rock to fracture or crack. Vertical stress is typically the largest stress force in a deep rock layer because it results from the overburden pressure. Therefore, vertical fractures are more commonly produced because it takes less force to move the rock to the side (vertical fracture) than to lift the overlying rock with a horizontal fracture. Vertical fractures also tend to parallel the maximum horizontal stress in the formation. Although many companies are moving toward horizontal well completions, Noble Energy is using vertical wells.

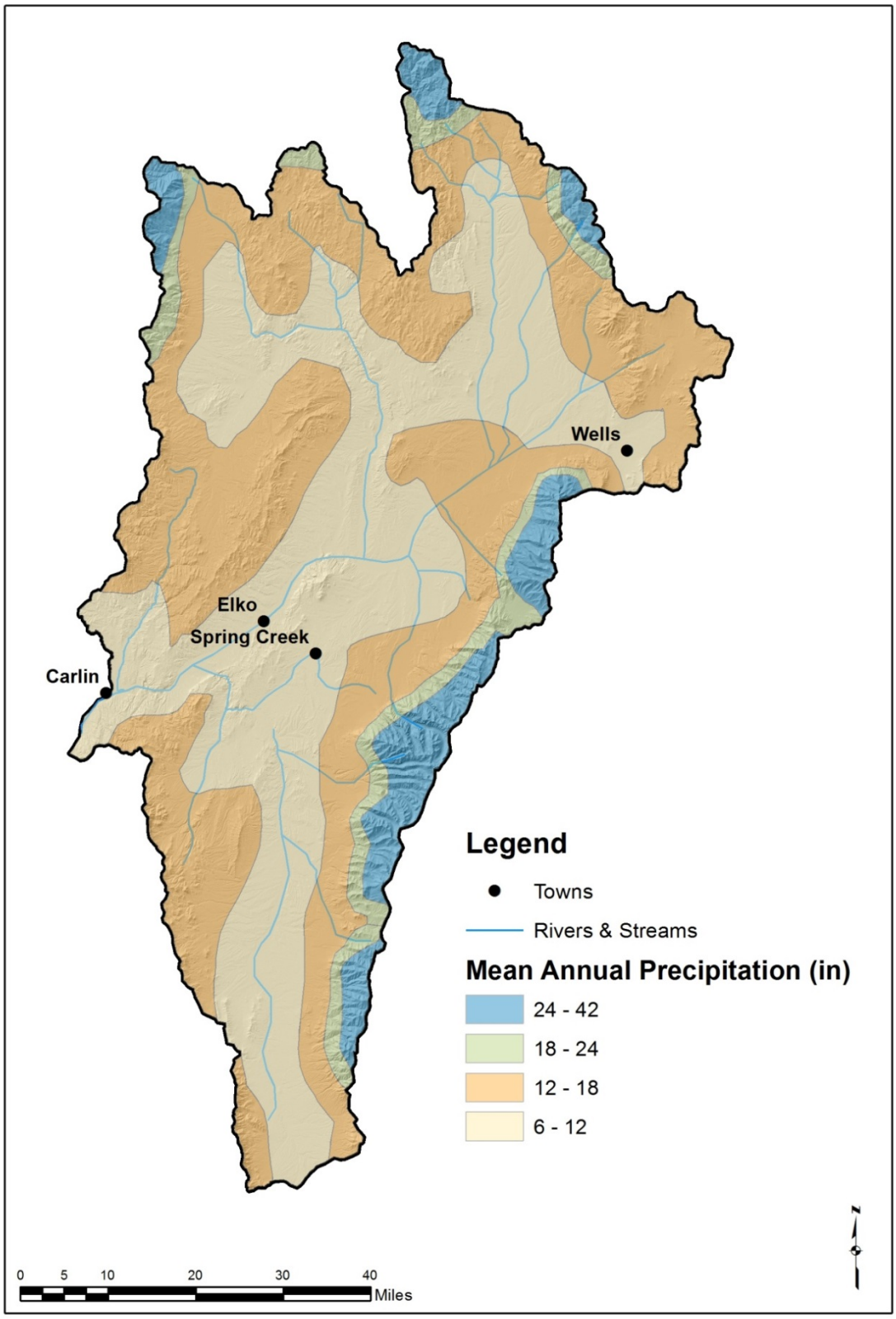

Figure 1-5. Distribution of mean annual precipitation (1981-2010) for upper Humboldt River Basin. Mean annual precipitation derived from 2.5 mile square grid (PRISM Climate Group, 2012).

The concept of fracturing rock within an oil reservoir is not new. One of the first efforts to enhance oil production came from Edward Roberts in 1864. Roberts developed a "petroleum torpedo" that consisted of tin cylinders filled with several pounds of gunpowder that were designed to detonate downhole to enhance oil production. In his patent, Roberts says, "In my improved method of increasing the capacity of wells, I fracture the rock containing the oil to some distance around the wells, thus creating artificial seams, and enabling me to connect the well thereby with seams containing the oil that would not have been otherwise reached by the well" (U.S. Patent No. 59,936, 1866).

Other companies have explored for oil from shale in northeastern Nevada. In 1916 near Elko, Nevada, Robert Catlin drilled a shaft that a short-lived plant used to pull oil from shale. Nevada's only successful oil-from-shale operation peaked in the early 1920s, but the plant then closed in the fall of 1924 because the oil was said to be too expensive to compete with other fossil oils of the time (Reno Gazette-Journal, 2014).

The first hydraulic fracturing experiment was performed in the Hugoton natural gas field in southwestern Kansas in 1946 by Stanolind Oil (Gold, 2014). Bob Fast, a petroleum engineer, used gasoline and napalm, which was readily available from World War II, as the hydraulic fracturing fluid. Although the experiment successfully fractured the limestone, it did not produce enough natural gas to be economically viable. J.B. Clark of Stanolind Oil then wrote and published a paper in *Transactions of the American Institute of Mining Engineers* to document the results and introduce the new technology (Montgomery and Smith, 2010). In 1949, a patent was issued to Halliburton Oil Well Cementing Company that granted them the exclusive right to the new "hydrafrac" process (Montgomery and Smith, 2010).

Early on, companies were using cross-linked gels as fracturing fluids because they had a higher capacity to carry the proppants that kept the fractures open. Gels have high viscosities and require higher fluid injection pressures than those typically used in slickwater operations because friction losses are greater. Slickwater fracture treatments have become the standard industry method. This treatment is termed "slickwater" because it uses water and friction-reducing agents, and therefore does not require the high pressurization that gel-based methods do.

Slickwater hydraulic fracturing fluid is generally made up of 99 percent water and sand (U.S. Department of Energy, 2009). When horizontal wells are used, the volume of water required per well ranges between 7 and 12 acre-ft (U.S. Department of Energy, 2009). Noble Energy uses vertical wells, which require significantly less water. For example, the amount of water used to hydraulically fracture Noble Energy's first well in northeastern Nevada (M2C-M2-21B) is 0.8 acre-ft. To gain a perspective on how much water this is, the total annual streamflow in the Humboldt River (near Carlin) is 316,000 acre-ft/yr (Plume and Smith, 2013). Total groundwater recharge is approximately 276,000 acre-ft/yr.

Hydraulic fracturing fluid (slickwater) contains multiple chemical constituents that each have a specific function. Typical hydraulic fracturing fluid may contain (< 1 percent) the following types of constituents:

- Water
- Friction reducer – used to reduce the friction losses of the fluid when injected
- Biocide – used to control the growth of microbes

- Surfactants – used to modify the surface tension and prevent emulsions
- Thickeners – gelatinous chemicals used to help carry the proppants
- Scale inhibitor – prevents mineral scale precipitates
- Acid – used to reduce the fracture initiation pressure
- Corrosion inhibitor – prevents corrosion of the acidic portion of the fluid on the well
- Cross-linker – maintains fluid viscosity as temperature increases
- Stabilizer – prevents clays from swelling
- Breaker – allows a delayed breakdown of the gel

Tables C-1 through C-3 list the fracking fluid chemicals used for wells Humboldt M2C-M2-21B, Humboldt M10C-M10-11B, and Huntington K1L-1V. The chemicals and concentrations are from FracFocus.org. Few organic carbon sorption coefficients (K_{oc}) and octanol-water partition coefficients (K_{ow}) are known. Maximum Contaminant Levels (MCLs), Risk Based Concentrations (RBCs), and Regional Screening Levels (RSLs) are identified to provide an indication of the health risks associated with the chemicals. Risk Based Concentrations, MCLs, and RSLs are from Material Safety Data Sheets (MSDSs) and Jackson (2013). The total water volume for HF fluids may include fresh water, produced water, and/or recycled water. Percentages for individual chemical constituents are based on the maximum potential concentration, and therefore the total may be over 100 percent. Calculation of maximum chemical concentration in the hydrofracking fluid by volume is calculated by dividing the maximum ingredient concentration by mass by the chemical specific gravity.

1.5 Literature Review

This section provides a review of the literature available that discusses the potential environmental effects of hydraulic fracturing. Although studies have focused on a range of environmental consequences—including shallow aquifer water quality and quantity, air quality, induced seismicity, and other impacts—this review focuses solely on the potential impacts to aquifers. Most of the studies associated with environmental impacts of hydraulic fracturing are relatively new (post-2009) but hydraulic fracturing has been going on since the 1940s.

Hydraulic fracturing can affect groundwater resources if there is both a high-permeability pathway and a hydraulic gradient that directs fluids toward aquifers. Most of the environmental assessments focus on high-permeability pathways. Gassiat *et al.* (2013) is one of the few studies that investigated the conditions that lead to permeable paths and the increased pressures that lead to an upward hydraulic gradient. Gassiat *et al.* (2013) developed a two-dimensional, single-phase, multispecies, density-dependent, finite-element numerical groundwater flow and mass transport model to simulate hydraulic fracturing in the vicinity of a permeable fault zone in a low-recharge, regional sedimentary basin with shallow groundwater flow. Their results showed that specific conditions are needed for the contamination of a shallow aquifer: a high-permeability fault, high overpressure in the shale unit, and hydrofracturing in the upper portion of the shale near the fault. Under these conditions, contaminants from the source (shale) unit could reach the shallow aquifer in less than 1,000 years following hydraulic fracturing at concentrations of solutes up to 90 percent of their initial concentration in the shale, which indicates that the impact on groundwater quality could be significant. The simulated conditions represent

hydraulic fracturing located directly adjacent to a high-permeability fault reaching depths of greater than 2 km that is connected to the near-surface environment. In Nevada, it is likely that faults of this nature would be associated with geothermal systems (i.e., outflow zones and hot springs).

Transport of contaminants through preexisting pathways has occurred in conventional oil and gas operations, but whether hydraulic fracturing is likely to enhance the problem remains to be determined (California Council on Science and Technology, 2014). Data concerning the existence of high-permeability pathways are limited. There are a few ongoing studies assessing the likelihood that these conditions can exist in deep geologic environments. In 2011, the U.S. Environmental Protection Agency (EPA) began research under its "Plan to Study the Potential Impacts of Hydraulic Fracturing on Drinking Water Resources." The purpose of the study is to assess the potential impacts of hydraulic fracturing on drinking water resources and to identify the driving factors that may affect the severity and frequency of such impacts. Scientists are focusing primarily on the hydraulic fracturing of shale formations to extract natural gas, with some assessment of other oil-and-gas-producing formations such as tight sands and coalbeds (U.S. EPA, 2012).

Halliburton Energy Services submitted a letter directly to the EPA to highlight key features that the EPA study should address (Jackson, 2013b). In particular, Jackson (2013b) suggests that the two conditions that are required for the upward migration of hydraulic fracturing fluids (upward gradient and high-permeability pathways) are mutually exclusive. The hypothesis is that natural upward head gradients occur only in low-permeability environments, such as shale plays.

The literature consists primarily of a few groups of competing and contentious studies, none of which provide direct evidence of fracturing leading to the contamination of groundwater (California Council on Science and Technology, 2014). However, the fact that no direct evidence has been found does not mean that additional research is not necessary. On the contrary, these conditions need to be investigated over the range of possible geologic conditions found in hydraulic fracturing operations.

Poor well construction is thought to have the highest likelihood of generating conditions that allow gas and fluid migration (Watson and Bachu, 2009). One factor that can lead to poor well construction is an incomplete cement job. Harrison (1983) suggests that overpressured annuli are a likely mechanism for groundwater being contaminated with produced gas or other formation fluids, even for wells that use a surface casing to protect shallow aquifers and particularly if the surface casing does not extend to a sufficient depth below the aquifer. Well barriers can also fail if the surface casing does not extend to a sufficient depth below the freshwater aquifer. During hydraulic fracturing operations, there has been concern that the expansion and contraction of the steel casing during the multiple stages of high-pressure injection may result in radial fracture and/or shear failure at the steel-concrete or concrete-rock interfaces (Carey *et al.*, 2012). Other factors that can create a pathway for hydraulic fracturing fluids to migrate upward include tectonic activity, subsidence events, radial cracking of the cement because of thermal and pressure fluctuations in the casings during production, and general degradation of the well structure because of age (Bonnet and Parfitis, 1996; Dusseault *et al.*, 2000; Brufatto *et al.*, 2003; Watson and Bachu 2009; Carey *et al.*, 2012). Corrosive subsurface environments can also pose a threat to cement and casings throughout the life of a well (Brufatto *et al.*, 2003; Chilingar and Endres, 2004). It is important to note that well integrity was addressed in the development of Nevada's regulations, which require before the use of intermediate casing, cement seals, cement bond logs, and pressure testing of casing to significantly reduce the potential for well failure. Given the very low probability of well failure in Nevada hydraulic fracturing operations, this study did not model the effects of well failure.

Myers (2012) was one of the first modeling studies to suggest that hydraulic fracturing fluid could migrate upward to shallow aquifers in tens to hundreds of years. The author admits that "the complexities of contaminant transport from hydraulically fractured shale to near-surface aquifers render estimates uncertain" and that "there is no data to verify either the pre- or post-fracking properties of the shale" (Myers, 2012). Others have disputed the underlying assumptions and parameterization used in the Myers (2012) study (Carter *et al.*, 2013; Vidic *et al.*, 2013). Vidic *et al.* (2013) note that the Myers (2012) modeling erroneously assumed that the hydraulic conductivity represents water-filled voids in the geological formations but that not all of the formations are water saturated. Vidic *et al.* (2013) also point out that the assumption of preexisting, 1,500-m-long vertical fractures is hypothetical and not based on geologic exploration.

Flewelling and Sharma (2014) evaluated the physical constraints on the upward migration of hydraulic fracturing fluid from shales (e.g., Marcellus, Bakken, and Eagle Ford) to shallow aquifers. They concluded that the upward migration of hydraulic fracturing fluid is unlikely because: 1) the stratigraphy above black shales is typically dominated by shales, siltstones, and mudstones, which have low permeability; 2) hydraulic fracturing affects a much smaller thickness of rock than that of the overburden; and 3) the natural upward hydraulic head gradients only exist in systems with low permeability, which inherently limit transport to timescales beyond 10^6 years.

Cai and Ofterdinger (2013) developed a three-dimensional discrete fracture model that represented data from a Bowland Shale gas exploration in Lancashire, United Kingdom, to determine the potential for migration to the overlying groundwater aquifer. Their results suggested that when induced fractures within the Bowland Shale are < 200 μm, migration of hydraulic fracturing fluid is unlikely. In situations with fracture apertures greater than 1,000 μm, the upward flux becomes very sensitive to upward fracture height growth and the hydraulic conductivity of the multilayered bedrock system. Migration times to the upper aquifer could be on the order of 100 years if the fracture aperture is greater than 1,000 μm.

Kissinger *et al.* (2013) conducted a modeling study to investigate the potential migration of hydraulic fracturing fluids through faults to shallow groundwater systems. The models were parameterized to reflect conditions in the North Rhine-Westphalia and Lower Saxony regions in Germany. Three scenarios were used to simulate the range of possible conditions at the site. In scenario 1, they found that short-term propagation of hydraulic-fracture fluid because of the high pressures induced by hydraulic fracturing activities leads to a maximum vertical migration length of 50 m if high-permeability faults are present. Scenario 2 investigated the long-term migration of hydraulic fracturing fluids and the results indicated that migration to the shallow aquifer (1,300 m above) is possible within 30 years if a strong vertical hydraulic head gradient and large fault permeability exist. Although transport was simulated in scenario 2, concentrations within the shallow aquifer were found to be 4,000 times smaller than the initial concentrations within the hydraulic fracturing zone. Scenario 3 simulations showed that a methane leak into the shallow layers through the overburden is only possible if several assumptions, which are considered to be conservative, are made. These assumptions include a high-permeability fault zone that intersects the source zone and shallow aquifer, low residual saturation, and low porosity. The authors noted that scenario 3 is highly unlikely because hydraulic fracturing operations probably would not be carried out in such an environment because oil would not exist in a zone that is intersected by a high-permeable fault.

Fisher and Warpinski (2011) investigated thousands of hydraulic fracturing treatments in the Barnett Shale in Texas, the Woodford Shale in Oklahoma, the Marcellus Shale in the northeastern United States, and the Eagle Ford Shale in south Texas. Their results indicated that the largest, directly measured, upward growth of all of these mapped fractures still places the fracture tops several thousand feet below the deepest known aquifer level in each of the reservoirs presented. Another important conclusion is that most of the larger fractures (both downward and upward) are a result of hydraulic fractures intercepting with natural faults. Note that the fracture heights were measured using microseismic tools that require displacement of a fracture. It is not clear if hydraulically stimulated fractures may have intersected a natural high-permeability fault that intersects a shallow aquifer, but fracture displacement was not measured. The authors acknowledged that high-permeability layers have a significant effect on fracture growth because they can either act as thief zones that accept fluid and reduce the fracture-driving forces or they can induce a large poroelastic backstress that clamps down on the fracture.

Davies *et al.* (2012) reviewed the heights (n = 1,170) of upward propagating hydraulic fractures from several thousand fracturing operations in the Marcellus, Barnett, Woodford, Eagle Ford, and Niobrara Shale sites. The maximum reported height is 1,929 ft (588 m). The probability of stimulated and natural hydraulic fractures extending vertically > 1,150 ft (350 m) is approximately 1 percent and 33 percent, respectively.

A more recent study (Flewelling *et al.*, 2013) analyzed the upward development of over 12,000 hydraulic fractures in North America using microseismic data. The maximum extent of the stimulated fracture height was less than 600 m above well perforations. A mathematical relationship was developed between the amount of hydraulic fracturing fluid used in the stimulation process and the fracture height. The relationship between stimulated fracture height and injection volume appears to be an upper bound because the empirical data generally falls below the predicted fracture heights. The primary conclusion of the Flewelling *et al.* (2013) study is that direct hydraulic communication between tight formations and shallow groundwater via induced fractures and faults is not a realistic expectation based on the limitations on fracture height growth.

Osborn *et al.* (2011) determined that there is a strong correlation between gas well location and methane contamination in shallow aquifers. Osborn *et al.* (2011) sampled water from 60 drinking-water wells in a gas producing region of northeastern Pennsylvania. They found that methane concentrations in wells increased with increasing proximity to gas wells. Isotopic ratios of the sampled gas indicated a thermogenic source for the gas and matched the geochemistry of gas from nearby production wells. Their research developed a lot of controversy because the migration mechanism for the shallow gas contamination could not be fully explained. There was no evidence of contamination of high TDS and/or hydraulic fracturing fluid in the shallow wells, but it is known that gas and liquid transport do not necessarily occur together or at similar timescales. Other investigators (Davies, 2011; Schon, 2011) hypothesized that gas leakage through well casings is more likely than a hydraulic fracturing process. Davies (2011) also suggested that high thermogenically derived methane concentrations may be preexisting, noting that such processes are already documented and well understood (Dyck and Dunn, 1986) for oil and gas producing formations and that a lack of evidence for fracturing fluids in the contaminated water supports ongoing natural processes. The only solid conclusion from the Osborn *et al.* (2011) study is that there is a strong correlation between gas well location and the appearance of shallow stray gas contamination.

Jackson *et al.* (2013a) sampled numerous water wells near Marcellus production well locations. They found ethane, propane, and methane and noted a thermogenic origin for the methane. The authors proposed that the most plausible mechanism for this was leakage caused by problems with the well casing and cementation and noted the number of violations recorded for well-construction issues in nearby production operations. In contrast, an isotopic study by Molofsky *et al.* (2013) stated that the isotopic ratios of methane found in Pennsylvania wells are more consistent with samples of shallower Upper Devonian Formation gas than with Marcellus Formation gas, which casts doubt on the source of the dissolved gas and the existence of connecting pathways.

Cardno ENTRIX (2012) reviewed ten years of hydraulic fracturing and gas production from oil and gas fields in the Los Angeles area. Microseismic data indicated that that hydraulically stimulated fractures were restricted to a distance of 7,700 ft (2,350 m) to the base of the freshwater zone. The study showed no impacts to groundwater quality through the migration of fracturing fluids, formation fluids, or methane gas, even though the formation includes faults and fractures connecting shallow formations to deeper formations. Additionally, no evidence was found of well casing failure when wells were constructed to industry standards. Therefore, no direct contamination occurred via stimulation or production activities.

Kell (2011) conducted one of the most extensive reviews of existing hydraulically induced groundwater-contamination data. This study focused primarily on Ohio and Texas and investigated over 16,000 horizontal hydraulic fracturing wells drilled between 1983 and 2008. The results showed that the literature provides no conclusive documentation of groundwater contamination resulting from the process of hydraulic fracturing.

Roy and Ryan (2013) advocate obtaining background field measurements of total dissolved gas pressure and gas isotopes in shallow groundwater aquifers prior to hydraulic fracturing so that changes in groundwater chemistry after fracking can be traced. Although not in widespread use, the authors suggest taking field measurements of the total dissolved pressure of the gas to provide useful information during investigations of the effects of natural gas development on groundwater.

Heilweil *et al.* (2013) demonstrated the benefit of sampling stream reaches for methane gas concentration and isotope characterization as a reconnaissance tool for delineating natural and anthropogenic methane in ground and surface water. Their study showed that methane injected into a stream was not immediately lost to the atmosphere, but remained in the stream for more than 6,600 ft (2,000 m). The implication is that measuring methane in gaining streams could provide a cost-effective, integrated measurement of groundwater quality.

King (2012) provides an introduction to fracking technique, background, regulation, and risk using existing case studies. The study is designed as a starting point for ongoing discussions on well design for minimizing environmental and health risks and the evolution of regulation and oversight in the fracking industry. One of the main conclusions is that properly constructed wells that are greater than 2,000 ft below ground surface depth pose little to no risk (less than 10^{-6}) of hydraulic fracturing fluid or thermogenic gas contamination in shallow ground and surface water. More likely causes of aquifer contamination include improperly sealed wells or surface spills and leaks.

Lange *et al.* (2013) evaluated the risk of groundwater contamination from hydraulic fracturing operations in the Munsterland Basin and the Lower Saxony Basin in Germany. Although the study focused on the geologic conditions found at the two sites in Germany, the recommendations were

generalized. The researchers focused on barrier effectiveness of different units of the overburden with respect to the migration of hydraulic fracturing fluids and methane, and considered fault zones to be the potential fluid pathway structures.

All Consulting (2012) provided a review of hydraulic fracturing in the Canadian Shale oil and natural gas plays. The report focused on the best management practices and potential pathways of fluid migration, the risk involved, and the past incidents that were attributed to hydraulic fracturing. Five hypothetical pathways from which hydraulic fracturing fluid could contaminant shallow aquifers were identified and analyzed. The analysis of each of these pathways demonstrates that it is highly improbable that fracture fluids or reservoir fluids would migrate from the production zone to a freshwater source as a result of hydraulic fracturing.

2.0 GEOLOGIC FRAMEWORK

2.1 HYDROGEOLOGIC UNITS

The many different geologic units shown on the geologic maps of Elko, Eureka, and White Pine Counties (Coats, 1987; Roberts *et al.*, 1967; and Hose *et al.*, 1976) are grouped, for the purposes of this study, into two general hydrogeologic groups—Cenozoic units above basement rock and Cenozoic units below basement (Plate 1 and Table 2-1). Cenozoic units above basement are further subdivided into six hydrogeologic units based on age and lithology. From oldest to youngest the units are: (1) older volcanic rocks of Oligocene and Eocene age, (2) Elko Formation of early Oligocene and late Eocene age, (3) Indian Well Formation of late Oligocene age, (4) younger volcanic rocks of Miocene and late Oligocene age, (5) Humboldt Formation of late Miocene age, and (6) alluvium of Holocene to Pliocene age. These six units overlie Cenozoic basement that is subdivided into five hydrogeologic units: (1) crystalline rocks of Tertiary, Cretaceous, Jurassic, and late Precambrian age; (2) older carbonate rocks of Devonian to Cambrian age; (3) thrusted clastic sedimentary rocks of Devonian to Ordovician age; (4) clastic sedimentary rocks of Pennsylvanian and Mississippian age; and (5) younger carbonate rocks of Permian and Pennsylvanian age. Descriptions of each of these units below are based on the county maps referred to above and on several area-specific geologic studies.

Oil well logs were used to further define the distribution of hydrogeologic units at depth in the project area. The Nevada Bureau of Mines and Geology maintains a file for each oil well that has been drilled in Nevada. These files are available online at: http://www.nbmg.unr.edu/Oil&Gas/NVWellInfo.html. There are 31 oil wells (most plugged and abandoned) in the project area-28 in Elko County and 3 in White Pine County (Plate 1 and Table 2-2). The information found in the files and used for this report includes lithologic logs (usually referred to as mudlogs), picks of formation tops, and intervals where drillstem tests were conducted and intervals of lost circulation. Drillstem tests are used to determine the permeability of an interval of the hole and even if the test is not successful, test results still provide qualitative information such as the amount of water produced during the test and the approximate altitude of the potentiometric surface of the interval. Intervals of lost circulation (drilling mud is being lost into the formation) provide qualitative evidence of relatively high permeability, especially when compared with intervals above and below where circulation was maintained.

2.1.1 Cenozoic Basement

Cenozoic basement forms the surface on which early Miocene, Oligocene, and Eocene hydrogeologic units were deposited and also forms the structural basin in which middle Miocene and later units accumulated. The distribution of the top of Cenozoic basement in the project area is presented in Figure 2-1 as contours of the altitude of the surface above and below sea level. The data points used to define this surface are altitudes of the top of Cenozoic basement in areas of outcrop and in the subsurface at 27 of the 31 oil wells in the project area. The contours of the top of Cenozoic basement is shown in Figure 2-1.

The most striking feature of the Cenozoic basement map is the deep, narrow structural basin that closely parallels the Ruby Mountains-Humboldt Range-Snake Mountains range fronts from southern Huntington Valley to the northern Marys River area, a distance of approximately 180 kilometers. Detachment faulting that resulted in uplift of the Ruby Mountains-East Humboldt Range-Snake Mountains and simultaneous formation of the adjacent structural basin to the west occurred in the middle Miocene (Wallace *et al.*, 2008, p. 58-63). Continuing volcanic

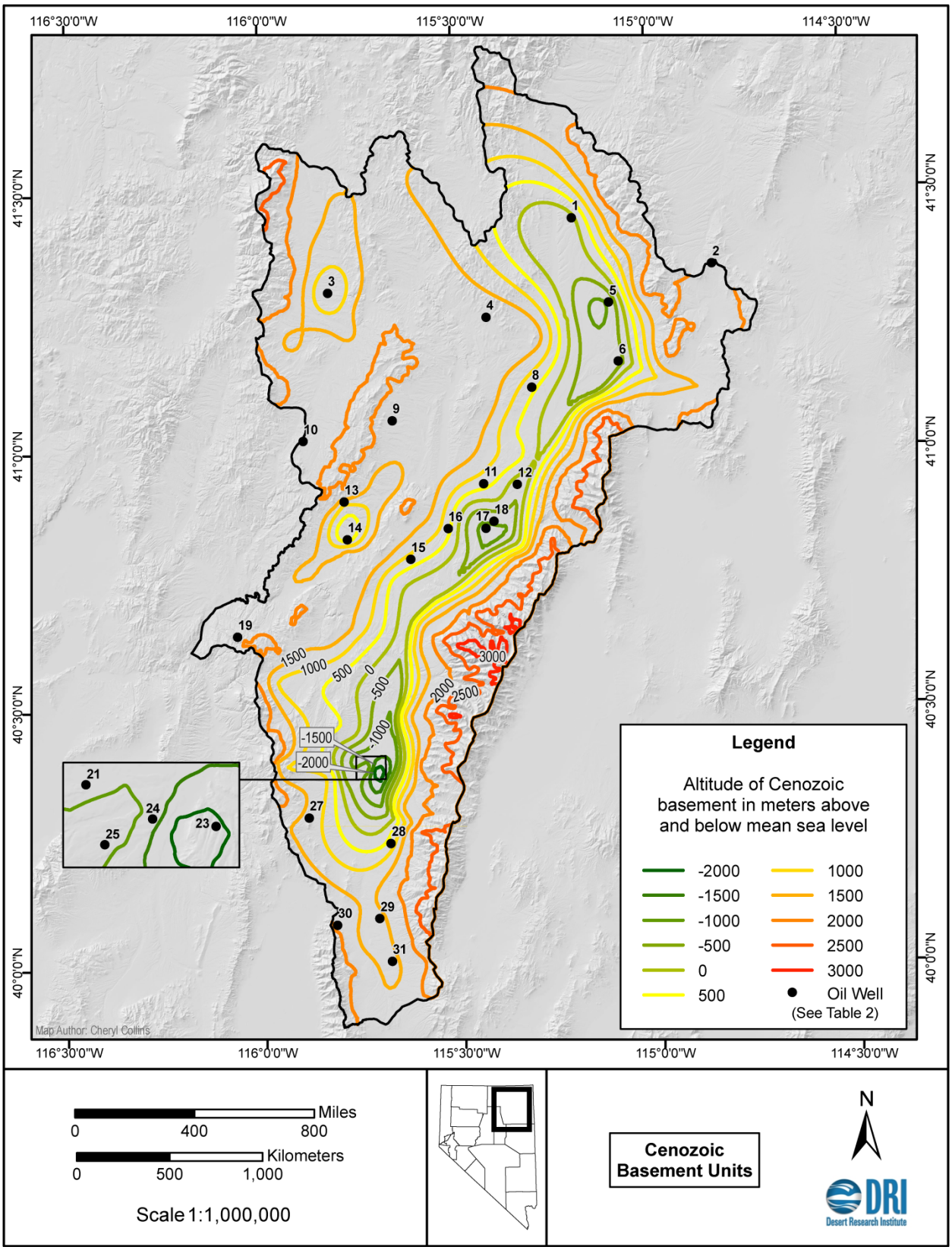

Figure 2-1. Distribution of Cenozoic basement in the upper Humboldt River basin, northeastern Nevada.

Table 2-1. Lithology, thickness, extent and water-bearing characteristics of hydrogeologic units in the upper Humboldt River Basin, Nevada. Sources of data for oil wells were the Nevada Bureau of Mines and Geology at http://web2.nbmg.unr.edu/Oil_and_Gas/list/oil/logs/Oil_and_Gas_by_API.htm and AMSTRAT[1] logs.

CENOZOIC UNITS				
Geologic Age	**Rock or Stratigraphic Unit**	**Hydrogeologic Unit**	**Lithology, Thickness, and Extent**	**Remarks**
Holocene, Pleistocene, and Pliocene	Alluvium, glacial outwash, and Hay Ranch Formation. Map units Qa, Qp, Qg, Qls, Qta, QTs, and QTls of Coats (1987, Plate 1).	Alluvium	Sorted and interbedded clay, sand, and gravel of stream floodplains less than 50 m thick. Poorly sorted to unsorted clay, silt, sand, gravel, and boulders of alluvial fans as much as 1,000 m thick. Includes glacial outwash on alluvial fans west of Ruby Mountains and East Humboldt Range.	Comprises shallow water-table aquifers and deeper confined aquifers. At oil well 1 porosity of gravel at depths 0-29 meters was 6-12 percent (AMSTRAT log D-2519). Oil well 24 penetrated in interval of lost circulation at depths 1,320-1,325 meters. Oil well 31 penetrated an interval of lost circulation at depths of 54-55 meters.
Late Miocene	Humboldt Formation. Map unit Ts3 of Coats (1987, Plate 1).	Humboldt Formation	Deposits of fluvial and lacustrine origin. Includes deposits of alluvial fans, stream flood plains, and shallow lakes. Deposits commonly are tuffaceous and interbedded with volcanic rocks. Exposed in northern and central parts of project area. Occurs at depths ranging from less than 100 to 1,400 meters in central and southern Huntington Valley. Thickness variable ranging from less than 100 m to nearly 2,000 m.	Comprises shallow water-table aquifers and deeper confined aquifers. Oil well 3 penetrated two intervals of lost circulation between depths of 152 and 327 meters. Oil well 6 penetrated an interval of lost circulation at depths of 1,189-1,289 meters. A drillstem test at oil well 7 at depths of 451-483 meters recovered 387 cubic meters of water, indicating moderate permeability. At oil well 14 porosity of sandstone and conglomerate was greater than 20 percent and porosity of interbedded tuff was low (AMSTRAT log D-4541). At oil well 16 porosity of conglomerate and sandstone was 12 to more than 20 percent at depths of 6-110 meters and less than 6 percent at greater depths (AMSTRAT log D-2713). At well 17 an interval of lost circulation was penetrated at depths of 1,820-1,856 meters. At oil well 26 a drillstem test at depths of 1,215-1,227 meters recovered 1,081 cubic meters of water and drilling mud. Oil well 31 penetrated three intervals of lost circulation at depths of 399-408, 411-418 and 448-452 meters.
Miocene and Late Oligocene	Jarbidge rhyolite and other volcanic rocks. Map units Ta_2, Ta_3, Tb, Tb_2, Tbc, Tbi, Tjr, Tpr, Tr_2, Tr_3, Tt_2, Tt_3, and Tts of Coats (1987, Plate 1).	Younger volcanic rocks	Rhyolitic and andesitic flows, welded and nonwelded tuff, and interbedded gravel. This unit is composed almost entirely of Jarbidge Rhyolite in northern parts of project area. Thickness as much as 2,000 ft (Coats, 1987, p. 62).	Permeability ranges over several orders of magnitude because of varied lithology and textures. Probable permeable intervals include gravel beds and fractured welded tuffs in eastern Jarbidge Mountains. Oil well 27 penetrated an interval of lost circulation in this unit at depths of 52-58 meters.

Table 2-1. Lithology, thickness, extent, and water-bearing characteristics of hydrogeologic units in the upper Humboldt River Basin, Nevada. Sources of data for oil wells were the Nevada Bureau of Mines and Geology at http://web2.nbmg.unr.edu/Oil_and_Gas/list/oil/logs/Oil_and_Gas_by_API.htm and AMSTRAT[1] logs (continued).

CENOZOIC UNITS				
Geologic Age	**Rock or Stratigraphic Unit**	**Hydrogeologic Unit**	**Lithology, Thickness, and Extent**	**Remarks**
Oligocene	Indian Well Formation. Map units Tw, Tg_2, and Ts_2 of Coats (1987, Plate 1).	Indian Well Formation	Conglomerate, sandstone, siltstone, mudstone, limestone, water-lain tuff, and rhyolitic to dacitic, nonwelded to densely welded tuff. Exposed in Pinion and Adobe Ranges and Elko and Peko Hills. Total thickness 350-640 meters in the Elko Hills and 1,015 meters in the Pinion Range. Penetrated by oil wells 7, 15, 17, and 18.	Possibly moderately to highly permeable because of coarse-grained intervals. Fractured welded tuff also may be permeable. Oil well 17 penetrated two intervals of lost circulation at depths of 2,009-2,018 and 2,231-2,243 meters. Both intervals consisted of welded tuff and interbedded sandstone and claystone. At oil well 21 results of three drillstem tests at depths of 1,743-1,773, 1,992-2,037 and 2,863-2,864 meters produced estimated altitudes of the potentiometric surface of 1,269, 805, and -990 meters, indicating a downward gradient between the Indian Well Formation and underlying Elko Formation. At oil well 22 results of three drillstem tests at depths of 1,414-1,433, 1,849-1,877, and 2,173-2,194 meters produced estimated altitudes of the potentiometric surface of 1,040, 1,376, and 1,608 meters, indicating an upward gradient between the Indian Well Formation and overlying Humboldt Formation. A drillstem test at oil well 25 at depths of 1,687-1,773 meters recovered 6 cubic meters of mud, indicating low permeability.
Late Eocene and Early Oligocene	Elko Formation and Eocene sedimentary rocks. Map units Ts1 and Tc of Coats (1987, Plate 1).	Elko Formation	Pebbly to bouldery limestone-clast conglomerate at base overlain by claystone, siltstone, shale, cherty limestone, sandstone, and tuff. Also includes four oil shale members. Exposed in and along edges of mountain ranges and occurs at differing depths in basins (see Table 2-2). Total thickness ranges from 760 meters in the Pinion Range and western Elko Hills to 1,500 meters in the eastern Elko Hills.	Permeability probably highly variable depending on lithology. Sandstone and limestone beds probably at least moderately permeable and fine-grained beds poorly permeable. AMSTRAT log D-4368 for oil well 3 indicates tuffs have no porosity and sandstone beds 3-30 meters thick have 6-18 percent porosity. Two drillstem tests at oil well 6 at depths of 1,969-1,971 and 2,348-2,369 meters recovered 335 and 27 cubic meters of drilling mud, respectively, indicating moderate to low permeability. A drillstem test at oil well 13 at depths of 529-546 meters recovered 72 meters of muddy water, indicating low permeability. Oil well 15 penetrated an interval of lost circulation at depths of 741-753 meters. At oil well 20, results of two drillstem tests at depths of 828-840 and 841-878 meters produced estimated altitudes of the potentiometric surface of 1,617 and 1,498 meters, respectively, indicating a downward vertical gradient.
Middle to Late Eocene	Volcanic rocks. Map units Tr_1, Ta_1, Tt_1, Tl and Ttsl of Coats (1987, Plate 1).	Older volcanic rocks	Ash-flow and air-fall tuffs, lava flows, and domes. Lithologies include basalt, andesite, dacite, latite, and rhyolite (Coats, 1987; Plate 1 and p. 51-67). Thickness uncertain.	Mostly impedes groundwater flow because tuffs weather to clay and because of interbedded fine-grained lake deposits. Absence of intervals of lost circulation in this unit at oil wells 9 and 10 also indicate low permeability.

Table 2-1. Lithology, thickness, extent, and water-bearing characteristics of hydrogeologic units in the upper Humboldt River Basin, Nevada. Sources of data for oil wells were the Nevada Bureau of Mines and Geology at http://web2.nbmg.unr.edu/Oil_and_Gas/list/oil/logs/Oil_and_Gas_by_API.htm and AMSTRAT[1] logs (continued).

CENOZOIC BASEMENT				
Geologic Age	**Rock or Stratigraphic Unit**	**Hydrogeologic Unit**	**Lithology, Thickness and Extent**	**Remarks**
Permian and Pennsylvanian	Ely Limestone, Moleen, Tomera, Carbon Ridge, and Schoonover Formations, Carlin Sequence and Strathearn Formation. Map units Pe, Pc, PPcs, PPl, and PPs of Coats (1987, Plate 1).	Younger carbonate rocks	Exposed in Diamond Mountains, Pinion Range, Elko Hills and Peko Hills, northern and southern Adobe Range, northern Independence Range and Snake Mountains. Forms top of Cenozoic basement in east-central parts of project area at oil wells 8, 11, 15, 16, and 18 and in southern Huntington Valley at oil wells 28 and 29. Consists of limestone, dolomite, and subordinate conglomerate, sandstone, siltstone and chert 1,300-1,700 meters thick in Pinion and Adobe Ranges, 58-210 meters thick in the Elko Hills, 1,050 meters thick in the Peko Hills and 350 meters thick in the Snake Mountains.	Unit is moderately to highly permeable and the site of several large springs in the canyon of the South Fork Humboldt River (Plume, 2013, p. 29). Oil well 9 penetrated four intervals of lost circulation at depths of 203-206, 297-299, 405-408, and 467-469 meters. Oil well 15 penetrated five intervals of lost circulation ranging from 3 to 168 meters thick at depths of 741-1,402 meters. Oil well 16 penetrated seven intervals of lost circulation ranging from less than 1 to 5 meters thick at depths of 961-1,561 meters. Also at oil well 15 a drillstem test at depths of 2,053-2,076 meters recovered 1,936 cubic meters of muddy water, indicating high permeability of the test interval.
Pennsylvanian and Mississippian	Diamond Peak Formation, Chainman Shale, Webb, Grossman, Banner, and Nelson Formations. Map units PMdp, Mc, Mw, MDg, Mbn, and Ma of Coats (1987, Plate 1).	Clastic rocks	Shale, sandstone, sandy limestone, conglomerate, and chert exposed extensively in western parts of project area. Thicknesses of 2,200 meters in Pinon Range, 1,220-1,520 meters in Elko Hills, 2,135 meters in northern Adobe Range and 675 meters in southern Snake Mountains.	Unit is poorly permeable and functions as a confining unit between younger and older carbonate rock aquifers. At oil well 9 four intervals of lost circulation penetrated at depths of 203-206, 297-299, 405-408, and 467-469 meters probably were thin sandstone or limestone beds. At oil well 23, a drillstem test at depths of 3,988-4,009 meters recovered 57 cubic meters of water and drilling mud, indicating low permeability. At oil well 31, a drillstem test at depths of 567-585 meters recovered 482 cubic meters of water, indicating fairly high permeability.
Devonian to Ordovician	Woodruff, Valmy, and Vinini Formations. Map units Dos, Dosl, Dw of Coats (1987, Plate 1)	Thrusted clastic rocks	Shale, siltstone, sandstone, quartzite, chert, and marine volcanic rocks. Upper plate of Roberts Mountains thrust. Structurally overlies various units of carbonate rocks that are part of the lower plate. Thickness approximately 675 meters in the Snake Mountains, 1,430 meters in Independence Mountains, 900 meters in the Pinyon Range, and 548 meters in the northern Adobe Range. Forms top of Cenozoic basement in northwest and north central parts of project area as far south as oil wells 3 and 4.	Impedes movement of groundwater. At oil well 3, AMSTRAT log D-4368 indicates porosity is less than 6 percent and shows intervals of lost circulation at depths of 1,923-1,938 and 2,118-2,133 meters.

Table 2-1. Lithology, thickness, extent, and water-bearing characteristics of hydrogeologic units in the upper Humboldt River Basin, Nevada. Sources of data for oil wells were the Nevada Bureau of Mines and Geology at http://web2.nbmg.unr.edu/Oil_and_Gas/list/oil/logs/Oil_and_Gas_by_API.htm and AMSTRAT[1] logs (continued).

CENOZOIC BASEMENT				
Geologic Age	**Rock or Stratigraphic Unit**	**Hydrogeologic Unit**	**Lithology, Thickness and Extent**	**Remarks**
Devonian to Middle Cambrian	Guilmette Formation, Devils Gate Limestone, Nevada Formation, Lone Mountain Dolomite, Roberts Mountains and Hanson Creek Formations, Eureka Quartzite, Pogonip Group, Windfall Formation, Dunderberg Shale, Hamburg Dolomite, Secret Canyon Shale, Geddes Limestone, Eldorado Dolomite, Pioche Shale Prospect Mountain Quartzite. Map units Dgd, Dd, DSrm, Dslm, DSd, DOd, SOd, SOh, Oe, Op, Cc, and Cpm of Coats (1987, Plate 1).	Older carbonate rocks	Intervals of limestone and dolomite interrupted by thinner intervals of shale, quartzite, and conglomerate. All units rarely present in a single mountain range. Underlie entire study area, but are concealed over large parts of mountain ranges by younger Cenozoic basement units. Thickness 2,600-5,500 meters in the Ruby Mountains, 3,000 meters in the Pinyon Range and Snake Mountains, and approximately 1,200 meters in the Independence Mountains. An oil well penetrated 1,370 meters of carbonate rocks from the Devils Gate Limestone to the Hanson Creek Formation at the north end of the Pinon Range (Coats, 1987, p. 13-47). Forms top of Cenozoic basement in eastern parts of project area at oil wells 1, 5, 6 and 17.	High permeability because of solution widening of fracture zones. Absence of perennial streams in watersheds even partly underlain by these rocks indicates high permeability. At oil well 8 AMSTRAT log D-2746 indicates low porosity; however, a drillstem test at depth of 1,532-1,549 meters recovered 1,366 cubic meters of drilling mud and water, indicating high permeability for this interval. Oil well 9 penetrated an interval of lost circulation at depths of 2,201-2,213 meters. Oil well 13 penetrated six intervals of lost circulation 6-100 meters thick at depths of 2,255-2,674 meters. Results of two drillstem tests at oil well 19 produced estimated altitude of potentiometric surface of 1,533 meters for both indicating little or no vertical hydraulic gradient. At oil well 27, a drillstem test at 1,696-1,740 meters recovered 480 cubic meters of drilling mud and water. At oil well 29, results of two drillstem tests at depths of 1,094-1,229 and 1,380-1,437 meters produced estimated altitudes of the potentiometric surface of 1,792 and 1,732 meters, respectively, indicating a downward vertical gradient. Oil well 29 also penetrated four intervals of lost circulation 3-98 meters thick at depths of 1,045-1,340 meters. At oil well 31 results of two drillstem tests at depths of 567-585 meters in clastic rocks and 746-759 meters in older carbonate rocks produced estimated altitudes of the potentiometric surface of 1,797 and 1,813 meters suggesting a slight upward gradient between the two units although the head difference of 16 meters is well within the uncertainty of the head values.
Tertiary, Jurassic, and Cambrian	Metamorphic and granitic intrusive rocks. Map units Cpm, Cpq, DCm, DOm, DPm, Jd, Jgr, Kgr, Mzgn, OCm, Oem, Pmc, Ps, Tgd, Tgr, and Ti of Coats (1987, Plate 1).	Crystalline rocks	Metamorphic rocks include marble, schist, and gneiss. They are metamorphosed carbonate and clastic sedimentary rocks of Paleozoic age in the central and northern Ruby Mountains and Elko Hills. Granitic rocks consist of granodiorite in the central Ruby Mountains and alaskite in the southern Independence Mountains. Can be much more extensive at depth than indicated by outcrop area.	Impedes the movement of groundwater and forms boundary of groundwater flow along the Ruby Mountains-East Humboldt Range mountain front and at depth along west dipping fault.

[1] AMSTRAT is the acronym for American Stratigraphic Company. AMSTRAT logs typically consist of a summary of subsurface information recorded during drilling of selected oil exploration wells. The logs include descriptions of lithology, porosity, intervals of lost circulation, drillstem tests, and results of coring. These logs are available for purchase from the following website: http://www.cslogsource.com/company/index.html.

activity and erosion of these mountain ranges and of those to the west 15-10 million years ago filled the basin with volcaniclastic sediments of fluvial and lacustrine origin. Altitudes of the basement rock range from 500 to 1,000 meters above sea level near its margins to more than 2,000 meters below sea level in its deepest parts.

2.1.1.1 Crystalline Rocks

Crystalline rocks span nearly the entire age range of all the other hydrogeologic units in the upper Humboldt River basin. They include regionally metamorphosed sedimentary rocks of Paleozoic and Precambrian age and granitic intrusive rocks of Eocene, Cretaceous, and Jurassic age. Crystalline rocks make up almost the entire northern Ruby Mountains and East Humboldt Range from approximately 10 miles south of Jiggs to a few miles southwest of Wells. It is likely that these rocks also occur at depth at least as far west as the axis of the structural basin along the west-sloping detachment fault. Crystalline rocks occur as a few scattered, intrusive bodies of small areal extent exposed in mountain ranges along the western side of the project area. Crystalline rocks are mostly impermeable, which is indicated by the numerous perennial streams that drain the Ruby Mountains and East Humboldt Range. Little high-altitude groundwater recharge occurs in areas where these rocks are exposed.

2.1.1.2 Older Carbonate Rocks

Older carbonate rocks consist of dolomite and limestone and subordinate shale and sandstone of Devonian to middle Cambrian age. This hydrogeologic unit is well exposed in two large outcrop areas: one at the south end of the Ruby Mountains and another in the Snake Mountains north of Wells. The unit is also exposed over smaller areas in the Pinion Range and Independence Mountains along the west side of the project area and in the Peko Hills in the north-central part.

Older carbonate rocks make up the main mass of the southernmost Ruby Mountains for a distance of approximately 40 kilometers. The stratigraphic thickness of this stack of relatively permeable rocks ranges from 2,600 to 5,500 meters and the rocks consistently dip to the east (Howard *et al.*, 1979; Nutt, 2000; and Nutt and Hart, 2004). The middle Cambrian parts of this stratigraphic section, exposed along the western foot of the Ruby Mountains, are underlain by the poorly permeable Prospect Mountain Quartzite (Howard *et al.*, 1979). The high permeability of the carbonate rocks in this area is indicated by the absence of perennial streams. This, combined with the eastward dip of the rocks, probably results in eastward groundwater flow from the west side of the Ruby Mountains to Ruby Valley east of the study area (Rush and Everett, 1966, p. 15; and Dudley, 1967, p. 88-98). Dudley (1967, p. 97) also found that the groundwater divide between the Huntington and Ruby Valleys may be as much as 2 miles west of the topographic divide between the two valleys. However, Dudley did not have the detailed geologic maps referred to above. It is probable that the hydrologic divide between the Huntington and Ruby Valleys is much farther west and runs along the western foot of the Ruby Mountains. This means that the Huntington Valley side of the Ruby Mountains potentially could be a recharge area for Ruby Valley and not Huntington Valley.

Older carbonate rocks crop out extensively on the west margins of the Snake Mountains in the northeast parts of the project area and are structurally overlain by thrusted clastic rocks. Older carbonate rocks also form the top of Cenozoic basement at oil wells 1, 5, and 6 at depths of 1,964, 2,655, and 2,496 meters, respectively, below the Marys River area just to the west of the Snake Mountains (Plate 1 and Table 2-2). The extensive presence of older carbonate rocks in the Snake Mountains and in the

Table 2-2. Depth and thickness of hydrogeologic units penetrated by oil wells, upper Humboldt River Basin, Nevada. Data from Nevada Bureau of Mines and Geology at http://web2.nbmg.unr.edu/Oil_and_Gas/list/oil/logs/Oil_and_Gas_by_API.htm

Well				Hydrogeologic unit		
Number on Plate 1	**API number**	**Altitude, meters**	**Depth, meters**	**Name in Table 2-1**	**Depth to top, meters**	**Thickness, meters**
1	27-007-05010	1,820	2,015	Alluvium	0	29
				Humboldt Formation	29	741
				Younger volcanic rocks	770	1,194
				Older carbonate rocks	1,964	>51
2	27-007-05245	2,017	2,694	Clastic rocks	0	2,112
				Older carbonate rocks	2,112	>852
3	27-007-05208	1,844	2,166	Alluvium	0	15
				Humboldt Formation	15	500
				Younger volcanic rocks	515	338
				Elko Formation	853	436
				Thrusted clastic rocks	1,289	>877
4	27-007-05233	1,852	3,048	Younger volcanic rocks	0	564
				Elko Formation	564	61
				Thrusted clastic rocks	625	1,341
				Clastic rocks	1,966	>1,082
5	27-007-05221	1,747	2,734	Humboldt Formation	0	838
				Younger volcanic rocks	838	213
				Elko Formation	1,051	1,603
				Older carbonate rocks	2,655	>79
6	27-007-05007	1,703	2,564	Humboldt Formation	0	1,692
				Elko Formation	1,691	805
				Older carbonate rocks	2,496	50
				Crystalline rocks	2,546	>18
7	27-007-05213	1,673	2,656	Humboldt Formation	0	610
				Indian Well Formation	610	491
				Younger volcanic rocks	1,100	222
				Elko Formation	1,323	>1333
8	27-007-05006	1,678	1,665	Humboldt Formation	0	1,012
				Younger carbonate rocks	1,012	78
				Clastic rocks	1,090	295
				Older carbonate rocks	1,385	>280
9	27-007-05232	1,839	3,832	Alluvium	0	26
				Older volcanic rocks	26	27
				Elko Formation	52	73
				Clastic rocks	125	1,688

Table 2-2. Depth and thickness of hydrogeologic units penetrated by oil wells, upper Humboldt River Basin, Nevada. Data from Nevada Bureau of Mines and Geology at http://web2.nbmg.unr.edu/Oil_and_Gas/list/oil/logs/Oil_and_Gas_by_API.htm (continued).

Well				Hydrogeologic unit		
Number on Plate 1	API number	Altitude, meters	Depth, meters	Name in Table 2-1	Depth to top, meters	Thickness, meters
				Older carbonate rocks	1,813	>2,019
10	27-007-05253	1,882	3,174	Humboldt Formation	0	37
				Older volcanic rocks	37	329
				Clastic rocks	366	2,764
				Older carbonate rocks	3,130	>44
11	27-007-05004	1,600	1,257	Alluvium	0	30
				Humboldt Formation	30	890
				Younger carbonate rocks	920	186
				Clastic rocks	1,106	>143
12	27-007-05224	1,632	2,286	Humboldt Formation	0	1,850
				Clastic rocks	1,850	>436
13	27-007-05234	1,801	2,702	Alluvium	0	35
				Younger volcanic rocks	35	258
				Elko Formation	293	286
				Clastic rocks	579	1,231
				Older carbonate rocks	1,810	>891
14	27-007-05209	1,579	1,728	Alluvium	0	12
				Humboldt Formation	12	305
				Younger volcanic rocks	317	963
				Clastic rocks	1,280	>448
15	27-007-05235	1,660	2,598	Humboldt Formation	0	24
				Younger volcanic rocks	24	341
				Indian Well Formation	366	244
				Elko Formation	610	155
				Younger carbonate rocks	765	>1833
16	27-007-05003	1,618	2,240	Alluvium	0	6
				Humboldt Formation	6	341
				Younger volcanic rocks	347	277
				Elko Formation	625	311
				Younger carbonate rocks	936	1,055
				Clastic rocks	1,990	>250
17	27-007-05274	1,631	2,774	Humboldt Formation	0	1,951
				Indian Well Formation	1,951	396
				Elko Formation	2,347	384
				Older carbonate rocks	2,731	>43

Table 2-2. Depth and thickness of hydrogeologic units penetrated by oil wells, upper Humboldt River Basin, Nevada. Data from Nevada Bureau of Mines and Geology at http://web2.nbmg.unr.edu/Oil_and_Gas/list/oil/logs/Oil_and_Gas_by_API.htm (continued).

Well				Hydrogeologic unit		
Number on Plate 1	API number	Altitude, meters	Depth, meters	Name in Table 2-1	Depth to top, meters	Thickness, meters
18	27-007-05272	1,650	3,563	Humboldt Formation	0	1,951
				Indian Well Formation	1,951	369
				Elko Formation	2,319	527
				Younger carbonate rocks	2,847	125
				Clastic rocks	2,972	>591
19	27-007-05248	1,943	2,758	Clastic rocks	0	1,371
				Older carbonate rocks	1,371	>1,387
20	27-007-05225	1,813	1,061	Indian Well Formation	0	582
				Elko Formation	582	>479
21	27-007-05217	1,694	3,337	Alluvium	0	641
				Humboldt Formation	641	896
				Indian Well Formation	1,536	1,223
				Elko Formation	2,759	148
				Clastic rocks	2,907	>430
22	27-007-05214	1,659	3,634	Alluvium	0	945
				Humboldt Formation	945	641
				Indian Well Formation	1,585	1,179
				Elko Formation	2,764	>870
23	27-007-05202	1,814	4,145	Cenozoic undivided	0	3,822
				Clastic rocks	3,822	>323
24	27-007-05227	1,671	3,062	Alluvium	0	1,425
				Indian Well Formation	1,425	1,225
				Elko Formation	2,650	46
				Younger carbonate rocks	2,696	>366
25	27-007-05223	1,687	3,145	Alluvium	0	1,036
				Humboldt Formation	1,036	799
				Indian Well Formation	1,835	655
				Clastic rocks	2,490	>655
26	27-007-05261	1,738	2,284	Alluvium	0	1,067
				Humboldt Formation	1,067	603
				Younger volcanic rocks	1,670	>614
27	27-007-05244	1,880	3,743	Younger volcanic rocks	0	165
				Clastic rocks	165	917
				Older carbonate rocks	1,082	1,250
				Clastic rocks	2,332	>1411

Table 2-2. Depth and thickness of hydrogeologic units penetrated by oil wells, upper Humboldt River Basin, Nevada. Data from Nevada Bureau of Mines and Geology at http://web2.nbmg.unr.edu/Oil_and_Gas/list/oil/logs/Oil_and_Gas_by_API.htm (continued).

Well				Hydrogeologic unit		
Number on Plate 1	API number	Altitude, meters	Depth, meters	Name in Table 2-1	Depth to top, meters	Thickness, meters
28	27-007-05252	1,815	1,267	Alluvium	0	521
				Elko Formation	521	640
				Younger carbonate rocks	1,161	>106
29	27-033-05278	1,826	1,904	Alluvium	0	294
				Humboldt Formation	294	127
				Younger carbonate rocks	421	30
				Clastic rocks	452	594
				Older carbonate rocks	1,045	>859
30	27-033-05320	1,914	2,161	Clastic rocks	0	988
				Older carbonate rocks	988	>1,173
31	27-033-05296	1,860	771	Alluvium	0	70
				Humboldt Formation	70	378
				Clastic rocks	448	192
				Older carbonate rocks	640	>131

subsurface to the west suggests the possibility of subsurface groundwater flow between this part of the project area and Thousand Springs Valley on the east side of the Snake Mountains, although previous studies have not identified such flow. However, a simple comparison of the occurrence of springs, both in the mountain block and on adjacent alluvial fans, using the Wells and Double Mountain 1:100,000 scale topographic maps indicates many more springs on the Thousand Springs Valley side of the Snake Mountains. This raises the possibility that the hydrologic divide between the Marys River area and Thousand Springs Valley could be some distance west of the topographic divide and that precipitation on the west side of the Marys River area might actually be a source of recharge to Thousand Springs Valley.

In addition to these surficial indications of the permeability of older carbonate rocks, data from several oil wells provide evidence of permeability at depth. Intervals of lost circulation were identified from mudlogs at: (1) a single interval at 2,201-2,213 meters in well 9; (2) six intervals at depths of 2,255-2,674 meters and ranging from 6 to 100 meters thick at well 13; and (3) four intervals at depths of 1,045-1,340 meters and ranging from 3 to 97 meters thick at well 29.

Altitudes of the potentiometric surface are estimated from final shut-in pressures recorded during pairs of drillstem tests at two wells. At well 19 the estimated altitude of the potentiometric surface was 1,533 meters for the depth intervals 1,381-1,434 meters and 1,490-1,600 meters, indicating little or no vertical gradient. At well 29 the estimated altitude of the potentiometric surface for the depth interval 1,094-1,229 meters was 1,792 meters and for the depth interval 1,380-1,437 meters was 1,732 meters, indicating a downward vertical gradient.

2.1.1.3 Thrusted Clastic Rocks

During the Devonian to middle Cambrian periods, what is now the eastern Great Basin was a continental margin along which carbonate rocks accumulated on the continental shelf and fine-grained clastic rocks accumulated in deeper water offshore. During early Mississippian and late Devonian periods, clastic rocks were thrust eastward (in modern coordinates) over coeval carbonate rocks along the continental shelf (Coats, 1987; p. 80-83). Along this fault, named the Roberts Mountains thrust, the older carbonate rocks are structurally overlain by the thrusted clastic rocks.

Thrusted clastic rocks are exposed in western parts of the project area in the Pinion and southern Adobe Ranges and extensively across the northern third of the project area between the Independence and Snake Mountains (Plate 1). This unit also forms the top of Cenozoic basement at oil wells 3 and 4. The presence of this unit at the northern end of the Adobe Range and at an isolated outcrop just west of Marys River and several miles north of oil well 8 suggests that the unit comprises the top of the Cenozoic basement in the project area as far south as the central Independence Mountains and northern Adobe Range and as far east as the western side of the Marys River area. Thrusted clastic rocks are at least 900 meters thick in the Pinion Range, 548 meters in the northern Adobe Range (Ketner and Ross, 1990), 1,430 meters in the southern Independence Mountains (Evans and Ketner, 1971), 675 meters in the Snake Mountains (Thorman *et al.*, 2010), at least 877 meters thick at oil well 3, and 1,341 meters thick at oil well 4.

This hydrogeologic unit is poorly permeable because it consists mostly of fine-grained sedimentary rocks. However, intervals of lost circulation were encountered during the drilling of oil well 3 at depths of 1,923-1,938 and 2,118-2,133 meters, indicating relatively higher permeability in two thin zones.

2.1.1.4 Clastic Rocks

A highland formed along the Devonian continental margin of what is now the eastern Great Basin during emplacement of thrusted clastic rocks along the Roberts Mountains thrust (see previous section). Erosion of this highland during the Pennsylvanian and Mississippian periods produced a sequence of clastic sedimentary rocks and subordinate carbonate rocks consisting mostly of the Mississippian Chainman Shale and Pennsylvanian and Mississippian Diamond Peak Formation. This unit is exposed extensively in western parts of the project area in the Pinion and Adobe Ranges and the Elko and Peko Hills. It also is exposed over smaller areas in the southern Ruby Mountains, Independence Mountains, and Snake Mountains. This unit forms the top of the Cenozoic basement in the subsurface at oil wells 21, 23, 25, 27, and 31 in southern Huntington Valley and at wells 9, 10, 13 and 14 in west-central parts of the project area (Plate 1). The thickness of this hydrogeologic unit is 2,200 meters in the Pinion Range (Smith and Ketner, 1978), 975 meters in the southern Ruby Mountains (Nutt, 2000), 1,220-1,520 meters in the Elko Hills (Solomon and Moore, 1982a and b), 2,135 meters in the northern Adobe Range (Ketner and Ross, 1990) and 675 meters in the southern Snake Mountains (Thorman *et al.*, 2010).

Clastic rocks form a thick impermeable confining unit between older and younger carbonate rocks. However, four intervals of lost circulation, possibly limestone or sandstone beds a few meters to more than 100 meters thick, at depths ranging from 203 to 469 meters in well 9 indicate a few zones of probably isolated permeability. The recovery of water and drilling mud during drillstem tests could indicate low permeability at oil well 23 and high permeability at oil well 31.

2.1.1.5 Younger Carbonate Rocks

Younger carbonate rocks are of Permian and Pennsylvanian age and consist of limestone and dolomite along with subordinate chert, shale, sandstone, and conglomerate. This hydrogeologic unit is exposed in mountain ranges throughout the project area. The largest areas of outcrop are in the northern Diamond Range, northern and southern ends of the Adobe Range, northern Independence Mountains and in the Snake Mountains. At depth, this hydrogeologic unit forms the top of the Cenozoic basement in east-central parts of the project area at oil wells 8, 11, 15, 16, and 18 and in southern Huntington Valley at wells 24, 28, and 29. Younger carbonate rocks are 1,500-1,700 meters thick in the Pinion Range (Smith and Ketner, 1978), 1,310 meters in the northern Adobe Range (Ketner and Ross, 1990), 58-210 meters in the Elko Hills (Solomon and Moore, 1982a and b), 1,050 meters in the Peko Hills (Ketner and Evans, 1988), and 350 meters in the Snake Mountains (Thorman *et al.*, 2010).

Younger carbonate rocks are exposed in the canyon of the South Fork Humboldt River, which is a few miles southwest of Elko at the northern mouth of the canyon. Several large springs discharge directly from this unit to the river channel over a reach of approximately eight kilometers. In October 1964, the combined discharge of these springs was 0.34 m^3/s (Rush and Everett, 1966, p. 23) and in 2008 and 2009, the discharge was 0.42 and 0.37 m^3/s (Plume and Smith, 2013, p. 29). Such large spring discharge distributed along a short reach of stream channel indicates that younger carbonate rocks are very permeable in this area. Numerous intervals of lost circulation were penetrated in younger carbonate rocks at depths ranging from 203 to 1,561 meters in oil wells 9, 15, and 16. The recovery of 1,936 cubic meters of muddy water during a drillstem test at well 15 also indicates that this unit can be highly permeable.

2.1.2 Cenozoic Units

2.1.2.1 Older Volcanic Rocks

Older volcanic rocks are of early Oligocene and Eocene age and are restricted to northwestern parts of the project area. This hydrogeologic unit consists almost entirely of rhyolitic to dacitic welded tuff, but also includes a few exposures of lava flows and ash-fall tuff of andesitic composition and exposures of the Frenchie Creek Rhyolite in the Elko Hills. Oil wells 9 and 10 penetrated 27 and 329 meters, respectively, of older volcanic rocks (Plate 1 and Table 2-2). The welded tuff in the northwest parts of the project area has the potential to be permeable because of its tendency to be fractured as a result of faulting. However, there are no reported measurements of permeability for these rocks.

2.1.2.2 Elko Formation

The hydrogeologic unit herein designated the Elko Formation includes two geologic units described by Coats (1987; Plate 1, p. 51, and pp. 54-55): a basal conglomerate of Eocene age and the Elko Formation proper that consists of volcaniclastic sedimentary rocks of late Eocene and Oligocene age. The conglomerate was deposited on a pre-Cenozoic erosion surface that consists of units of Cenozoic basement. The conglomerate consists of a clayey matrix containing pebbles and boulders derived from underlying Cenozoic basement units. The conglomerate ranges from 20 to 90 meters thick, although it is missing in some areas. Where the Elko Formation is exposed in the Pinion Range and Elko Hills it consists of 760-1,500 meters of interbedded sandstone, siltstone, claystone, and shale and includes several units of oil shale and cherty limestone near its base (Coats, 1987, p. 54-55). Elsewhere, this hydrogeologic unit is exposed as scattered outcrops in mountain ranges of the western part of the project

area and to a lesser extent in mountain ranges in northeastern parts (Plate 1). The Elko Formation also has been identified in the subsurface where oil wells have been drilled (Plate 1 and Table 2-2). Logs for these wells indicate that the Elko Formation is missing in some areas, but where it is present it ranges from a few hundred meters thick in western and central parts of the project area to more than 1,000 meters in northeastern parts.

Most likely, the transmissivity of the Elko Formation is relatively low mainly because of its fine-grained lithology and clayey matrix of the basal conglomerate. Oil well number 20 penetrated 479 meters of the Elko Formation below a depth of 582 meters (Plate 1 and Table 2-2). Analyses of drillstem tests conducted at depths of 828-840 and 841-878 meters yielded transmissivity values of 0.4 and 0.05 m^2/day (values from USGS, Carson City, NV files). Recovery of water and drilling mud during drillstem tests at oil wells 6 and 13 indicate low to moderate permeability.

2.1.2.3 Indian Well Formation

The Indian Well Formation consists of tuffaceous sedimentary rocks of lacustrine and fluvial origin. At its type section on the west side of Huntington Valley it is 1,015 meters thick and consists of a sequence of sandstone, tuff, and interbedded limestone (Smith and Ketner, 1976b, p.23-25). The Indian Well Formations is exposed as several outcrop areas that are mostly along the west side of Huntington Valley but also over a small area in the Elko Hills. At its outcrop area in the Elko Hills it is 270 meters thick (Solomon and Moore, 1982a). Its thickness ranges from 244 to 491 meters at oil wells 7, 15, 17, and 18 (Plate 1 and Table 2-2). These five occurrences appear to mark the northern extent of the Indian Well Formation in the project area because it is not found in outcrop and is not penetrated by oil wells farther north. In Huntington Valley, the Indian Well Formation has been identified in oil wells 20, 21, 22, 24, and 25 where it occurs at depths ranging from land surface to 1,425-1,835 meters and its thickness ranges from 582 to 1,179 meters (Plate 1 and Table 2-2). According to the mudlog for well 18, the Indian Well Formation consists of welded tuff and sandstone with fractures ranging from partly open to cemented. The open fractures could be an indication of at least moderate permeability.

Oil well 17 penetrated two intervals of lost circulation between depths of 2,009 and 2,243 meters. Both intervals consisted of welded tuff and interbedded sandstone and claystone. A drillstem test at oil well 25 recovered 6 cubic meters of drilling mud, indicating low permeability. At oil well 21, estimates of the potentiometric surface for three drillstem tests indicate a downward hydraulic gradient between the Indian Well Formation and underlying Elko Formation (Table 2-1). A few kilometers away at oil well 23, estimates of the potentiometric surface for three drillstem tests indicate an upward hydraulic gradient between the Indian Well Formation and overlying Humboldt Formation.

2.1.2.4 Younger Volcanic Rocks

Younger volcanic rocks are of Miocene and late Oligocene age and are extensive in the Pinion Range and Jarbidge Mountains. They also occur at scattered outcrops in the Elko Hills and Adobe Range. This hydrogeologic unit consists of rhyolitic to andesitic lava flows, welded and nonwelded tuff and interbedded gravel. In the northern most parts of the project area, this unit consists almost entirely of the Jarbidge Rhyolite but includes older flows, ignimbrite, and tuff as well. Younger volcanic rocks in the Pinon Range consist of ignimbrite and lesser amounts of rhyolitic to dacitic lava flows. Younger volcanic rocks were penetrated by oil wells 1, 3, 4, 5, 7, 13, 14, 15, 16, 26, and 27 from at or near land surface to depths ranging from 300 to 1,670 meters. The thickness of this unit can be as much as 760 meters (Coats, 1987, p. 62). The only interval of lost circulation reported for this unit during the drilling of oil wells in the project area was at well 27. Overall, it is most likely that this hydrogeologic unit is poorly permeable.

2.1.2.5 Humboldt Formation

Detachment faulting that resulted in uplift of the Ruby Mountains-East Humboldt Range-Snake Mountains and the simultaneous formation of an adjacent deep, structural basin to the west occurred in the middle Miocene (Wallace *et al.*, 2008, p. 58-63). Erosion of these mountain ranges and of the Pinion and Adobe Ranges to the west 15-10 million years ago filled the structural basin with volcaniclastic lacustrine and fluvial sediments that are named the Humboldt Formation (Coats, 1987, p. 63). These sediments are tuffaceous throughout and consist of a lower section of volcanic ash and tuff and an upper section of siltstone, sandstone, and conglomerate. The Humboldt Formation is exposed extensively in lowlands adjacent to the Humboldt River and its tributaries in central and northern parts of the project area (Plate 1). In southern Huntington Valley, it underlies alluvium at depths that range from less than 100 meters in the far south to over 1,000 meters near Jiggs. The thickness of the Humboldt Formation ranges from 300 to 500 meters in central and western parts of the project area but thickens to 600 to 1,950 meters farther east in the deepest parts of the structural basin.

Where it is exposed or covered only by a thin veneer of alluvium, the Humboldt Formation functions as a shallow water-table aquifer and one or more deeper confined aquifers. At depth, such as in southern Huntington Valley, it may either function as a confining unit or as a confined aquifer. Oil wells 3, 6, 17, and 31 penetrated intervals of lost circulation at depths ranging from 153 to 1,856 meters. Recovery of water and drilling mud during drillstem tests at oil wells 7 and 26 indicate moderate to high permeability. Overall, the Humboldt Formation may be more permeable than older Cenozoic units.

2.1.2.6 Alluvium

Alluvium is of Holocene, Pleistocene, and Pliocene age and consists of unsorted clay, silt, sand, gravel, and boulders on alluvial fans and sorted and interbedded clay, silt, sand, gravel, and boulders along stream flood plains. The source of this alluvium is the erosion of the mountain ranges of the project area that began with uplift of the Ruby and Snake Mountains and East Humboldt Range during the Miocene period. In addition to erosion of these mountains, glaciation during the past 300,000 years produced large quantities of outwash, part of which was deposited on pediment slopes adjacent to the mountains and much of which was transported out of the upper Humboldt River basin by the Humboldt River.

The Ruby Mountains, East Humboldt Range, and northern Independence Mountains were glaciated during two substages: the Lamoille and Angel Lake from 300,000 to 130,000 and 110,000 to 10,000 years ago, respectively (Sharp, 1938; Coats, 1987, p. 71; and Howard, 2000). During both substages, glacial outwash deposits accumulated on pediment surfaces underlain by the Humboldt Formation adjacent to the Ruby Mountains and East Humboldt Range as far as 6 to 9 kilometers south of Jiggs (Sharp, 1938). Outwash also accumulated in the northernmost parts of the Independence Mountains (Sharp, 1938; and Coats, 1987, p. 71). In addition to outwash deposits, glaciation in Lamoille Canyon deposited moraines as far as one mile north of the canyon mouth during the Lamoille substage (Sharp, 1938, p. 303–304 and 319; and Howard, 2000). Outwash deposits of the Lamoille substage consist of sand and gravel near the mouth of Lamoille Canyon and, with increasing distance from the canyon mouth, sand, gravel, and interbedded sandstone (Howard, 2000).

In northern parts of the project area, alluvium is mostly restricted to thin, well sorted fluvial deposits along stream flood plains. These deposits are probably never more than a few tens of meters thick and along the Humboldt River channel they function as a shallow water-table aquifer that does not seem to be hydraulically connected with underlying aquifers in the Humboldt Formation (Plume and

Smith, 2013, p. 36). In Huntington Valley alluvium occupies not only stream flood plains, but also the alluvial slopes on each side of the valley. The reason for the much greater extent of alluvium in this part of the project area is not clear. Perhaps the South Fork Humboldt River and its main tributary Huntington Creek were not as efficient as the Humboldt River at transporting sediment out of the area. In southern Huntington Valley, the thickness of alluvium ranges from 70 to 1,425 meters. It functions as a shallow water-table aquifer along the valley axis and becomes progressively deeper toward valley margins.

2.2 STRUCTURAL FEATURES

The most common structural features that affect groundwater flow in the project area are faults. Faults can affect groundwater flow in two ways: (1) they can form a barrier to groundwater flow either by juxtaposing permeable rocks against impermeable ones or by forming a fine-grained impermeable gouge along the fault plane; or (2) they can enhance permeability by fracturing rocks along the fault zone. However, hydrologic evidence (mainly the water levels in wells) is normally not sufficiently detailed to evaluate the effects of a fault. Despite this lack of evidence, there are a few examples of the effects of faults in the project area.

Some of the oldest faulting in the project area is along the Roberts Mountains thrust, which placed thrusted clastic rocks over older carbonate rocks during the Devonian period and later (Plate 1). Thrusted clastic rocks are poorly permeable, which enhances runoff from upland areas and prevents recharge to carbonate rocks. At depth, they function as a confining unit overlying older carbonate rocks.

The Ruby Mountains-East Humboldt Range-Snake Mountains were uplifted by a west-dipping listric fault during Miocene period.[1] Movement along this fault resulted in the formation of a deep structural basin in which sediments that were eroded from the uplifted mountains were deposited in the basin as the Humboldt Formation and alluvium (Plate 1 and Figure 2-1). This fault is exposed along parts of the mountain ranges and elsewhere is concealed by alluvium or the Humboldt Formation (Plate 1). The hydrologic importance of this fault is that Cenozoic hydrogeologic units are either faulted against (pre-Miocene units) or deposited against (Miocene and later) impermeable crystalline rocks. Either way, crystalline rocks form a hydrologic boundary along this fault from the mountain fronts westward at depth at least as far as the axis of the deep structural basin.

Several large springs are located in the lower canyon of the South Fork Humboldt River where it cuts through the Elko Hills. In October 1964 and 2008 and November 2009, these springs were discharging at 0.34, 0.42, and 0.37 m^3/s, respectively (Rush and Everett, 1966, p.23; and Plume and Smith, 2013, p. 29). Except for a thin prism of alluvium along the river channel, carbonate rocks of Permian and Pennsylvanian age and clastic rocks of Pennsylvanian and Mississippian age are the only hydrogeologic units exposed in this part of the canyon. All contacts between these two units are high-angle faults that juxtapose the carbonate and clastic rocks (Smith and Ketner, 1978). Therefore, the locations of the springs are a result of a combination of the high permeability of the carbonate rocks and the low permeability of the clastic rocks that are faulted against the carbonate rocks.

Another example of structural control of groundwater flow is in the southern Ruby Mountains, which are mostly underlain by a thick section of east-dipping older carbonate rocks. This section is underlain by impermeable east-dipping Prospect Mountain Quartzite and Secret Canyon Shale (Howard

[1] A listric fault is one that dips steeply at shallow depths and flattens at greater depth. The sense of movement along listric faults is normal.

et al., 1979; and Nutt and Hart, 2004) along and near the western mountain front. The eastward dip, especially of the underlying impermeable rocks, of this section is probably the main reason for eastward flow of groundwater recharge to Ruby Valley even though numerous faults must also play a part.

2.3 HYDROGEOLOGIC SECTIONS

Three hydrogeologic sections numbered 1-1', 2-2', and 3-3' are presented on Plate 2 and their locations are shown on Plate 1. The sections are numbered to correspond with the three Noble Energy exploration areas in the project area.

Section 1-1' is oriented east-west and extends from the crest of the Pinion Range across Huntington Valley through Noble Energy Area 1 to the Crest of the Ruby Mountains. Geologic sources for this section are Smith and Ketner (1972), Willden and Kistler (1969), and oil well 21. Younger volcanic rocks exposed in the Pinion Range overlie Cenozoic that consists of younger carbonate rocks, which are underlain at depth by clastic rocks and older carbonate rocks. The simplified distribution of Cenozoic basement units shown on the section is undoubtedly more complicated because of faulting. The east side of Huntington Valley and the adjacent uplands are underlain by Cenozoic basement that consists of crystalline rocks of the Ruby Mountains metamorphic core complex. Cenozoic hydrogeologic units in the deepest part of the structural basin beneath Huntington Valley are 2,907 meters thick and consist of 641 meters of alluvium, 896 meters of Humboldt Formation, 1,223 meters of Indian Well Formation, and 148 meters of Elko Formation (well 21, Table 2-2).

Section 2-2' extends south-southeast for approximately 12 kilometers, and then bends east-west across Lamoille and Starr Valleys and Noble Energy Area 2 to the crest of the Ruby Mountains. Geologic sources for this section are Coats (1987), Hess *et al.* (2011), Howard *et al.* (1979), Ketner (1990), interpretation of proprietary seismic data from Noble Energy, and oil well 18.

There are two possible scenarios for the distribution of Cenozoic basement adjacent to and just west of the Ruby Mountains range front. The first, and more likely scenario is shown on the hydrogeologic sections plate (Plate 2, Section 2-2') is that the outcrop of younger carbonate rocks near the Ruby Mountains range front (Howard et al., 1979) is a relatively small and isolated body that was detached from the main mass of younger carbonate rocks during extensional faulting and is now enclosed in the Humboldt Formation. In this scenario, the top of Cenozoic basement is still younger carbonate rocks, but they are juxtaposed at depth against rocks of the Ruby Mountains metamorphic core complex. This interpretation is also supported by the three-dimensional seismic data collected by Noble Energy.

The second, and less likely alternative is that younger carbonate rocks form the top of Cenozoic basement along this section from its western end to the Ruby Mountains range front. This interpretation is based on an outcrop of younger carbonate rocks (Strathearn Formation) that is exposed approximately one mile west of the range front (Howard et al., 1979). Crystalline rocks of the metamorphic core complex form the top of Cenozoic basement from the range front to the Ruby Mountains crest. Younger carbonate rocks are at relatively shallow depths at the western end of the section, deepen to the east to 2,847 meters at oil well 18, and then become progressively shallow until they are exposed at the Ruby Mountains range front. The Elko and Indian Well Formations overlie younger carbonate rocks along this part of the section.

Section 3-3' extends east-southeast from the crest of the Independence Mountains across the North Fork area and southern Jarbidge Mountains to oil well 4, and then bends southeast across the Marys River area, Noble Energy Area 3, and southern Snake Mountains to the Wood Hills east of Wells. Geologic sources for this section are Coats (1987) and oil wells 3, 4, and 6. Thrusted clastic rocks form the top of Cenozoic basement along Section 3-3' in the Independence Mountains at depths of 1,289 and 625 meters at oil wells 3 and 4, respectively, and at an isolated outcrop approximately two kilometers west of Marys River. Based on these four occurrences, thrusted clastic rocks are inferred to form the top of the Cenozoic basement over a large part of the project area from the Independence Mountains to the west side of the Marys River area. Granitic rocks of Tertiary age (crystalline rocks) have intruded the small outcrop of thrusted clastic rocks and are exposed as two small outcrops. This body of intrusive rocks is inferred to extend to great depth and to be more extensive than the two outcrops. Cenozoic hydrogeologic units along this part of Section 3-3' consist of the Elko Formation and overlying younger volcanic rocks and Humboldt Formation, all of which are offset by several normal faults, including the Independence Mountains range front fault.

Older carbonate rocks form the top of Cenozoic basement at a depth of 2,496 meters in the structural basin at oil well 6. However, this unit is only 50 meters thick at the well and is underlain by crystalline rocks that extend to uncertain depths. Older carbonate rocks and crystalline rocks are inferred to extend westward across the Marys River area as far as the normal fault on the west side of the basin. Cenozoic units in the basin consist of the Elko Formation, the overlying Humboldt Formation, and thin prisms of alluvium at land surface.

Thrusted clastic rocks form the top of Cenozoic basement at depths of at least 500 meters from the Snake Mountains range front fault eastward to the Wood Hills. These rocks are underlain by older carbonate rocks and crystalline rocks. Cenozoic units along this part of the section consist of the Elko Formation overlain by the Humboldt Formation and alluvium.

3.0 REGIONAL HYDROGEOLOGY

3.1 GROUNDWATER BUDGET

The upper Humboldt groundwater system (Figure 3-1) is defined by nine hydrographic areas (HAs) including:

- Marys River Area (42)
- Starr Valley Area (43)
- North Fork Area (44)
- Lamoille Valley (45)
- South Fork Area (46)
- Huntington Valley (47)
- Dixie Creek-Tenmile Creek Area (48)
- Elko Segment (49)
- Susie Creek Area (50)

Precipitation is the primary source of groundwater recharge within the study area. The majority of precipitation comes as winter snowfall on the mountain ranges with smaller amounts falling as rain. A certain portion of the snowmelt will infiltrate and provide water for one of the following processes (Heilweil and Brooks, 2011):

1. Discharge to mountain springs
2. Baseflow to mountain streams
3. Groundwater recharge to the adjacent basin-fill aquifer
4. Groundwater recharge to consolidated bedrock aquifers

This analysis focuses on the latter two processes that ultimately control the amount of water that recharges the groundwater system.

Groundwater discharges in a variety of forms:

1. Phreatophyte evapotranspiration (ET)
2. Interbasin Flow
3. Streamflow accretion
4. Regional groundwater springs
5. Groundwater pumping

A groundwater budget was developed for annual average conditions representing current (last decade) conditions. Given that the area's ranching and farming developed as early as the 1870s and groundwater pumping for municipal and agricultural purposes developed in the early part of the 20th century, the hydrologic system is likely in a state of quasi-equilibrium (fluid sources and sinks do not change significantly from year to year).

3.1.1 Groundwater Recharge

A summary of groundwater recharge estimates from eight groundwater studies is presented in Table 3-1. As is typical with recharge estimates, there is significant variability in the estimated recharge, which ranges between 152,500 to 477,000 acre-ft/yr.

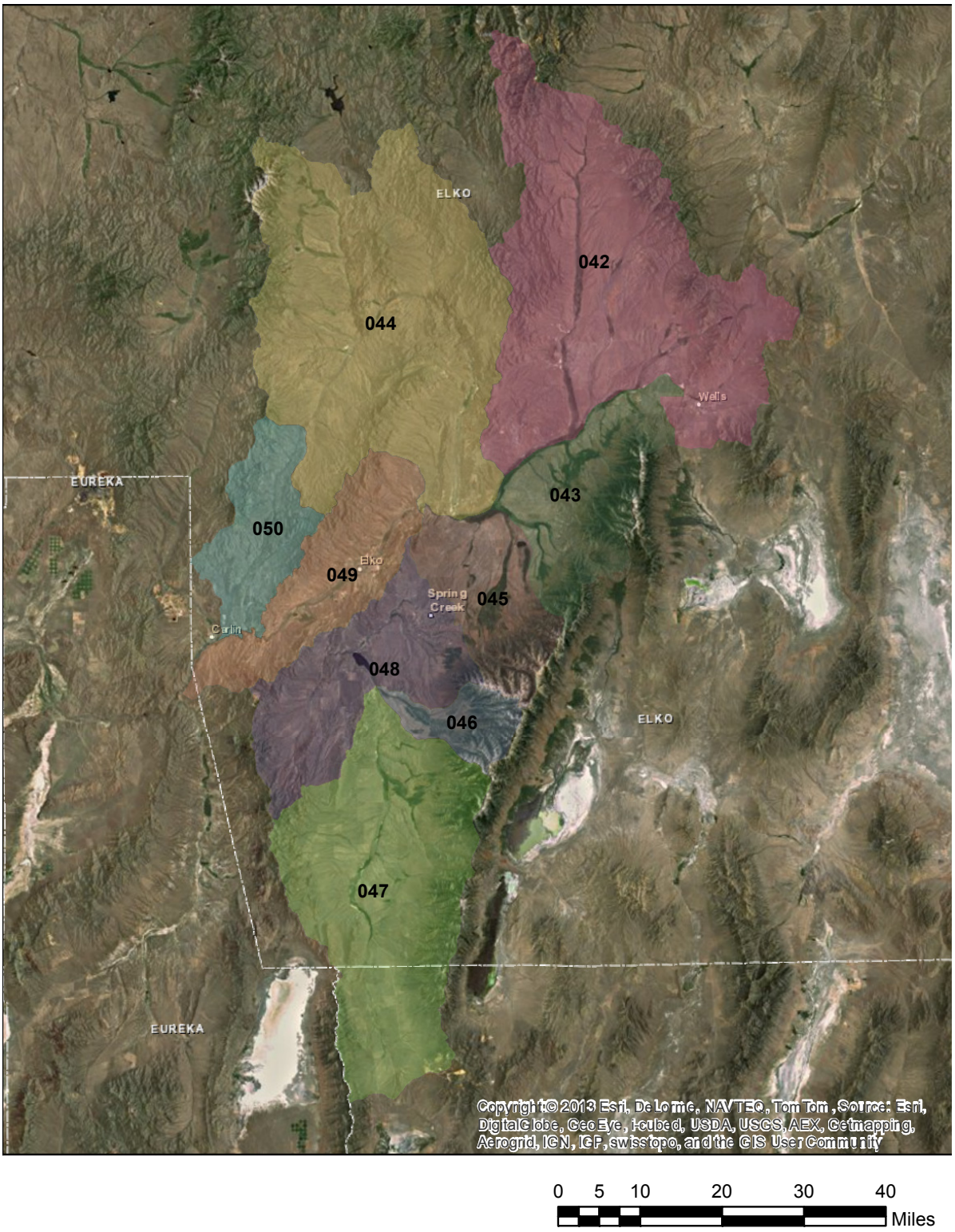

0 5 10 20 30 40 Miles

Figure 3-1. Upper Humboldt groundwater system including the hydrographic areas Marys River Area (42), Starr Valley Area (43), North Fork Area (44), Lamoille Valley (45), South Fork Area (46), Huntington Valley (47), Dixie Creek-Tenmile Creek Area (48), Elko Segment (49), and Susie Creek Area (50).

Table 3-1. Estimated mountain-block recharge for hydrographic basins within the upper Humboldt region.

Mountain Block Recharge										
	Hydrographic Basin									
Source	**Marys River Area 42 (afy)**	**Starr Valley Area 43 (afy)**	**North Fork Area 44 (afy)**	**Lamoille Valley 45 (afy)**	**South Fork Area 46 (afy)**	**Huntington Valley 47 (afy)**	**Dixie Creek-Tenmile Creek Area 48 (afy)**	**Elko Segment 49 (afy)**	**Susie Creek Area 50 (afy)**	**Total (afy)**
Nowlin, 1986						15,000				
Rush and Everett, 1966					3,000	14,000	13,000			
Eakin and Lamke, 1966			83,000					13,000		
State of Nevada, 1971	54,000	26,000	58,000	36,000	4,000	14,000	13,000	7,400	8,000	220,400
Masbruch, 2011a (In-place + runoff)	51,000	42,000	46,000	17,000	13,000	48,000	28,000	3,600	6,100	254,700
Masbruch, 2011a (In-place only)	31,000	18,000	30,000	5,900	8,700	45,000	5,800	2,900	5,200	152,500
Maxey-Eakin, 1949 - Calculated	48,000	31,000	56,000	29,000	20,000	49,000	13,000	7,000	7,000	260,000
Epstein, 2010 Calculated	73,000	98,000	71,000	65,000	52,000	83,000	18,000	10,000	7,000	477,000
Best Estimate	54,000	44,000	52,000	35,000	20,000	54,700	16,000	8,000	7,000	290,700

Rush and Everett (1966) developed groundwater recharge estimates for the southern portion of the upper Humboldt River Basin (South Fork Area, Huntington Valley, and Dixie Creek-Tenmile Creek Area) based primarily on estimates of phreatophyte ET. Four ET units are identified in the study: (1) wet meadow, (2) dry meadow, (3) rabbitbrush and greasewood, and (4) rabbitbrush and big sage. Discharge rates are estimated as the product of the area for each ET unit and ET rate. Evapotranspiration rates are 0.75, 0.5, 0.3, and 0.2 ft/yr for the wet meadow, dry meadow, rabbitbrush-greasewood, and rabbitbrush-sage units, respectively. The authors note that the wet meadow units are typically irrigated during the growing season, so the groundwater discharge estimates represent the remaining part of the year. Groundwater recharge is estimated to be 3,000, 14,000, and 13,000 acre-ft/yr for the South Fork Area, Huntington Valley, and Dixie Creek-Tenmile Creek Area, respectively.

Eakin and Lamke (1966) developed groundwater recharge estimates for what they call the headwaters for the upper Humboldt River (Marys River Area, Starr Valley Area, North Fork Area, and Lamoille Valley). Their recharge estimate is also based on estimates of phreatophyte discharge. Three ET units are developed: (1) wet, (2) intermediate, and (3) residual lowland. Evapotranspiration rates are 0.5, 0.4, and 0.1 ft/yr for the wet, intermediate, and lowland areas, respectively. Recharge rates are presented for the four hydrographic areas combined as 83,000 acre-ft/yr. A groundwater recharge estimate of 13,000 acre-ft/yr is also presented for the Elko hydrographic basin.

State of Nevada (1971) use an empirical approach that assumes a percentage of average annual precipitation will recharge the groundwater reservoir. They refer to Eakin *et al.* (1951) for the empirical method rather than the more traditional Maxey and Eakin (1949) reference, but the resulting equations are the same. For the hydrographic areas in the headwaters of the Humboldt River, they estimate groundwater

recharge to be 54,000, 26,000, 58,000, 36,000 acre-ft/yr for Marys River, Starr Valley Area, North Fork Area, and Lamoille Valley, respectively. For the southern areas, they estimate recharge is 4,000, 14,000, and 13,000 acre-ft/yr for the South Fork Area, Huntington Valley, and Dixie-Tenmile Creek Area, respectively. They estimate recharge of 7,400 and 8,000 acre-ft/yr for the Elko Segment and Susie Creek Area, respectively.

Independent calculations of groundwater recharge using the Maxey and Eakin (1949) method are performed here. Theoretically, the results should be identical to the estimates presented by the State of Nevada (1971) because the same empirical equations are used. In our analysis, we used a digital version of the Hardman precipitation map that was originally developed in 1936, but later updated by the Nevada State Engineer's office in the 1970s. Given the advances in geographic information system processing of spatial datasets, we assume that our analysis is more accurate. For the hydrographic areas in the headwaters of the Humboldt River, groundwater recharge is estimated to be 48,000, 31,000, 56,000, and 29,000 acre-ft/yr for Marys River, Starr Valley Area, North Fork Area, and Lamoille Valley, respectively. For the southern areas, recharge is 20,000, 49,000, and 13,000 acre-ft/yr for the South Fork Area, Huntington Valley, and Dixie-Tenmile Creek Area, respectively. Recharge is estimated as 7,000 and 7,000 acre-ft/yr for the Elko Segment and Susie Creek Area, respectively. The State of Nevada (1971) points out that the empirical estimates may be too large in some cases because recharge might be rejected and ultimately flow out of the basin in streams. Rejected recharge is likely in mountainous regions associated with volcanic, intrusive, or metamorphic rocks of lower permeability. Low-permeability rocks dominate most of the hydrographic areas except the southern portion of Huntington Valley and in the Elko Segment.

Nowlin (1986) developed a comprehensive database for the State of Nevada to highlight regions of poor water quality. The database also included groundwater recharge estimates for individual hydrographic areas when available. Groundwater recharge of 15,000 acre-ft/yr is estimated for Huntington Valley, but the technical methods are not provided.

Epstein *et al.* (2010) developed a bootstrap brute-force recharge model that is similar to the Maxey and Eakin (1949) empirical approach. The Epstein *et al.* (2010) method relies on the PRISM precipitation map (PRISM Climate Group, 2012) and was calibrated using 90 hydrographic areas with independently derived recharge estimates. This method yields significantly more recharge than the Maxey and Eakin (1949) method at 73,000, 98,000, 71,000, and 65,000 acre-ft/yr for Marys River, Starr Valley Area, North Fork Area, and Lamoille Valley, respectively. For the southern areas, recharge is 52,000, 83,000, and 18,000 acre-ft/yr for the South Fork Area, Huntington Valley, and Dixie-Tenmile Creek Area, respectively. They estimate recharge of 10,000 and 7,000 acre-ft/yr for the Elko Segment and Susie Creek Area, respectively.

Masbruch (2011a) estimated groundwater recharge based on a regional-scale water balance method known as the Basin Characterization Model (BCM) (Flint and Flint, 2007). The BCM is a distributed-parameter, water-balance accounting model used to identify areas that have the climatic and geologic conditions to allow precipitation to become potential runoff or potential in-place recharge and to estimate the amount of each. In-place recharge is calculated as the volume of water per time that percolates through the soil zone past the root zone and becomes net infiltration to consolidated rock or unconsolidated deposits. Runoff may infiltrate the subsurface, undergo ET farther downslope, or become streamflow. The BCM does not track or route this streamflow runoff. Total groundwater recharge from precipitation is the sum of in-place recharge and the runoff that infiltrates into the subsurface (a percentage of total BCM runoff).

Because many of the upper Humboldt River Basin streams are gaining because of high water tables, two sets of BCM generated recharge results are presented. First, total recharge is presented that represents in-place recharge and recharge derived from runoff generation. In-place recharge is also presented as a separate estimate and is likely a more accurate representation of regional groundwater recharge.

The BCM model generated in-place recharge estimates are most useful for the development of a groundwater model. Their estimates for Marys River, Starr Valley Area, North Fork Area, and Lamoille Valley are 31,000, 18,000, 30,000, and 5,900 acre-ft/yr, respectively. For the South Fork Area, Huntington Valley, and Dixie-Tenmile Creek Area, recharge estimates are 8,700, 45,000, and 5,800 acre-ft/yr, respectively. For the Elko Segment and Susie Creek Area, recharge estimates are 2,900 and 5,200 acre-ft/yr, respectively.

3.1.2 Phreatophyte Evapotranspiration

Phreatophyte ET areas were delineated using methods developed in Plume and Smith (2013). Evapotranspiration areas were mapped using Landsat imagery, the National Agricultural Imagery Program (NAIP), and a digital elevation model (DEM).

Evapotranspiration discharge areas were classified into five categories similar to the method of Plume and Smith (2013):

1. Phreatophytic shrublands
2. Riparian areas
3. Meadows
4. Irrigated croplands
5. Open water

A Modified-Soil Adjusted Vegetation Index (MSAVI) was computed from Landsat imagery (Qi *et al.*, 1994) using the approach of Plume and Smith (2013). The image from July 11, 2008, was used to minimize the effects of precipitation on vegetation greenness. The MSAVI was used to identify areas of open water, phreatophytic shrublands, meadows, and riparian ET units according to the thresholds shown in Table 3-2. The MSAVI cannot distinguish between meadows or irrigated croplands, so agricultural areas had to be manually digitized using aerial photos. Areas with MSAVI greater than 0.315 located outside of the irrigated cropland were classified as meadows. Figure 3-2 shows the distribution of ET units. The areas are consistent (+/- 10 percent) with the Plume and Smith (2013) results. Some differences are to be expected because manual digitization was required for some of the ET units.

Net ET rates are needed for each plant category. These rates were taken from Welch *et al.* (2007), which were derived for a hydrologic study in eastern Nevada. Net ET rates used for the upper Humboldt River Basin are: phreatophytic shrublands, 0.3 ft/yr; riparian areas, 3.3 ft/yr; meadows, 1.7 ft/yr; and open water, 4.3 ft/yr. Similar to the net ET rate for phreatophytes, the net irrigation water requirement (NIWR) of an irrigated crop is the rate at which water must be applied for a crop to grow. It is calculated as the crop ET minus the sum of precipitation runoff and deep percolation. The NIWR rates for alfalfa and highly managed pasture grass are 2.4 ft/yr for the Marys River Area, 2.4 ft/yr for the Starr Valley Area, 2.2 ft/yr for the North Fork Area, 2.3 ft/yr for Lamoille Valley, 2.5 ft/yr for the South Fork Area, 2.4 ft/yr for Huntington Valley, 2.8 ft/yr for the Dixie Creek-Tenmile Creek Area, and 2.6 ft/yr for the Elko Segment.

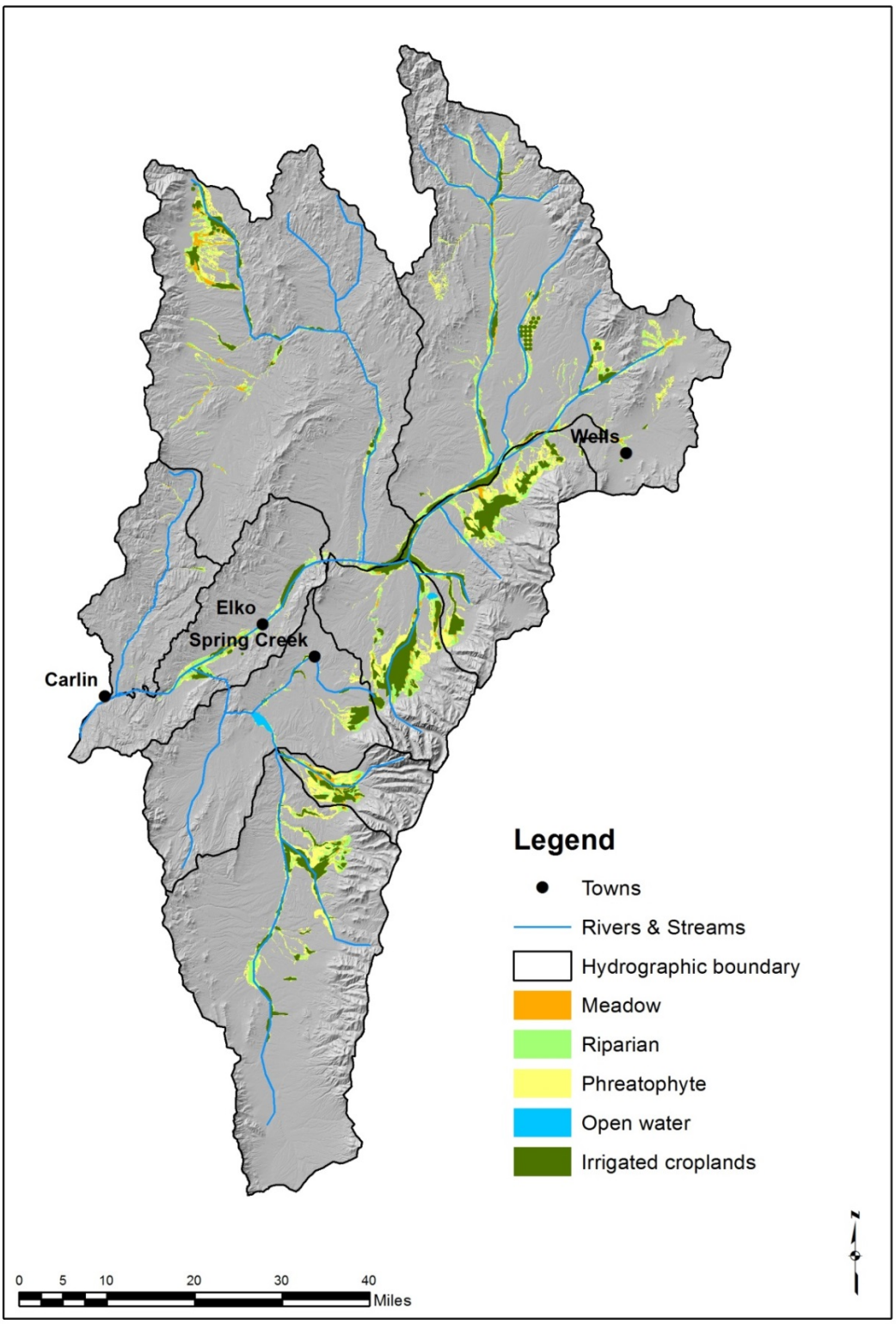

Figure 3-2. Evapotranspiration units delineated using Landsat imagery from July 11, 2008.

Table 3-2. MSAVI thresholds used in the evapotranspiration analysis (taken from Plume and Smith, 2013).

ET Unit	MSAVI Threshold
Irrigated croplands	>= 0.315
Meadows	>= 0.316
Riparian areas	0.165 - 0.315
Phreatophytic shrublands	0.135 - 0.165
Xerophytes	0.025 - 0.135
Open water	< 0.025

Volumes of net ET are presented for each hydrographic area and are shown in Table 3-3. Total net ET for all hydrographic basins is 484,069 acre-ft/yr. Groundwater supplies a large majority of the phreatophyte, riparian, and meadow ET and totals 280,441 acre-ft/yr. Phreatophyte shrubland represents 25,921 acre-ft/yr or nine percent of the nonagricultural ET. Riparian ET is the largest consumer of groundwater (78 percent of nonagricultural ET) at 218,384 acre-ft/yr. Meadows use 36,136 acre-ft/yr, which represents 13 percent of the groundwater-derived ET. Open water ET is presumably derived from surface water and represents 9,628 acre-ft/yr.

Table 3-3. Phreatophyte evapotranspiration area and annual discharge volume for each of the vegetation units.

	Phreatophyte		Riparian		Meadows		Irrigated Croplands		Open Water		
Hydrographic area	Area (acres)	Volume (acres-ft/yr)	Area (acres)	Volume (acres-ft/yr)	Area (acres)	Volume (acres-ft/yr)	Area (acres)	Volume (acres-ft/yr)	Area (acres)	Volume (acres-ft/yr)	Total
Marys River (042)	22,464	6,739	18,529	61,145	6,707	11,402	11,145	26,749	93	398	106,433
Starr Valley (043)	15,568	4,670	9,617	31,735	2,429	4,130	18,675	44,820	3	13	85,370
North Fork (044)	13,026	3,908	9,712	32,049	5,149	8,753	10,313	22,688	122	525	67,922
Lamoille Valley (045)	10,032	3,010	7,913	26,112	1,983	3,371	16,920	38,915	429	1,844	73,251
South Fork (046)	4,596	1,379	3,646	12,031	2,300	3,910	4,388	10,970	0	0	28,290
Huntington Valley (047)	13,682	4,105	8,573	28,290	1,055	1,794	12,083	28,998	10	41	63,228
Dixie Creek-Tenmile Creek (048)	3,150	945	2,079	6,859	234	397	3,515	9,841	1,478	6,354	24,396
Elko Segment (049)	2,527	758	5,076	16,750	1,254	2,132	4,154	10,800	105	453	30,893
Susie Creek (050)	1,357	407	1,034	3,413	145	247	87	219	0	0	4,286
Total	86,402	25,921	66,177	218,384	21,256	36,136	81,279	194,000	2,239	9,628	484,069

3.1.3 Interbasin Flow

Figure 3-3 shows the two locations where groundwater is known to exit the basins. Higher permeability carbonate rocks located at the south end of the Ruby Mountains facilitate groundwater recharge. Plume (2009) noted the eastward dip of the carbonate rocks, which likely results in groundwater flow from the west side of the southern Ruby Mountains to Ruby Valley east of the study area where numerous large springs emanate from the eastern base of the Ruby Mountains. Rush and Everett (1966) estimated 10,000 acre-ft/yr of groundwater discharge to Ruby Valley. Plume and Smith (2013) revised this estimate using Darcy's law and estimated that the flow rate to Ruby Valley is approximately 4,000 acre-ft/yr. This study used the Maxey and Eakin (1949) method to calculate groundwater recharge at the southern end of the Ruby Mountains, which is associated with carbonate rocks (Figure 3-3). This method yielded 13,600 acre-ft/yr of recharge in this region. Clearly there is uncertainty in the amount of interbasin flow toward Ruby Valley, but 4,000 acre-ft/yr is considered to be the best estimate.

Plume and Smith (2013) developed an estimate of groundwater flow approximately 10 miles upstream of the point that the Humboldt River exits the study area (southwest portion of the Elko Segment hydrographic area). They estimated 100 acre-ft/yr of subsurface outflow in this segment, but the flood-plain deposits are roughly twice as wide in this region. Therefore, subsurface flow is estimated to be approximately 50 acre-ft/yr where the Humboldt River exits the Elko Segment. Total subsurface flow from the study area is estimated to be 4,050 acre-ft/yr. A majority of this subsurface flow (4,000 acre-ft/yr) is exiting at the southern end of the Ruby Mountains and a small amount (50 acre-ft/yr) beneath and adjacent to the Humboldt River in the Elko Segment.

3.1.4 Streamflow Accretions/Depletions

Groundwater discharges to most of the streams within the study area. Plume and Smith (2013) conducted late fall measurements of streamflow to determine the amount of groundwater seepage occurring in the tributary streams and in the Humboldt River. Two sets of seepage runs were conducted. The first was conducted in October 2008 and the second in November 2009. Groundwater discharge to streams was calculated by differencing the downstream and upstream flows with the influences from tributary flows removed. The results of the Plume (2013) seepage analysis is shown in Table 3-4.

Table 3-4. Estimated gains/losses for streams by hydrographic area segment.

Segment	2008 Gain/Loss (cfs)	2009 Gain/Loss (cfs)	Average (cfs)
Marys River Area	-3	-8	-6
Starr Valley Area	0	0	0
North Fork	5	8	7
Lamoille Valley	-4	-5	-5
Huntington Valley	0	1	0.5
South Fork	15	13	14
Humboldt River	3.4	8.2	6

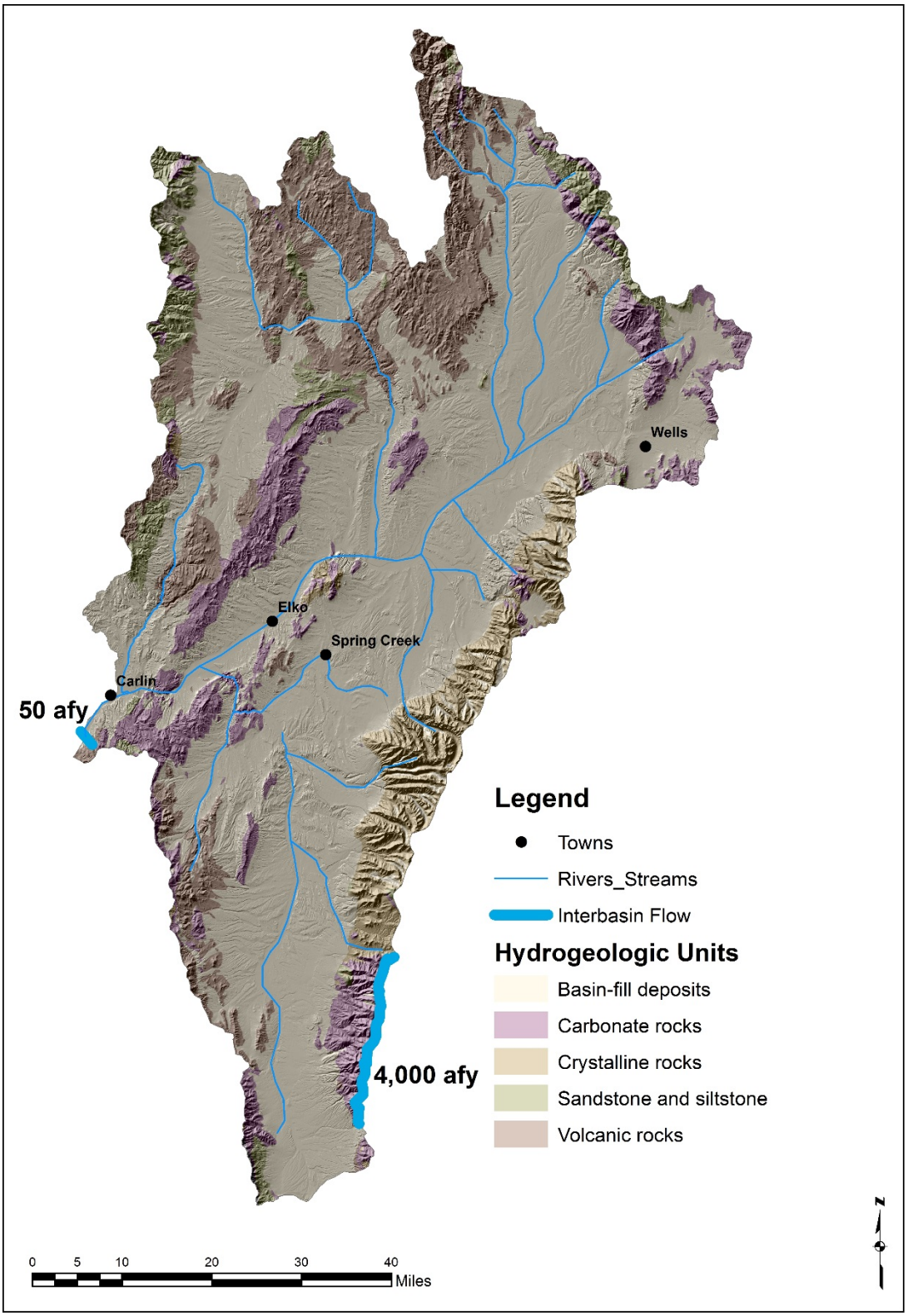

Figure 3-3. Location of groundwater interbasin flow zones and hydrogeologic units.

Three of the hydrographic areas had either insignificant gains or were losing. These include Marys River Area, Starr Valley Area, and Lamoille Valley. Four other areas indicate net groundwater discharge, including North Fork, Huntington Valley, South Fork, and the main stem of the Humboldt River. Average groundwater discharge for North Fork, Huntington Valley, South Fork, and the main stem of the Humboldt River is 7, 0.5, 14, and 6 cfs, respectively.

The largest groundwater discharge is in the South Fork Humboldt River below the South Fork Reservoir and above the confluence with the main stem of the Humboldt River. According to Plume (2013), this region (Figure 3-4) contains numerous springs discharging from carbonate and clastic sedimentary rocks. In October 1964, this reach of the river gained approximately 12 cfs (Rush and Everett, 1966). In 2008 and 2009, the gains were approximately 15 cfs and 13 cfs, respectively. Although groundwater discharges to Huntington Creek south of Jiggs, the stream losses upstream made up a majority of that volume in 2008 and 2009.

3.1.5 Springs

Springs associated with regional groundwater flow were digitized from U.S. Geological Survey 1:24,000 topographic maps. Springs located in the higher elevations were excluded because they are thought to be controlled by local groundwater flow and not considered part of the regional flow system. Figure 3-5 shows the regional springs. Surface elevations were extracted from the 30 m DEM for use in the groundwater model. Masbruch (2011b) developed estimates of spring discharge for each hydrographic area. Table 3-5 shows the spring discharge estimates. The total spring flow is 20,700 acre-ft/yr for all hydrographic areas.

Table 3-5. Estimated spring discharge by hydrographic basin (Masbruch, 2011b).

HA #	Hydrographic Area	Spring Discharge (acre-ft/yr)
42	Marys River Area	1,300
43	Starr Valley Area	-
44	North Fork Area	3,200
45	Lamoille Valley	1,500
46	South Fork Area	1,500
47	Huntington Valley	3,500
48	Tenmile Creek Area	-
49	Elko Segment	9,700
50	Susie Creek Area	-
	Total:	**20,700**

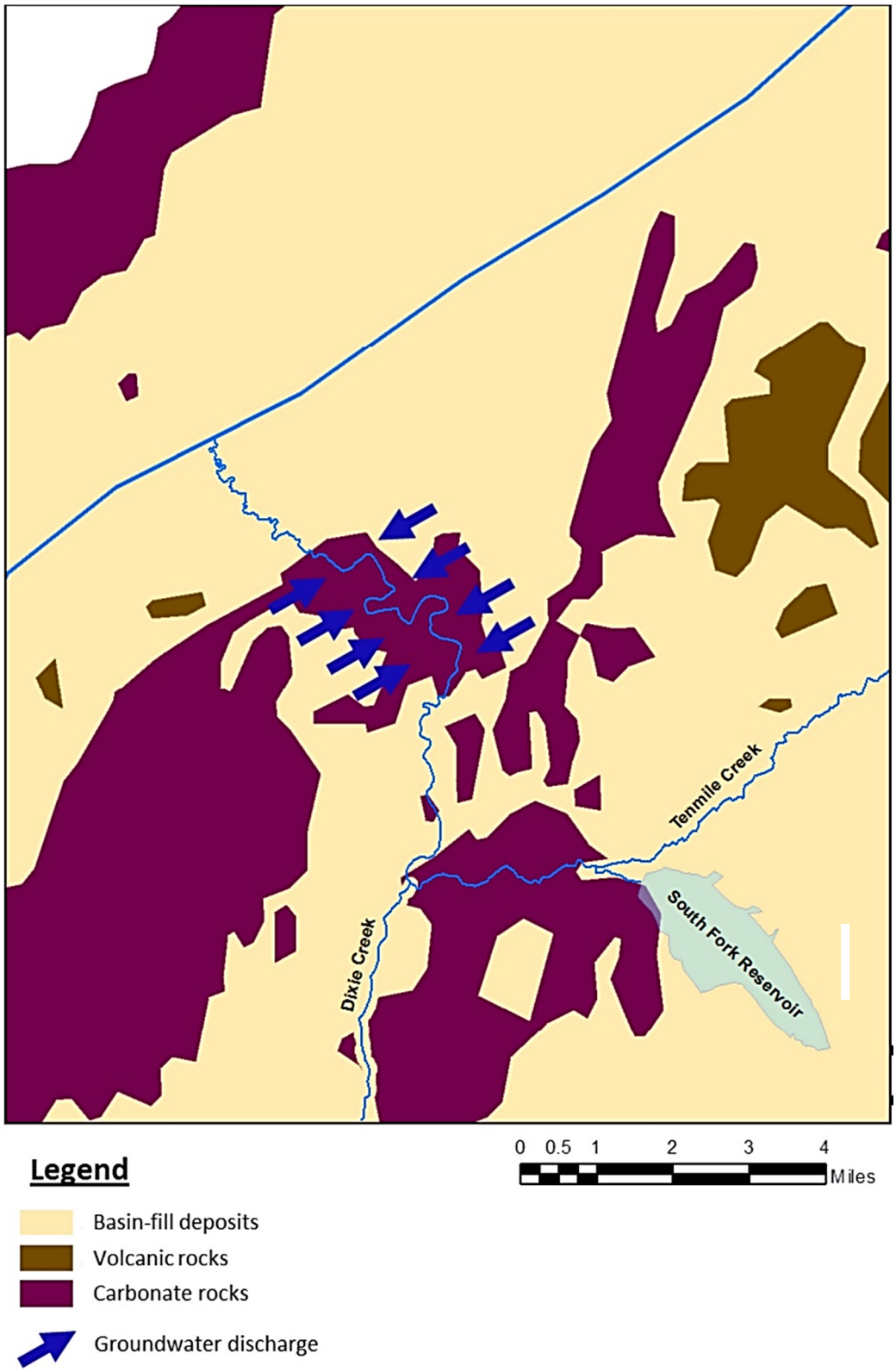

Figure 3-4. Location of groundwater discharge to the South Fork Humboldt River.

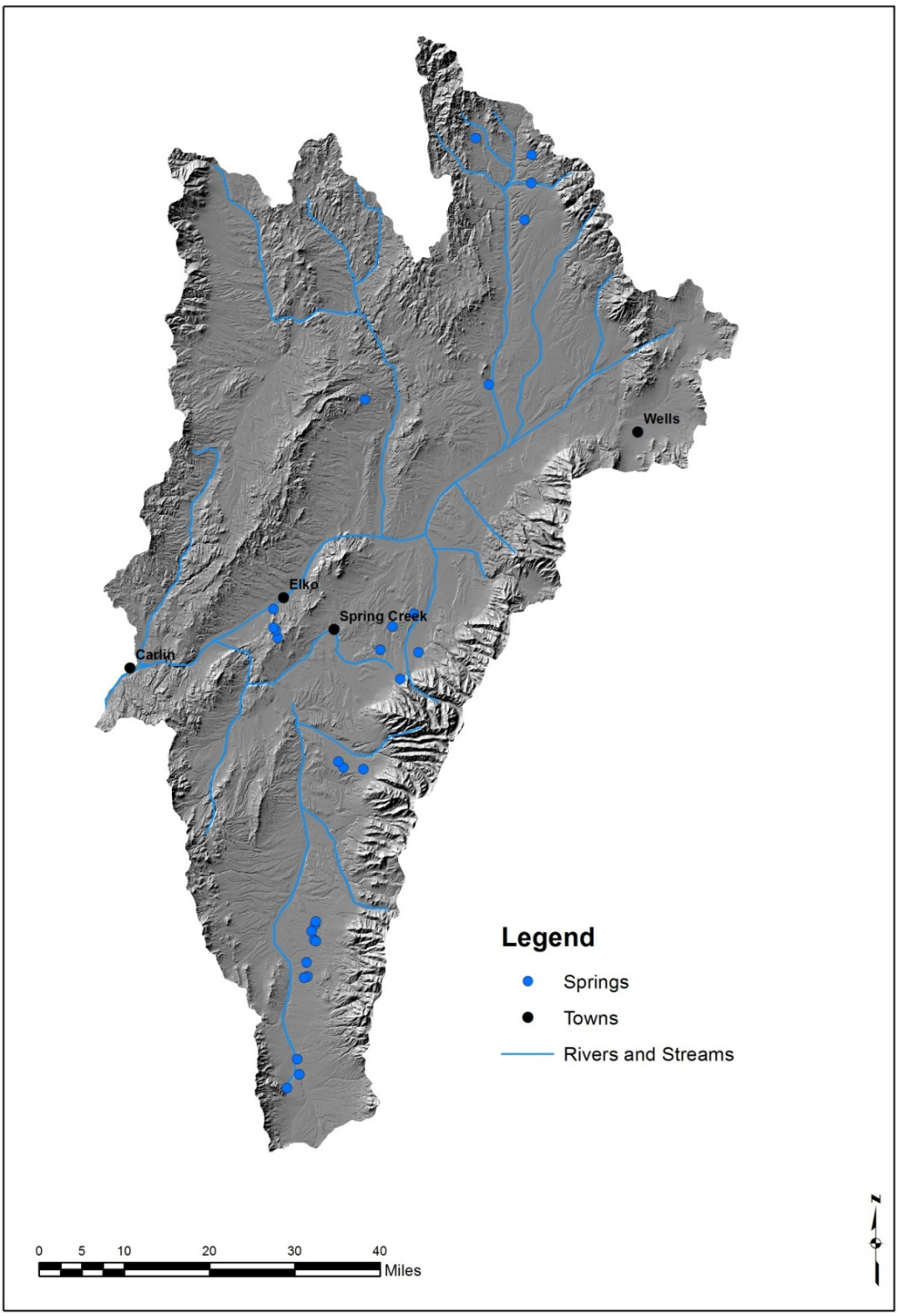

Figure 3-5. Regional groundwater springs in the study area.

3.1.6 Groundwater Pumping

Groundwater pumping in the upper Humboldt River Basin is used for municipal purposes and to irrigate agricultural crops and golf courses. Aerial photography is used to digitize the location of 32 center pivots and three golf courses. Imagery mosaics are from the ArcGIS online imagery mosaic collection and represent different time periods between 2010 and 2011. Figure 3-6 shows the locations of the pumping wells.

Pumping rates for agricultural plots and golf courses are determined based on the digitized area and the NIWR. The NIWR represents the total ET rate minus annual precipitation. Values of NIWRs for crops in each hydrographic area in Nevada are presented at the NDWR website. The NIWR rates for alfalfa are used for the center pivots and turf grass for golf courses.

Pumping estimates for municipal purposes are determined based on population and per capita water usage. Per capita water use is estimated to be 0.4 acre-ft/yr (Prudic *et al.*, 2006). Populations for Lamoille, Wells, Spring Creek, and Elko are determined from the 2010 census (http://quickfacts.census.gov/qfd/states). For Elko and Spring Creek, multiple wells are used to ensure that single-well groundwater pumping did not exceed 1,000 gal/min.

A total of 44 wells were developed to represent pumping within the study area (Table 3-6). The pumping wells shown in Table 3-6 are not meant to represent actual wells. The well locations and pumping rates are meant to represent generalized pumping features on a regional basis and should provide a good approximation of the average annual pumping.

3.1.7 System-wide Groundwater Budget

A best-estimate of the system-wide groundwater budget is presented in Table 3-7. Expert judgment was used to determine the best estimate for groundwater recharge in each hydrographic basin based on the regional geology, the accuracy of the methodology, and the overall regional water balance. Total recharge is assumed to be approximately 283,700 acre-ft/yr for all nine hydrographic basins (Marys River Basin [050] is not included in the model domain and is therefore not included in the groundwater budget shown in Table 3-7). Groundwater is assumed to provide 64 percent of the riparian ET with the remainder coming from surface water. This partitioning was determined by simply adjusting the contribution from groundwater until the overall groundwater budget was in balance.

Groundwater discharges as phreatophyte ET (phreatophyte shrubland, meadows, and riparian zones), interbasin flow, groundwater pumping, stream accretions, and springs. Phreatophyte ET represents the largest discharge term at 73 percent, or 202,000 acre-ft/yr. The next largest discharge of groundwater is accretions to streams at 13 percent, or 36,000 acre-ft/yr. Spring discharge is 21,000 acre-ft/yr, or eight percent. Groundwater pumping represents 13,000 acre-ft/yr, or five percent, and interbasin flow out of the basin is only one percent, or 4,000 acre-ft/yr.

3.2 Generalized Groundwater Flow Directions

The occurrence and movement of groundwater in the upper Humboldt River Basin is described in detail in Plume (2009). Shallow groundwater levels and flow directions were interpreted using groundwater levels in 161 wells measured by personnel from the USGS, Nevada Division of Water Resources, and Newmont Mining Corporation during the spring and summer 2007. Water levels ranged

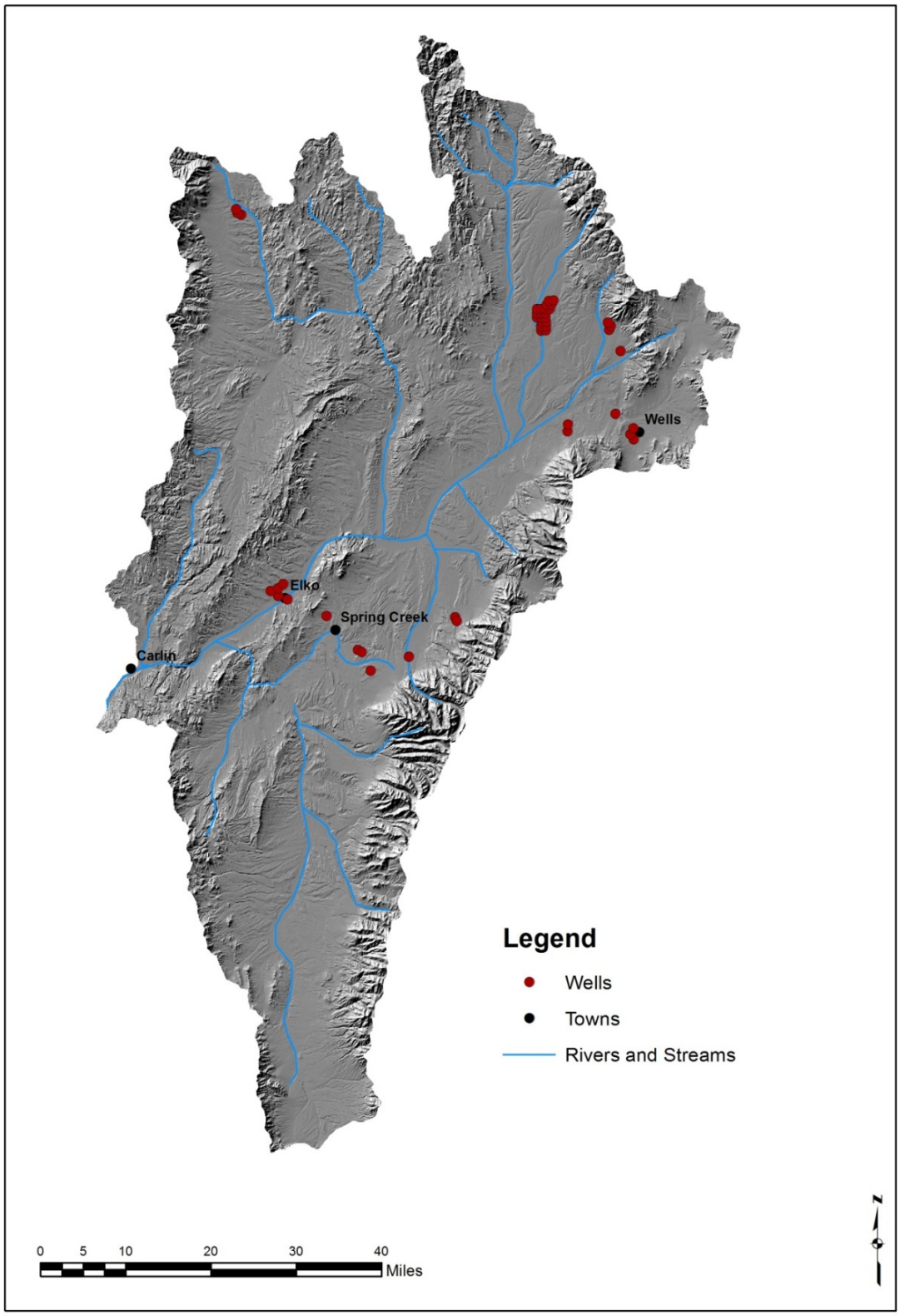

Figure 3-6. Groundwater pumping wells in the study area.

Table 3-6. Estimated well pumping for municipal, agricultural, and golf course wells.

Well #	Type	Area (acres)	Population	Rate (AFA/person)	Rate (ft/yr)	Vol Rate (AFA)	Hydrographic Area
0	Center pivot	72			2.4	173	Marys River
1	Golf course	33			2.2	72	Marys River
2	Wells	-	1,292	0.4		517	Marys River
3	Center pivot	37			2.4	88	Starr Valley
4	Center pivot	122			2.4	292	Marys River
5	Center pivot	122			2.4	292	Marys River
6	Center pivot	122			2.4	292	Marys River
7	Center pivot	62			2.4	150	Marys River
8	Center pivot	104			2.4	249	Starr Valley
9	Center pivot	104			2.4	249	Starr Valley
10	Center pivot	113			2.3	259	Lamoille Valley
11	Center pivot	113			2.3	259	Lamoille Valley
12	Lamoille	-	105	0.4		42	Lamoille Valley
13	Spring Creek	-	4,120	0.4		1,648	Dixie Creek
14	Spring Creek	-	4,120	0.4		1,648	Dixie Creek
15	Spring Creek	-	4,120	0.4		1,648	Dixie Creek
44	Spring Creek Golf Course	54			2.6	141	Dixie Creek
16	Elko	-	4,847	0.4		1,939	Elko Segment
17	Elko	-	4,847	0.4		1,939	Elko Segment
18	Elko	-	4,847	0.4		1,939	Elko Segment
19	Elko	-	4,847	0.4		1,939	Elko Segment
20	Elko Golf Course	140			2.5	350	Elko Segment
21	Center pivot	122			2.4	292	Marys River
22	Center pivot	122			2.4	292	Marys River
23	Center pivot	122			2.4	292	Marys River
24	Center pivot	122			2.4	292	Marys River
25	Center pivot	122			2.4	292	Marys River
26	Center pivot	122			2.4	292	Marys River
27	Center pivot	122			2.4	292	Marys River
28	Center pivot	122			2.4	292	Marys River
29	Center pivot	122			2.4	292	Marys River
30	Center pivot	122			2.4	292	Marys River
31	Center pivot	122			2.4	292	Marys River
32	Center pivot	122			2.4	292	Marys River
33	Center pivot	122			2.4	292	Marys River
34	Center pivot	122			2.4	292	Marys River
35	Center pivot	122			2.4	292	Marys River
36	Center pivot	122			2.4	292	Marys River
37	Center pivot	122			2.4	292	Marys River

Table 3-6. Estimated well pumping for municipal, agricultural, and golf course wells (continued).

Well #	Type	Area (acres)	Population	Rate (AFA/person)	Rate (ft/yr)	Vol Rate (AFA)	Hydrographic Area
38	Center pivot	122			2.4	292	Marys River
39	Center pivot	122			2.4	292	Marys River
40	Center pivot	122			2.4	292	Marys River
41	Center pivot	104			2.2	228	North Fork
42	Center pivot	104			2.2	228	North Fork
43	Center pivot	104			2.2	228	North Fork
					Total:	**22,657**	

Table 3-7. Estimated groundwater budget.

INPUTS	
Item	**Amount (acre-ft/yr)**
Groundwater Recharge	
Marys River (042)	54,000
Starr Valley (043)	44,000
North Fork (044)	52,000
Lamoille Valley (045)	35,000
South Fork (046)	20,000
Huntington Valley (047)	54,700
Tenmile Creek (048)	16,000
Elko Segment (049)	8,000
TOTAL:	**283,700**

OUTPUTS	
Item	**Amount (acre-ft/yr)**
Phreatophyte ET	
Marys River (042)	57,000
Starr Valley (043)	29,000
North Fork (044)	33,000
Lamoille Valley (045)	23,000
South Fork (046)	13,000
Huntington Valley (047)	24,000
Tenmile Creek (048)	6,000
Elko Segment (049)	14,000
Interbasin Flow	4,050
Groundwater Pumping	22,700
Streamflow Accretions	
North Fork (044)	5,000
Main Stem Humboldt River	18,000
Huntington Valley (047)	2,000
South Fork (046)	11,000
Springs	
Marys River (042)	1,300
Starr Valley (043)	-
North Fork (044)	3,200
Lamoille Valley (045)	1,500
South Fork (046)	1,500
Huntington Valley (047)	3,500
Tenmile Creek (048)	-
Elko Segment (049)	9,700
TOTAL:	282,500
Difference	1,200

from at or near land surface in younger basin-fill deposits along stream flood plains to 300-400 ft below land surface in older basin-fill deposits mostly along basin margins. Water-level contours in feet above sea level primarily reflect groundwater levels in older and younger basin-fill deposits, but also may reflect water levels in unconfined carbonate rock aquifers (Figure 3-7).

Groundwater moves through permeable zones driven by hydraulic head gradient from areas of recharge to areas of discharge. Recharge occurs mostly along mountain fronts, but also occurs in mountainous areas underlain by carbonate rocks. Discharge occurs mostly on valley floors by transpiration by phreatophytes, groundwater seepage to channels and springs (and subsequent evaporation), and pumpage. The main discharge area in the upper Humboldt River Basin is the river flood plain, which can be as much as one mile wide.

In Huntington Valley and the South Fork Area, groundwater flow is from the western base of the Ruby Mountains toward Huntington Creek and its confluence with the South Fork Humboldt River. In Huntington Valley, groundwater also flows from the eastern base of the Diamond Mountains and Pinon Range toward Huntington Creek. Water-level gradients range from 200 feet per mile adjacent to the Ruby Mountains to 10 feet per mile between the Pinon Range and Huntington Creek (Plate 1). This range of gradients either indicates that more recharge originates from the Ruby Mountains than from mountain ranges on the west side of the valley or that basin-fill deposits on the east side of the valley are less permeable than those on the west side. Rush and Everett (1966, p. 26-27) noted that basin-fill deposits on the east side of Huntington Valley are saturated to near land surface and that potential recharge is rejected and leaves the area as streamflow. The sharp, upstream inflections of water-level contours along the axis of Huntington Valley indicate that groundwater discharges to the channel of Huntington Creek. However, groundwater also flows northward along the axis of the valley along gradients of 5-10 feet per mile.

The high permeability of carbonate rocks likely results in recharge rather than runoff, which is indicated by the absence of perennial streams in the southern Ruby Mountains (Figure 2-1 and Plate 1). This combined with the eastward dip of the rocks probably results in groundwater flow from the west side of the southern Ruby Mountains to Ruby Valley east of the study area where numerous large springs emanate from the eastern base of the Ruby Mountains (Rush and Everett, 1966, p. 15; Dudley, 1967, p. 88-98). Dudley (1967, p. 97) also determined that the groundwater divide between Huntington and Ruby Valleys may be as much as two miles west of the topographic divide between the two valleys, which suggests that most of the high-altitude precipitation in the southern Ruby Mountains does not recharge the upper Humboldt River Basin.

Groundwater flow from Huntington Valley and the South Fork Area continues northward into the Dixie Creek-Tenmile Creek Area. Additionally, groundwater flows west and northwest from the recharge area along the mountain front of the Ruby Mountains and north and northeast from the Pinon Range. A low topographic divide separates the Dixie Creek-Tenmile Creek Area from Lamoille Valley to the northeast. A group of unnamed hills separates the Dixie Creek-Tenmile Creek Area from the Humboldt River downstream from Elko. The water-level contours on Plate 1 indicate that groundwater flows northwest through these hills to the river flood plain.

In Lamoille Valley and Starr Valley Area, groundwater flow is from a recharge area along the base of the Ruby Mountains, which are composed entirely of low-permeability crystalline rocks. As a result, groundwater recharge is predominantly from infiltration of runoff from the mountains as it crosses

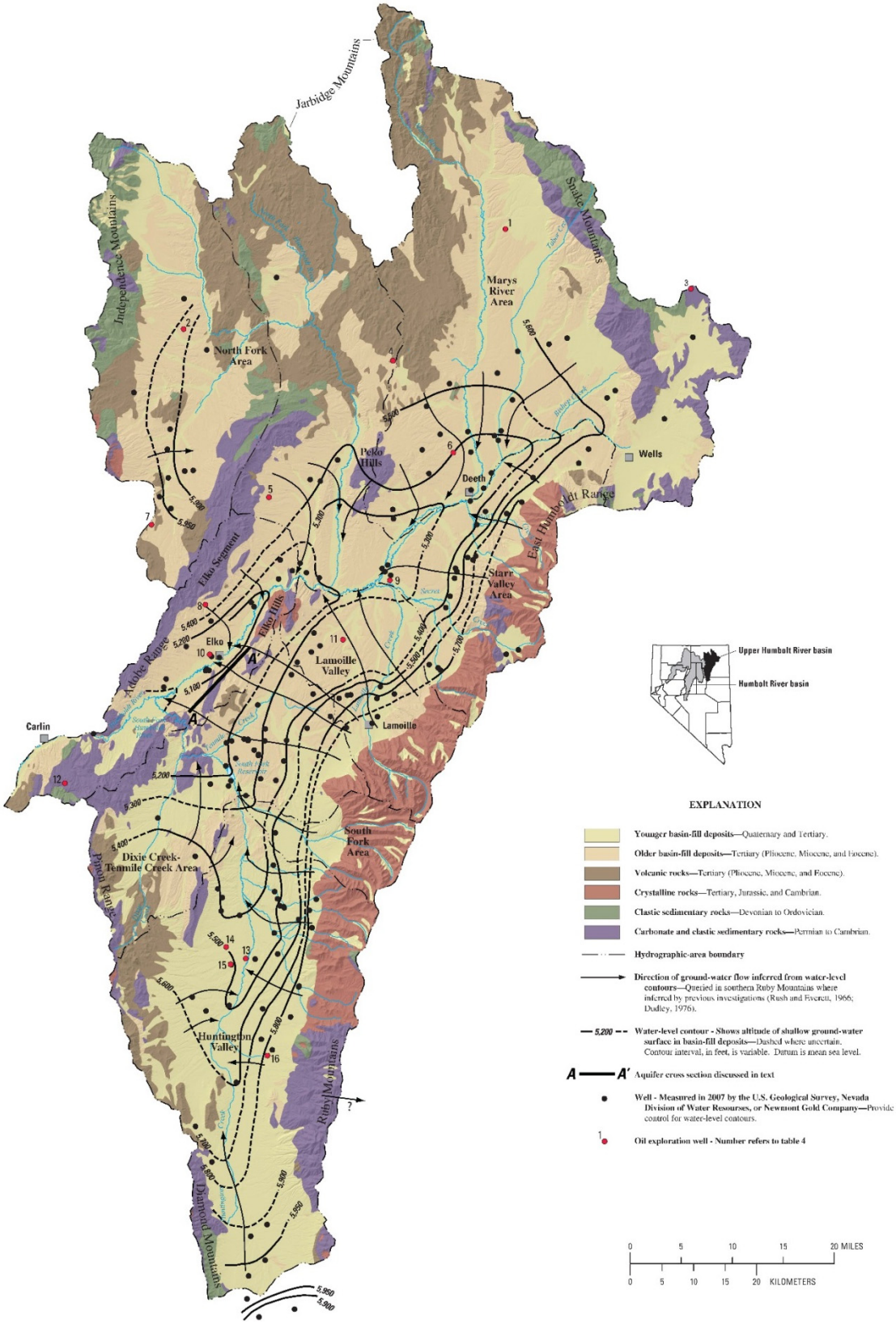

Figure 3-7. Groundwater levels and flow directions in the basin-fill deposits of the upper Humboldt River Basin, northeastern Nevada. Modified from Plume (2009).

the pediment between the mountains and Humboldt River flood plain. A portion of the water leaves the two basins as runoff because aquifers in both valleys are saturated to near land surface and have limited storage available for recharge (Eakin and Lamke, 1966, p. 31).

Groundwater flow is to the northwest in Lamoille Valley and to the west in the Starr Valley Area. Water-level gradients range from 50-100 feet per mile adjacent to the mountains to 10-30 feet per mile near the Humboldt River flood plain. Groundwater flow in the Marys River Area is generally southward to the Humboldt River. The lower reaches of Marys River are ephemeral and water-level contours have no upstream inflection unlike other streams in the study area. Near the Humboldt River flood plain, water-level gradients are approximately 20 feet per mile.

The North Fork Area consists of upper and lower topographic basins that are connected by streamflow through a canyon in the northern Adobe Range. The upper basin consists of an east sloping pediment of flat-lying to tilted older basin-fill deposits overlain by a thin cover of younger basin-fill deposits (A.R. Wallace, U.S. Geological Survey, oral communication, 2008), as much as five miles wide, between the Independence Mountains to the west and Double Mountain and the Adobe Range to the east. Sparse water-level data indicate that groundwater flow is eastward from a recharge area along the eastern base of the Independence Mountains. Water-level data are not sufficient to determine whether the direction of groundwater flow on the east side of the area moves northeastward parallel with the Adobe Range or continues eastward through the range. The first possibility would require a sharp change in the direction of flow from eastward to northeastward. The second does not seem likely because the principle rock types of the Adobe Range are 4,000-5,500 ft of poorly permeable shale and sandstone of the Diamond Peak Formation and Chainman Shale (Figure 3-7).

Groundwater flow in the lower part of the North Fork Area is southeastward from the Adobe Range and southwestward from the Peko Hills toward the North Fork Humboldt River, which is indicated by the 5,300 and 5,400 ft water-level contours, and then southward along the basin axis toward the Humboldt River (Figure 3-7). The Peko Hills are underlain by the Diamond Peak Formation, Chainman Shale, and by older and younger carbonate rocks.

Sharp upstream inflections of the water-level contours indicate that the Humboldt River gains flow from groundwater seepage from a few miles west of Wells to the west boundary of the study area. Water-level gradients along the flood plain range from approximately 7 to 30 feet per mile east of the Elko Hills. Groundwater flow in the Elko Segment (Elko Hills to the west boundary of the study area) is to the southeast from the Adobe Range and northwest from the Dixie Creek-Tenmile Creek Area through the unnamed hills between the Elko Hills and the South Fork Humboldt River. Streamflow gains of the river in the Elko Segment are approximately 6,600 acre-ft/yr. This groundwater seepage to the river channel primarily moves through a 10-mile-wide section of the unnamed hills (Figure 3-7) under a water-level gradient of 40 feet per mile.

4.0 REGIONAL GROUNDWATER MODEL

4.1 INTRODUCTION

A numerical three-dimensional groundwater flow model of the upper Humboldt River Basin is developed to guide configuration and parameterization of specific components of the local-scale flow and transport models (see Appendix B). The objective of the regional model is to estimate the three-dimensional distribution of hydraulic head given the independent calculations of the regional groundwater budget presented earlier in this report, the estimated hydraulic parameters of the regional hydrogeologic units, and the water level observations at 148 wells throughout the upper Humboldt River Valley. The regional model provides the head distribution on which head boundary conditions, hydraulic gradients, and groundwater flow directions for the local models of groundwater flow and transport can be inferred.

4.2 ASSUMPTIONS

- The system is in quasi-equilibrium and can be represented by steady-state conditions based on current annual estimates of hydraulic stresses.
- Groundwater flow at the regional scale can be described by the continuum approach.
- The spatial distribution of hydraulic conductivity is defined by the configuration of hydrogeologic units.
- Regional hydrogeologic units are internally homogeneous or can be divided into homogeneous zones with respect to hydraulic properties.
- All components of the groundwater budget are estimated independently of the model and are used as input.

4.3 MODEL CONSTRUCTION

The regional flow model uses the public-domain MODFLOW-2005 (Version 1.10.00) finite-difference groundwater modeling code and supporting modular flow packages (Harbaugh, 2005). Hydrographic areas 42, 43, 44, 45, 46, 47, 48, and 49 (as discussed in Section 3 of this report) are all included in their entirety within the 4,360 square mile model domain. The mesh is aligned with the Universal Transverse Mercator coordinate system (UTM Zone 11, NAD83, meters) and is horizontally discretized into 121 columns and 211 rows (Table 4-1). Cell dimensions are 1,000 m in both the easting and northing directions. All model cells outside the basin boundary are inactive and all cells inside the boundary are active. Each model layer includes 11,279 active cells, resulting in 372,207 active cells in the model. The timescales of the processes under investigation span 10 to 10^3 years and are considered to undergo few changes within that time. Therefore, steady-state conditions are assumed for the regional groundwater flow model.

Table 4-1. Horizontal coordinates of the regional flow model mesh. Coordinates are given at cell centers.

Corner	Row	Column	Easting (m)	Northing (m)
Northwest	1	1	570,000	4,627,000
Southeast	211	121	690,000	4,417,000

The majority of the perimeter boundary is treated as no-flow based on the assumption that interbasin groundwater flow is an insignificant component of the groundwater budget. However, Plume (2009) suggests that recharge on high-permeability, east-dipping carbonate rocks that form the southern Ruby Mountains may exit the basin as groundwater flow eastward toward Ruby Valley at a rate of approximately 4,000 acre-ft/yr (approximately 1.5 percent of the total basin outflow). Flow out of the model domain through this boundary is simulated using the Modflow WEL module. The configuration of the perimeter boundary is shown in Figure 4-1.

Thirty-three model layers are used, with the elevation of the top of the model defined by the topography of the water table surface and the base set at an elevation of 4,500 m below mean sea level (AMSL). The configuration of the water table is approximated by contouring water level measurements in 148 shallow wells (Plume, 2009) within the basin (Figure 4-1). Head data from most of these wells are also used as head observations, but wells located in the mountain blocks are not included, as described below.

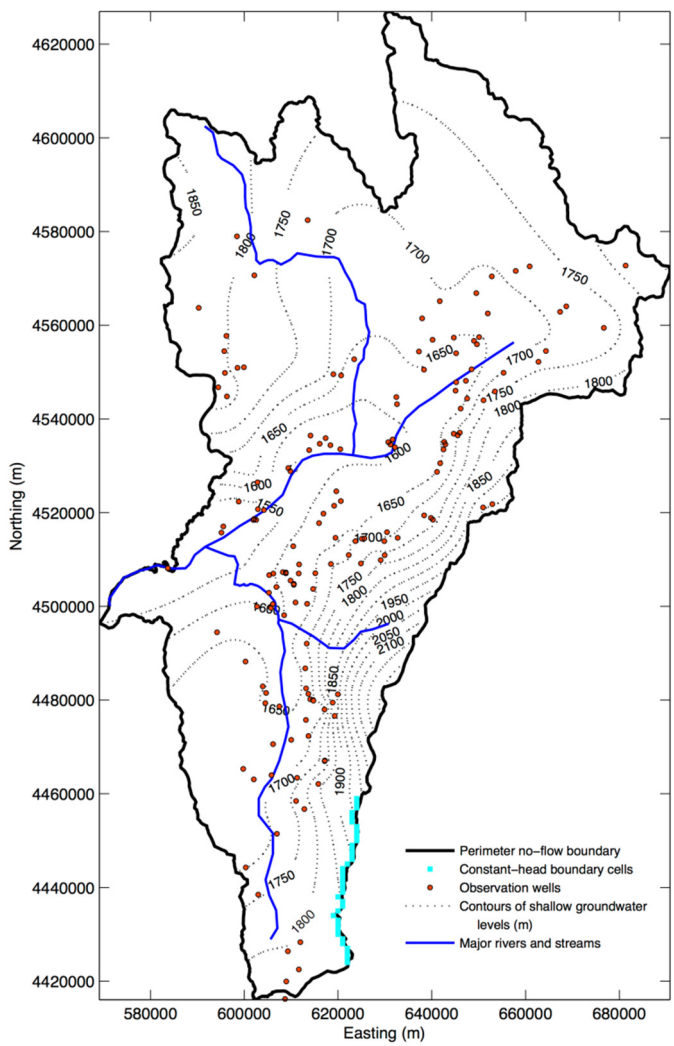

Figure 4-1. Map view of the regional flow model domain showing perimeter boundary, constant-head boundary cells, observation wells, contours of shallow groundwater levels, and major rivers and streams.

Virtually all of the wells are located within the major valleys of the basin and their water levels represent heads in laterally continuous shallow aquifers represented in layer 1 of the regional flow model. Although very few in number, water levels measured in the adjacent mountain ranges reflect conditions in higher elevation valleys that are not simulated in the regional model. Two of these wells are located in the southern Snake Mountains and five in the Ruby Mountains. These wells are included for contouring purposes and to maintain a trend of higher groundwater level elevations along the range fronts, but they are not used as head observations in the model.

Model layer thicknesses are selected to balance maximizing simulation accuracy at the depths of interest with computational efficiency (Figure 4-2 and Table 4-2). Model layer elevations do not conform to HGU elevations (described below) owing to the irregular shapes and large variations in thickness of the hydrogeologic units that underlie the basin. The base elevation was selected to include Paleozoic carbonate units below the volcanic and other sedimentary rocks that fill the deep Miocene structural basin. The finite difference equations of flow are solved using Modflow's preconditioned conjugate gradient (PCG) package that uses convergence criteria for the simulations of 0.01 m for head change and 0.01 m^3/day for residuals.

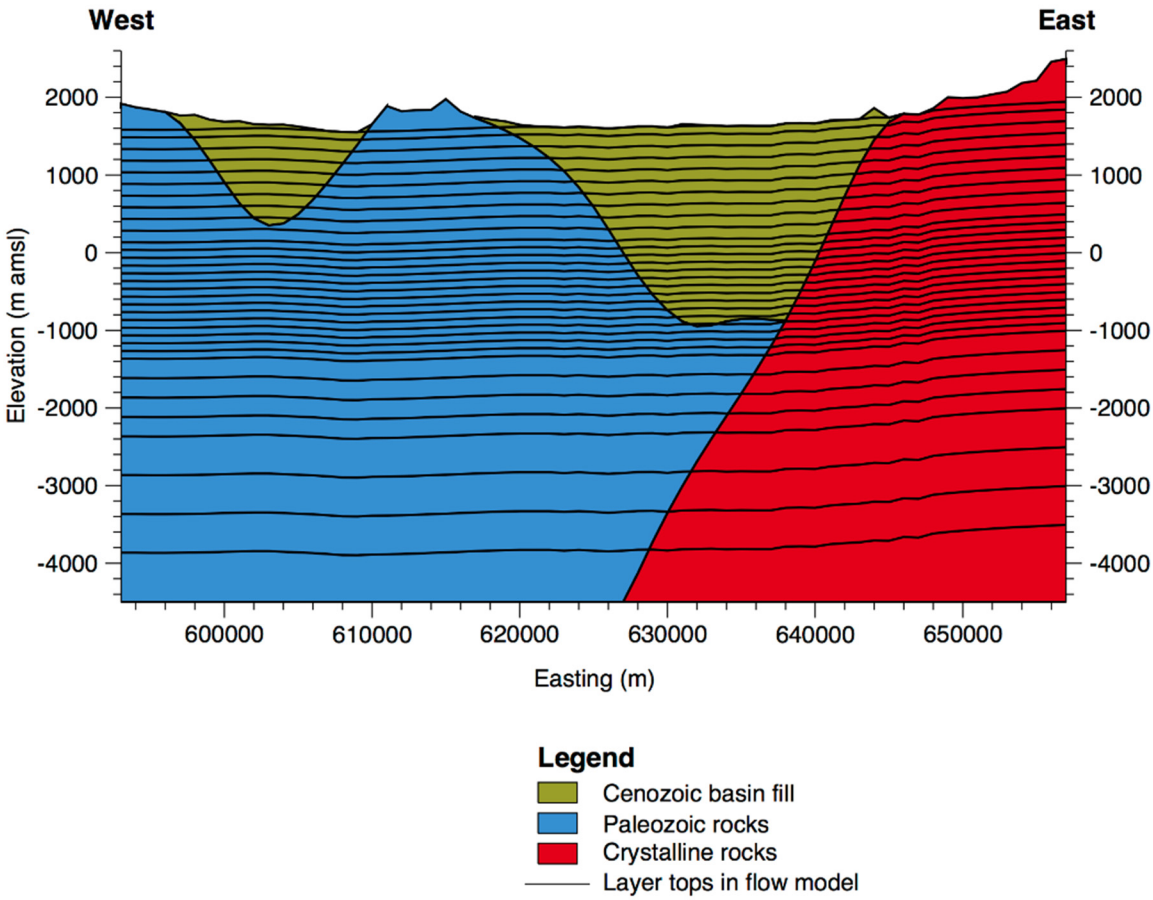

Figure 4-2. Configuration of layers in the regional flow model using a West-East profile at 4,525,000 m North (model row 103) as an example. Layer thicknesses are given in Table 4-2. The ten units in the regional hydrogeologic framework model are combined into three units for illustrative purposes.

Table 4-2. Layer thicknesses in the regional flow model.

Model Layer Number	Thickness (m)
1 (top)	100
2 to 10	150
11 to 25	100
26 to 29	250
30 to 32	500
33 (base)	558 to 1,473

4.4 HYDROGEOLOGIC UNITS

Subsurface hydrogeologic units in the upper Humboldt River Basin vary greatly in thickness and lateral extent, which is consistent with geologic basins across the Great Basin. Cenozoic units deposited within the deep and narrow Miocene structural basin that extends from southern Huntington Valley to the northern Marys River Area (Plume, 2009) pinch out at the margins of the basin, whereas underlying Paleozoic rocks extend under a much broader area. Additionally, crystalline rocks in the Ruby Mountains outcrop on the eastern edge of the basin, but also underlie eastern portions of the Cenozoic basement. This relatively complicated hydrogeologic framework prevents the use of simple horizontal model layers to represent HGUs or zones of hydraulic conductivity. Instead, the regional flow model uses the Hydrogeologic-Unit Flow (HUF) package (Anderman and Hill, 2000) within Modflow to represent the geometry and define the hydraulic parameters of hydrogeologic units that are independent of flow model layers. The HUF package averages the hydraulic parameters of hydrogeologic units that are present in each cell of the flow model based on their relative volumes within the cell. The impact of averaging parameters of independent HGUs that share flow model cells, which is an issue that is inherent to the HUF approach, is minimized by using thin flow-model layers, particularly at the targeted depths of the local-scale models.

The conceptual regional framework model includes 10 hydrogeologic units of the 11 described in Section 2 of this report. The older and younger volcanic rocks are combined into a single volcanic unit because their similar lithologic characteristics and locations within the basin are presumed to provide similar hydraulic characteristics. Therefore, the conceptual hydrogeologic framework includes four Paleozoic units, five Cenozoic units, and one crystalline rock unit. The differentiation of these units is based on stratigraphic relationships, lithology, and potential water-bearing characteristics as described in Section 2. Note that crystalline rocks are included only in the northern and central Ruby Mountains and the east Humboldt Range. Isolated intrusive bodies in the basin are not included. Each hydrogeologic unit is assigned a value of hydraulic conductivity and vertical anisotropy that represents the associated rock type. Faults are not expressly included as hydraulic features because of the lack of information about their hydraulic properties. However, several faults are included through the juxtaposition of hydrogeologic units, including the Miocene listric fault located along the western margin of the Ruby Mountains and the Roberts Mountain thrust fault in the North Fork area.

The conceptual hydrogeologic framework was built using mapped geologic outcrops (Coats, 1987) and information from 29 oil and gas exploration boreholes obtained from the Nevada Bureau of Mining and Geology. Lithologic, stratigraphic, and geophysical data for Noble Energy boreholes M2C and M10C in Exploration Area 2 were provided by Noble Energy, Inc. Section 2 of this report describes these data and the basis for hydrogeologic interpretations made to develop the hydrogeologic framework. Three-dimensional top surfaces for each hydrogeologic unit were developed in MATLAB® (The MathWorks, Inc.)—a programming environment for numerical computation and visualization—using spatially registered elevations from outcrops and borehole logs. The biharmonic spline interpolation method was used to fit unit surfaces to known data points because it generates smooth surfaces while still honoring all data points. Faults are not directly included in the conceptual framework model. Considering the limited availability of subsurface data (31 boreholes covering approximately 4,360 mi^2) adjustments to the simulated surfaces were necessary in areas of extremely sparse data. These adjustments were accomplished by generating profiles through the model and establishing control points consistent with observed stratigraphic and structural relationships to guide further rounds of interpolation. Figure 4-3 shows these profiles through the conceptual hydrogeologic framework model at Noble Exploration Areas 1 and 2, and just south of Noble Exploration Area 3 (where borehole control is better).

4.5 Recharge, Discharge, and Boundary Flow

Recharge from precipitation is simulated as linear arrangements of groundwater injection wells located at the interfaces between consolidated rock units that form the highlands and unconsolidated rocks that fill the basins (Figure 4-4). Recharge is added to the top model layer using the Modflow WEL package. Individual well recharge rates are determined from the recharge estimates for each of the eight hydrographic areas described in Section 3.1 and the geometric arrangement of wells adjacent to a given mountain block using the GMS Modflow preprocessor. This approach to simulating recharge was taken because simulating areal recharge over low-permeability mountain blocks would add additional modeling complexity that was considered beyond the scope of the objectives of the regional-scale model.

Groundwater discharge occurs as withdrawals from pumping wells, baseflow to major rivers and streams, regional groundwater springs, and evapotranspiration from phreatophytes (Figures 4-5 and 4-6). The methods used for determining all discharge volumes are described in Section 3.1. Groundwater pumping at 45 production wells is simulated in layer 1 using the Modflow WEL package. Baseflow is simulated using the Modflow DRN package and is included only for rivers and streams that are thought to be gaining streams. Losing streams are considered a minor component of the regional water budget. The 29 springs located in major valleys that discharge from alluvial or carbonate units are considered part of the regional flow system and are also simulated using the DRN package. Data are not available for annual discharge volumes for these springs, so they could not be used as observations to calibrate the model. Hydraulic conductivity is set to 1.0 m/d for calculating all drain conductance values, which is consistent with fluvial sediments (Freeze and Cherry, 1979). Discharge from ET is simulated as negative recharge from layer 1 using the Modflow RCH package.

All perimeter boundaries are no flow, with the exception of the southern end of the Ruby Mountains. At that southern end, groundwater flows eastward toward Ruby Valley through eastward-dipping Cambrian to Devonian carbonate rocks at an estimated rate of approximately 4,000 acre-ft/yr

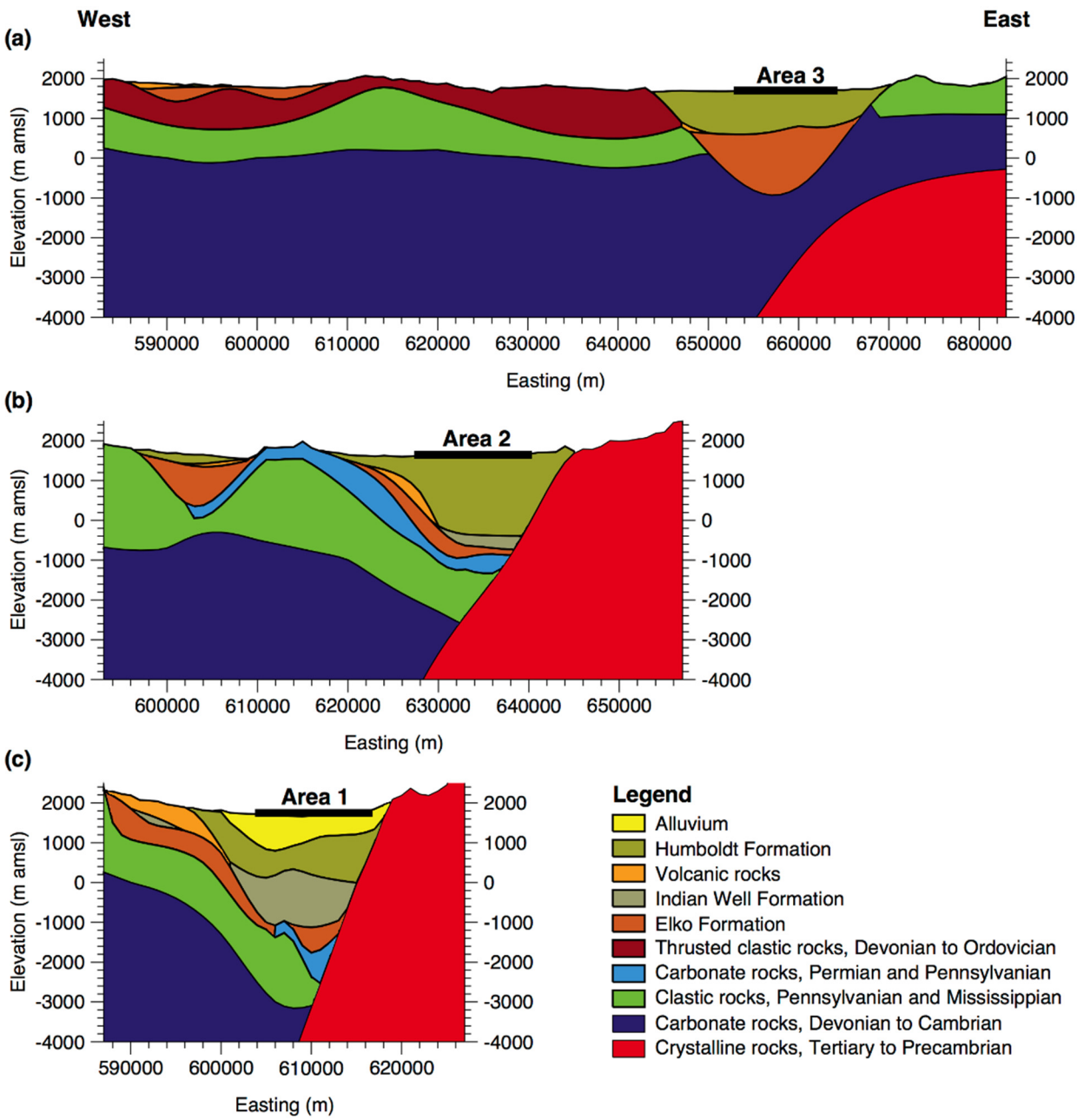

Figure 4-3. West-east profiles through the conceptual regional hydrogeologic framework of the upper Humboldt River basin at (a) 4,564,000 m north, (b) 4,525,000 m north, and (c) 4,473,000 m north. The profiles pass through Noble Exploration Areas 3, 2, and 1, respectively.

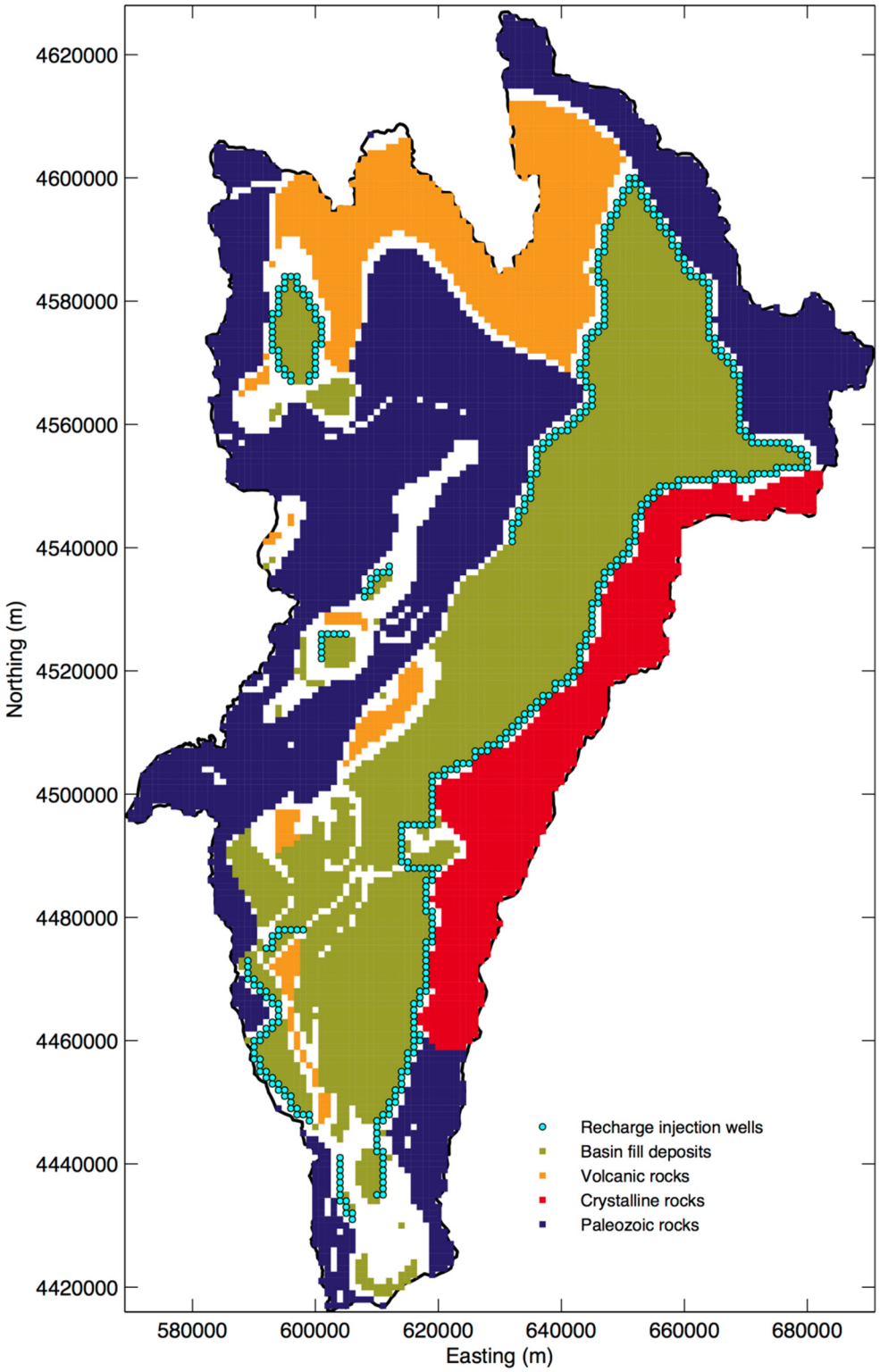

Figure 4-4. Locations of recharge injection wells used to simulate mountain front recharge at the margins of basin-fill deposits and hydrogeologic classes that comprise greater than 95 percent of cell thickness in layer 1 of the flow model. Areas within the model domain are shown as white indicate cells where no single hydrogeologic class exceeds 95 percent of cell thickness in layer 1.

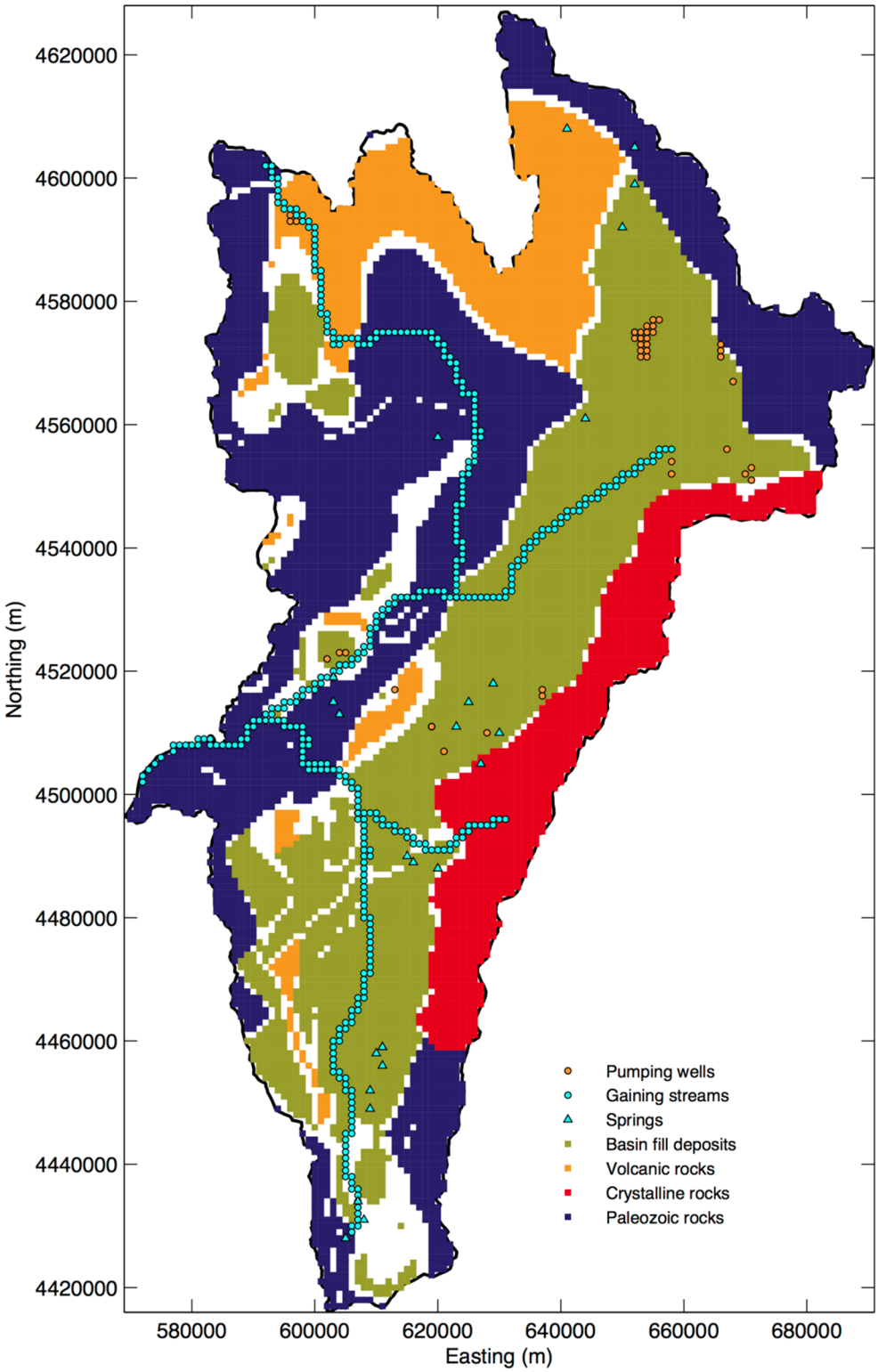

Figure 4-5. Locations of pumping wells, streams, springs and hydrogeologic units that comprise greater than 95 percent of cell thickness in layer 1 of the flow model. Areas within the model domain are shown as white indicate cells where no single hydrogeologic unit exceeds 95 percent of cell thickness in layer 1.

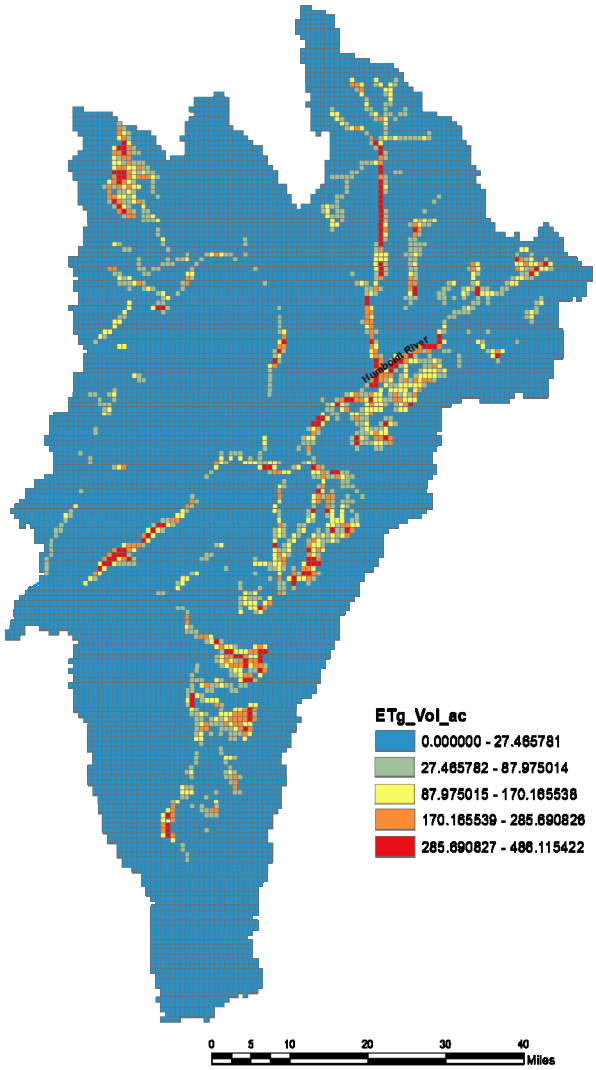

Figure 4-6. Distribution of groundwater evapotranspiration simulated in the regional flow model.

(Plume, 2009). This is simulated using the Modflow WEL module. Wells in 36 cells aligned along the eastern model boundary are configured to remove groundwater from layers 1 and 2, simulating this eastward flow within the top 250 m of the saturated zone (shown on Figure 4-1).

4.6 RESULTS

A manual trial-and-error approach is taken for model calibration using observed heads as the calibration values. Hydraulic parameters are adjusted until a reasonable fit of the model to the observations is obtained. Although observations from throughout the basin are included (with the exception of seven wells located at higher elevations in the southern Snake Mountains and Ruby Mountains that were described previously) and equally weighted, emphasis is placed on matching heads near Area 2, where the local models are based. Although all observations are located in shallow aquifers that are simulated as layer 1 of the regional model, the local models address groundwater flow at depths of 1,500 meters or more below land surface. Unfortunately, reliable head data are not available at these

great depths and so the regional model can provide only approximations of heads that are consistent with the conceptualizations of the groundwater budget and regional flow. Furthermore, the manual calibration approach used here is consistent with the objective of the regional model but does not guarantee the statistically best model fit throughout the basin.

Twenty-two hydraulic parameters were calibrated using the root mean squared error (RMSE) between observed heads h_o and corresponding simulated heads h_s as the measure of model goodness of fit. The RMSE is defined as:

$$RMSE = \left[\frac{1}{n}\sum_{i=1}^{n}(h_o - h_s)_i^2\right]^{1/2} \tag{4-1}$$

where n is the number of head observations.

Because of the lack of aquifer hydraulic testing in the upper Humboldt River Basin, values of hydraulic conductivity were assumed to be consistent with hydraulic testing and modeling results for similar hydrogeologic environments in other northern Nevada basins (Prudic, 2007; Plume, 1996; Plume, 2009; Plume and Smith, 2013) and for general categories of rock type (Freeze and Cherry, 1979; Domenico and Schwartz, 1997). The calibrated values are listed in Table 4-3. The Humboldt Formation and Devonian to Cambrian Carbonate Rocks are divided into two hydraulic conductivity zones to address calibration issues (Figure 4-7).

Table 4-3. Values of calibrated model parameters.

Parameter	Value
Horizontal hydraulic conductivity, *K* (m/d)	
Alluvium	10.0
Humboldt Formation, zone 1	0.5
Humboldt Formation, zone 2	0.1
Volcanic rocks	0.03
Indian Well Formation	0.10
Elko Formation	0.005
Thrusted clastic rocks, Devonian to Ordovician	0.01
Carbonate rocks, Permian and Pennsylvanian	0.01
Clastic rocks, Pennsylvanian and Mississippian	0.01
Carbonate rocks, Devonian to Cambrian, zone 1	0.15
Carbonate rocks, Devonian to Cambrian, zone 2	0.10
Crystalline rocks	0.005
Vertical Anisotropy[a]	
Alluvium	10.0
Humboldt Formation, zones 1 and 2	10.0
Volcanic rocks	10.0
All other hydrogeologic units	1.0

[a]Ratio of *K* in the horizontal direction to *K* in the vertical direction

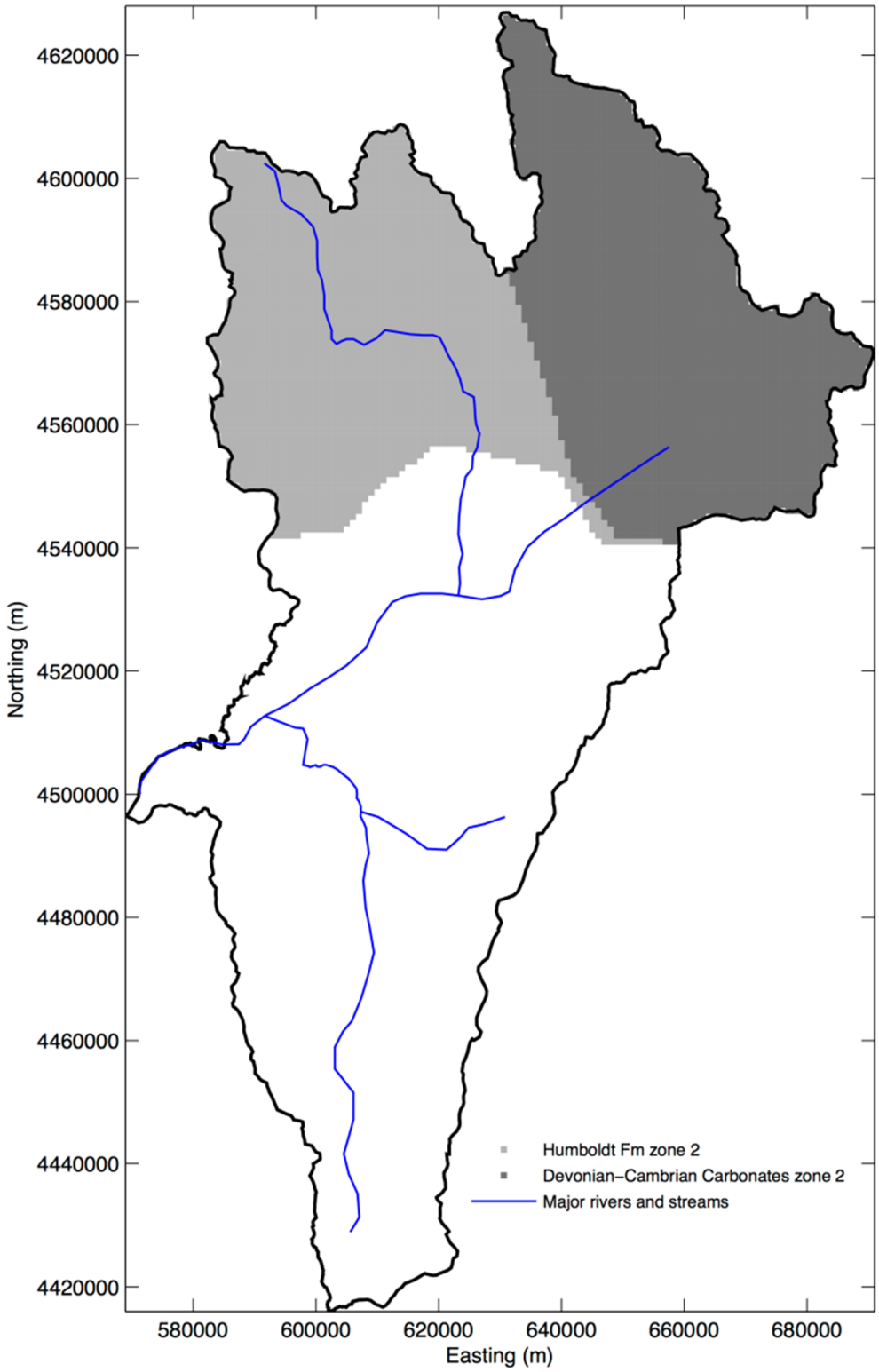

Figure 4-7. Location of hydraulic conductivity zones. Zone 2 of the Humboldt Formation also includes the area defined by Zone 2 of the Devonian to Cambrian carbonates. The remainder of the domain (shown with no shading) represents Zone 1 for both units.

Zone 2 of the Devonian to Cambrian Carbonate Rocks is assigned a lower hydraulic conductivity than the bulk of this unit to reduce unrealistically high transmissivity values associated with its great thickness in the Marys River Area. Zone 2 of the Humboldt Formation is also assigned a lower hydraulic conductivity to improve the fit of the model-to-head observations in the northern portion of the domain. However, there is no direct evidence to suggest that values of hydraulic conductivity are lower.

Vertical anisotropy is defined only for the three shallowest basin-fill units (Table 4-3). Stratification of these unconsolidated rocks is more likely to reduce vertical conductivity relative to horizontal conductivity as compared to deeper, fractured, and faulted consolidated carbonate and clastic rocks.

Observed heads plotted against simulated heads for the calibrated model show that the average head error of 53 meters is approximately 10 percent of the range in heads simulated over the entire model (Figure 4-8). Although the random distribution of heads around the 1:1 line suggests that the head simulation is relatively unbiased, heads are generally underestimated in the southern Marys River and North Fork areas and overestimated in portions of Huntington Valley and the Dixie Creek-Tenmile Creek Area.

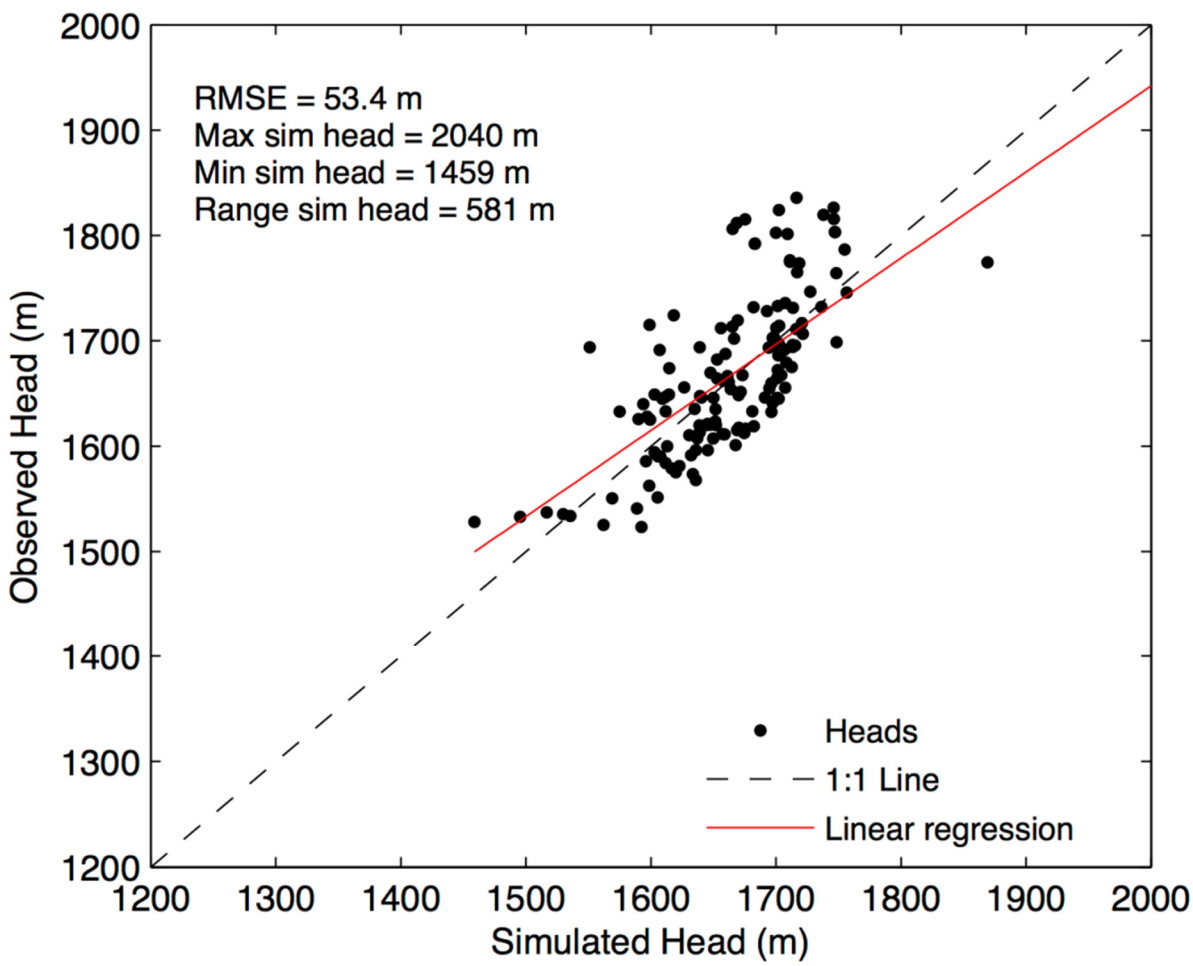

Figure 4-8. Plot of simulated heads against observed heads in the shallow aquifer.

The groundwater budget for the simulation indicates a discrepancy between input and output components of less than 0.001 percent (Table 4-4), which shows that the components of the budget simulated by the flow model adequately represent the groundwater budget presented in Section 3.1. The small differences between calculated and simulated flow rates for the baseflow and pumping components result from model-simulated capture of baseflow to the Humboldt River by production wells located near Elko.

Heads simulated in layer 1 show that the model qualitatively represents the major features of the groundwater flow system as depicted by water levels mapped in the shallow aquifer. As expected, simulated flow occurs from recharge areas at higher elevations in the mountain blocks to low alluvial plains with ultimate discharge to downstream reaches of the Humboldt River and other major streams (Figure 4-9). Drawdowns associated with groundwater pumping for municipal and irrigation uses are evident near Elko and in the Marys River Area. These drawdowns are overestimated because the resolution of the model is not fine enough to account for lateral variation in hydraulic conductivity in near-surface aquifers.

The general pattern of groundwater flow in the upper layers of the model near Exploration Area 2 is from recharge areas in the highlands of the Ruby Mountains toward lower elevations adjacent to the Humboldt River where groundwater enters the river as baseflow (Figure 4-10). Contours of head parallel the southwest-northeast orientation of both the river and mountain front and indicate a horizontal component of groundwater flow that is directed northeast to north. The horizontal component of flow at greater depths shifts toward a predominantly northwest direction—as is evident by the head contours plotted for model layer 20—which corresponds to the approximate 2,400 m depth of the Elko Formation. The horizontal component of flow from this depth to the base of the model remains directed toward the northwest.

Table 4-4. Calculated groundwater budget and budget simulated by the regional model.

	Calculated Rate[a]		**Simulated Rate**
Input Components	**(ac-ft/yr)**	**(m^3/d)**	**(m^3/d)**
Recharge	283,700	958,080	958,102
Total In	283,700	958,080	958,102
Output Components			
Baseflow and springs	56,700	191,481	195,887
Evapotranspiration	199,000	672,041	671,360
Interbasin Flow	4,000	13,508	13,508
Pumping	22,700	76,660	77,347
Total Out	282,400	953,690	958,102
In - Out	1,300		0
Percent Discrepancy	0.460%		0.000%

[a]See calculation of groundwater budget in Section 3.1

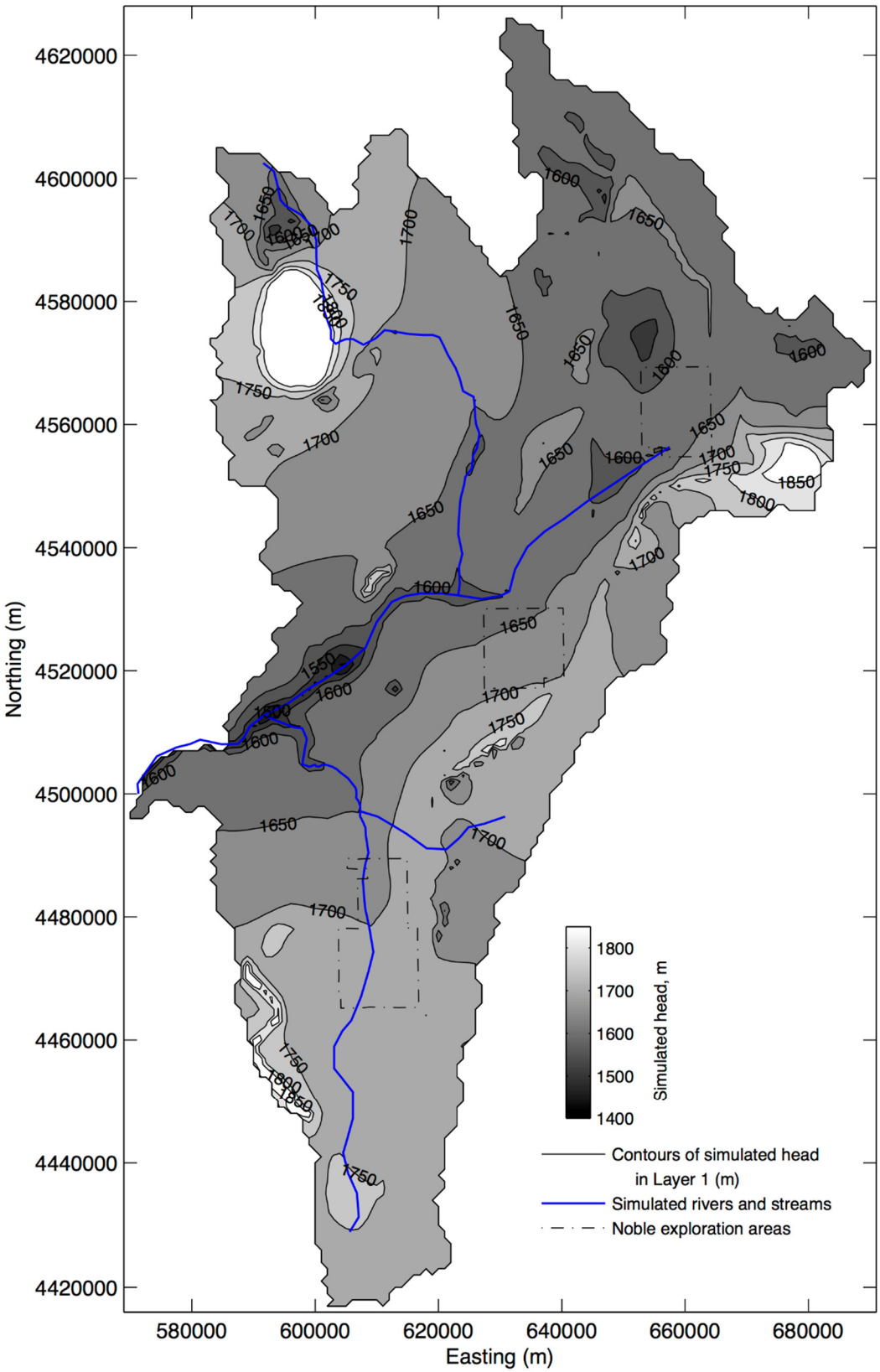

Figure 4-9. Heads simulated in layer 1 of the regional model.

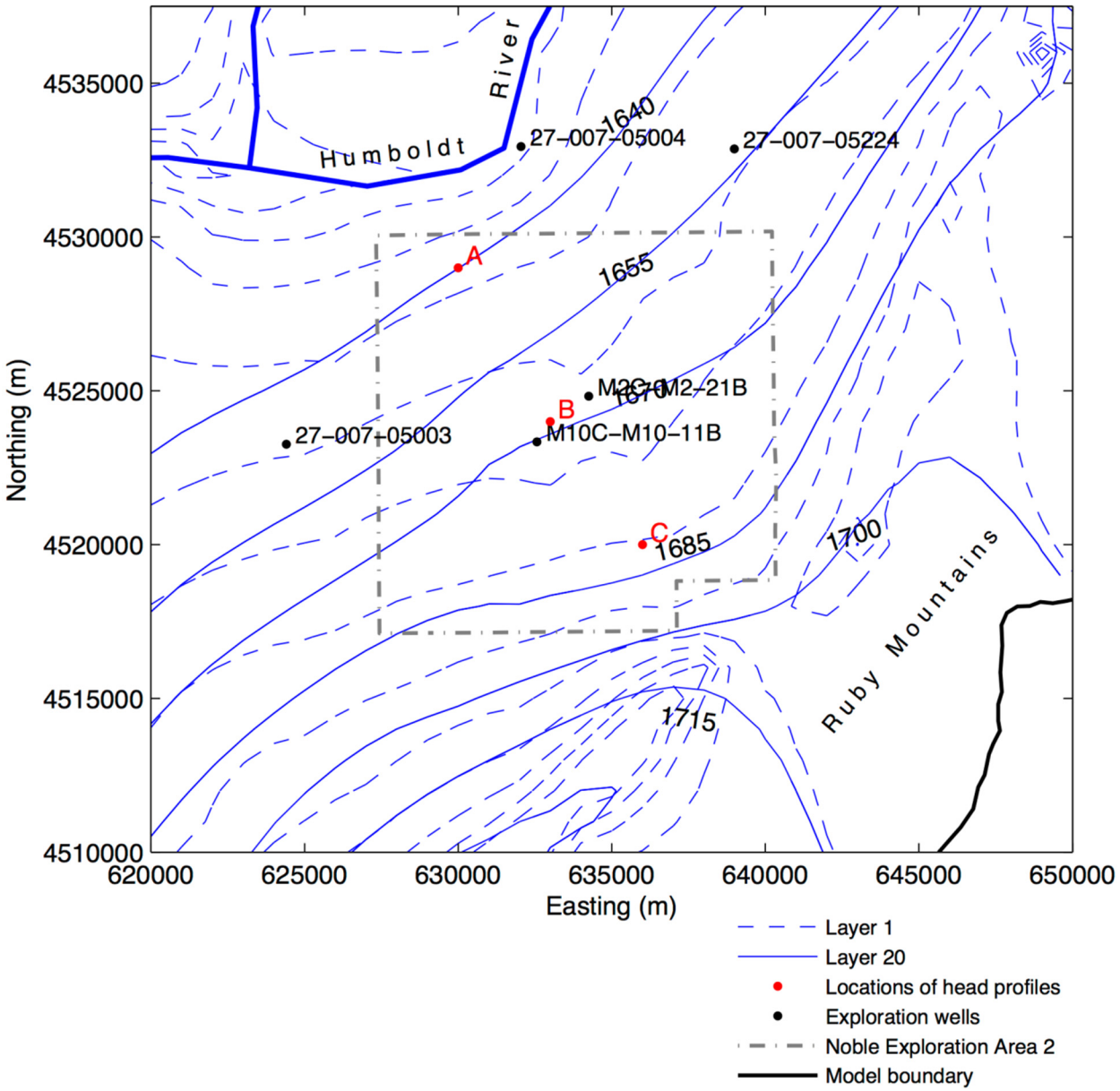

Figure 4-10. Contours of simulated heads in layer 1 (near-surface aquifer) and layer 20 (approximate elevation range of -815 to -715 m) in the vicinity of Exploration Area 2. The Elko Formation is simulated in layer 20 in this area. The locations of the vertical head profiles plotted in Figure 4-11 are shown in red. For clarity, contours in the Ruby Mountains are not shown.

The vertical head profiles shown in Figure 4-11 illustrate how the vertical components of the hydraulic gradients vary with depth in the groundwater flow system near Exploration Area 2. At Point A in the northwest corner of Area 2 (approximately down-hydraulic-gradient of Noble Energy wells M2C and M10C), heads increase with increasing depth in the upper portion of the flow system, which indicates upward flow in the Humboldt Formation toward the discharge zone of the Humboldt River. The break in slope in the profile at an elevation of 478 m represents the contact with the underlying Elko Formation, which is estimated to be 482 m thick at this location. In contrast, heads decline 2.7 m from the base of the Elko Formation to the base of the model (-4,500 m elevation), which indicates that even though there is a component of the gradient directed vertically downward, horizontal flow dominates in the Paleozoic section.

The flow pattern is similar near the center of Area 2 (represented as Point B in Figure 4-11), but two important differences are evident. First, the effect of a greater thickness of basin fill is reflected in the greater depth of the inflection point in the head profile and a thicker section of vertically upward directed flow. Here, the Elko Formation lies between -857 and -1,065 m elevation. Second, below the Elko Formation, the decline in head with increasing depth is of a greater magnitude than seen at Point A to the

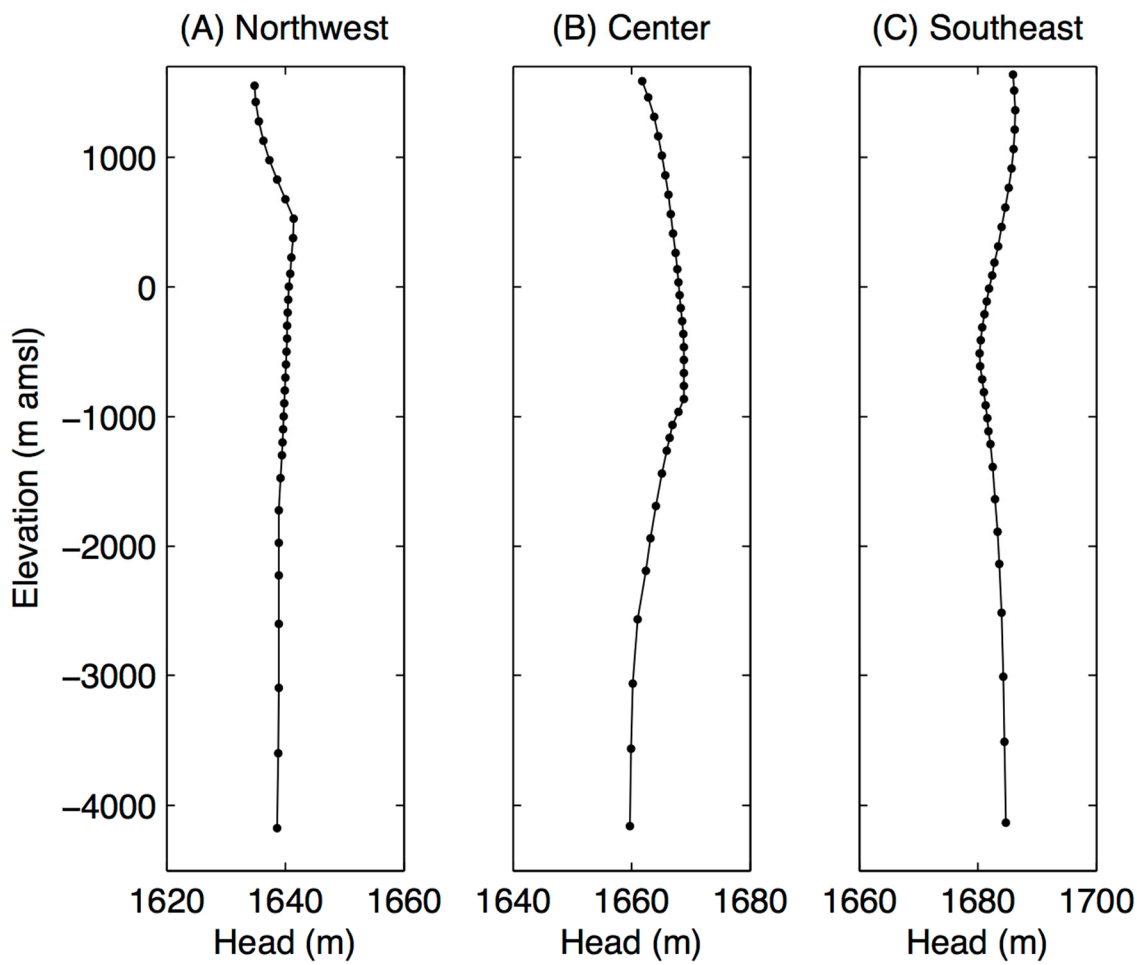

Figure 4-11. Vertical profiles of simulated head at three locations in Exploration Area 2. The locations are shown in Figure 4-10.

northwest, which indicates the stronger influence of groundwater recharge in the Ruby Mountains to the southeast. The southeast corner of Area 2 is less than 4 km from the face of the Ruby Mountains. The proximity to this recharge area combined with basin-fill sediments that rapidly thin toward the southeast causes a shift to greater downward flow in the upper portion of the basin (represented as Point C in Figure 4-11). At this location, the Miocene basin is bounded below by crystalline rocks that extend from an elevation of -560 m to the base of the model. The head profile in this section reflects the contrast between low-conductivity crystalline rocks and more conductive carbonate rocks to the northwest and more conductive basin fill at higher elevations in the section.

4.7 SENSITIVITY ANALYSIS

The regional flow model uses a single continuum approach to simulate groundwater flow by assigning a single regional value of hydraulic conductivity to each of the hydrogeologic units within the upper Humboldt River Basin. Fractures, faults, bedding, and other internal features that might affect groundwater flow are not explicitly simulated but are implicit to the averaged estimates of *K*. The only exceptions to this regional approach are the Humboldt Formation and the Devonian to Cambrian carbonates, which were each assigned two *K* zones as described above. The continuum approach is maintained within each of these zones. In contrast, a dual-continuum approach is used in the local models to more accurately represent the critical role that fractures play in groundwater flow and transport at the local scale. These models assign independent values of *K* to fractures and to the rock matrix that differ from the values assigned to the same units in the regional model, though together an equivalent value of *K* can be estimated for the unit that is consistent with the regional values. The dual-continuum approach used for the local models is fully described in the next section of this report. Although values of *K* are chosen to be consistent with the rock types that comprise the regional hydrogeologic framework, the final values are determined through model calibration that considers heads throughout the entire basin.

For these reasons, *K* values in the regional model may not be identical to *K* values assigned to hydrogeologic units specific to the local scale of Area 2. A sensitivity analysis illustrates the impacts that a range of *K* in the regional model (covering four orders of magnitude) has on heads simulated in Area 2 (Figure 4-12). Heads are evaluated at the three locations (shown in Figure 4-10) in model layers 12, 22, and 28, which correspond to elevations at Point 2 of 37, -964, and -1,939 m AMSL, respectively. The upper elevation is near the top of the local models and in the Elko Formation at Point A and the Humboldt Formation at Points B and C. The middle elevation is in the Paleozoic section at Point A, the Elko Formation at Point B, and crystalline rocks at Point C. The lower elevation is in the Paleozoic section at Points A and B and in crystalline rocks at Point C.

The northwest corner of Area 2 is down-hydraulic-gradient of wells M2C and M10C as represented by Point A. Heads in the Elko Formation and below show little variation with depth here (Figures 4-11 and 4-12), which indicates that the vertical component of groundwater flow is minimal. Adjustment of *K* from 10^{-2} m/d downward to 10^{-6} m/d leads to congruent reductions in head to a maximum of 8.5 m at all three elevations, as shown on Figure 4-12 (A). This indicates that vertical gradients do not change appreciably, but that horizontal gradients may increase from upgradient areas. Near M2C and M10C head increases by 7.7 m in the Humboldt Formation and is reduced by 1 m in the Elko Formation and 13.8 m in the Paleozoic section, as shown on Figure 4-12 (B). The simulation of lower *K* in the Elko Formation leads to a corresponding increase in the vertically downward directed

gradient. This is expected because the vertical gradient is higher in this area and the impact of reducing *K* in the Elko Formation serves to further increase it. The consequences for groundwater flow velocity depend on the interplay of these two factors. Heads farther southeast show a similar pattern of increase in the Humboldt Formation, as shown on Figure 4-12 (C). The two lower elevations at Point C are located within crystalline rocks that are not considered a significant contributor to the flow system.

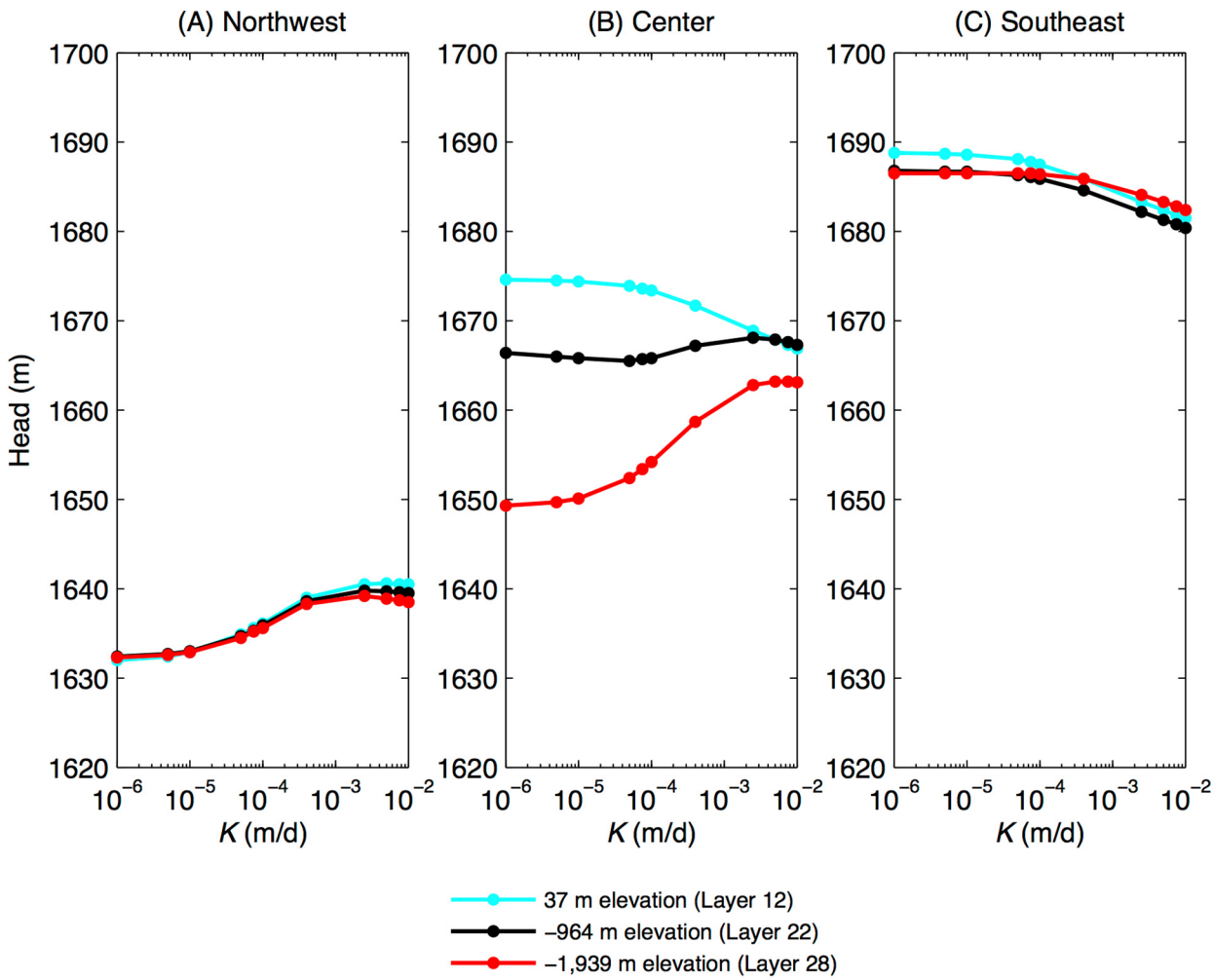

Figure 4-12. Plots of the variation of simulated head in Exploration Area 2 against a range of hydraulic conductivity values assigned to the Elko Formation in the regional flow model. The calibrated value is 5.0×10^{-3} m/d. Heads are plotted for three elevations that correspond to the range of elevations simulated in the local flow and transport models. The locations of these three points in Exploration Area 2 are shown in Figure 4-10.

5.0 GEOCHEMISTRY AND WATER QUALITY

5.1 Role of Geochemistry in the Project

Given Nevada's constitutional mandate to protect all "waters of the State," the NDOM and NDEP have requested access to nonproprietary groundwater data and information gathered by Noble Energy during exploration. The AQUA Program was established "to gather and share data and information on groundwater and geological conditions associated with the fate and transport of chemicals used for hydraulic fracturing" in a Memorandum of Understanding (MOU) between NDOM, NDEP, DRI, and Noble Energy (MOU, 2013).

The Desert Research Institute is supporting Noble Energy in its monitoring program in the upper Humboldt River Basin by providing quality assurance of sampling and laboratory activities and analyses, evaluating the usefulness of additional geochemical and isotopic parameters for monitoring and hydrologic characterization of flow paths, and collecting geochemical and isotopic parameters for springs in the project area (Figure 5-1). A data report (Hershey *et al.*, 2014) presents the analytical results from September 2013 through November 2014 for samples collected by DRI and Tetra Tech, Inc., (Tetra Tech) for Noble Energy in Exploration Area 1 (Huntington), Area 2 (Humboldt), and Area 3 (Marys River) as required for the AQUA Program in Section II.F.2 of the MOU (MOU, 2013). These data are evaluated and interpreted here.

5.2 Parameter Selection

A summary of the selected chemical and isotopic parameters and their purposes, as described below, is presented in Table 5-1. The natural gas components methane, ethane, and propane were selected for analysis in the monitoring program because they are associated with petroleum, they will degas when the pressure is lowered, and they may migrate more quickly than the target crude oil. The total petroleum hydrocarbons (TPH) separated into diesel range organics (TPH-DRO) and gasoline range organics (TPH-GRO) and the hydrocarbons benzene, ethylbenzene, toluene, and xylenes, which are refined at higher temperatures from crude oil were chosen because the presence of these chemicals in groundwater indicates ground-surface activities, as does the presence of methyl tert-butyl ether (MTBE, a gasoline additive).

The chemical parameters and constituents of water—including temperature, electrical conductivity (EC), pH, total dissolved solids (TDS), dissolved cations (Ca, Mg, Na, K, B, Ba, Li, Sr), anions (alkalinity [HCO_3, CO_3], Cl, SO_4, NO_3, F, Br,), and SiO_2—are used to chemically characterize groundwater prior to hydraulic fracturing activities and to identify potential water contamination after hydraulic fracturing activities. Water from the target shale units is likely to be very high in TDS and chemically different from local groundwater (e.g., Rowan *et al.*, 2011; Engle *et al.*, 2012). If shale water were to mix with local groundwater, changes in the chemical character of the local groundwater would be evident.

Shale often has elevated, naturally occurring radioactivity from the presence of uranium and its daughter products. The target shale units in the exploration areas are expected to have uranium and its daughter products. The radioactivity analyses of gross alpha, gross beta, radium-226, and radium-228 are used to identify the mixing of target shale water with local groundwater. These analyses have been shown to be an effective tracer of shale water in the Marcellus Shale in Pennsylvania (e.g., Rowan *et al.*, 2011; Engle *et al.*, 2012). Because uranium and its daughter products are also present in the granitic rock of the Ruby Mountains, it is important to establish the natural background radioactivity in the exploration areas prior to hydraulic fracturing of the target shale.

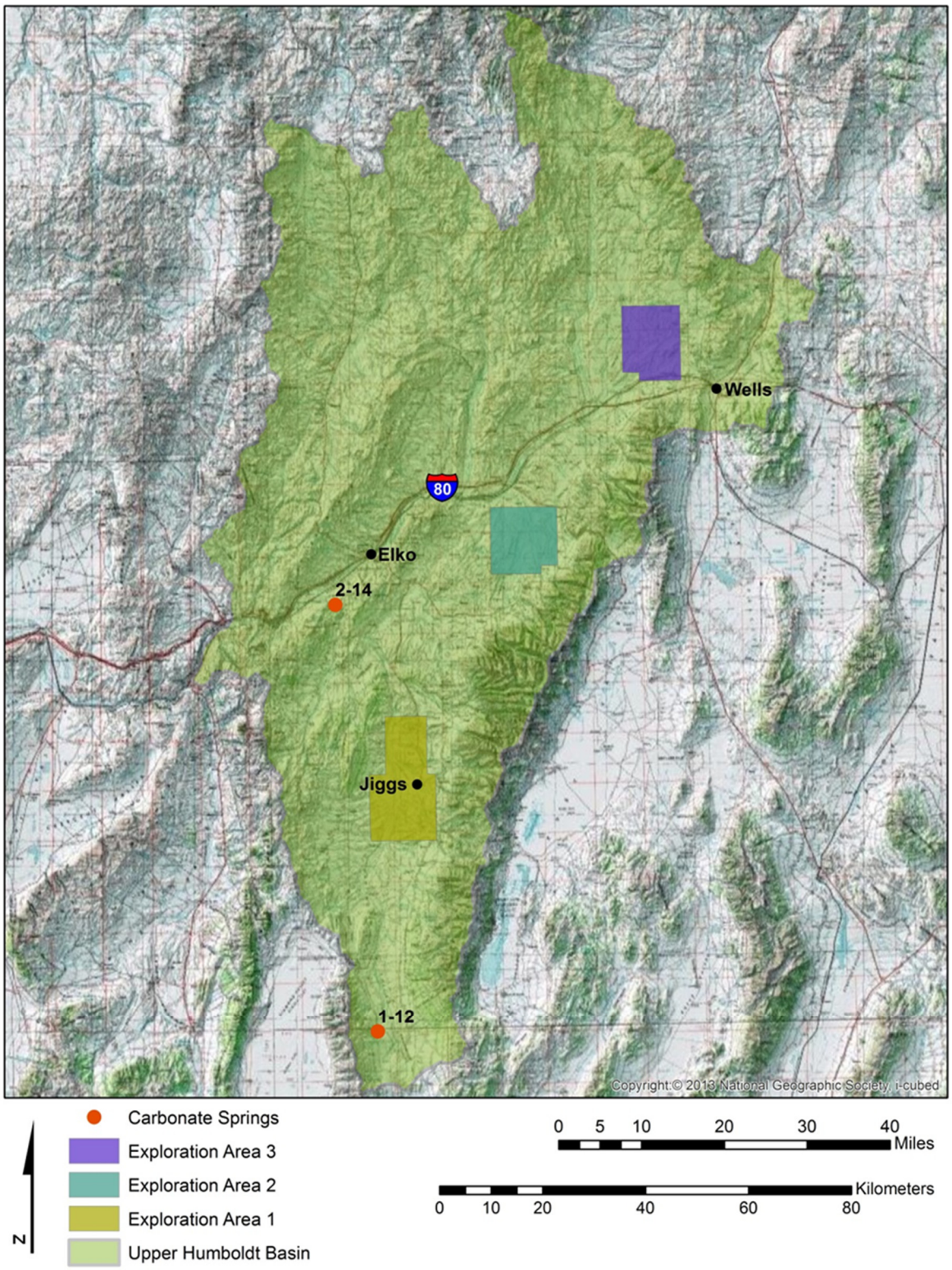

Figure 5-1. Noble Energy exploration areas in the upper Humboldt River Basin and sample locations outside the vicinity of the exploration areas.

Table 5-1. Chemical and isotopic parameters and the purpose these parameters were selected for the aquifer quality assessment program.

Parameter or Constituent	Purpose
Methane, Ethane, Propane	Early indicators of crude oil release
Diesel Range Organics	Refined hydrocarbon release from earth-surface activities
Gasoline Range Organics	Refined hydrocarbon release from earth-surface activities
MTBE, Benzene, Toluene, Ethylbenzene, Xylenes	Refined hydrocarbon release from earth-surface activities
Temperature, Electrical Conductivity, pH	Characterize local groundwater, identify mixing of shale water
Ca, Mg, Na, K, Li, B, Ba, Sr	Characterize local groundwater, identify mixing of shale water
Alkalinity, Cl, SO_4, Br, NO_3, F, SiO_2, Total Dissolved Solids	Characterize local groundwater, identify mixing of shale water
Gross Alpha, Gross Beta, Radium-226, Radium-228	Establish natural background in local groundwater, identify mixing of shale water
δ^2H, $\delta^{18}O$, $\delta^{13}C$ DIC water	Characterize local groundwater, identify mixing of shale water
δ^2H, $\delta^{13}C$ methane	Identify source of methane: biogenic or thermogenic
Ne, Ar, Kr, Xe, ^4He	Identify source of natural gas, characterize local groundwater, identify mixing of shale water
R/R_a ($[^3He/^4He]_{groundwater}$ / $[^3He/^4He]_{atmosphere}$)	Identify source of natural gas, characterize local groundwater, identify mixing of shale water
Methanol, Ethanol, Isopropanol, 2-Butoxyethanol, Acrylonitrile, Glycerol, Ethylene Glycol, Propylene Glycol, Ammonium Persulfate	Indicators of hydraulic fracturing fluid release

The stable isotopes of water, δ^2H and $\delta^{18}O$, and dissolved inorganic carbon (DIC) in water, $\delta^{13}C$, are used to isotopically characterize local groundwater prior to hydraulic fracturing activities and to identify potential water contamination after hydraulic fracturing activities. It is assumed that water from the target shale units will have substantially different isotopic signatures (e.g., Sharma *et al.*, 2011; Engle *et al.*, 2012) compared with local groundwater because the target shale water originated from precipitation that fell under different climatic conditions than more recently recharged local groundwater. Stable isotopes will be collected to characterize the local groundwater and to identify changes in the isotopic signatures of local groundwater in the event that water from the target shale units mixes with the local groundwater.

Two distinct processes produce hydrocarbon gas: biogenic and thermogenic degradation of organic matter. Isotopic tracers of methane ($\delta^{13}C$, δ^2H) are used to identify whether the hydrocarbon gas is of biogenic or thermogenic origin. Biogenic gas is formed at shallow depths and low temperatures by anaerobic bacterial decomposition of sedimentary organic matter. Thermogenic gas is formed at deeper depths by either thermal cracking of sedimentary organic matter into hydrocarbon liquids and gas or thermal cracking of oil at high temperatures into gas. The occurrence of biogenic gas is unrelated to the processes that form oil. Each process produces a different isotopic signature of methane, so the isotopic signatures can be used to identify whether the methane came from deep target shale units or from the near surface (e.g., Jackson *et al.*, 2013).

The abundance of noble gases and the isotopic composition of helium are used to distinguish between potential sources of natural gas and different fluids, such as shallow groundwater and water from target shale units (e.g., Jackson *et al.*, 2013). Dissolved noble-gas concentrations in water depend on the temperature and pressure at which the gas exchange with the atmosphere occurs. When precipitation recharges and becomes groundwater, it is isolated from the atmosphere and retains its noble-gas concentration from the time of recharge and does not change as groundwater flows. Helium, on the other hand, can increase in concentration as groundwater flows because it is produced by radioactive decay of uranium and thorium in aquifer rocks and can also come from upward diffusion from the Earth's mantle. The source of helium in groundwater can be evaluated by examining the ratio of helium-3 and helium-4 isotopes. Helium-4 is also a major component of thermogenic natural gas.

A variety of chemicals may be used to hydraulically fracture shale to increase the production of hydrocarbons (e.g., http://fracfocus.org/chemical-use/what-chemicals-are-used). Many of these chemicals are used in very low concentrations or break down quickly and may not be useful for identifying hydraulic fracturing fluids in groundwater. Based on the list of hydraulic fracturing chemicals provided by Noble Energy in the MOU, an analytical suite of chemicals was developed to identify the occurrence of hydraulic fracturing chemicals in groundwater. The chemicals that were analyzed include short-chained alcohols, glycerins, glycols, ammonium persulfate, and acrylonitrile. These chemicals were selected because they might be used in sufficient quantities during hydraulic fracturing to be detected in groundwater or be breakdown products of hydraulic fracturing chemicals that are sufficiently long-lived and in sufficient quantities to be detected in groundwater.

5.3 Sampling Procedures

Pre-hydraulic-fracturing samples were collected from 35 locations in Exploration Area 1 (Huntington) near Jiggs, Nevada (Figure 5-2); from nine locations in Exploration Area 2, (Humboldt) near Lamoille, Nevada (Figure 5-3); and from 15 locations in Exploration Area 3, (Marys River), northwest of Wells, Nevada (Figure 5-4). Samples were collected from 17 locations in Exploration Area 2 (Figure 5-5) after initial hydraulic fracturing activities, including a sample from one of the exploration wells. Additionally, two springs that flow from carbonate-rock outcrops in the greater Elko County area (1-12 and 2-14, Figure 5-1) were sampled to chemically and isotopically characterize groundwater in carbonate aquifers that underlie the targeted hydrocarbon-containing shale formations in the centers of the valleys.

Prior to collecting water samples, domestic, stock, and irrigation wells were pumped roughly for 10 to 20 minutes, or until approximately one to three well volumes were removed (when well construction information was available), and until temperature, EC, and pH stabilized. Well samples were collected as close to the wellhead as possible. Spring samples were collected as close to the spring orifice as possible. Samples from diffuse seeps that did not have a clear spring orifice were collected at the most convenient location. Samples were collected in various plastic or glass bottles and preserved as required by the different laboratory protocols and standard analytical methods. Samples for noble gas analyses were collected using the copper tube method (http://www.noblegaslab.utah.edu/pdfs/cu_tube_sampling.pdf). Because noble gas samples must be collected without being exposed to the atmosphere to obtain good analytical results, samples could not be collected at all locations. Water samples were kept at approximately 4 °C, except the noble gas samples, until they could be delivered to the different laboratories.

Filtering is conducted to remove suspended or larger-sized colloidal particles from the water sample prior to analysis that could affect the analysis. Samples collected by Tetra Tech were not filtered. Samples collected for major and trace ions were filtered in the field (0.45 µm) by DRI. Chemical constituents that pass through a 0.45 µm filter are operationally considered to be dissolved, whereas unfiltered samples are considered to represent the total chemical load. Water samples collected for metals analysis including the major cations (Ca, Mg, Na, K) and trace metal ions (e.g., Cr, Mn, Fe, Co, Ni, Cu, etc.) are acidified in the field to preserve the sample (keep the metals in solution), usually with concentrated nitric acid. If the sample is not filtered, when the acid preservative is added to the water sample, residual particles can dissolve, which increases the concentrations of metals in the sample. Groundwater samples collected from a properly constructed well that was purged adequately and at sufficiently low pumping rates should have minimal suspended or large-sized colloidal particles. Therefore, the total and dissolved metals concentrations should be comparable. However, in surface-water samples (e.g., springs and streams), there can be more suspended and colloidal particles. In this case, the total and dissolved metals concentrations may not be comparable. The need to filter metals samples to remove larger particles is dependent on the turbidity of the sample. When turbidity is below 5-10 NTU (Matanoski and Murarka, 1997; Yeskis and Zavala, 2002), filtering may not be necessary. For this project, turbidity is currently not being measured prior to sampling.

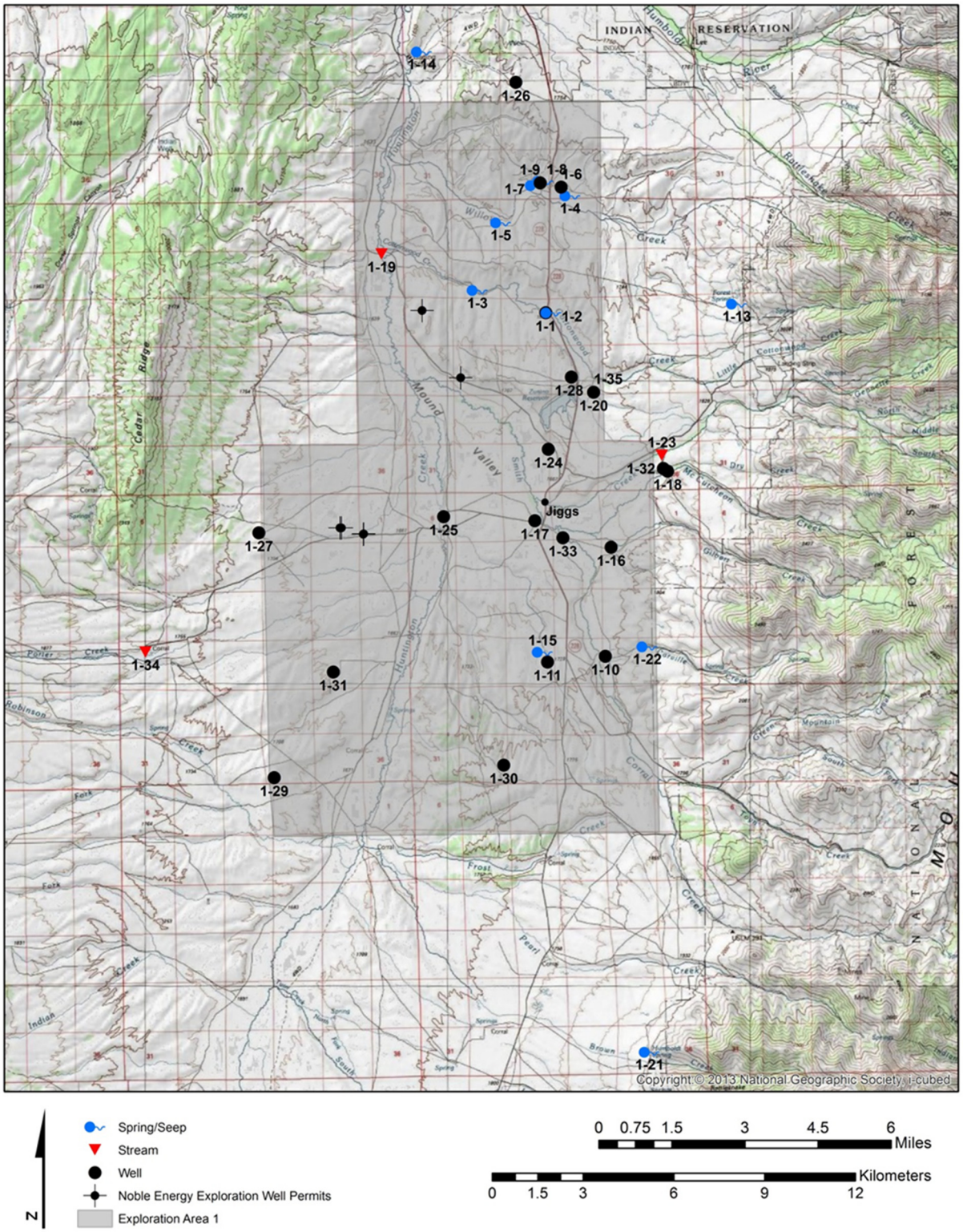

Figure 5-2. Noble Energy Exploration Area 1 (Huntington): pre-hydraulic-fracturing, water-quality sample locations.

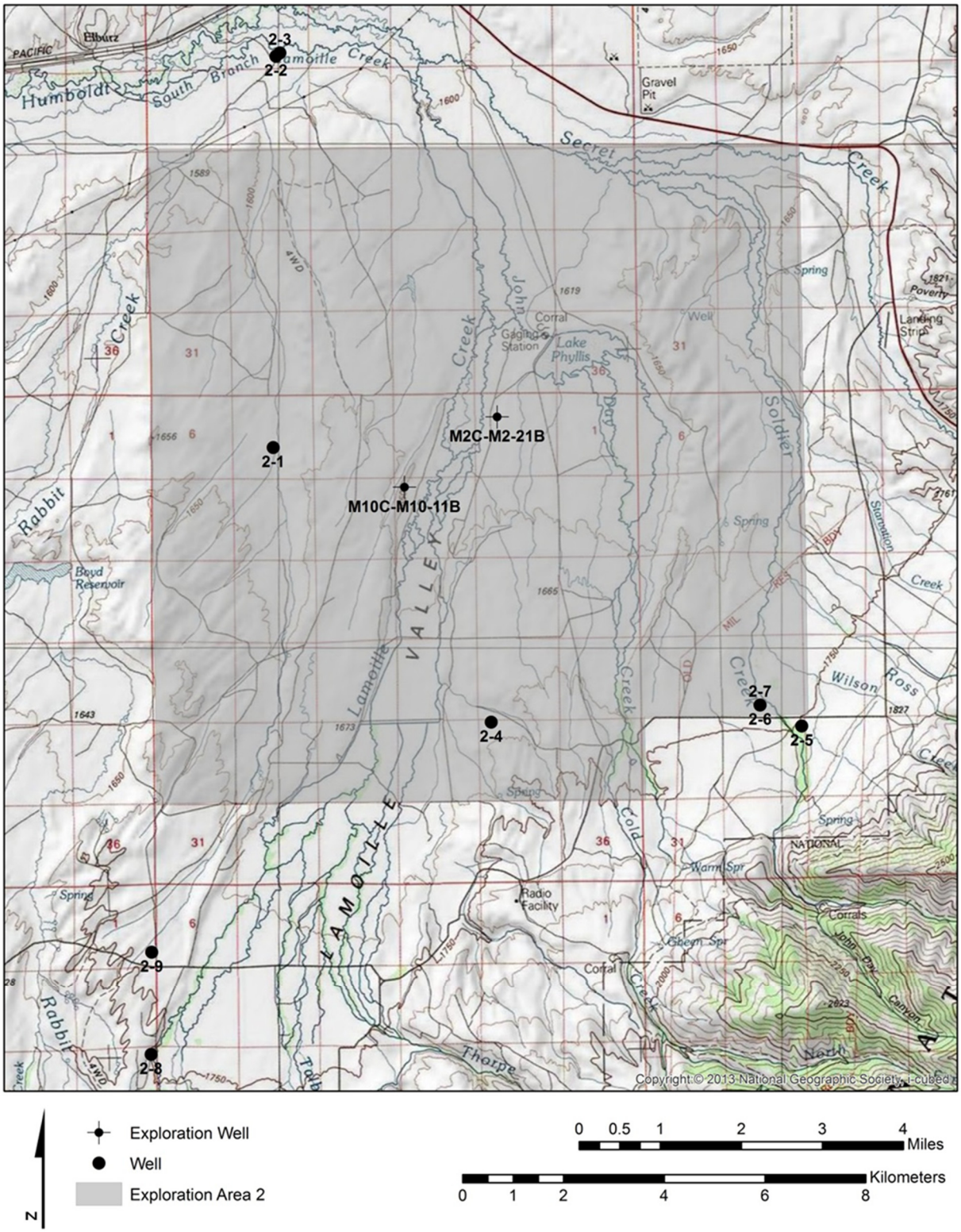

Figure 5-3. Noble Energy Exploration Area 2 (Humboldt): pre-hydraulic-fracturing, water-quality sample locations.

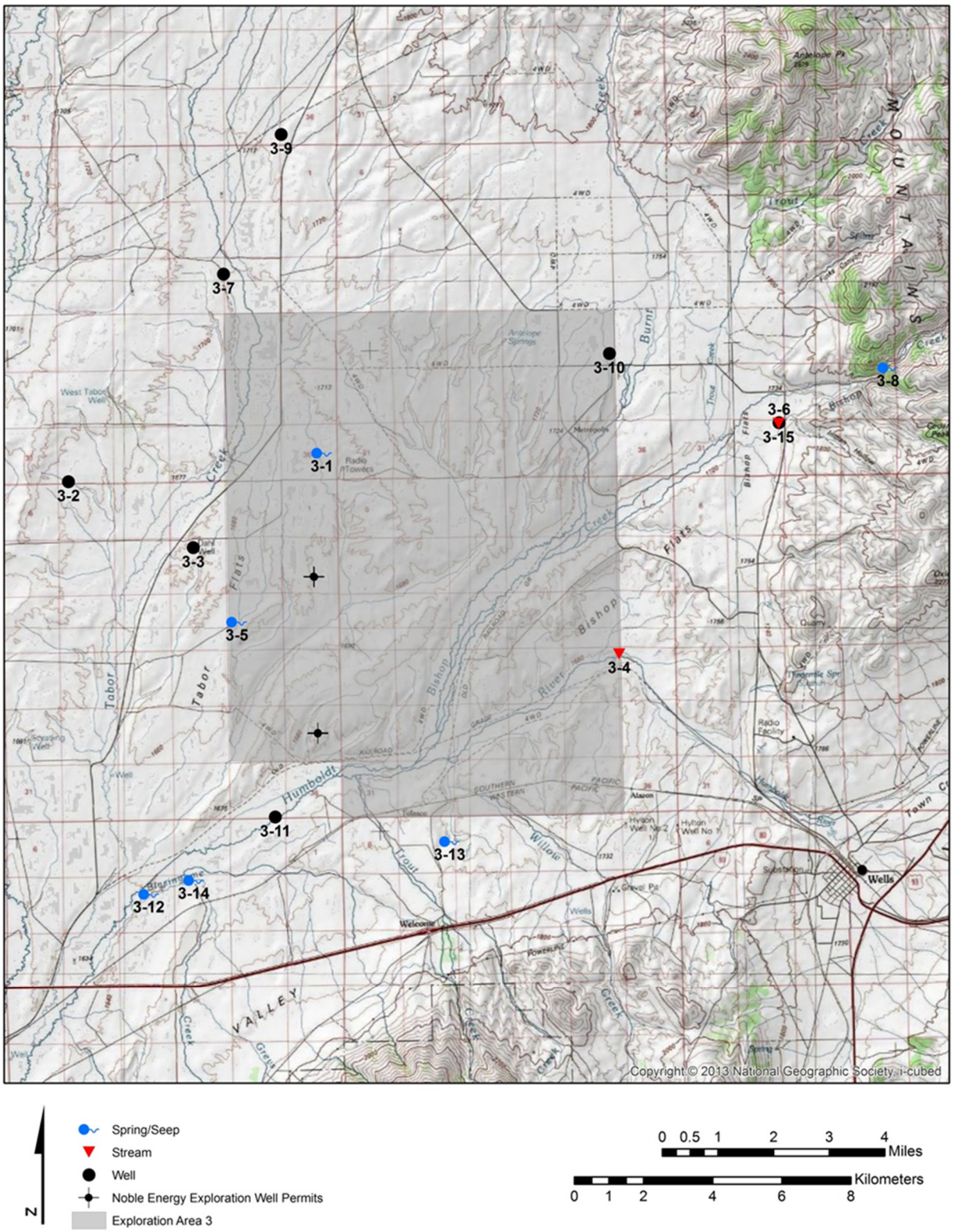

Figure 5-4. Noble Energy Exploration Area 3 (Marys River): pre-hydraulic-fracturing, water-quality sample locations.

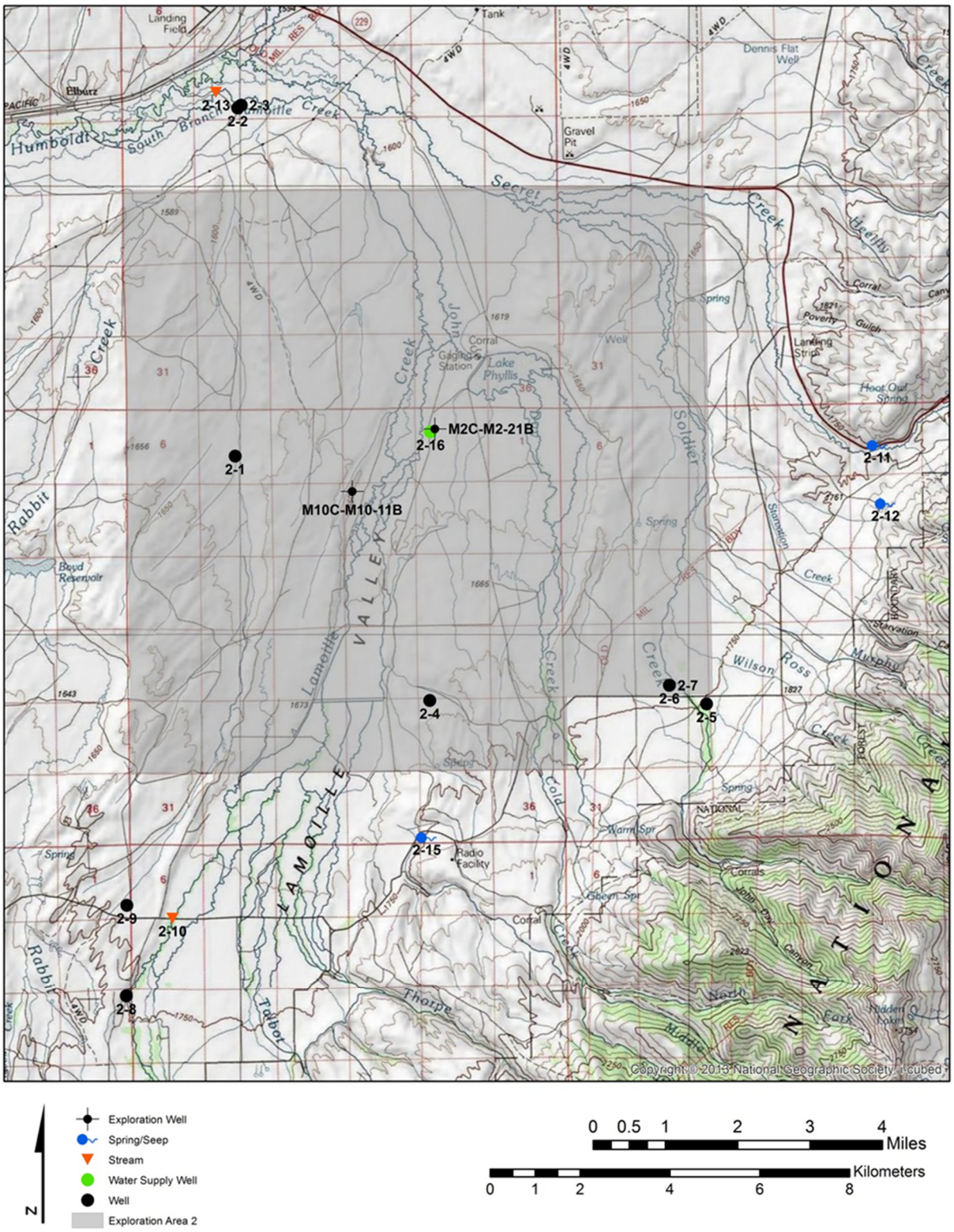

Figure 5-5. Noble Energy Exploration Area 2 (Humboldt): post-hydraulic-fracturing, water-quality sample locations.

Samples were analyzed for a suite of chemical, isotopic, and radiochemical parameters to establish background concentrations (pre-hydraulic fracturing) and to identify any potential contamination (post-hydraulic fracturing). Table 5-2 lists the field parameters and analyses conducted by Tetra Tech as specified in Table 1 in the Memorandum of Understanding (MOU) between the State of Nevada Division of Minerals and Division of Environmental Protection, the Desert Research Institute, and Noble Energy and as requested by the U.S. Bureau of Land Management (BLM) for an environmental assessment (EA) in exploration Area 1 (Huntington). Table 5-3 lists the field parameters and analyses conducted by DRI: DRI analyses include the same analyses as Tetra Tech (in all exploration areas) to assess the quality of the

Table 5-2. Chemical and isotopic parameters, units, analytical methods, and laboratories for water samples collected by Tetra Tech, Inc.

Parameter or Constituent (All Exploration Areas)	**Units**	**Method**	**Laboratory**
Temperature	°C		
Field Electrical Conductivity	µS/cm		
Field pH	pH units		
Field Filtration		No	
Ca, Mg, Na, K, Li	mg/L	6010C	TestAmerica
Cl, SO_4, F, Br	mg/L	300.0	TestAmerica
Alkalinity	mg/L as $CaCO_3$	SM 2320B	TestAmerica
Methane, Ethane, Propane	µg/L	RSK-175	TestAmerica
Diesel Range Organics	µg/L	8015C	TestAmerica
Gasoline Range Organics	µg/L	8015C	TestAmerica
Benzene, Toluene, Ethylbenzene, Xylenes	µg/L	8260B	TestAmerica
$\delta^{13}C$ Methane	‰		Dolan Integration Group
$\delta^{2}H$ Methane	‰		Dolan Integration Group
Parameter or Constituent (Area 1 BLM EA)	**Units**	**Method**	**Laboratory**
Temperature	°C		
Field Electrical Conductivity	µS/cm		
Field pH	pH units		
Field Filtration		No	
Ca, Mg, Na, K, Li, B, Sr	mg/L	6010C	TestAmerica
Ba	mg/L	200.8	TestAmerica
Cl, SO_4, F, Br	mg/L	300.0	TestAmerica
Alkalinity	mg/L as $CaCO_3$	SM 2320B	TestAmerica
Total Dissolved Solids	mg/L	SM 2540C	TestAmerica
Methane, Ethane, Propane	µg/L	RSK-175	TestAmerica
Diesel Range Organics	µg/L	8015C	TestAmerica
Gasoline Range Organics	µg/L	8015C	TestAmerica
Benzene, Toluene, Ethylbenzene, Xylenes, Acrylonitrile	µg/L	8260B	TestAmerica
Radium-226	pCi/L	904	TestAmerica
Gross Alpha, Gross Beta	pCi/L	9310	TestAmerica

Table 5-3. Chemical and isotopic parameters, units, analytical methods, and laboratories for water samples collected by DRI.

Parameter or Constituent	Units	Method	Laboratory
Temperature	°C	-	-
Field Electrical Conductivity	µS/cm	-	-
Field pH	pH units	-	-
Field Filtration	-	0.45 µm	-
Lab Electrical Conductivity	µS/cm	SM 2510 B	DRI Water Laboratory, Silver State Analytical
Lab pH	pH units	SM 4500 H+ B	DRI Water Laboratory, Silver State Analytical
Ca, Mg, Na, K, Li	mg/L	SM 3111B	DRI Water Laboratory, Silver State Analytical
Cl, SO_4, Br	mg/L	EPA 300.0	DRI Water Laboratory, Silver State Analytical
NO_3	mg N/L	SM 4500-NO3 F	DRI Water Laboratory, Silver State Analytical
SiO_2	mg/L	EPA 370.1	DRI Water Laboratory, Silver State Analytical
Alkalinity	mg/L as $CaCO_3$	USGS I 1030-85 SM 2320 B	DRI Water Laboratory, Silver State Analytical
F	mg/L	SM 4500F C	DRI Water Laboratory, Silver State Analytical
B, Ba, Sr	mg/L	EPA 200.8	DRI Water Laboratory, Silver State Analytical
Total Dissolved Solids	mg/L	SM 2540 C	DRI Water Laboratory, Silver State Analytical
Methane, Ethane, Propane	µg/L	RSK-175	Alpha Analytical
Diesel Range Organics	µg/L	SW8015B/C Ext	Alpha Analytical
Gasoline Range Organics	µg/L	SW8015B/C / SW8260B	Alpha Analytical
MTBE, Benzene, Toluene, Ethylbenzene, Xylenes	µg/L	SW8260B	Alpha Analytical
Gross Alpha, Gross Beta	pCi/L	EPA 900.0	Eurofins Eaton Analytical
Radium-226	pCi/L	RA-226 GA	Eurofins Eaton Analytical
Radium-228	pCi/L	RA-228 GA	Eurofins Eaton Analytical
δ^2H, $\delta^{18}O$, $\delta^{13}C$ DIC water	‰	Isotope Ratio Mass Spectrometry	UC Davis, University of Waterloo
δ^2H, $\delta^{13}C$ methane	‰	Isotope Ratio Mass Spectrometry	UC Davis, University of Waterloo
Ne, Ar, Kr, Xe	ccSTP/g	Quadrupole Mass Spectrometry	University of Utah
^4He	ccSTP/g	Sector-field Mass Spectrometry	University of Utah
R/R_a ($[^3He/^4He]_{groundwater}$ / $[^3He/^4He]_{atmosphere}$)	-	Sector-field Mass Spectrometry	University of Utah
Methanol, Ethanol, Isopropanol, 2-Butoxyethanol, Acrylonitrile	mg/L	Gas Chromatography Flame Ionization Detection	DRI Organic Analysis Laboratory
Glycerol, Ethylene Glycol, Propylene Glycol, Ammonium Persulfate	mg/L	Liquid Chromatography Mass Spectrometry	DRI Organic Analysis Laboratory

analytical results between the different laboratories. In addition to the MOU analyses, DRI collected samples for additional tracers to characterize local groundwater, establish natural background of radioactivity in local groundwater, identify mixing of shale water, identify the source of natural gas, and/or identify hydraulic fracturing fluid release (Table 5-1). For the Area 1 BLM EA, the full suite of Tetra Tech and DRI analyses (i.e., Table 5-3) were divided between Tetra Tech and DRI laboratories. All of the laboratories listed in Tables 5-2 and 5-3 are certified by the State of Nevada for the standard methods listed. There are no standard methods or State of Nevada certification programs for the isotopic ratio analyses that were conducted by the University of California, Davis; the University of Waterloo; and Dolan Integration Group. Neither are there standard methods nor State of Nevada certification programs for the noble-gas analyses that were conducted by the University of Utah or for the alcohols, glycols, glycerol, acrylonitrile, and ammonium persulfate analyses that were conducted by the DRI Organic Analysis Laboratory.

5.4 QA Comparison of Tetra Tech and DRI Samples

A subset of field duplicate samples collected by Tetra Tech for Noble Energy was also collected by DRI to assess the quality of the analytical results between the different laboratories. Duplicate sampling and analyses were conducted for methane, ethane, propane, TPH-GRO, TPH-DRO, benzene, ethylbenzene, toluene, xylenes, cations, anions, and trace elements. Samples collected by Tetra Tech were analyzed by TestAmerica (Table 5-2), Samples collected by DRI were analyzed by Alpha Analytical, the DRI Water Laboratory, and/or Silver State Analytical Laboratories (Table 5-3).

5.4.1 Methane, Ethane, and Propane

For methane, ethane, and propane, both TestAmerica and Alpha Analytical used method RSK-175, so water samples were collected in the field without headspace. In the laboratory, a headspace was prepared by displacing 10 percent of the water with high-purity helium. The bottle was shaken for five minutes and a headspace sample was injected into a gas chromatographic column where the gaseous components were separated and detected by either a thermal conductivity detector, a flame ionization detector, or an electron capture detector. The concentration of dissolved gas in the water sample was determined by using the Henry's law constant, the concentrations of the gas in the headspace, the bottle volume, and temperature of the sample (http://www.epa.gov/region1/info/testmethods/pdfs/RSKsop175v2.pdf). TestAmerica had method detection limits of 0.218 μg/L, 0.573 μg/L, and 0.560 μg/L for methane, ethane, and propane, respectively, with a reporting limit of 5.0 μg/L. Alpha Analytical had a method detection limit of 5.0 μg/L each for methane, ethane, and propane with a reporting limit of 10 μg/L.

For methane, TestAmerica and Alpha Analytical reported seven duplicate results above their respective reporting limits. Of these seven results, Alpha Analytical had six results with higher concentrations than TestAmerica. The percent error for the seven duplicate analyses ranged from 27 to 98 percent (Table 5-4). Figure 5-6 shows the Alpha Analytical methane concentrations compared with the TestAmerica methane concentrations, a one-to-one line, and ±25 percent recovery limits as error bars. At four additional sample locations, Alpha Analytical and/or TestAmerica reported values for methane above the reporting limit, above their respective detection limits but below their reporting limits, or below their detection limits (Table 5-4).

Table 5-4. Comparison between duplicate TestAmerica (TestA) and Alpha Analytical (Alpha) results for methane and ethane. The bottom section of the table reports the duplicate results for methane and ethane above their reporting limits, above their detection limits but below their reporting limits, or below their detection limits.

	Methane	**Ethane**
TestAmerica and Alpha Detected	7	2
Percent Difference	27-98	35-53
TestAmerica Detection Limit (µg/L)	<0.218	<0.573
TestAmerica Reporting Limit (µg/L)	<5.0	<5.0
Alpha Detection Limit (µg/L)	<5.0	<5.0
Alpha Reporting Limit (µg/L)	<10.0	<10.0

Water-quality Sample Location	**Methane**		**Ethane**	
	Alpha (µg/L)	**TestA (µg/L)**	**Alpha (µg/L)**	**TestA (µg/L)**
1-24	32	<0.218	8.0J	<0.218
2-4	5.0J	0.715J		
3-3			<5.0	1.71J
3-11	<5.0	1.90J		
3-12	<5.0	2.08J		

J = less than reporting limit but greater than detection limit; concentration is approximate.

For ethane, TestAmerica and Alpha Analytical reported two duplicate results above the reporting limits. For these results, Alpha Analytical had one result with a higher concentration than TestAmerica. The percent error for the two duplicate analyses ranged from 35 to 53 percent. Figure 5-7 shows the Alpha Analytical ethane concentrations compared with the TestAmerica ethane concentrations, a one-to-one line, and ±25 percent recovery limits as error bars. At two additional locations, Alpha Analytical and/or TestAmerica reported values for ethane above their respective detection limits but below their reporting limits or below the detection limit (Table 5-4). Propane was not detected in any sample locations by TestAmerica or Alpha Analytical.

5.4.2 TPH DRO and TPH GRO

For TPH DRO and TPH GRO, both TestAmerica and Alpha Analytical used method 8015C, gas chromatography-flame ionization detection (http://www.epa.gov/epawaste/hazard/testmethods/sw846/pdfs/8015c.pdf). TestAmerica had method detection limits of 0.03 mg/L and 0.01 mg/L for DRO and GRO, respectively, with reporting limits of 0.24 and 0.025 mg/L. Alpha Analytical had a method detection limit of 0.25 mg/L for both DRO and GRO with a reporting limit of 0.5 mg/L (Table 5-5). For TPH, TestAmerica and Alpha Analytical reported no duplicate results above their respective reporting

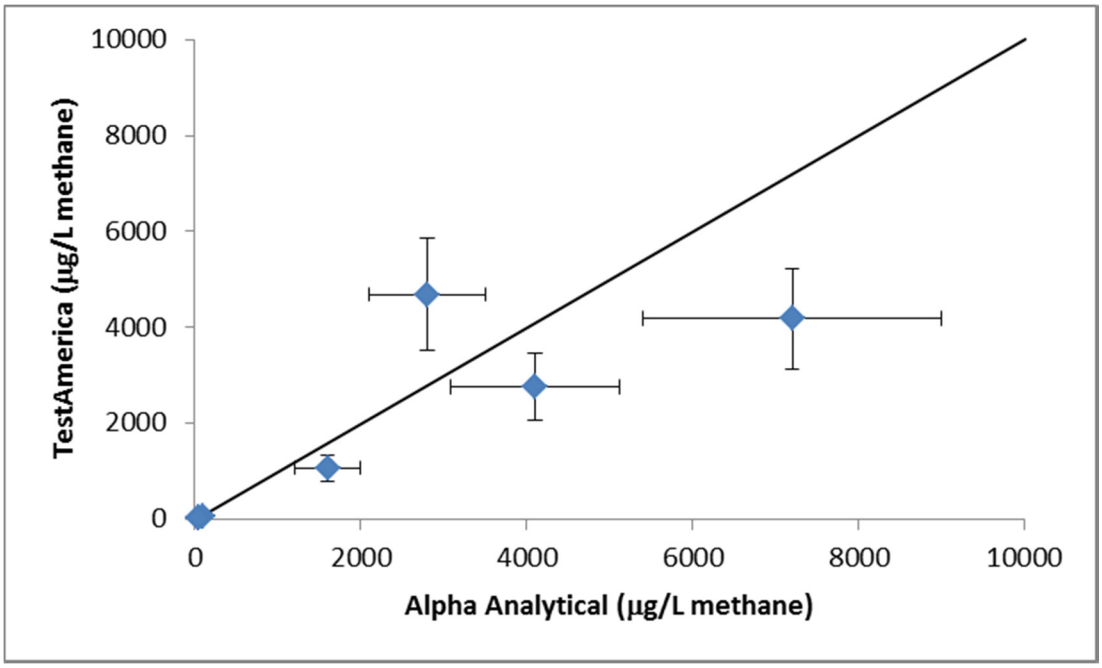

Figure 5-6. Comparison of methane concentrations between Alpha Analytical and TestAmerica for seven sampling locations with measureable methane and a one-to-one line for reference. Error bars are ±25 percent recovery limits.

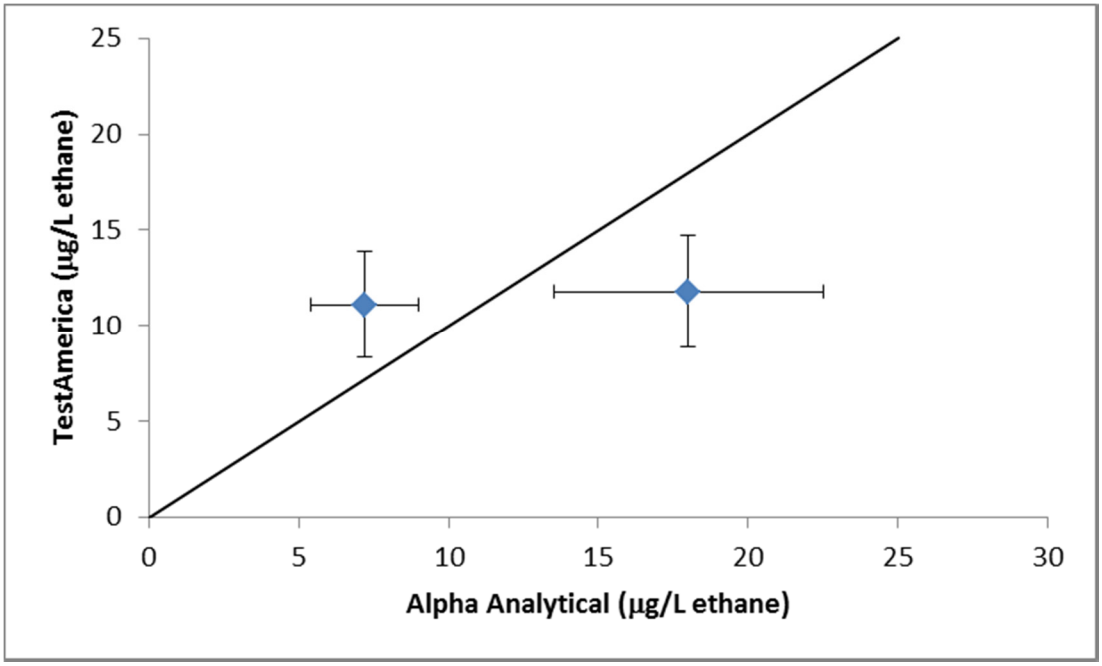

Figure 5-7. Comparison of ethane concentrations between Alpha Analytical and TestAmerica for two sampling locations with measureable ethane and a one-to-one line for reference. Error bars are ±25 percent recovery limits.

Table 5-5. Comparison between duplicate TestAmerica (TestA) and Alpha Analytical (Alpha) results for TPH DRO and TPH GRO. The bottom section of the table reports duplicate results above their detection limits but below their reporting limits or below their detection limits.

	TPH-DRO	TPH-GRO
TestAmerica and Alpha Detected	0	0
Percent Difference	0	0
TestAmerica Detection Limit (mg/L)	<0.03	<0.01
TestAmerica Reporting Limit (mg/L)	<0.24	<0.025
Alpha Detection Limit (mg/L)	<0.25	<0.25
Alpha Reporting Limit (mg/L)	<0.50	<0.50

Water-quality Sample Location	TPH-DRO		TPH-GRO	
	Alpha (mg/L)	TestA (mg/L)	Alpha (mg/L)	TestA (mg/L)
1-28	<0.25	0.0562J		
3-1	<0.25	0.0377J		
3-11			<0.25	0.014J

J = less than reporting limit, but greater than detection limit; concentration is approximate.

limits. At two locations, TestAmerica reported values for DRO above the detection limit but below their reporting limits, whereas Alpha Analytical did not report any values above the detection limit. At one location, TestAmerica reported a value for GRO above the detection limit but below their reporting limit, whereas Alpha Analytical did not report a value above the detection limit (Table 5-5). In summary, the results are consistent between the laboratories, given their different detection and reporting limits.

5.4.3 Benzene, Ethylbenzene, Toluene, and Xylene

For benzene, ethylbenzene, toluene, and xylene, both TestAmerica and Alpha Analytical used method 8206B, gas chromatography-mass spectrometry (http://www.epa.gov/waste/hazard/testmethods/sw846/pdfs/8260b.pdf). TestAmerica had method detection limits of 0.16 µg/L for benzene and ethylbenzene, 0.17 µg/L for toluene, and 0.19 µg/L for total xylene. They had reporting limits of 1.0 µg/L for benzene, ethylbenzene, and toluene and 2.0 µg/L for xylene. Alpha Analytical had a method detection limit of 0.5 µg/L and a reporting limit of 1.0 µg/L for each volatile organic compound. Both TestAmerica and Alpha Analytical reported no detections in the duplicate samples above their respective reporting limits. At two locations, TestAmerica reported values for toluene above the detection limit but below their reporting limits, whereas Alpha Analytical did not report any values above their detection limit (Table 5-6).

Table 5-6. Comparison between duplicate TestAmerica (TestA) and Alpha Analytical (Alpha) results for benzene, ethylbenzene, toluene, and xylene. The bottom section of the table reports duplicate results above their detection limits but below their reporting limits or below their detection limits.

	Toluene
TestAmerica and Alpha Detected	0
Percent Difference	0
TestAmerica Detection Limit (μg/L)	<0.17
TestAmerica Reporting Limit (μg/L)	<1.0
Alpha Detection Limit (μg/L)	<0.50
Alpha Reporting Limit (μg/L)	<1.0

Water-quality Sample Location	**Toluene**	
	Alpha (mg/L)	**TestA (mg/L)**
3-6	<0.5	0.325 J
3-9	<0.5	0.181 J

J = less than reporting limit but greater than detection limit; concentration is approximate.

5.4.4 Cations, Anions, and Trace Elements

Eight different ions were analyzed in duplicate by three different labs for DRI and by TestAmerica in sufficient quantities to compare the results between the laboratories. In most cases, there was good agreement between well, spring, and stream filtered samples that were analyzed by the DRI Water Laboratory, Alpha Analytical, or Silver State Analytical Laboratories and the unfiltered samples analyzed by TestAmerica. Comparisons for Ca, Na, Li, and B are presented below for demonstrative purposes. Comparisons for the remaining ions, Mg, K, Sr, and HCO_3 are presented in Appendix QA for completeness.

Figure 5-8 compares the results for Ca from 28 locations (24 wells, 3 springs, 1 stream). There is good agreement between the DRI labs and TestAmerica for Ca. There were an equal number of DRI lab results (14) that were greater than the TestAmerica results and TestAmerica results that were greater than DRI lab results. The percent differences ranged from 0 to 31 percent (Table 5-7), excluding two locations with greater than 50 percent difference (location 3-3: DRI Lab = 10.6 mg/L, TestAmerica = 0.72 mg/L, 93 percent difference; location 2-1: DRI Lab = 0.57 mg/L, TestAmerica = 3.17 mg/L, 82 percent difference).

A comparison of the results for Na for 28 locations (24 wells, 3 springs, 1 stream) shows good agreement between the DRI labs and TestAmerica (Figure 5-9). However, only five DRI results were greater than TestAmerica results, whereas 23 TestAmerica results were greater than DRI results. The

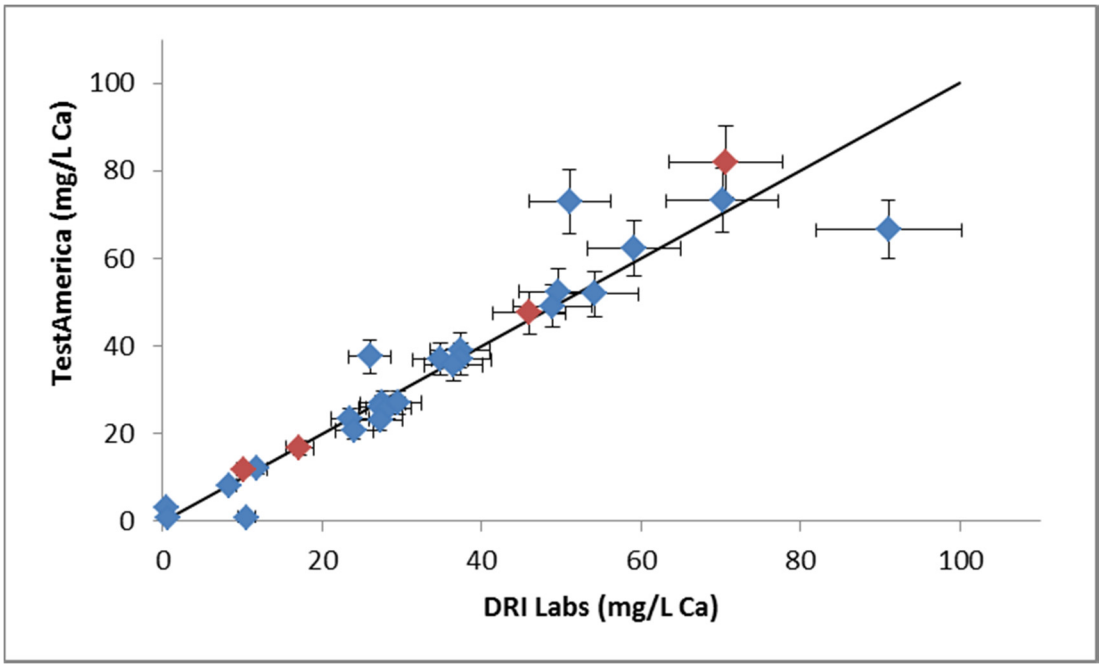

Figure 5-8. Comparison of Ca ion concentration between DRI labs and TestAmerica for 28 sampling locations with measureable Ca concentrations and a one-to-one line for reference. Wells are blue diamonds; springs and steams are red diamonds. Error bars are ±10 percent recovery limits.

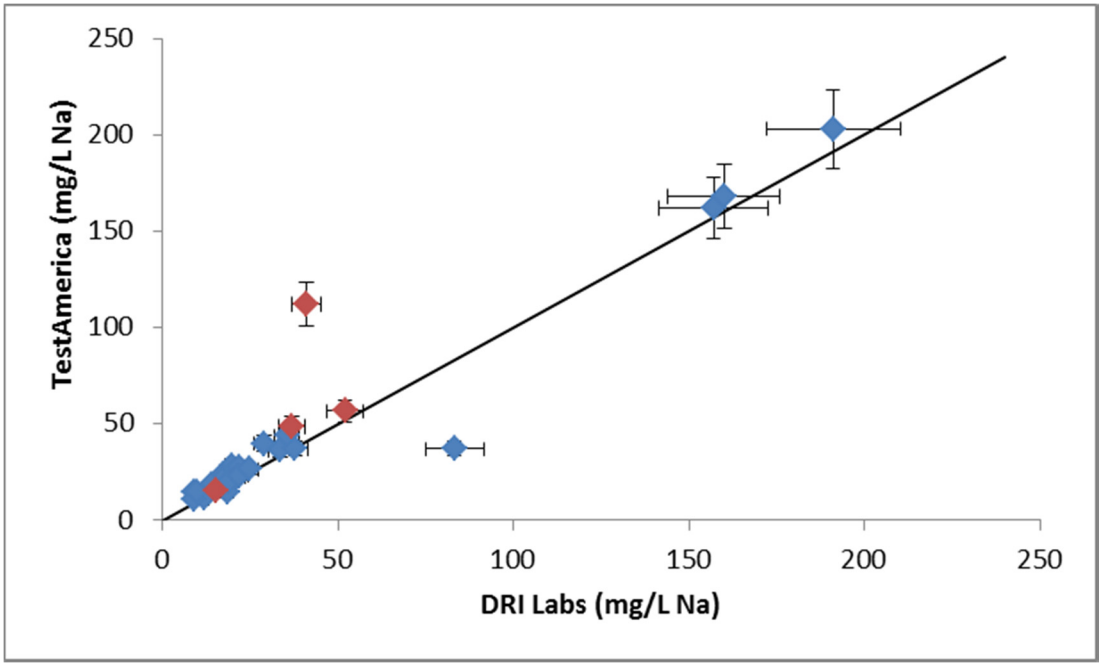

Figure 5-9. Comparison of Na ion concentration between DRI labs and TestAmerica for 28 sampling locations with measureable Na concentrations and a one-to-one line for reference. Wells are blue diamonds; springs and steams are red diamonds. Error bars are ±10 percent recovery limits.

Table 5-7. Comparison between duplicate DRI labs and TestAmerica results for Ca, Na, Li, and B. The bottom section of the table reports duplicate results with a greater than 50 percent difference between DRI labs and TestAmerica results.

	Ca	Na	Li	B
TestAmerica and DRI Labs Detected	28	28	12	5
Percent Difference	0-31	1-36	5-50	5-33
TestAmerica Reporting Limit (mg/L)	<0.2	<1	<0.01	<0.1
DRI Water Reporting Limit (mg/L)	<0.1	<0.1	<0.01	<0.01
Alpha Reporting Limit (mg/L)	<0.5	<0.5	<0.005	<0.1
Silver State Reporting Limit (mg/L)	<0.1	<0.1	<0.001	<0.01
DRI Labs > TestAmerica	14	5	2	4
TestAmerica > DRI Labs	14	23	10	1

	> 50 % difference											
	Ca			Na			Li			B		
Water-quality Sample Location	DRI (mg/L)	Test A (mg/L)	% Diff.	DRI (mg/L)	Test A (mg/L)	% Diff.	DRI (mg/L)	Test A (mg/L)	% Diff.	DRI (mg/L)	Test A (mg/L)	% Diff.
1-25							0.016	0.047	66			
2-1	0.57	3.17	82									
3-3	10.6	0.721	93									
3-11				83.2	36.9	56				0.5	0.126	75
3-12				41	112	63	0.014	0.053	74			

percent differences ranged from 0 to 36 percent (Table 5-7), excluding two locations with percent differences greater than 50 percent (location 3-12: DRI Lab = 41.2 mg/L, TestAmerica = 112 mg/L, 63 percent difference; location 3-11: DRI Lab = 83.2 mg/L, TestAmerica = 36.9 mg/L, 56 percent difference).

Figure 5-10 compares results for Li for 12 locations (10 wells, 2 springs). There is good agreement between the DRI labs and TestAmerica (Figure 5-10). However, only two DRI results were greater than the TestAmerica results, whereas 10 TestAmerica results were greater than the DRI results. The percent differences ranged from 0 to 50 percent (Table 5-7), excluding two locations with percent differences greater than 50 percent (location 3-12: DRI Lab = 0.014 mg/L, TestAmerica = 0.053 mg/L, 74 percent difference; location 1-25: DRI Lab = 0.016 mg/L, TestAmerica = 0.047 mg/L, 66 percent difference).

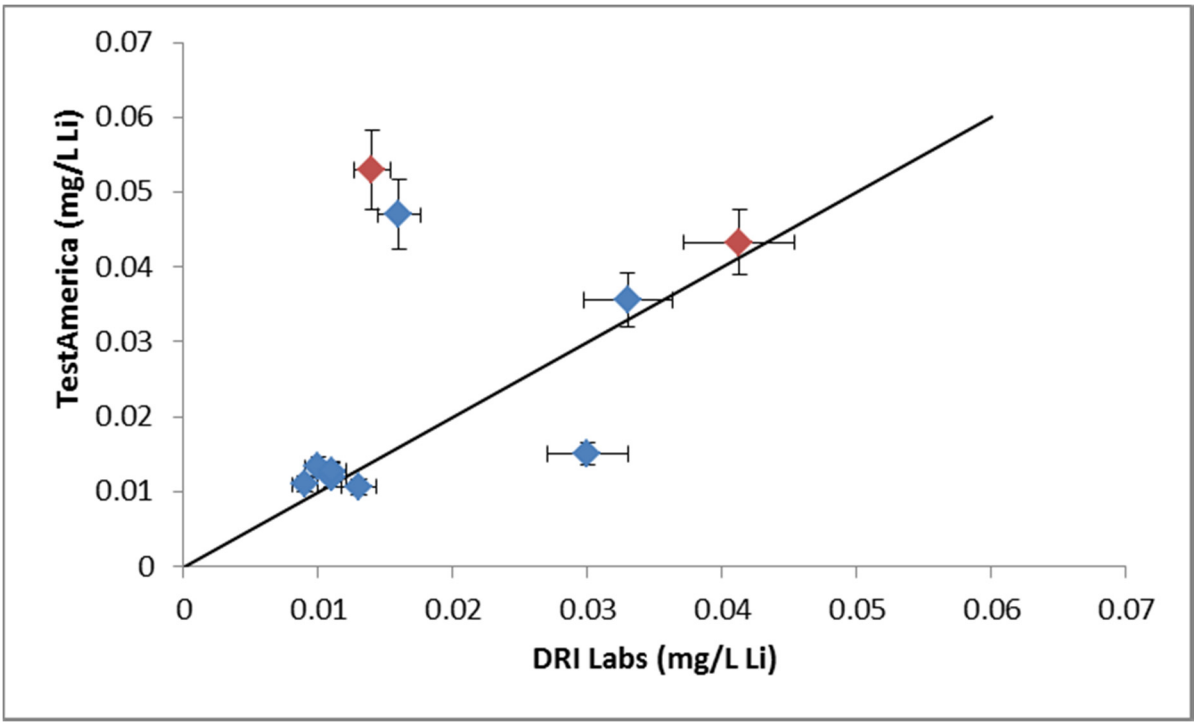

Figure 5-10. Comparison of Li ion concentration between DRI labs and TestAmerica for 12 sampling locations with measureable Li concentrations and a one-to-one line for reference. Wells are blue diamonds; springs are red diamonds. Error bars are ±10 percent recovery limits.

A comparison of the results for B for five locations (five wells) shows good agreement between the DRI labs and TestAmerica (Figure 5-11). However, only one TestAmerica result was greater than the DRI results, whereas four DRI results were greater than TestAmerica results. The percent differences ranged from 5 to 33 percent (Table 5-7), excluding one location with a percent difference greater than 50 percent (location 3-11: DRI Lab = 0.5 mg/L, TestAmerica = 0.126 mg/L, 75 percent difference).

5.5 Hydrochemical and Isotopic Characterization

5.5.1 Characteristics of Shallow Groundwater, Springs, and Streams

5.5.1.1 Major-ion Composition

The chemical composition of natural waters is largely the result of mineral dissolution and precipitation reactions. These are controlled by physical and chemical conditions that are influenced by atmospheric and biologic processes. Although some of the waters sampled from the three areas have similar chemical characteristics, overall differences between the areas are apparent. The majority of samples from all three areas have salinity below 500 mg/L TDS (Figure 5-12). However, water of higher salinity also occurs in 13 samples in Areas 1 through 3. Along with lower salinity, Area 2 water is almost exclusively a Ca-HCO_3 type (with two exceptions discussed below). Conversely, Area 3 waters include both Ca-HCO_3 and Na-HCO_3 types, and the majority of Area 1 samples are a mixed cation-HCO_3 between the Ca and Na end members (Figure 5-13). There is a correlation between the Na-HCO_3 facies and higher salinity, which indicates the interaction of water with volcanic rocks.

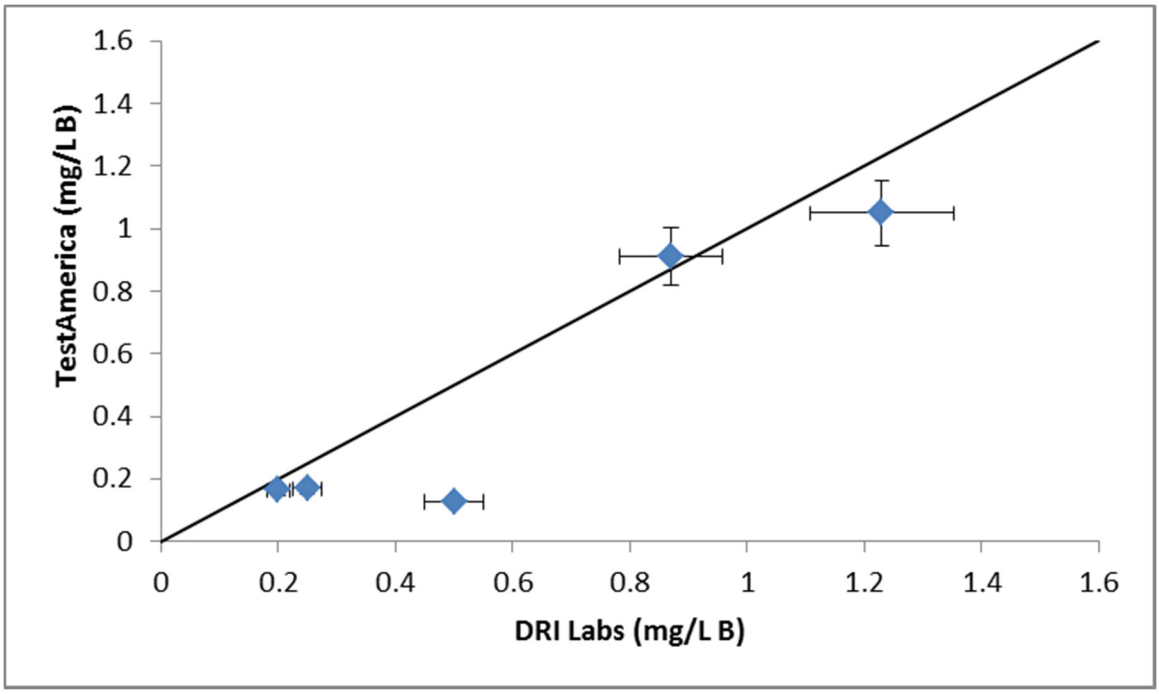

Figure 5-11. Comparison of B ion concentration between DRI labs and TestAmerica for five sampling locations with measureable B concentrations and a one-to-one line for reference. Wells are blue diamonds; error bars are ±10 percent recovery limits.

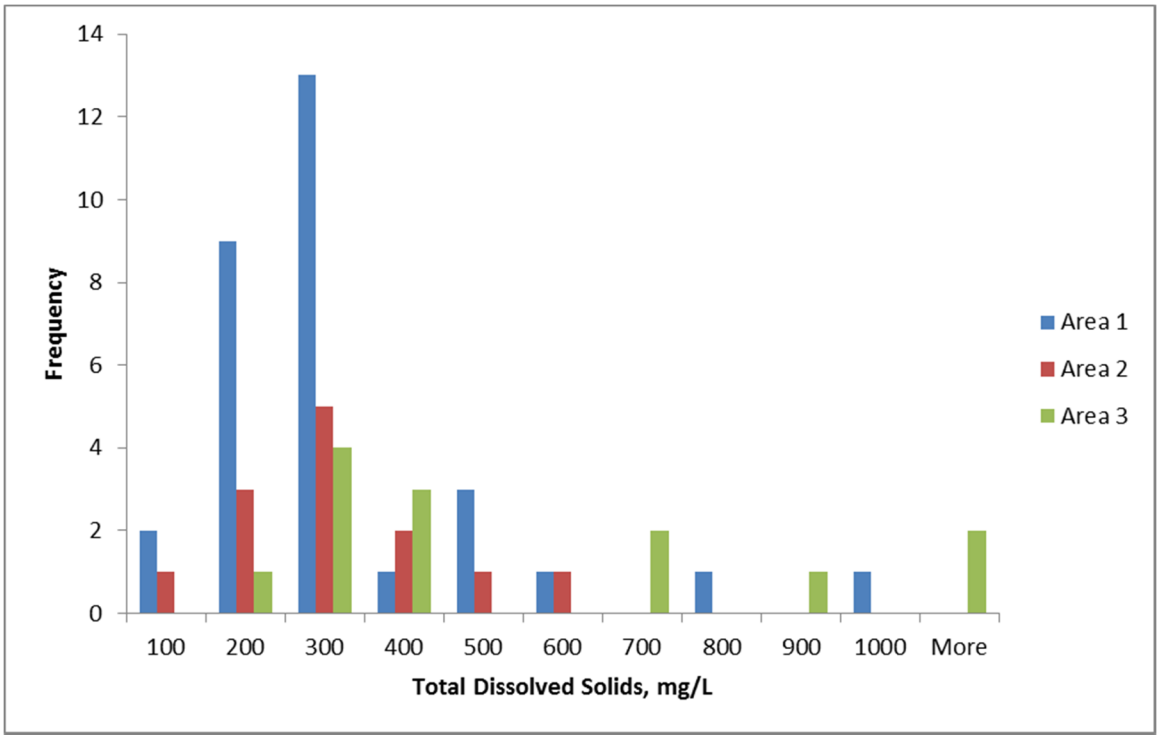

Figure 5-12. Total dissolved solids content of springs, streams, and groundwater sampled from the three study areas.

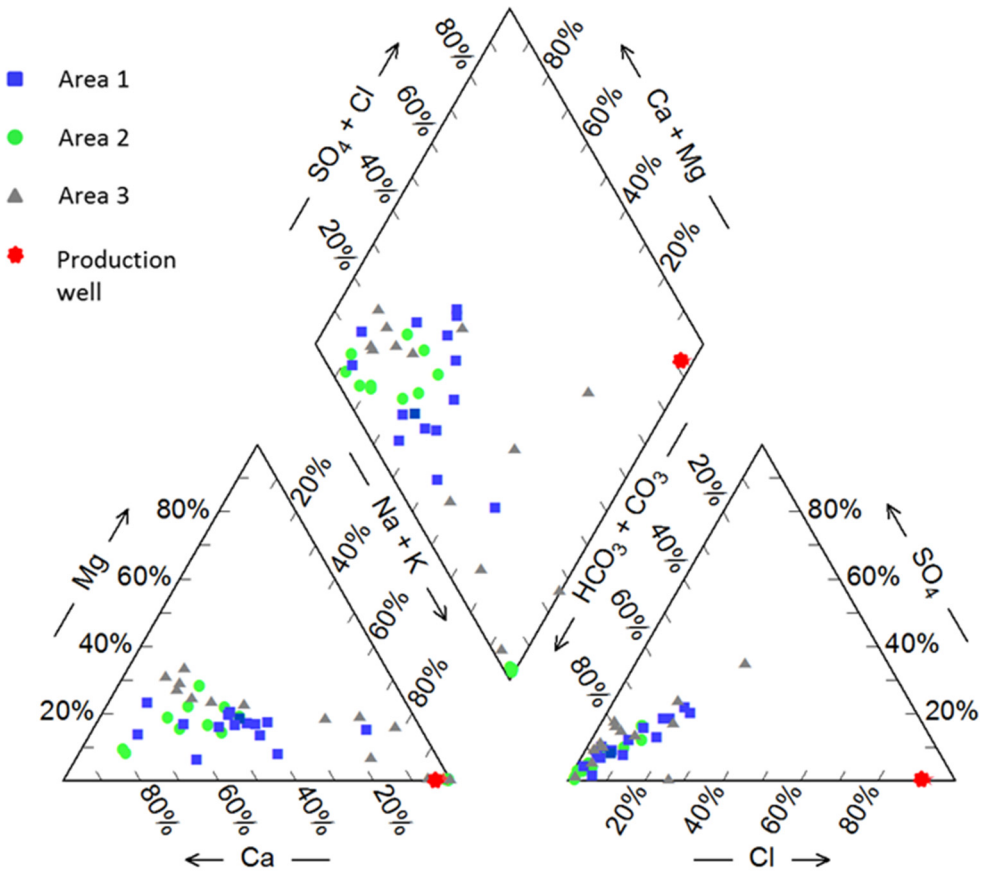

Figure 5-13. Piper diagram plotting the relative major-ion percentages for water sampled from Areas 1, 2, and 3 and the production well.

The decomposition of silicate minerals by interaction with water and CO_2—a process known as silicate hydrolysis—produces clays and enriches the water in Ca, Na, HCO_3, and SiO_2. As Ca and HCO_3 increase, the increasing solution concentration causes calcium to precipitate as calcite, which leads to a higher proportion of sodium in the water. The rate of decomposition depends on the primary silicate mineralogy and grain size, with fine-grained and glassy volcanics being more soluble than coarse-grained minerals found in intrusive igneous rocks such as granite. The major-ion compositions of the water samples suggest that there is more interaction between water and volcanic rock in Area 3 than in the other areas, and more interaction in Area 1 than in Area 2. The lower salinity, Ca-HCO_3 water present in all areas indicates this water type has minimal volcanic rock contact, which suggests interaction with coarse grained silicates and carbonate minerals. Carbonate dust and limestone rock are common sources of calcium. The carbonate spring 1-12 is a reasonable representation of water that has been influenced primarily by contact with carbonate rock. The cation composition of the other carbonate spring, 2-14, suggests water from that spring has also interacted with silicate rock (Appendix A).

When silicate weathering is rapid relative to CO_2 uptake, pH rises, which decreases calcite solubility and results in more complete precipitation of calcite. This leads to a high pH Na-HCO_3 water, such as observed at the alkaline spring sample 3-13. High pH and Na-HCO_3 composition also describes well 3-3 chemistry in Area 3 and the two anomalous samples from Area 2, which were mentioned previously. These well samples differ from the alkaline spring in having relatively low salinity (the TDS

of 3-13 is more than 3,000 mg/L, whereas 3-3, 2-1, and 2-16 are 400-600 mg/L), but they exhibit similar significant methane concentrations. The carbon and hydrogen isotopic ratios that identify this methane as biogenic in origin are discussed in a separate section below. Microbial production of CH_4 from acetate fermentation also produces CO_2 (CH_3COOH $CH_4 + CO_2$), which increases the alkalinity in the associated water and affects the major-ion composition of the water. The resulting high pH, Na-HCO_3 water is similar to the characteristics created by rapid silicate weathering. A combination of silicate weathering and acetate fermentation likely accounts for the high pH waters observed, particularly the high salinity water at 3-13.

In stark contrast to the stream, spring, and shallow groundwater in the area, the water collected from the production reservoir in well M2C in Area 2 is a distinctive Na-Cl brackish water (Figure 5-13). The salinity is much higher than the other water samples at greater than 8,500 mg/L and it is the only water dominated by the chloride anion.

5.5.1.2 Stable Isotopic Composition of Water

The majority of the δ^2H and $\delta^{18}O$ data from the area waters plot close to the global meteoric water line, which indicates that they are consistent with meteoric water that has not undergone evaporation or geothermal alteration (Figures 5-14a and b). Several springs in Area 3 are exceptions to this, being enriched in $\delta^{18}O$ relative to δ^2H, which is consistent with isotopic fractionation during evaporation.

The large spread in stable isotopic composition indicates different recharge conditions, which likely reflects different condensation temperatures from different recharge elevations. The waters with more depletion in heavy isotopes (more negative ratios) would be associated with condensation under cooler conditions at higher elevations. Isotopically depleted water is located in all three areas and primarily associated with groundwater. This suggests that portions of the groundwater systems in the Huntington, Lamoille, and Wells areas are recharged at high elevation in the nearby mountain ranges.

As part of an isotopic investigation of minerals, including fluid inclusions, Fricke *et al.* (1992) reported an estimated isotopic composition for modern meteoric water in the Elko area as -16 ‰ $\delta^{18}O$ and -119 ‰ δ^2H (Figures 5-14a and b). This estimate is at the heavy-isotope enriched end of the range of waters sampled for this study. Mariner *et al.* (1983) relied on the general δ^2H map of Sheppard *et al.* (1969) to conclude that most precipitation in the northern Great Basin should range from approximately -130 to -110 ‰ in δ^2H. This range encompasses most of the samples reported here. Mariner *et al.* (1983) also observed that a few hot springs near Elko are at -145‰, which is significantly depleted compared with that range. Jewell *et al.* (1994) investigated waters in Area 3 near Wells and found cold springs and well waters to range from -140 to -125 ‰ in δ^2H and -17.1 to -15.9 ‰ in $\delta^{18}O$. In contrast to the cool waters, thermal waters in the Wells area were observed to be more depleted in δ^2H (from -147 to -137 ‰) and enriched $\delta^{18}O$ values compared to those predicted by the Meteoric Water Line (Jewell *et al.*, 1994). Although others attributed the δ^2H depletion to recharge during a previous colder climate (Mariner *et al.*, 1983), Jewell *et al.* (1994) analyzed velocity estimates and the isotopic composition of high-elevation spring water and precipitation elsewhere in the Great Basin (Jacobson *et al.*, 1983) and concluded that even the most isotopically depleted hot spring waters did not represent a signal from a cooler climate 12,000 years ago.

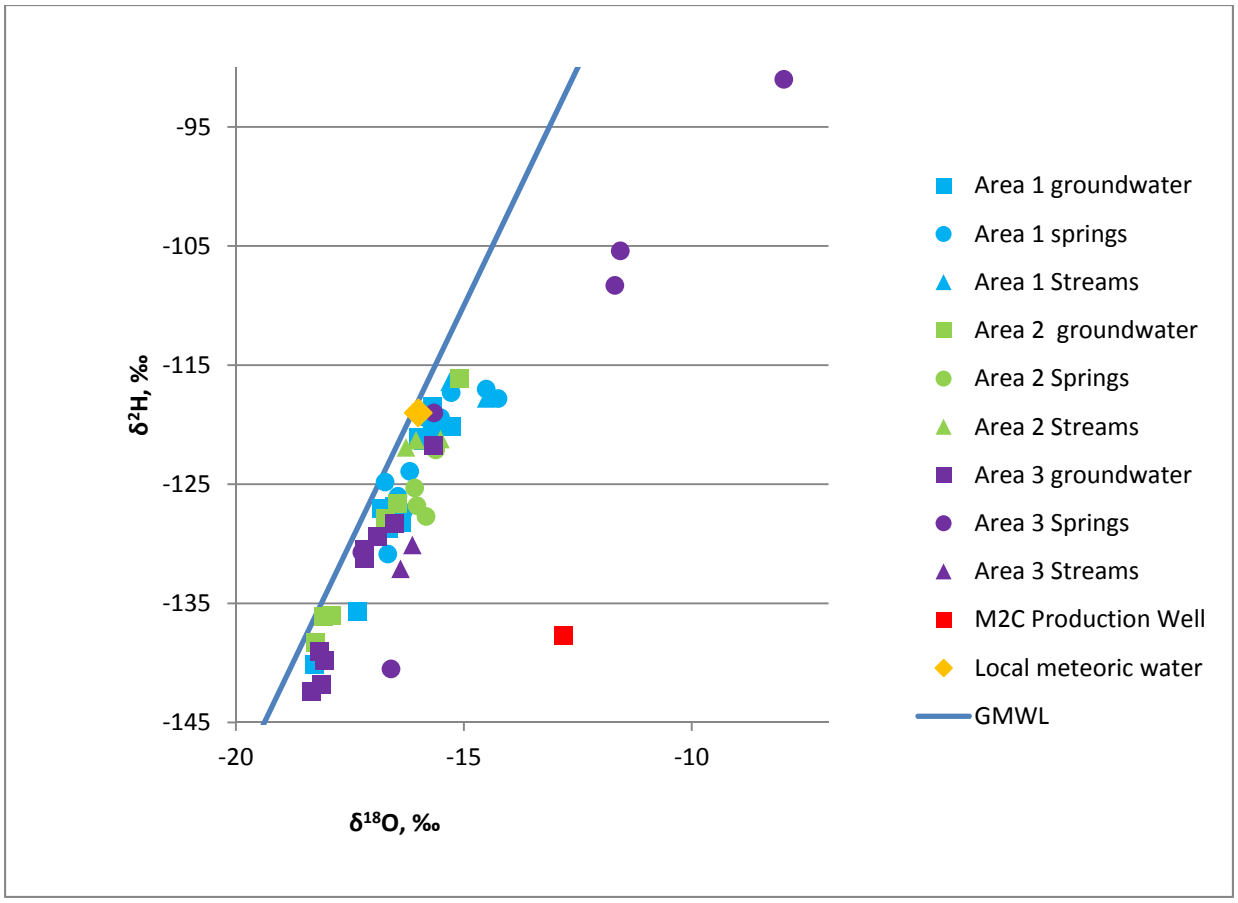

Figure 5-14a. Oxygen ($\delta^{18}O$) and hydrogen ($\delta^{2}H$) stable isotope compositions of the area samples shown with the Global Meteoric Water Line and an estimate of local meteoric water from Fricke *et al.* (1992). Figure 5-14b provides an expanded view of the majority of samples.

5.5.1.3 Radionuclides

Many of the samples have detectable amounts of gross alpha and gross beta radioactivity, which reflect the dissolution of natural radionuclides that occur in rocks such as ^{40}K and members of the uranium and thorium decay series. Gross alpha activity is generally below the U.S. EPA Primary Drinking Water Standard limit of 15 pCi/L, though five sample sites in Area 1 and one in Area 2 have higher activities. The gross alpha standard is exclusive of uranium and radon, so those constituents would need to be determined and subtracted for a rigorous comparison to the regulation.

One spring sample in Area 1 has a gross beta activity in excess of the screening value of 50 pCi/L. The gross beta drinking water standard is dose based, so determining an activity limit requires knowing the responsible radionuclide(s). Potassium-40 and several members of the uranium and thorium decay series are beta producers. Radium-226 was detected in one spring sample in Area 3 and ^{228}Ra was detected in two spring samples from Area 1. All of these detections were at activities below the drinking water standard of 5 pCi/L.

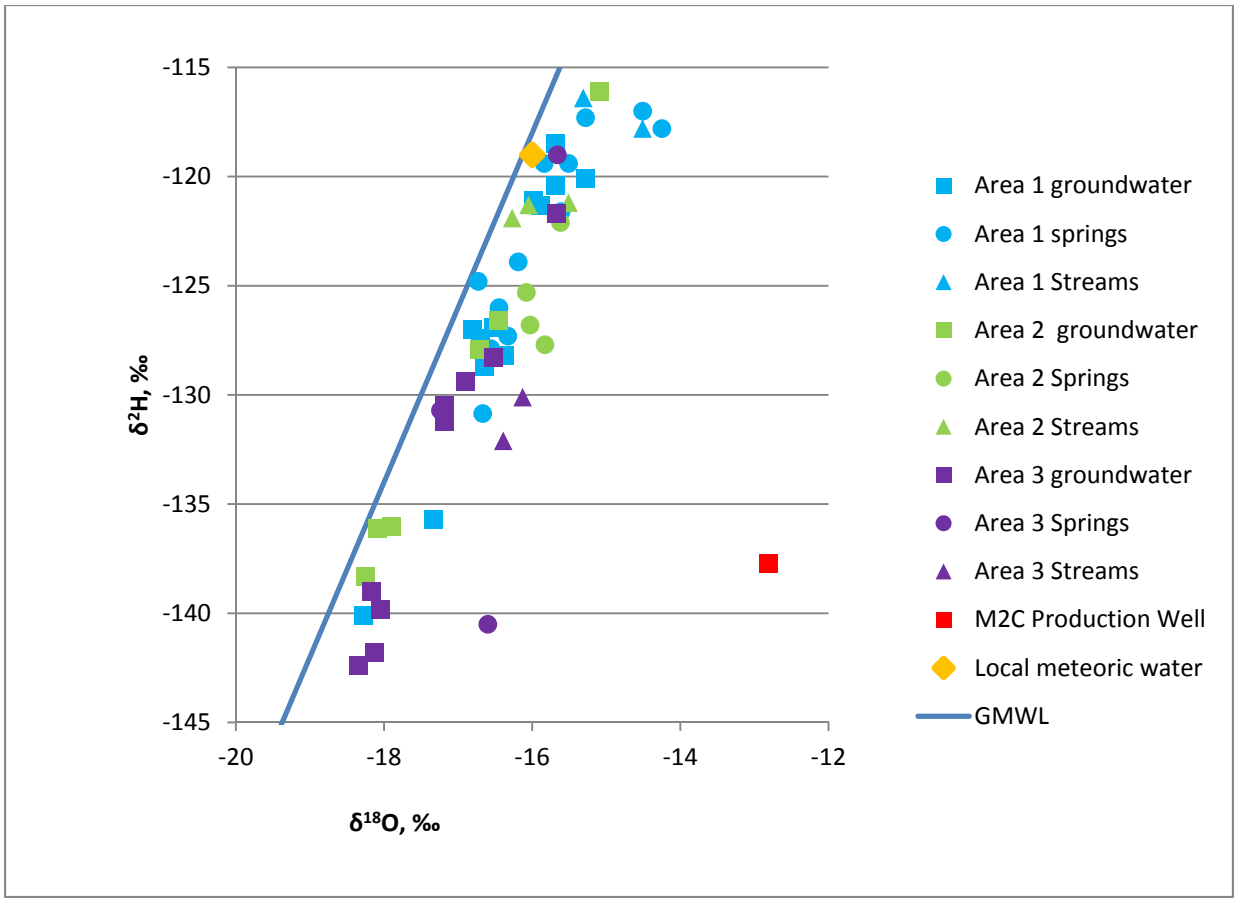

Figure 5-14b. Oxygen ($\delta^{18}O$) and hydrogen ($\delta^{2}H$) stable isotope compositions of the area samples shown with the Global Meteoric Water Line and an estimate of local meteoric water from Fricke *et al.* (1992). This graph excludes several heavy-isotope enriched samples shown in Figure 5-14a.

5.5.1.4 Methane

Methane is observed in a number of water samples (Figure 5-15). In the majority of samples, the concentration is very low (less than 100 µg/L). For reference, The Office of Surface Mining Reclamation and Enforcement (Eltschlager *et al.*, 2001) recommends the following action levels for methane dissolved in water:

- > 28 mg/L (28,000 µg/L) should trigger immediate ventilation to prevent potentially explosive conditions
- > 10 mg/L but < 28 mg/L (> 10,000 µg/L but < 28,000 µg/L) merits warning well users to avoid ignition sources and consider ventilation/remediation; one sample had results meeting this threshold
- < 10 mg/L (10,000 µg/L) in water requires no action

These action levels were developed in response to the possibility of explosive levels of methane developing in wells or structures and are based on the solubility of methane in water at standard temperature and pressure (STP). Methane will exsolve from water under STP conditions at dissolved

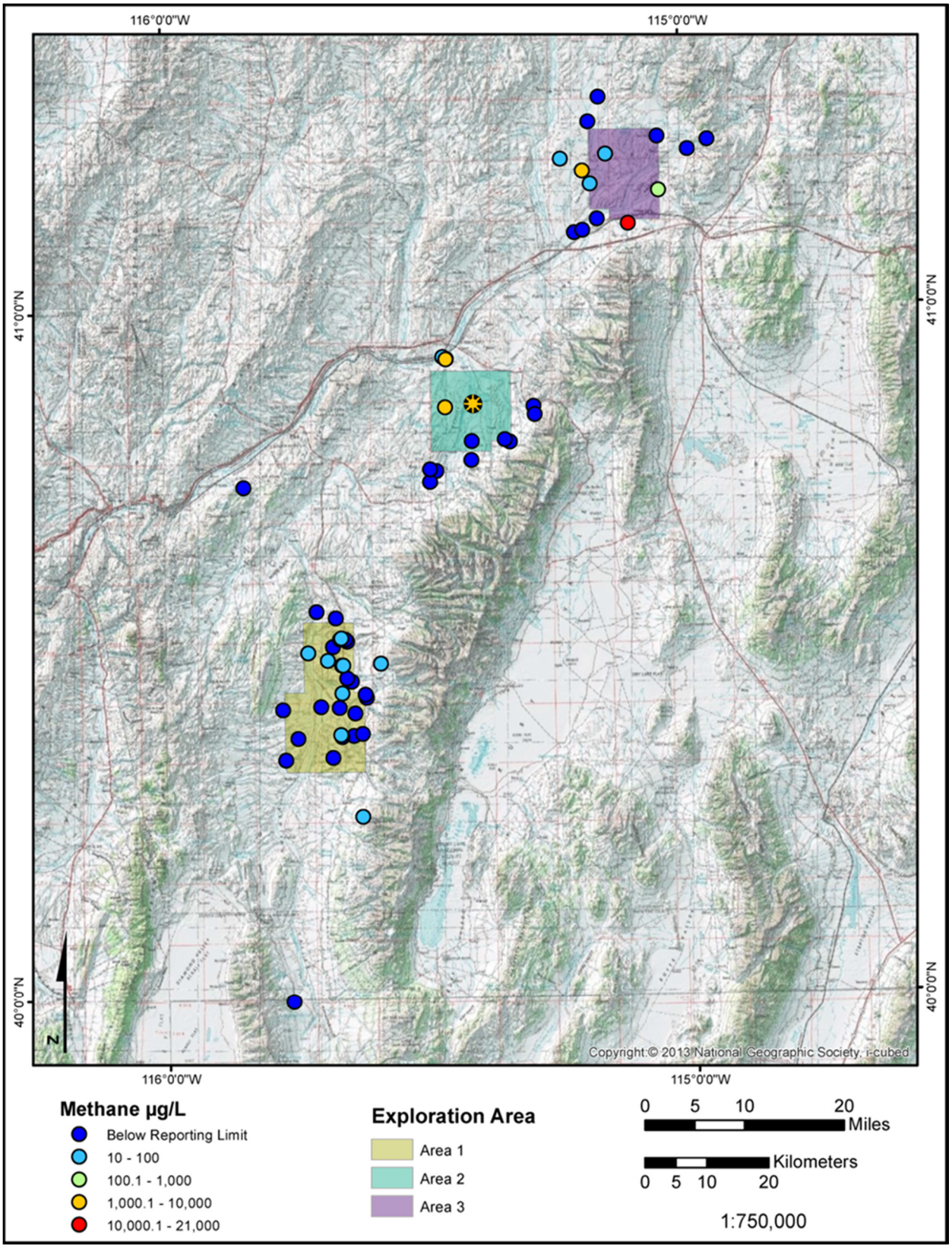

Figure 5-15. Dissolved methane measured in area water samples. The production well is indicated by the starred circle in Area 2.

concentrations between 28 and 30 mg/L. Standard temperature is 0 °C (32 °F) and standard pressure is considered at sea level. At the general altitude of the study area (5,000 ft above sea level), the solubility of methane decreases approximately in half to 14.5 mg/L.

Of the 35 collection locations in Area 1, eight have naturally occurring methane concentrations higher than the analytical reporting limit. These concentrations range from 16.7 to 79.6 µg/L. In Area 2, four of the 16 locations were above the reporting limit for methane. Although one of these Area 2 locations is below 100 µg/L, the others are significantly higher. In Area 3, six locations have methane above the reporting limit and three of these are greater than 100 µg/L.

A wide range of stable carbon isotopic compositions are associated with the methane detections. There are several samples with a heavy carbon isotope signature (less negative $\delta^{13}C$), which indicates thermogenic methane from hydrocarbon-bearing rock. These are from Areas 1 and 3 and they are associated with low methane concentrations (less than 100 µg/L) (Figure 5-16). The natural migration of minute amounts of gas from deep reservoirs is possible, but the heavier hydrocarbons such as ethane and propane that often accompany thermogenic methane are below detection in these samples. The relationship between the $\delta^{13}C$ and $\delta^{2}H$ of methane is associated with different methane origins (Whiticar, 1999). None of the samples are consistent with a thermogenic source (Figure 5-17) when considering both

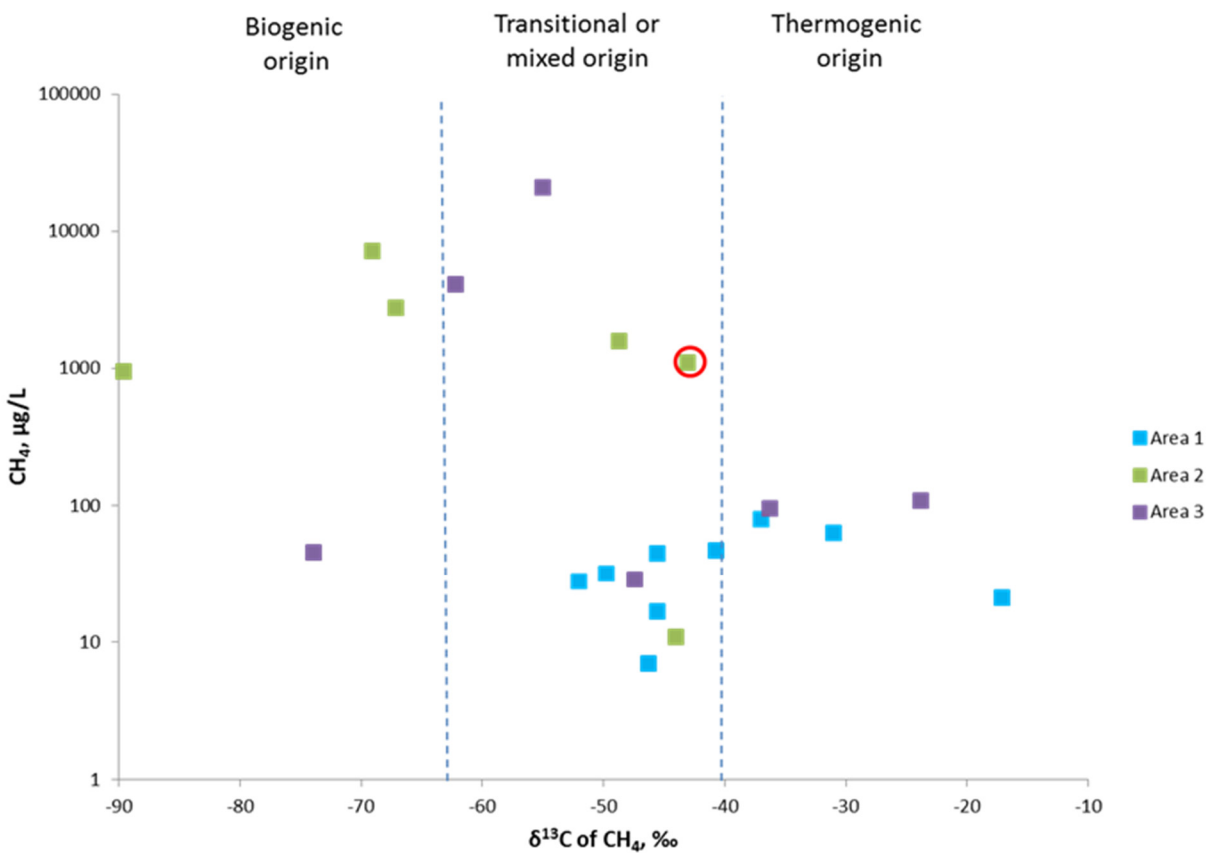

Figure 5-16. Relationship between methane concentration (log scale) and $\delta^{13}C$ composition of the methane. The association of $\delta^{13}C$ values and source of the methane are based on general signatures from Jackson *et al.* (2013). The red circle identifies the water sample collected from the production well, M2C-M2-21B.

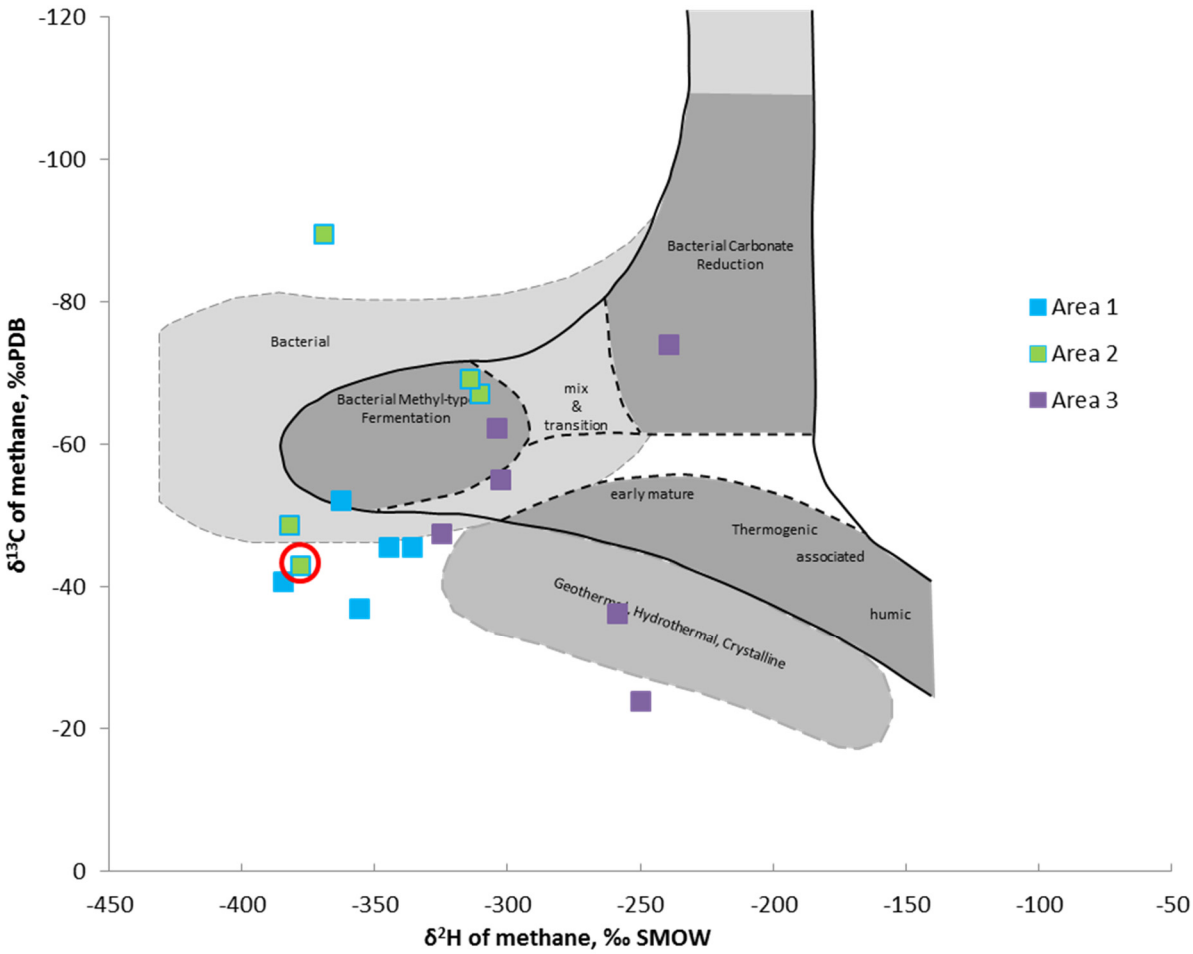

Figure 5-17. Classification of methane origin based on $\delta^{13}C$ CH_4 and δ^2H CH_4 from Whiticar (1999). The red circle identifies the water sample collected from the production well, M2C-M2-21B.

$\delta^{13}C$ and δ^2H. The majority of samples from all areas have methane $\delta^{13}C$ and δ^2H compositions that are consistent with biogenic origins, though two samples from Area 3 have a geothermal signature. Although these two sampling sites (one spring and one stream) do not have elevated water temperatures, hot springs are found in Area 3.

The highest methane values for which stable carbon isotopic data are also available were measured in an alkaline spring in Area 3, the pre- and post-fracking samples from well 2-1, and wells 2-2 and 3-3. The carbon and hydrogen isotopic compositions of these samples are consistent with a biogenic methane source (Figures 5-16 and 5-17). Other samples from all three exploration areas also contain biogenic methane. Based on the stable carbon isotopic composition of methane versus that of dissolved carbon in water (Figure 5-18), the majority of biogenic methane in the samples is derived by the process of acetate fermentation. Although the more depleted carbon isotopes in the methane from wells 2-1, 3-2, and 3-3 suggest that biologically driven CO_2 reduction ($CO_2 + 4H_2 \rightarrow CH_4 + 2H_2O$) may affect these waters, the heavy-isotope enrichment (less negative) of the $\delta^{13}C$ of the dissolved inorganic carbon is consistent with acetate fermentation whereby microbially produced CO_2 is enriched in ^{13}C as the methane is depleted (Baldassare *et al.*, 2014). The combined characteristics of high-alkalinity heavy $\delta^{13}C$

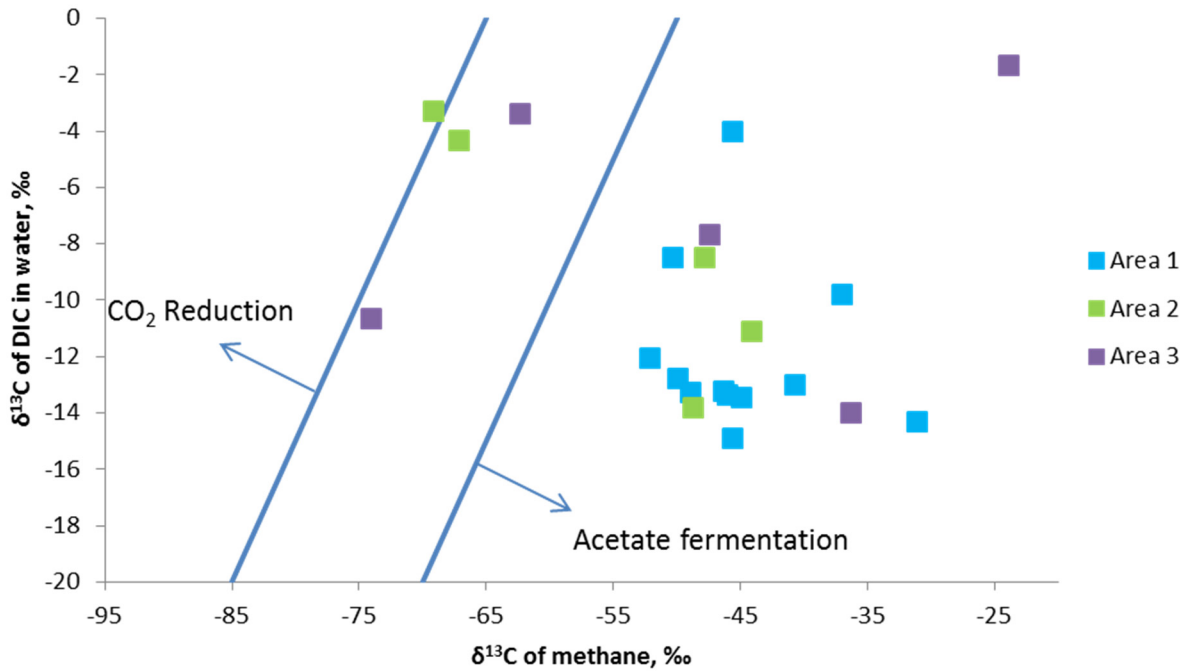

Figure 5-18. Relationship between $\delta^{13}C$ CH_4 and $\delta^{13}C$ DIC-H_2O used by Clark and Fritz (1997) to identify the pathway for methanogenesis.

in the dissolved inorganic carbon in the water, very light (depleted) $\delta^{13}C$ and $\delta^{2}H$ in the methane, and a very low ethane to methane ratio are consistent with acetate fermentation by microbial processes as the source of the methane. The only water sample with a methane concentration above the action level is from 3-13, the highly alkaline spring in Area 3. As described above, the data currently available for this spring are consistent with a biogenic methane origin.

5.5.1.5 Noble Gases

Noble gas samples were collected from 20 locations, including two locations approximately two months after hydraulic fracturing in Area 2 and a sample from Lamoille Creek upstream of the fractured wells. The equilibrium concentrations of noble gases dissolved in water depend on the temperature at the time of groundwater recharge and the Henry's Law solubility of each noble gas (Mazor, 1991). This process is called air-water solubility. Air-water solubility is a function of recharge temperature and recharge altitude (e.g., http://pubs.usgs.gov/sir/2009/5057/section3.html, July 15, 2015).

Neon does not have significant subsurface sources so the neon concentration in groundwater is representative of the air-water solubility at the temperature and altitude of recharge. Neon concentrations in groundwater before hydraulic fracturing ranged from 1.4×10^{-7} to 3.4×10^{-7} ccSTP/g (Figure 5-19). The sample from Lamoille Creek had a neon concentration of 1.7×10^{-7} ccSTP/g that was consistent with the air-water solubility at the sample altitude of collection and temperature (1,646 m above mean sea level [5,400 ft], 16.8 °C). The maximum possible concentration of neon in fresh water at sea level for standard temperature (0 °C) is 2.4×10^{-7} ccSTP/g. The observed neon concentrations above the maximum value (not considering recharge temperature and altitude, which reduce dissolved equilibrium concentrations) likely result from entrainment of excess air: "Excess air is thought to result from a fluctuating water table

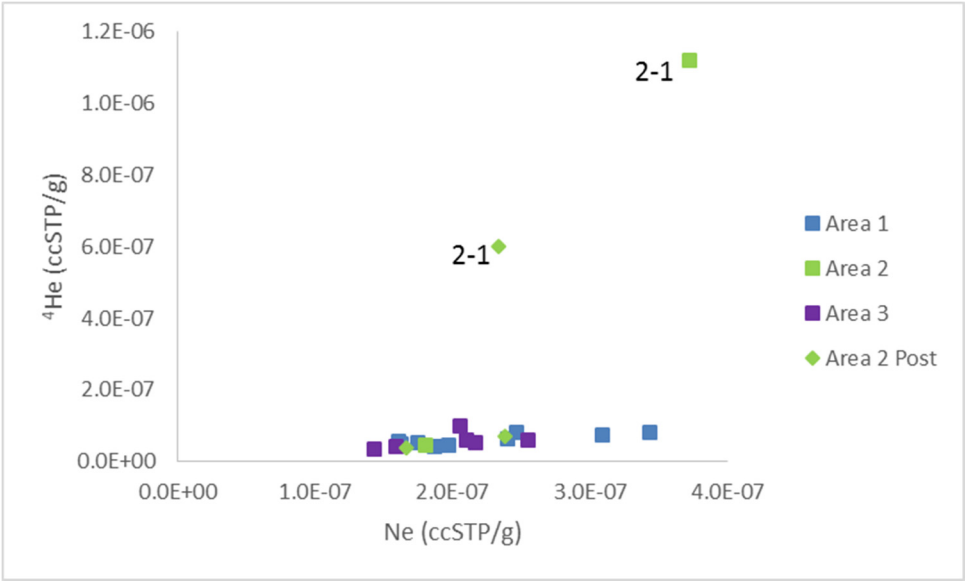

Figure 5-19. ^{4}He versus Ne for samples from exploration areas 1, 2, and 3. Ne and ^{4}He concentrations are consistent with air-water solubility and excess air except for two samples from location 2-1. Elevated 4He concentrations in location 2-1 (and helium isotopic ratios) are consistent with water in contact with an older and/or uranium-rich geologic formations.

entraining air bubbles or from recharge water trapping air bubbles near the water table. These air bubbles dissolve into groundwater as groundwater migrates below the water table and hydrostatic pressure increases" (http://pubs.usgs.gov/sir/2009/5057/section3.html, July 15, 2015).

Helium has two stable isotopes ^{3}He and ^{4}He. Most helium in the environment is ^{4}He (natural abundance 99.999866 percent, http://education.jlab.org/itselemental/iso002.html, July 15, 2015). Helium concentrations in groundwater originate from several sources, including air-water solubility, radiogenic sources in the subsurface, and from the mantle. Most ^{4}He concentrations ranged from 3.6 x 10^{-8} to 9.95 x 10^{-8} ccSTP/g (Figure 5-19), excluding two samples from the same location with much higher ^{4}He concentration (location 2-1, 1.1 x10^{-6} and 6.0 x 10^{-7} ccSTP/g). The sample from Lamoille Creek had a ^{4}He concentration of 3.8 x10^{-8} ccSTP/g that was consistent with the air-water solubility at the altitude of sample collection and temperature. The maximum possible concentration of helium in fresh water at sea level for standard temperature (0 °C) is 5.0 x 10^{-8} ccSTP/g. Almost all of the samples have ^{4}He concentrations greater than the maximum possible concentration from air-water solubility.

Helium R/Ra values, where R is the measured ^{3}He/^{4}He of a sample and Ra is the ^{3}He/^{4}He of air (Ra = 1.4 x 10^{-6}), are used to distinguish different sources of helium. Surface waters should have an R/Ra value of 1. The upstream Lamoille Creek sample has an R/Ra value of 0.99. Although most of the samples have ^{4}He concentrations greater than the maximum possible, most also have R/Ra values close to 1. This, along with neon and argon concentrations, show that ^{4}He in the samples is from air-water solubility and excess air. The two samples from location 2-1 with elevated ^{4}He concentrations also have low R/Ra values (0.13 and 0.14), which are consistent with water in contact with an older and/or uranium-rich geologic formation where ^{4}He is created by the decay of very long-lived isotopes of uranium and thorium. One other sample, location 1-1, has a ^{4}He concentration that is slightly higher than

air-water solubility, but consistent with the other sample locations. This sample has the highest R/Ra value (2.48), which indicates more ^{3}He than the other samples and suggests a small component of mantle helium.

5.5.1.6 Refined Hydrocarbons and Hydraulic Fracturing Components

Only a few samples had detectable refined hydrocarbons or hydraulic fracturing components. Toluene in the drilling water supply well, location 2-16, is the only analysis with refined hydrocarbons above the analytical reporting limit. This sample was collected after hydrofracturing in MC2, but there is no pre-fracturing sample for comparison. Toluene is one of a group of volatile aromatic compounds typically found in petroleum products. It was one of the most frequently detected volatile organic compounds in samples from aquifers studied as part of the National Water-Quality Assessment (NAWQA) Program (Zogorski *et al.*, 2006). For perspective, the toluene concentration measured in the drilling supply well is 17 µg/L, whereas the Safe Drinking Water Act maximum contaminant level for toluene is 1 mg/L (1,000 µg/L).

The majority of the chemicals analyzed that could possibly be in a hydraulic fracturing fluid were below the minimum detection limit in the water samples. Exceptions include six samples (three from Area 1 and three from Area 3) with low levels of propylene glycol and one sample from Area 3 with a low level of ammonium persulfate. The propylene glycol analytical results are noted by the laboratory as possibly reflecting contamination, even though the instrument used was cleaned and recalibrated prior to the reported analyses. Propylene glycol is used in the chemical, food, and pharmaceutical industries as an additive. Ammonium persulfate is a strong oxidizer used for etching and bleaching. It is very soluble in water and it will disassociate into ammonium and persulfate (which degrades to sulfate), so there is no regulation for ammonium persulfate.

5.5.2 Characteristics of Formation Water from the Oil Production Zone

Analytical results are available for one water sample from the hydrocarbon reservoir. This sample is from well M2C-M2-21B, which was drilled in Area 2. This sample was collected from the oil-water separator which is located after the wellhead. In addition to impacts to the chemical and isotopic characteristics as a result of processes associated with the oil-water separator (which also heats the fluid), fluids were used during the drilling and fracturing of the well and are unlikely to have been completely purged from the subsurface. These factors combine to suggest that the water collected from M2C-M2-21B at the oil-water separator may not be fully representative of the natural subsurface groundwater in the reservoir. Nonetheless, differences between the M2C-M2-21B water and shallow groundwater are evident.

5.5.2.1 Major-ion Composition of Water from the Oil Production Zone

Groundwater from the production well is much more saline than any other water sampled for the study, with a brackish TDS of 8,527 mg/L. The water is a Na-Cl type, so it is also chemically distinct from all the ground-, spring, and surface waters sampled (Figure 5-13). The chloride concentration is significantly higher in M2C-M2-21B than any other water sample (Figure 5-20). Other distinctive characteristics of the M2C-M2-21B groundwater are higher SiO_2, F, Sr, Li, Ba, and B than the other waters sampled in Areas 1, 2, and 3. This is consistent with a greater degree of rock-water interaction as a result of higher temperature and longer residence time.

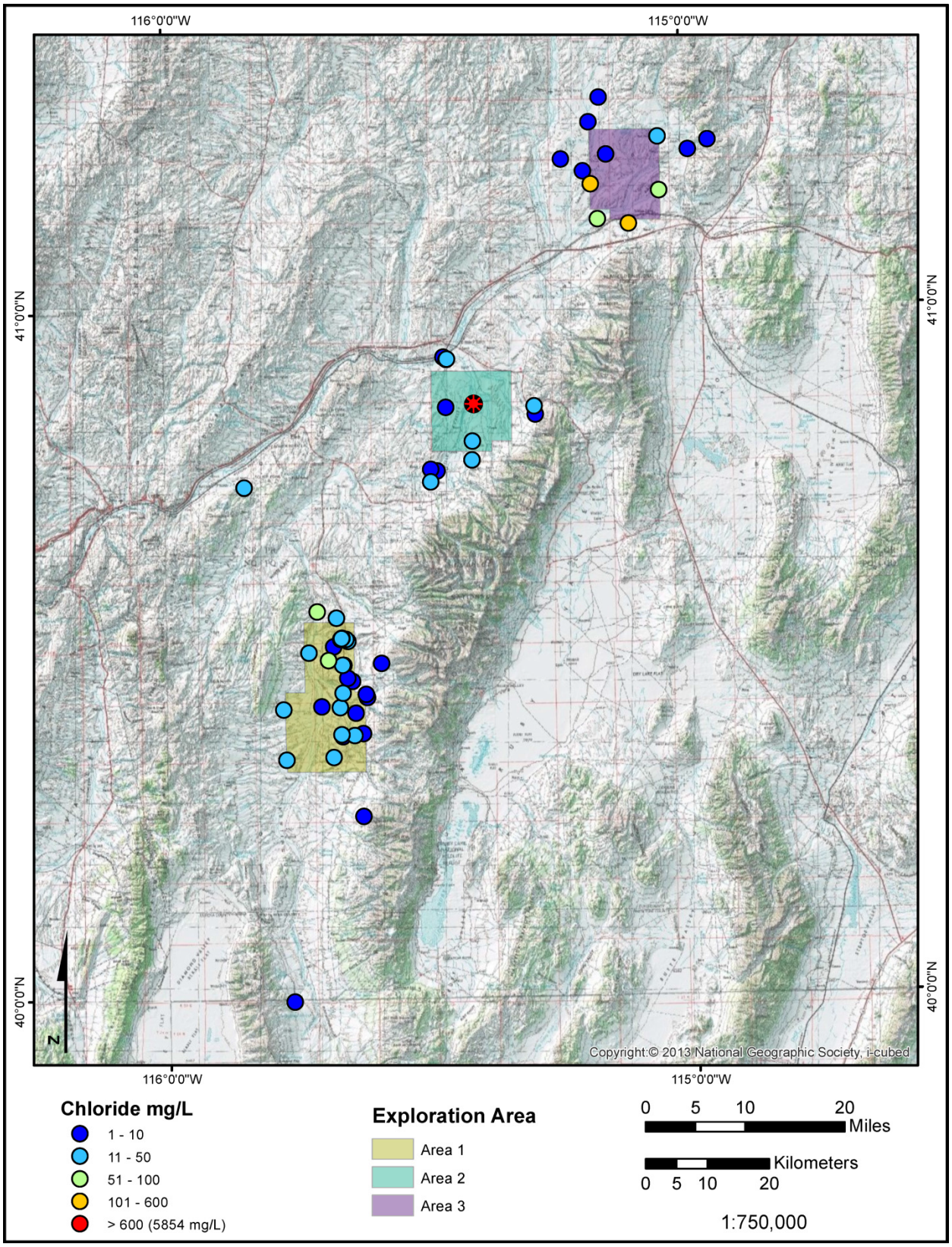

Figure 5-20. Dissolved chloride distribution in area waters.

5.5.2.2 Stable Isotopic Composition of Water from the Oil Production Zone

The hydrogen and oxygen stable isotopic composition of water separated from the production fluid is markedly enriched in the heavy isotope of oxygen relative to meteoric water (Figures 5-14a and b). The enriched $\delta^{18}O$ observed for waters collected from M2C-M2-21B may reflect exchange with oxygen-bearing minerals during a long residence time for the water in the production reservoir under elevated temperatures. Oxygen is much more abundant in rock minerals than hydrogen so that the isotopes of oxygen are more commonly affected by exchange reactions. Oxygen isotopic enrichment of a water by exchange with minerals requires high temperatures and substantial residence time, and therefore is not commonly observed in near-surface water, though it is not uncommon in the waters of geothermal systems. The fluid temperature at depth in the target shales is unknown, but based on an average geothermal gradient (25 °C/1 Km), the fluid temperature in the target shales at 10,000 ft would be roughly 90 °C. The measured fluid temperature at the wellhead was 30.76 °C (87.36 °F), which is consistent with typical heat loss for a fluid as it travels from depth to the land surface. Evaporation of water in the separator could also account for heavy isotope enrichment of oxygen, but would additionally affect hydrogen. Considering the slope of typical evaporative enrichment, the original groundwater composition (prior to evaporation) would be more depleted in heavy isotopes than other groundwater sampled in the area. Therefore, whether the stable isotopic composition of M2C-M2-21B is a result of exchange processes in the reservoir or evaporation in the separator, it is unique compared to other groundwater in the area.

5.5.2.3 Radionuclides in Water from the Oil Production Zone

Gross alpha and particularly gross beta are elevated in water from the production well, which is consistent with observations of fluids from other petroleum reservoirs. The high concentration of dissolved K (524 mg/L) suggests that the decay of ^{40}K contributes to the gross beta, along with the uranium and thorium isotopes that are often associated with hydrocarbon reservoirs. Both radium isotopes are also present.

5.5.2.4 Methane Dissolved in Water from the Oil Production Zone

Although higher than the majority of waters sampled, the methane concentration dissolved in water from the production well is not distinct compared with that observed in several other locations in the study area (Figure 5-21). It is possible that the conditions in the separator may cause methane to be removed from solution. In contrast to the methane results, the substantive concentrations of the higher-chain hydrocarbons ethane and propane are unique to the production well. For the few other water samples with reportable ethane, the methane/ethane ratios range from 300 to 2,000. The methane to ethane ratio at M2C-M2-21B is 0.85. A propane concentration above the reporting limit is unique to the production well.

The carbon and hydrogen isotopic data from the production well water do not exhibit the degree of heavy isotope enrichment (less negative values) that is typical of thermogenic, reservoir methane (Figures 5-16 and 5-17). Recall that this water was collected from the oil-water separator at the wellhead, and that significant amounts of fluid were used during the drilling and fracturing of the well. The source of the drilling water is well 2-16, which contains measurable methane of biogenic origin. The isotopic data suggest that the methane dissolved in water collected from the oil-water separator at M2C-M2-21B is unlikely to be representative of the reservoir gas.

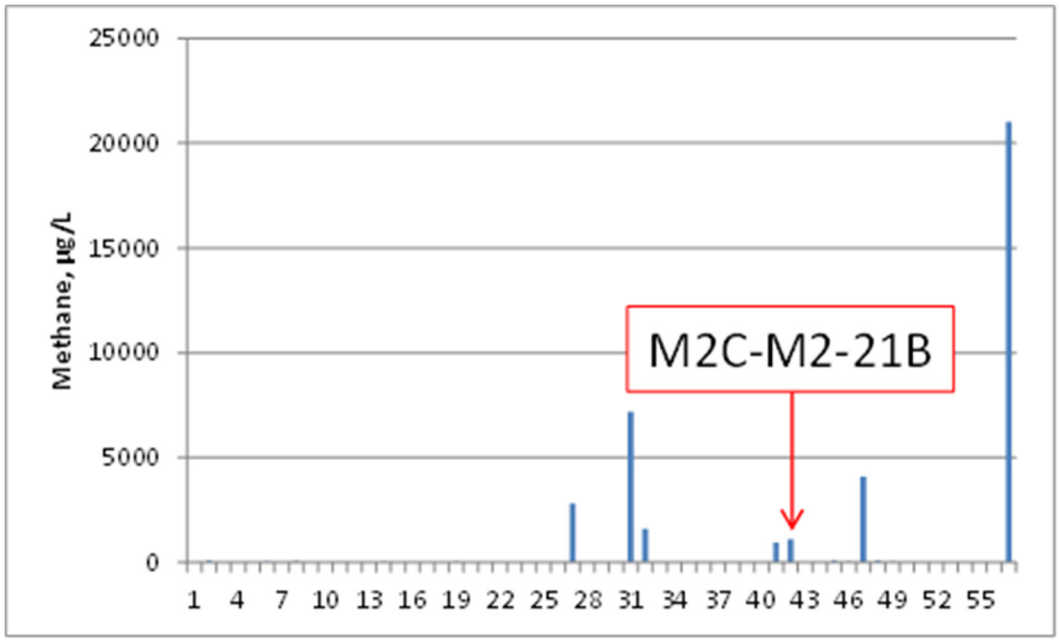

Figure 5-21. Methane concentrations for the samples with reported results. The majority are below the detection limit.

5.5.2.5 Noble Gases in Water from the Oil Production Zone

One sample for noble gas analysis was collected from the M2C exploration well in Area 2 on September 25, 2014, which was approximately six months after hydraulic fracturing. The sample was collected from a sampling point in the oil-water separator because a sampling port was not available at the wellhead. The noble gas sample from M2C had high inlet pressure from large amounts of CO_2 in the sample, so liquid nitrogen had to be used to extract the sample. Using liquid nitrogen to extract the sample does not allow for krypton and xenon concentrations to be measured. Neon and argon concentrations from M2C are anomalously lower by two to three orders of magnitude than groundwater samples, which is well below the accepted concentrations for atmospheric noble gases in fresh water (Mazor, 1991) and well below reported concentrations for other natural gas reservoirs (e.g., Hunt et al., 2012). The ^{4}He concentration (6.2 x 10^{-8} ccSTP/g) is consistent with other samples from exploration areas 1, 2, and 3. Because of the anomalous neon and argon concentrations, the noble gas concentrations have likely been affected by the oil-water separator and are not representative of the resource or host shale formation (Figure 5-22).

5.5.2.6 Refined Hydrocarbons and Hydraulic Fracturing Components in Water from the Oil Production Zone

The water from the production well contains chemicals that are consistent with refined hydrocarbons associated with activities at the ground surface. The chemicals TPH-DRO; TPH-GRO; benzene; toluene; ethylbenzene; and m- , p-, and o-xylene are all indicative of petroleum derivatives and are present in the water that was separated from the fluid collected at M2C-M2-21B. The benzene and toluene concentrations are above the Safe Drinking Water Act MCLs. The presence of benzene, ethylbenzene, and the xylenes is unique to the production well. Of the analytical suite of chemicals chosen because of their possible use in hydraulic fracturing fluids, the chemicals methanol, ethanol, and 2-butoxyethanol were detected in M2C-M2-21B.

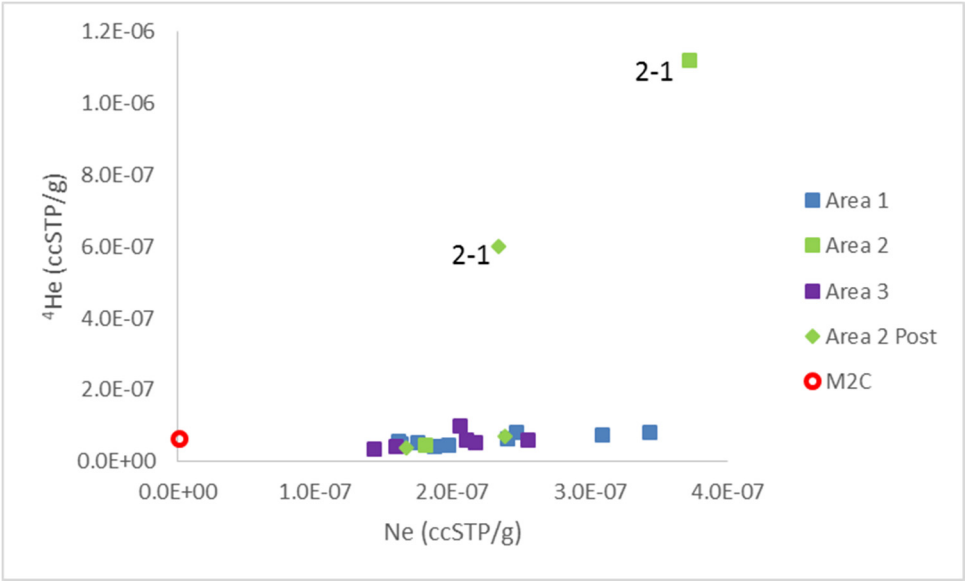

Figure 5-22. ^{4}He versus Ne for samples from exploration areas 1, 2, and 3 and exploration well M2C.

5.5.3 Comparison of Pre- and Post-hydraulic-fracturing Samples

Pre- and post-hydraulic-fracturing samples were collected in Area 2 from nine locations by Tetra Tech, with two of these also sampled by DRI (Table 5-8). No systematic differences between the pre- and post-hydraulic-fracturing samples are evident (comparison of Tetra Tech and DRI analytical results are presented in the QA Section). Major ions, salinity as indicated by electrical conductivity, and radioactivity as indicated by gross alpha and gross beta are similar before and after fracturing (Figures 5-23, 5-24, and 5-25). Other ions and the stable isotopes of water and dissolved inorganic carbon are also consistent before and after hydraulic fracturing. Differences in sample temperature are observed, but some are warmer after hydraulic fracturing, whereas others are cooler (Figure 5-26).

The majority of methane analyses are unchanged because the measurements are below the analytical limit of detection both before and after fracturing (Table 5-8). Of the three sample pairs with methane concentrations above 100 µg/L, two have higher concentrations after the hydraulic fracturing of exploration well M2C-M2-21B (Figure 5-27). The combined Tetra Tech and DRI datasets are not consistent for one of these locations, 2-1. The post-fracturing DRI sample for location 2-1 shows more than double the methane concentration, but the Tetra Tech post-fracturing analysis is 10 percent lower than the pre-fracturing result for the same well. The stable isotopic composition of the dissolved methane at 2-1 is consistent with a biogenic source both pre- and post-fracturing, with the δ^{13}C analysis identical within the analytical error bounds (-67.18‰ pre-fracturing and -69.14‰ post-fracturing). A very large increase in the methane concentrations reported by Tetra Tech (from 62 µg/L pre-fracturing to 1,070 µg/L post-fracturing) is also observed at location 2-2. A duplicate DRI sample post-fracturing generally confirms the post-fracturing measurement (at a value of 1,600 µg/L, the 25 percent error bars of the analyses overlap), but there is no confirmatory second analysis for the pre-fracturing sample. The δ^{13}C composition of the methane from 2-2 is more enriched in heavy isotopes than many biogenic gases, but the δ^{13}C-δ^{2}H relationship remains consistent with the bacterial zone identified by Whiticar (1999) (Figure 5-17).

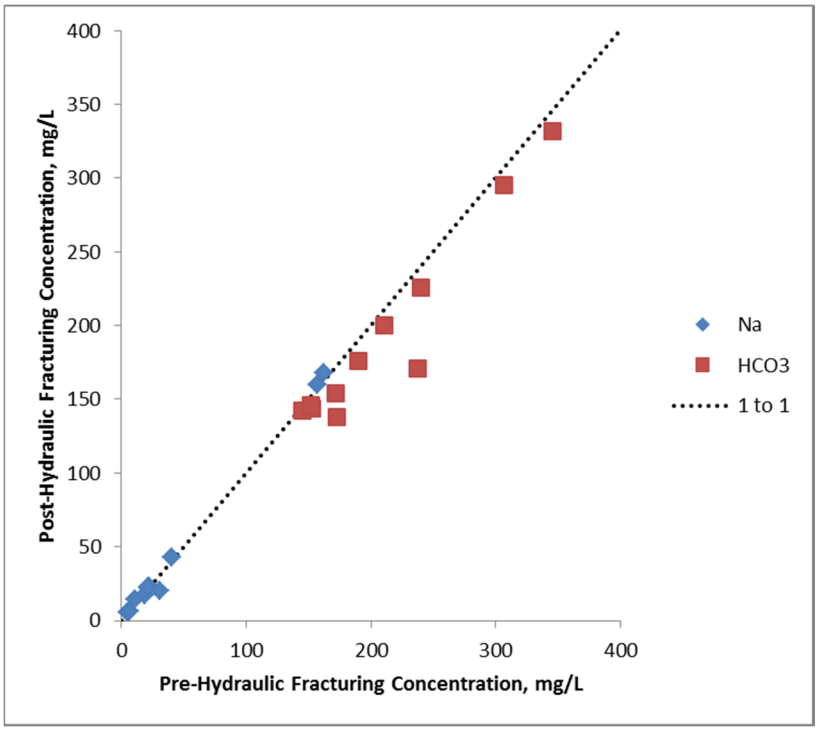

Figure 5-23. Comparison of pre- and post-hydraulic-fracturing analyses of Area 2 waters for Na and HCO^3.

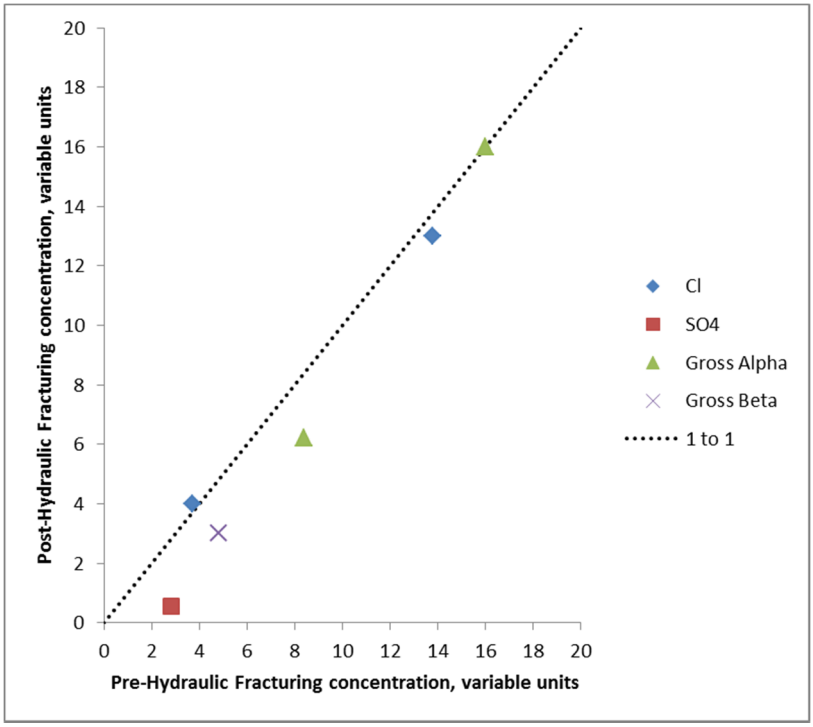

Figure 5-24. Comparison of pre- and post-hydraulic-fracturing analyses of Area 2 waters for the ions Cl and SO_4 (units of mg/L) and radioactivity as gross alpha and gross beta (units of pCi/L).

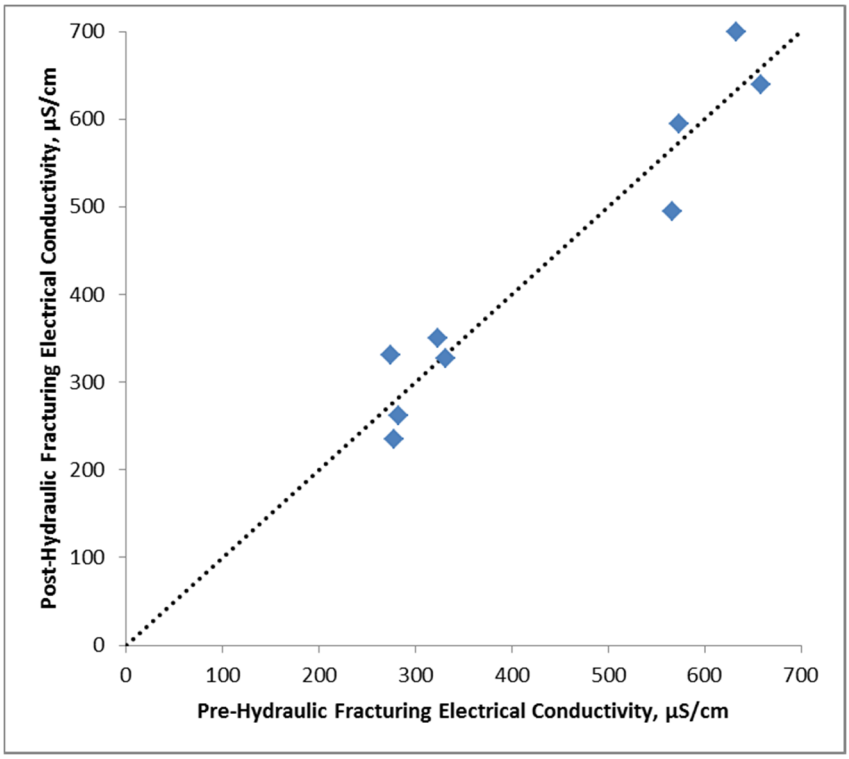

Figure 5-25. Comparison of pre- and post-hydraulic-fracturing analyses of electrical conductivity in Area 2 waters. The dotted line follows a one-to-one relationship for comparison.

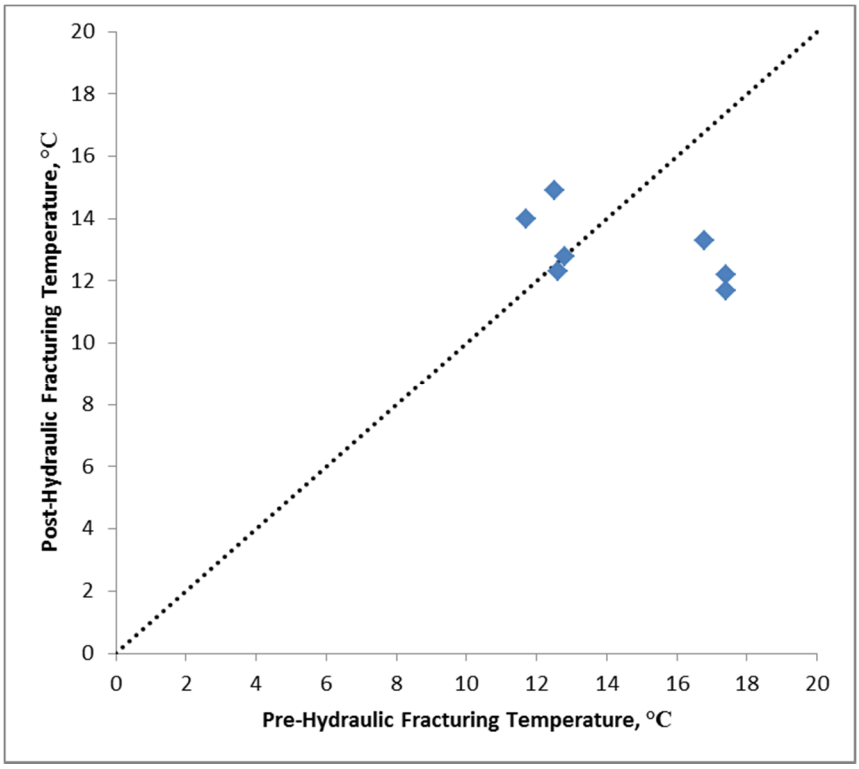

Figure 5-26. Pre- and post-hydraulic-fracturing sample temperatures for Area 2 waters. The dotted line follows a one-to-one relationship for comparison.

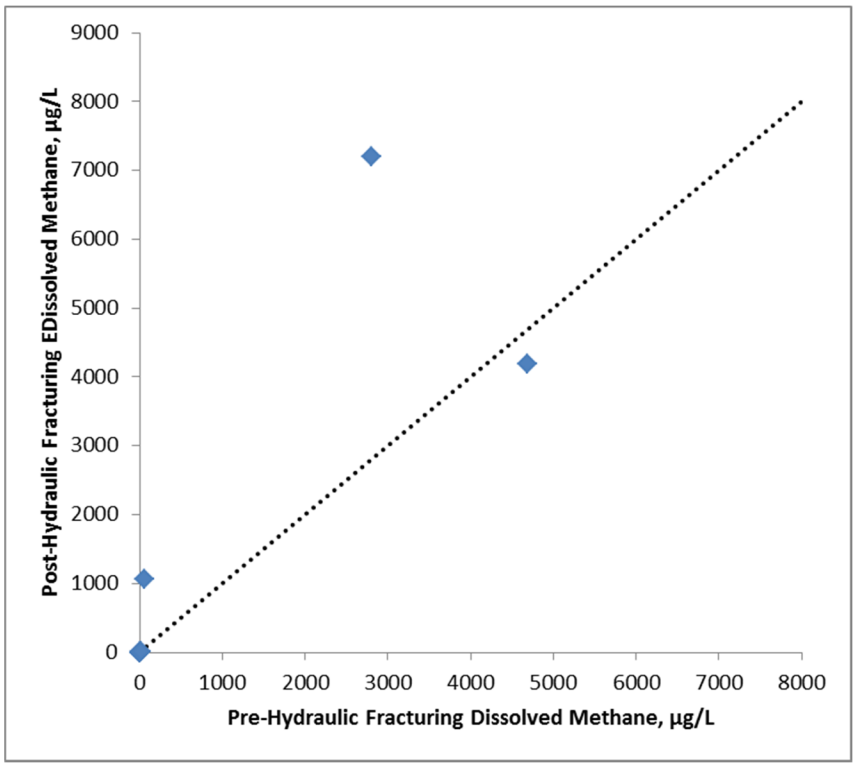

Figure 5-27. Pre- and post-hydraulic-fracturing methane concentrations in waters from Area 2. The dotted line follows a one-to-one relationship for comparison.

5.5.4 Parameter Recommendations for Monitoring

There are numerous differences between the groundwater sample from the producing horizon in the M2C-M2-21B production well and shallow groundwater, springs, and surface water in the area. The water sample collected post-hydraulic fracturing at the M2C-M2-21B production well (from the oil-water separator) suggests that indicators of potential incursion of reservoir-associated fluids into the near-surface environment include temperature, TDS, major-ion composition, oxygen isotopic ratio, trace elements, and C2 and C3 hydrocarbons. Indicators of industrial ground-surface activities present in the sampled production fluid include benzene, ethylbenzene, and the xylenes. Compounds in the M2C-M2-21B water sample that are associated with fluids used for hydraulic fracturing or their breakdown products include, methanol, ethanol, and 2-butoxyethanol. Of the above monitoring parameters, TDS, as indicated by the surrogate measurement of electrical conductivity, can be easily and quickly measured in the field and would be a useful indicator of a shallow groundwater or surface water mixing with reservoir fluid. Laboratory measurements of chloride and propane would be additional useful monitoring analytes, as would the hydraulic fracturing fluid chemicals listed above. Although temperature can be measured in the field, the pre- and post-hydraulic-fracturing samples in Area 2 indicate temporal variations in temperature, which are perhaps seasonally related, that render it problematic as an indicator.

Methane would be a poor choice as an indicator of the impact of production water on near-surface water. Biogenic methane is present in numerous groundwater and spring samples at concentrations similar to and greater than those observed in the production-well groundwater. Isotopic analyses of carbon and hydrogen should always accompany methane analyses to distinguish biogenic and thermogenic sources.

Table 5-8. Pre- and post-hydraulic-fracturing chemical and isotopic parameter analytical results for Exploration Area 2, Humboldt.

Agency (Units)	Location ID	Sample Date	Lab pH	Lab EC (µS/cm)	Ca (dissolved) (mg/L)	Mg (dissolved) (mg/L)	Na (dissolved) (mg/L)	K (dissolved) (mg/L)	HCO_3 (mg/L)	CO_3 (mg/L)	Cl (mg/L)	SO_4 (mg/L)	TDS (mg/L)	B (mg/L)	Ba (dissolved) (mg/L)
DRI	2-1	9/4/2013	9.61	632	0.57	0.06	157	1.8	238	82.8	3.7	2.8	435	0.86	ND
DRI	2-1	6/23/2014	9.50	700	0.61	ND	160	1.5	171	120	4.0	0.57	390	0.87	ND

Agency (Units)	Location ID	Sample Date	Li (dissolved) (mg/L)	SiO_2 (mg/L)	NO_3 - N (mg/L)	F (mg/L)	Br (mg/L)	Gross Alpha (pCi/L)	Gross Beta (pCi/L)	Methane (µg/L)	Ethane (µg/L)	$\delta^{13}C$ CH_4 (‰)	$\delta^{2}H$ CH_4 (‰)	$\delta^{13}C$ DIC Water (‰)	$\delta^{2}H$ Water (‰)	$\delta^{18}O$ Water (‰)
DRI	2-1	9/4/2013	<0.01	54.3	<0.01	3.73	0.02	16	11	2800*	7.2	-67.18*	-310.6*	-4.35	-136.0	-17.90
DRI	2-1	6/23/2014	0.01	49	ND	3.9	ND	16	ND	7200*	18	-69.14*	-314.0*	-3.29	-136.1	-18.09

Agency (Units)	Location ID	Sample Date	Lab pH	Lab EC (µS/cm)	Ca (dissolved) (mg/L)	Mg (dissolved) (mg/L)	Na (dissolved) (mg/L)	K (dissolved) (mg/L)	HCO_3 (mg/L)	CO_3 (mg/L)	Cl (mg/L)	SO_4 (mg/L)	TDS (mg/L)	B (mg/L)	Ba (dissolved) (mg/L)
DRI	2-4	9/4/2013	7.98	323	37.4	6.7	21.6	2.4	152	ND	13.8	26.2	207	0.05	ND
DRI	2-4	6/23/2014	7.90	350	26	6.5	22	3.4	146	ND	13	25	190	0.11	0.055

Agency (Units)	Location ID	Sample Date	Li (dissolved) (mg/L)	SiO_2 (mg/L)	NO_3 - N (mg/L)	F (mg/L)	Br (mg/L)	Gross Alpha (pCi/L)	Gross Beta (pCi/L)	Methane (µg/L)	Ethane (µg/L)	$\delta^{13}C$ CH_4 (‰)	$\delta^{2}H$ CH_4 (‰)	$\delta^{13}C$ DIC Water (‰)	$\delta^{2}H$ Water (‰)	$\delta^{18}O$ Water (‰)
DRI	2-4	9/4/2013	0.01	29.1	0.07	0.21	0.06	8.4	4.8	<10.0	<10.0	-56.6 Q	-212.4 Q	-10.33	-126.6	-16.46
DRI	2-4	6/23/2014	0.01	25	ND	ND	ND	6.2	3	5.0 J	<5.0	NC	NC	-9.90	-127.9	-16.72

*methane identified as biogenic origin by $\delta^{13}C$ CH_4 and $\delta^{2}H$ CH_4.
J = result is less than the reporting limit but greater than or equal to the method detection limit and the concentration is an approximate value.
NC = not collected.
ND = none detected (below minimum detection limit).
Q = concentration below limit of quantification.

Table 5-8. Pre- and post-hydraulic-fracturing chemical and isotopic parameter analytical results for Exploration Area 2, Humboldt (continued).

Agency (Units)	Location ID	Sample Date	Field pH	Field EC (µS/cm)	Temperature (˚C)	Ca (total) (mg/L)	Mg (total) (mg/L)	Na (total) (mg/L)	K (total) (mg/L)	HCO_3 (mg/L)	CO_3 (mg/L)	Li (total) (mg/L)	Methane (µg/L)	Ethane (µg/L)
TT	2-1	9/4/2013	9.96	658	11.7	3.17	0.695	162	ND	190	106	0.0113	4690	11.1
TT	2-1	6/23/2014	9.70	640	14.0	0.84	0.039 J	168	1.93 J	176	105	0.0062 J	4190	11.8
TT	2-2	9/4/2013	7.79	566	17.4	70.6	10.4	30.6	3.77	307	ND	ND	62	<0.573
TT	2-2	6/23/2014	7.30	495	12.2	73.0	11.9	20.1	5.25	295	ND	0.0107	1070	<0.573
TT	2-3	9/4/2013	7.54	573	16.8	81.5	12.5	21.5	5.26	346	ND	ND	12.2	<0.573
TT	2-3	6/23/2014	7.45	595	13.3	90.9	14.2	22.3	5.78	332	ND	0.0096 J	7.54	<0.573
TT	2-4	9/4/2013	8.16	331	12.8	36.9	6.58	22.5	ND	153	ND	ND	<0.218	<0.573
TT	2-4	6/23/2014	7.60	327	12.8	37.5	6.99	23.0	2.59 J	144	ND	0.0061 J	0.715 J	<0.573
TT	2-5	9/4/2013	7.25	282	12.5	34.9	5.20	18.6	ND	172	ND	ND	<0.218	<0.573
TT	2-5	6/25/2014	6.60	262	14.9	34.8	5.24	17.4	0.954 J	154	ND	0.0035 J	<0.218	<0.573
TT	2-6	9/4/2013	7.09	278	12.6	44.8	4.18	5.31	ND	173	ND	ND	<0.218	<0.573
TT	2-6	6/25/2014	6.50	235	12.3	42.7	4.04	5.28	0.865 J	138	ND	ND	<0.218	<0.573
TT	2-7	9/4/2013	8.93	274	17.4	50.4	7.57	10.9	ND	211	ND	ND	<0.218	<0.573
TT	2-7	7/1/2014	7.60	331	11.7	50.7	8.06	14.2	1.39 J	200	ND	ND	<0.218	<0.573
TT	2-8	10/8/2013	NC	NC	NC	42.0	7.75	6.34	ND	145	ND	ND	<0.218	<0.573
TT	2-8	6/25/2014	7.58	288	13.9	43.9	8.54	6.35	1.28 J	142	ND	ND	<0.218	<0.573
TT	2-9	10/8/2013	NC	NC	NC	43.7	8.02	40.7	ND	240	ND	ND	<0.218	<0.573
TT	2-9	6/25/2014	7.70	430	15.6	46.5	9.00	42.5	1.35 J	226	ND	0.0068 J	<0.218	<0.573

Considerable variability in methane concentrations reported for duplicate samples by different laboratories is observed, which suggests that quantitative measurements are difficult at the low concentrations observed in the study area. Very low levels of ethane have also been detected in several shallow samples, so ethane is not considered an ideal reservoir indicator. However, propane is unique to the reservoir fluid.

Compounds associated with refining and hydrofracturing are present in the production-zone water and rare in the near-surface water. Nonetheless, the detection of toluene, TPH-DRO, TPH-GRO, ammonium persulfate, ethylene glycol, propylene glycol, and glycerol in pre-hydraulic-fracturing samples show the difficulties of relying on characterizing trace contaminants as indicators of drilling and fracturing activities. Benzene, ethylbenzene, the xylenes, methanol, ethanol, and 2-butoxethanol are uniquely observed in the production fluids and are better choices to identify drilling and hydraulic fracturing chemicals.

6.0 MIGRATION POTENTIAL FOR HYDRAULIC FRACTURING FLUIDS AND NATURAL GAS

The Elko Formation is the current target for exploration as an oil reservoir in the project areas. The conditions in Area 2 and at two recent Noble exploration wells in particular, M2C and M10C, are used to assess the potential for contaminant migration from hydraulic fracturing operations. Despite this local focus, the emphasis is on identifying the factors that are important for either contributing to or controlling migration so that the results may be generalized to other areas.

The processes, pathways, and conditions found in Exploration Area 2 are summarized in an event-tree diagram in Figure 6-1. The various branches describe the design condition and the other possibilities if fracturing does not occur as designed, with subsequent limbs bracketing the uncertainty in subsurface conditions that can affect transport along a pathway. Select combinations on the event tree are analyzed using numerical models of flow and transport (see Appendix B). Not every combination required a full computer model analysis and those that did were deliberately biased toward exploring failure scenarios with conditions that favor transport. This allows the identification of conditions and parameters that are key to controlling the migration of hydraulic fracturing fluids in the subsurface, which provides the opportunity to control operations to minimize the probability of transport. When potential significant transport pathways are identified, the failure bias is relaxed to incorporate more realistic transport processes (such as sorption of contaminants) to more realistically understand potential consequences. An additional sensitivity analysis was performed for each pathway to explore the impact of various model parameters and conceptualizations on transport behavior.

6.1 MIGRATION POTENTIAL UNDER OIL PRODUCTION

Once hydraulic fracturing is completed, the well may go into production or may be shut in. Because oil production is the primary incentive, it is the more likely outcome. Oil production will establish a hydraulic gradient toward the wellbore that will limit the potential for migration of fluids in any other direction. Therefore, for most of the upper portion of the event-tree diagram (Figure 6-1), migration would be limited and no further assessment is needed (Scenarios OP1, OP2, and OP3). The only two exceptions would be (1) intermittent oil production because of poor economic or operational conditions or (2) natural gas (methane) vertical migration caused by lower fluid pressures during pumping (Scenario OP4 - methane migration).

6.1.1 Methane Migration

Although it is not a consequence of hydraulic fracturing, the possible vertical migration of gaseous methane is an additional contaminant migration process associated with hydrocarbon production. Oil production creates a zone of low fluid pressure surrounding the borehole that allows dissolved methane in the formation water to come out of solution as a gas. This can only happen if the fluid pressure is lowered below the vapor pressure of dissolved methane in the liquid phase. While pumping continues, this gas is drawn toward the well. Once the well is shut in, remaining gaseous methane may move vertically along a density gradient (See Figure 6-2).

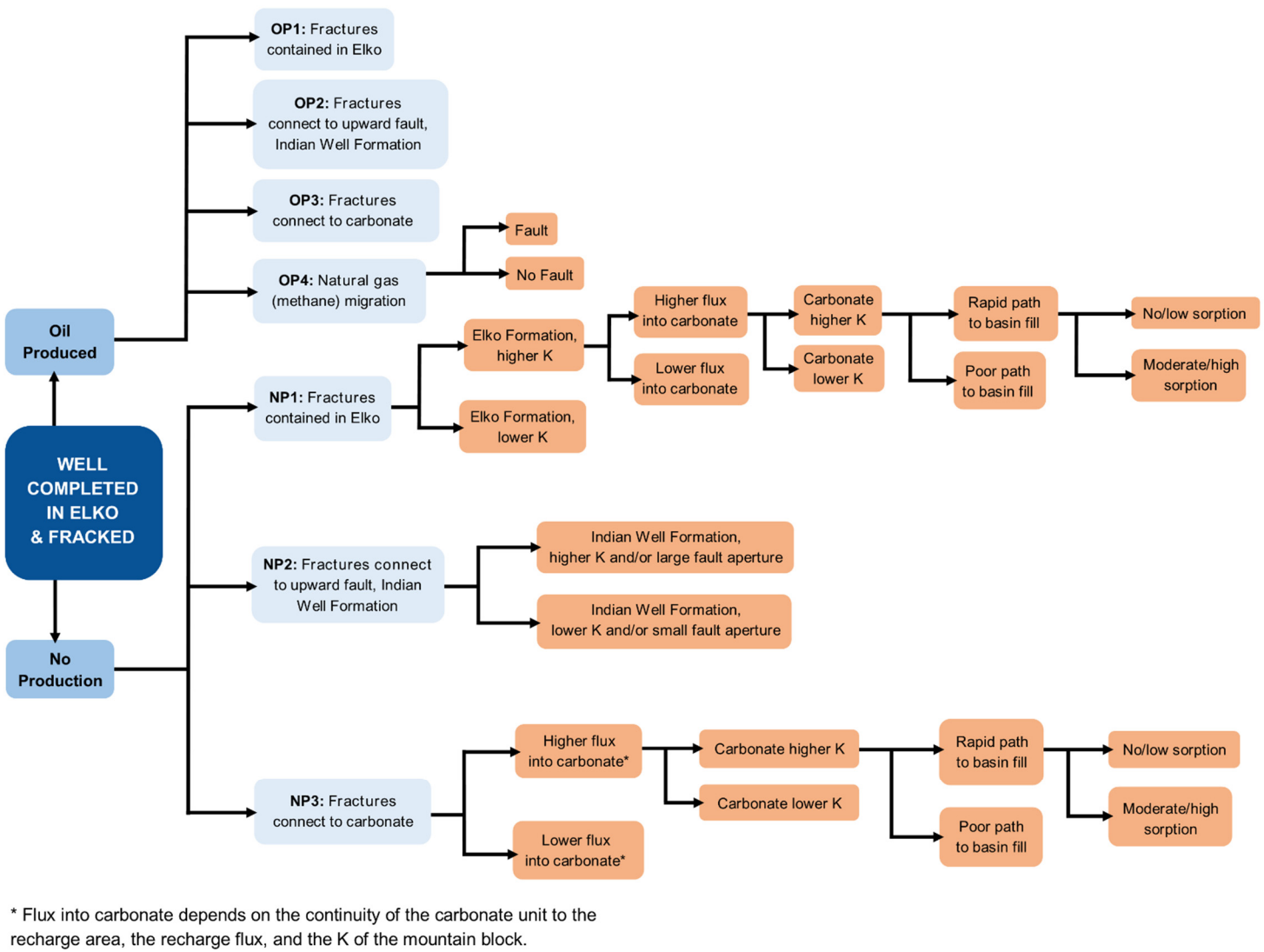

Figure 6-1. Event-tree diagram used for the evaluation of hydraulic fracturing fluid migration. OP1, -2, and -3 were not analyzed with a numerical model.

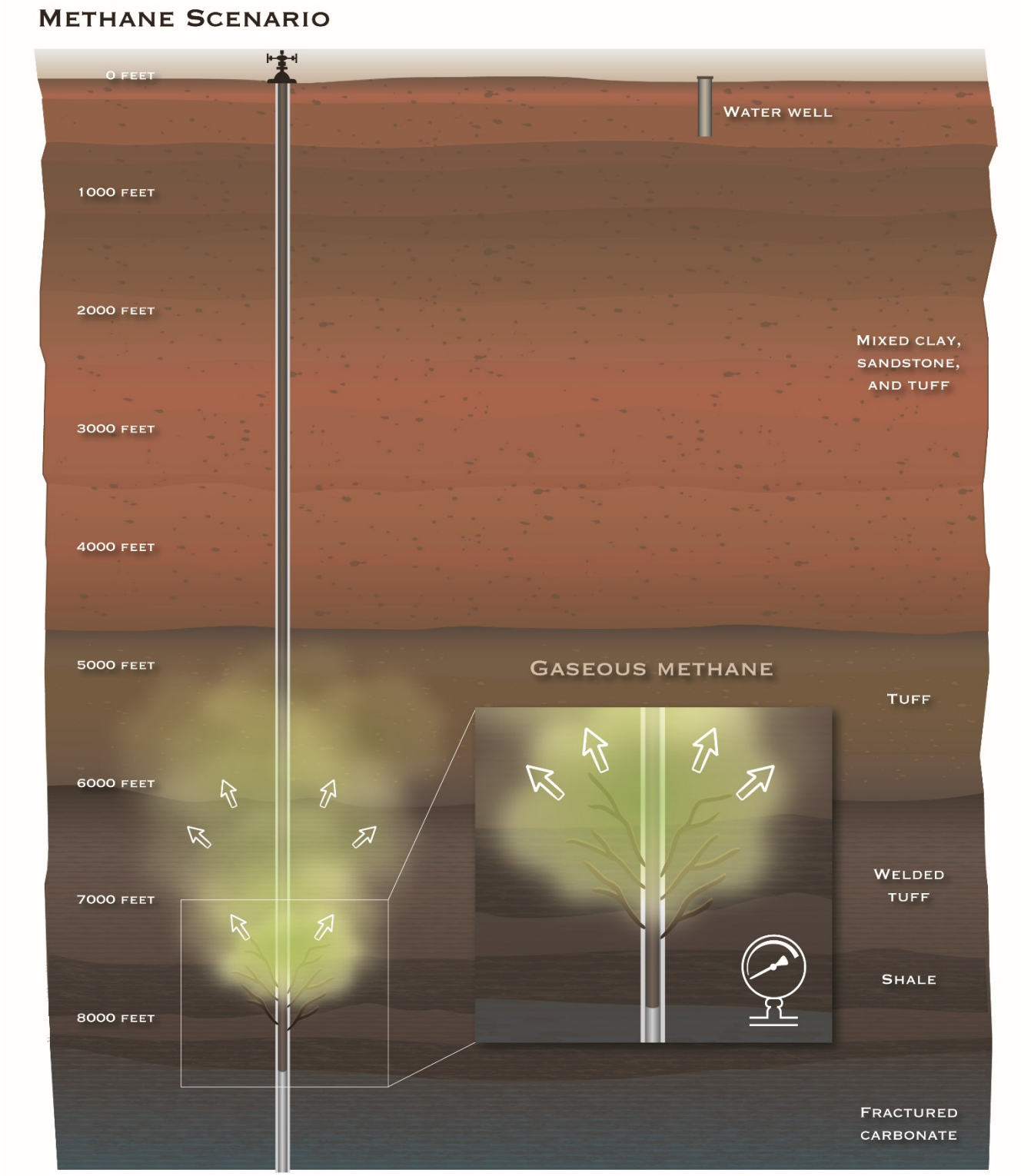

Figure 6-2. Methane degassing scenario (OP4). Dissolved methane in the targeted shale formation degasses as formation pressure drops because of pumping. Gaseous methane is transported vertically along a density gradient.

The methane gas migration scenario (NP4) was evaluated in detail using multiphase modeling techniques (see Appendix B). Two conditions were simulated to represent (1) a highly transmissive and steeply dipping fault that projects upward from the contact between the Elko and Indian Well Formations to the shallow aquifer and (2) no faults located between the Elko Formation and the shallow aquifer.

In both simulations, methane gas redissolves before reaching the shallow aquifer. Because of lower fluid pressures caused by oil production, immediately after methane gas is formed it migrates short distances vertically along a density gradient and to a lesser extent laterally under capillary pressures. As gas-phase methane migrates to cells with low concentrations of dissolved methane, it enters the liquid phase (redissolves) where it is effectively immobilized because of the low fluid-phase permeability. In the simulation without a vertical fault, methane gas migrates a total vertical distance of approximately 2,500 ft in 70 years before redissolving and becoming immobile. In the simulation that includes a high-permeability vertical fault, methane gas migrates a total vertical distance of 6,500 ft in 70 years before redissolving and becoming immobile. In both cases, vertical migration terminates before reaching the shallow basin-fill aquifer.

6.2 Migration Potential under Shut-In Conditions

If a well is shut in because oil is not found, then natural hydraulic conditions will govern flow. The generalized conceptual model for natural groundwater flow conditions is shown in Figure 6-3. Groundwater recharge occurs in the higher elevation mountain block and downward flow dominates in the Metamorphic Core Complex. The higher-permeability carbonate units tend to focus flow laterally toward the west side of the valley. If the western faults are of high enough permeability, upward flow can occur toward the shallow aquifer to ultimately discharge in local springs or in the Humboldt River. These conditions were explored in the computer models to determine the impact on the timing and magnitude of hydraulic fracturing fluid concentrations reaching shallow aquifers.

The Elko Formation thickness and its relationship to hydraulic fracture extent are particularly important for the transport of hydraulic fracturing fluids. In the vicinity of the two explorations wells, the top of the Elko Formation is between 7,500 and 9,500 ft below land surface (Figure 6-4). The thickness of the Elko Formation is also variable, being approximately 700 ft at M2C and 560 ft at M10C (Figure 6-4). Three paths are identified on the event tree and examined by numerical models for the condition of no oil production after hydraulic fracturing. The NP1 path explores the possibility of hydraulically induced fractures being contained in the Elko Formation. The NP2 path explores the possibility of a hydraulically induced fracture intersecting a natural vertical fault that extends upward to the Indian Well Formation. The NP3 path examines the impact of hydraulically induced fractures extending into the carbonate unit below the Elko Formation.

The intention of hydraulic fracturing in the well is to fracture the low-permeability oil shale members of the formation to enhance production to the well. There is no economic incentive to expend energy or materials to fracture beyond the targeted oil zone and connecting to permeable aquifers is counterproductive to the purpose of enhancing production from the oil shale. As a result, the expectation is that the hydraulic fracturing operation will be designed to contain the fractures within the Elko Formation (scenario NP1). This is consistent with the observation that the "vast majority of stimulated hydraulic fractures have a very limited vertical extent of < 100 m (330 ft)" (Davies *et al.*, 2012). Therefore, the design condition is that hydraulic fracturing fluids will be contained within the Elko Formation at the conclusion of the fracturing process.

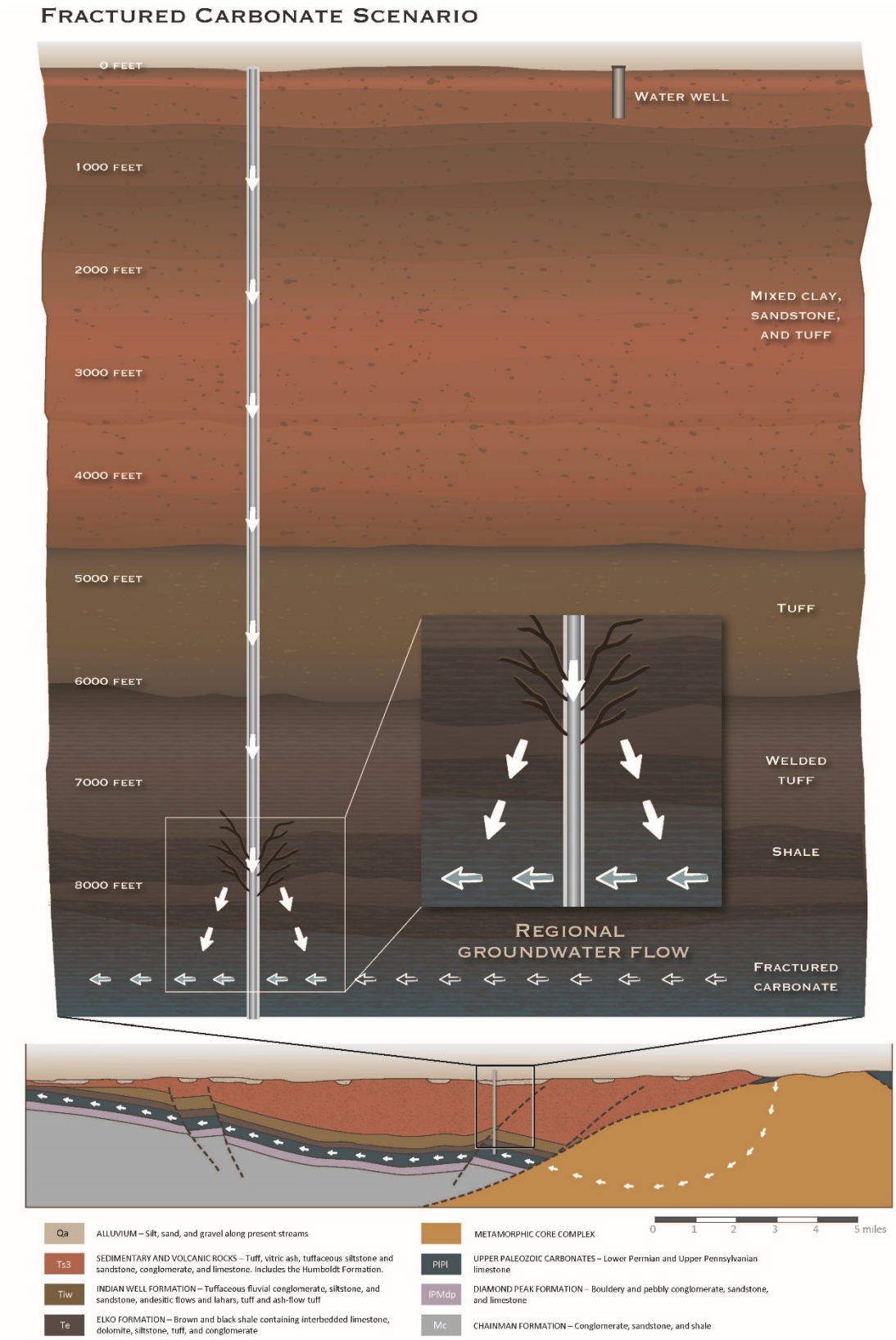

Figure 6-3. Conceptual model of the regional groundwater flow system in the upper Humboldt River Valley.

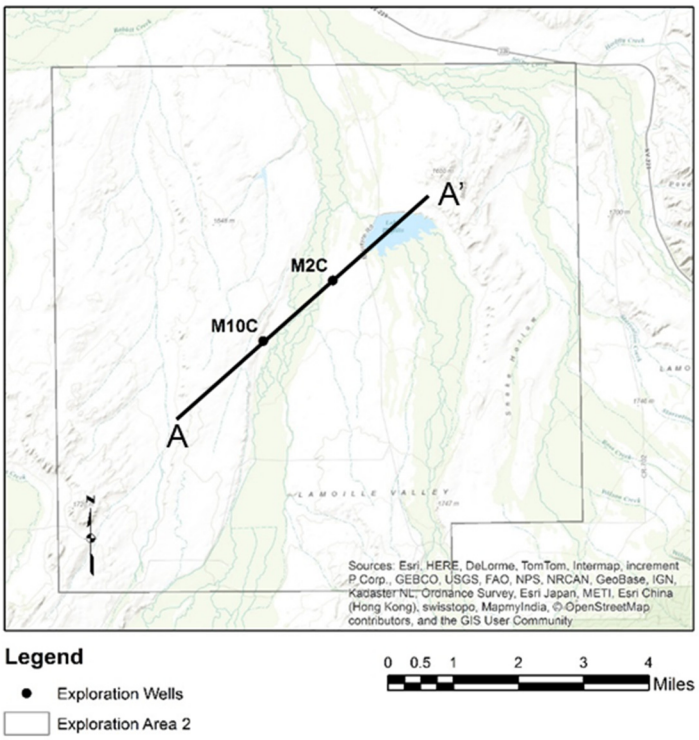

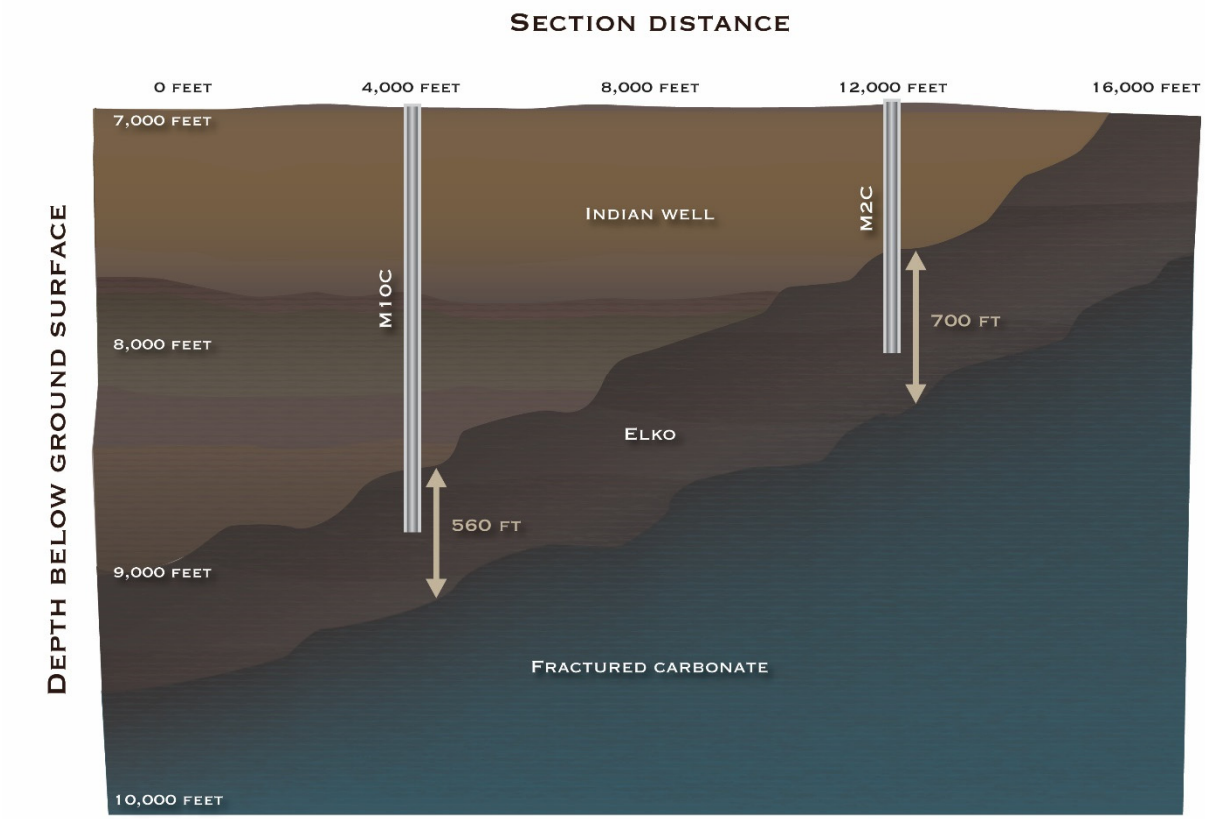

Figure 6-4. Geologic cross section within exploration area 2.

Permeability is an important parameter that governs the ability of hydraulic fracturing fluid to migrate. Permeability is a measure of the ability of water to transmit through subsurface materials. Sometimes hydrogeologists use the term hydraulic conductivity interchangeably with permeability. Strictly speaking, permeability is a property of porous media, whereas hydraulic conductivity is a function of permeability and the fluid. Permeability can be converted to hydraulic conductivity if the fluid viscosity and density are known. This distinction is important because oil field reservoir engineers typically use permeability, whereas hydrogeologists use hydraulic conductivity. The units of permeability are generally presented in darcies (or millidarcies), whereas hydraulic conductivity is presented in m/day (or cm/sec).

Generally, the permeability of oil shale formations is very low, which is evident by the accumulation of oil and the need for fracturing. But the Elko Formation has a variable character that contains not only shale, but also sandstones and a limestone-clast conglomerate that are probably at least moderately permeable. Table 6-1 provides a summary of hydraulic conductivity values for the Elko Formation. A total of 46 side-core samples were taken from the two exploration wells. Laboratory analysis yielded hydraulic conductivities ranging between 1×10^{-10} to 2×10^{-5} m/day and a geometric mean of 9×10^{-8} m/day. Laboratory analysis of hydraulic conductivity can be unreliable because the samples are highly disturbed and may not be representative of in-situ conditions. Drillstem tests within the Elko Formation from other exploration activities yielded a range of 2×10^{-4} to 5×10^{-4} with a geometric mean of 3×10^{-4}. It is difficult to determine the applicability of the drillstem tests because detailed lithology is not known for these wells and may represent hydraulic properties of other nonshale units (e.g., siltstone and limestone). For reference, Neuzil (1994) estimates the range in hydraulic conductivity for shale to be 10^{-11} to 10^{-4} m/day. Freeze and Cherry (1979) limit the range from 10^{-8} to 10^{-4} m/day.

Depending on the thickness of the various lithologies and their spatial distribution relative to the hydraulic fractures, none of which can be known with certainty throughout the area, fluid migration during shut-in conditions could be characterized by very low permeability (10^{-7} m/day) or moderate permeability (10^{-4} m/day) in the Elko Formation. If design conditions exist and the hydraulic fractures are contained within the Elko Formation with very low permeabilities, then computer modeling of flow and transport (see Appendix B) indicates that the migration of hydraulic fracturing fluid would not occur toward the carbonate unit and/or Indian Well Formation within 1,000 years. There is no time limit in Nevada's water quality regulations, but 1,000 years is adopted here as a timescale of concern, which is consistent with the timeframe used by the State of Nevada to evaluate contaminant migration in other settings, such as through the Federal Facility Agreement and Consent Order with the U.S. Department of Energy and Department of Defense.

If moderate permeability exists and migration of fracturing fluids is through the Elko Formation on a timescale of concern or if hydraulic fracturing operations do not occur per the expected design condition and create fractures extending vertically out of the production horizon, then the potential for transport in formations above and below the Elko Formation must be considered. Overlying the Elko Formation is the Indian Well Formation and beneath the Elko Formation are carbonate rocks. The Indian Well Formation may contain permeable horizons in coarse-grained intervals of sandstone, limestone, and welded tuff. Younger carbonate rocks (Permian and Pennsylvanian age) underlie the Elko Formation in the area of the two exploration wells. These rocks are characterized as moderately to highly permeable and may function as a pathway for groundwater flow from the mountain highlands to discharge through

Table 6-1. Shale permeability summary.

Source	K_{min} (m/day)	K_{max} (m/day)	K_{mean} (m/day)	Notes
Side-core laboratory tests	1×10^{-10}	2×10^{-5}	9×10^{-8}	Small sample size, disturbed sample, not in-situ
Drillstem tests	2×10^{-4}	5×10^{-4}	3×10^{-4}	Detailed lithologic composition not known (e.g., shale, siltstone, limestone)
Freeze and Cherry, 1979 - Shale	1×10^{-8}	1×10^{-4}	n/a	
Neuzil, 1994 - Shale	1×10^{-11}	1×10^{-4}	n/a	
Source zone model	1×10^{-7}	8×10^{-5}	n/a	Minimum based on geometric mean of side-core analysis and maximum based on expert judgement and an assessment of the drillstem tests, porosity, and fracture density

overlying, shallow aquifers and ultimately into the Humboldt River. Migration through either the Indian Well Formation or younger carbonate would occur in response to regional groundwater flow paths (as explored in the regional model in Chapter 4 and in Appendix B) and is subject to substantial uncertainty in the hydraulic properties (permeability and porosity) of the rocks because of sparse data.

The following sections first explore the release and migration of hydraulic fracturing fluids within the Elko Formation (Scenario NP1). Under this condition, migration of hydraulic fracturing fluid is initially governed by the permeability of the Elko Formation, and then other conditions that control the magnitude of deep circulation of fluids (e.g., permeable pathways to the carbonate, and then upward to the basin fill). Next, the model is used to address the possibility of migration to the overlying Indian Well Formation through vertical transmissive faults (Scenario NP2). In this case, migration is governed by the permeability in the Indian Well Formation. Scenario NP3 is similar to NP1, but the initial assumption is that hydraulically induced fractures extend directly into the carbonate. In this case, the features controlling transport are similar to Scenario NP1. Each section evaluates the consequence of the pathway in terms of hydraulic fracturing fluid migration.

6.2.1 Fractures Contained in Elko Formation – Scenario NP1

According to Davies *et al.* (2012), a vast majority of hydraulic fractures will be limited in the vertical extent to approximately less than 300 ft. Under these conditions, hydraulic fractures would be limited to the Elko Formation and migration toward adjacent geologic units will be controlled primarily by the permeability of the Elko Formation. Computer modeling of flow and transport indicates that migration does not occur on a timescale of concern if the Elko permeability is on the order of 10^{-7} m/day. If the Elko Formation permeability is on the order of 10^{-4} m/day, migration to adjacent geologic units could occur within timescales of interest (~1,000 years, as described above). Migration through a moderately permeable Elko Formation to the underlying carbonate unit is on the order of 100 years for conservative solutes.

The hydraulic head gradient in Exploration Area 2 is down, which directs flow to the carbonate unit located beneath the Elko Formation. Computer models were constructed to evaluate the migration potential from the Elko Formation to the carbonate unit that may act as a conduit for regional flow. The concept of the potential migration pathway is illustrated in Figure 6-3 (Scenario NP1).

If hydraulic fracturing fluid enters the underlying carbonate unit, migration is controlled by the fluid flux in the carbonate unit. Groundwater recharge from the mountainous region is the primary control on the carbonate flux. A variety of factors influence the groundwater recharge into the carbonate unit including:

- Disconnection or connection of the deep carbonate to the outcrop in the Ruby Mountains
- Magnitude of mountain-block recharge
- Hydraulic conductivity of the carbonate unit
- Hydraulic conductivity of the metamorphic core complex
- Hydraulic conductivity of the basin fill aquifer (Tertiary sediments)

Features that enhance a permeable connection between the recharge in the upper elevations and deep groundwater flow will increase the flow in the carbonate. As the connection or permeability in the mountain block decreases, shallow groundwater recharge is directed to the shallow basin fill aquifer and deep flow decreases.

If the flux rate into the carbonate is high enough, then transport is governed by the hydraulic conductivity of the carbonate unit. In the case of low carbonate hydraulic conductivity (10^{-2} m/day), transport is limited and does not occur within the timescale of concern (1,000 years). If the carbonate hydraulic conductivity is above 1 m/day, transport to the shallow aquifer will not be restricted.

Under conditions of higher hydraulic conductivity in the carbonate, transport to the shallow basin-fill aquifer may occur if there is a rapid pathway. Such a pathway would occur if there are permeable vertical faults located on the west side of the valley. Faults have been interpreted based on deep borehole information but the permeability of the faults is not known. If the fault apertures are small enough (10^{-4} m), permeability is limited and transport to the shallow aquifer does not occur.

The conditions of significant carbonate flux and a permeable pathway to the shallow aquifer need to be in place for migration of hydraulic fracturing fluid to shallow aquifers to occur in less than 1,000 years. Even under these conditions, transport processes can significantly reduce or eliminate migration to the shallow aquifer. The most important factors governing migration are the chemical constituents of interest and their sorption, the available contaminant mass, matrix diffusion, dispersion, degradation capacity, and maximum contaminant levels.

Dissolved solutes fall into two broad classes: conservative and reactive. Conservative solutes do not react with aquifer material nor do they degrade. Many chemical species adsorb to mineral particles, which causes a solute front to advance more slowly than water molecules. The rate of solute movement can be determined by the retardation equation:

$$v_c = \frac{v_w}{1 + \frac{\rho_b K_d}{\theta}} \tag{6-1}$$

where v_w is the average linear velocity of pure water (L/T), v_c is the velocity of solute front (L/T), ρ_b is the bulk density of the aquifer material (M/L^3), θ is the porosity, and K_d is the distribution coefficient (sorption coefficient) that describes the magnitude of sorption for a specific solute and aquifer material (L^3/M). The denominator in Equation 6-1 is referred to as the retardation factor because it describes the ratio at which the solute movement is slowed compared with water.

Synthetic organic chemicals can be adsorbed by organic carbon that resides in aquifer material. Sorption coefficients for these chemicals can be estimated as the product of the soil-water partition coefficient (K_{oc}) and the fraction of organic carbon in an aquifer. Other relationships have been developed between a chemical's octanol-water partition coefficient (K_{ow}), which is a measure of an organic chemical's ability to dissolve in water, and K_{oc}. Soil-water partition and octanol-water partition coefficients are presented when available for a few of the chemicals used in the hydraulic fracturing process (see Tables C-1, C-2, and C-3). The octanol-water and soil-water partition coefficients are not known for many of the hydraulic fracturing chemicals.

For reference, retardation coefficients were calculated for chemicals used in the hydraulic fracturing process (see Tables C-1 through C-3) and other selected contaminants (Figure 6-5). In the context of the migration pathway analysis, those chemicals with retardation factors greater than 10 effectively become immobile in timescales of concern (1,000 years). For the chemicals shown in Figure 6-5, 61 percent have retardation factors greater than 10 and can be considered immobile species.

For the purposes of the solute transport modeling, ethanol is used as a surrogate chemical because it has negligible sorption (R = 1.2). Ethylene glycol monobutyl ether (R = 2.1) and 2,2-Dibromo-3-nitrilopropionamide have moderate sorption (R = 5.6) and were included in a sensitivity analysis to determine the impact of increased sorption on the transport behavior.

The mass of chemical compounds available for migration after hydraulic fracturing depends on the amount injected and the amount subsequently removed during flowback testing. Some quantity of injected chemicals will remain in the subsurface after flowback testing, but that amount is variable and depends on many conditions and processes, and therefore cannot be predicted. Given that uncertainty, the modeling conservatively ignores the flowback process of contaminant removal, which results in calculated concentrations that are higher than expected.

Many chemical species degrade quickly through biodegradation processes. Also known as natural attenuation, biodegradation serves to lower contaminant concentrations over time, which decreases the potential for migration to the shallow aquifer. Degradation capacity is dependent on many factors, including temperature, pH, and general geochemical conditions in the subsurface. Unfortunately, little information is known regarding the degradation capacity of the chemicals used in the hydraulic fracturing process. It is therefore difficult to quantify the impact of degradation on the migration potential and is not included explicitly in the transport modeling.

The transport of solutes in fractured media is controlled by a process known as matrix diffusion. Matrix diffusion is the redistribution of a contaminant into a matrix block by transverse molecular diffusion. The net result is retardation of solute plumes by up to two orders of magnitude (McKay *et al.*, 1993) in addition to sorption effects. In other words, matrix diffusion could potentially slow the migration of hydraulic fracturing fluid such that migration would not occur within 1,000 years.

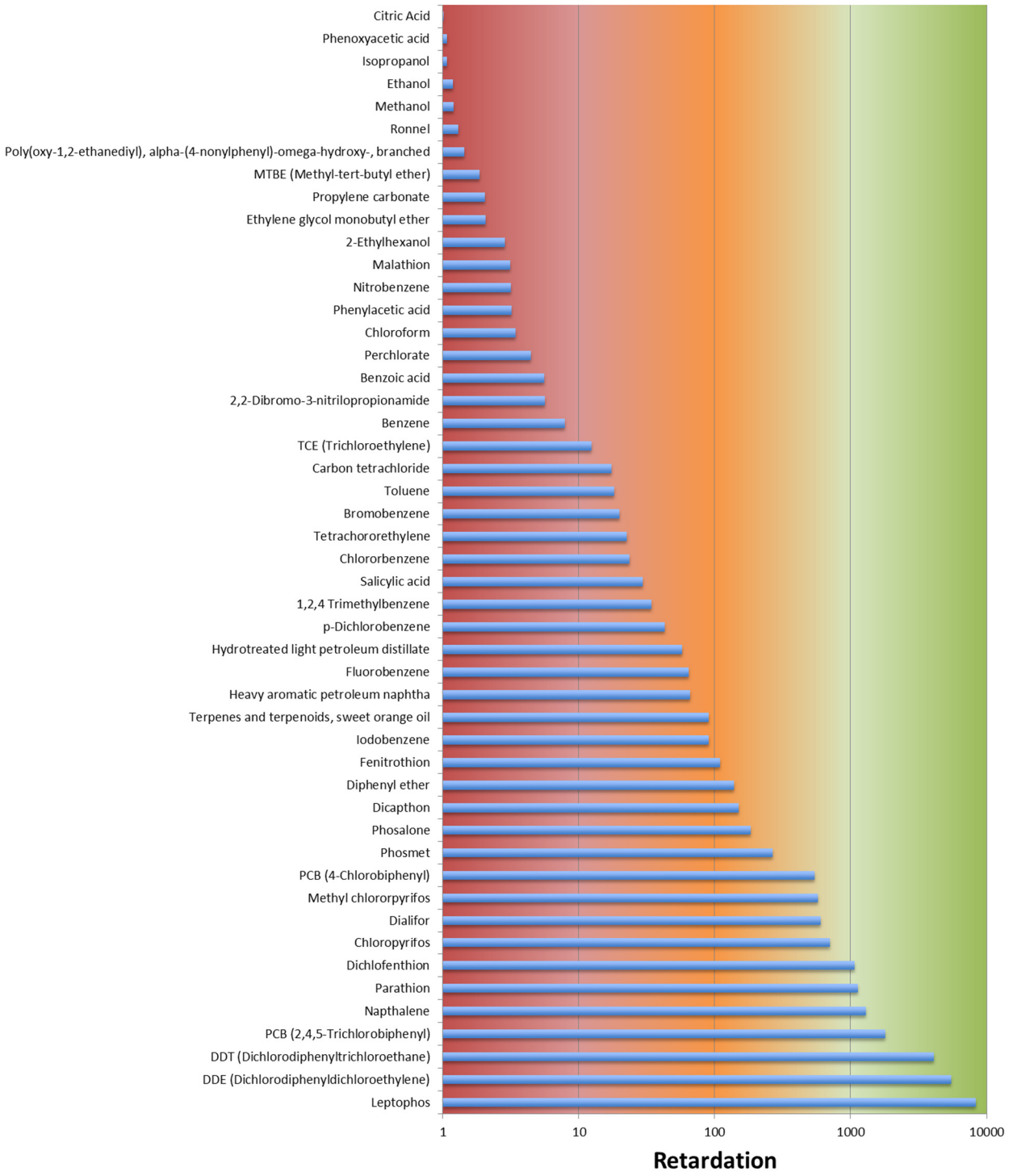

Figure 6-5. Retardation factors for selected chemicals within the carbonate system.

Matrix diffusion rates are dependent on matrix porosity, fracture aperture, and the size of the solute molecule. Tracer tests are generally needed to accurately quantify matrix diffusion rates, which would be intractable for all of the chemical species of interest. The transport modeling assumed moderate matrix diffusion rates in the Elko Formation but none in the other geologic units. Increasing matrix diffusion rates in all fractured units would decrease the migration potential. Because the information is not available to quantify the magnitude of matrix diffusion, the model predictions rely on conservative assumptions that favor transport.

The Maximum Contaminant Level (MCL) is the maximum concentration of a chemical that is allowed in public drinking water systems. The MCL is established by the U.S. Environmental Protection Agency (EPA). Generally, the migration potential for contaminants is evaluated by comparing predicted concentrations within a timeframe of interest with an MCL for specific chemicals of interest, but the MCLs are not available for many of the hydraulic fracturing chemicals.

A sensitivity analysis was performed to determine the impact of various hydraulic parameters, transport parameters, and geologic conceptualizations on hydraulic fracturing fluid migration. The 13 simulations are detailed in Table 6-2. Migration potential of hydraulic fracturing fluids is determined by monitoring simulated concentrations at aquifer depths that are shallower than 600 feet. In many simulations, concentrations were not detectable in the shallow aquifer and as such breakthrough curves are not presented. Although the timescale of concern is 1,000 years, the time horizon for the simulations is 2,000 years to fully assess transport results. Three metrics are used to quantify migration behavior to the shallow aquifer. Initial breakthrough time is calculated as the time in which relative concentrations (C/C_0) exceed 10^{-4}. Peak breakthrough is the time at which peak breakthrough occurs within the first 600 ft of the shallow aquifer and peak concentration is the relative peak concentration (C/C_0).

Six of the 13 simulations did yield breakthrough to the shallow aquifer within the 1,000 year timescale of concern. Two scenarios (Case 5: Low carbonate K, and Case 7: Low basin fill K) resulted in unrealistically high heads in the mountain block, so solute transport was not simulated. Four other cases (Case 3: Low recharge, Case 6: High basin fill K, Case 9: Small fault aperture, and Case 13: Increased sorption) did not result in transport to the shallow aquifer within 1,000 years. The low recharge case (Case 3) results in significantly lower fluid velocities in the carbonate unit. Case 6 (High basin fill K) directs most of the mountain-block recharge into the shallow aquifer, which reduces the fluid flux to the deeper units including the carbonate unit. Case 9 (Small fault aperture) reduces the permeability of the faults located on the west side of the valley, which restricts fluid flow upward to the shallow aquifer. Case 13 (Increased sorption) reduces the effective solute velocity because of increased reactivity.

Seven of the scenarios resulted in migration to the shallow aquifer within the timescale of concern. The base simulation (Case 1) represents the most likely hydraulic and transport parameter values and resulted in an initial breakthrough to the shallow aquifer in just under 700 years. Peak breakthrough occurred at 943 years with a relative concentration of 2×10^{-4}. Maximum concentrations of ethanol at this magnitude are below detectable limits.

Doubling mountain block recharge (from 0.003 to 0.006 m/day) increases deep fluid flux and decreases the migration time to the shallow aquifer (Case 2). Initial breakthrough to the shallow aquifer occurred at 400 years. Peak breakthrough occurred at 559 years with a relative concentration of 2×10^{-4}. Maximum concentrations of ethanol at this magnitude are below detectable limits.

Table 6-2. Summary of flow and transport simulations performed for Scenario NP1 (Fractures contained in Elko Formation) and associated hydraulic and transport parameters and breakthrough results to the shallow aquifer.

#	Simulation	Notes	Recharge (m/day)	Carbonate K (m/day)	Basin Fill K (m/day)	Fault Aperture (m)	Metamorphic K (m/day)	Retardation (-)	Initial Breakthrough (years)	Peak Breakthrough (years)	Peak Concentration (C/C_0)
1	Base Scenario		0.003	3	1	0.001	0.005	1.2	697	943	2.4E-04
2	High Recharge		0.006	3	1	0.001	0.005	1.2	400	559	2.2E-04
3	Low Recharge	1	0.0009	3	1	0.001	0.005	1.2	n/a	n/a	n/a
4	High Carbonate K		0.003	40	1	0.001	0.005	1.2	562	775	2.6E-04
5	Low Carbonate K	2	0.003	0.01	1	0.001	0.005	1.2	n/a	n/a	n/a
6	High Basin Fill K		0.003	3	2	0.001	0.005	1.2	1132	1500	2.2E-04
7	Low Basin Fill K	2	0.003	3	0.01	0.001	0.005	1.2	n/a	n/a	n/a
8	Large Fault Aperture		0.003	3	1	0.01	0.005	1.2	636	873	2.9E-04
9	Small Fault Aperture		0.003	3	1	0.0001	0.005	1.2	1428	1967	3.8E-05
10	High MMC K		0.003	3	1	0.001	0.05	1.2	419	605	3.1E-04
11	Low MMC K		0.003	3	1	0.001	0.0005	1.2	889	1191	1.9E-04
12	Carbonate Connectivity	3	0.003	3	1	0.001	0.005	1.2	282	425	2.6E-04
13	Increased Sorption	4	0.003	3	1	0.001	0.005	2.1	1147	1491	1.6E-04

Notes:

1. Simulation did not result in transport to the surface within 2,000 years, breakthrough curves not presented.
2. Parameters resulted in unrealistic heads in the mountain block, transport was not simulated.
3. Carbonate connectivity case assumes carbonate unit is continuous from depth to the surface in the Ruby Mountains.
4. Increased sorption case simulates ethylene glycol monobutyl ether versus the ethanol for all other simulations.

Increasing the carbonate hydraulic conductivity from 3 to 40 m/day increases fluid flux and solute velocities (Case 4). Initial breakthrough to the shallow aquifer occurred at 562 years. Peak breakthrough occurred at 775 years with a relative concentration of 3×10^{-4}. Maximum concentrations of ethanol at this magnitude are below detectable limits.

Increasing the fault aperture for faults occurring on the west side of the valley allows for increased upward fluid flow and more rapid migration to the shallow aquifer (Case 8). Initial breakthrough to the shallow aquifer occurred at 636 years. Peak breakthrough occurred at 873 years with a relative concentration of 3 x 10^{-4}. Maximum concentrations of ethanol at this magnitude are below detectable limits.

Similar to Case 2 (High recharge) increasing the hydraulic conductivity (0.005 to 0.05 m/day) of the metamorphic core complex (Ruby Mountains) increases deep fluid flow to the carbonate unit and increases fluid flux and solute velocities (Case 10). Initial breakthrough to the shallow aquifer occurred at 419 years. Peak breakthrough occurred at 605 years with a relative concentration of 3 x 10^{-4}. Maximum concentrations of ethanol at this magnitude are below detectable limits.

Lowering the hydraulic conductivity (0.005 to 0.0005 m/day) of the metamorphic core complex (Ruby Mountains) decreases deep fluid flow to the carbonate unit and reduces fluid flux and solute velocities (Case 11). Initial breakthrough to the shallow aquifer occurred at 889 years. Peak breakthrough occurred at 1,191 years with a relative concentration of 2 x 10^{-4}. Maximum concentrations of ethanol at this magnitude are below detectable limits.

An additional simulation was performed to test another conceptualization of the carbonate connection to land surface as shown in Figure 6-6 (Case 12). The preferred conceptualization is that the carbonate unit terminates against the range-front fault on the east side of the valley, in agreement with three-dimensional seismic data. An alternate, lower probability, interpretation is that the carbonate rocks are continuous from the carbonate outcrops in the Ruby Mountains to the deep subsurface below the valley. Introducing this direct connection of a high permeable unit from land surface to depth allows for increased deep fluid flux and solute velocities. This scenario results in the earliest initial breakthrough to the shallow aquifer at 282 years. Peak breakthrough occurred at 425 years with a relative concentration of 3 x 10^{-4}. Maximum concentrations of ethanol at this magnitude are below detectable limits.

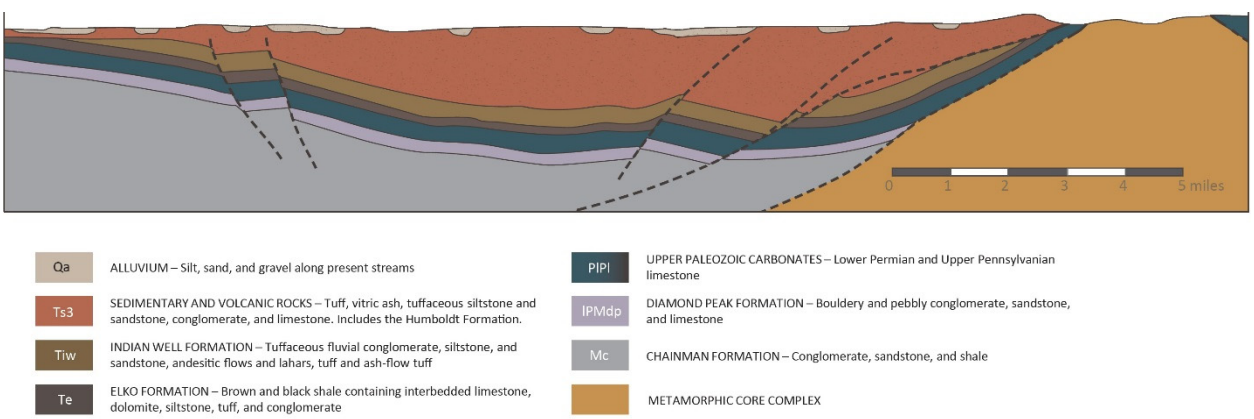

Figure 6-6. Conceptual model for the NP1 scenario in which fractures are contained in the Elko Formation. Injected hydraulic fracturing fluid migrates through moderate permeability shale into the underlying carbonate formation, where it is transported along a regional flow path.

6.2.2 Fractures Connect to Upward Fault in Indian Well Formation: Scenario NP2

Although hydraulic gradients are generally downward in Exploration Area 2, upward migration potential was investigated. In this scenario, it was assumed that hydraulic fractures penetrate upward into the overlying Indian Well Formation and connect with a hypothetical preexisting or reactivated fault zone. Although a connection between the hydraulically induced fracture and fault is made, the induced pressure from the hydraulic fracturing operation is assumed to be only enough to transport fluid to the end of the hydraulically induced fracture. Migration through the naturally occurring faults is simulated under a natural flow regime and an initial concentration at the base of the fault (Figure 6-7).

For Scenario NP2, none of the nine simulations resulted in migration of hydraulic fracturing fluid to the shallow aquifer within timescales of concern (1,000 years). For most simulations, migration occurred vertically through the fault only as far as the thickness of the Indian Well Formation. In one case, the permeability of the Tertiary sediments was reduced, which forced more fluid through the Indian Well Formation. This resulted in a small amount of lateral transport but no significant vertical transport. The variation of fault parameters, system recharge, and formation conductivities had only a minor effect on migration pathways.

6.2.3 Fractures Connect to Carbonate: Scenario NP3

As noted above, there is no economic incentive to expend energy or materials to fracture beyond the targeted oil zone and connecting to permeable aquifers is counterproductive to the purpose of enhancing production from the oil shale. As a result, the expectation is that the hydraulic fracturing operation will be designed to contain the fractures within the Elko Formation.

The likelihood of hydraulically stimulated fractures extending beyond the target zone is investigated. Davies *et al.* (2012) reviewed the heights (n = 1,170) of upward propagating hydraulic fractures from several thousand fracturing operations in the Marcellus, Barnett, Woodford, Eagle Ford, and Niobrara Shale sites. Stimulated fracture height is controlled by many factors, including fluid injection volume, local stress field, rock material properties (e.g., Young's modulus), and natural variations in lithology. Figure 6-8 shows the probability of nonexceedance against downward propagating stimulated fracture heights (Davies *et al.*, 2012). Stimulated fractures that propagate downward are of interest because the carbonate unit lies beneath the Elko Formation and may have high permeability. For reference, the average full- and half-thickness of the Elko Formation are plotted. If a stimulated fracture is initiated at the top of the Elko Formation, there is a 95 percent probability that it will not extend into the carbonate unit. Likewise, if a fracture is initiated at the midpoint of the Elko Formation there is an 82 percent probability that it will not extend into the carbonate unit.

Natural variations in lithology tend to provide natural barriers to propagation because of higher confining stress or high permeability, which allows the fluid to bleed off (Fisher and Warpinski, 2011; Davies *et al.*, 2012). King *et al.* (2008) noted that in the Barnett Shale the Viola and Ellenberger Limestone (i.e., carbonate) located below the Barnett Shale can limit the downward propagation of hydraulic fractures.

Flewelling *et al.* (2013) analyzed the upward development of over 12,000 hydraulic fractures in North America using microseismic data. A mathematical relationship was developed between the amount of hydraulic fracturing fluid used in the stimulation process and fracture height. Although the Flewelling *et al.* (2013) study focused solely on upward propagating fractures, understanding bounds on fracture

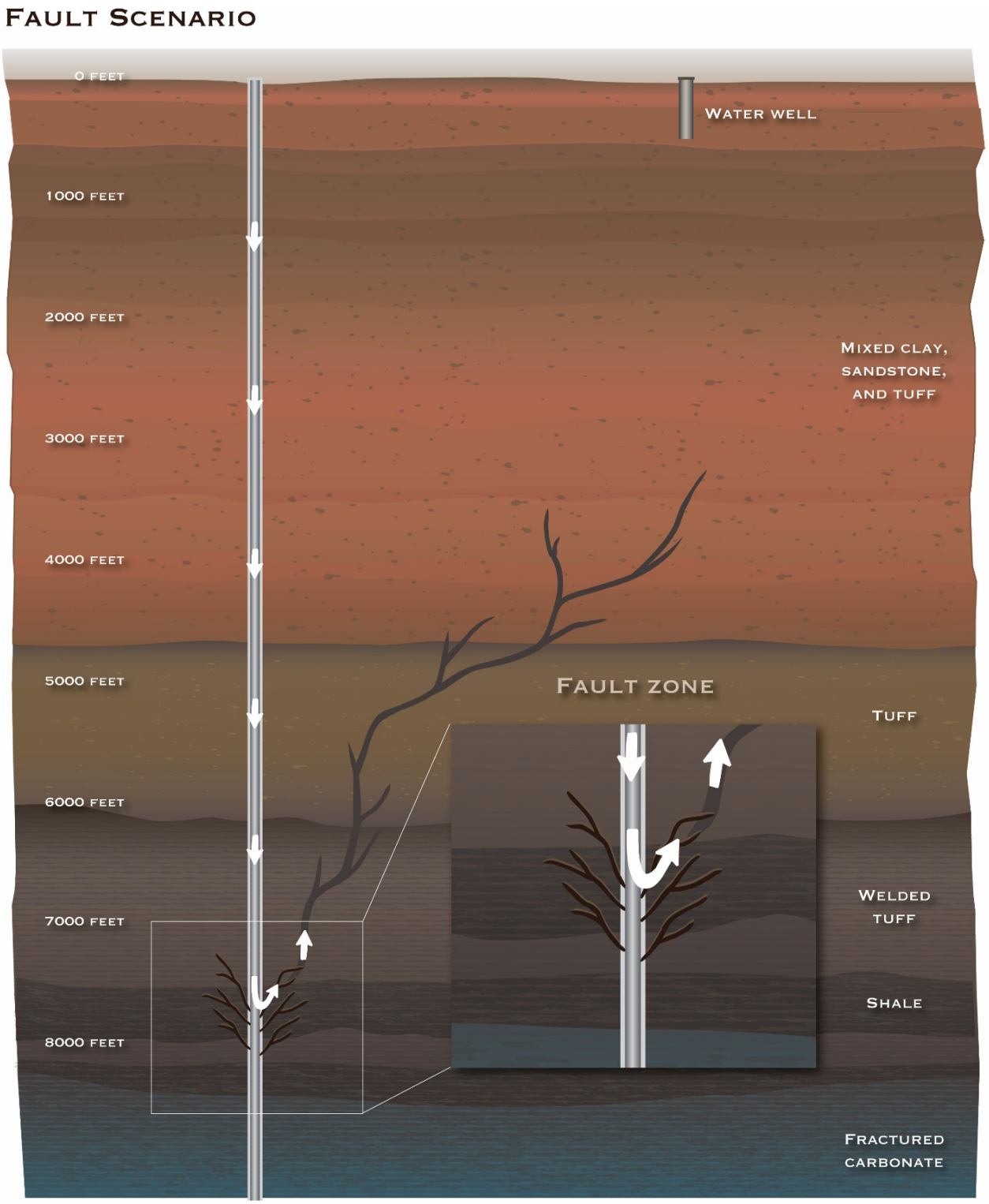

Figure 6-7. Scenario NP2: Fractures connect to an upward fault to the Indian Well Formation.

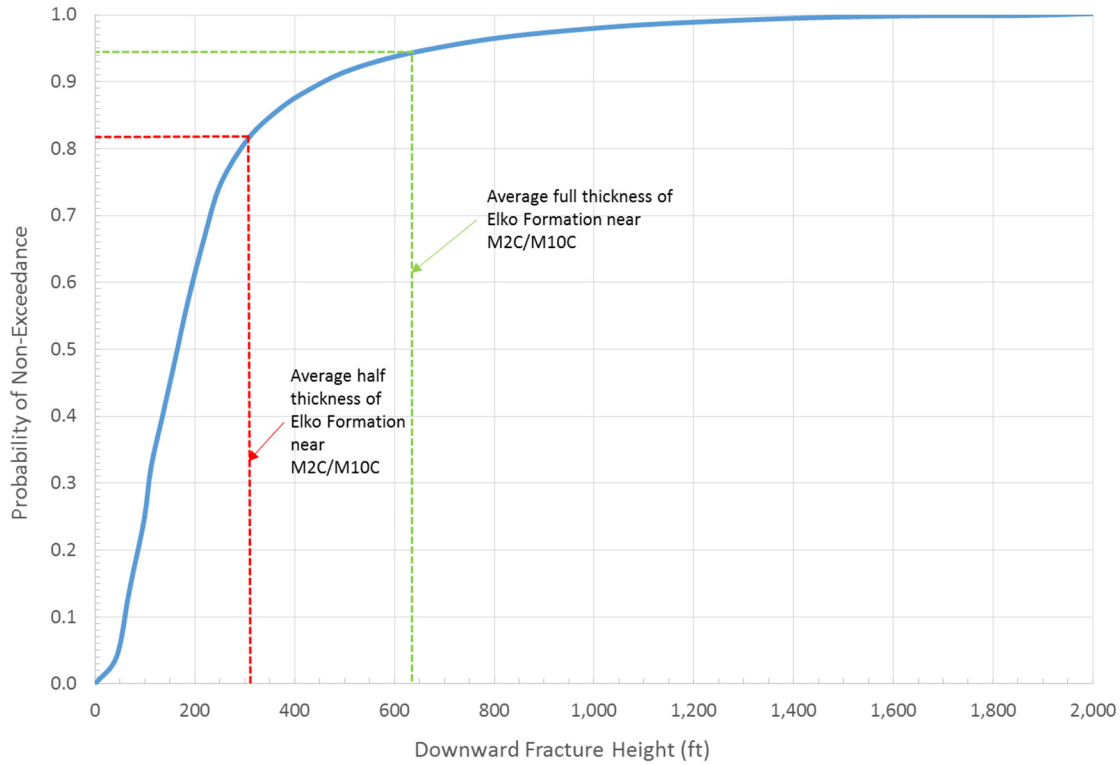

Figure 6-8. Probability of nonexceedance against downward propagating stimulated fracture height (ft). Adapted from Davies *et al.*, 2012.

growth may be useful. Figure 6-9 shows the observed upward fracture heights versus hydraulic fracture fluid volume injection and the functional relationship between injection volume and fracture height, which appears to be an upper bound. For reference, the average injection volume (300,000 gallons) for the three stimulation operations conducted by Noble Energy in the upper Humboldt River Basin are plotted. The observed fracture heights range from less than 1 m (3 ft) to 300 m (1,000 ft).

Although the likelihood of stimulated fractures extending into the carbonate unit is low, it is a possibility. Flow and transport models were used to evaluate the potential migration of hydraulic fracturing fluid under the condition that stimulated fractures extend into the carbonate unit. The models initiated hydraulic fracturing fluid at the top of the carbonate unit and allowed for migration under natural conditions.

Similar to the NP1 event (fractures contained in Elko) a sensitivity analysis was performed to determine the impact of various hydraulic parameters, transport parameters, and geologic conceptualizations on hydraulic fracturing fluid migration. The 13 simulations are detailed in Table 6-3. The primary difference between the NP1 event (Section 6.2.1) and NP3 is that the hydraulically induced fractures are allowed to connect directly to the carbonate unit. As noted above there is there is a 95 percent probability that fractures will not extend into the carbonate unit, but this event calculates the migration behavior should it occur. The results of this event are analogous to the NP1 event, but the calculated travel times to the shallow aquifer do not include transport within the Elko Formation. This effectively reduces the travel times by the 50 to 100 years required to travel through the Elko formation.

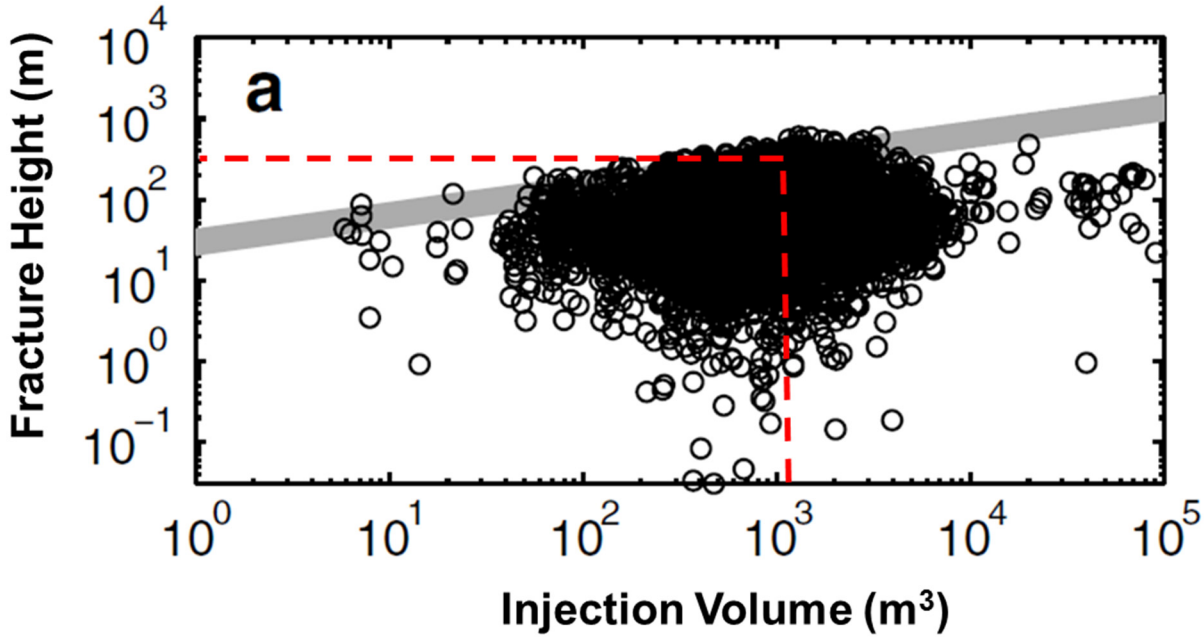

Figure 6-9. Observed upward fracture heights versus hydraulic fracture fluid volume injection. The thick gray line represents the functional relationship between injection volume and fracture height developed by Flewelling *et al.*, 2013. The dashed red line represents the average injection volume used by Noble Energy in the three stimulation operations.

Six of the 13 simulations yield breakthrough to the shallow aquifer within the timescale of concern (1,000 years). Two scenarios (Case 5: Low carbonate K, and Case 7: Low basin fill K) resulted in unrealistically high heads in the mountain block, so solute transport was not simulated. Four other cases (Case 3: Low recharge, Case 6: High basin fill K, Case 9: Small fault aperture, and Case 13: Increased sorption) did not result in transport to the shallow aquifer within 1,000 years. The low recharge case (Case 3) results in significantly lower fluid velocities in the carbonate unit. Case 6 (High basin fill K) directs most of the mountain-block recharge into the shallow aquifer which reduces the fluid flux to the deeper units including the carbonate unit. Case 9 (Small fault aperture) reduces the permeability of the faults located on the west side of the valley restricting fluid flow upward to the shallow aquifer. Case 13 (Increased sorption) reduces the effective solute velocity due to increased reactivity.

Seven of the scenarios resulted in migration to the shallow aquifer within the timescale of concern. The base simulation (Case 1) represents the most likely hydraulic and transport parameter values and resulted in an initial breakthrough to the shallow aquifer in 632 years. Peak breakthrough occurred at 838 years with a relative concentration of 4×10^{-4}. Maximum concentrations of ethanol at this magnitude are below detectable limits. Recall that the effect of flowback testing is not included in the model and would result in even lower concentrations.

Doubling mountain block recharge (from 0.003 to 0.006 m/day) increases deep fluid flux and decreases the migration time to the shallow aquifer (Case 2). Initial breakthrough to the shallow aquifer occurred at 347 years. Peak breakthrough occurred at 460 years with a relative concentration of 4×10^{-4}. Maximum concentrations of ethanol at this magnitude are below detectable limits.

Table 6-3. Summary of flow and transport simulations performed for Scenario NP3 (fractures connect to carbonate) and associated hydraulic and transport parameters and breakthrough results to the shallow aquifer.

#	Simulation	Notes	Recharge (m/day)	Carbonate K (m/day)	Basin Fill K (m/day)	Fault Aperture (m)	Metamorphic K (m/day)	Retardation (-)	Initial Breakthrough (years)	Peak Breakthrough (years)	Peak Concentration (C/C_0)
1	Base Scenario		0.003	3	1	0.001	0.005	1.2	632	838	3.520E-04
2	High Recharge		0.006	3	1	0.001	0.005	1.2	347	460	4.101E-04
3	Low Recharge	1	0.0009	3	1	0.001	0.005	1.2	n/a	n/a	n/a
4	High Carbonate K		0.003	40	1	0.001	0.005	1.2	501	671	4.079E-04
5	Low Carbonate K	2	0.003	0.01	1	0.001	0.005	1.2	n/a	n/a	n/a
6	High Basin Fill K		0.003	3	2	0.001	0.005	1.2	1055	1395	2.894E-04
7	Low Basin Fill K	2	0.003	3	0.01	0.001	0.005	1.2	n/a	n/a	n/a
8	Large Fault Aperture		0.003	3	1	0.01	0.005	1.2	572	770	4.359E-04
9	Small Fault Aperture		0.003	3	1	0.0001	0.005	1.2	1334	1857	4.706E-05
10	High MMC K		0.003	3	1	0.001	0.05	1.2	365	499	5.050E-04
11	Low MMC K		0.003	3	1	0.001	0.0005	1.2	816	1085	2.639E-04
12	Carbonate Connectivity	3	0.003	3	1	0.001	0.005	1.2	235	320	5.112E-04
13	Increased Sorption	4	0.003	3	1	0.001	0.005	2.1	1064	1387	2.379E-04

Notes:

1. Simulation did not result in transport to the surface within 2000 years, breakthrough curves not presented.
2. Parameters resulted in unrealistic heads in the mountain block, transport was not simulated.
3. Carbonate connectivity case assumes carbonate unit is continuous from depth to the surface in the Ruby Mountains.
4. Increased sorption case simulates ethylene glycol monobutyl ether versus the ethanol for all other simulations.

Increasing the carbonate hydraulic conductivity from 3 to 40 m/day increases fluid flux and solute velocities (Case 4). Initial breakthrough to the shallow aquifer occurred at 501 years. Peak breakthrough occurred at 671 years with a relative concentration of 4×10^{-4}. Maximum concentrations of ethanol at this magnitude are below detectable limits.

Increasing the fault aperture for faults occurring on the west side of the valley allows for increased upward fluid flow and more rapid migration to the shallow aquifer (Case 8). Initial breakthrough to the shallow aquifer occurred at 572 years. Peak breakthrough occurred at 770 years with a relative concentration of 4×10^{-4}. Maximum concentrations of ethanol at this magnitude are below detectable limits.

Similar to Case 2 (High recharge), increasing the hydraulic conductivity (0.005 to 0.05 m/day) of the metamorphic core complex (Ruby Mountains) increases deep fluid flow to the carbonate unit and increases fluid flux and solute velocities (Case 10). Initial breakthrough to the shallow aquifer occurred at

365 years. Peak breakthrough occurred at 499 years with a relative concentration of 5 x 10^{-4}. Maximum concentrations of ethanol at this magnitude are below detectable limits.

Lowering the hydraulic conductivity (0.005 to 0.0005 m/day) of the metamorphic core complex (Ruby Mountains) decreases deep fluid flow to the carbonate unit and reduces fluid flux and solute velocities (Case 11). Initial breakthrough to the shallow aquifer occurred at 816 years. Peak breakthrough occurred at 1,085 years with a relative concentration of 3 x 10^{-4}. Maximum concentrations of ethanol at this magnitude are below detectable limits.

An additional simulation was performed to test another conceptualization of the carbonate connection to land surface as shown in Figure 6-5 (Case 12). The preferred conceptualization is that the carbonate unit terminates against the range-front fault on the east side of the valley, which is in agreement with three-dimensional seismic data. The alternative conceptualization of the carbonate unit continuing upward to land surface, for a continuous carbonate pathway from the outcrops in the Ruby Mountains to the deep valley, is investigated as a low probability scenario. Introducing this direct connection of a high permeable unit from land surface to depth allows for increased deep fluid flux and solute velocities. This scenario results in the earliest initial breakthrough to the shallow aquifer occurred at 235 years. Peak breakthrough occurred at 320 years with a relative concentration of 3 x 10^{-4}. Maximum concentrations of ethanol at this magnitude are below detectable limits.

7.0 CONCLUSIONS/RECOMMENDATIONS

The following conclusions and recommendations can be drawn from this Interim Final Study. As described in the MOU establishing the AQUA Program, additional data might be collected if future oil and gas development occurs in the exploration areas that will be incorporated in any future updates to this work.

- Water-quality monitoring established a pre-fracturing baseline for surface water and groundwater in the exploration areas. The constituents measured include those present in natural gas associated with petroleum reservoirs, refined hydrocarbons, and related chemical compounds associated with surface exploration activities, compounds associated with generic hydraulic fracturing fluids, and chemical, isotopic, and radiochemical constituents found in water. Surface and groundwater samples collected prior to and following hydraulic fracturing in Exploration Area 2 do not indicate any significant changes in water-quality parameters between pre- and post-fracturing samples.
- Sampling of shallow wells, springs, and surface water indicates that low levels of biogenically derived dissolved methane occur naturally throughout the upper Humboldt Basin, making methane problematic as an indicator of reservoir fluids. Any methane monitoring should include isotopic analysis of carbon and hydrogen to distinguish biogenic and thermogenic (oil reservoir) sources.
- Useful markers for monitoring the incursion of reservoir-associated fluids into the near-surface environment are Total Dissolved Solids (or the related field measurement of electrical conductivity), chloride, and propane. Methanol, ethanol, and 2-butoxyethanol can be used as indicators of hydraulic fracturing fluids.
- The detection of trace levels of a variety of refined hydrocarbons and chemicals that are often associated with hydraulic fracturing fluids (e.g., ammonium persulfate, ethylene glycol, propylene glycol, and glycerol) in pre-hydraulic-fracturing samples in some surface water and near-surface groundwater locations show the difficulties of relying on analyses near analytical detection limits as indicators of drilling and fracturing impacts.
- Scenarios for the possible migration of hydraulic fracturing fluids to shallow groundwater in Exploration Area 2 are identified. The scenarios account for a conceptual groundwater model of the upper Humboldt Basin (based on geologic, hydraulic, and chemical data) and the processes, pathways, and conditions that control potential migration of fracturing fluids from the Elko Formation. The outcome for many of the scenarios is that hydraulic fracturing fluid remains contained within the Elko Formation for at least 1,000 years (a timeframe used by the State of Nevada to evaluate contaminant migration in other settings, such as through the Federal Facility Agreement and Consent Order with the U.S. Department of Energy and Department of Defense). Furthermore, for scenarios in which migration out of the Elko Formation occurs, the concentrations of hydraulic fracturing fluids once transported to the shallow aquifer are expected to be below EPA-approved analytical detection limits.
- Scenario conditions that lead to fracturing fluids being contained within the Elko Formation include the following: hydrocarbon production from the exploration well that creates a hydraulic gradient toward the well and prevents migration away from the Elko Formation; hydraulic fractures that are restricted to the Elko Formation; low hydraulic conductivity in the Elko

Formation; and moderate to strong sorptive, diffusive, and degradation properties for the chemicals used in hydraulic fracturing.

- Methane migration from the producing formation (Elko) into shallow aquifers is not likely to occur according to results of a natural-gas transport model.
- Migration of fracturing fluids upward is limited in local-scale transport models, even when hydraulic fractures are assumed to connect to the Indian Well Formation (located just above the Elko Formation). This finding is consistent with the downward hydraulic gradient of the regional groundwater flow model for Exploration Area 2.
- Assuming the moderate hydraulic conductivity of the Elko Formation (which is consistent with some drillstem measurements), simulations result in fluid movement downward to the carbonate, even when hydraulic fractures are constrained to the Elko Formation. A literature review of typical hydraulic fracture lengths suggests a greater than five percent probability that such fractures could extend into the underlying carbonate and facilitate fluid movement. Once in the carbonate, the fate of fracturing fluids depends on a number of factors. Migration to shallow aquifers will not occur within a 1,000 year timeframe if recharge to the carbonate aquifer is low, the hydraulic conductivity is low, the connection between the carbonate and shallow units is limited, or the sorption of chemicals of concern is high.
- The breakthrough of fracture fluids to the shallow aquifer is simulated under conditions of moderate to high recharge to the carbonate aquifer, reasonably high hydraulic conductivity, good connection between the carbonate and shallow aquifers, and less chemical sorption. This breakthrough does not occur for at least 400 years. In all simulations, even those that assume a direct hydrofracture connection to the carbonate, chemical concentrations in the shallow aquifer are very low, being three to four orders of magnitude lower than the initial concentration in the fracturing fluid. These concentrations would be even lower if the impact of flowback testing had been included. Putting this into context for three particular hydraulic fracturing chemicals, the peak concentrations are all below EPA-approved analytical detection limits.
- Although the modeling results indicate that it is likely that hydraulic fracturing fluids will be retained in the deep subsurface for 1,000 years or more and that when migration is simulated under a combined set of specific conditions the consequence is low (being below analytical detection limits), data collection during oil exploration activities might be able to resolve the presence or absence of characteristics that are important for transport.

8.0 REFERENCES

2013 Annual Update of the Expanded Pipeline Groundwater Flow Model: Barrick Cortez Inc., HC66 Box 1250, Crescent Valley, NV 89821-1250. Prepared by Geomega Inc., 2525 28th Street, Suite 200, Boulder, Colorado, 80301.

2013 Update of Carlin Trend Numerical Groundwater Flow Model: Itasca Denver, Inc.

Advanced Well Stimulation Technologies in California, An Independent Review of Scientific and Technical Information: California Council on Science and Technology, Lawrence Berkeley National Laboratory Pacific Institute, ISBN # 978-1-930117-93-8, August, 2014.

All Consulting, 2012. The Modern Practices of Hydraulic Fracturing – A Focus on Canadian Resources, Prepared for PTAC, p. 229.

Anderman, E.R. and M.C. Hill, 2000. MODFLOW-2000, the U.S. Geological Survey Modular Ground-Water Model -Documentation of the Hydrogeologic-Unit Flow (HUF) Package. U.S. Geological Survey Open-File Report 2000-342.

Anna, L.O., L.N.R. Roberts, and C.J. Potter. Geologic Assessment of Undiscovered Oil and Gas in the Paleozoic–Tertiary Composite Total Petroleum System of the Eastern Great Basin, Nevada and Utah, Chapter 2 of Geologic Assessment of Undiscovered Oil and Gas Resources of the Eastern Great Basin Province, Nevada, Utah, Idaho, and Arizona: U.S. Geological Survey Digital Data Series DDS–69–L.

Arthur, J.D., B. Bohm, and M. Layne, 2008. Consulting Hydraulic Fracturing Considerations for Natural Gas Wells of the Marcellus Shale: The Ground Water Protection Council Annual Forum, Cincinnati, Ohio, 2008.

Baldassare, F.J., M.A. McCaffrey, and J.A. Harper, 2014. A geochemical context for stray gas investigations in the northern Appalachian Basin: Implications of analyses of natural gases from Neogene-through-Devonian-age strata. AAPG Bulletin, v. 98(2), pp.341-372.

Bear, J., 1972. Dynamics of Fluids in Porous Media. New York, NY: Elsevier Publishing Co.

Beardsmore, G.R. and J.P. Cull, 2002. *Crustal heat flow: a guide to measurement and modeling.* Cambridge University Press.

Ben-Naceur, K., 1989. Chapter 3: Modeling of Hydraulic Fractures: Dowell Schlumberger.

Berger, D.L., 2000. Water Budgets for Pine Valley, Carico Lake Valley and Upper Reese River Valley Hydrographic Areas Middle Humboldt River Basin, North-Central Nevada Methods for Estimation and Results: U.S. Department of the Interior U.S. Geological Survey and Nevada Division of Water Resources, Water-Resources Investigations Report 99-4272.

Bláha, K. and P. Rusnak, 2004. SIDS Initial Assessment Report for SIAM 19, Ethanol: UNEP Publications, Berlin, Germany.

Boyer, E., B. Swistock, J. Clark, M. Madden, and D. Rizzo, 2011. The Impact of Marcellus Gas Drilling on Rural Drinking Water Supplies (p. 28). Retrieved from http://www.rural.palegislature.us/documents/reports/Marcellus_and_drinking_water_2011_rev.pdf

Brantley, S.L., D. Yoxtheimer, S. Arjmand, P. Grieve, R. Vidic, J. Pollak, G.T. Llewellyn, J. Abad, and C. Simon, 2014. Water Resource Impacts during Unconventional Shale Gas Development: the Pennsylvania Experience. *International Journal of Coal Geology*, doi:10.1016/j.coal.2013.12.017.

Bredehoeft, J.D., 1963. Hydrogeology of the Lower Humboldt River Basin, Nevada: Water Resources Bulletin No. 21, State of Nevada Department of Conservation and Natural Resources, Carson City, Nevada and Technical Report No. 3, the Desert Research Institute, University of Nevada, Reno, Nevada.

Bredehoeft, J.D., 2012. Comment on the Hydrogeology of Proposed Cadiz Project: Center for Biological Diversity & National Parks Conservation Association

Brufatto, C., J. Cochran, L. Conn, D. Power, S.Z.A.A. El-Zeghaty, B. Fraboulet, T. Griffin, S. James, T. Munk, F. Justus, J. Levine, C. Montgomery, D. Murphy, J. Pfeiffer, T. Pornpoch, and L. Rishmani, 2003. From Mud to Cement-Building Gas Wells. Oilf. Rev., pp. 62-76.

Buscheck, T.A., N.D. Rosenberg, J. Gansemer, and Y. Sun, 2002. Thermohydrologic behavior at an underground nuclear waste repository at Yucca Mountain, NV, *Water Resources Research*, 38 (3), 10, pp. 1-17.

Cai, Z. and U. Ofterdinger, 2013. Numerical assessment of potential impacts of hydraulically fractured Bowland Shale on overlying aquifers: Groundwater Research Group, School of Planning Architecture and Civil Engineering, Queen's University Belfast, Belfast BT9 5AG, Northern Ireland, UK.

California Council on Science and Technology, 2014. Advanced Well Stimulation Technologies in California – An Independent Review of Scientific and Technical Information, Lawrence Berkeley National Laboratory Pacific Institute, p. 400.

Cardno ENTRIX, 2012. Hydraulic Fracturing Study, PXP Inglewood Oil Field, 206 p. Los Angeles, CA.

Carey, A.E. and D.E. Prudic, 1996. Documentation of Model Input and Output Values for Simulation of Pumping Effects in Paradise Valley, A Basin Tributary to the Humboldt River, Humboldt County, Nevada: Supplement to U.S. Geological Survey Professional Paper 1409-F, *U.S. Geological Survey* Open-File Report 92-491, Carson City, Nevada.

Carey, J.W., K. Lewis, S. Kelkar, and G.A. Zyvoloski, 2013. Geomechanical Behavior of Wells in Geologic Sequestration. *Energy Procedia*, 37, pp. 5642-5652, doi:10.1016/j.egypro.2013.06.486.

Carter, K.M., N. Kresic, P. Muller, and L.F. Vittorio, 2013. Technical Rebuttal to Article Claiming a Link between Hydraulic Fracturing and Groundwater Contamination: Pennsylvania Council of Professional Geologists and the Pennsylvania Geological Survey.

Chapman, E.C., R.C. Capo, B.W. Stewart, C.S. Kirby, R.W. Hammack, K.T. Schroeder, and H.M. Edenborn, 2012. Geochemical and Strontium Isotope Characterization of Produced Waters from Marcellus Shale Natural Gas Extraction. *Environmental Science & Technology*, 46(6), pp. 3545-53, doi:10.1021/es204005g.

Cikes, M., 2000. Long-Term Hydraulic-Fracture Conductivities Under Extreme Conditions: *Society of Petroleum Engineers, Production & Facilities*, v. 15, pp. 255-261.

Clark, I. and P. Fritz, 1997. Environmental Isotopes in Hydrogeology. CRC Press, New York.

Coats, R.R., 1987. Geology of Elko County, Nevada: Nevada Bureau of Mines and Geology Bulletin 101, p. 112, scale 1:250,000.

Coolbaugh, M., R. Zehner, C. Creemer, D. Blackwell, G. Oppliger, D. Sawatzky, G. Blewitt, A. Pancha, M. Richards, L. Shevenell, G. Raines, G. Johnson, T. Minor, and T. Boyd, 2005. "Geothermal potential of the Great Basin region, Western United States." Nevada Bureau of Mining and Geology, Map 151.

Daneshy, A., 1990. Hydraulic Fracturing To Improve Production: Daneshy Consultants International, Tech 101.

Davies, R.J., 2011. Methane Contamination of Drinking Water Caused by Hydraulic Fracturing Remains Unproven. *Proceedings of the National Academy of Sciences of the United States of America*, 108(43), pp. E871-E871, doi:10.1073/pnas.1113299108.

Davies, R.J., G. Foulger, A. Bindley, and P. Styles, 2013. Induced Seismicity and Hydraulic Fracturing for the Recovery of Hydrocarbons. *Marine and Petroleum Geology*, 45, pp. 171-185.

Davies, R.J., S.A. Mathias, J. Moss, S. Hustoft, and L. Newport, 2012. Hydraulic Fractures: How far can they go? *Marine and Petroleum Geology*, 37(1), pp. 1-6, doi:10.1016/j.marpetgeo.2012.04.001.

Dettinger, M.D., J.R. Harrill, D.L. Schmidt, and J.W. Hess, 1995. Distribution of Carbonate-Rock Aquifers and the Potential for Their Development, Southern Nevada and Adjacent Parts of California, Arizona, and Utah: Water-Resources Investigations Report 91-4146, U.S. Geological Survey and the Desert Research Institute.

Diersch, H.J., 2014. *FEFLOW (Version 6.2) [Computer program]. DHI-WASY, Berlin, Germany.*

Digiulio, D.C., R.T. Wilkin, C. Miller, and G. Oberly, 2011. DRAFT: Investigation of Ground Water Contamination near Pavillion, Wyoming. US Environmental Protection Agency. pp. 121.

Domenico, P.A., and F.W. Schwartz, 1997. Physical and Chemical Hydrogeology. John Wiley & Sons, Inc., New York.

Dudley, W.W., Jr., 1967. Hydrogeology and ground-water flow system of the central Ruby Mountains, Nevada: Urbana, University of Illinois, doctoral thesis, 107 p.

Dusseault, M.B., M.N. Gray, and P.A. Nawrocki, 2000. Why Oilwells Leak: Cement Behavior and Long-Term Consequences. In SPE International Oil and Gas Conference and Exhibition, SPE 64733 (p. 8). Beijing, China: Society of Petroleum Engineers.

Dyck, W. and E. Dunn, 1986. Helium and Methane Anomalies in Domestic Well Waters in Southwestern Saskatchewan Canada, and Their Relationship to Other Dissolved Constituents, Oil and Gas Fields, and Tectonic Patterns. *Journal of Geophysical Research*, 91(5), pp. 343-353.

Eakin, T.E., G.B. Maxey, T.W. Robinson, J.C. Fredericks, and O.J. Loeltz, 1951. State of Nevada Office of the State Engineer, Water Resources Bulletin No. 12, Contributions to the Hydrology of Eastern Nevada, in cooperation with the U.S. Geological Survey, 160p.

Eakin, T.E. and R.D. Lamke, 1966. Hydrologic Reconnaissance of the Humboldt River Basin, Nevada: State of Nevada Department of Conservation and Natural Resources and the U.S. Geological Survey, Water Resources Bulletin No. 32.

Eltschlager, K.K., J.W. Hawkins, W.C. Ehler, and F. Baldassare, 2001. Technical Measures for the Investigation and Mitigation of Fugitive Methane Hazards in Areas of Coal Mining. U.S. Department of Interior, Office of Surface Mining Reclamation and Enforcement, Appalachian Regional Coordinating Center, Pittsburgh, PA.

Engelder, T., 2012. Capillary Tension and Imbibition Sequester Frack Fluid in Marcellus Gas Shale. *Proceedings of the National Academy of Sciences of the United States of America*, 109(52), E3625; author reply E3626.

Engle, M.A., E.L. Rowan, T.F. Kraemer, and A.L. Bates, 2012. Geochemical and hydrologic controls on produced water geochemistry from shale gas reservoirs. Paper No. 125-6, *Geological Society of America* Abstracts with Programs. 44(7), p. 314.

Environmental Assessment for the Marys River Oil and Gas Exploration Project, 2014, United States Department of the Interior Bureau of Land Management, p. 224.

Epstein, B., Pohll, G.M., Huntington, J. and Carroll, R.W.H. 2010. Development and uncertainty analysis of an empirical recharge prediction model for Nevada's desert basins. Nevada Water Resources Association. 5(1): 1-22.

Evans, J.G., and K.B. Ketner, 1971. Geologic map of the Swales Mountain quadrangle and part of the Adobe Summit quadrangle, Elko County, Nevada: U.S. Geological Survey Miscellaneous Geologic Investigations Map I-667, scale 1:24,000.

Fisher K. and N. Warpinski, 2011. Hydraulic Fracture-Height Growth: Real Data: Society of Petroleum Engineers.

Fisher, J.B., 2014. Hydraulic Fracturing in Nevada: University of Tulsa and Lithochimeia, LLC. Presentation.

Fisher, K. and N. Warpinski, 2012. Hydraulic-Fracture-Height Growth: Real Data. *Society of Petroleum Engineers Production and Operations*, 27(1), pp. 8-19.

Flewelling, S.A. and M. Sharma, 2014. Constraints on Upward Migration of Hydraulic Fracturing Fluid and Brine. *Groundwater*, 52, pp. 9-19.

Flewelling, S.A., M.P. Tymchak, and N. Warpinski, 2013. Hydraulic Fracture Height Limits and Fault Interactions in Tight Oil and Gas Formations. *Geophysical Research Letters*, 40(14), pp. 3602-3606, doi:10.1002/grl.50707.

Flewelling, S.A., M.P. Tymchak, and N. Warpinski, 2013. Hydraulic fracture height limits and fault interactions in tight oil and gas formations. *Geophysical Research Letters*, 40(14), pp. 3602-3606.

Flint, A.L. and L.E. Flint, 2007. Application of the basin characterization model to estimate in-place recharge and runoff potential in the Basin and Range carbonate-rock aquifer system, White Pine County, Nevada, and adjacent areas in Nevada and Utah. U.S. Geological Survey Scientific Investigations Report 2007-5099, p. 20.

Freeze, R.A. and J.A. Cherry, 1979. Groundwater, Prentice-Hall, Inc., Englewood Cliffs, New Jersey, p. 604

Freyss, H., P. Guieze, N. Varotsis, A. Khakoo, K. Lestelle, and D. Simper. PVT Analysis of Oil Reservoirs. Reservoir Engineering, Technical Review, 37, pp. 4-15.

Fricke, H.C., S.M. Wickham, and J.R. O'Neil, 1992. Oxygen and hydrogen isotopic evidence for meteoric water infiltration during mylonitization and uplift in the Ruby Mountains-East Humboldt Range core complex, Nevada. Contributions to *Mineralogy and Petrology III*. pp. 203-221.

Gassiat, C., T. Gleeson, R. Lefebvre, and J. McKenzie, 2013. Hydraulic Fracturing in Faulted Sedimentary Basins: Numerical Simulation of Potential Contamination of Shallow Aquifers Over Long Time Scales. *Water Resources Research*, 49, pp. 8310-8327.

Gold, R., 2014. The Boom – How Fracking Ignited the American Energy Revolution and Changed the World, Simon and Schuster, New York, NY, p. 366.

Gordalla, B.C., U. Ewers, and F.H. Frimmel, 2013. Hydraulic Fracturing: a Toxicological Threat for Groundwater and Drinking-water? *Environmental Earth Science*, 70, pp. 3875-3893.

Hao Y., Y. Sun, and J.J. Nitao, 2012. Overview of NUFT: A Versatile Numerical Model for Simulating Flow and Reactive Transport in Porous Media, in Groundwater Reactive Transport Models, F. Zhang, G.T. Yeh, and J.C. Parker eds. Oak Park, IL: Bentham Science Publishers.

Harbaugh, A.W., 2005. MODFLOW-2005: the U.S. Geological Survey Modular Ground-Water Model-the Ground-Water Flow Process. U.S. Geological Survey Techniques and Methods 6-A16.

Harrill, J.R. and D.E. Prudic, 1998. Aquifer Systems in the Great Basin Region of Nevada, Utah, and Adjacent States Summary Report: U.S. Geological Survey Professional Paper 1409-A.

Harrison, S.S., 1983. Evaluating System for Ground-Water Contamination Hazards Due to Gas-Well Drilling on the Glaciated Appalachian Plateau. *Ground Water*, 21(6), pp. 689–700.

Harrison, S.S., 1985. Contamination of Aquifers by Overpressuring the Annulus of Oil and Gas Wells. *Ground Water*, 23(3), pp. 317-324, doi: 10.1111/j.1745-6584.1985.tb00775.

Heilweil, V.M. and L.E. Brooks, 2011. Conceptual Model of the Great Basin Carbonate and Alluvial Aquifer System: U.S. Department of the Interior U.S. Geological Survey, Scientific Investigations Report 2010–5193.

Heilweil, V.M., B.J. Stolp, B.A. Kimball, D.D. Susong, T.M. Marston, and P.M. Gardner, 2013. A Stream-Based Methane Monitoring Approach for Evaluating Groundwater Impacts Associated with Unconventional Gas Development. *Groundwater*, 51, pp. 511-524.

Hershey, R.L., S. Rybarski, J.M. Thomas, and G. Pohll, 2014. Water-Quality Data, Hydraulic Fracturing in the Upper Humboldt River Basin, Aquifer Quality Assessment Program, Report 2. Desert Research Institute, Division of Hydraulic Sciences, Publication No. 41259.

Hess, R.H., M.A. Henson, D.A. Davis, S.H. Limerick, S.S. Siewe, and M. Niles, 2011. Oil and Gas Well Information for Nevada – 2011 Update, Nevada Bureau of Mines and Geology Open File Report 11-6.

Horton, G.A., 2000. Humboldt River Chronology Volume 1 Overview: An Overview and Chronological History of the Humboldt River and Related Water Issues: A Publication in the Nevada Water Basin Information and Chronology Series, Nevada Division of Water Planning, p. 201.

Hose, R.K., M.C. Blake, and R.M. Smith, 1976. Geology and mineral resources of White Pine County, Nevada: Nevada Bureau of Mines and Geology Bulletin 85, p. 105, scale 1:250,000.

Houghton, J.G., C.M. Sakamoto, and R.O. Gifford, 1975. Nevada's weather and climate. Nevada Bureau of Mines and Geology Special Publication 2, p. 78.

Howard, K.A., 2000. Geologic map of the Lamoille quadrangle, Elko County, Nevada. Nevada Bureau of Mines and Geology Map 125.

Howard, K.A., R.W. Kistler, A.W. Snoke, and R. Willden, 1979. Geologic map of the Ruby Mountains, Nevada: U.S. Geological Survey Miscellaneous Investigations Map I-1136, scale 1:125,000.

Hunt, A.G., T.H. Darrah, R.J. Poreda, 2012. Determining the source and genetic fingerprint of natural gases using noble gas geochemistry: A northern Appalachian Basin case study. AAPG Bulletin 96:1785-1811.

Hydraulic Fracturing Study, PXP Inglewood Oil Field, 2012. Cardno ENTRIX, 10940 Wilshire Blvd., Suite 1525, Los Angeles, California.

Jackson, R.B., A. Vengosh, T.H. Darrah, N.R. Warner, A. Down, R.J. Poreda, S.G. Osborn, K. Zhao, and J.D. Karr, 2013a. Increased Stray Gas Abundance in a Subset of Drinking Water Wells near Marcellus Shale Gas Extraction. *Proceedings of the National Academy of Sciences of the United States of America*, 110(28), pp. 11250-11255, doi:10.1073/pnas.1221635110. www.pnas.org/cgi/doi/10.1073/pnas.1221635110

Jackson, R.B., S.G. Osborn, A. Vengosh, and N.R. Warner, 2011. Reply to Davies: Hydraulic Fracturing Remains a Possible Mechanism for Observed Methane Contamination of Drinking Water. *Proceedings of the National Academy of Sciences of the United States of America*, 108(43), pp. E872–E872, doi:10.1073/pnas.1113768108.

Jackson, R.E., A.W. Gorody, B. Mayer, J.W. Roy, M.C. Ryan, and D.R. Van Stempvoort, 2013b. Groundwater Protection and Unconventional Gas Extraction: The Critical Need for Field-Based Hydrogeological Research. *Groundwater*, 51(4), pp. 488-510, doi:10.1111/gwat.12074.

Jackson, T.C., 2013a. Comments of Halliburton Energy Services Inc. on: "Science Advisory Board Consultation on the Study of the Potential Impacts of Hydraulic Fracturing on Drinking Water Resources: Progress Report, Environmental Protection Agency": Comments submitted on behalf of Halliburton Energy Systems, Inc.

Jacobson, R.L., N.L. Ingraham, and M.E. Campana, 1983. Isotope Hydrology of a Basin and Range Geothermal System. Desert Research Institute, Water Resources Center, Publication No. 41087.

Jewell, P.W., T.A. Rahn, and J.R. Bowman, 1994. Hydrology and chemistry of thermal waters near Wells, Nevada. *Ground Water,* 32 (4), pp. 657-665.

Kell, S., 2011. State Oil and Gas Agency Groundwater Investigations and Their Role in Advancing Regulatory Reforms, a Two-State Review: Ohio and Texas. Groundwater Protection Council, http://www.gwpc.org/sites/default/files/State%20Oil%20%26%20Gas%20Agency%20Groundwater%20Investigations.pdf

Ketner, K.B. and J.G. Evans, 1988. Geologic map of the Peko Hills, Elko County, Nevada: U.S. Geological Survey Miscellaneous Investigations Map I-1902, scale 1:24,000.

Ketner, K.B., 1990. Geologic map of the Elko Hills, Elko County, Nevada: U.S. Geological Survey Miscellaneous Investigations Map I-2082.

Ketner, K.B., 1998. Geologic map of the southern Independence Mountains, Elko County, Nevada: U.S. Geological Survey Geologic Investigations Map I-2629, scale 1:24,000.

Ketner, K.B., and R.J. Ross, 1990. Geologic map of the northern Adobe Range, Elko County, Nevada: U.S. Geological Survey Miscellaneous Investigations Map I-2081, scale 1:24,000.

Kim, J., and G.J. Moridis, 2012. Gas Flow Tightly Coupled to Elastoplastic Geomechanics for Tight and Shale Gas Reservoirs: Material Failure and Enhanced Permeability. *In: Proc. Americas Unconventional Resources Conference*, Pittsburgh, PA.

Kim, J., E.S. Um, and G.J. Moridis, 2014. SPE 168578 Fracture Propagation, Fluid Flow, and Geomechanics of Water-Based Hydraulic Fracturing in Shale Gas Systems and Electromagnetic Geophysical Monitoring of Fluid Migration. *In: Proc. Society of Petroleum Engineers Hydraulic Fracturing Technology Conference*, Woodlands, TX.

King, G.E., 2012. Hydraulic Fracturing 101: What Every Representative, Environmentalist, Regulator, Reporter, Investor, University Researcher, Neighbor, and Engineer Should Know About Estimating Frac Risk and Improving Frac Performance in Unconventional Gas and Oil Wells, *Society of Petroleum Engineers,* Publication 152596, p. 80.

King, G.E., L. Haile, J. Shuss, T.A. Dobkins, 2008. Increasing Fracture Path Complexity and Controlling Downward Fracture Growth in the Barnett Shale. *Society of Petroleum Engineers,* Publication 119896.

Kissinger, A., R. Helmig, A. Ebigbo, H. Class, T. Lange, M. Sauter, M. Heitfeld, J. Klunker, and W. Jahnke, 2013. Hydraulic fracturing in unconventional gas reservoirs: risks in the geological system, part 2: Modelling the transport of fracturing fluids, brine and methane. *Environmental Earth Science*, 70(8), pp. 3855-3873, doi:10.1007/s12665-013-2578-6.

LaBolle, E.M., 2006. RWHet: Random walk particle model for simulating transport in heterogeneous media, Version 3.2 User's Manual and Program Documentation.

LaBolle, E.M., and G.E. Fogg, 2001. Role of molecular diffusion in contaminant migration and recovery in an alluvial aquifer system. *Transport in Porous Media*, 42, pp. 155-179.

LaBolle, E.M., G.E. Fogg, and A.F.B. Tompson, 1996. Random-walk simulation of transport in heterogeneous porous media: Local mass conservation problem and implementation methods. *Water Resources Research*, 32(3), pp. 583-593.

LaBolle, E.M., J. Quastel, G.E. Fogg, and J. Gravner, 2000. Diffusion processes in composite porous media and their numerical integration by random walks: Generalized stochastic differential equations with discontinuous coefficients. *Water Resources Research*, 36(3), pp. 651-662.

Lange, T., M. Sauter, M. Heitfeld, K. Schetelig, K. Brosig, W. Jahnke, A. Kissinger, R. Helmig, A. Ebigbo, and H. Class, 2013. Hydraulic fracturing in unconventional gas reservoirs: risks in the geological system part 1. *Environmental Earth Science*, 70, pp. 3839-3853.

Lei, G., 2012. Producing Gas-Oil Ratio Performance of Conventional and Unconventional Reservoirs: Norwegian University of Science and Technology Department of Petroleum Engineering and Applied Geophysics, p. 92.

Liu, H.H., G.S. Bodvarsson, and L. Pan, 2000. Determination of particle transfer in random walk particle methods for fractured porous media. *Water Resources Research*, 36(3), pp. 707-713.

Liu, T., M. Marongiu-Porcu, C. Ehlig-Economides, and M.J. Economides, 2013. A Study of Transversely vs. Longitudinally Fractured Wells in a Moderate-permeability Gas Reservoir. *Journal of Engineering Research*, 1 pp. 139-156.

Maguire-Boyle S.J., D.J Garner, J.E. Heimann, L. Gao, A.W Orbaek, and A.R. Barron, 2014. Automated method for determining the flow of surface functionalized nanoparticles through a hydraulically fractured mineral formation using plasmonic silver nanoparticles. *Environmental Science: Processes & Impacts*, 16(2) pp. 220-231, doi:10.1039/c3em00718a.

Mariner, R.H., T.S. Presser, and W.C. Evans, 1983. Geochemistry of active geothermal systems in the northern Basin and Range Province. In Geothermal Resources Council, The Role of Heat in the Development of Energy and Mineral Resources in the Northern Basin and Range Province, Special Report No. 13, Davis, California, pp. 95-119.

Masbruch, M.D., 2011a. Appendix 4: Current Study Groundwater Recharge Estimates for Predevelopment Conditions and Ranges of Previously Reported Estimates of Groundwater Recharge for Each Hydrographic Area within the Great Basin Carbonate and Alluvial Aquifer System Study Area. In: Conceptual Model of the Great Basin Carbonate and Alluvial Aquifer System. V.M. Heilweil and L.E. Brookes (Eds.). U.S Geological Survey Scientific Investigations Report 2010-5193.

Masbruch, M.D., 2011b. Appendix 5: Current Study Groundwater Discharge Estimates for Predevelopment Conditions and Ranges of Previously Reported Estimates of Groundwater Discharge for Each Hydrographic Area within the Great Basin Carbonate and Alluvial Aquifer System Study Area. In: Conceptual Model of the Great Basin Carbonate and Alluvial Aquifer System. V.M. Heilweil and L.E. Brookes (Eds.). U.S Geological Survey Scientific Investigations Report 2010-5193.

Matanoski, G.M. and I.P. Murarka, 1997. To Filter, or Not to Filter; that is the Question. A letter to the Honorable Carol M. Browner, U.S. Environmental Protection Agency, EEC-LTR-97-011. http://nepis.epa.gov/Exe/ZyNET.exe/2000PF5K.txt?ZyActionD=ZyDocument&Client=EPA&Index=1995%20Thru%201999&Docs=&Query=&Time=&EndTime=&SearchMethod=1&TocRestrict=n&Toc=&TocEntry=&QField=&QFieldYear=&QFieldMonth=&QFieldDay=&UseQField=&IntQFieldOp=0&ExtQFieldOp=0&XmlQuery=&File=D%3A\ZYFILES\INDEX%20DATA\95THRU99\TXT\00000017\2000PF5K.txt&User=ANONYMOUS&Password=anonymous&SortMethod=h|&MaximumDocuments=1&FuzzyDegree=0&ImageQuality=r75g8/r75g8/x150y150g16/i425&Display=p|f&DefSeekPage=x&SearchBack=ZyActionL&Back=ZyActionS&BackDesc=Results%20page&MaximumPages=1&ZyEntry=1

Mavor, M., 2014. Reservoir Fluid Properties Required for Low-Permeability Oil Reservoir Analysis: Search and Discovery Article #80363. Presentation given at Geoscience Technology Workshop,

Hydrocarbon Charge Considerations in Liquid-Rich Unconventional Petroleum Systems, Vancouver, BC, Canada, November 5, 2013.

Maxey, G.B. and T.E. Eakin, 1949. Ground water in White River Valley, White Pine, Nye, and Lincoln Counties, Nevada. No. 8, State of Nevada Office of the State Engineer prepared in cooperation with the United State Department of the Interior Geological Survey, Carson City, Nevada.

Mazor, E., 1991. Applied Chemical and Isotopic Groundwater Hydrology. Halsted Press, New York.

McKay, L.D., R.W. Gillham, and J.A. Cherry, 1993. Field experiments in a fractured clay till: 2. Solute and colloid transport. *Water Resources Research*, 29(12).

Modern Shale Gas Development in the United States: A Primer: Ground Water Protection Council Oklahoma City, Oklahoma and ALL Consulting, Tulsa, Oklahoma, 2009. Prepared for: Department of Energy Office of Fossil Energy and National Energy Technology Laboratory, DE-FG26-04NT15455.

Molofsky, L.J., J.A. Connor, A.S. Wylie, T. Wagner, S.K. Farhat, 2013. Evaluation of methane sources in groundwater in northeastern Pennsylvania. *Groundwater* 51(3), pp. 333–349.

Montgomery, C.T. and M.B. Smith, 2010. Hydraulic Fracturing: History of an Enduring Technology. Journal of Petroleum Technology, 62(12), pp. 26-32.

MOU, 2013. Memorandum of Understanding between the State of Nevada by the Nevada Division of Minerals and Nevada Division of Environmental Protection and Desert Research Institute and Noble Energy, Inc., p. 14.

Myers, T., 2012. Potential Contaminant Pathways from Hydraulically Fractured Shale to Aquifers. *Ground Water*, 50(6), pp. 872-82, doi: 10.1111/j.1745-6584.2012.00933.x.

Neuzil, C.E., 1994. How permeable are clays and shales? *Water Resources Research*, 30(2), pp. 145-150.

Nevada Division of Environmental Protection, 2010. http://ndep.nv.gov/docs_10/nev95019_f10.pdf

Nevada State Senate Bill No. 390, 2014, Senators Segerblom and Jones. Joint Sponsors Assemblymen Bobzien and Daly, p. 3.

Newmark, R.L., W.D. Daily, K.R. Kyle, and A.L. Ramirez, 1997. Monitoring DNAPL Pumping Using Integrated Geophysical Techniques, DOE report, Lawrence Livermore National Laboratory.

Nitao, J.J., 2000a. Reference Manual for the NUFT Flow and Transport Code, Version 3.0, UCRL-MA-130651-REV-1. Livermore, CA: Lawrence Livermore National Laboratory.

Nitao, J.J., 2000b. User's Manual for the USNT Module of the NUFT Code, Version 3.0, UCRL-MA-130643-REV-2. Livermore, CA: Lawrence Livermore National Laboratory.

Nitao, J.J., 2004. User's manual for the US1P module of the NUFT flow and transport code, Lawrence Livermore National Laboratory.

Nowlin, J.O., 1986. Ground-Water Quality in Nevada: a Proposed Monitoring Program: United States Department of the Interior Geological Survey, Carson City, Nevada, p. 248.

Nutt, C.J. and K.S. Hart, 2004. Geologic map of the Big Bald Mountain quadrangle and part of the Tognini Spring quadrangle, White Pine County, Nevada: Nevada Bureau of Mines and Geology Map 145, scale 1:24,000.

Nutt, C.J., 2000. Geologic map of the Alligator Ridge area, including the Buck Mountain East and Mooney Basin Summit quadrangles and parts of the Sunshine Well NE and Long Valley Slough quadrangles, White Pine County, Nevada: U.S. Geological Survey Geologic Investigation Series Map I-2691, scale 1:24,000.

Osborn, S.G., A. Vengosh, N.R. Warner, and R.B. Jackson, 2011a. Methane Contamination of Drinking Water Accompanying Gas-well Drilling and Hydraulic Fracturing. *Proceedings of the National Academy of Sciences of the United States of America,* 108(20), pp. 8172-8176, doi:10.1073/pnas.1100682108.

Pan, L. and G.S. Bodvarsson, 2002. Modeling transport in fractured porous media with the random-walk particle method: The transient activity range and the particle transfer probability. *Water Resources Research*, 38, p. 6, doi:10.1029/2001WR000901.

Phase I Hydrologic Data for the Groundwater Flow and Contaminant Transport Model of Corrective Action Unit 97: Yucca Flat/Climax Mine, Nevada Test Site, Nye County, Nevada: Revision No.: 0, 2006, U.S. Department of Energy, Contract No. DE-AC52-03NA99205.

Plume, R.W. and J.L. Smith, 2013. Properties of Basin-Fill Deposits, a 1971-2000 Water Budget, and Surface-Water-Groundwater Interactions in the Upper Humboldt River Basin, Northeastern Nevada. U.S. Geological Survey Scientific Investigations Report 2013-5077. http://pubs.usgs.gov/sir/2013/5077/

Plume, R.W., 1996. Hydrogeologic framework of the Great Basin region of Nevada, Utah, and adjacent states. Regional Aquifer System Analysis, U.S. Geological Survey Professional Paper 1409-B.

Plume, R.W., 2003. Ground-Water Use, Locations of Production Wells, and Areas Irrigated Using Ground Water in 1998, Middle Humboldt River Basin, North-Central Nevada: U.S. Department of the Interior U.S. Geological Survey and Nevada Division of Water Resources, Water-Resources Investigations Report 03–4227.

Plume, R.W., 2009. Hydrogeologic Framework and Occurence and Movement of Ground Water in the Upper Humboldt River Basin, Northeastern Nevada. U.S. Geological Survey Scientific Investigations Report 2009-5014.

PRISM Climate Group, 2012. Oregon State University, http://prism.oregonstate.edu, created July 10, 2012.

Proposed Regulation of the Division of Minerals of the Commission on Mineral Resources, 2014. LCB File No. ROU-14: Authority: §§1-16 and 19, NRS 522.040 and 522.119; §17, NRS 522.040 and 522.150; §18, NRS 534A.090.

Prudic, D.E., 2007, "Evaluating Cumulative Effects of Groundwater Withdrawals on Streamflow": A dissertation submitted in partial fulfillment of the requirements for the degree of Doctor of Philosophy in Hydrogeology, University of Nevada, Reno, p. 348.

Prudic, D.E., 2012. "Evaluating Cumulative Effects of Groundwater Withdrawals on Flows in the Humboldt River": Presentation, March 7, 2012, *Nevada Water Resources Association Annual Meeting*, Las Vegas, Nevada.

Prudic, D.E., J.R. Harrill, and T.J. Burbey, 1995. Conceptual Evaluation of Regional Ground-Water Flow in the Carbonate-Rock Province of the Great Basin, Nevada, Utah, and Adjacent States: Regional Aquifer System Analysis, U.S. Geological Survey Professional Paper 1409-D.

Prudic, D.E., R.G. Niswonger, and R.W. Plume, 2006. Trends in Streamflow on the Humboldt River between Elko and Imlay, Nevada: U.S. Department of the Interior U.S. Geological Survey, Scientific Investigations Report 2005-5199.

Qi, J.C., A.R., Kerr, Y.H., and Sorooshian, Soroosh, 1994. A modified soil adjusted vegetation index: *Remote Sensing of Environment*, op. 119–126.

Rahman, M.M. and M K. Rahman, 2010. A Review of Hydraulic Fracture Models and Development of an Improved Pseudo-3D Model for Stimulating Tight Oil/Gas Sand. *Energy Sources*, Part A, 32, pp. 1416-1436, Taylor & Francis Group, LLC.

Reeves, D.M., R. Parashar, K. Pohlmann, C. Russell, and J. Chapman, 2014. Development and calibration of dual-permeability flow models with discontinuous fault networks. *Vadose Zone Journal*, doi:10.2136/vzj2013.10.0183.

Reinicke, A., E. Rybacki, S. Stanchits, E. Huenges, and G. Dresen, 2010. Hydraulic fracturing stimulation techniques and formation damage mechanisms-Implications from laboratory testing of tight sandstone-proppant systems. *Chemie der Erde*, 70, pp. 107-117.

Reno Gazette Journal, 2014. Fracking hits home in Nevada, Article published April 15, 2014, http://www.rgj.com/story/tech/environment/2014/04/13/fracking-hits-home-nevada/7649293/, accessed July 17, 2014.

Roberts, E.A.L., 1866. U.S. Patent No. 59, 936. Washington, DC: U.S. Patent and Trademark Office.

Roberts, R.J., K.M. Montgomery, and R.W. Lehrer, 1967. Geology and mineral resources of Eureka County, Nevada. Nevada Bureau of Mines and Geology Bulletin 64, p. 152, 1:250,000.

Romero, D.J., P.P. Valko, and M.J. Economides, 2002. The Optimization of the Productivity Index and the Fracture Geometry of a Stimulated Well with Fracture Face and Choke Skins. *Society of Petroleum Engineers Inc. International Symposium and Exhibition on Formation Damage Control,* Lafayette, Louisiana, February 20-21.

Romero, D.J., P.P. Valko, and M.J. Economides, 2003. Proppant flow-back, over-displacement or polymer damage. Society of Petroleum Engineers Inc. February 2003 *Society of Petroleum Engineers Production & Facilities*.

Rowan, E.L., M.A. Engle, and T.F. Kraemer, 2011. Formation waters from reservoirs in the Appalachian basin, New York, Pennsylvania, and West Virginia: Observations on major and minor element, and radium geochemistry. Paper No. 236-2, *GSA Annual Meeting*, Minneapolis, October 9-12.

Roy, J.W. and M.C. Ryan, 2013. Effects of Unconventional Gas Development on Groundwater: A Call for Total Dissolved Gas Pressure Field Measurements. *Groundwater*, 51, p. 3.

Rozell, D.J., and S.J. Reaven, 2012. Water Pollution Risk Associated with Natural Gas Extraction from the Marcellus Shale. *Society for Risk Analysis*, 32(8), pp. 1382-1393, doi:10.1111/j.1539-6924.2011.01757.x.

Rush, F.E. and D.E. Everett, 1966. Water Resources Appraisal of the Huntington Valley Area, Elko and White Pine Counties, Nevada: Nevada Department of Conservation and Natural Resources Water Resources Reconnaissance Series, Report 35.

Safety Data Sheet – Extended, 2011. Prepared in accordance with Annex II of REACH Regulation (EC) No. 1907/2006, Regulation (EC) 1272/2008 and regulation (EC) 453/2010, 2-ethylhexanol (octanol), Oltchim, S. A. Technical & Development Department, Valcea, Romania: http://www.petkim.com.tr/Userfiles/File/uretim/ithal_urunler/MSDS/2EH_MSDS.pdf

Safety Data Sheet according to Regulation (EC) No. 1907/2006 (REACH) and Regulation (CE) 453/2010, Azichem, Goito, Italy: http://www.azichem.com

Scherpenisse, W., K. Wit, A.E. Zweers, G. Shoei, and A. Van Wolfswinkel, 1994. Predicting Gas Saturation Buildup during Depressurization of a North Sea Oil Reservoir. *Society of Petroleum Engineers*, 28842, p. 11.

Schon, S.C., 2011. Hydraulic Fracturing Not Responsible for Methane Migration. Letter to Proceedings of the National Academy of Sciences, 108(37), pp. E664–E664, doi:10.1073/pnas.1107960108.

Schumer, R and G. Pohll, 2014. Preliminary Assessment of Hydraulic Fracturing Fluid Concentrations and Hydrologic Conditions in Noble Development Area #2, Upper Humboldt River Basin, Phase I report.

Schwartz, F.W., 2013, Folk Beliefs and Fracking: *Groundwater*: Editorial, 51.

Sharma, S., M.L. Mulder, H.M. Edenborn, and R.W. Hammack, 2011. Stable isotope fingerprinting of co-produced waters associated with Marcellus shale natural gas extraction. Paper No. 236-7, *GSA Annual Meeting*, Minneapolis, October 9-12.

Sharp, R.P., 1938. Pleistocene glaciation in the Ruby-East Humboldt Range, northeastern Nevada: *Journal of Geomorphology*, 1(4), pp. 296-323.

Sheppard, S.M., R.L. Nielsen, and H.P. Taylor Jr., 1969. Oxygen and hydrogen isotope ratios of clay and minerals from porphyry copper deposits. *Economic Geology*, 64, pp. 755-777.

Smith, J.F., Jr., and K.B. Ketner, 1972. Generalized geologic map of the Carlin, Dixie Flats, Pine Valley and Robinson Mountain quadrangles, Elko and Eureka Counties, Nevada: U.S. Geological Survey Miscellaneous Field Studies Map MF-481, scale 1:125,000.

Smith, J.F., Jr., and K.B. Ketner, 1975. Stratigraphy of Paleozoic rocks in the Carlin-Pinon Range area, Nevada: U.S. Geological Survey Professional Paper 867-A, p. 87.

Smith, J.F., Jr., and K.B. Ketner, 1975. Stratigraphy of post-Paleozoic rocks and summary of resources in the Carlin-Pinon Range area, Nevada: U.S. Geological Survey Professional Paper 867-B, p. 48.

Solomon, B.J., and S.W. Moore, 1982a. Geology and Oil Shale Deposits of the Elko East Quadrangle, Elko County, Nevada, U.S. Geological Survey Map MF-1410.

Solomon, B.J., and S.W. Moore, 1982b. Geology and Oil Shale Deposits of the Elko West Quadrangle, Elko County, Nevada, U.S. Geological Survey Map MF-1421.

State of Nevada, 1971. Water Planning Report No. 3, Nevada State Engineer's Office, 97 p.

Study of the Potential Impacts of Hydraulic Fracturing on Drinking Water Resources: Progress Report: U.S. Environmental Protection Agency, Office of Research and Development Washington, DC, 2012, EPA/601/R-12/011.

Thamke, J.N. and B.D. Smith, 2014. Delineation of Brine Contamination in and near the East Poplar Oil Field, Fort Peck Indian Reservation, Northeastern Montana, 2004–09: U.S. Department of the Interior U.S. Geological Survey, Scientific Investigations Report 2014–5024.

The Modern Practices of Hydraulic Fracturing: A Focus on Canadian Resources: ALL Consulting, LLC, Tulsa, Oklahoma, 2012.

Thorman, C.H., W.E. Brooks, K.B. Ketner, and R.F. Dubiel, Preliminary geologic map of the Oxley Peak area, Elko County, Nevada – 2nd Edition, Nevada Bureau of Mines and Geology.

Tompson, A.F.B., G.B. Hudson, D.K. Smith, and J.R. Hunt, 2006. Analysis of Radionuclide Migration through a 200-m Vadose Zone following a 16-Year Infiltration Event, *Advances in Water Resources*, 29(2), pp. 281–292.

Tsimpanogiannis, I.N. and Y.C. Yortsos, 2002. Model for the Gas Evolution in a Porous Medium Driven by Solute Diffusion. *AIChE Journal*, 48, pp. 2690-2710.

United States Department of Energy, 2009. Modern Shale Gas, Development in the Unites States: A Primer, 116p.

United States Environmental Protection Agency (US EPA), (1987), Report to Congress: Management of Wastes from the Exploration, Development, and Production of Crude Oil, Natural Gas, and Geothermal Energy.

United States Environmental Protection Agency, 2012. Study of the Potential Impacts of Hydraulic Fracturing on Drinking Water Resources – Progress Report, 278p.

Urbancic, T. and K. Mountjoy, 2011. Microseismic Monitoring Increases Efficiency and Performance in Liquids-Rich Plays: Special Report: Reservoir Characterization, by The American Oil & Gas Reporter.

Valkó, P.P., 2006. HF2D Frac Design Spreadsheet: Harold Vance Department Petroleum Engineering, Texas A&M University.

Vengosh, A., N. Warner, R. Jackson, and T. Darrah, 2013. The effects of shale gas exploration and hydraulic fracturing on the quality of water resources in the United States. *Procedia Earth and Planetary Science*, 7, p. 863-866.

Vidic, R.D., S.L. Brantley, J.M. Vandenbossche, D. Yoxtheimer, and J.D. Abad, 2013. Impact of Shale Gas Development on Regional Water Quality. *Science*, 340(6134), 1235009, doi:10.1126/science.1235009.

Wallace, A.R., M.E. Perkins, and R.J. Fleck, 2008. Late Cenozoic paleogeographic evolution of northeastern Nevada: Evidence from the sedimentary basins. *Geosphere*, 4(1), doi: 10.1130/GES00114.1.

Warner, N.R., R.B. Jackson, T.H. Darrah, S.G. Osborn, A. Down, K. Zhao, A. White, and A. Vengosh, 2012b. Reply to Engelder: Potential for Fluid Migration from the Marcellus Formation Remains Possible. *Proceedings of the National Academy of Sciences of the United States of America*, 109(52), E3626–E3626.

Warner, N.R., T.M. Kresse, P.D. Hays, A. Down, J.D. Karr, R.B. Jackson, and A. Vengosh, 2013. Geochemical and Isotopic Variations in Shallow Groundwater in Areas of the Fayetteville Shale Development, Northcentral Arkansas. *Applied Geochemistry*, 35, pp. 207-220, doi:10.1016/j.apgeochem.2013.04.013.

Warpinski, N., 2009. Microseismic Monitoring: Inside and Out. *Society of Petroleum Engineers,* 118537.

Water for Nevada, Nevada's Water Resources: State of Nevada Water Planning Report, Report No. 3, State Engineer's Office, 1971, p. 97.

Watson, T. and S. Bachu, 2009. Evaluation of the Potential for Gas and CO2 Leakage along Wellbores. SPE Drill. *Complet.,* 21(1), pp. 115-126.

Wesnousky, S.G., A.D. Barron, R.W. Briggs, S.J. Caskey, S. Kumar, and L. Owen, 2005. Paleoseismic Transect Across the Northern Great Basin. *Journal of Geophysical Research*, 110, B05408.

Welch, A.H., D.J. Bright, and L.A. Knochenmus, 2007, Water resources of the basin and range carbonate-rock aquifer system, White Pine County, Nevada, and adjacent areas in Nevada and Utah: U.S. Geological Survey Scientific Investigations Report 2007–5261, 96 p.

White, 2004. Evaluation of Impacts to Underground Sources of Drinking Water by Hydraulic Fracturing of Coalbed Methane Reservoirs: Appendix A, EPA 816-R-04-003, Department of Energy.

Whiticar, M.J., 1999. Carbon and hydrogen isotope systematics of bacterial formation and oxidation of methane. *Chemical Geology*, 161, pp. 291-314.

Willden, R., and R.W. Kistler, 1969. Geologic map of the Jiggs quadrangle, Elko County, Nevada: U.S. Geological Survey Geological Quadrangle Map GQ-859, scale 1:62,500.

Wright, C.A., R.A. Conant, G.M. Golich, P.L. Bondor, A.S. Murer, and C.A. Dobie, 1995. Hydraulic Fracture Orientation and Production/Injection Induced Reservoir Stress Changes in Diatomite Waterfloods. In Proceedings: *Society of Petroleum Engineers Western Regional Meeting*, pp. 139-152, Bakersfield, California.

Yager, R.M. and J.C. Fountain, 2001. Effect of Natural Gas Exsolution on Specific Storage in a Confined Aquifer Undergoing Water Level Decline. *Ground Water*, 39, pp. 517-525.

Yeskis, D., and B. Zavala, 2002. Ground-Water Sampling Guidelines for Superfund and RCRA Project Managers. U.S. Environmental Protection Agency, Ground Water Forum Issue Paper, Office of Solid Waste and Emergency Response, EPA 542-S-02-001.

Zhang, Y., E.M. LaBolle, D.M. Reeves, and C. Russell, 2012. Development of RWHet to Simulate Contaminant Transport in Fractured Porous Media, DOE/NV/0000939-01, DRI Report No. 45244.

Zhang, Y., M. Person, J. Rupp, K. Ellett, M.A. Celia, C.W. Gable, B. Bowen, J. Evans, K. Bandilla, P. Mozley, T. Dewers, and T. Elliot, 2013. Hydrogeologic Controls on Induced Seismicity in Crystalline Basement Rocks due to Fluid Injection into Basal Reservoirs. *Groundwater*, 51, pp. 525-538.

Zheng, C., and G.D. Bennett, 2002. *Applied contaminant transport modeling* (Vol. 2). New York: Wiley-Interscience.

Zogorski, J.S., 2006. The Quality of Our Nation's Water-Volatile organic compounds in the Nation's ground water and drinking-water supply wells. U.S. Geological Survey Circular 1292, p. 101.

APPENDIX A: CHEMICAL AND ISOTOPIC PARAMETERS FOR UPPER HUMBOLDT RIVER BASIN WELLS, SPRINGS, AND STREAMS

Table A-1. Field and laboratory parameters and radionuclides for upper Humboldt River Basin wells, springs, and streams.

Agency (Units)	Location ID	Sample Date	Field pH	Lab pH	Field EC (µS/cm)	Lab EC (µS/cm)	Temperature (˚C)	Gross Alpha (pCi/L)	Gross Beta (pCi/L)	^{226}Ra (pCi/L)	^{228}Ra (pCi/L)
Area 1 Pre-hydraulic Fracturing											
TT	1-1	3/31/2014	6.35	NC	394	NC	10.6	NC	NC	NC	NC
DRI	1-1	3/31/2014	NC	7.10	NC	382	NC	<3	<3	<0.42	<0.82
TT	1-2	3/31/2014	7.10	NC	416	NC	2.9	4.55	2.09	NC	0.289 U
TT	1-3	3/31/2014	7.40	NC	727	NC	6.7	6.47	6.37	NC	0.323 U
TT	1-4	3/31/2014	7.45	NC	354	NC	9.4	9.56	4.13	NC	0.372 U
TT	1-5	3/31/2014	7.96	NC	208	NC	18.3	3.05	2.59	NC	0.407 U
TT	1-6	3/31/2014	7.62	NC	254	NC	13.3	NC	NC	NC	NC
TT	1-7	4/1/2014	7.42	NC	570	NC	10.0	23.6	4.23	NC	0.563
TT	1-8	4/1/2014	7.89	NC	828	NC	10.0	13.5 G	8.38	NC	0.365 U
TT	1-9	4/1/2014	7.55	NC	365	NC	13.3	NC	NC	NC	NC
TT	1-10	4/1/2014	7.48	NC	332	NC	6.6	NC	NC	NC	NC
TT	1-11	4/1/2014	7.05	NC	363	NC	11.7	NC	NC	NC	NC
DRI	1-12	4/2/2014	7.54	7.86	333	339	17.1	9.0	6.8	<0.44	<0.89
TT	1-13	4/7/2014	7.64	NC	152	NC	13.9	3.0	0.2	NC	NC
TT	1-13	4/18/2014	6.72	NC	157	NC	13.1	3.39	3.88	NC	0.034 U
DRI	1-13	4/18/2014	NC	NC	NC	NC	NC	NC	NC	NC	NC
TT	1-14	4/18/2014	7.35	NC	1380	NC	10.6	83.0 G	30.2 G	NC	0.725
DRI	1-15	4/18/2014	8.76	8.65	968	1020	22.2	3.2	76	<0.37	<0.88
DRI	1-16	9/22/2014	NC	7.04	NC	149	NC	<3	<3	<0.36	<0.78
TT	1-16	9/22/2014	7.6	NC	144	NC	12.5	NC	NC	NC	NC
DRI	1-17	9/22/2014	NC	7.05	NC	530	NC	37	15	<0.44	<0.5
TT	1-17	9/22/2014	7.70	NC	583	NC	15.1	NC	NC	NC	NC
DRI	1-18	9/22/2014	6.66	7.11	271	249	14.4	8.8	4.5	<0.32	<0.74
TT	1-18	9/22/2014	NC	NC	NC	NC	NC	NC	NC	NC	NC
DRI	1-19	9/23/2014	NC	7.70	NC	553	NC	16	9.7	<0.33	<0.85

Table A-1. Field and laboratory parameters and radionuclides for upper Humboldt River Basin wells, springs, and streams (continued).

Agency (Units)	Location ID	Sample Date	Field pH	Lab pH	Field EC (µS/cm)	Lab EC (µS/cm)	Temperature (˚C)	Gross Alpha (pCi/L)	Gross Beta (pCi/L)	^{226}Ra (pCi/L)	^{228}Ra (pCi/L)
TT	1-19	9/23/2014	7.55	NC	564	NC	15.7	NC	NC	NC	NC
DRI	1-20	9/23/2014	NC	7.10	NC	255	NC	14	6.2	<0.3	<0.73
TT	1-20	9/23/2014	7.55	NC	220	NC	19.8	NC	NC	NC	NC
DRI	1-21	9/23/2014	7.28	7.51	NC	365	12.4	<3	<3	<0.38	<0.74
DRI	1-22	9/24/2014	NC	7.74	NC	198	13.9	7.8	<3	<0.31	<0.69
DRI	1-23	9/24/2014	NC	7.56	NC	67	17.4	<3	<3	<0.34	<0.68
DRI	1-24	9/29/2014	NC	7.14	NC	264	NC	8.9	<3	<0.34	<1
TT	1-24	9/29/2014	7.20	NC	279	NC	13.8	NC	NC	NC	NC
DRI	1-25	9/29/2014	NC	7.37	NC	339	NC	8.0	6.3	<0.3	<0.83
TT	1-25	9/29/2014	7.49	NC	344	NC	17.6	NC	NC	NC	NC
DRI	1-26	10/7/2014	NC	7.76	NC	335	NC	10	<3	<0.27	<0.84
TT	1-26	10/7/2014	8.08	NC	327	NC	16.4	NC	NC	NC	NC
DRI	1-27	10/7/2014	NC	7.63	NC	407	NC	12	4	<0.39	<0.57
TT	1-27	10/7/2014	7.98	NC	409	NC	14.5	NC	NC	NC	NC
DRI	1-28	10/20/2014	NC	7.08	NC	287	NC	20	4.1	<0.35	<0.87
TT	1-28	10/20/2014	7.22	NC	288	NC	12.1	NC	NC	NC	NC
DRI	1-29	10/20/2014	NC	7.95	NC	279	NC	5.6	7.1	<0.36	<0.48
TT	1-29	10/20/2014	8.31	NC	289	NC	12.7	NC	NC	NC	NC
DRI	1-30	10/21/2014	NC	7.91	NC	254	NC	10	<3	<0.31	<0.77
TT	1-30	10/21/2014	8.31	NC	269	NC	16.9	NC	NC	NC	NC
TT	1-31	10/20/2014	8.30	NC	363	NC	13.7	NC	NC	NC	NC
TT	1-32	9/23/2014	7.48	NC	221	NC	15.7	NC	NC	NC	NC
TT	1-33	9/22/2014	7.33	NC	252	NC	13.2	NC	NC	NC	NC
TT	1-34	9/22/2014	7.46	NC	357	NC	12.3	NC	NC	NC	NC
TT	1-35	9/23/2014	7.55	NC	220	NC	19.8	NC	NC	NC	NC
TT	1-36	11/12/2014	7.09	NC	113	NC	13.1	NC	NC	NC	NC
TT	1-37	11/12/2014	7.26	NC	114	NC	11.6	NC	NC	NC	NC

Table A-1. Field and laboratory parameters and radionuclides for upper Humboldt River Basin wells, springs, and streams (continued).

Agency (Units)	Location ID	Sample Date	Field pH	Lab pH	Field EC (µS/cm)	Lab EC (µS/cm)	Temperature (˚C)	Gross Alpha (pCi/L)	Gross Beta (pCi/L)	^{226}Ra (pCi/L)	^{228}Ra (pCi/L)
Area 1 Post-Hydraulic Fracturing											
TT	1-1	2/25/2015	7.33	7.77 HF	388	374	7.4	NC	NC	NC	NC
TT	1-1	3/12/2015	7.50	NC	388	NC	8.7	NC	NC	NC	NC
DRI	1-2	6/8/2015	NC	NC	NC	NC	NC	<3	3.4	<0.41	<0.73
TT	1-2	3/4/2015	7.77	7.05 HF	286	272	2.8	NC	NC	NC	NC
TT	1-2	3/25/2015	7.87	NC	311	NC	7.7	NC	NC	NC	NC
DRI	1-3	6/8/2015	NC	NC	NC	NC	NC	10	25	<0.33	<0.49
TT	1-3	3/4/2015	7.71	7.79 HF	691	589	3.9	NC	NC	NC	NC
TT	1-3	3/25/2015	7.79	NC	664	NC	8.2	NC	NC	NC	NC
DRI	1-4	6/9/2015	NC	NC	NC	NC	NC	6.7	4.7	<0.32	<0.71
TT	1-4	2/25/2015	7.85	8.11 HF	343	338	10.3	NC	NC	NC	NC
DRI	1-5	6/9/2015	NC	NC	NC	NC	NC	<3	5.2	<0.34	<0.60
TT	1-5	3/9/2015	8.41	NC	206	NC	18.1	NC	NC	NC	NC
TT	1-6	2/25/2015	7.61	7.83 HF	254	255	13.4	NC	NC	NC	NC
DRI	1-7	6/9/2015	NC	NC	NC	NC	NC	15	10	<0.38	<0.83
TT	1-7	2/26/2015	7.94	8.05 HF	552	510	10.8	NC	NC	NC	NC
DRI	1-8	6/9/2015	NC	NC	NC	NC	NC	10	8.1	<0.32	<0.79
TT	1-8	2/26/2015	8.14	8.05 HF	464	425	8.0	NC	NC	NC	NC
TT	1-8	3/12/2015	8.16	NC	482	NC	8.4	NC	NC	NC	NC
TT	1-9	2/26/2015	7.99	8.01 HF	364	343	13.4	NC	NC	NC	NC
TT	1-10	2/23/2015	8.07	7.85 HF	334	339	7.1	NC	NC	NC	NC
TT	1-11	2/23/2015	7.56	7.90 HF	358	349	11.5	NC	NC	NC	NC
DRI	1-13	6/8/2015	NC	NC	NC	NC	NC	<3	<3	<0.36	<0.76
TT	1-13	6/8/2015	7.66	7.91 HF	146	160	19.2	NC	NC	NC	NC
TT	1-13	8/17/2015	7.96	NC	NC	NC	19.3	NC	NC	NC	NC
DRI	1-14	6/8/2015	NC	NC	NC	NC	NC	32	48	<0.29	<0.73
TT	1-14	6/8/2015	7.50	8.08 HF	1254	974	19.2	NC	NC	NC	NC

Table A-1. Field and laboratory parameters and radionuclides for upper Humboldt River Basin wells, springs, and streams (continued).

Agency (Units)	Location ID	Sample Date	Field pH	Lab pH	Field EC (µS/cm)	Lab EC (µS/cm)	Temperature (˚C)	Gross Alpha (pCi/L)	Gross Beta (pCi/L)	^{226}Ra (pCi/L)	^{228}Ra (pCi/L)
TT	1-16	3/31/2015	7.65	8.29 HF	144	140	10.3	NC	NC	NC	NC
DRI	1-17	2/11/2015	NC	7.05	NC	383	NC	15	4.5	<0.36	<0.84
TT	1-17	2/11/2015	7.71	7.62 HF	382	347	8.9	NC	NC	NC	NC
DRI	1-18	2/11/2015	NC	7.00	NC	247	NC	5.5	4.2	<3.0	<0.47
TT	1-18	2/11/2015	7.63	7.58 HF	248	240	11.2	NC	NC	NC	NC
DRI	1-19	2/11/2015	NC	7.76	NC	362	NC	9.0	8.6	<0.45	<0.88
TT	1-19	2/11/2015	8.11	8.07 HF	366	321	9.1	NC	NC	NC	NC
TT	1-19	3/12/2015	8.15	NC	361	NC	8.8	NC	NC	NC	NC
DRI	1-20	2/10/2015	NC	7.11	NC	249	NC	8.9	8.7	<0.32	<0.69
TT	1-20	2/10/2015	7.59	7.63 HF	254	242	9.5	NC	NC	NC	NC
DRI	1-24	2/11/2015	NC	7.10	NC	272	NC	6.8	<3	<0.33	<0.66
TT	1-24	2/11/2015	7.67	7.60 HF	277	262	12.6	NC	NC	NC	NC
DRI	1-25	2/10/2015	NC	7.23	NC	354	NC	<3	8.7	<0.35	<0.67
TT	1-25	2/10/2015	7.72	7.76 HF	363	332	7.3	NC	NC	NC	NC
TT	1-25	3/12/2015	7.80	NC	357	NC	9.4	NC	NC	NC	NC
TT	1-26	6/30/2015	7.9	7.86 HF	349	352	16.7	NC	NC	NC	NC
TT	1-27	5/12/2015	8.21	8.10 HF	406	347	13.5	NC	NC	NC	NC
TT	1-28	2/10/2015	7.60	7.47 HF	288	282	11.9	NC	NC	NC	NC
TT	1-29	6/24/2015	7.97	8.13 HF	282	285	12.8	NC	NC	NC	NC
TT	1-29	8/12/2015	8.21	NC	296	NC	20.6	NC	NC	NC	NC
TT	1-30	5/12/2015	8.30	8.11 HF	268	265	17.2	NC	NC	NC	NC
TT	1-31	6/24/2015	7.67	8.04 HF	355	336	13.0	NC	NC	NC	NC
TT	1-32	2/11/2015	7.47	7.53 HF	222.2	217	12.5	NC	NC	NC	NC
TT	1-33	3/31/2015	7.99	7.81 HF	257	246	8.2	NC	NC	NC	NC
TT	1-34	7/23/2015	7.55	7.63 HF	267	272	11.4	NC	NC	NC	NC
TT	1-35	2/10/2015	8.04	7.91 HF	213	218	11.1	NC	NC	NC	NC
TT	1-36	12/3/2014	7.24	NC	141	NC	13.2	NC	NC	NC	NC

Table A-1. Field and laboratory parameters and radionuclides for upper Humboldt River Basin wells, springs, and streams (continued).

Agency (Units)	Location ID	Sample Date	Field pH	Lab pH	Field EC (µS/cm)	Lab EC (µS/cm)	Temperature (˚C)	Gross Alpha (pCi/L)	Gross Beta (pCi/L)	^{226}Ra (pCi/L)	^{228}Ra (pCi/L)
TT	1-36	2/18/2015	7.56	7.40 HF	120	129	12.4	NC	NC	NC	NC
TT	1-36	3/3/2015	7.43	NC	119	NC	11.7	NC	NC	NC	NC
TT	1-37	12/3/2014	7.34	NC	114	NC	13.8	NC	NC	NC	NC
TT	1-37	2/18/2015	7.80	7.43 HF	110	120	13.5	NC	NC	NC	NC
TT	1-37	3/3/2015	7.41	NC	110	NC	13.4	NC	NC	NC	NC
Area 2 Pre-hydraulic Fracturing											
DRI	2-1	9/4/2013	NC	9.61	NC	632	NC	16	11	<0.49	<0.95
TT	2-1	9/4/2013	9.96	NC	658	NC	11.7	NC	NC	NC	NC
TT	2-1	10/8/2013	NC	NC	NC	NC	NC	NC	NC	NC	NC
TT	2-2	9/4/2013	7.79	NC	566	NC	17.4	NC	NC	NC	NC
TT	2-3	9/4/2013	7.54	NC	573	NC	16.8	NC	NC	NC	NC
DRI	2-4	9/4/2013	NC	7.98	NC	323	NC	8.4	4.8	<0.45	<0.83
TT	2-4	9/4/2013	8.16	NC	331	NC	12.8	NC	NC	NC	NC
TT	2-5	9/4/2013	7.25	NC	282	NC	12.5	NC	NC	NC	NC
TT	2-6	9/4/2013	7.09	NC	278	NC	12.6	NC	NC	NC	NC
TT	2-7	9/4/2013	8.93	NC	274	NC	17.4	NC	NC	NC	NC
TT	2-8	10/8/2013	NC	NC	NC	NC	NC	NC	NC	NC	NC
TT	2-9	10/8/2013	NC	NC	NC	NC	NC	NC	NC	NC	NC
Area 2 Post-hydraulic Fracturing											
DRI	2-1	6/23/2014	NC	9.50	NC	700	NC	16	<3	<0.95	<2.1
TT	2-1	6/23/2014	9.70	NC	640	NC	14.0	NC	NC	NC	NC
DRI	2-2	6/23/2014	NC	7.40	NC	520	NC	<3	5.7	<0.33	<0.88
TT	2-2	6/23/2014	7.30	NC	495	NC	12.2	NC	NC	NC	NC
TT	2-3	6/23/2014	7.45	NC	595	NC	13.3	NC	NC	NC	NC
DRI	2-4	6/23/2014	NC	7.90	NC	350	NC	6.2	3	<0.36	<0.7
TT	2-4	6/23/2014	7.60	NC	327	NC	12.8	NC	NC	NC	NC
TT	2-5	6/25/2014	6.60	NC	262	NC	14.9	NC	NC	NC	NC

Table A-1. Field and laboratory parameters and radionuclides for upper Humboldt River Basin wells, springs, and streams (continued).

Agency (Units)	Location ID	Sample Date	Field pH	Lab pH	Field EC (µS/cm)	Lab EC (µS/cm)	Temperature (˚C)	Gross Alpha (pCi/L)	Gross Beta (pCi/L)	^{226}Ra (pCi/L)	^{228}Ra (pCi/L)
TT	2-6	6/25/2014	6.50	NC	235	NC	12.3	NC	NC	NC	NC
TT	2-7	7/1/2014	7.60	NC	331	NC	11.7	NC	NC	NC	NC
TT	2-8	6/25/2014	7.58	NC	288	NC	13.9	NC	NC	NC	NC
TT	2-9	6/25/2014	7.70	NC	430	NC	15.6	NC	NC	NC	NC
DRI	2-10	4/1/2014	8.08	8.08	220	220	9.3	<3	<3	<0.43	<0.82
DRI	2-10	6/23/2014	7.96	7.90	123	140	16.8	<3	<3	<0.31	<0.72
DRI	2-11	6/25/2014	8.04	7.90	354	370	21.8	<3	<3	<0.36	<0.78
DRI	2-12	6/24/2014	8.01	7.90	352	410	19.4	6.9	<3	<0.48	<0.67
DRI	2-13	6/24/2014	8.32	8.20	338	360	22.8	5.7	<3	<0.4	<0.54
DRI	2-14	6/24/2014	7.20	7.50	530	600	16.0	6.9	6.1	<0.34	<0.51
DRI	2-15	9/5/2014	7.88	7.91	316	305	13.0	<3	<3	<0.29	<0.71
DRI	2-16	9/25/2014	9.64	9.63	370	506	19.5	7.9	9.9	<0.57	<1.3
DRI	M2C-M2-21B	9/25/2014	6.39	6.58	4447	12440	54.0	36	1200	11	14
	M10C-M10-11B	-----	-----	-----	-----	-----	-----	-----	-----	-----	-----
Area 2 One-Year Post Hydraulic Fracturing											
TT	2-1	7/16/2015	9.68	9.58 HF	652	630	12.7	NC	NC	NC	NC
DRI	2-2	3/18/2015	NC	7.48	NC	462	NC	<3	4.6	<0.28	<0.70
TT	2-2	3/18/2015	7.90	7.99 HF	471	408	10.6	NC	NC	NC	NC
TT	2-2	4/9/2015	8.02	NC	459	NC	13.3	NC	NC	NC	NC
TT	2-3	3/18/2015	7.81	8.02 HF	615	514	9.4	NC	NC	NC	NC
TT	2-3	4/9/2015	7.85	NC	609	NC	8.2	NC	NC	NC	NC
DRI	2-4	3/18/2015	NC	7.98	NC	330	NC	<3	<3	<0.38	<0.74
TT	2-4	3/18/2015	8.25	8.16 HF	329	325	9.9	NC	NC	NC	NC
DRI	2-5	3/19/2015	NC	7.15	NC	277	NC	7.7	<3	<0.41	<0.84
TT	2-5	3/19/2015	7.77	7.76 HF	277	295	8.9	NC	NC	NC	NC
TT	2-6	3/24/2015	7.77	7.46 HF	293	278	9.7	NC	NC	NC	NC

Table A-1. Field and laboratory parameters and radionuclides for upper Humboldt River Basin wells, springs, and streams (continued).

Agency (Units)	Location ID	Sample Date	Field pH	Lab pH	Field EC (µS/cm)	Lab EC (µS/cm)	Temperature (˚C)	Gross Alpha (pCi/L)	Gross Beta (pCi/L)	^{226}Ra (pCi/L)	^{228}Ra (pCi/L)
TT	2-7	3/19/2015	7.85	8.13 HF	342	327	10.0	NC	NC	NC	NC
TT	2-8	3/17/2015	7.63	8.12 HF	292	270	10.1	NC	NC	NC	NC
TT	2-9	3/24/2015	8.13	7.91 HF	431	393	11.5	NC	NC	NC	NC
DRI	2-13	3/19/2015	8.25	8.36	421	421	14.4	9.2	3.3	<0.36	<0.82
Area 3 Pre-hydraulic Fracturing											
DRI	3-1	9/3/2014	NC	8.09	NC	354	NC	<3	15	<0.53	<1.2
TT	3-1	9/3/2014	7.97	NC	542	NC	14.3	NC	NC	NC	NC
DRI	3-2	9/3/2014	NC	8.38	NC	258	NC	<3	15	<0.52	<0.67
TT	3-2	9/3/2014	8.13	NC	273	NC	16.2	NC	NC	NC	NC
DRI	3-3	9/3/2014	NC	9.53	NC	791	NC	<3	7	<0.37	<0.71
TT	3-3	9/3/2014	9.47	NC	845	NC	14.8	NC	NC	NC	NC
DRI	3-4	9/4/2014	8.59	8.61	928	889	17.6	<3	15	<0.34	<0.78
DRI	3-5	9/5/2014	9.69	9.58	1252	1215	15.1	<3	36	<0.32	<0.92
DRI	3-6	9/30/2014	NC	7.32	NC	594	NC	<3	6.2	<0.36	<0.7
TT	3-6	9/30/2014	7.55	NC	606	NC	15.9	NC	NC	NC	NC
DRI	3-7	9/30/2014	NC	7.70	NC	387	NC	5.5	3.3	<0.37	<0.79
TT	3-7	9/30/2014	7.99	NC	394	NC	11.9	NC	NC	NC	NC
DRI	3-8	9/30/2014	7.16	7.52	489	493	38.2	11	4.4	4.5	<0.7
DRI	3-9	10/8/2014	NC	7.78	NC	331	NC	22	<3	<0.42	<0.95
TT	3-9	10/8/2014	7.9	NC	333	NC	15.0	NC	NC	NC	NC
DRI	3-10	10/21/2014	NC	7.66	NC	397	9.9	11	<3	<0.32	<0.78
TT	3-10	10/29/2014	5.67	NC	395	NC	12.6	NC	NC	NC	NC
DRI	3-11	10/21/2014	NC	7.99	NC	1018	NC	4.9	4.5	<0.29	<0.66
TT	3-11	10/21/2014	8.22	NC	1070	NC	13.8	NC	NC	NC	NC
TT	3-12	10/21/2014	7.86	NC	696	NC	12.4	NC	NC	NC	NC
DRI	3-12	10/22/2014	NC	7.59	NC	652	NC	11	<3	<0.34	<0.51
DRI	3-13	10/22/2014	NC	9.04	NC	5510	15.4	<3	26	<0.36	<0.8

Table A-1. Field and laboratory parameters and radionuclides for upper Humboldt River Basin wells, springs, and streams (continued).

Agency (Units)	Location ID	Sample Date	Field pH	Lab pH	Field EC (µS/cm)	Lab EC (µS/cm)	Temperature (˚C)	Gross Alpha (pCi/L)	Gross Beta (pCi/L)	^{226}Ra (pCi/L)	^{228}Ra (pCi/L)
TT	3-14	10/21/2014	8.10	NC	708.9	NC	11.9	NC	NC	NC	NC
TT	3-15	9/30/2014	8.44	NC	620	NC	17.3	NC	NC	NC	NC
TT	3-16	12/8/2014	8.35	NC	344	NC	12.2	NC	NC	NC	NC
TT	3-17	12/8/2014	8.00	NC	407	NC	8.2	NC	NC	NC	NC
TT	3-18	12/8/2014	7.90	NC	447	NC	6.2	NC	NC	NC	NC
TT	3-19	12/8/2014	7.98	NC	2388	NC	71.7	NC	NC	NC	NC
TT	3-19	1/6/2015	7.73	NC	2359	NC	61.7	NC	NC	NC	NC
TT	3-20	12/8/2014	7.80	NC	1169	NC	11.0	NC	NC	NC	NC
TT	3-20	1/6/2015	7.90	NC	1168	NC	11.6	NC	NC	NC	NC

DRI = Desert Research Institute
EC = electrical conductivity
G = the minimum detection concentration of the sample is greater than the requested reporting limit
NC = not collected
$R/R_a = (^3He/^4He)_{groundwater} / (^3He/^4He)_{atmosphere}$
TT = Tetra Tech
U = result is less than the sample detection limit

Table A-2. Major-ion chemistry and total dissolved solids for upper Humboldt River Basin wells, springs, and streams.

Agency (Units)	Location ID	Sample Date	Ca (dissolved) (mg/L)	Ca (total) (mg/L)	Mg (dissolved) (mg/L)	Mg (total) (mg/L)	Na (dissolved) (mg/L)	Na (total) (mg/L)	K (dissolved) (mg/L)	K (total) (mg/L)	HCO_3 (mg/L)	CO_3 (mg/L)	Cl (mg/L)	SO_4 (mg/L)	TDS (mg/L)
Area 1 Pre-Hydraulic Fracturing															
TT	1-1	3/31/2014	NC	36.9	NC	8.84	NC	36.3	NC	3.74	161	ND	21.8	35.1	265
DRI	1-1	3/31/2014	34.8	NC	8.03	NC	33.5	NC	3.3	NC	159	ND	21.9	34.3	274
TT	1-2	3/31/2014	NC	30.0	NC	7.35	NC	55.5	NC	4.11	205	ND	9.42	37.9	266
TT	1-3	3/31/2014	NC	70.7	NC	16.1	NC	51.8	NC	10.0	185	ND	84.9	114	452
TT	1-4	3/31/2014	NC	33.0	NC	8.35	NC	35.4	NC	<0.237	176	ND	14.5	24.2	226
TT	1-5	3/31/2014	NC	25.1	NC	1.43	NC	16.6	NC	4.44	109	ND	6.4	9.12	166
TT	1-6	3/31/2014	NC	29.1	NC	6.07	NC	15.2	NC	<0.237	112	ND	12.5	18.3	183
TT	1-7	4/1/2014	NC	50.9	NC	13.3	NC	59.6	NC	3.66	268	ND	21.5	40.3	376
TT	1-8	4/1/2014	NC	58.4	NC	29.1	NC	103	NC	12.1	462	ND	40.4	34.0	571
TT	1-9	4/1/2014	NC	46.4	NC	8.03	NC	22.2	NC	<0.237	181	ND	10.4	19.9	235 H
TT	1-10	4/1/2014	NC	30.0	NC	6.7	NC	33.1	NC	<0.237	133	ND	16.5	30.1	232 H
TT	1-11	4/1/2014	NC	4.34	NC	7.66	NC	30.1	NC	<0.237	207	ND	6.65	9.82	225 H
DRI	1-12	4/2/2014	49.1	NC	10.2	NC	8.07	NC	1.07	NC	190	ND	4.9	17.3	203
TT	1-13	4/7/2014	NC	11.8	NC	3.17	NC	15.0	NC	<0.237	74	ND	5.12	6.52	107
DRI	1-13	4/18/2014	10.2	NC	3.09	NC	15.1	NC	2.57	NC	NC	NC	NC	NC	NC
TT	1-14	4/18/2014	NC	109	NC	20	NC	201	NC	26.4	366	ND	66.0 B	328	976
DRI	1-15	4/18/2014	34.1	NC	21.5	NC	184	NC	17.7	NC	519	25.4	41.9	68.1	799
DRI	1-16	9/22/2014	11.9	NC	2.86	NC	9.2	NC	7.1	NC	73	ND	3.6	5.89	110
TT	1-16	9/22/2014	NC	11.9	NC	3.05	NC	14.4	NC	1.64 J	76	ND	NC	NC	NC
DRI	1-17	9/22/2014	59.1	NC	10.9	NC	37.8	NC	7.8	NC	210	ND	39.9	59.4	488
TT	1-17	9/22/2014	NC	62.3	NC	10.7	NC	37.3	NC	2.35 J	212 B	ND	NC	NC	NC
DRI	1-18	9/22/2014	23.5	NC	5.7	NC	17.3	NC	7.2	NC	127	ND	6.32	9.4	92
TT	1-18	9/22/2014	NC	23.4	NC	5.31	NC	23.2	NC	1.94 J	127 B	ND	NC	NC	NC
DRI	1-19	9/23/2014	46.0	NC	12.4	NC	52.0	NC	14.1	NC	293	ND	22.2	20.8	475
TT	1-19	9/23/2014	NC	47.5	NC	12.0	NC	56.6	NC	10.9	292 B	ND	NC	NC	NC

Table A-2. Major-ion chemistry and total dissolved solids for upper Humboldt River Basin wells, springs, and streams (continued).

Agency (Units)	Location ID	Sample Date	Ca (dissolved) (mg/L)	Ca (total) (mg/L)	Mg (dissolved) (mg/L)	Mg (total) (mg/L)	Na (dissolved) (mg/L)	Na (total) (mg/L)	K (dissolved) (mg/L)	K (total) (mg/L)	HCO_3 (mg/L)	CO_3 (mg/L)	Cl (mg/L)	SO_4 (mg/L)	TDS (mg/L)
DRI	1-20	9/23/2014	27.6	NC	7.2	NC	18.4	NC	6.9	NC	127	ND	4.32	7.67	251
TT	1-20	9/23/2014	NC	26.9	NC	6.69	NC	14.7	NC	2.20 J	129 B	ND	NC	NC	NC
DRI	1-21	9/23/2014	61.2	NC	6.7	NC	11.8	NC	0.5	NC	220	ND	2.96	7.65	280
DRI	1-22	9/24/2014	17.6	NC	3.27	NC	17.7	NC	5.3	NC	84	ND	7.89	14.1	110
DRI	1-23	9/24/2014	6.4	NC	1.33	NC	2.2	NC	5.8	NC	34	ND	1.22	0.40	81
DRI	1-24	9/29/2014	27.4	NC	6.82	NC	17.8	NC	6.9	NC	103	ND	15.8	22.8	220
TT	1-24	9/29/2014	NC	25.9	NC	6.39	NC	19.1	NC	2.91 J	106 B	ND	NC	NC	NC
DRI	1-25	9/29/2014	28.3	NC	3.24	NC	35.4	NC	10.2	NC	185	ND	5.03	11.3	280
TT	1-25	9/29/2014	NC	25.8	NC	2.88	NC	43.6	NC	7.36	183	ND	NC	NC	NC
DRI	1-26	10/7/2014	37.3	NC	2.09	NC	19.7	NC	3.13	NC	107	ND	23.2	28.6	200
TT	1-26	10/7/2014	NC	39.0	NC	2.09	NC	28.0 B	NC	3.05	104 B	ND	NC	NC	NC
DRI	1-27	10/7/2014	49.6	NC	8.08	NC	17.8	NC	6.59	NC	171	ND	23.3	24.1	262
TT	1-27	10/7/2014	NC	52.4	NC	7.9	NC	22.4 B	NC	6.26	165	ND	NC	NC	NC
DRI	1-28	10/20/2014	24.0	NC	6.09	NC	20.7	NC	2.2	NC	122	ND	9.2	18.3	168
TT	1-28	10/20/2014	NC	20.7	NC	4.93	NC	26.1	NC	1.9 J	127	ND	NC	NC	NC
DRI	1-29	10/20/2014	27.3	NC	4.82	NC	21.9	NC	6.9	NC	112	ND	12.9	25.6	200
TT	1-29	10/20/2014	NC	23.1	NC	3.84	NC	27.3	NC	6.33	120	ND	NC	NC	NC
DRI	1-30	10/21/2014	29.5	NC	4.61	NC	14.1	NC	2.8	NC	107	ND	12.8	17.3	150
TT	1-30	10/21/2014	NC	27.0	NC	4.04	NC	18.2	NC	2.77 J	109	ND	NC	NC	NC
TT	1-31	10/20/2014	NC	35.4	NC	6.56	NC	18.5	NC	6.46	98	ND	NC	NC	NC
TT	1-32	9/23/2014	NC	19.4	NC	4.23	NC	21.0	NC	1.57 J	115	ND	NC	NC	NC
TT	1-33	9/22/2014	NC	22.7	NC	5.01	NC	23.6	NC	2.31 J	116	ND	NC	NC	NC
TT	1-34	9/22/2014	NC	36.0	NC	7.62	NC	29.9	NC	5.53	145	ND	NC	NC	NC
TT	1-35	9/23/2014	NC	19.3	NC	5.31	NC	19.1	NC	1.83 J	114	ND	NC	NC	NC
TT	1-36	11/12/2014	NC	8.4	NC	2.11	NC	12.4	NC	2.49 J	55	ND	NC	NC	NC
TT	1-37	11/12/2014	NC	8.4	NC	2.09	NC	13.4	NC	2.39 J	62	ND	NC	NC	NC

Table A-2. Major-ion chemistry and total dissolved solids for upper Humboldt River Basin wells, springs, and streams (continued).

Agency (Units)	Location ID	Sample Date	Ca (dissolved) (mg/L)	Ca (total) (mg/L)	Mg (dissolved) (mg/L)	Mg (total) (mg/L)	Na (dissolved) (mg/L)	Na (total) (mg/L)	K (dissolved) (mg/L)	K (total) (mg/L)	HCO_3 (mg/L)	CO_3 (mg/L)	Cl (mg/L)	SO_4 (mg/L)	TDS (mg/L)
Area 1 Post-Hydraulic Fracturing															
TT	1-1	2/25/2015	NC	35.0	NC	8.19	NC	34.2	NC	3.43	159	ND	20.3 B	28.2	265
DRI	1-2	6/8/2015	NC	NC	NC	NC	NC	NC	NC	NC	NC	NC	NC	NC	90
TT	1-2	3/4/2015	NC	21.0	NC	5.16	NC	34.3	NC	3.42	148	ND	5.19	16.8	191
DRI	1-3	6/8/2015	NC	NC	NC	NC	NC	NC	NC	NC	NC	NC	NC	NC	310
TT	1-3	3/4/2015	NC	62.1	NC	15.2	NC	53.5	NC	5.00	129	ND	79.2	83.9	416
DRI	1-4	6/9/2015	NC	NC	NC	NC	NC	NC	NC	NC	NC	NC	NC	NC	190
TT	1-4	2/25/2015	NC	30.5	NC	7.52	NC	33.0	NC	2.21 J	161	ND	12.0 B	19.5	227
DRI	1-5	6/9/2015	NC	NC	NC	NC	NC	NC	NC	NC	NC	NC	NC	NC	132
TT	1-6	2/25/2015	NC	27.5	NC	5.57	NC	13.9	NC	1.71 J	108	ND	10.8 B	15.4	177
DRI	1-7	6/9/2015	NC	NC	NC	NC	NC	NC	NC	NC	NC	NC	NC	NC	275
TT	1-7	2/26/2015	NC	48.2	NC	12.5	NC	54.5	NC	3.49	260	ND	19.6	39.9	362
DRI	1-8	6/9/2015	NC	NC	NC	NC	NC	NC	NC	NC	NC	NC	NC	NC	215
TT	1-8	2/26/2015	NC	44.7	NC	11.8	NC	40.5	NC	2.51 J	233	ND	14.1	31.4	297
TT	1-9	2/26/2015	NC	44.4	NC	7.65	NC	20.6	NC	1.96 J	179	ND	10.3	21.5	231
TT	1-10	2/23/2015	NC	27.8	NC	6.39	NC	32.3	NC	2.21 J	134	ND	14.8 B	28.3	228
TT	1-11	2/23/2015	NC	41.3	NC	7.37	NC	29.3	NC	1.59 J	205	ND	5.89 B	9.68	214
DRI	1-13	6/8/2015	NC	NC	NC	NC	NC	NC	NC	NC	NC	NC	NC	NC	50
TT	1-13	6/8/2015	NC	11.6 B	NC	3.04 B	NC	16.3	NC	1.35 J	65	ND	5.47	7.33	118
DRI	1-14	6/8/2015	NC	NC	NC	NC	NC	NC	NC	NC	NC	NC	NC	NC	655
TT	1-14	6/8/2015	NC	98.4	NC	18.8 B	NC	188	NC	30.9	388	ND	64.7	230	852
TT	1-16	3/31/2015	NC	11.5	NC	3.19	NC	15.0	NC	1.66 J	77	ND	3.46	5.52	104
DRI	1-17	2/11/2015	49.7	NC	9.2	NC	43.3	NC	<0.01	NC	200	ND	28.1	22.8	248
TT	1-17	2/11/2015	NC	46.9	NC	8.68	NC	30.9	NC	1.93 J	210	ND	12.6	17.6	247 H
DRI	1-18	2/11/2015	25.1	NC	6.1	NC	32.7	NC	<0.01	NC	132	ND	23.9	10.7	157
TT	1-18	2/11/2015	NC	24.5	NC	5.92	NC	24.0	NC	1.90 J	135	ND	5.89	8.64	138 H

Table A-2. Major-ion chemistry and total dissolved solids for upper Humboldt River Basin wells, springs, and streams (continued).

Agency (Units)	Location ID	Sample Date	Ca (dissolved) (mg/L)	Ca (total) (mg/L)	Mg (dissolved) (mg/L)	Mg (total) (mg/L)	Na (dissolved) (mg/L)	Na (total) (mg/L)	K (dissolved) (mg/L)	K (total) (mg/L)	HCO_3 (mg/L)	CO_3 (mg/L)	Cl (mg/L)	SO_4 (mg/L)	TDS (mg/L)
DRI	1-19	2/11/2015	37.9	NC	9.7	NC	42.5	NC	1.7	NC	185	ND	23.2	27.1	239
TT	1-19	2/11/2015	NC	36.4	NC	9.35	NC	30.7	NC	4.29	188	ND	12.8	20.9	232 H
DRI	1-20	2/10/2015	27.1	NC	7.0	NC	40.4	NC	<0.01	NC	132	ND	48.4	8.39	162
TT	1-20	2/10/2015	NC	25.6	NC	6.68	NC	18.0	NC	1.89 J	135	ND	4.1	6.44	158 H
DRI	1-24	2/11/2015	28.3	NC	7.2	NC	31.0	NC	0.08	NC	107	ND	28.2	27.4	204
TT	1-24	2/11/2015	NC	26.6	NC	6.74	NC	19.1	NC	2.81 J	107	ND	14.8	21.1	189 H
DRI	1-25	2/10/2015	30.5	NC	3.3	NC	61.5	NC	6.9	NC	195	ND	22.5	12.4	279
TT	1-25	2/10/2015	NC	28.8	NC	3.04	NC	47.4	NC	7.94	204	ND	6.49	9.27	279 H
TT	1-26	6/30/2015	NC	41.3	NC	2.2	NC	28.5	NC	2.85 J	114	ND	24.2	32.6	230
TT	1-27	5/12/2015	NC	51.8	NC	8.69 B	NC	22.6	NC	6.28	178	ND	22.6 B	22.4	278
TT	1-28	2/10/2015	NC	22.7	NC	5.58	NC	29.2	NC	2.1 J	131	ND	9.7	18.2	179 H
TT	1-29	6/24/2015	NC	22.2	NC	3.92	NC	27.7	NC	6.22	122	ND	13.0	25.5 B	225
TT	1-30	5/12/2015	NC	30.4	NC	4.76 B	NC	20.1	NC	3.1	115	ND	10.9 B	14.5	169
TT	1-31	6/14/2015	NC	33.0	NC	6.55	NC	18.5	NC	6.23	100	ND	35.5	27.9 B	254
TT	1-32	2/11/2015	NC	19.4	NC	4.79	NC	22.2	NC	1.51 J	121	ND	4.48	7.92	138 H
TT	1-33	3/31/2015	NC	22.4	NC	5.38	NC	24.5	NC	2.31 J	126	ND	9.79	14.4	174
TT	1-34	7/23/2015	NC	26.6	NC	6.43	NC	19.8	NC	4.75	120	ND	11.3	20.6	196
TT	1-35	2/10/2015	NC	18.9	NC	5.45	NC	20.9	NC	1.7 J	118	ND	3.36	6.35	140
TT	1-36	2/18/2015	NC	7.97	NC	2.1	NC	13.3 B	NC	2.37 J	58	ND	8.30 B	2.98 J	107 H
TT	1-37	2/18/2015	NC	7.37	NC	1.98	NC	13.2 B	NC	2.26 J	57	ND	4.04 B	2.29 J	107 H
Area 2 Pre-Hydraulic Fracturing															
DRI	2-1	9/4/2013	0.75	NC	0.06	NC	157	NC	1.8	NC	238	82.8	3.7	2.8	435
TT	2-1	9/4/2013	NC	3.17	NC	0.695	NC	162	NC	<0.237	190	106.2	3.74	<5	NC
TT	2-2	9/4/2013	NC	70.6	NC	10.4	NC	30.6	NC	3.77	307	ND	13.6	17.8	NC
TT	2-3	9/4/2013	NC	81.5	NC	12.5	NC	21.5	NC	5.26	346	ND	10.7	15.4	NC
DRI	2-4	9/4/2013	37.4	NC	6.7	NC	21.6	NC	2.4	NC	152	ND	13.8	26.2	207

Table A-2. Major-ion chemistry and total dissolved solids for upper Humboldt River Basin wells, springs, and streams (continued).

Agency (Units)	Location ID	Sample Date	Ca (dissolved) (mg/L)	Ca (total) (mg/L)	Mg (dissolved) (mg/L)	Mg (total) (mg/L)	Na (dissolved) (mg/L)	Na (total) (mg/L)	K (dissolved) (mg/L)	K (total) (mg/L)	HCO_3 (mg/L)	CO_3 (mg/L)	Cl (mg/L)	SO_4 (mg/L)	TDS (mg/L)
TT	2-4	9/4/2013	NC	36.9	NC	6.58	NC	22.5	NC	<0.237	153	ND	13.6	25.2	NC
TT	2-5	9/4/2013	NC	34.9	NC	5.2	NC	18.6	NC	<0.237	172	ND	<3	7.25	NC
TT	2-6	9/4/2013	NC	44.8	NC	4.18	NC	5.31	NC	<0.237	173	ND	<3	<5	NC
TT	2-7	9/4/2013	NC	50.4	NC	7.57	NC	10.9	NC	<0.237	211	ND	<3	7.89	NC
TT	2-8	10/8/2013	NC	42	NC	7.75	NC	6.34	NC	<0.237	145	ND	11.5	13.8	NC
TT	2-9	10/8/2013	NC	43.7	NC	8.02	NC	40.7	NC	<0.237	240	ND	5.25	29.4	NC
Area 2 Post-Hydraulic Fracturing															
DRI	2-1	6/23/2014	0.61	NC	<0.5	NC	160	NC	1.5	NC	171	120	4.0	0.57	390
TT	2-1	6/23/2014	NC	0.842	NC	0.0386 J	NC	168	NC	1.93 J	176	105	NC	NC	NC
DRI	2-2	6/23/2014	51	NC	12	NC	19	NC	4.9	NC	293	ND	6.6	10	290
TT	2-2	6/23/2014	NC	73.0	NC	11.9	NC	20.1	NC	5.25	295	ND	NC	NC	NC
TT	2-3	6/23/2014	NC	90.9	NC	14.2	NC	22.3	NC	5.78	332	ND	NC	NC	NC
DRI	2-4	6/23/2014	26	NC	6.5	NC	22	NC	3.4	NC	146	ND	13	25	190
TT	2-4	6/23/2014	NC	37.5	NC	6.99	NC	23.0	NC	2.59 J	144	ND	NC	NC	NC
TT	2-5	6/25/2014	NC	34.8	NC	5.24	NC	17.4	NC	0.954 J	154	ND	NC	NC	NC
TT	2-6	6/25/2014	NC	42.7	NC	4.04	NC	5.28	NC	0.865 J	138	ND	NC	NC	NC
TT	2-7	7/1/2014	NC	50.7	NC	8.06 B	NC	14.2	NC	1.390 J	200	ND	NC	NC	NC
TT	2-8	6/25/2014	NC	43.9	NC	8.54	NC	6.35	NC	1.28 J	142	ND	NC	NC	NC
TT	2-9	6/25/2014	NC	46.5	NC	9	NC	42.5	NC	1.35 J	226	ND	NC	NC	NC
DRI	2-10	4/1/2014	37.2	NC	2.54	NC	5.16	NC	1.2	NC	130	ND	2.4	5.4	138
DRI	2-10	6/23/2014	16	NC	0.97	NC	1.9	NC	1.6	NC	89	ND	0.71	1.9	71
DRI	2-11	6/25/2014	32	NC	5.2	NC	23	NC	1.7	NC	171	ND	12	16	220
DRI	2-12	6/24/2014	36	NC	12	NC	16	NC	1.8	NC	232	ND	6.5	7.4	210
DRI	2-13	6/24/2014	38	NC	6.7	NC	11	NC	2.2	NC	220	ND	3.3	5	190
DRI	2-14	6/24/2014	51	NC	14	NC	33	NC	8.2	NC	317	ND	12	25	300
DRI	2-15	9/5/2014	37.2	NC	5.5	NC	14.4	NC	1.7	NC	127	ND	12.8	16	322
DRI	2-16	9/25/2014	1.43	NC	0.025	NC	112	NC	6.8	NC	103	101	2.87	1.12	508

Table A-2. Major-ion chemistry and total dissolved solids for upper Humboldt River Basin wells, springs, and streams (continued).

Agency (Units)	Location ID	Sample Date	Ca (dissolved) (mg/L)	Ca (total) (mg/L)	Mg (dissolved) (mg/L)	Mg (total) (mg/L)	Na (dissolved) (mg/L)	Na (total) (mg/L)	K (dissolved) (mg/L)	K (total) (mg/L)	HCO_3 (mg/L)	CO_3 (mg/L)	Cl (mg/L)	SO_4 (mg/L)	TDS (mg/L)
DRI	M2C-M2-21B	9/25/2014	56.8	NC	3.62	NC	3390	NC	524	NC	791	ND	5854	11.1	8527
	M10C-M10-11B	-----	-----	-----	-----	-----	-----	-----	-----	-----	-----	-----	-----	-----	-----
Area 2 One-Year Post Hydraulic Fracturing															
TT	2-1	7/16/2015	NC	0.817	NC	0.0292 J	NC	163.0 B	NC	2.35 J B	192	95	4.02	0.312 J	424
DRI	2-2	3/18/2015	65.7	NC	9.51	NC	29.5	NC	3.53	NC	276	ND	8.07	16.4	246
TT	2-2	3/18/2015	NC	65.6	NC	9.68	NC	24.4	NC	3.9	282	ND	6.64 B	12.7	291
TT	2-3	3/18/2015	NC	90.9	NC	13.4	NC	23.3	NC	6.05	364	ND	11.0 B	19.0	393
DRI	2-4	3/18/2015	47.1	NC	6.38	NC	19.0	NC	2.09	NC	151	ND	15.3	30.8	184
TT	2-4	3/18/2015	NC	89.1	NC	13.3	NC	23.2	NC	5.9	153	ND	12.0 B	24.1	212
DRI	2-5	3/19/2015	40.2	NC	4.68	NC	14.1	NC	0.61	NC	163	ND	2.62	8.51	157
TT	2-5	3/19/2015	NC	34.5	NC	5.19	NC	20.3	NC	0.974 J	171	ND	2.83 J B	7.14	231
TT	2-6	3/24/2015	NC	48.3	NC	5.17	NC	5.83	NC	1.11 J	183	ND	1.89 J	2.6 J	195
TT	2-7	3/19/2015	NC	51.3	NC	7.76	NC	11.3	NC	1.27 J	217	ND	2.71 J B	7.51	201
TT	2-8	3/17/2015	NC	42.9	NC	7.95	NC	6.26	NC	1.18 J	138	ND	10.8	13.3	187
TT	2-9	3/24/2015	NC	43.6	NC	8.17	NC	41.1	NC	1.37 J	233	ND	4.6	25.9	268
DRI	2-13	3/19/2015	69.0	NC	10.6	NC	15.8	NC	2.51	NC	246	2	7.75	16.2	238
Area 3 Pre-Hydraulic Fracturing															
DRI	3-1	9/3/2014	17.2	NC	7.9	NC	36.9	NC	20.7	NC	195	ND	3.42	14.8	290
TT	3-1	9/3/2014	NC	16.7	NC	7.44	NC	48.6	NC	15.1	204	ND	NC	NC	NC
DRI	3-2	9/3/2014	8.4	NC	1.8	NC	29.0	NC	22.5	NC	140	ND	3.53	5.87	239
TT	3-2	9/3/2014	NC	8.11	NC	1.31	NC	39.8	NC	17.3	148	2	NC	NC	NC
DRI	3-3	9/3/2014	10.6	NC	0.2	NC	191	NC	6.4	NC	307	86	5.09	2.7	634
TT	3-3	9/3/2014	NC	0.721	NC	0.035 J	NC	203	NC	3.04	211	137	NC	NC	NC
DRI	3-4	9/4/2014	28.1	NC	21.9	NC	135	NC	27.1	NC	378	5	66.9	77.6	827
DRI	3-5	9/5/2014	17.7	NC	24	NC	201	NC	50.6	NC	207	48	137	223	1182

Table A-2. Major-ion chemistry and total dissolved solids for upper Humboldt River Basin wells, springs, and streams (continued).

Agency (Units)	Location ID	Sample Date	Ca (dissolved) (mg/L)	Ca (total) (mg/L)	Mg (dissolved) (mg/L)	Mg (total) (mg/L)	Na (dissolved) (mg/L)	Na (total) (mg/L)	K (dissolved) (mg/L)	K (total) (mg/L)	HCO_3 (mg/L)	CO_3 (mg/L)	Cl (mg/L)	SO_4 (mg/L)	TDS (mg/L)
DRI	3-6	9/30/2014	70.2	NC	18.5	NC	24.8	NC	10.9	NC	300	ND	10.0	46.5	348
TT	3-6	9/30/2014	NC	73.2	NC	18.1	NC	26.3 B	NC	7.72	325	ND	NC	NC	NC
DRI	3-7	9/30/2014	48.9	NC	15.2	NC	12.0	NC	7.1	NC	220	ND	5.0	21.5	272
TT	3-7	9/30/2014	NC	49.1	NC	14.5	NC	11.4 ^ B	NC	3.18	222	ND	NC	NC	NC
DRI	3-8	9/30/2014	65.0	NC	18.3	NC	15.7	NC	8.9	NC	264	ND	6.75	44.9	328
DRI	3-9	10/8/2014	36.5	NC	14.0	NC	9.1	NC	5.06	NC	176	ND	5.25	15.4	200
TT	3-9	10/8/2014	NC	35.7	NC	13.5	NC	10.9 B	NC	4.99	174 B	ND	NC	NC	NC
DRI	3-10	10/21/2014	54.2	NC	17.1	NC	9.7	NC	4.1	NC	205	ND	10.1	29.7	242
TT	3-10	10/29/2014	NC	51.8 ^	NC	15.4	NC	14.2 ^B	NC	4.23	212	ND	NC	NC	NC
DRI	3-11	10/21/2014	91.0	NC	28.9	NC	83.2	NC	8.5	NC	383	ND	62.9	116	612
TT	3-11	10/21/2014	NC	66.5	NC	17.7	NC	36.9	NC	5.62	305	ND	NC	NC	NC
TT	3-12	10/21/2014	NC	82.0	NC	25.7	NC	112	NC	5.29	428	3	NC	NC	NC
DRI	3-12	10/22/2014	70.6	NC	19.6	NC	41.0	NC	4.5	NC	336	ND	27.8	45.0	396
DRI	3-13	10/22/2014	<1	NC	<1	NC	1240	NC	64.4	NC	2001	264	518	<0.1	3336
TT	3-14	10/21/2014	NC	58.4	NC	15.8	NC	49.0	NC	3.08	354	ND	NC	NC	NC
TT	3-15	9/30/2014	NC	71.0	NC	21.6	NC	28.4 B	NC	7.47	332	7	NC	NC	NC
TT	3-16	12/8/2014	NC	15.7	NC	13.1	NC	30.7	NC	15.3	188	ND	NC	NC	NC
TT	3-17	12/8/2014	NC	44.9	NC	18.7	NC	10.1	NC	56.7	218	ND	NC	NC	NC
TT	3-18	12/8/2014	NC	51.6	NC	20.8	NC	97.4	NC	5.6	243	ND	NC	NC	NC
TT	3-19	12/8/2014	NC	11.1	NC	1.33	NC	577	NC	23.1	1415	ND	NC	NC	NC
TT	3-20	12/8/2014	NC	75.0	NC	43.7	NC	120.0	NC	12.5	458	ND	NC	NC	NC

DRI = Desert Research Institute
B = compound was found in the blank and sample
H = sample was prepped or analyzed beyond the specified holding time
J = result is less than the reporting limit but greater than or equal to the method detection limit and the concentration is an approximate value

NC = not collected
ND = none detected (below minimum detection limit)
TT = Tetra Tech
^ = instrument related quality check exceeds the control limits

Table A-3. Trace elements, SiO_2, and NO_3-N for upper Humboldt River Basin wells, springs, and streams.

Agency (Units)	Location ID	Sample Date	B (mg/L)	Ba (dissolved) (mg/L)	Ba (total) (mg/L)	Li (dissolved) (mg/L)	Li (total) (mg/L)	Sr (dissolved) (mg/L)	Sr (total) (mg/L)	SiO_2 (mg/L)	NO_3 - N (mg/L)	F (mg/L)	Br (mg/L)
Area 1 Pre-hydraulic Fracturing													
TT	1-1	3/31/2014	<0.00437	NC	0.154	NC	0.0133	NC	0.321	NC	NC	<0.5	<0.2
DRI	1-1	3/31/2014	0.07	0.14	NC	0.01	NC	0.26	NC	57.0	1.17	0.16	0.08
TT	1-2	3/31/2014	0.112	NC	0.0606	NC	<0.00261	NC	0.229	NC	NC	<0.5	<0.2
TT	1-3	3/31/2014	<0.00437	NC	0.106	NC	<0.00261	NC	0.609	NC	NC	<0.5	0.424
TT	1-4	3/31/2014	<0.00437	NC	0.583	NC	<0.00261	NC	0.227	NC	NC	<0.5	<0.2
TT	1-5	3/31/2014	<0.00437	NC	0.00433	NC	<0.00261	NC	0.150	NC	NC	<0.5	<0.2
TT	1-6	3/31/2014	<0.00437	NC	0.0545	NC	<0.00261	NC	0.174	NC	NC	<0.5	<0.2
TT	1-7	4/1/2014	0.111	NC	0.0686	NC	<0.00261	NC	0.33	NC	NC	<0.5	<0.2
TT	1-8	4/1/2014	0.194	NC	0.128	NC	0.0172	NC	0.495	NC	NC	0.582	0.262
TT	1-9	4/1/2014	<0.00437	NC	0.088	NC	<0.00261	NC	0.234	NC	NC	<0.5	<0.2
TT	1-10	4/1/2014	<0.00437	NC	0.0852	NC	0.0181	NC	0.271	NC	NC	<0.5	<0.2
TT	1-11	4/1/2014	<0.00437	NC	0.102	NC	0.141	NC	0.291	NC	NC	<0.5	<0.2
DRI	1-12	4/2/2014	0.04	0.12	NC	<0.01	NC	0.13	NC	12.1	0.93	0.08	0.02
TT	1-13	4/7/2014	<0.1	NC	0.0164	NC	<0.01	NC	0.0924	NC	NC	<0.5	<0.2
TT	1-13	4/18/2014	NC	NC	NC	NC	NC	NC	NC	NC	NC	NC	NC
DRI	1-13	4/18/2014	0.05	0.02	NC	0.01	NC	0.09	NC	NC	NC	NC	NC
TT	1-14	4/18/2014	0.393 B	NC	0.163	NC	0.196	NC	0.509	NC	NC	1.42 J	0.761
DRI	1-15	4/18/2014	0.51	0.03	NC	0.06	NC	0.55	NC	NC	0.59	0.98	0.24
DRI	1-16	9/22/2014	<0.01	0.02	NC	0.03	NC	0.093	NC	42.5	0.17	0.17	<0.01
TT	1-16	9/22/2014	0.0417 J B	NC	NC	NC	0.0151 B	NC	0.093	NC	NC	NC	NC
DRI	1-17	9/22/2014	<0.01	0.097	NC	<0.001	NC	0.33	NC	53.1	0.70	0.35	0.152
TT	1-17	9/22/2014	0.0722 J B	NC	NC	NC	0.0133 B	NC	0.342	NC	NC	NC	NC
DRI	1-18	9/22/2014	<0.01	0.037	NC	<0.001	NC	0.2	NC	35.3	0.78	0.20	<0.01
TT	1-18	9/22/2014	0.0674 J B	NC	NC	NC	0.00637 J B	NC	0.190	NC	NC	NC	NC
DRI	1-19	9/23/2014	0.26	0.06	NC	<0.001	NC	0.42	NC	30.2	0.08	0.71	<0.01

Table A-3. Trace elements, SiO_2, and NO_3-N for upper Humboldt River Basin wells, springs, and streams (continued).

Agency (Units)	Location ID	Sample Date	B (mg/L)	Ba (dissolved) (mg/L)	Ba (total) (mg/L)	Li (dissolved) (mg/L)	Li (total) (mg/L)	Sr (dissolved) (mg/L)	Sr (total) (mg/L)	SiO_2 (mg/L)	NO_3 - N (mg/L)	F (mg/L)	Br (mg/L)
.	1-19	9/23/2014	0.273 B	NC	NC	NC	0.059 B	NC	0.418	NC	NC	NC	NC
DRI	1-20	9/23/2014	0.07	0.04	NC	<0.001	NC	0.22	NC	38.7	2.58	0.20	<0.01
TT	1-20	9/23/2014	0.0768 J B	NC	NC	NC	0.0105 B	NC	0.197	NC	NC	NC	NC
DRI	1-21	9/23/2014	0.01	0.005	NC	<0.001	NC	0.24	NC	20.4	0.06	0.08	<0.01
DRI	1-22	9/24/2014	0.02	0.05	NC	0.014	NC	0.18	NC	42.9	0.50	0.30	<0.01
DRI	1-23	9/24/2014	<0.01	<0.001	NC	0.04	NC	0.05	NC	19.1	0.01	0.08	<0.01
DRI	1-24	9/29/2014	0.08	0.14	NC	<0.001	NC	0.24	NC	62.9	1.37	0.18	0.0604
TT	1-24	9/29/2014	0.0421 J	NC	NC	NC	0.015	NC	0.223	NC	NC	NC	NC
DRI	1-25	9/29/2014	0.2	<0.001	NC	0.016	NC	0.125	NC	99.4	0.14	2.20	0.0264
TT	1-25	9/29/2014	0.164	NC	NC	NC	0.047	NC	0.118	NC	NC	NC	NC
DRI	1-26	10/7/2014	0.067	0.03	NC	0.011	NC	0.18	NC	35.0	3.05	0.386	0.105
TT	1-26	10/7/2014	0.0601 J	NC	NC	NC	0.0118	NC	0.196	NC	NC	NC	NC
DRI	1-27	10/7/2014	0.109	0.086	NC	0.011	NC	0.22	NC	57.8	0.355	0.339	0.078
TT	1-27	10/7/2014	0.0807 J	NC	NC	NC	0.0126	NC	0.246	NC	NC	NC	NC
DRI	1-28	10/20/2014	<0.5	0.094	NC	0.007	NC	0.18	NC	33.1	1.76	0.236	0.0484
TT	1-28	10/20/2014	0.0619 J	NC	NC	NC	0.00834 J	NC	0.164	NC	NC	NC	NC
DRI	1-29	10/20/2014	<0.5	0.043	NC	0.011	NC	0.15	NC	70.9	0.122	0.467	0.0413
TT	1-29	10/20/2014	0.0968 J	NC	NC	NC	0.0118	NC	0.144	NC	NC	NC	NC
DRI	1-30	10/21/2014	<0.5	0.124	NC	0.009	NC	0.47	NC	26.3	1.45	0.486	0.0587
TT	1-30	10/21/2014	0.0424 J	NC	NC	NC	0.011	NC	0.446	NC	NC	NC	NC
TT	1-31	10/20/2014	0.0807 J	NC	NC	NC	0.0151	NC	0.226	NC	NC	NC	NC
TT	1-32	9/23/2014	0.0629 J B	NC	NC	NC	0.00926 J B	NC	0.167	NC	NC	NC	NC
TT	1-33	9/22/2014	0.0512 J B	NC	NC	NC	0.0254 B	NC	0.176	NC	NC	NC	NC
TT	1-34	9/22/2014	0.146 B	NC	NC	NC	0.010 B	NC	0.245	NC	NC	NC	NC
TT	1-35	9/23/2014	0.0798 J B	NC	NC	NC	0.00772 J B	NC	152	NC	NC	NC	NC
TT	1-36	11/12/2014	0.0332 J	NC	NC	NC	0.021	NC	0.0872	NC	NC	NC	NC
TT	1-37	11/12/2014	0.033 J	NC	NC	NC	0.0161	NC	0.0809	NC	NC	NC	NC

Table A-3. Trace elements, SiO_2, and NO_3-N for upper Humboldt River Basin wells, springs, and streams (continued).

Agency (Units)	Location ID	Sample Date	B (mg/L)	Ba (dissolved) (mg/L)	Ba (total) (mg/L)	Li (dissolved) (mg/L)	Li (total) (mg/L)	Sr (dissolved) (mg/L)	Sr (total) (mg/L)	SiO_2 (mg/L)	NO_3 - N (mg/L)	F (mg/L)	Br (mg/L)
Area 1 Post-hydraulic Fracturing													
TT	1-1	2/25/2015	0.0744 J	NC	0.141	NC	0.00972 J	NC	0.283	24.2	1.07	0.227 J	NC
DRI	1-2	6/8/2015	0.069 J	0.06	NC	NC	NC	0.16	NC	NC	NC	NC	NC
TT	1-2	3/4/2015	0.0952 J	NC	0.0497	NC	<0.00261	NC	0.170	16.1	<0.019	0.310 J	<0.113
DRI	1-3	6/8/2015	0.205 J	0.21	NC	NC	NC	0.7	NC	NC	NC	NC	NC
TT	1-3	3/4/2015	0.121	NC	0.138	NC	0.00544 J	NC	0.460	21.6	0.0221 J	0.203 J	0.357
DRI	1-4	6/9/2015	0.072 J	0.05	NC	NC	NC	0.18	NC	NC	NC	NC	NC
TT	1-4	2/25/2015	0.0663 J	NC	0.0611	NC	0.00673 J	NC	0.195	20.7	0.945	0.325 J	NC
DRI	1-5	6/9/2015	0.035 J	0.006 J	NC	NC	NC	0.12	NC	NC	NC	NC	NC
TT	1-6	2/25/2015	0.022 J	NC	0.0506	NC	0.00335 J	NC	0.153	19.0	0.987	0.208 J	NC
DRI	1-7	6/9/2015	0.09 J	0.06	NC	NC	NC	0.28	NC	NC	NC	NC	NC
TT	1-7	2/26/2015	0.114	NC	0.0672	NC	0.00752 J	NC	0.302	22.0	2.45	0.507	NC
DRI	1-8	6/9/2015	0.116 J	0.06	NC	NC	NC	0.27	NC	NC	NC	NC	NC
TT	1-8	2/26/2015	0.0864 J	NC	0.0634	NC	0.0062 J	NC	0.287	21.2	1.08	0.460 J	NC
TT	1-9	2/26/2015	0.0485 J	NC	0.0838	NC	0.00352 J	NC	0.218	15.9	2.17	0.152 J	NC
TT	1-10	2/23/2015	58.5 J	NC	0.0814	NC	0.015	NC	0.255	23.4	0.994	0.365 J	NC
TT	1-11	2/23/2015	0.0808 J	NC	0.097	NC	0.0146	NC	0.279	15.1	0.557	0.324 J	NC
DRI	1-13	6/8/2015	0.081 J	0.02	NC	NC	NC	0.09	NC	NC	NC	NC	NC
TT	1-13	6/8/2015	0.0538 J B	NC	0.0227 B	NC	0.0104	NC	0.0968 B	15.7	0.898	0.138 J	<0.113
DRI	1-14	6/8/2015	0.5	0.05	NC	NC	NC	0.41	NC	NC	NC	NC	NC
TT	1-14	6/8/2015	0.5 B	NC	0.139 B	NC	0.224	NC	0.476 B	60.0	<0.019	1.71	0.31
TT	1-16	3/31/2015	0.0446 J	NC	0.0329	NC	0.0148	NC	0.0926	18.2	0.174	0.213 J	<0.113
DRI	1-17	2/11/2015	0.18	0.101	NC	0.01	NC	0.31	NC	37.0	0.15	0.21	<0.005
TT	1-17	2/11/2015	0.065 J	NC	0.111	NC	0.00701 J	NC	0.275	20.9	0.112	0.242 J B	NC
DRI	1-18	2/11/2015	0.23	0.044	NC	0.006	NC	0.22	NC	25.7	0.88	0.21	<0.005
TT	1-18	2/11/2015	0.0064 J	NC	0.0518	NC	0.00432 J	NC	0.202	16.3	0.923	0.232 J B	NC

Table A-3. Trace elements, SiO_2, and NO_3-N for upper Humboldt River Basin wells, springs, and streams (continued).

Agency (Units)	Location ID	Sample Date	B (mg/L)	Ba (dissolved) (mg/L)	Ba (total) (mg/L)	Li (dissolved) (mg/L)	Li (total) (mg/L)	Sr (dissolved) (mg/L)	Sr (total) (mg/L)	SiO_2 (mg/L)	NO_3 - N (mg/L)	F (mg/L)	Br (mg/L)
DRI	1-19	2/11/2015	0.22	0.038	NC	0.021	NC	0.30	NC	25.7	<0.1	0.31	<0.005
TT	1-19	2/11/2015	0.0931 J	NC	0.045	NC	0.0153	NC	0.276	16.8	<0.019	0.355 J B	NC
DRI	1-20	2/10/2015	0.30	0.038	NC	0.005	NC	0.22	NC	25.5	2.77	0	<0.005
TT	1-20	2/10/2015	0.0798 J	NC	0.0448	NC	<0.00261	NC	0.190	15.7	2.59	0.267 J B	NC
DRI	1-24	2/11/2015	0.18	0.097	NC	0.01	NC	0.26	NC	37.4	1.61	0.18	<0.005
TT	1-24	2/11/2015	0.041 J	NC	0.109	NC	0.00797 J	NC	0.229	26.7	1.73	0.194 J B	NC
DRI	1-25	2/10/2015	0.40	0.003	NC	0.037	NC	0.14	NC	48.4	0.10	2.39	<0.005
TT	1-25	2/10/2015	0.188	NC	0.00221 J	NC	0.0416	NC	0.126	42.6	0.0345 J	2.45 B	NC
TT	1-26	6/30/2015	0.0597 J	Nc	0.0318	Nc	0.014	NC	0.191	15.8	3.18	0.265 J	0.139 J
TT	1-27	5/12/2015	0.0794 J	NC	0.0897	NC	0.0144	NC	0.233 B	28.6	0.393	0.397 J	<0.113
TT	1-28	2/10/2015	0.0708 J	NC	0.1	NC	0.00357 J	NC	0.182	14.0	1.91	0.140 J B	NC
TT	1-29	6/24/2015	0.104	NC	0.0422	NC	0.174	NC	0.140	27.6	0.0865 J	0.292 J	<0.113
TT	1-30	5/12/2015	0.0491 J	NC	0.137	NC	0.0095 J	NC	0.495 B	11.8	1.28	0.288 J	<0.113
TT	1-31	6/24/2015	0.0869 J	NC	0.0279	NC	0.0192	NC	0.216	28.5	2.39	0.209	0.190 J
TT	1-32	2/11/2015	0.0607 J	NC	0.0404	NC	0.0063 J	NC	0.168	14.9	0.639	0.181 J B	NC
TT	1-33	3/31/2015	0.0555 J	NC	0.0716	NC	0.0223	NC	0.174	21.0	0.33	0.275 J	<0.113
TT	1-34	7/23/2015	0.0904 J	NC	0.120	NC	0.00963 J	NC	0.191	22.6 F1	0.0888 J	0.204 J	<0.113
TT	1-35	2/10/2015	0.0779 J	NC	0.0281	NC	0.00359 J	NC	0.148	16.4	0.957	0.370 J B	NC
TT	1-36	2/18/2015	0.0367 J	NC	0.0686	NC	0.0204	NC	NC	24.8	0.0343 J	0.295 J	NC
TT	1-37	2/18/2015	0.0372 J	NC	0.0432	NC	0.0155	NC	NC	27.7	0.0442 J	0.371 J	NC
Area 2 Pre-Hydraulic Fracturing													
DRI	2-1	9/4/2013	0.86	<0.005	NC	<0.01	NC	NC	NC	54.3	<0.01	3.73	0.02
TT	2-1	9/4/2013	NC	NC	NC	NC	0.0113	NC	NC	NC	NC	3.3	<0.2
TT	2-2	9/4/2013	NC	NC	NC	NC	<0.00261	NC	NC	NC	NC	<0.5	<0.2
TT	2-3	9/4/2013	NC	NC	NC	NC	<0.00261	NC	NC	NC	NC	<0.5	<0.2
DRI	2-4	9/4/2013	0.05	<0.005	NC	0.01	NC	NC	NC	29.1	0.07	0.21	0.06

Table A-3. Trace elements, SiO_2, and NO_3-N for upper Humboldt River Basin wells, springs, and streams (continued).

Agency (Units)	Location ID	Sample Date	B (mg/L)	Ba (dissolved) (mg/L)	Ba (total) (mg/L)	Li (dissolved) (mg/L)	Li (total) (mg/L)	Sr (dissolved) (mg/L)	Sr (total) (mg/L)	SiO_2 (mg/L)	NO_3 - N (mg/L)	F (mg/L)	Br (mg/L)
TT	2-4	9/4/2013	NC	NC	NC	NC	<0.00261	NC	NC	NC	NC	<0.5	<0.2
TT	2-5	9/4/2013	NC	NC	NC	NC	<0.00261	NC	NC	NC	NC	<0.5	<0.2
TT	2-6	9/4/2013	NC	NC	NC	NC	<0.00261	NC	NC	NC	NC	<0.5	<0.2
TT	2-7	9/4/2013	NC	NC	NC	NC	<0.00261	NC	NC	NC	NC	<0.5	<0.2
TT	2-8	10/8/2013	NC	NC	NC	NC	<0.00261	NC	NC	NC	NC	<0.5	<0.2
TT	2-9	10/8/2013	NC	NC	NC	NC	<0.00261	NC	NC	NC	NC	<0.5	<0.2
Area 2 Post-hydraulic Fracturing													
DRI	2-1	6/23/2014	0.87	0.055	NC	0.0074	NC	<0.02	NC	49	<0.25	3.9	<0.25
TT	2-1	6/23/2014	0.911	NC	NC	NC	0.00622 J	NC	0.00689 J	NC	NC	NC	NC
DRI	2-2	6/23/2014	0.13	0.055	NC	0.013	NC	0.26	NC	31	<0.25	0.26	<0.25
TT	2-2	6/23/2014	0.0782 J	NC	NC	NC	0.0107	NC	0.313	NC	NC	NC	NC
TT	2-3	6/23/2014	0.0942 J	NC	NC	NC	0.00964 J	NC	0.368	NC	NC	NC	NC
DRI	2-4	6/23/2014	0.11	0.055	NC	0.01	NC	0.25	NC	25	<0.25	<0.25	<0.25
TT	2-4	6/23/2014	0.0513 J	NC	NC	NC	0.00614 J	NC	0.295	NC	NC	NC	NC
TT	2-5	6/25/2014	0.0394 J	NC	NC	NC	0.0035 J	NC	0.161	NC	NC	NC	NC
TT	2-6	6/25/2014	0.0198 J	NC	NC	NC	<0.00261	NC	0.146	NC	NC	NC	NC
TT	2-7	7/1/2014	0.0397 J B	NC	NC	NC	<0.00261	NC	0.211	NC	NC	NC	NC
TT	2-8	6/25/2014	0.0209 J	NC	NC	NC	<0.00261	NC	0.241	NC	NC	NC	NC
TT	2-9	6/25/2014	0.237	NC	NC	NC	0.00683 J	NC	0.278	NC	NC	NC	NC
DRI	2-10	4/1/2014	0.02	0.02	NC	<0.01	NC	0.11	NC	13.4	<0.01	0.05	<0.02
DRI	2-10	6/23/2014	<0.1	0.0075	NC	<0.005	NC	0.059	NC	6.7	<0.25	<0.25	<0.25
DRI	2-11	6/25/2014	0.12	0.070	NC	0.015	NC	0.21	NC	32	1.3	0.4	<0.25
DRI	2-12	6/24/2014	<0.1	0.10	NC	0.0075	NC	0.25	NC	22	<0.25	<0.25	<0.25
DRI	2-13	6/24/2014	<0.1	0.028	NC	0.0061	NC	0.19	NC	17	<0.25	<0.25	<0.25
DRI	2-14	6/24/2014	0.17	0.13	NC	0.060	NC	0.58	NC	22	0.36	0.65	<0.25
DRI	2-15	9/5/2014	0.08	0.0423	NC	0.0035	NC	0.17	NC	25.7	1.1	0.14	<0.05

Table A-3. Trace elements, SiO_2, and NO_3-N for upper Humboldt River Basin wells, springs, and streams (continued).

Agency (Units)	Location ID	Sample Date	B (mg/L)	Ba (dissolved) (mg/L)	Ba (total) (mg/L)	Li (dissolved) (mg/L)	Li (total) (mg/L)	Sr (dissolved) (mg/L)	Sr (total) (mg/L)	SiO_2 (mg/L)	NO_3 - N (mg/L)	F (mg/L)	Br (mg/L)
DRI	2-16	9/25/2014	0.33	<0.001	NC	0.05	NC	0.007	NC	113	0.01	3.43	<0.01
DRI	M2C-M2-21B	9/25/2014	15.0	10.8	NC	19.2	NC	46.7	NC	192	<0.001	24.1	<0.01
	M10C-M10-11B		-----	-----	-----	-----	-----	-----	-----	-----	-----	-----	-----
Area 2 One-Year Post Hydraulic Fracturing													
DRI	2-1	7/16/2015	0.836	NC	<0.000576	NC	0.0106	NC	0.00625 J B	25.0 B	<0.019	4.16	<0.113
DRI	2-2	3/18/2015	0.11	0.05	NC	0.006	NC	0.28	NC	27.2	<0.1	0.33	0.048
TT	2-2	3/18/2015	0.0959 J	NC	0.05	NC	0.01	NC	0.248	13.8	<0.019	0.307 J	<0.113
TT	2-3	3/18/2015	0.099 J	NC	0.0618	NC	0.0109	NC	0.342	15.7	0.0531 J	0.352 J	<0.113
DRI	2-4	3/18/2015	0.03	0.05	NC	0.005	NC	0.29	NC	22.5	<0.1	0.16	0.060
TT	2-4	3/18/2015	0.0983 J	NC	0.0597	NC	0.00844 J	NC	0.336	15.4	<0.019	0.271 J	<0.113
DRI	2-5	3/19/2015	0.02	0.06	NC	0.003	NC	0.16	NC	25.5	0.34	0.16	0.029
TT	2-5	3/19/2015	0.0461 J	NC	0.0559 B	NC	0.004 J	NC	0.154	13.8	0.464	0.243 J	<0.113
TT	2-6	3/24/2015	0.0172 J	NC	0.0349 B	NC	<0.00261	NC	0.146	10.2	0.0729 J	<0.06	<0.113
TT	2-7	3/19/2015	0.0301 J	NC	0.0373 B	NC	0.00338 J	NC	0.199	10.1	0.383	0.112 J	<0.113
Area 3 Pre-Hydraulic Fracturing													
DRI	3-1	9/3/2014	0.20	0.0129	NC	0.0413	NC	0.21	NC	51.2	<0.001	0.43	<0.05
TT	3-1	9/3/2014	0.0992 J	NC	NC	NC	0.0433	NC	0.202	NC	NC	NC	NC
DRI	3-2	9/3/2014	0.25	0.033	NC	0.033	NC	0.15	NC	58.8	0.002	0.51	<0.05
TT	3-2	9/3/2014	0.168	NC	NC	NC	0.0356	NC	0.141	NC	NC	NC	NC
DRI	3-3	9/3/2014	1.23	0.0056	NC	0.0024	NC	0.01	NC	72.5	<0.001	9.26	<0.05
TT	3-3	9/3/2014	1.05	NC	NC	NC	<0.00261	NC	0.0126	NC	NC	NC	NC
DRI	3-4	9/4/2014	0.48	0.214	NC	0.131	NC	0.71	NC	66.7	<0.001	1.05	<0.05
DRI	3-5	9/5/2014	0.62	0.0222	NC	0.066	NC	0.31	NC	11.7	<0.001	1.16	<0.05
DRI	3-6	9/30/2014	0.13	0.15	NC	<0.001	NC	0.35	NC	46.3	0.43	0.41	0.0353
TT	3-6	9/30/2014	0.0913 J	NC	NC	NC	0.0422	NC	0.349	NC	NC	NC	NC
DRI	3-7	9/30/2014	0.06	0.18	NC	<0.001	NC	0.19	NC	42.1	0.16	0.17	0.0198

Table A-3. Trace elements, SiO_2, and NO_3-N for upper Humboldt River Basin wells, springs, and streams (continued).

Agency (Units)	Location ID	Sample Date	B (mg/L)	Ba (dissolved) (mg/L)	Ba (total) (mg/L)	Li (dissolved) (mg/L)	Li (total) (mg/L)	Sr (dissolved) (mg/L)	Sr (total) (mg/L)	SiO_2 (mg/L)	NO_3 - N (mg/L)	F (mg/L)	Br (mg/L)
TT	3-7	9/30/2014	0.0327 J	NC	NC	NC	0.00638 J	NC	0.179	NC	NC	NC	NC
DRI	3-8	9/30/2014	0.08	0.19	NC	<0.001	NC	0.48	NC	37.8	30	0.73	23.4
DRI	3-9	10/8/2014	0.047	0.14	NC	0.011	NC	0.21	NC	49.9	0.277	0.373	0.0218
TT	3-9	10/8/2014	0.0324 J	NC	NC	NC	0.0128	NC	0.231	NC	NC	NC	NC
DRI	3-10	10/21/2014	<0.5	0.166	NC	0.006	NC	0.23	NC	42.5	0.885	0.262	0.0543
TT	3-10	10/29/2014	0.041 J	NC	NC	NC	0.00749 J	NC	0.260	NC	NC	NC	NC
DRI	3-11	10/21/2014	0.5	0.2	NC	0.048	NC	0.42	NC	24.6	<0.1	0.62	0.214
TT	3-11	10/21/2014	0.126	NC	NC	NC	0.00932 J	NC	0.345	NC	NC	NC	NC
TT	3-12	10/21/2014	0.502	NC	NC	NC	0.053	NC	0.417	NC	NC	NC	NC
DRI	3-12	10/22/2014	<0.5	0.075	NC	0.014	NC	0.33	NC	39.9	0.267	0.551	0.1
DRI	3-13	10/22/2014	22.8	0.083	NC	0.001	NC	0.08	NC	76	<0.1	78.0	<0.02
TT	3-14	10/21/2014	0.220	NC	NC	NC	0.0132	NC	0.290	NC	NC	NC	NC
TT	3-15	9/30/2014	0.0903 J	NC	NC	NC	0.0746	NC	0.451	NC	NC	NC	NC
TT	3-16	12/8/2014	0.0619 J	NC	NC	NC	0.057	NC	0.102	NC	NC	NC	NC
TT	3-17	12/8/2014	0.0244 J	NC	NC	NC	0.0112	NC	0.284	NC	NC	NC	NC
TT	3-18	12/8/2014	0.0242 J	NC	NC	NC	0.0095 J	NC	0.278	NC	NC	NC	NC
TT	3-19	12/8/2014	1.37	NC	NC	NC	1.25	NC	0.395	NC	NC	NC	NC
TT	3-20	12/8/2014	0.493	NC	NC	NC	0.0901	NC	0.629	NC	NC	NC	NC

DRI = Desert Research Institute
B = compound was found in the blank and sample
J = result is less than the reporting limit but greater than or equal to the method detection limit and the concentration is an approximate value

NC = not collected
TT = Tetra Tech

Table A-4. Methane, ethane, propane, methane isotopes, and noble gases for upper Humboldt River Basin wells, springs, and streams.

Agency (Units)	Location ID	Sample Date	Methane (µg/L)	Ethane (µg/L)	Propane (µg/L)	$\delta^{13}C$ CH_4 (‰)	$\delta^{2}H$ CH_4 (‰)	Ar (ccSTP/g)	Ne (ccSTP/g)	Kr (ccSTP/g)	Xe (ccSTP/g)	^{4}He (ccSTP/g)	R/R_a
Area 1 Pre-hydraulic Fracturing													
TT	1-1	3/31/2014	<0.218	<0.573	<0.560	NC	NC	NC	NC	NC	NC	NC	NC
DRI	1-1	3/31/2014	NC	NC	NC	-49.95	Q	4.11E-04	3.09E-07	8.67E-08	1.19E-08	7.44E-08	2.48
TT	1-2	3/31/2014	16.7	<0.573	<0.560	NC	NC	NC	NC	NC	NC	NC	NC
DRI	1-2	3/31/2014	NC	NC	NC	-45.61	-344.8	3.80E-04	1.86E-07	8.36E-08	1.36E-08	4.11E-08	0.98
TT	1-3	3/31/2014	79.6	<0.573	<0.560	NC	NC	NC	NC	NC	NC	NC	NC
DRI	1-3	3/31/2014	NC	NC	NC	-37.03	-355.7	NA	NA	NA	NA	NA	NA
TT	1-4	3/31/2014	<0.218	<0.573	<0.560	NC	NC	NC	NC	NC	NC	NC	NC
DRI	1-4	3/31/2014	NC	NC	NC	-45.98	Q	3.36E-04	1.97E-07	7.54E-08	1.14E-08	4.62E-08	1.15
TT	1-5	3/31/2014	<0.218	<0.573	<0.560	NC	NC	NC	NC	NC	NC	NC	NC
DRI	1-5	3/31/2014	NC	NC	NC	-48.93	Q	NC	NC	NC	NC	NC	NC
TT	1-6	3/31/2014	<0.218	<0.573	<0.560	NC	NC	NC	NC	NC	NC	NC	NC
TT	1-7	4/1/2014	<0.218	<0.573	<0.560	NC	NC	NC	NC	NC	NC	NC	NC
DRI	1-7	4/1/2014	NC	NC	NC	-44.96	Q	NC	NC	NC	NC	NC	NC
TT	1-8	4/1/2014	47.4	<0.573	<0.560	NC	NC	NC	NC	NC	NC	NC	NC
DRI	1-8	4/1/2014	NC	NC	NC	-40.75	-384.1	NC	NC	NC	NC	NC	NC
TT	1-8	5/13/2014	NC	NC	NC	-52.7	BAL	NC	NC	NC	NC	NC	NC
TT	1-9	4/1/2014	<0.218	<0.573	<0.560	NC	NC	NC	NC	NC	NC	NC	NC
TT	1-10	4/1/2014	<0.218	<0.573	<0.560	NC	NC	NC	NC	NC	NC	NC	NC
TT	1-11	4/1/2014	<0.218	<0.573	<0.560	NC	NC	NC	NC	NC	NC	NC	NC
DRI	1-12	4/2/2014	<5.0	<5.0	<5.0	-50.32	Q	3.20E-04	1.79E-07	7.63E-08	1.13E-08	5.84E-08	0.79
TT	1-13	4/7/2014	63.5	<0.573	<0.560	NC	NC	NC	NC	NC	NC	NC	NC
DRI	1-13	4/18/2014	NC	NC	NC	-31.05	BAL	NC	NC	NC	NC	NC	NC
TT	1-14	4/18/2014	0.64 J	<0.573	<0.560	NC	NC	NC	NC	NC	NC	NC	NC
DRI	1-14	4/18/2014	NC	NC	NC	-18.24	BAL	NC	NC	NC	NC	NC	NC
DRI	1-15	4/18/2014	21	<5.0	<5.0	-17.14	BAL	NC	NC	NC	NC	NC	NC

Table A-4. Methane, ethane, propane, methane isotopes, and noble gases for upper Humboldt River Basin wells, springs, and streams (continued).

Agency (Units)	Location ID	Sample Date	Methane (µg/L)	Ethane (µg/L)	Propane (µg/L)	$\delta^{13}C$ CH_4 (‰)	$\delta^{2}H$ CH_4 (‰)	Ar (ccSTP/g)	Ne (ccSTP/g)	Kr (ccSTP/g)	Xe (ccSTP/g)	^{4}He (ccSTP/g)	R/R_a
DRI	1-16	9/22/2014	<5.0	<5.0	<5.0	NC	NC	1.67E-04	1.61E-07	4.16E-08	5.48E-09	5.51E-08	1.01
TT	1-16	9/22/2014	ND	ND	ND	NC	NC	NC	NC	NC	NC	NC	NC
DRI	1-17	9/22/2014	<5.0	<5.0	<5.0	NC	NC	NC	NC	NC	NC	NC	NC
TT	1-17	9/22/2014	ND	ND	ND	NC	NC	NC	NC	NC	NC	NC	NC
DRI	1-18	9/22/2014	<5.0	<5.0	<5.0	NC	NC	NC	NC	NC	NC	NC	NC
TT	1-18	9/22/2014	ND	ND	ND	NC	NC	NC	NC	NC	NC	NC	NC
DRI	1-19	9/23/2014	45	<5.0	<5.0	-45.59	-335.8	NC	NC	NC	NC	NC	NC
TT	1-19	9/23/2014	22.7	ND	ND	NC	NC	NC	NC	NC	NC	NC	NC
DRI	1-20	9/23/2014	<5.0	<5.0	<5.0	NC	NC	5.01E-04	3.43E-07	1.08E-07	1.49E-08	8.20E-08	1.22
TT	1-20	9/23/2014	ND	ND	ND	NC	NC	NC	NC	NC	NC	NC	NC
DRI	1-21	9/23/2014	28	<5.0	<5.0	-52.10	-362.7	NC	NC	NC	NC	NC	NC
DRI	1-22	9/24/2014	7.0 J	<5.0	<5.0	-46.30	-224.4 Q	NC	NC	NC	NC	NC	NC
DRI	1-23	9/24/2014	<5.0	<5.0	<5.0	NC	NC	NC	NC	NC	NC	NC	NC
DRI	1-24	9/29/2014	32	8.0 J	<5.0	-49.77	-264.8 Q	3.87E-04	2.40E-07	9.05E-08	1.19E-08	6.25E-08	0.84
TT	1-24	9/29/2014	ND	ND	ND	NC	NC	NC	NC	NC	NC	NC	NC
DRI	1-25	9/29/2014	<5.0	<5.0	<5.0	NC	NC	NC	NC	NC	NC	NC	NC
TT	1-25	9/29/2014	ND	ND	ND	NC	NC	NC	NC	NC	NC	NC	NC
DRI	1-26	10/7/2014	<5.0	<5.0	<5.0	NC	NC	3.28E-04	1.75E-07	8.08E-08	1.16E-08	5.25E-08	0.92
TT	1-26	10/7/2014	ND	ND	ND	NC	NC	NC	NC	NC	NC	NC	NC
DRI	1-27	10/7/2014	<5.0	<5.0	<5.0	NC	NC	NC	NC	NC	NC	NC	NC
TT	1-27	10/7/2014	ND	ND	ND	NC	NC	NC	NC	NC	NC	NC	NC
DRI	1-28	10/20/2014	<5.0	<5.0	<5.0	NC	NC	NC	NC	NC	NC	NC	NC
TT	1-28	10/20/2014	ND	ND	ND	NC	NC	NC	NC	NC	NC	NC	NC
DRI	1-29	10/20/2014	<5.0	<5.0	<5.0	NC	NC	3.00E-04	2.46E-07	6.80E-08	9.07E-09	7.91E-08	0.93
TT	1-29	10/20/2014	ND	ND	ND	NC	NC	NC	NC	NC	NC	NC	NC
DRI	1-30	10/21/2014	<5.0	<5.0	<5.0	NC	NC	3.16E-04	1.62E-07	7.89E-08	1.03E-08	4.85E-08	0.80

Table A-4. Methane, ethane, propane, methane isotopes, and noble gases for upper Humboldt River Basin wells, springs, and streams (continued).

Agency (Units)	Location ID	Sample Date	Methane (µg/L)	Ethane (µg/L)	Propane (µg/L)	$\delta^{13}C$ CH_4 (‰)	$\delta^{2}H$ CH_4 (‰)	Ar (ccSTP/g)	Ne (ccSTP/g)	Kr (ccSTP/g)	Xe (ccSTP/g)	^{4}He (ccSTP/g)	R/R_a
TT	1-30	10/21/2014	ND	ND	ND	NC	NC	NC	NC	NC	NC	NC	NC
TT	1-31	10/20/2014	0.247 J	<0.573	<0.560	NC	NC	NC	NC	NC	NC	NC	NC
TT	1-32	9/23/2014	ND	ND	ND	NC	NC	NC	NC	NC	NC	NC	NC
TT	1-33	9/22/2014	ND	ND	ND	NC	NC	NC	NC	NC	NC	NC	NC
TT	1-34	9/22/2014	ND	ND	ND	NC	NC	NC	NC	NC	NC	NC	NC
TT	1-35	9/23/2014	ND	ND	ND	NC	NC	NC	NC	NC	NC	NC	NC
TT	1-36	11/12/2014	13.4	<0.573	<0.560	NC	NC	NC	NC	NC	NC	NC	NC
TT	1-37	11/12/2014	253	<0.573	<0.560	NC	NC	NC	NC	NC	NC	NC	NC
Area 1 Post-Hydraulic Fracturing													
TT	1-1	2/25/2015	1.18 J	<0.573	<0.560	NC	NC	NC	NC	NC	NC	NC	NC
DRI	1-2	6/8/2015	NC	NC	NC	-43.72	-223.8	3.15E-04	1.51E-07	7.23E-08	9.08E-09	3.60E-08	0.989
TT	1-2	3/4/2015	38.8	<0.573	<0.560	NC	NC	NC	NC	NC	NC	NC	NC
DRI	1-3	6/8/2015	NC	NC	NC	-37.81	-267.4	NC	NC	NC	NC	NC	NC
TT	1-3	3/4/2015	53.0	<0.573	<0.560	NC	NC	NC	NC	NC	NC	NC	NC
DRI	1-4	6/9/2015	NC	NC	NC	NC	NC	3.32E-04	1.78E-07	8.15E-08	1.09E-08	4.20E-08	1.148
TT	1-4	2/25/2015	<0.218	<0.573	<0.560	NC	NC	NC	NC	NC	NC	NC	NC
DRI	1-5	6/9/2015	NC	NC	NC	NC	NC	NC	NC	NC	NC	NC	NC
TT	1-6	2/25/2015	<0.218	<0.573	<0.560	NC	NC	NC	NC	NC	NC	NC	NC
DRI	1-7	6/9/2015	NC	NC	NC	NC	NC	NC	NC	NC	NC	NC	NC
TT	1-7	2/26/2015	<0.218	<0.573	<0.560	NC	NC	NC	NC	NC	NC	NC	NC
DRI	1-8	6/9/2015	NC	NC	NC	-43.01	-296.8	NC	NC	NC	NC	NC	NC
TT	1-8	2/26/2015	1.62 J	<0.573	<0.560	NC	NC	NC	NC	NC	NC	NC	NC
TT	1-9	2/26/2015	<0.218	<0.573	<0.560	NC	NC	NC	NC	NC	NC	NC	NC
TT	1-10	2/23/2015	<0.218	<0.573	0.793 J	NC	NC	NC	NC	NC	NC	NC	NC
TT	1-11	2/23/2015	<0.218	<0.573	<0.560	NC	NC	NC	NC	NC	NC	NC	NC
DRI	1-13	6/8/2015	NC	NC	NC	-50.82	-354.9	NC	NC	NC	NC	NC	NC

Table A-4. Methane, ethane, propane, methane isotopes, and noble gases for upper Humboldt River Basin wells, springs, and streams (continued).

Agency (Units)	Location ID	Sample Date	Methane (µg/L)	Ethane (µg/L)	Propane (µg/L)	$\delta^{13}C$ CH_4 (‰)	$\delta^{2}H$ CH_4 (‰)	Ar (ccSTP/g)	Ne (ccSTP/g)	Kr (ccSTP/g)	Xe (ccSTP/g)	^{4}He (ccSTP/g)	R/R_a
TT	1-13	6/8/2015	41.8	<0.573	<0.560	NC	NC	NC	NC	NC	NC	NC	NC
DRI	1-14	6/8/2015	NC	NC	NC	NC	NC	NC	NC	NC	NC	NC	NC
TT	1-14	6/8/2015	9.95	<0.573	<0.560	NC	NC	NC	NC	NC	NC	NC	NC
DRI	1-16	3/31/2015	<0.218	<0.573	<0.560	NC	NC	NC	NC	NC	NC	NC	NC
DRI	1-17	2/11/2015	<5.0	<5.0	<5.0	NC	NC	4.24E-04	2.77E-07	9.79E-08	1.38E-08	6.41E-08	1.91
TT	1-17	2/11/2015	<0.218	<0.573	<0.560	NC	NC	NC	NC	NC	NC	NC	NC
DRI	1-18	2/11/2015	<5.0	<5.0	<5.0	NC	NC	3.52E-04	1.99E-07	8.60E-08	1.23E-08	9.07E-08	1.06
TT	1-18	2/11/2015	<0.218	<0.573	<0.560	NC	NC	NC	NC	NC	NC	NC	NC
DRI	1-19	2/11/2015	31	<5.0	<5.0	-46.95	-304.7	NC	NC	NC	NC	NC	NC
TT	1-19	2/11/2015	21.1	<0.573	<0.560	NC	NC	NC	NC	NC	NC	NC	NC
DRI	1-20	2/10/2015	<5.0	<5.0	<5.0	NC	NC	4.92E-04	3.29E-07	1.04E-07	1.45E-08	7.27E-08	1.22
TT	1-20	2/10/2015	<0.218	<0.573	<0.560	NC	NC	NC	NC	NC	NC	NC	NC
DRI	1-24	2/11/2015	<5.0	<5.0	<5.0	NC	NC	3.85E-04	2.72E-07	8.65E-08	1.24E-08	6.42E-08	0.83
TT	1-24	2/11/2015	<0.218	<0.573	<0.560	NC	NC	NC	NC	NC	NC	NC	NC
DRI	1-25	2/10/2015	22	<5.0	<5.0	-71.49	-342.4	3.82E-04	2.61E-07	9.57E-08	1.40E-08	3.32E-06	0.44
TT	1-25	2/10/2015	12.6	<0.573	<0.560	NC	NC	NC	NC	NC	NC	NC	NC
TT	1-26	6/30/2015	<0.218	<0.573	<0.560	NC	NC	NC	NC	NC	NC	NC	NC
TT	1-27	5/12/2015	<0.218	<0.573	<0.560	NC	NC	NC	NC	NC	NC	NC	NC
TT	1-28	2/10/2015	<0.218	<0.573	<0.560	NC	NC	NC	NC	NC	NC	NC	NC
TT	1-30	5/12/2015	<0.218	<0.573	<0.560	NC	NC	NC	NC	NC	NC	NC	NC
TT	1-32	2/11/2015	<0.218	<0.573	<0.560	NC	NC	NC	NC	NC	NC	NC	NC
TT	1-33	3/31/2015	<0.218	<0.573	<0.560	NC	NC	NC	NC	NC	NC	NC	NC
TT	1-34	7/23/2015	<0.218	<0.573	<0.560	NC	NC	NC	NC	NC	NC	NC	NC
TT	1-35	2/10/2015	<0.218	<0.573	<0.560	NC	NC	NC	NC	NC	NC	NC	NC
TT	1-36	12/4/2014	NC	NC	NC	-21.8	NC	NC	NC	NC	NC	NC	NC
TT	1-36	2/18/2015	40.9	<0.573	<0.560	NC	NC	NC	NC	NC	NC	NC	NC

Table A-4. Methane, ethane, propane, methane isotopes, and noble gases for upper Humboldt River Basin wells, springs, and streams (continued).

Agency (Units)	Location ID	Sample Date	Methane (µg/L)	Ethane (µg/L)	Propane (µg/L)	$\delta^{13}C$ CH_4 (‰)	$\delta^{2}H$ CH_4 (‰)	Ar (ccSTP/g)	Ne (ccSTP/g)	Kr (ccSTP/g)	Xe (ccSTP/g)	^{4}He (ccSTP/g)	R/R_a
TT	1-37	12/3/2014	NC	NC	NC	-94.7	BAL	NC	NC	NC	NC	NC	NC
TT	1-37	2/18/2015	124	<0.573	<0.560	NC	NC	NC	NC	NC	NC	NC	NC
Area 2 Pre-hydraulic Fracturing													
DRI	2-1	9/4/2013	2800	7.2	<10.0	-67.18	-310.6	4.85E-04	3.73E-07	1.08E-07	1.52E-08	1.12E-06	0.136
TT	2-1	9/4/2013	4690	11.1	<0.560	NC	NC	NC	NC	NC	NC	NC	NC
TT	2-1	10/8/2013	NC	NC	NC	-78.8	-315	NC	NC	NC	NC	NC	NC
TT	2-2	9/4/2013	62	<0.573	<0.560	NC	NC	NC	NC	NC	NC	NC	NC
TT	2-3	9/4/2013	12.2	<0.573	<0.560	NC	NC	NC	NC	NC	NC	NC	NC
DRI	2-4	9/4/2013	<10.0	<10.0	<10.0	-56.6 Q	-212.4 Q	3.26E-04	1.80E-07	7.61E-08	1.12E-08	4.41E-08	0.945
TT	2-4	9/4/2013	<0.218	<0.573	<0.560	NC	NC	NC	NC	NC	NC	NC	NC
TT	2-5	9/4/2013	<0.218	<0.573	<0.560	NC	NC	NC	NC	NC	NC	NC	NC
TT	2-6	9/4/2013	<0.218	<0.573	<0.560	NC	NC	NC	NC	NC	NC	NC	NC
TT	2-7	9/4/2013	<0.218	<0.573	<0.560	NC	NC	NC	NC	NC	NC	NC	NC
TT	2-8	10/8/2013	<0.218	<0.573	<0.560	NC	NC	NC	NC	NC	NC	NC	NC
TT	2-9	10/8/2013	<0.218	<0.573	<0.560	NC	NC	NC	NC	NC	NC	NC	NC
Area 2 Post-hydraulic Fracturing													
DRI	2-1	6/23/2014	7200	18	<5.0	-69.14	-314.0	3.90E-04	2.34E-07	8.74E-08	1.03E-08	6.01E-07	0.13
TT	2-1	6/23/2014	4190	11.8	<0.560	NC	NC	NC	NC	NC	NC	NC	NC
DRI	2-2	6/23/2014	1600	<5.0	<5.0	-48.72	-382.2	NC	NC	NC	NC	NC	NC
TT	2-2	6/23/2014	1070	<0.573	<0.560	NC	NC	NC	NC	NC	NC	NC	NC
TT	2-3	6/23/2014	7.54	<0.573	<0.560	NC	NC	NC	NC	NC	NC	NC	NC
DRI	2-4	6/23/2014	5.0 J	<5.0	<5.0	NC	NC	3.43E-04	2.38E-07	7.30E-08	9.17E-09	7.08E-08	0.95
TT	2-4	6/23/2014	0.715 J	<0.573	<0.560	NC	NC	NC	NC	NC	NC	NC	NC
TT	2-5	6/25/2014	<0.218	<0.573	<0.560	NC	NC	NC	NC	NC	NC	NC	NC
TT	2-6	6/25/2014	<0.218	<0.573	<0.560	NC	NC	NC	NC	NC	NC	NC	NC
TT	2-7	7/1/2014	<0.218	<0.573	<0.560	NC	NC	NC	NC	NC	NC	NC	NC

Table A-4. Methane, ethane, propane, methane isotopes, and noble gases for upper Humboldt River Basin wells, springs, and streams (continued).

Agency (Units)	Location ID	Sample Date	Methane (µg/L)	Ethane (µg/L)	Propane (µg/L)	$\delta^{13}C$ CH_4 (‰)	$\delta^{2}H$ CH_4 (‰)	Ar (ccSTP/g)	Ne (ccSTP/g)	Kr (ccSTP/g)	Xe (ccSTP/g)	^{4}He (ccSTP/g)	R/R_a
TT	2-8	6/25/2014	<0.218	<0.573	<0.560	NC	NC	NC	NC	NC	NC	NC	NC
TT	2-9	6/25/2014	<0.218	<0.573	<0.560	NC	NC	NC	NC	NC	NC	NC	NC
DRI	2-10	4/1/2014	<5.0	<5.0	<5.0	-47.8	Q	3.24E-04	1.66E-07	7.81E-08	1.21E-08	3.78E-08	0.99
DRI	2-10	6/23/2014	5.0 J	<5.0	<5.0	NC	NC	NC	NC	NC	NC	NC	NC
DRI	2-11	6/25/2014	<5.0	<5.0	<5.0	NC	NC	NC	NC	NC	NC	NC	NC
DRI	2-12	6/24/2014	7.0 J	<5.0	<5.0	NC	NC	NC	NC	NC	NC	NC	NC
DRI	2-13	6/24/2014	11	<5.0	<5.0	-44.07	-292.5 Q	NC	NC	NC	NC	NC	NC
DRI	2-14	6/24/2014	<5.0	<5.0	<5.0	NC	NC	2.86E-04	1.56E-07	5.59E-08	8.12E-09	8.20E-08	1.19
DRI	2-15	9/5/2014	<5.0	<5.0	<5.0	NC	NC	NC	NC	NC	NC	NC	NC
DRI	2-16	9/25/2014	960	<5.0	<5.0	-89.64	-368.9	NC	NC	NC	NC	NC	NC
DRI	M2C-M2-21B	9/25/2014	1100	1300	1100	-43.08	-377.8	6.79E-07	1.53E-09	N	N	6.16E-08	1.61
	M10C-M10-11B	-----	-----	-----	-----	-----	-----	-----	-----	-----	-----	-----	-----
Area 2 One-Year Post Hydraulic Fracturing													
TT	2-1	7/16/2015	4510	11.6	<0.560	NC	NC	NC	NC	NC	NC	NC	NC
TT	2-1	7/23/2015	NC	NC	NC	-78.3	-304	NC	NC	NC	NC	NC	NC
DRI	2-2	3/18/2015	42	<5.0	<5.0	-43.24	-274.6	NC	NC	NC	NC	NC	NC
TT	2-2	3/18/2015	23.6	<0.573	<0.560	NC	NC	NC	NC	NC	NC	NC	NC
TT	2-3	3/18/2015	3.23 J	<0.573	<0.560	NC	NC	NC	NC	NC	NC	NC	NC
DRI	2-4	3/18/2015	<5.0	<5.0	<5.0	NC	NC	3.09E-04	1.93E-07	6.61E-08	8.03E-09	4.34E-08	0.94
TT	2-4	3/18/2015	1.53 J	<0.573	<0.560	NC	NC	NC	NC	NC	NC	NC	NC
DRI	2-5	3/19/2015	<5.0	<5.0	<5.0	NC	NC	4.23E-04	2.48E-07	8.77E-08	1.30E-08	5.96E-08	2.778
TT	2-5	3/19/2015	<0.218	<0.573	<0.560	NC	NC	NC	NC	NC	NC	NC	NC
TT	2-6	3/24/2015	<0.218	<0.573	<0.560	NC	NC	NC	NC	NC	NC	NC	NC
TT	2-7	3/19/2015	<0.218	<0.573	<0.560	NC	NC	NC	NC	NC	NC	NC	NC
TT	2-8	3/17/2015	<0.218	<0.573	<0.560	NC	NC	NC	NC	NC	NC	NC	NC
TT	2-9	3/24/2015	<0.218	<0.573	<0.560	NC	NC	NC	NC	NC	NC	NC	NC

Table A-4. Methane, ethane, propane, methane isotopes, and noble gases for upper Humboldt River Basin wells, springs, and streams (continued).

Agency (Units)	Location ID	Sample Date	Methane (µg/L)	Ethane (µg/L)	Propane (µg/L)	$\delta^{13}C$ CH_4 (‰)	$\delta^{2}H$ CH_4 (‰)	Ar (ccSTP/g)	Ne (ccSTP/g)	Kr (ccSTP/g)	Xe (ccSTP/g)	^{4}He (ccSTP/g)	R/R_a
DRI	2-13	3/19/2015	<5.0	<5.0	<5.0	NC	NC	3.26E-04	1.70E-07	8.13E-08	1.16E-08	3.70E-08	1.00
Area 3 Pre-Hydraulic Fracturing													
DRI	3-1	9/3/2014	95	<5.0	<5.0	-36.33	-258.4	NC	NC	NC	NC	NC	NC
DRI	3-1	9/3/2014	NC	NC	NC	NC	NC	NC	NC	NC	NC	NC	NC
TT	3-1	9/3/2014	74.7	<0.573	<0.560	NC	NC	NC	NC	NC	NC	NC	NC
TT	3-1	10/1/2014	NC	NC	NC	BAL	BAL	NC	NC	NC	NC	NC	NC
DRI	3-2	9/3/2014	46	<5.0	<5.0	-74.00	-239.1	3.93E-04	2.05E-07	9.76E-08	1.35E-08	9.95E-08	0.49
DRI	3-2	9/3/2014	NC	NC	NC	NC	NC	NC	NC	NC	NC	NC	NC
TT	3-2	9/3/2014	33.8	<0.573	<0.560	NC	NC	NC	NC	NC	NC	NC	NC
TT	3-2	10/1/2014	NC	NC	NC	-75.7	BAL	NC	NC	NC	NC	NC	NC
DRI	3-3	9/3/2014	4100	<5.0	<5.0	-62.28	-304.1	NC	NC	NC	NC	NC	NC
DRI	3-3	9/3/2014	NC	NC	NC	NC	NC	NC	NC	NC	NC	NC	NC
TT	3-3	9/3/2014	2760	1.71 J	<0.560	NC	NC	NC	NC	NC	NC	NC	NC
DRI	3-4	9/4/2014	110	<5.0	<5.0	-23.90	-249.7 Q	NC	NC	NC	NC	NC	NC
DRI	3-4	9/4/2014	NC	NC	NC	NC	NC	NC	NC	NC	NC	NC	NC
DRI	3-5	9/5/2014	29	<5.0	<5.0	-47.43	-324.5	2.60E-04	1.43E-07	6.73E-08	8.69E-09	3.55E-08	0.95
DRI	3-6	9/30/2014	<5.0	<5.0	<5.0	NC	NC	3.04E-04	1.59E-07	7.32E-08	9.57E-09	4.05E-08	1.00
TT	3-6	9/30/2014	ND	ND	ND	NC	NC	NC	NC	NC	NC	NC	NC
DRI	3-7	9/30/2014	<5.0	<5.0	<5.0	NC	NC	3.70E-04	2.17E-07	8.91E-08	1.31E-08	5.14E-08	1.07
TT	3-7	9/30/2014	<0.218	<0.573	<0.560	NC	NC	NC	NC	NC	NC	NC	NC
DRI	3-8	9/30/2014	<5.0	<5.0	<5.0	NC	NC	NC	NC	NC	NC	NC	NC
DRI	3-9	10/8/2014	<5.0	<5.0	<5.0	NC	NC	3.66E-04	2.11E-07	9.03E-08	1.28E-08	6.00E-08	0.84
TT	3-9	10/8/2014	<0.218	<0.573	<0.560	NC	NC	NC	NC	NC	NC	NC	NC
DRI	3-10	10/21/2014	<5.0	<5.0	<5.0	NC	NC	4.48E-04	2.55E-07	9.52E-08	1.26E-08	5.87E-08	1.41
TT	3-10	10/29/2014	<0.218	<0.573	<0.560	NC	NC	NC	NC	NC	NC	NC	NC
DRI	3-11	10/21/2014	<5.0	<5.0	<5.0	NC	NC	NC	NC	NC	NC	NC	NC
TT	3-11	10/21/2014	1.9 J	<0.573	<0.560	NC	NC	NC	NC	NC	NC	NC	NC

Table A-4. Methane, ethane, propane, methane isotopes, and noble gases for upper Humboldt River Basin wells, springs, and streams (continued).

Agency (Units)	Location ID	Sample Date	Methane (µg/L)	Ethane (µg/L)	Propane (µg/L)	$\delta^{13}C$ CH_4 (‰)	$\delta^{2}H$ CH_4 (‰)	Ar (ccSTP/g)	Ne (ccSTP/g)	Kr (ccSTP/g)	Xe (ccSTP/g)	^{4}He (ccSTP/g)	R/R_a
TT	3-11	12/3/2014	NC	NC	NC	-59.5	BAL	NC	NC	NC	NC	NC	NC
TT	3-12	10/21/2014	2.08 J	<0.573	<0.560	NC	NC	NC	NC	NC	NC	NC	NC
DRI	3-12	10/22/2014	<5.0	<5.0	<5.0	NC	NC	NC	NC	NC	NC	NC	NC
DRI	3-13	10/22/2014	21000	11	<5.0	-55.05	-302.3	1.18E-04	2.25E-08	N	N	7.73E-06	0.13
TT	3-14	10/21/2014	<0.218	<0.573	<0.560	NC	NC	NC	NC	NC	NC	NC	NC
TT	3-15	9/30/2014	4.4 J	ND	ND	NC	NC	NC	NC	NC	NC	NC	NC
TT	3-16	12/8/2014	0.324 J	<0.573	<0.560	NC	NC	NC	NC	NC	NC	NC	NC
TT	3-17	12/8/2014	<0.218	<0.573	<0.560	NC	NC	NC	NC	NC	NC	NC	NC
TT	3-18	12/8/2014	70.7	<0.573	<0.560	NC	NC	NC	NC	NC	NC	NC	NC
TT	3-19	12/8/2014	47.1	3.73 J	1.34 J	NC	NC	NC	NC	NC	NC	NC	NC
TT	3-20	12/8/2014	19.2	<0.573	0.884 J	NC	NC	NC	NC	NC	NC	NC	NC

BAL = below analytical limit
DRI = Desert Research Institute
J = result is less than the reporting limit but greater than or equal to the method detection limit and the concentration is an approximate value
N = Value not available because liquid nitrogen was necessary on inlet because of large amounts of CO2 gas in sample

NA = Sample was collected but could not be analyzed
NC = not collected
ND = none detected (below minimum detection limit)
Q = concentration below limit of quantification
$R/R_a = (^{3}He/^{4}He)_{groundwater} / (^{3}He/^{4}He)_{atmosphere}$
TT = Tetra Tech

Table A-5. TPH, MTBE, benzene, toluene, ethylbenzene, xylene, and stable isotopes of water for upper Humboldt River Basin wells, springs, and streams.

Agency (Units)	Location ID	Sample Date	TPH-DRO (mg/L)	TPH-GRO (mg/L)	MTBE (µg/L)	Benzene (µg/L)	Toluene (µg/L)	Ethylbenzene (µg/L)	m,p-Xylene (µg/L)	o-Xylene (µg/L)	Xylenes Total (µg/L)	$\delta^{13}C$ DIC Water (‰)	$\delta^{2}H$ Water (‰)	$\delta^{18}O$ Water (‰)
Area 1 Pre-Hydraulic Fracturing														
TT	1-1	3/31/2014	<0.239	<0.25	NC	<0.16	<0.17	<0.16	NC	NC	<0.19	NC	NC	NC
DRI	1-1	3/31/2014	NC	NC	NC	NC	NC	NC	NC	NC	NC	-12.80	-120.1	-15.28
TT	1-2	3/31/2014	<0.241	<0.25	NC	<0.16	<0.17	<0.16	NC	NC	<0.19	NC	NC	NC
DRI	1-2	3/31/2014	NC	NC	NC	NC	NC	NC	NC	NC	NC	-14.91	-117.3	-15.28
TT	1-3	3/31/2014	<0.239	<0.25	NC	<0.16	<0.17	<0.16	NC	NC	<0.19	NC	NC	NC
DRI	1-3	3/31/2014	NC	NC	NC	NC	NC	NC	NC	NC	NC	-9.82	-117.0	-14.51
TT	1-4	3/31/2014	<0.237	<0.25	NC	<0.16	<0.17	<0.16	NC	NC	<0.19	NC	NC	NC
DRI	1-4	3/31/2014	NC	NC	NC	NC	NC	NC	NC	NC	NC	-13.37	-123.9	-16.19
TT	1-5	3/31/2014	<0.239	<0.25	NC	<0.16	<0.17	<0.16	NC	NC	<0.19	NC	NC	NC
DRI	1-5	3/31/2014	NC	NC	NC	NC	NC	NC	NC	NC	NC	-13.27	-126.0	-16.45
TT	1-6	3/31/2014	<0.245	<0.25	NC	<0.16	<0.17	<0.16	NC	NC	<0.19	NC	NC	NC
TT	1-7	4/1/2014	<0.240	<0.25	NC	<0.16	<0.17	<0.16	NC	NC	<0.19	NC	NC	NC
DRI	1-7	4/1/2014	NC	NC	NC	NC	NC	NC	NC	NC	NC	-13.44	-121.6	-15.61
TT	1-8	4/1/2014	<0.238	<0.25	NC	<0.16	<0.17	<0.16	NC	NC	<0.19	NC	NC	NC
DRI	1-8	4/1/2014	NC	NC	NC	NC	NC	NC	NC	NC	NC	-13.01	-119.4	-15.51
TT	1-9	4/1/2014	<0.243	<0.25	NC	<0.16	<0.17	<0.16	NC	NC	<0.19	NC	NC	NC
TT	1-10	4/1/2014	<0.240	<0.25	NC	<0.16	<0.17	<0.16	NC	NC	<0.19	NC	NC	NC
TT	1-11	4/1/2014	<0.238	<0.25	NC	<0.16	<0.17	<0.16	NC	NC	<0.19	NC	NC	NC
DRI	1-12	4/2/2014	<0.25	<0.25	<0.5	<0.5	<0.5	<0.5	<0.5	<0.5	NC	-8.50	-124.8	-16.73
TT	1-13	4/7/2014	<0.238	<0.25	NC	<0.16	<0.17	<0.16	<0.34	<0.19	<0.19	NC	NC	NC
DRI	1-13	4/18/2014	NC	NC	NC	NC	NC	NC	NC	NC	NC	-14.32	-127.9	-16.56
TT	1-14	4/18/2014	<0.0319	<0.01	NC	<0.16	<0.17	<0.16	<0.34	<0.19	<0.19	NC	NC	NC
DRI	1-14	4/18/2014	NC	NC	NC	NC	NC	NC	NC	NC	NC	-10.22	-130.9	-16.67
DRI	1-15	4/18/2014	<0.25	<0.25	<0.5	<0.5	<0.5	<0.5	<0.5	<0.5	NC	-10.04	-117.8	-14.25
DRI	1-16	9/22/2014	<0.25	<0.25	<0.5	<0.5	<0.5	<0.5	<0.5	<0.5	NC	-14.57	-127.0	-16.81

Table A-5. TPH, MTBE, benzene, toluene, ethylbenzene, xylene, and stable isotopes of water for upper Humboldt River Basin wells, springs, and streams (continued).

Agency (Units)	Location ID	Sample Date	TPH-DRO (mg/L)	TPH-GRO (mg/L)	MTBE (µg/L)	Benzene (µg/L)	Toluene (µg/L)	Ethylbenzene (µg/L)	m,p-Xylene (µg/L)	o-Xylene (µg/L)	Xylenes Total (µg/L)	$\delta^{13}C$ DIC Water (‰)	$\delta^{2}H$ Water (‰)	$\delta^{18}O$ Water (‰)
TT	1-16	9/22/2014	ND	ND	NC	ND	ND	ND	NC	NC	ND	NC	NC	NC
DRI	1-17	9/22/2014	<0.25	<0.25	<0.5	<0.5	<0.5	<0.5	<0.5	<0.5	NC	-14.50	-120.4	-15.68
TT	1-17	9/22/2014	ND	ND	NC	ND	ND	ND	NC	NC	ND	NC	NC	NC
DRI	1-18	9/22/2014	<0.25	<0.25	<0.5	<0.5	<0.5	<0.5	<0.5	<0.5	NC	-17.56	-121.3	-15.89
TT	1-18	9/22/2014	ND	ND	NC	ND	ND	ND	NC	NC	ND	NC	NC	NC
DRI	1-19	9/23/2014	<0.25	<0.25	<0.5	<0.5	<0.5	<0.5	<0.5	<0.5	NC	-4.00	-117.8	-14.51
TT	1-19	9/23/2014	ND	ND	NC	ND	ND	ND	NC	NC	ND	NC	NC	NC
DRI	1-20	9/23/2014	<0.25	<0.25	<0.5	<0.5	<0.5	<0.5	<0.5	<0.5	NC	-17.69	-118.5	-15.68
TT	1-20	9/23/2014	ND	ND	NC	ND	ND	ND	NC	NC	ND	NC	NC	NC
DRI	1-21	9/23/2014	<0.25	<0.25	<0.5	<0.5	<0.5	<0.5	<0.5	<0.5	NC	-12.04	-119.4	-15.84
DRI	1-22	9/24/2014	<0.25	<0.25	<0.5	<0.5	<0.5	<0.5	<0.5	<0.5	NC	-13.23	-127.3	-16.33
DRI	1-23	9/24/2014	<0.25	<0.25	<0.5	<0.5	<0.5	<0.5	<0.5	<0.5	NC	-11.91	-116.4	-15.31
DRI	1-24	9/29/2014	<0.25	<0.25	<0.5	<0.5	<0.5	<0.5	<0.5	<0.5	NC	-12.13	-128.2	-16.38
TT	1-24	9/29/2014	ND	ND	NC	ND	ND	ND	NC	NC	ND	NC	NC	NC
DRI	1-25	9/29/2014	<0.25	<0.25	<0.5	<0.5	<0.5	<0.5	<0.5	<0.5	NC	-6.17	-140.1	-18.28
TT	1-25	9/29/2014	ND	ND	NC	ND	ND	ND	NC	NC	ND	NC	NC	NC
DRI	1-26	10/7/2014	<0.25	<0.25	<0.5	<0.5	<0.5	<0.5	<0.5	<0.5	NC	-12.32	-135.7	-17.34
TT	1-26	10/7/2014	<0.031	<0.01	NC	<0.16	<0.17	<0.16	NC	NC	<0.19	NC	NC	NC
DRI	1-27	10/7/2014	<0.25	<0.25	<0.5	<0.5	<0.5	<0.5	<0.5	<0.5	NC	-10.38	-128.7	-16.65
TT	1-27	10/7/2014	<0.031	<0.01	NC	<0.16	<0.17	<0.16	NC	NC	<0.19	NC	NC	NC
DRI	1-28	10/20/2014	<0.25	<0.25	<0.5	<0.5	<0.5	<0.5	<0.5	<0.5	NC	-14.78	-121.1	-15.99
TT	1-28	10/20/2014	0.0562 J*	<0.01	NC	<0.16	<0.17	<0.16	NC	NC	<0.19	NC	NC	NC
DRI	1-29	10/20/2014	<0.25	<0.25	<0.5	<0.5	<0.5	<0.5	<0.5	<0.5	NC	-11.94	-127.4	-16.70
TT	1-29	10/20/2014	<0.0309	<0.01	NC	<0.16	<0.17	<0.16	NC	NC	<0.19	NC	NC	NC
DRI	1-30	10/21/2014	<0.25	<0.25	<0.5	<0.5	<0.5	<0.5	<0.5	<0.5	NC	-10.61	-126.9	-16.53
TT	1-30	10/21/2014	<0.031	<0.01	NC	<0.16	<0.17	<0.16	NC	NC	<0.19	NC	NC	NC
TT	1-31	10/20/2014	<0.031	<0.01	NC	<0.16	<0.17	<0.16	NC	NC	<0.19	NC	NC	NC
TT	1-32	9/23/2014	ND	ND	NC	ND	ND	ND	NC	NC	ND	NC	NC	NC

Table A-5. TPH, MTBE, benzene, toluene, ethylbenzene, xylene, and stable isotopes of water for upper Humboldt River Basin wells, springs, and streams (continued).

Agency (Units)	Location ID	Sample Date	TPH-DRO (mg/L)	TPH-GRO (mg/L)	MTBE (µg/L)	Benzene (µg/L)	Toluene (µg/L)	Ethylbenzene (µg/L)	m,p-Xylene (µg/L)	o-Xylene (µg/L)	Xylenes Total (µg/L)	$\delta^{13}C$ DIC Water (‰)	$\delta^{2}H$ Water (‰)	$\delta^{18}O$ Water (‰)
TT	1-33	9/22/2014	0.0317 J	ND	NC	ND	ND	ND	NC	NC	ND	NC	NC	NC
TT	1-34	9/22/2014	ND	ND	NC	ND	ND	ND	NC	NC	ND	NC	NC	NC
TT	1-35	9/23/2014	ND	ND	NC	ND	ND	ND	NC	NC	ND	NC	NC	NC
TT	1-36	11/12/2014	<0.0310	<0.01	NC	<0.16	<0.17	<0.16	NC	NC	<0.19	NC	NC	NC
TT	1-37	11/12/2014	<0.0312	<0.01	NC	<0.16	<0.17	<0.16	NC	NC	<0.19	NC	NC	NC
Area 1 Post-Hydraulic Fracturing														
TT	1-1	2/25/2015	<0.0312	<0.01	NC	<0.16	<0.17	<0.16	NC	NC	<0.19	NC	NC	NC
DRI	1-2	6/8/2015	NC	NC	NC	NC	NC	NC	NC	NC	NC	-13.74	-115.7	-14.98
TT	1-2	3/4/2015	0.0980 J B	<0.01	NC	<0.16	<0.17	<0.16	NC	NC	<0.19	NC	NC	NC
DRI	1-3	6/8/2015	NC	NC	NC	NC	NC	NC	NC	NC	NC	-7.16	-91.3	-8.97
TT	1-3	3/4/2015	0.0588 J B	<0.01	NC	<0.16	<0.17	<0.16	NC	NC	<0.19	NC	NC	NC
DRI	1-4	6/9/2015	NC	NC	NC	NC	NC	NC	NC	NC	NC	-14.31	-123.4	-16.20
TT	1-4	2/25/2015	<0.0312	<0.01	NC	<0.16	<0.17	<0.16	NC	NC	<0.19	NC	NC	NC
DRI	1-5	6/9/2015	NC	NC	NC	NC	NC	NC	NC	NC	NC	-13.62	-127.2	-16.68
TT	1-6	2/25/2015	<0.0312	<0.01	NC	<0.16	<0.17	<0.16	NC	NC	<0.19	NC	NC	NC
DRI	1-7	6/9/2015	NC	NC	NC	NC	NC	NC	NC	NC	NC	NC	-121.3	-15.65
TT	1-7	2/26/2015	<0.0310	<0.01	NC	<0.16	<0.17	<0.16	NC	NC	<0.19	NC	NC	NC
DRI	1-8	6/9/2015	NC	NC	NC	NC	NC	NC	NC	NC	NC	-13.60	-121.3	-15.80
TT	1-8	2/26/2015	<0.0311	<0.01	NC	<0.16	<0.17	<0.16	NC	NC	<0.19	NC	NC	NC
TT	1-9	2/26/2015	<0.0315	<0.01	NC	<0.16	<0.17	<0.16	NC	NC	<0.19	NC	NC	NC
TT	1-10	2/23/2015	<0.0310	<0.01	NC	<0.16	<0.17	<0.16	NC	NC	<0.19	NC	NC	NC
TT	1-11	2/23/2015	<0.0314	<0.01	NC	<0.16	<0.17	<0.16	NC	NC	<0.19	NC	NC	NC
DRI	1-13	6/8/2015	NC	NC	NC	NC	NC	NC	NC	NC	NC	-13.09	-127.9	-16.49
TT	1-13	6/8/2015	<0.0314	<0.01	<0.25	<0.16	0.547 J	<0.16	NC	NC	<0.19	NC	NC	NC
DRI	1-14	6/8/2015	NC	NC	NC	NC	NC	NC	NC	NC	NC	-11.25	-126.9	-16.09
TT	1-14	6/8/2015	0.0684 J	<0.01	<0.25	<0.16	<0.17	<0.16	NC	NC	<0.19	NC	NC	NC
DRI	1-16	3/31/2015	0.0497 J	<0.01	<0.25	<0.16	<0.17	<0.16	NC	NC	<0.19	NC	NC	NC

Table A-5. TPH, MTBE, benzene, toluene, ethylbenzene, xylene, and stable isotopes of water for upper Humboldt River Basin wells, springs, and streams (continued).

Agency (Units)	Location ID	Sample Date	TPH-DRO (mg/L)	TPH-GRO (mg/L)	MTBE (µg/L)	Benzene (µg/L)	Toluene (µg/L)	Ethylbenzene (µg/L)	m,p-Xylene (µg/L)	o-Xylene (µg/L)	Xylenes Total (µg/L)	$\delta^{13}C$ DIC Water (‰)	$\delta^{2}H$ Water (‰)	$\delta^{18}O$ Water (‰)
DRI	1-17	2/11/2015	<0.25	<0.25	<0.5	<0.5	<0.5	<0.5	<0.5	<0.5	NC	-14.22	-119.1	-15.46
TT	1-17	2/11/2015	<0.0310	0.0123 J	NC	<0.16	<0.17	<0.16	NC	NC	<0.19	NC	NC	NC
DRI	1-18	2/11/2015	<0.25	<0.25	<0.5	<0.5	<0.5	<0.5	<0.5	<0.5	NC	-17.29	-119.1	-15.83
TT	1-18	2/11/2015	<0.0310	<0.01	NC	<0.16	<0.17	<0.16	NC	NC	<0.19	NC	NC	NC
DRI	1-19	2/11/2015	<0.25	<0.25	<0.5	<0.5	<0.5	<0.5	<0.5	<0.5	NC	-8.54	-118.1	-15.29
TT	1-19	2/11/2015	<0.0310	<0.01	NC	<0.16	<0.17	<0.16	NC	NC	<0.19	NC	NC	NC
DRI	1-20	2/10/2015	<0.25	<0.25	<0.5	<0.5	<0.5	<0.5	<0.5	<0.5	NC	-17.53	-117.4	-15.68
TT	1-20	2/10/2015	0.0470 J	<0.01	NC	<0.16	<0.17	<0.16	NC	NC	<0.19	NC	NC	NC
DRI	1-24	2/11/2015	<0.25	<0.25	<0.5	<0.5	<0.5	<0.5	<0.5	<0.5	NC	-11.89	-126.0	-16.31
TT	1-24	2/11/2015	<0.0310	<0.01	NC	<0.16	<0.17	<0.16	NC	NC	<0.19	NC	NC	NC
DRI	1-25	2/10/2015	<0.25	<0.25	<0.5	<0.5	5.6	<0.5	<0.5	<0.5	NC	-6.28	-139.5	-18.24
TT	1-25	2/10/2015	<0.0309	0.013 J	NC	<0.16	8.56	<0.16	NC	NC	<0.19	NC	NC	NC
TT	1-26	6/30/2015	<0.0324	<0.01	<0.25	<0.16	<0.17	<0.16	NC	NC	<0.19	NC	NC	NC
TT	1-27	5/12/2015	<0.0310	<0.01	<0.25	<0.16	<0.17	<0.16	NC	NC	<0.19	NC	NC	NC
TT	1-28	2/10/2015	<0.0310	<0.01	NC	<0.16	<0.17	<0.16	NC	NC	<0.19	NC	NC	NC
TT	1-29	6/24/2015	<0.0314	<0.01	<0.25	<0.16	<0.17	<0.16	NC	NC	<0.19	NC	NC	NC
TT	1-30	5/12/2015	<0.0311	<0.01	NC	<0.16	<0.17	<0.16	NC	NC	<0.19	NC	NC	NC
TT	1-31	6/24/2015	<0.0317	<0.01	<0.25	<0.16	<0.17	<0.16	NC	NC	<0.19	NC	NC	NC
TT	1-32	2/11/2015	0.558	<0.01	NC	<0.16	<0.17	<0.16	NC	NC	<0.19	NC	NC	NC
TT	1-33	3/31/2015	0.0503 J	<0.01	<0.25	<0.16	<0.17	<0.16	NC	NC	<0.19	NC	NC	NC
TT	1-34	7/23/2015	<0.0316	<0.01	<0.25	<0.16	3.15	<0.16	NC	NC	<0.19	NC	NC	NC
TT	1-35	2/10/2015	<0.0309	<0.01	NC	<0.16	<0.17	<0.16	NC	NC	<0.19	NC	NC	NC
TT	1-36	12/4/2014	0.0648 J	<0.01	NC	<0.16	<0.17	<0.16	NC	NC	<0.19	NC	NC	NC
TT	1-36	2/18/2015	0.0439 J	<0.01	NC	<0.16	<0.17	<0.16	NC	NC	<0.19	NC	NC	NC
TT	1-37	2/18/2015	<0.0312	<0.01	NC	<0.16	<0.17	<0.16	NC	NC	<0.19	NC	NC	NC
Area 2 Pre-Hydraulic Fracturing														
DRI	2-1	9/4/2013	<0.25	<0.25	<0.5	<0.5	<0.5	<0.5	<0.5	<0.5	NC	-4.35	-136.0	-17.90

Table A-5. TPH, MTBE, benzene, toluene, ethylbenzene, xylene, and stable isotopes of water for upper Humboldt River Basin wells, springs, and streams (continued).

Agency (Units)	Location ID	Sample Date	TPH-DRO (mg/L)	TPH-GRO (mg/L)	MTBE (µg/L)	Benzene (µg/L)	Toluene (µg/L)	Ethylbenzene (µg/L)	m,p-Xylene (µg/L)	o-Xylene (µg/L)	Xylenes Total (µg/L)	$\delta^{13}C$ DIC Water (‰)	$\delta^{2}H$ Water (‰)	$\delta^{18}O$ Water (‰)
TT	2-1	9/4/2013	<0.245	<0.01	NC	<0.16	<0.17	<0.16	NC	NC	NC	NC	NC	NC
TT	2-1	10/8/2013	NC	NC	NC	NC	NC	NC	NC	NC	NC	NC	NC	NC
TT	2-2	9/4/2013	<0.245	<0.01	NC	<0.16	<0.17	<0.16	NC	NC	<0.19	NC	NC	NC
TT	2-3	9/4/2013	<0.245	<0.01	NC	<0.16	<0.17	<0.16	NC	NC	<0.19	NC	NC	NC
DRI	2-4	9/4/2013	<0.25	<0.25	<0.5	<0.5	<0.5	<0.5	<0.5	<0.5	NC	-10.33	-126.6	-16.46
TT	2-4	9/4/2013	<0.245	<0.01	NC	<0.16	<0.17	<0.16	NC	NC	NC	NC	NC	NC
TT	2-5	9/4/2013	<0.240	<0.25	NC	<0.16	<0.17	<0.16	NC	NC	<0.19	NC	NC	NC
TT	2-6	9/4/2013	<0.241	<0.25	NC	<0.16	<0.17	<0.16	NC	NC	<0.19	NC	NC	NC
TT	2-7	9/4/2013	<0.246	<0.25	NC	<0.16	<0.17	<0.16	NC	NC	<0.19	NC	NC	NC
TT	2-8	10/8/2013	<0.0309	<0.01	NC	<0.16	<0.17	<0.16	NC	NC	<0.19	NC	NC	NC
TT	2-9	10/8/2013	<0.0313	<0.01	NC	<0.16	<0.17	<0.16	NC	NC	<0.19	NC	NC	NC
Area 2 Post-Hydraulic Fracturing														
DRI	2-1	6/23/2014	<0.25	<0.25	<0.5	<0.5	<0.5	<0.5	<0.5	<0.5	NC	-3.29	-136.1	-18.09
TT	2-1	6/23/2014	0.0360 J	<0.01	NC	<0.16	<0.17	<0.16	NC	NC	<0.19	NC	NC	NC
DRI	2-2	6/23/2014	<0.25	<0.25	<0.5	<0.5	<0.5	<0.5	<0.5	<0.5	NC	-13.84	-116.1	-15.09
TT	2-2	6/23/2014	<0.241	<0.01	NC	<0.16	<0.17	<0.16	NC	NC	<0.19	NC	NC	NC
TT	2-3	6/23/2014	<0.243	<0.01	NC	<0.16	<0.17	<0.16	NC	NC	<0.19	NC	NC	NC
DRI	2-4	6/23/2014	<0.25	<0.25	<0.5	<0.5	<0.5	<0.5	<0.5	<0.5	NC	-9.90	-127.9	-16.72
TT	2-4	6/23/2014	<0.240	<0.01	NC	<0.16	<0.17	<0.16	NC	NC	<0.19	NC	NC	NC
TT	2-5	6/25/2014	<0.0311	<0.01	NC	<0.16	<0.17	<0.16	NC	NC	<0.19	NC	NC	NC
TT	2-6	6/25/2014	<0.0310	<0.01	NC	<0.16	<0.17	<0.16	NC	NC	<0.19	NC	NC	NC
TT	2-7	7/1/2014	<0.0309	<0.01	NC	<0.16	<0.17	<0.16	NC	NC	<0.19	NC	NC	NC
TT	2-8	6/25/2014	<0.245	<0.01	NC	<0.16	<0.17	<0.16	NC	NC	<0.19	NC	NC	NC
TT	2-9	6/25/2014	<0.245	<0.01	NC	<0.16	<0.17	<0.16	NC	NC	<0.19	NC	NC	NC
DRI	2-10	4/1/2014	<0.25	<0.25	<0.5	<0.5	<0.5	<0.5	<0.5	<0.5	NC	-8.48	-121.3	-16.05
DRI	2-10	6/23/2014	<0.25	<0.25	<0.5	<0.5	<0.5	<0.5	<0.5	<0.5	NC	-6.94	-121.9	-16.27
DRI	2-11	6/25/2014	<0.25	<0.25	<0.5	<0.5	<0.5	<0.5	<0.5	<0.5	NC	-11.83	-127.7	-15.83

Table A-5. TPH, MTBE, benzene, toluene, ethylbenzene, xylene, and stable isotopes of water for upper Humboldt River Basin wells, springs, and streams (continued).

Agency (Units)	Location ID	Sample Date	TPH-DRO (mg/L)	TPH-GRO (mg/L)	MTBE (µg/L)	Benzene (µg/L)	Toluene (µg/L)	Ethylbenzene (µg/L)	m,p-Xylene (µg/L)	o-Xylene (µg/L)	Xylenes Total (µg/L)	$\delta^{13}C$ DIC Water (‰)	$\delta^{2}H$ Water (‰)	$\delta^{18}O$ Water (‰)
DRI	2-12	6/24/2014	<0.25	<0.25	<0.5	<0.5	<0.5	<0.5	<0.5	<0.5	NC	-11.55	-122.1	-15.62
DRI	2-13	6/24/2014	<0.25	<0.25	<0.5	<0.5	<0.5	<0.5	<0.5	<0.5	NC	-11.12	-121.2	-15.51
DRI	2-14	6/24/2014	<0.25	<0.25	<0.5	<0.5	<0.5	<0.5	<0.5	<0.5	NC	-2.72	-126.8	-16.03
DRI	2-15	9/5/2014	<0.25	<0.25	<0.5	<0.5	<0.5	<0.5	<0.5	<0.5	NC	-12.21	-125.3	-16.08
DRI	2-16	9/25/2014	<0.25	<0.25	<0.5	<0.5	17	<0.5	<0.5	<0.5	NC	-6.33	-138.3	-18.25
DRI	M2C-M2-21B	9/25/2014	1.3 C L	18	<20 V	3800	4000	170	700	350	NC	-1.91	-137.7	-12.81
	M10C-M10-11B	-----	-----	-----	-----	-----	-----	-----	-----	-----	-----	-----	-----	-----
Area 2 One-Year Post Hydraulic Fracturing														
TT	2-1	7/16/2015	<0.0315	<0.01	<0.25	<0.16	<0.17	<0.16	NC	NC	<0.19	NC	NC	NC
DRI	2-2	3/18/2015	<0.25	<0.25	<0.5	<0.5	<0.5	<0.5	<0.5	<0.5	NC	-13.33	-108.1	-13.53
TT	2-2	3/18/2015	<0.0311	<0.01	<0.25	<0.16	<0.17	<0.16	NC	NC	<0.19	NC	NC	NC
TT	2-3	3/18/2015	<0.0309	<0.01	<0.25	<0.16	<0.17	<0.16	NC	NC	<0.19	NC	NC	NC
DRI	2-4	3/18/2015	<0.25	<0.25	<0.5	<0.5	<0.5	<0.5	<0.5	<0.5	NC	-10.64	-126.7	-16.62
TT	2-4	3/18/2015	<0.0310	<0.01	<0.25	<0.16	<0.17	<0.16	NC	NC	<0.19	NC	NC	NC
DRI	2-5	3/19/2015	<0.25	<0.25	<0.5	<0.5	<0.5	<0.5	<0.5	<0.5	NC	-14.83	-121.9	-16.41
TT	2-5	3/19/2015	<0.0310	<0.01	<0.25	<0.16	<0.17	<0.16	NC	NC	<0.19	NC	NC	NC
TT	2-6	3/24/2015	<0.0310	<0.01	<0.25	<0.16	<0.17	<0.16	NC	NC	<0.19	NC	NC	NC
TT	2-7	3/19/2015	<0.0311	<0.01	<0.25	<0.16	<0.17	<0.16	NC	NC	<0.19	NC	NC	NC
TT	2-8	3/17/2015	<0.0309	<0.01	<0.25	<0.16	<0.17	<0.16	NC	NC	<0.19	NC	NC	NC
TT	2-9	3/24/2015	<0.0312	<0.01	<0.25	<0.16	<0.17	<0.16	NC	NC	<0.19	NC	NC	NC
DRI	2-13	3/19/2015	<0.25	<0.25	<0.5	<0.5	<0.5	<0.5	<0.5	<0.5	NC	-9.21	-111.7	-14.45
Area 3 Pre-Hydraulic Fracturing														
DRI	3-1	9/3/2014	<0.25	<0.25	<0.5	<0.5	<0.5	<0.5	<0.5	<0.5	NC	-14.01	-105.4	-11.57
DRI	3-1	9/3/2014	NC	NC	NC	NC	NC	NC	NC	NC	NC	NC	-108.3	-11.69

Table A-5. TPH, MTBE, benzene, toluene, ethylbenzene, xylene, and stable isotopes of water for upper Humboldt River Basin wells, springs, and streams (continued).

Agency (Units)	Location ID	Sample Date	TPH-DRO (mg/L)	TPH-GRO (mg/L)	MTBE (µg/L)	Benzene (µg/L)	Toluene (µg/L)	Ethylbenzene (µg/L)	m,p-Xylene (µg/L)	o-Xylene (µg/L)	Xylenes Total (µg/L)	δ^{13}C DIC Water (‰)	δ^{2}H Water (‰)	δ^{18}O Water (‰)
TT	3-1	9/3/2014	0.0377 J	<0.01	NC	<0.16	<0.17	<0.16	NC	NC	<0.19	NC	NC	NC
DRI	3-2	9/3/2014	<0.25	<0.25	<0.5	<0.5	<0.5	<0.5	<0.5	<0.5	NC	-10.67	-141.8	-18.13
DRI	3-2	9/3/2014	NC	NC	NC	NC	NC	NC	NC	NC	NC	NC	-139.8	-18.05
TT	3-2	9/3/2014	<0.0309	<0.01	NC	<0.16	<0.17	<0.16	NC	NC	<0.19	NC	NC	NC
DRI	3-3	9/3/2014	<0.25	<0.25	<0.5	<0.5	<0.5	<0.5	<0.5	<0.5	NC	-3.37	-139.0	-18.17
DRI	3-3	9/3/2014	NC	NC	NC	NC	NC	NC	NC	NC	NC	NC	-142.4	-18.35
TT	3-3	9/3/2014	<0.0313	<0.01	NC	<0.16	<0.17	<0.16	NC	NC	<0.19	NC	NC	NC
DRI	3-4	9/4/2014	<0.25	<0.25	<0.5	<0.5	<0.5	<0.5	<0.5	<0.5	NC	-1.66	-130.1	-16.13
DRI	3-4	9/4/2014	NC	NC	NC	NC	NC	NC	NC	NC	NC	NC	-132.1	-16.39
DRI	3-5	9/5/2014	<0.25	<0.25	<0.5	<0.5	<0.5	<0.5	<0.5	<0.5	NC	-7.66	-91.0	-7.98
DRI	3-6	9/30/2014	<0.25	<0.25	<0.5	<0.5	<0.5	<0.5	<0.5	<0.5	NC	-6.42	-128.3	-16.53
TT	3-6	9/30/2014	ND	ND	NC	ND	0.325 J	ND	NC	NC	ND	NC	NC	NC
DRI	3-7	9/30/2014	<0.25	<0.25	<0.5	<0.5	<0.5	<0.5	<0.5	<0.5	NC	-10.18	-130.5	-17.18
TT	3-7	9/30/2014	<0.0309	<0.01	NC	<0.16	<0.17	<0.16	NC	NC	<0.19	NC	NC	NC
DRI	3-8	9/30/2014	<0.25	<0.25	<0.5	<0.5	<0.5	<0.5	<0.5	<0.5	NC	-3.80	-130.7	-17.24
DRI	3-9	10/8/2014	<0.25	<0.25	<0.5	<0.5	<0.5	<0.5	<0.5	<0.5	NC	-10.27	-131.2	-17.19
TT	3-9	10/8/2014	<0.0309	<0.01	NC	<0.16	0.181 J	<0.16	NC	NC	<0.19	NC	NC	NC
DRI	3-10	10/21/2014	<0.25	<0.25	<0.5	<0.5	<0.5	<0.5	<0.5	<0.5	NC	-10.73	-129.4	-16.90
TT	3-10	10/29/2014	<0.031	<0.01	NC	<0.16	<0.17	<0.16	NC	NC	<0.19	NC	NC	NC
DRI	3-11	10/21/2014	<0.25	<0.25	<0.5	<0.5	<0.5	<0.5	<0.5	<0.5	NC	-10.90	-121.7	-15.67
TT	3-11	10/21/2014	<0.0311	0.014 J	NC	<0.16	<0.17	<0.16	NC	NC	<0.19	NC	NC	NC
TT	3-12	10/21/2014	<0.0315	<0.01	NC	<0.16	<0.17	<0.16	NC	NC	<0.19	NC	NC	NC
DRI	3-12	10/22/2014	<0.25	<0.25	<0.5	<0.5	<0.5	<0.5	<0.5	<0.5	NC	-12.89	-119.0	-15.66
DRI	3-13	10/22/2014	<0.25	<0.25	<0.5	<0.5	<0.5	<0.5	<0.5	<0.5	NC	-1.96	-140.5	-16.60
TT	3-14	10/21/2014	<0.0309	<0.01	NC	<0.16	<0.17	<0.16	NC	NC	<0.19	NC	NC	NC
TT	3-15	9/30/2014	ND	ND	NC	ND	ND	ND	NC	NC	ND	NC	NC	NC

Table A-5. TPH, MTBE, benzene, toluene, ethylbenzene, xylene, and stable isotopes of water for upper Humboldt River Basin wells, springs, and streams (continued).

Agency (Units)	Location ID	Sample Date	TPH-DRO (mg/L)	TPH-GRO (mg/L)	MTBE (µg/L)	Benzene (µg/L)	Toluene (µg/L)	Ethylbenzene (µg/L)	m,p-Xylene (µg/L)	o-Xylene (µg/L)	Xylenes Total (µg/L)	δ^{13}C DIC Water (‰)	δ^{2}H Water (‰)	δ^{18}O Water (‰)
TT	3-16	12/8/2014	<0.0308	38.8	NC	<0.16	<0.17	<0.16	NC	NC	<0.19	NC	NC	NC
TT	3-17	12/8/2014	<0.0309	<0.01	NC	<0.16	<0.17	<0.16	NC	NC	<0.19	NC	NC	NC
TT	3-18	12/8/2014	0.0316 J	<0.01	NC	<0.16	<0.17	<0.16	NC	NC	<0.19	NC	NC	NC
TT	3-19	12/8/2014	0.257	61.6	NC	11.9	6.88	0.603 J	NC	NC	5.04	NC	NC	NC
TT	3-20	12/8/2014	<0.0311	<0.01	NC	<0.16	<0.17	<0.16	NC	NC	<0.19	NC	NC	NC

DRI = Desert Research Institute
NC = not collected
ND = none detected (below minimum detection limit)
TBA = to be analyzed
TT = Tetra Tech
* = relative percent difference of the lab control sample and lab control sample duplicate exceeds the control limits.

C = reported concentration includes additional compounds uncharacteristic of common fuels and lubricants.
J = result is less than the reporting limit but greater than or equal to the method detection limit and the concentration is an approximate value.
L = DRO concentration may include contributions from heavier-end hydrocarbons that elute in the DRO range.
V = reporting limits were increased due to high concentration of target analytes.

Table A-6. Hydraulic-fracturing chemical tracers for upper Humboldt River Basin wells, springs, and streams.

Agency (Units)	Location ID	Sample Date	Methanol (mg/L)	Ethanol (mg/L)	Isopropanol (mg/L)	Glycerol (mg/L)	Ethylene Glycol (mg/L)	Propylene Glycol (mg/L)	2-Butoxyethanol (mg/L)	Acrylonitrile (mg/L)	Ammonium Persulfate (mg/L)
Area 1 Pre-hydraulic Fracturing											
TT	1-1	3/31/2014	NC	NC	NC	NC	NC	NC	NC	NC	NC
DRI	1-1	3/31/2014	<2.0	<2.0	<2.0	<0.5	<0.5	<0.5	<0.5	<2.0	<1.0
TT	1-2	3/31/2014	NC	NC	NC	NC	NC	NC	NC	NC	NC
DRI	1-2	3/31/2014	<2.0	<2.0	<2.0	<0.5	<0.5	<0.5	<0.5	<2.0	<1.0
TT	1-3	3/31/2014	NC	NC	NC	NC	NC	NC	NC	NC	NC
DRI	1-3	3/31/2014	<2.0	<2.0	<2.0	<0.5	<0.5	<0.5	<0.5	<2.0	<1.0
TT	1-4	3/31/2014	NC	NC	NC	NC	NC	NC	NC	NC	NC
DRI	1-4	3/31/2014	<2.0	<2.0	<2.0	<0.5	<0.5	<0.5	<0.5	<2.0	<1.0
TT	1-5	3/31/2014	NC	NC	NC	NC	NC	NC	NC	NC	NC
DRI	1-5	3/31/2014	<2.0	<2.0	<2.0	<0.5	<0.5	<0.5	<0.5	<2.0	<1.0
TT	1-6	3/31/2014	NC	NC	NC	NC	NC	NC	NC	NC	NC
TT	1-7	4/1/2014	NC	NC	NC	NC	NC	NC	NC	NC	NC
DRI	1-7	4/1/2014	<2.0	<2.0	<2.0	<0.5	<0.5	<0.5	<0.5	<2.0	<1.0
TT	1-8	4/1/2014	NC	NC	NC	NC	NC	NC	NC	NC	NC
DRI	1-8	4/1/2014	<2.0	<2.0	<2.0	<0.5	<0.5	<0.5	<0.5	<2.0	<1.0
TT	1-9	4/1/2014	NC	NC	NC	NC	NC	NC	NC	NC	NC
TT	1-10	4/1/2014	NC	NC	NC	NC	NC	NC	NC	NC	NC
TT	1-11	4/1/2014	NC	NC	NC	NC	NC	NC	NC	NC	NC
DRI	1-12	4/2/2014	<2.0	<2.0	<2.0	<0.5	<0.5	<0.5	<0.5	<2.0	<1.0
TT	1-13	4/7/2014	NC	NC	NC	NC	NC	NC	NC	<0.0014	NC
DRI	1-13	4/18/2014	<2.0	<2.0	<2.0	<0.5	<0.5	<0.5	<0.5	<2.0	<1.0
TT	1-14	4/18/2014	NC	NC	NC	NC	NC	NC	NC	<0.0014	NC
DRI	1-14	4/18/2014	<2.0	<2.0	<2.0	<0.5	<0.5	<0.5	<0.5	<2.0	<1.0
DRI	1-15	4/18/2014	<2.0	<2.0	<2.0	<0.5	<0.5	<0.5	<0.5	<2.0	<1.0
DRI	1-16	9/22/2014	<2.0	<2.0	<2.0	<0.5	<0.5	<0.5	<0.5	<2.0	<1.0

Table A-6. Hydraulic fracturing chemical tracers for upper Humboldt River Basin wells, springs, and streams (continued).

Agency (Units)	Location ID	Sample Date	Methanol (mg/L)	Ethanol (mg/L)	Isopropanol (mg/L)	Glycerol (mg/L)	Ethylene Glycol (mg/L)	Propylene Glycol (mg/L)	2-Butoxyethanol (mg/L)	Acrylonitrile (mg/L)	Ammonium Persulfate (mg/L)
TT	1-16	9/22/2014	NC	NC	NC	NC	NC	NC	NC	NC	NC
DRI	1-17	9/22/2014	<2.0	<2.0	<2.0	<0.5	<0.5	<0.5	<0.5	<2.0	<1.0
TT	1-17	9/22/2014	NC	NC	NC	NC	NC	NC	NC	NC	NC
DRI	1-18	9/22/2014	<2.0	<2.0	<2.0	<0.5	<0.5	1.945 P	<0.5	<2.0	<1.0
TT	1-18	9/22/2014	NC	NC	NC	NC	NC	NC	NC	NC	NC
DRI	1-19	9/23/2014	<2.0	<2.0	<2.0	<0.5	<0.5	<0.5	<0.5	<2.0	<1.0
TT	1-19	9/23/2014	NC	NC	NC	NC	NC	NC	NC	NC	NC
DRI	1-20	9/23/2014	<2.0	<2.0	<2.0	<0.5	<0.5	2.327 P	<0.5	<2.0	<1.0
TT	1-20	9/23/2014	NC	NC	NC	NC	NC	NC	NC	NC	NC
DRI	1-21	9/23/2014	<2.0	<2.0	<2.0	<0.5	<0.5	<0.5	<0.5	<2.0	<1.0
DRI	1-22	9/24/2014	<2.0	<2.0	<2.0	<0.5	<0.5	<0.5	<0.5	<2.0	<1.0
DRI	1-23	9/24/2014	<2.0	<2.0	<2.0	<0.5	<0.5	<0.5	<0.5	<2.0	<1.0
DRI	1-24	9/29/2014	<2.0	<2.0	<2.0	<0.5	<0.5	<0.5	<0.5	<2.0	<1.0
TT	1-24	9/29/2014	NC	NC	NC	NC	NC	NC	NC	NC	NC
DRI	1-25	9/29/2014	<2.0	<2.0	<2.0	<0.5	<0.5	1.967 P	<0.5	<2.0	<1.0
TT	1-25	9/29/2014	NC	NC	NC	NC	NC	NC	NC	NC	NC
DRI	1-26	10/7/2014	<2.0	<2.0	<2.0	<0.5	<0.5	<0.5	<0.5	<2.0	<1.0
TT	1-26	10/7/2014	NC	NC	NC	NC	NC	NC	NC	NC	NC
DRI	1-27	10/7/2014	<2.0	<2.0	<2.0	<0.5	<0.5	<0.5	<0.5	<2.0	<1.0
TT	1-27	10/7/2014	NC	NC	NC	NC	NC	NC	NC	NC	NC
DRI	1-28	10/20/2014	<2.0	<2.0	<2.0	<0.5	<0.5	<0.5	<0.5	<2.0	<1.0
TT	1-28	10/20/2014	NC	NC	NC	NC	NC	NC	NC	NC	NC
DRI	1-29	10/20/2014	<2.0	<2.0	<2.0	<0.5	<0.5	<0.5	<0.5	<2.0	<1.0
TT	1-29	10/20/2014	NC	NC	NC	NC	NC	NC	NC	NC	NC
DRI	1-30	10/21/2014	<2.0	<2.0	<2.0	<0.5	<0.5	<0.5	<0.5	<2.0	<1.0
TT	1-30	10/21/2014	NC	NC	NC	NC	NC	NC	NC	NC	NC

Table A-6. Hydraulic fracturing chemical tracers for upper Humboldt River Basin wells, springs, and streams (continued).

Agency (Units)	Location ID	Sample Date	Methanol (mg/L)	Ethanol (mg/L)	Isopropanol (mg/L)	Glycerol (mg/L)	Ethylene Glycol (mg/L)	Propylene Glycol (mg/L)	2-Butoxyethanol (mg/L)	Acrylonitrile (mg/L)	Ammonium Persulfate (mg/L)
TT	1-31	10/20/2014	NC	NC	NC	NC	NC	NC	NC	NC	NC
TT	1-32	9/23/2014	NC	NC	NC	NC	NC	NC	NC	NC	NC
TT	1-33	9/22/2014	NC	NC	NC	NC	NC	NC	NC	NC	NC
TT	1-34	9/22/2014	NC	NC	NC	NC	NC	NC	NC	NC	NC
TT	1-35	9/23/2014	NC	NC	NC	NC	NC	NC	NC	NC	NC
TT	1-36	11/12/2014	NC	NC	NC	NC	NC	NC	NC	NC	NC
TT	1-37	11/12/2014	NC	NC	NC	NC	NC	NC	NC	NC	NC
Area 1 Post-Hydraulic Fracturing											
TT	1-1	2/25/2015	NC	NC	NC	NC	NC	NC	NC	NC	NC
DRI	1-2	6/8/2015	<2.0	<2.0	<2.0	<0.5	<0.5	<0.5	<0.5	<2.0	<1.0
TT	1-2	3/4/2015	NC	NC	NC	NC	NC	NC	NC	NC	NC
DRI	1-3	6/8/2015	<2.0	<2.0	<2.0	<0.5	<0.5	<0.5	<0.5	<2.0	<1.0
TT	1-3	3/4/2015	NC	NC	NC	NC	NC	NC	NC	NC	NC
DRI	1-4	6/9/2015	<2.0	<2.0	<2.0	<0.5	<0.5	<0.5	<0.5	<2.0	<1.0
TT	1-4	2/25/2015	NC	NC	NC	NC	NC	NC	NC	NC	NC
DRI	1-5	6/9/2015	<2.0	<2.0	<2.0	<0.5	<0.5	<0.5	<0.5	<2.0	<1.0
TT	1-6	2/25/2015	NC	NC	NC	NC	NC	NC	NC	NC	NC
DRI	1-7	6/9/2015	<2.0	<2.0	<2.0	<0.5	<0.5	<0.5	<0.5	<2.0	<1.0
TT	1-7	2/26/2015	NC	NC	NC	NC	NC	NC	NC	NC	NC
DRI	1-8	6/9/2015	<2.0	<2.0	<2.0	<0.5	<0.5	<0.5	<0.5	<2.0	<1.0
TT	1-8	2/26/2015	NC	NC	NC	NC	NC	NC	NC	NC	NC
TT	1-9	2/26/2015	NC	NC	NC	NC	NC	NC	NC	NC	NC
TT	1-10	2/23/2015	NC	NC	NC	NC	NC	NC	NC	NC	NC
TT	1-11	2/23/2015	NC	NC	NC	NC	NC	NC	NC	NC	NC
DRI	1-13	6/8/2015	<2.0	<2.0	<2.0	<0.5	<0.5	<0.5	<0.5	<2.0	<1.0
TT	1-13	6/8/2015	NC	NC	NC	NC	NC	NC	NC	NC	NC

Table A-6. Hydraulic fracturing chemical tracers for upper Humboldt River Basin wells, springs, and streams (continued).

Agency (Units)	Location ID	Sample Date	Methanol (mg/L)	Ethanol (mg/L)	Isopropanol (mg/L)	Glycerol (mg/L)	Ethylene Glycol (mg/L)	Propylene Glycol (mg/L)	2-Butoxyethanol (mg/L)	Acrylonitrile (mg/L)	Ammonium Persulfate (mg/L)
DRI	1-14	6/8/2015	<2.0	<2.0	<2.0	<0.5	<0.5	<0.5	<0.5	<2.0	<1.0
TT	1-14	6/8/2015	NC	NC	NC	NC	NC	NC	NC	NC	NC
TT	1-16	3/31/2015	NC	NC	NC	NC	NC	NC	NC	NC	NC
DRI	1-17	2/11/2015	<2.0	<2.0	<2.0	<0.5	<0.5	<0.5	<0.5	<2.0	<1.0
TT	1-17	2/11/2015	NC	NC	NC	NC	NC	NC	NC	NC	NC
DRI	1-18	2/11/2015	<2.0	<2.0	<2.0	<0.5	<0.5	<0.5	<0.5	<2.0	<1.0
TT	1-18	2/11/2015	NC	NC	NC	NC	NC	NC	NC	NC	NC
DRI	1-19	2/11/2015	<2.0	<2.0	<2.0	<0.5	<0.5	<0.5	<0.5	<2.0	<1.0
TT	1-19	2/11/2015	NC	NC	NC	NC	NC	NC	NC	NC	NC
DRI	1-20	2/10/2015	<2.0	<2.0	<2.0	<0.5	<0.5	<0.5	<0.5	<2.0	<1.0
TT	1-20	2/10/2015	NC	NC	NC	NC	NC	NC	NC	NC	NC
DRI	1-24	2/11/2015	<2.0	<2.0	<2.0	<0.5	<0.5	<0.5	<0.5	<2.0	<1.0
TT	1-24	2/11/2015	NC	NC	NC	NC	NC	NC	NC	NC	NC
DRI	1-25	2/10/2015	<2.0	<2.0	<2.0	<0.5	<0.5	<0.5	<0.5	<2.0	<1.0
TT	1-25	2/10/2015	NC	NC	NC	NC	NC	NC	NC	NC	NC
TT	1-26	6/30/2015	NC	NC	NC	NC	NC	NC	NC	NC	NC
TT	1-27	5/12/2015	NC	NC	NC	NC	NC	NC	NC	NC	NC
TT	1-28	2/10/2015	NC	NC	NC	NC	NC	NC	NC	NC	NC
TT	1-29	6/24/2015	NC	NC	NC	NC	NC	NC	NC	NC	NC
TT	1-30	5/12/2015	NC	NC	NC	NC	NC	NC	NC	NC	NC
TT	1-31	6/24/2015	NC	NC	NC	NC	NC	NC	NC	NC	NC
TT	1-32	2/11/2015	NC	NC	NC	NC	NC	NC	NC	NC	NC
TT	1-33	3/31/2015	NC	NC	NC	NC	NC	NC	NC	NC	NC
TT	1-34	7/23/2015	NC	NC	NC	NC	NC	NC	NC	NC	NC
TT	1-35	2/10/2015	NC	NC	NC	NC	NC	NC	NC	NC	NC
TT	1-36	2/18/2015	NC	NC	NC	NC	NC	NC	NC	NC	NC

Table A-6. Hydraulic fracturing chemical tracers for upper Humboldt River Basin wells, springs, and streams (continued).

Agency (Units)	Location ID	Sample Date	Methanol (mg/L)	Ethanol (mg/L)	Isopropanol (mg/L)	Glycerol (mg/L)	Ethylene Glycol (mg/L)	Propylene Glycol (mg/L)	2-Butoxyethanol (mg/L)	Acrylonitrile (mg/L)	Ammonium Persulfate (mg/L)
TT	1-37	2/18/2015	NC	NC	NC	NC	NC	NC	NC	NC	NC
Area 2 Pre-hydraulic Fracturing											
DRI	2-1	9/4/2013	<2.0	<2.0	<2.0	<0.5	<0.5	<0.5	<0.5	<2.0	<1.0
TT	2-1	9/4/2013	NC	NC	NC	NC	NC	NC	NC	NC	NC
TT	2-2	9/4/2013	NC	NC	NC	NC	NC	NC	NC	NC	NC
TT	2-3	9/4/2013	NC	NC	NC	NC	NC	NC	NC	NC	NC
DRI	2-4	9/4/2013	<2.0	<2.0	<2.0	<0.5	<0.5	<0.5	<0.5	<2.0	<1.0
TT	2-4	9/4/2013	NC	NC	NC	NC	NC	NC	NC	NC	NC
TT	2-5	9/4/2013	NC	NC	NC	NC	NC	NC	NC	NC	NC
TT	2-6	9/4/2013	NC	NC	NC	NC	NC	NC	NC	NC	NC
TT	2-7	9/4/2013	NC	NC	NC	NC	NC	NC	NC	NC	NC
TT	2-8	10/8/2013	NC	NC	NC	NC	NC	NC	NC	NC	NC
TT	2-9	10/8/2013	NC	NC	NC	NC	NC	NC	NC	NC	NC
Area 2 Post-hydraulic Fracturing											
DRI	2-1	6/23/2014	<2.0	<2.0	<2.0	<0.5	<0.5	<0.5	<0.5	<2.0	<1.0
TT	2-1	6/23/2014	NC	NC	NC	NC	NC	NC	NC	NC	NC
DRI	2-2	6/23/2014	<2.0	<2.0	<2.0	<0.5	<0.5	<0.5	<0.5	<2.0	<1.0
TT	2-2	6/23/2014	NC	NC	NC	NC	NC	NC	NC	NC	NC
TT	2-3	6/23/2014	NC	NC	NC	NC	NC	NC	NC	NC	NC
DRI	2-4	6/23/2014	<2.0	<2.0	<2.0	<0.5	<0.5	<0.5	<0.5	<2.0	<1.0
TT	2-4	6/23/2014	NC	NC	NC	NC	NC	NC	NC	NC	NC
TT	2-5	6/25/2014	NC	NC	NC	NC	NC	NC	NC	NC	NC
TT	2-6	6/25/2014	NC	NC	NC	NC	NC	NC	NC	NC	NC
TT	2-7	7/1/2014	NC	NC	NC	NC	NC	NC	NC	NC	NC
TT	2-8	6/25/2014	NC	NC	NC	NC	NC	NC	NC	NC	NC
TT	2-9	6/25/2014	NC	NC	NC	NC	NC	NC	NC	NC	NC

Table A-6. Hydraulic fracturing chemical tracers for upper Humboldt River Basin wells, springs, and streams (continued).

Agency (Units)	Location ID	Sample Date	Methanol (mg/L)	Ethanol (mg/L)	Isopropanol (mg/L)	Glycerol (mg/L)	Ethylene Glycol (mg/L)	Propylene Glycol (mg/L)	2-Butoxyethanol (mg/L)	Acrylonitrile (mg/L)	Ammonium Persulfate (mg/L)
DRI	2-10	4/1/2014	<2.0	<2.0	<2.0	<0.5	<0.5	<0.5	<0.5	<2.0	<1.0
DRI	2-10	6/23/2014	<2.0	<2.0	<2.0	<0.5	<0.5	<0.5	<0.5	<2.0	<1.0
DRI	2-11	6/25/2014	<2.0	<2.0	<2.0	<0.5	<0.5	<0.5	<0.5	<2.0	<1.0
DRI	2-12	6/24/2014	<2.0	<2.0	<2.0	<0.5	<0.5	<0.5	<0.5	<2.0	<1.0
DRI	2-13	6/24/2014	<2.0	<2.0	<2.0	<0.5	<0.5	<0.5	<0.5	<2.0	<1.0
DRI	2-14	6/24/2014	<2.0	<2.0	<2.0	<0.5	<0.5	<0.5	<0.5	<2.0	<1.0
DRI	2-15	9/5/2014	<2.0	<2.0	<2.0	<0.5	<0.5	<0.5	<0.5	<2.0	<1.0
DRI	2-16	9/25/2014	<2.0	<2.0	<2.0	<0.5	<0.5	<0.5	<0.5	<2.0	<1.0
DRI	M2C-M2-21B	9/25/2014	33.10	13.40	<2.0	<0.5	<0.5	<0.5	5.58	<2.0	<1.0
	M10C-M10-11B	-----	-----	-----	-----	-----	-----	-----	-----	-----	-----
Area 2 One-Year Post Hydraulic Fracturing											
TT	2-1	7/16/2015	NC	NC	NC	NC	NC	NC	NC	NC	NC
DRI	2-2	3/18/2015	<2.0	<2.0	<2.0	<0.5	<0.5	<0.5	<0.5	<2.0	<1.0
TT	2-2	3/18/2015	NC	NC	NC	NC	NC	NC	NC	NC	NC
TT	2-3	3/18/2015	NC	NC	NC	NC	NC	NC	NC	NC	NC
DRI	2-4	3/18/2015	<2.0	<2.0	<2.0	<0.5	<0.5	<0.5	<0.5	<2.0	<1.0
TT	2-4	3/18/2015	NC	NC	NC	NC	NC	NC	NC	NC	NC
DRI	2-5	3/19/2015	<2.0	<2.0	<2.0	<0.5	<0.5	<0.5	<0.5	<2.0	<1.0
TT	2-5	3/19/2015	NC	NC	NC	NC	NC	NC	NC	NC	NC
TT	2-6	3/24/2015	NC	NC	NC	NC	NC	NC	NC	NC	NC
TT	2-7	3/19/2015	NC	NC	NC	NC	NC	NC	NC	NC	NC
TT	2-8	3/17/2015	NC	NC	NC	NC	NC	NC	NC	NC	NC
TT	2-9	3/24/2015	NC	NC	NC	NC	NC	NC	NC	NC	NC
Area 3 Pre-hydraulic Fracturing											
DRI	3-1	9/3/2014	<2.0	<2.0	<2.0	<0.5	<0.5	<0.5	<0.5	<2.0	<1.0

Table A-6. Hydraulic fracturing chemical tracers for upper Humboldt River Basin wells, springs, and streams (continued).

Agency (Units)	Location ID	Sample Date	Methanol (mg/L)	Ethanol (mg/L)	Isopropanol (mg/L)	Glycerol (mg/L)	Ethylene Glycol (mg/L)	Propylene Glycol (mg/L)	2-Butoxyethanol (mg/L)	Acrylonitrile (mg/L)	Ammonium Persulfate (mg/L)
TT	3-1	9/3/2014	NC	NC	NC	NC	NC	NC	NC	NC	NC
DRI	3-2	9/3/2014	<2.0	<2.0	<2.0	<0.5	<0.5	1.883 P	<0.5	<2.0	<1.0
TT	3-2	9/3/2014	NC	NC	NC	NC	NC	NC	NC	NC	NC
DRI	3-3	9/3/2014	<2.0	<2.0	<2.0	<0.5	<0.5	<0.5	<0.5	<2.0	<1.0
TT	3-3	9/3/2014	NC	NC	NC	NC	NC	NC	NC	NC	NC
DRI	3-4	9/4/2014	<2.0	<2.0	<2.0	<0.5	<0.5	<0.5	<0.5	<2.0	<1.0
DRI	3-5	9/5/2014	<2.0	<2.0	<2.0	<0.5	<0.5	<0.5	<0.5	<2.0	<1.0
DRI	3-6	9/30/2014	<2.0	<2.0	<2.0	<0.5	<0.5	1.566 P	<0.5	<2.0	1.46
TT	3-6	9/30/2014	NC	NC	NC	NC	NC	NC	NC	NC	NC
DRI	3-7	9/30/2014	<2.0	<2.0	<2.0	<0.5	<0.5	2.782 P	<0.5	<2.0	<1.0
TT	3-7	9/30/2014	NC	NC	NC	NC	NC	NC	NC	NC	NC
DRI	3-8	9/30/2014	<2.0	<2.0	<2.0	<0.5	<0.5	<0.5	<0.5	<2.0	<1.0
DRI	3-9	10/8/2014	<2.0	<2.0	<2.0	<0.5	<0.5	<0.5	<0.5	<2.0	<1.0
TT	3-9	10/8/2014	NC	NC	NC	NC	NC	NC	NC	NC	NC
DRI	3-10	10/21/2014	<2.0	<2.0	<2.0	<0.5	<0.5	<0.5	<0.5	<2.0	<1.0
TT	3-10	10/29/2014	NC	NC	NC	NC	NC	NC	NC	NC	NC
DRI	3-11	10/21/2014	<2.0	<2.0	<2.0	<0.5	<0.5	<0.5	<0.5	<2.0	<1.0
TT	3-11	10/21/2014	NC	NC	NC	NC	NC	NC	NC	NC	NC
TT	3-12	10/21/2014	NC	NC	NC	NC	NC	NC	NC	NC	NC
DRI	3-12	10/22/2014	<2.0	<2.0	<2.0	<0.5	<0.5	<0.5	<0.5	<2.0	<1.0
DRI	3-13	10/22/2014	<2.0	<2.0	<2.0	<0.5	<0.5	<0.5	<0.5	<2.0	<1.0
TT	3-14	10/21/2014	NC	NC	NC	NC	NC	NC	NC	NC	NC
TT	3-15	9/30/2014	NC	NC	NC	NC	NC	NC	NC	NC	NC
TT	3-16	12/8/2014	NC	NC	NC	NC	NC	NC	NC	NC	NC
TT	3-17	12/8/2014	NC	NC	NC	NC	NC	NC	NC	NC	NC
TT	3-18	12/8/2014	NC	NC	NC	NC	NC	NC	NC	NC	NC

Table A-6. Hydraulic fracturing chemical tracers for upper Humboldt River Basin wells, springs, and streams (continued).

Agency (Units)	Location ID	Sample Date	Methanol (mg/L)	Ethanol (mg/L)	Isopropanol (mg/L)	Glycerol (mg/L)	Ethylene Glycol (mg/L)	Propylene Glycol (mg/L)	2-Butoxyethanol (mg/L)	Acrylonitrile (mg/L)	Ammonium Persulfate (mg/L)
TT	3-19	12/8/2014	NC	NC	NC	NC	NC	NC	NC	NC	NC
TT	3-20	12/8/2014	NC	NC	NC	NC	NC	NC	NC	NC	NC

DRI = Desert Research Institute

NC = not collected

P = possible contamination of laboratory equipment or sample vials

TT = Tetra Tech

THIS PAGE INTENTIONALLY LEFT BLANK

APPENDIX B: MIGRATION POTENTIAL TRANSPORT MODELING

A variety of computer models were developed to test the migration potential of subsurface methane gas and hydraulic fracturing fluid toward shallow drinking water resources. The transport modeling was done in addition to the regional groundwater flow model described in Section 4.0. To the extent possible, the regional groundwater flow model was used to define local boundary conditions for the other models used to calculate migration potential.

Three types of transport models were constructed to evaluate some of the scenarios outlined in Section 6.0. These models can be described conceptually as:

- *Local Scale Source Term Model* – This is a local scale, three-dimensional flow and transport model that is centered on Noble wells M2C and M10C. The NUFT (Nitao, 2004) simulator is used to simulate flow and RWHet (LaBolle, 2006) for solute transport away from the hydraulic fracturing zone into adjacent geologic units.
- *Regional Cross-sectional Model* – This is a regional scale two-dimensional model that simulates flow and transport using the FEFLOW simulator (DHI, 2012). This model is used to determine the migration potential to shallow drinking water resources.
- *Vertical Gas Transport Model* – This is a two-dimensional model centered on Noble wells M2C and M10C using the TOUGH2 simulator (Pruess, 2012) to simulate methane gas migration upward from the hydraulic fracturing.

A convolution technique is used to integrate the results of the local scale source term model with the regional cross-sectional model. In particular, the convolution method was used for the special case of the local scale model in which hydraulic fracturing fluid migrated from the Elko Formation to the carbonate unit. This only occurs for the case of a higher hydraulic conductivity in the Elko formation that permits transport to the lower carbonate unit. A convolution is a mathematical technique that integrates the effects of the more detailed source term release into the regional cross-sectional model. In this way, the source term loading to the carbonate aquifer can be "convolved" with the regional solution to predict the effects of the slow release of hydraulic fracturing fluid to the lower carbonate unit and then migration downgradient.

The convolution technique combines the results of the local scale model and the cross-sectional regional scale model. The local scale model, which computes transport in a dual-continua framework and also allows for diffusional mass exchange between matrix and fracture, is used to generate inputs to the cross-sectional model. This is done by placing a horizontal control plane at the interface between the Carbonates and the Elko Formation. Contaminant particles are released in the hydraulic fractures (50 meters in height and placed centrally within the Elko Formation), and the percentage of particles passing the horizontal control plane is recorded for each year up to a maximum simulation period of 2,000 years. This simulation is done separately for well 2C and well 10C. This appendix documents the construction of the models and results that were used to estimate the migration potential for many of the scenarios presented in Section 6.0.

B.1 LOCAL SCALE FLOW AND TRANSPORT MODEL

B.1.1 Introduction

A local scale model is developed for the area surrounding the boreholes M2C and M10C located in the Noble Energy Lease Area 2. The model is designed to study the configuration of flow through the Elko Formation and adjoining units and assess the likelihood of contaminant migration from the hydraulically fractured zones of the shale unit. The regional groundwater flow model (see Section 4) provides the distribution of hydraulic head and estimates of the hydraulic gradient and flow direction that are used to guide the construction, parameterization, and application of boundary conditions for the local scale model. The local scale model uses a dual continuum approach to simulate flow contributions from primary porosity of the rock and secondary porosity of interconnected rock fractures. A separate transport model that uses the dual-continuum flow solutions is used to assess the potential extent and pathways of contaminant migration associated with chemicals introduced by the hydraulic fracturing process.

B.1.2 Model Construction

The local scale model is three-dimensional with a grid that is approximately oriented in the direction of flow inferred from the regional groundwater flow model. This rotated grid allows for larger distances between the sources zone (i.e., the zone of initial release of contaminants) and the downgradient boundary while constraining the model in the lateral direction to reduce computational complexity. The total length of the model is 3,600 m along the direction of flow with boreholes M2C and M10C located one-third (1200 m) of the distance from the upgradient boundary and two-thirds (2400 m) of the distance to the downgradient boundary. The large distance between the source release area and downgradient boundary (> 2 km) allows for spatial analysis of the evolving contaminant plume for identification of potential pathways for migrating contaminants. The width of the model is also 3,600 m such that each lateral boundary is located approximately 500 m from the nearest borehole. The vertical extent of the model is constant and ranges from sea level down to -3,000 m AMSL. The lower model boundary extends below to the Cenozoic basement, and therefore allows for the inclusion of a large volume of highly conductive carbonates in the model. The Elko Formation, which varies in depth over the model extent, ranges approximately between 650 m and 900 m from the top of the model in the vicinity of borehole M2C and between 900 m and 1,100 m from the top of the model in the vicinity of borehole M10C.

The model domain in the context of geological units and wells M2C and M10C is shown by the yellow box in Figure B-1. All surfaces in Figure B-1 represent the top elevation of each geologic unit, except the top surface that denotes the land surface elevation. The top surfaces of each unit are displayed in a hot and cold scale and denote (from the top): younger volcanics, the Indian Well Formation, Elko Formation, three carbonate rock units, and the Cenozoic basement. The rotation applied to the model boundaries is 45 degrees east counterclockwise. The direction of the hydraulic gradient in this rotated domain is almost parallel to the lateral faces (aligned to the northwest) of the model. The UTM coordinates (UTM Zone 11, NAD83) of the domain vertices and boreholes are given in Table B-1. The model is discretized uniformly in all three directions to generate the three-dimensional grid for numerical computations. The cell size in the *x*- and *y*-directions is fixed at 80 m, which results in 45 cells in each of these two directions. The cell size in the vertical direction is fixed at 50 m resulting in 60 equally spaced layers. The total number of cells in the model equals 121,500.

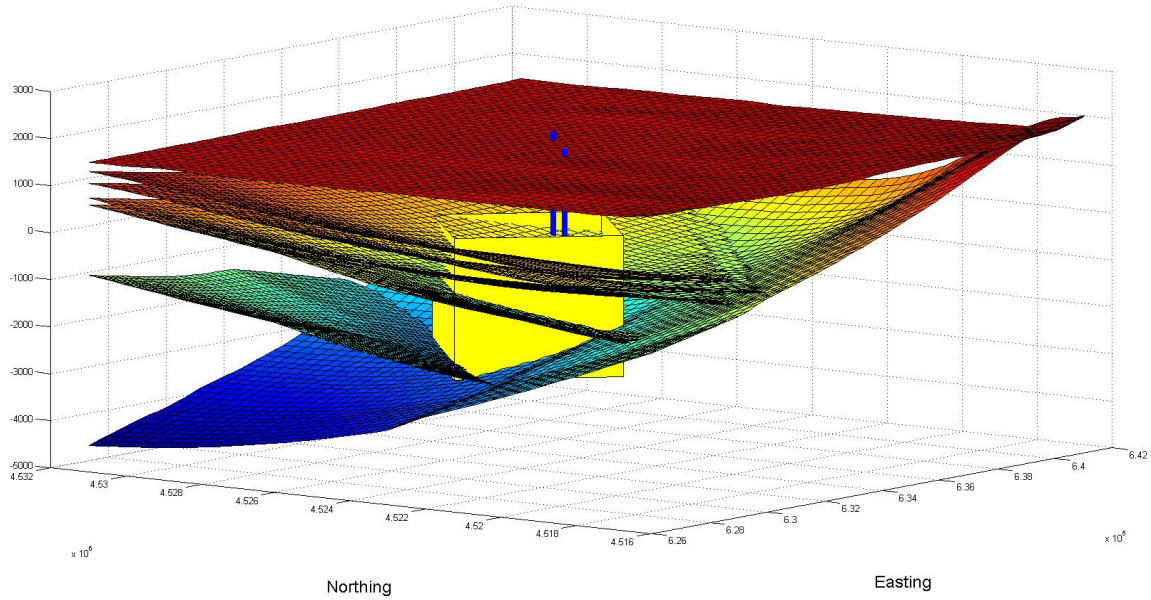

Figure B-1. Vertical and horizontal extent of the local scale model (depicted by the yellow box) shown alongside topographical surfaces of different geologic units and the location of two wells (M2C and M10C) in Area 2.

The flow model is solved using nonisothermal unsaturated-saturated flow and transport (NUFT), which is an integrated finite-difference code to simulate flow in multi-phase, multi-continua environments (Nitao, 2004). The steady state flow field from NUFT is input into a Lagrangian transport simulator, Random Walk in Heterogeneous (RWHet) Porous Media (LaBolle, 2006), to provide transport estimates of dissolved solutes.

It is important to note the two main assumptions used to develop this model:

1. The model does not account for production from wells M2C and M10C after hydraulic fracturing that would capture some of the transport mass.
2. Production from wells M2C and M10C locally decreases the hydraulic gradient and reduces velocities of contaminants within the zone of well influence.

Therefore, the results from the local scale model represent scenarios in which the downgradient migration of contaminants is accelerated relative to other possible scenarios.

Table B-1. UTM coordinates of local scale model vertices and location of the boreholes.

	Easting (m)	**Northing (m)**
Southern Vertex	633017.0	4522131.0
Eastern Vertex	635562.6	4524676.6
Northern Vertex	633017.0	4527222.2
Western Vertex	630471.4	4524676.6
Borehole M2C	634420.4	4525068.1
Borehole M10C	632556.0	4523339.0

B.1.3 Boundary Conditions

The regional groundwater flow model provides a basis for assigning hydraulic boundary conditions to the local scale model. The regional scale model contains grid cells with a greater horizontal discretization than the local scale model and variable vertical discretization. This necessitates a linear interpolation of head values in the regional scale model—which range from approximately 1,635 m to 1,680 m—via a MATLAB® script to assign values of hydraulic head for each individual cell on the six boundary faces of the local scale model. Figure B-2 shows the simulated hydraulic head distribution from the regional model for the local model domain. The values of head assigned to the boundary cells are held constant throughout time and the flux of water through the model depends on head values assigned to the boundary cells and the geometry and hydraulic parameters assigned to each geologic unit. The boreholes are passive in the model because active pumping is not simulated for the wells. Instead, the boreholes are used to place the hydraulic fractures and initial contaminant release in the model.

B.1.4 Hydraulic Properties and Transport Parameters

The geologic units present in the local scale model consist of five groups: 1) volcanics, 2) Indian Well Formation, 3) Elko Formation, 4) carbonates, or 5) basement rock. The value of hydraulic conductivity of each of these five rock types is guided by the calibrated results of the regional groundwater flow model, with some exceptions as remarked in Table B-2. The distribution of conductivity between the matrix and the fracture continua for various rock types is selected by considering: a) dominant rock type(s) delineated from the Noble Energy borehole mudlogs, b) fracture intensity in the Noble Energy fracture data analysis report, and c) the trend in porosity values.

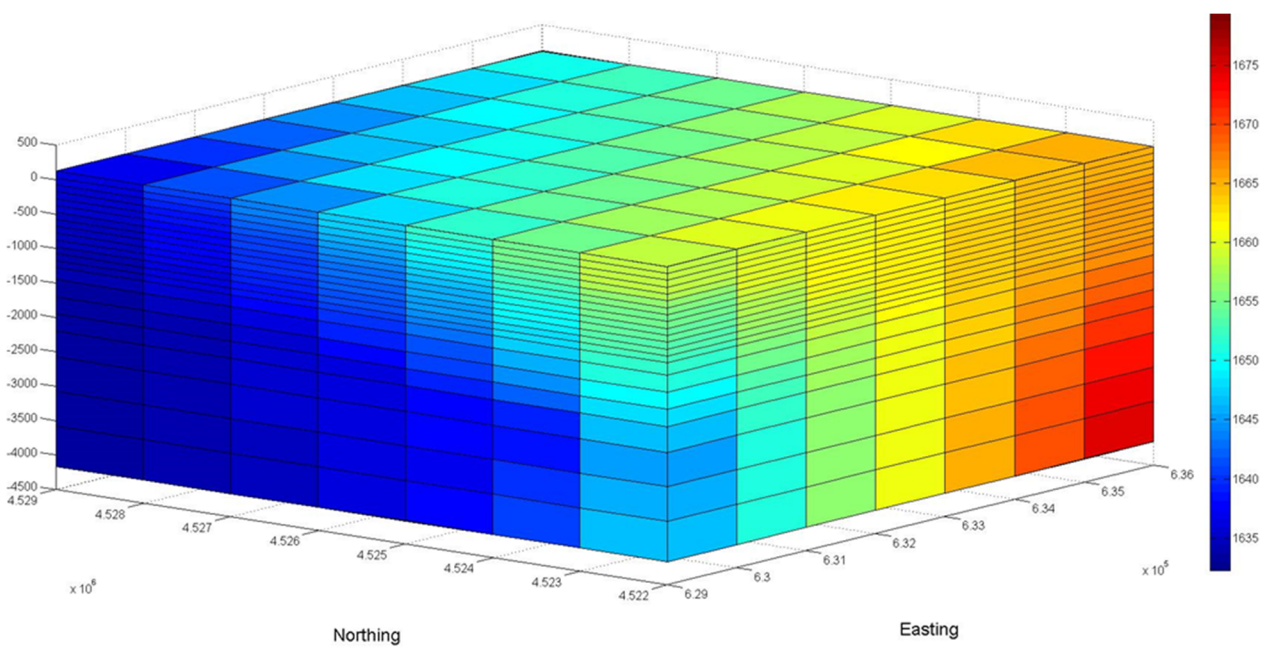

Figure B-2. Distribution of hydraulic head extracted from the regional groundwater flow model at and around the location of the local scale flow and transport model. The datum for this figure is fixed at sea level. These head values provide the boundary conditions for all six faces of the local scale model.

Table B-2. Hydraulic properties of various rock types in the local scale flow and transport model.

	Hydraulic Conductivity [m/s]		Porosity [-]		Fracture Aper. [10^{-6} m]	Fracture Spac. [m]	Remarks
	Matrix	Fracture	Matrix	Fracture			
Volcanics	2.78e-07	6.94e-08	0.20	0.001	50	1.26	Conductivity based on calibrated value given in Table 4-3 and an 80/20 split between the matrix and fracture continua. Value of K_z in an order smaller.
Indian Well Formation	2.89e-07	2.89e-07	0.18	0.001	50	0.96	Conductivity based on average value inferred from the drillstem test (Section 5) and a 50/50 split between the matrix and fracture continua.
Elko Formation	5.00e-11	9.50e-10	0.16	0.001	50	1.16	Conductivity based on 10^{-9} m/s and a 5/95 split between the matrix and fracture continua.
Carbonates	8.68e-08	1.65e-06	0.02	0.005	100	0.20	Conductivity based on calibrated value given in Table 4-3 and a 5/95 split between the matrix and fracture continua.
Basement rock	5.00e-12	9.50e-11	0.02	0.001	50	2.00	Conductivity based on 10^{-10} m/s and a 5/95 split between the matrix and fracture continua.
Hydraulically fractured cells	5.00e-11	1.00e-06	0.16	0.002	700	1.00	High value of conductivity assigned to the fractures; matrix values are unchanged from Elko Formation.

Porosity values assigned to the matrix continuum are guided by the porosity logs (see Schumer and Pohll, 2014), whereas porosity values for the fractures are largely unknown and assigned to the fracture continuum on the order of 10^{-3}. These fracture porosity values are based partially on the fracture intensity of the geologic units and past experience in assigning properties of discrete fracture networks to continuum grids. Lower porosity values translate to a more restricted volume through which the fluid must flow, and therefore they generate higher values of velocity for a given volumetric flow rate.

Fracture spacing—which is used in the dual-continuum flow model as well as the algorithm used to simulate molecular diffusion between rock matrix and fractures—is computed using the Noble Energy fracture data analysis report by counting only the faults, open fractures, and partially open fractures. For the carbonates with sparse data, fracture spacing is assigned a high value based on the numbers reported for carbonates at the Nevada National Security Site (Reeves *et al.*, 2014). Smaller values of fracture spacing (a high density of fractures) promotes diffusional mass exchange between the matrix and fracture continua by enhancing surface area for particles to diffuse back and forth through each continua. Fracture aperture is unknown and a relatively small value of 50 microns is assigned to most of the rock units to account for a mix of open and partially open fractures. Fracture-dominated carbonate rocks are given a higher value of fracture aperture (100 microns). Similar to fracture spacing, smaller values of fracture aperture enhance diffusional mass exchange from fractures to the matrix.

The hydraulically fractured cells in the Elko Formation are assigned modified hydraulic property values to account for the presence of stimulated fractures. These fractures are oriented north to south to honor the stress field measurements from borehole breakouts as summarized in the Noble Energy fracture data analysis report. The horizontal length of stimulated fractures are fixed at 300 m and fracture height is assumed to be 50 m for the purposes of the local scale model. Larger fracture heights are investigated with the cross-sectional regional model by assuming hydraulic fractures extend directly into the carbonate unit. The model cells in which hydraulic fractures are assumed to be present are assigned a high conductivity of 10^{-6} m/s in the fracture continuum. The conductivity of the matrix continuum is unaltered from the Elko Formation values. The fracture spacing and fracture porosity are given a slightly higher value than unfractured Elko Formation cells. Aperture values of the hydraulically stimulated fractures are computed using the following expressions developed by optimizing well productivity given pay zone constraints (e.g., reservoir geometry and permeability) (Romero *et al.*, 2002):

$$w = \left(\frac{C_{fDopt} V_f k}{h k_f} \right)^{1/2} \tag{B-1}$$

where:

$$C_{fd} = \frac{k_f w}{k x_f} \tag{B-2}$$

Here, w is the fracture width (aperture), C_{fd} is a dimensionless fracture conductivity that serves as a design parameter governing the productivity of the reservoir, k_f is the fracture permeability governed by permeability of the proppant material, x_f is the fracture half-length, k is the reservoir permeability, h is the height of the pay zone (thickness of Elko Formation), and V_f is the volume of the hydraulically induced fracture and it is estimated according to the total volume of injected fluid.

The optimized value of C_{fd} is usually very close to 1.6 (Romero *et al.*, 2002) and is used here to estimate the aperture of the hydraulic fractures. Values used for other variables in Equation B-1 are: V_f = 300,000 gallon = 1134 m^3; k_f = 200 darcies, $k = 10^{-5}$ darcies; and h = 200 m. Substituting these values in Equation B-1 and rounding the result to the nearest multiple of 100 microns yields an aperture value of 700 microns for hydraulic fractures. The values of various properties for all rock types and the hydraulically stimulated fractured cells are shown in Table B-2.

The transport simulations are conducted by assuming a nonsorbing contaminant ($K_d = 0$) with a low-diffusion coefficient to provide conservative estimates of contaminant migration. The value of the free water molecular diffusion coefficient applied to the conservative contaminant is fixed at 5×10^{-10} m^2/s, which is representative of moderate- to large-sized molecules. This value is further multiplied by 0.2 (to model the formation factor for all rock types) to produce an effective diffusion coefficient of 10^{-10} m^2/s. The longitudinal and transverse dispersivity in the model is fixed at 5 m.

B.1.5 Subsurface Flow Simulation

The local scale flow models are developed using the US1P module in NUFT, which simulates single-phase, variably saturated fluid flow (Nitao, 2004). The dual-permeability option in US1P is used to simulate pressure disequilibrium between matrix and fracture continua that arise from differential hydraulic properties in the two continua. As described by Nitao (2000a,b) and Hao *et al.* (2012), NUFT is a suite of multi-phase, multi-component models for numerical solution of nonisothermal fluid flow and dissolved species transport in porous media with application to subsurface contaminant transport problems. The distinct modules are embedded in a single code to use a common set of utility routines and input file formats. The NUFT has been used in numerous applications ranging from designing nuclear waste repositories (e.g., Buscheck *et al.*, 2002) to analyzing contaminant remediation (e.g., Newmark *et al.*, 1997) or contaminant migration (e.g., Tompson *et al.*, 2006) to studying variably saturated flow systems with complex flow patterns (e.g., Reeves *et al.*, 2014).

In general, NUFT solves the three-dimensional continuum balance equations for the conservation of fluid and species mass, fluid momentum, and thermal energy (Nitao, 2004). It may be applied to either single-continuum or dual-continua conceptualizations of the porous medium. In the continuum-based approach, the flow domain is discretized into grid blocks that have effective property values. The balance equations are discretized in space using the integrated, finite difference method and in time using the fully implicit backward Euler method. The resulting nonlinear system of equations is solved at each time step using the Newton-Raphson method. The US1P module is designed to simulate the flow of liquid phase under isothermal, variably saturated conditions, as commonly described by the Richards equation (e.g., Bear, 1972; Hao *et al.*, 2012). Conceptualizing the system as 100 percent water saturated, NUFT simulations are conducted to establish steady-state conditions for the local scale model.

The dual continuum approach used in the local scale flow model distinguishes flow contributions (and corresponding velocities) between matrix and fractures. This approach is particularly important for geologic units where both porous rock and fractures are likely to significantly contribute to flow. Reducing either of these geologic units to a single continuum in a numerical model would likely result in unrealistic predictions of contaminant migration (e.g., assigning the entire hydraulic conductivity from the regional scale model to the fracture continuum would lead to unrealistically high velocities and overpredict transport, whereas assigning the entire hydraulic conductivity from the regional scale model to the matrix continuum would lead to underpredicting transport). The application of saturated initial and

boundary conditions generate steady-state head values between fractures and the matrix that are in equilibrium (i.e., the head distribution shown in Figure B-3 is the same for each continuum), yet the flow field solution defines flow contributions for each continuum. Steady-state, cell-by-cell flows for each continuum are extracted from the NUFT solutions and input into the RWHet transport model.

B.1.6 Simulation of Contaminant Transport

Contaminant transport through large-scale fractured media is typically quantified by particle-tracking based Lagrangian solvers through the inclusion of dual-domain mass transfer algorithms that probabilistically determine particle transfer between fractures and unfractured matrix blocks. The fully Lagrangian methods are considered superior to the standard Eulerian solvers in simulating transport in regional-scale fractured media because of their computational efficiency (LaBolle *et al.*, 1996; Liu *et al.*, 2000), the subflow grid-scale resolution of the concentrations, and the construction of sample pathways for the underlying stochastic processes.

A mature, fully Lagrangian transport simulator, RWHet Porous Media (LaBolle, 2006), is used to simulate particle trajectories through NUFT dual-permeability flow-field solutions. The RWHet solves an advection-dispersion equation through the NUFT dual-permeability flow fields that includes the processes of advection, dispersion, retardation (LaBolle *et al.*, 1996, 2000, 2001; LaBolle, 2006), and dual-domain (i.e., fracture-matrix) mass transfer (Zhang *et al.*, 2012; Reeves *et al.*, 2014). The RWHet incorporates advanced smoothing algorithms that accurately simulate particle transport between adjacent cells with sharp contrasts in hydraulic conductivity, velocity, and dispersion/diffusion coefficients. For the dual-continuum transport simulations, RWHet requires input of cell-by-cell flow terms for matrix, fracture, and fracture-matrix nodes; matrix and fracture porosity, retardation, and longitudinal and transverse dispersion coefficients; fracture spacing and aperture; effective diffusion coefficients; and the initial distribution of particles.

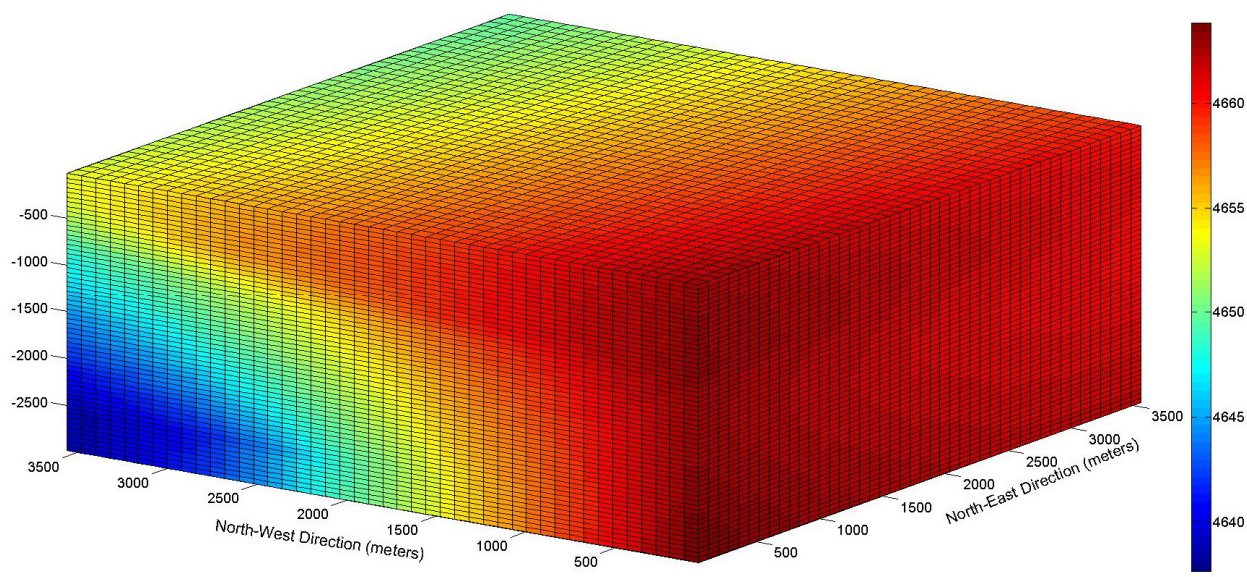

Figure B-3. Simulated distribution of hydraulic head at steady state for the local scale flow and transport model. The datum is fixed at the bottom of the model (3,000 meters below sea level). The model grid discretization is fixed at dx = dy = 80 m, and dz = 50 m.

The particle-based transfer probability approach of Pan and Bodvarsson (2002) is incorporated into RWHet as a subroutine to describe dual-domain mass transfer. This approach idealizes a fractured medium as a series of equally spaced, fracture-separated, uniform matrix blocks and uses geometric and hydraulic properties of the fracture and matrix blocks in the computation of forward (i.e., fracture-matrix) and backward (i.e., matrix-fracture) transition probabilities for diffusing particles (Figure B-4). The forward and backward transition probabilities change with the time elapsed because the release of particles affects the concentration gradient between the fractures and the matrix. The numerical implementation of the Pan and Bodvarsson (2002) algorithm in RWHet is comprehensively documented and tested in Zhang *et al.* (2012).

B.1.7 Local Scale Model Results

The local scale model assumes that the height of the hydraulic fractures to 50 m, which is approximately the median value of downward propagating fractures as determined by Davies *et al.* (2012). The total thickness of the Elko Formation near well M2C is approximately 250 m and 150 m for M2C and M10C, respectively (see Figure B-5). Therefore, the hydraulic fractures are completely contained in the Elko Formation for wells with at least 50 m of vertical distance between the hydraulic fracturing zone and the overlying Indian Well Formation or the underlying carbonates.

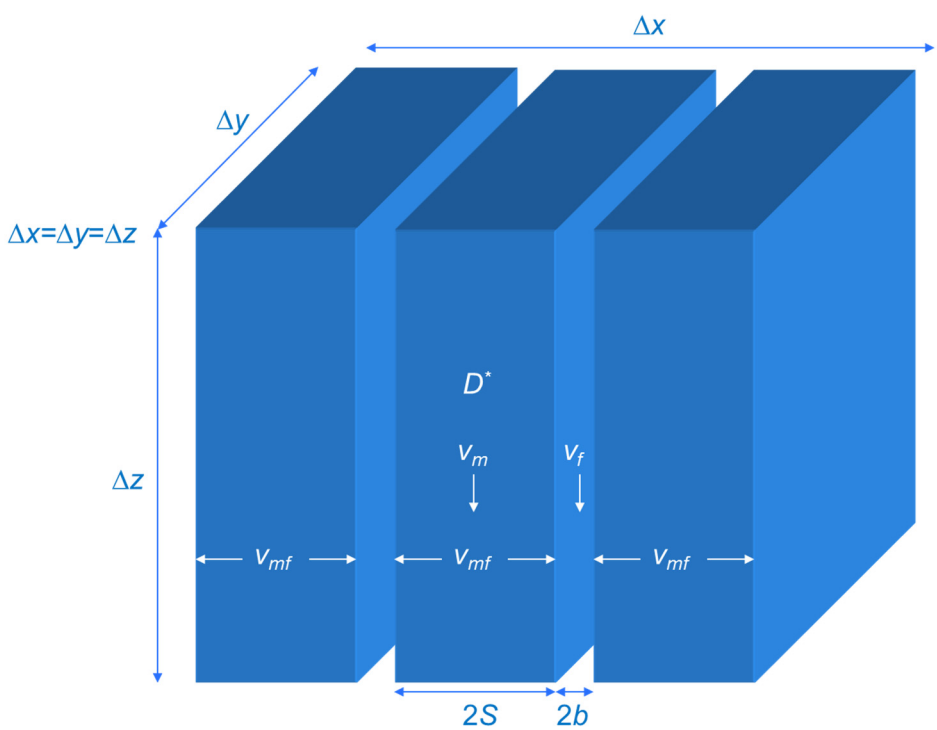

Figure B-4. Conceptual model of vertical flow through a cube containing parallel-plate fractures of velocity vf and aperture 2b separated by porous matrix blocks of constant thickness 2S with vertical velocity vm. The fracture-to-matrix velocity is denoted by v_{mf}. The effective diffusion coefficient D* is the product of the free water diffusion coefficient for a specific radionuclide and tortuosity formation factor specific to rock type. The dual-domain algorithm of Pan and Bodvarsson (2002) takes these geometric, diffusion, and velocity parameters into account during the computation of forward and backward transition probabilities.

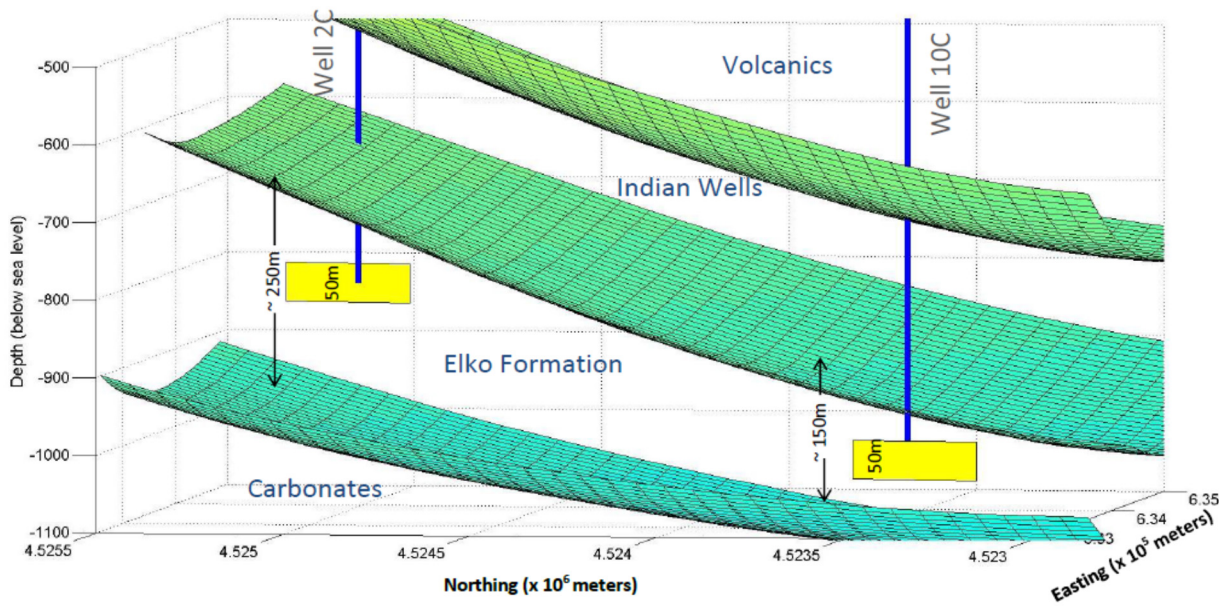

Figure B-5. Illustration of the surfaces of different geologic units, placement of the wells, and hydraulic fractures of height 50 meters included in the local scale model.

Flow solutions were computed using NUFT by running the model to steady-state conditions. The total amount of water moving through the system approximately equals 0.103 m^3/s (2,730 acre-feet per year) with very little variation between the cases. The NUFT flow fields are converted to velocity by RWHet and particle trajectories are computed throughout the model domain of 2,000 years. A total of 100,000 particles of identical mass equally divided between wells M2C and M10C are used in each scenario with an initial release condition in the fracture continuum at the beginning of the simulation.

The initial release of particles is well mixed over all the hydraulic-fracture cells with no bias in distribution either along the length or height of the hydraulic fractures. The particles move through the system as nonsorbing contaminants with a somewhat weak diffusion process between matrix and fracture continua (modeled by a relatively low value of 10^{-10} m^2/s for diffusion coefficient). The diffusion of particles to the lower velocities of the matrix continuum serves as a retention mechanism in fractured rock masses. Therefore, a lower diffusion coefficient minimizes the transfer of particles from higher velocity fractures to the rock matrix. The transport assessments are conservative in nature (because of the low diffusion coefficient and absence of adsorption/absorption) with likely outcomes exhibiting slower migration rates and lower mass breakthroughs than the simulated results for the majority of the chemicals introduced into the subsurface during the hydraulic fracturing process.

When the hydraulic fractures are fully contained in the Elko Formation, the low velocities within the Elko Formation restrict particle release to the carbonate unit, but mass is released during the 2,000 year simulation. Specific breakthrough curves are not presented for mass movement between the Elko Formation and the lower carbonate unit because these results are presented in the next section as integrated results once they are convoluted with the cross-sectional regional model.

B.2 Cross-sectional Regional Scale Flow and Transport Model

The cross-sectional regional model was used to calculate the migration potential of hydraulic fracturing fluids under various hypothetical scenarios. In all cases, this model simulates a condition in which no oil is produced from the hydraulically fractured well. In this case, hydraulic fracturing fluid migration is allowed to move with the ambient hydraulic gradients.

In terms of the scenario tree (Figure 6-1) in Section 6, this model is used to represent the three primary scenarios under the no oil production portion of the tree including:

1. Fractures contained in the Elko Formation
2. Fractures connect to upward fault in Indian Well Formation
3. Fractures connect to carbonate

In scenario #1 where the fractures are contained in the Elko formation, migration only occurs toward the lower carbonate unit when higher permeabilities are assumed in the Elko. Under these conditions migration of hydraulic fracturing fluids is simulated using both the local scale model convoluted with the cross-sectional model. The cross-sectional regional model does not explicitly simulate the movement of hydraulic fracturing fluids from the Elko Formation to the carbonate unit. Instead, the cross-sectional regional model assumes the initial mass concentration is placed at a node just below the contact between the Elko Formation and the carbonate unit. The migration potential of hydraulic fracturing fluid is simulated for 2,000 years.

The second scenario was used to test hypothesis related to transport along a fault zone in the Indian Well Formation and Tertiary sediments. The model is set up such that hydraulically induced fractures connect to a preexisting fault. The model places a mass-concentration representative of fracking fluids in a fault in the Indian Well Formation near its lower boundary and simulates single-phase transport as a conservative tracer.

The third scenario assumes that hydraulic fractures connect directly to the lower carbonate unit. Simulations in this case are similar to the first scenario, but transport of hydraulic fracturing fluids to the lower carbonate unit is not delayed by the slow migration through the Elko Formation. Therefore, these simulations are not convoluted with the local source term model.

B.2.1 General Model Design

All simulations assumed fully saturated conditions as two-dimensional vertical systems in FEFLOW (DHI, 2012). The FEFLOW is a finite element modeling program for groundwater systems that simulates flow, heat, and mass transport according to general equations defined for each, which are respectively:

$$L(h) = S\frac{\partial h}{\partial t} - \nabla * \left(Kf_{\mu}B * (\nabla h + \Theta e)\right) - Q \tag{B-3}$$

$$L(T) = S\frac{\partial T}{\partial t} + q * \nabla T - \nabla * (B\Lambda * \nabla T) + \Phi(T - T_0) - Q \tag{B-4}$$

$$L(C) = S\frac{\partial C}{\partial t} + q * \nabla C - \nabla * (B\varepsilon D * \nabla C) + \Phi C - Q \tag{B-5}$$

where h is hydraulic head, T is heat, C is contaminant mass, S is storativity, t is time, K is hydraulic conductivity, B is aquifer thickness, f_μ is a fluid viscosity function, Θ is effective saturation, e is the void ratio, ε is porosity, Q is discharge, q is Darcy velocity, Λ is thermal conductivity, Φ is the velocity potential, and D is hydrodynamic dispersion. These equations are adjusted by FEFLOW as appropriate depending on the dimensionality of the simulation and flow can be modeled through either a porous media or as a free fluid.

The model mesh created for these scenarios follows the cross-sectional representation of the upper Humboldt River Basin that intersects Exploration Area 2, which is discussed in Section 2.3 and explained again here for clarity. The transect begins in the east in the Ruby Mountains, intersects Noble Energy well M2C-M2-21B in Exploration Area 2, and terminates near the Humboldt River. Two geologic interpretations for this cross section are presented and modeled in this report such that the more likely interpretation (Figure B-6a) is used as the base scenario for sensitivity analysis and the less likely interpretation (Figure B-6b) is modeled only once to highlight the difference in transport resulting from this alternate interpretation. For both interpretations, formation thicknesses and porosities are taken from Noble Energy borehole logs and assumed to be constant. Hydraulic conductivities for all formations (Table B-3) are taken from a combination of literature values and drillstem test analyses in those formations from previously drilled wells basin wide, as discussed in Section 2.

A fluid-flux (Neumann type) boundary condition on the eastern surface of the mesh represents recharge into the carbonate formation and basin fill deposits. In both the fractured carbonate scenario and the fault connectivity scenario, recharge values were varied for sensitivity over a range of 0.0009-0.006 m/d, taken from the span of possible values from several estimates of mountain block recharge into the basin, as discussed in Section 3.1.1. A constant hydraulic head (Dirichlet type) boundary condition was placed on the upper bounds to the west near the Humboldt River intersection and set as the approximate elevation of the river (1,600 m) (Figure B-7).

Table B-3. Base model parameters.

Formation	Hydraulic Conductivity (m/d)	Porosity	Thermal Conductivity (J/m/s/K)
Alluvium	4.0	0.5	2.9
Sedimentary and Volcanic Rocks	1.0	0.35	2.0
Indian Well Formation	0.1	0.2	1.7
Elko Formation	0.0005	0.2	2.9
Upper Paleozoic Carbonates	3.0	0.03	3.4
Diamond Peak Formation	1.0	0.05	3.4
Chainman Formation	0.0005	0.05	2.9
Metamorphic Core Complex	0.005	0.01	3.4

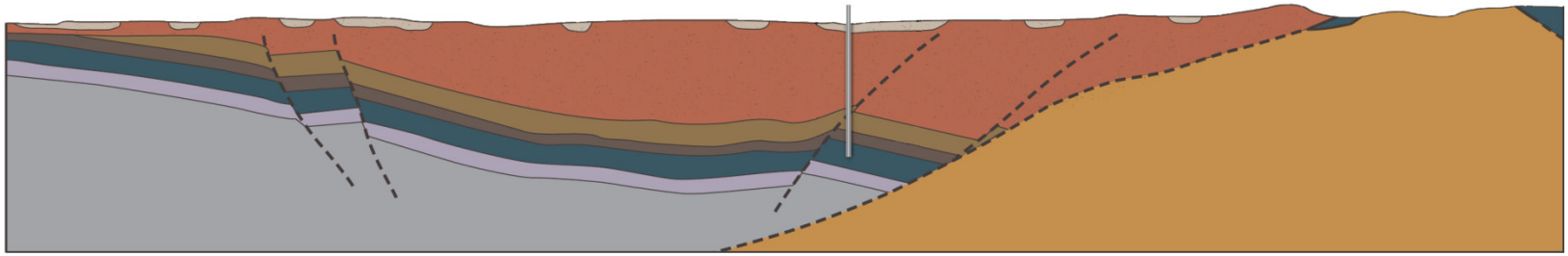

Figure B-6a. Upper Humboldt River cross section used as basis for FEFLOW model domain.

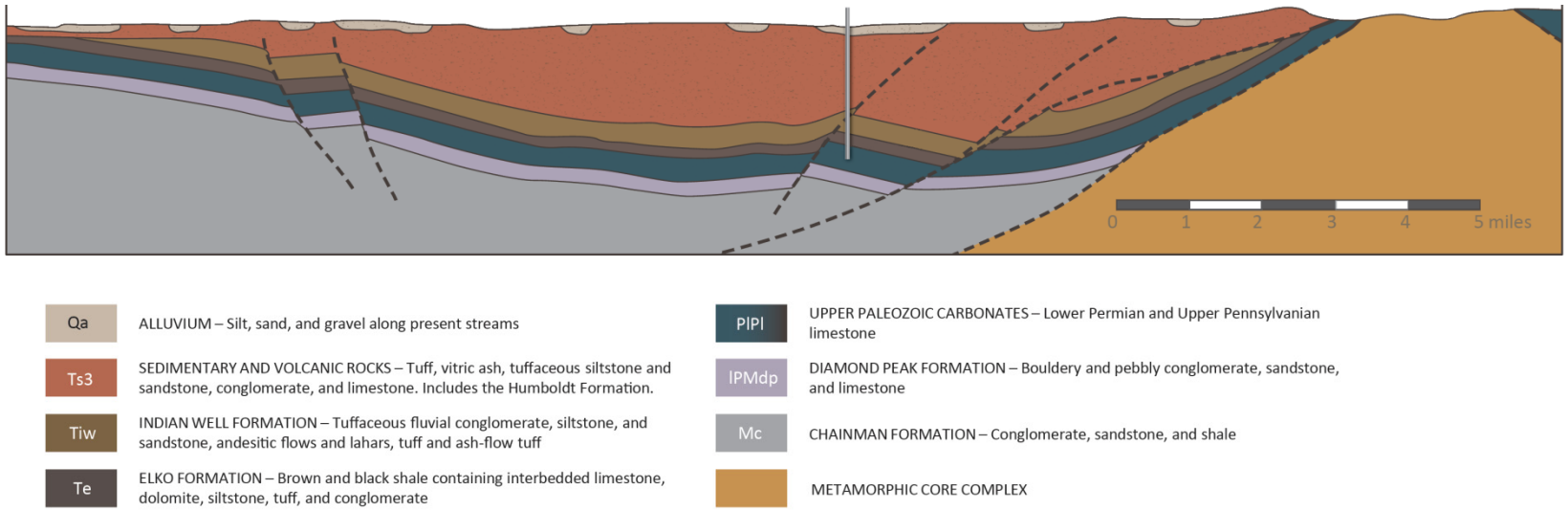

Figure B-6b. Upper Humboldt River Basin alternative geology cross section used as basis for FEFLOW model domain.

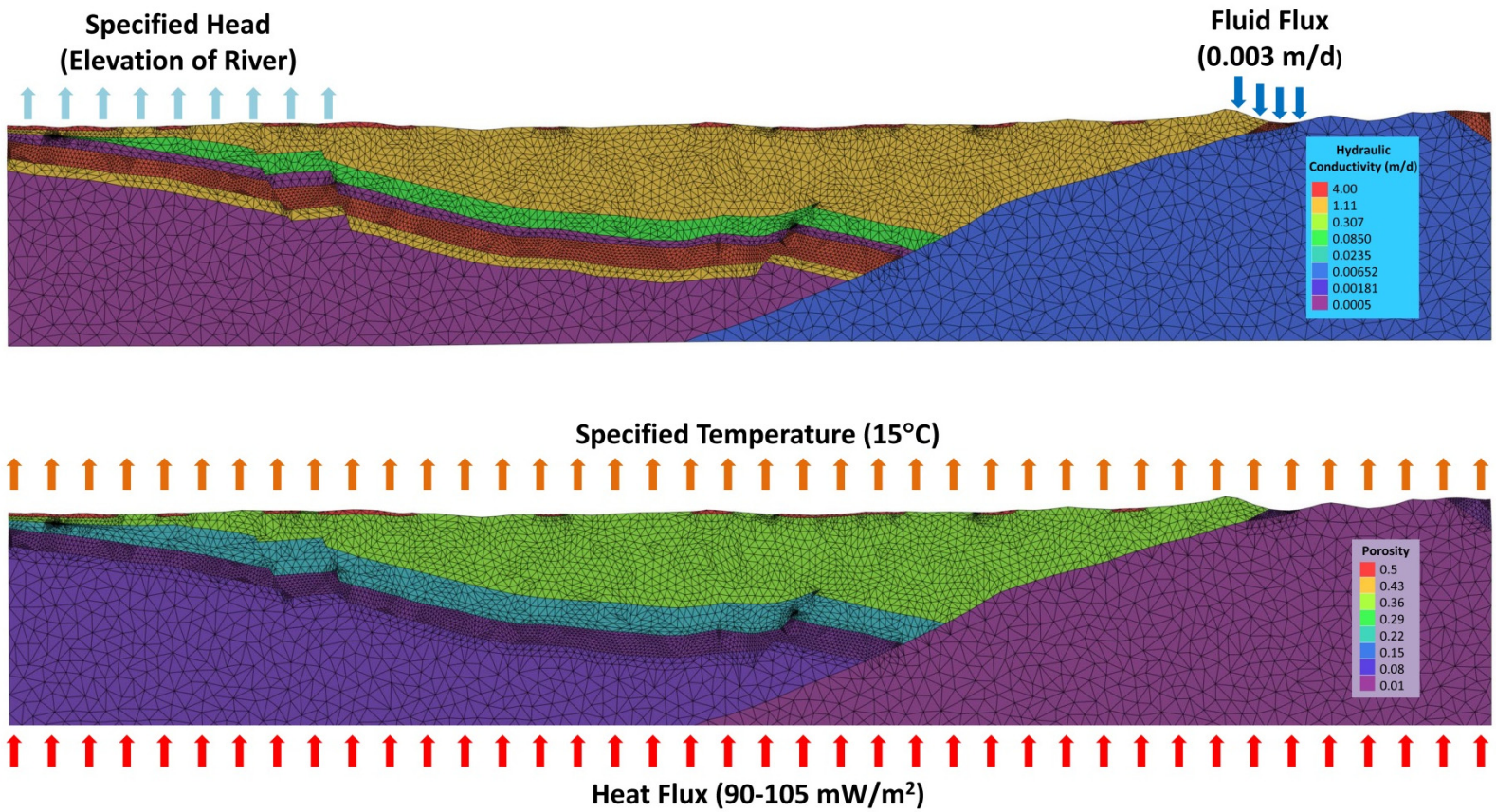

Figure B-7. Boundary conditions and parameters for FEFLOW simulations.

Formation temperatures were derived through the placement of a heat-flux (Neumann type) boundary condition along the lower bounds of the model and a constant-temperature (Dirichlet type) boundary condition along the upper bounds of the model. Heat-flux values for the basin range from 90-105 W/m^2 as determined from geothermal potential data for the Great Basin region (Coolbaugh *et al.*, 2005) and were set accordingly, with variation within that range to adjust for unrealistic resulting temperatures along the western boundary. The constant temperature boundary was set to 15 °C to be representative of surface air temperatures (Figure B-7). Thermal conductivities for all formations were taken from literature values (Beardsmore and Cull, 2001, p. 104). Longitudinal dispersivity for all formations was set to 30 m, which was taken from a range of possible literature values appropriate for the scale of observation (Zheng and Bennett, 2002) and selected because it resulted in the most stable simulation. Transverse dispersivity was assumed to be one-tenth of this value.

Subsurface fault data is limited away from the borehole and hypothetical faults were placed to be consistent with a typical basin and range structure. Although several faults affect basin structure, only one is modeled here as a discrete feature and potential flow path. The fault is conceptually modeled as an open rectangular slit with a constant length and width and the hydraulic aperture is varied for sensitivity over a range of 0.0001-0.01 m. Because the width of the fault is held constant through all scenarios and because frictional factors and asperities are ignored, the cross-sectional area varies proportionally with the hydraulic aperture.

The base model scenario was simulated five times to account for the range of sorption coefficients across the variety of chemicals present in fracking fluids. Organic compounds can be sorbed to organic carbon present in the aquifer at varying rates that depend largely on the molecular structure of the compound. This process causes some solutes to migrate through the aquifer at a much slower rate than the groundwater that is transporting them (Fetter, 2000). The sorption parameters used are representative of ethanol (very low sorption), ethylene glycol monobutyl ether (low sorption), 2,2-dibromo-3-nitrilopropionamide (moderate sorption), hydrotreated light petroleum distillate (high sorption), and naphthalene (very high sorption). Sorption was calculated in FEFLOW using a linear adsorption isotherm such that:

$$C^* = \kappa C \tag{B-6}$$

where C^* is the concentration of adsorbed species in units of mass per solid volume, κ is the Henry sorptivity coefficient, and C is the concentration of the dissolved species in units of mass per fluid volume. The sorptivity coefficient κ is more often expressed in terms of the distribution coefficient K_d, where K_d is the product of the sorptivity coefficient and the bulk density of the porous media, which was assumed to be 2.65 g/cm^3 for all formations. For organic compounds, K_d can be calculated from the soil organic carbon/water coefficient (K_{oc}) of the compound and the fraction of organic carbon of a soil or aquifer surface (f_{oc}), where:

$$K_d = K_{oc} f_{oc} \tag{B-7}$$

and for which K_{oc} and f_{oc} are determined experimentally (Fetter, 2000). Values of K_{oc} and f_{oc} were taken from literature values (Table B-4).

Table B-4. Sorption parameters used for the sensitivity study.

Sorption Degree	Compound	K_{oc} (ml/g)	K_d (ml/g) Carbonate (f_{oc} = 0.0008)	K_d (ml/g) Humboldt (f_{oc} = 0.0006)	K_d (ml/g) Elko (f_{oc} = 0.0158)	K_d (ml/g) Indian Well (f_{oc} = 0.0091)
Negligible	Ethanol	2.7	0.00216	0.00162	0.04266	0.02457
Low	Ethylene glycol monobutyl ether	15	0.012	0.009	0.237	0.1365
Moderate	2,2-Dibromo-3-nitrilopropionamide	65	0.052	0.039	1.027	0.5915
High	Hydrotreated light petroleum distillate	800	0.64	0.48	12.64	7.28
Very High	Naphthalene	18200	14.56	10.92	287.56	165.62

In all cases a normalized initial mass is used. Breakthrough curve results can be scaled to represent specific chemical concentrations used in the hydraulic fracturing process. The initial solute concentration is also subject to the equilibrium condition with the concentration of the adsorbed species as calculated using Equation B-6. Therefore, initial concentrations were scaled based on the value of κ for each constituent such that the total initial species mass in the model domain was equal for all simulations.

B.2.2 Carbonate Model Design

Model sensitivity was tested using nine scenarios (Table B-5) and varying the conductivity of the carbonate and basin fill formations, recharge volume, and fault aperture. For each scenario, the flow model component was run without mass transport until steady-state flow conditions were achieved. Missing from those scenarios listed in Table B-5 is a simulation with a decreased hydraulic conductivity of the Tertiary sediments. For this scenario, initial steady-state conditions showed unrealistic heads in the mountain block, and therefore the mass transport simulation was not run. In addition to the simulations detailed below, the parameters listed for Simulation 1 were also used to model the effects of increasing sorption as well as the alternate geologic interpretation presented in Figure B-6b.

Table B-5. Parameters for fractured carbonate transport simulations.

Simulation	Recharge (m/d)	Hydraulic conductivity of carbonate (m/d)	Hydraulic conductivity of Tertiary sediments (m/d)	Hydraulic conductivity of metamorphic rocks (m/d)	Hydraulic aperture of fault (m)
1	0.003	3	1	0.005	0.001
2	0.006	3	1	0.005	0.001
3	0.0009	3	1	0.005	0.001
4	0.003	40	1	0.005	0.001
5	0.003	0.01	1	0.005	0.001
6	0.003	3	2	0.005	0.001
7	0.003	3	0.01	0.005	0.001
8	0.003	3	1	0.005	0.01
9	0.003	3	1	0.005	0.0001
10	0.003	3	1	0.05	0.001
11	0.003	3	1	0.0005	0.001

B.2.3 Fault Zone Model Design

The cross-sectional model was also used to test hypothesis related to transport along a fault zone in the Indian Well Formation and Tertiary sediments. The model is set up so that hydraulically induced fractures connect to a preexisting fault. The model places a mass concentration representative of fracking fluids in a fault in the Indian Well Formation near its lower boundary and simulates single-phase transport as a conservative tracer.

The same model mesh is used here, with the same hydraulic and thermal conductivities, porosities, and boundary conditions (see Section B.2.1). A fault was placed such that the base of the fault is within the Indian Well Formation and within 400 feet of the contact between the upper boundary of the Elko Shale and the wellbore, which is the distance calculated to be the maximum potential fracture extent given the volume of water injected by the equation derived in Flewelling *et al.* (2013), and assuming five injection periods. Although the fault zone placement in this scenario differs from the carbonate transport scenario, it is conceptually modeled in the same way and the hydraulic aperture is varied for sensitivity over the same range of values (0.0001-0.01 m). Nine simulations were again run, this time varying the conductivities of the Indian Well Formation and the Tertiary sediments, recharge, and fault aperture for sensitivity (Table B-6). Simulations were run to steady state before the addition of a 1 mg/L concentration at the base of the fault zone, and then allowed to run for 500 years. Effects of sorption were not considered for this scenario.

Table B-6. Parameters for fault connectivity scenario.

Simulation	Recharge (m/d)	Hydraulic conductivity of Indian Well (m/d)	Hydraulic conductivity of Tertiary sediments (m/d)	Hydraulic conductivity of metamorphic rocks (m/d)	Hydraulic aperture of fault (m)
1	0.003	0.1	1	0.005	0.001
2	0.006	0.1	1	0.005	0.001
3	0.003	54	1	0.005	0.001
4	0.003	0.0001	1	0.005	0.001
5	0.003	0.1	2	0.005	0.001
6	0.003	0.1	1	0.005	0.01
7	0.003	0.1	1	0.05	0.001

B.2.4 Cross Sectional Model Results

Migration potential of hydraulic fracturing fluids was determined by monitoring simulated concentrations at aquifer depths shallower than 600 ft. In many simulations concentrations were not detectable in the shallow aquifer, and therefore breakthrough curve results are not presented. The time horizon for the simulations varied depending on the transport behavior within the individual simulation over a range of 500 to 2,000 years. In some cases simulation times were extended for plotting purposes to achieve a full breakthrough curve.

B.2.4.1 Scenario 1 – Fractures Contained in Elko

As noted above the cross-sectional regional model was used to simulate eleven scenarios that represent differing values of recharge, hydraulic conductivity of carbonate, hydraulic conductivity of Tertiary sediments, hydraulic aperture, and cross-sectional area of faults (see Table B-5 for detail). The base scenario was also simulated with five sorption coefficients to represent the range expected across the variety of chemicals present in fracking fluids. Additionally, the parameters used in the base scenario were also used to simulate potential transport in a cross section of an alternative geologic interpretation. Therefore, a total of 16 simulations were constructed.

Of the eleven scenarios simulated, two resulted in unrealistic heads in the mountain block, and transport was therefore not simulated. A third scenario did not result in any contaminant the shallow aquifers during a simulation period of 2,000 years. These three scenarios are:

- Simulation 3 has very low recharge value (0.0009 m/d compared to 0.003 m/d and 0.006 m/d for other scenarios);
- Simulation 5 has very low hydraulic conductivity of carbonate (0.01 m/d compared to 3 m/d or 40 m/d for other scenarios), which results in unrealistic heads in the mountain block; and
- Simulation 7 has very low hydraulic conductivity of Tertiary sediments (0.01 m compared to 1 m/d or 2 m/d for other scenarios), which results in unrealistic heads in the mountain block.

Additionally, no trace of contaminant was found to reach the shallow aquifers when the moderate sorption (K_{oc} = 65), high sorption (K_{oc} = 800), and very high sorption (K_{oc} = 18200) coefficients were used. Therefore, results are only presented for:

- Eight of the eleven scenarios (1, 2, 4, 6, 7, 8, 9, 10, and 11)
- Two of the five sorption coefficients (negligible and low)
- Alternative geologic interpretation

The breakthrough plots showing normalized concentration (computed concentration as a fraction of the initial concentration) for these combinations of simulation runs, as convolved for well 10C. Because of the greater thickness of the Elko formation at well 2C, convolution results in longer arrival times and reduced peak concentrations of contaminants originating from that well. For clarity, only the convolved results for well 10C are shown here. It is important to note that the concentration values reported in these figures are the maximum simulated concentration only within the upper 600 ft of the shallow aquifers.

Simulation 10 (high value of conductivity of the metamorphic core complex) results in highest peak concentration of contaminants, followed closely by Simulation 8. This simulation run has a fault aperture value of 0.01 m that is 10 times more than the value of 0.001 m used for other scenarios. However, a higher fault aperture value does not necessarily lead to a significantly faster first arrival time or time to peak. In fact, the breakthrough plots have a time shift of only approximately 10 percent between Simulation 1 and Simulation 8 (Figure B-8).

Fast arrival times are observed for Simulations 2, 4, and 10. These three simulations are characterized by a high recharge value, a high value of conductivity of carbonate, and a high value of conductivity of the metamorphic core complex, respectively. Arrival times are significantly delayed for Simulation 6, which is the scenario with high value of hydraulic conductivity in the tertiary sediments. High value of recharge or changes to the conductivity of tertiary sediments also leads to reduction in peak concentration and associated thicker tails of the breakthrough plots (Figure B-8).

Increasing the K_{oc} values reduces the peak concentration and increases the arrival times as one would expect. However, the amount of reduction in peak concentration does not follow a linear trend with increasing K_{oc} values. The peak concentration values of breakthrough curves are very sensitive to increasing K_{oc} at the low range and less so when the increase occurs at higher range. The increase in arrival times as the K_{oc} values change follow a more regular pattern, with large changes in arrival time when a significant shift occurs in the K_{oc} values (Figure B-9).

By far, the most rapid arrival time occurs with the simulation using the alternative geologic interpretation. Although the hydrologic parameters used for this simulation are the same as those used in Simulation 1, the result is a time shift of approximately 60 percent between breakthrough curves (Figure B-10). However, the difference in peak concentration between these two simulations is negligible.

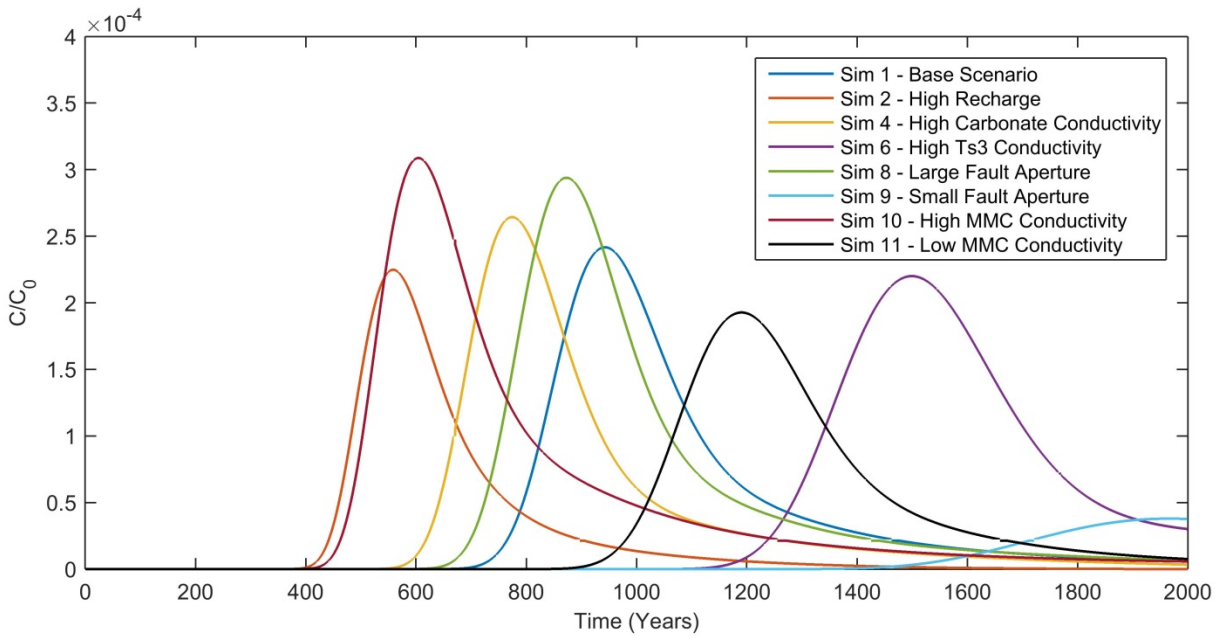

Figure B-8. Breakthrough curves generated by convoluting results from the local scale model with the results obtained for Simulations 1, 2, 4, 6, 8, 9, 10, and 11 of the cross sectional regional model.

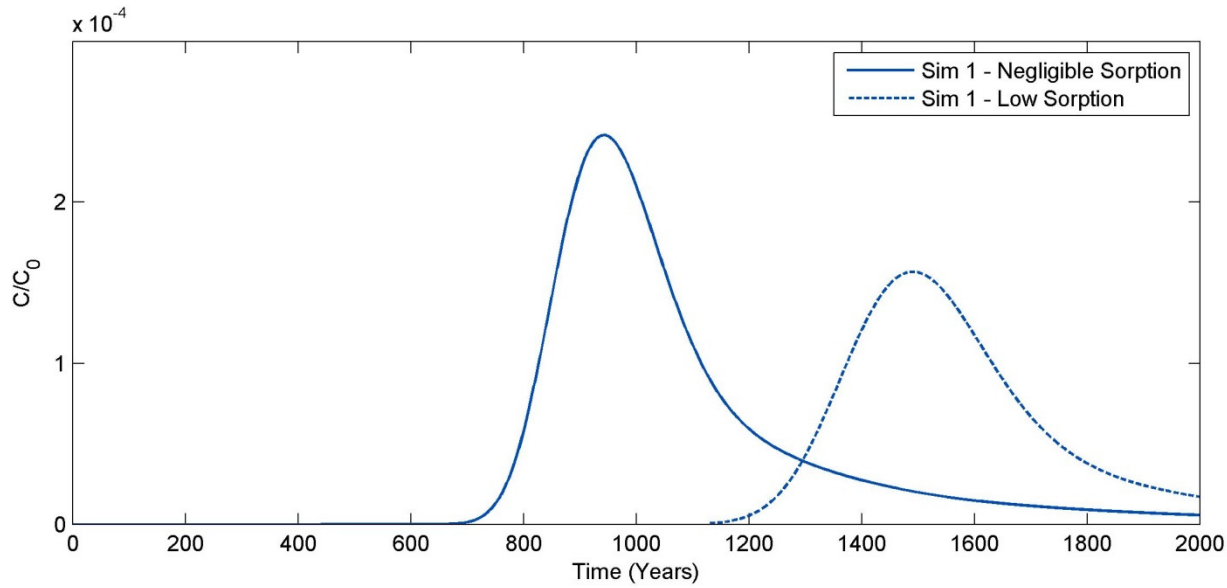

Figure B-9. Breakthrough curves generated by convoluting results from the local scale model with the results obtained for Simulation 1 of the cross sectional regional model using negligible and low sorption parameters.

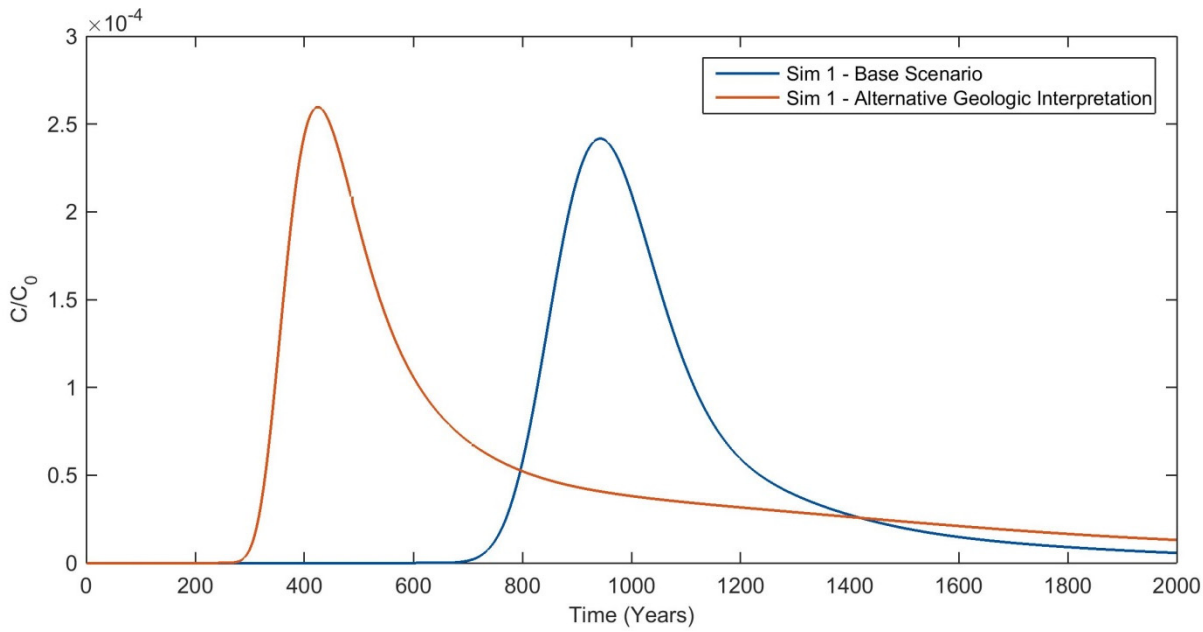

Figure B-10. Breakthrough curves generated by convoluting results from the local scale model with the results obtained for Simulation 1 of the cross sectional regional model and the alternative geologic interpretation.

In addition to the results presented here, a set of simulations was conducted where the hydraulic conductivity in the Elko Formation was reduced by two orders of magnitude in the local scale model (i.e., matrix and fracture conductivity for Elko Formation was changed to 5.00e-13 m/s and 9.50e-12 m/s respectively). This reduction in the conductivity values strongly altered the hydraulic head and velocity field in the local scale model resulting in 100 percent containment of particles released from well 2C and containment of more than 99.9 percent particles released from well 10C (for negligible, low, and moderately sorbing compounds) during the 2,000 years simulation period.

B.2.4.2 Scenario 2 – Indian Well Fault Zone

For this scenario, none of the nine simulations showed any concentration present in the shallow water aquifer after a period of 500 years. The hydraulic gradient in the Elko Formation near the borehole is generally downward and no simulated combination of hydraulic parameters resulted in flow upward through the fault. Instead, the majority of the tracer was transported laterally through the Indian Well Formation, downward through the Elko formation toward the carbonate, or simply trapped within the Elko Formation. Although the variation of fault parameters, system recharge, and formation conductivities did affect the preferential flow path for migration, none made vertical migration through the fault either more likely or more preferred over the lateral flow path (Figure B-11).

B.2.4.3 Scenario 3 – Fractures Connecting to Carbonate

When hydraulic fractures are connected directly to the carbonate unit migration to the carbonate unit is assumed to occur instantaneously. Therefore, the breakthrough curves to the shallow aquifer are similar to Scenario 1 (Fractures Contained in Elko), but breakthrough occurs more rapidly.

Similar to Scenario 1, nine scenarios were simulated that represent differing values of recharge, hydraulic conductivity of carbonate, hydraulic conductivity of Tertiary sediments, hydraulic aperture, and cross-sectional areas of the faults (see Table B-5 for detail). The base scenario was simulated with five sorption coefficients to represent the range expected across the variety of chemicals present in fracking fluids. Additionally, the parameters used in the base scenario were also used to simulate potential transport in a cross section of an alternative geologic interpretation. Therefore, a total of 16 simulations were constructed.

Of the 11 simulated scenarios, two resulted in unrealistic heads in the mountain block, and therefore transport was not simulated. A third scenario did not result in any contaminant the shallow aquifers during a simulation period of 2,000 years. These three scenarios are:

- Simulation 3 has very low recharge value (0.0009 m/d compared to 0.003 m/d and 0.006 m/d for other scenarios);
- Simulation 5 has very low hydraulic conductivity of carbonate (0.01 m/d compared to 3 m/d or 40 m/d for other scenarios), which results in unrealistic heads in the mountain block; and
- Simulation 7 has very low hydraulic conductivity of Tertiary sediments (0.01 m compared to 1 m/d or 2 m/d for other scenarios), which results in unrealistic heads in the mountain block.

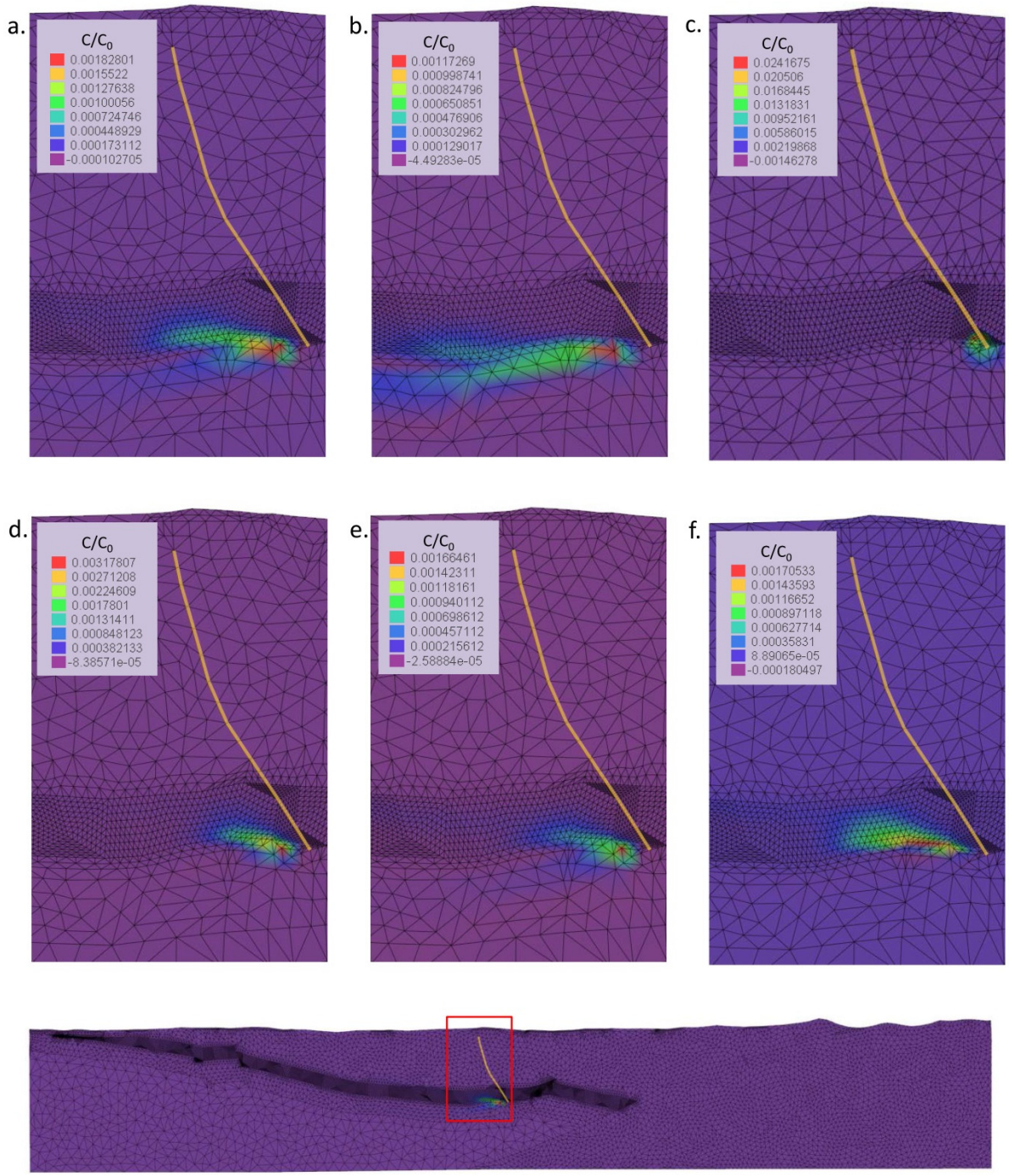

Figure B.11. Results of fault connectivity simulations with the relevant area magnified from full model domain; a) Simulation 1: Base model; b) Simulation 2: Recharge = 0.06 m/d; c) Simulation 4: Indian Well K = 0.0001 m/d; d) Simulation 5: Ts3 K = 2 m/d; e) Simulation 6: Fault aperture = 0.01 m; and f) Simulation 7: MMC K = 0.05 m/d. Simulation 3 not pictured.

Additionally, no trace of contaminant was found to reach the shallow aquifers when the moderate sorption (K_{oc} = 65), high sorption (K_{oc} = 800), and very high sorption (K_{oc} = 18200) coefficients were used. Therefore, results are only presented for:

- Eight of the 11 scenarios (1, 2, 4, 6, 7, 8, 9, 10, and 11)
- Two of the five sorption coefficients (negligible and low)
- Alternative geologic interpretation

The breakthrough plots showing normalized concentration (computed concentration as a fraction of the initial concentration) for these simulation runs are shown in Figure B-12, whereas a comparison of the breakthrough curves for low and negligible sorption and the alternative geologic interpretation are shown in Figures B-13 and B-14, respectively. As in Scenario 1, concentration reported in these figures the maximum simulated concentration in the upper 600 ft of the shallow aquifers.

The result of instantaneously placing hydraulic fracturing fluids directly in the carbonate unit is more rapid migration and larger concentrations in the shallow aquifer. Using Simulation 1 as an example, breakthrough arrives approximately 65 years earlier and a peak concentration nearly 50 percent greater as compared to migration from well 10C.

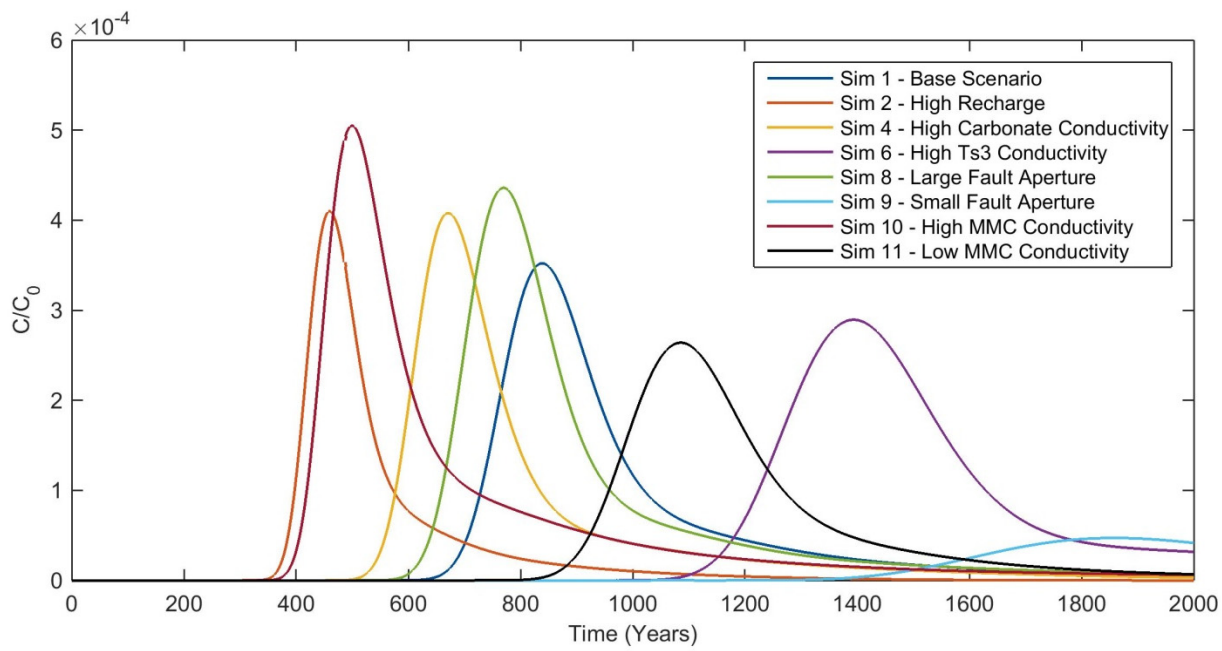

Figure B-12. Breakthrough curves generated by the cross-sectional regional model assuming instant migration from the Elko Formation to the carbonate unit (i.e., hydraulic fractures extend into carbonate unit) for Simulations 1, 2, 4, 6, 8, 9, 10, and 11.

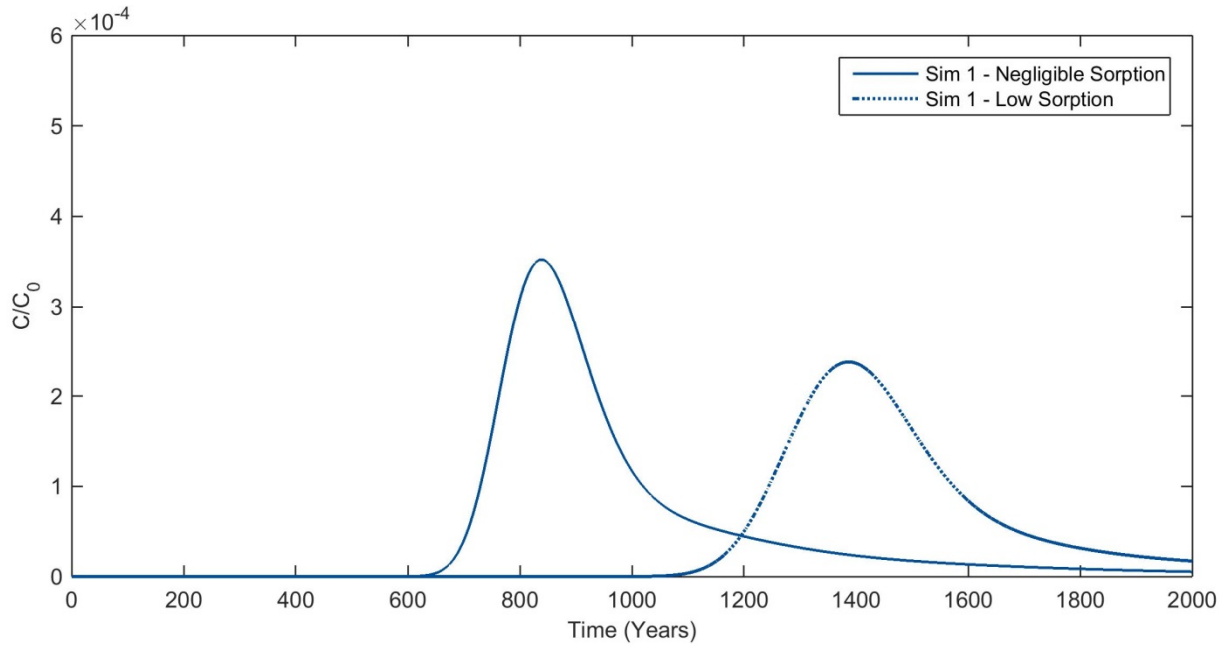

Figure B-13. Breakthrough curves generated by the cross-sectional regional model assuming instant migration from the Elko Formation to the carbonate unit for Simulation 1 using negligible and low sorption parameters.

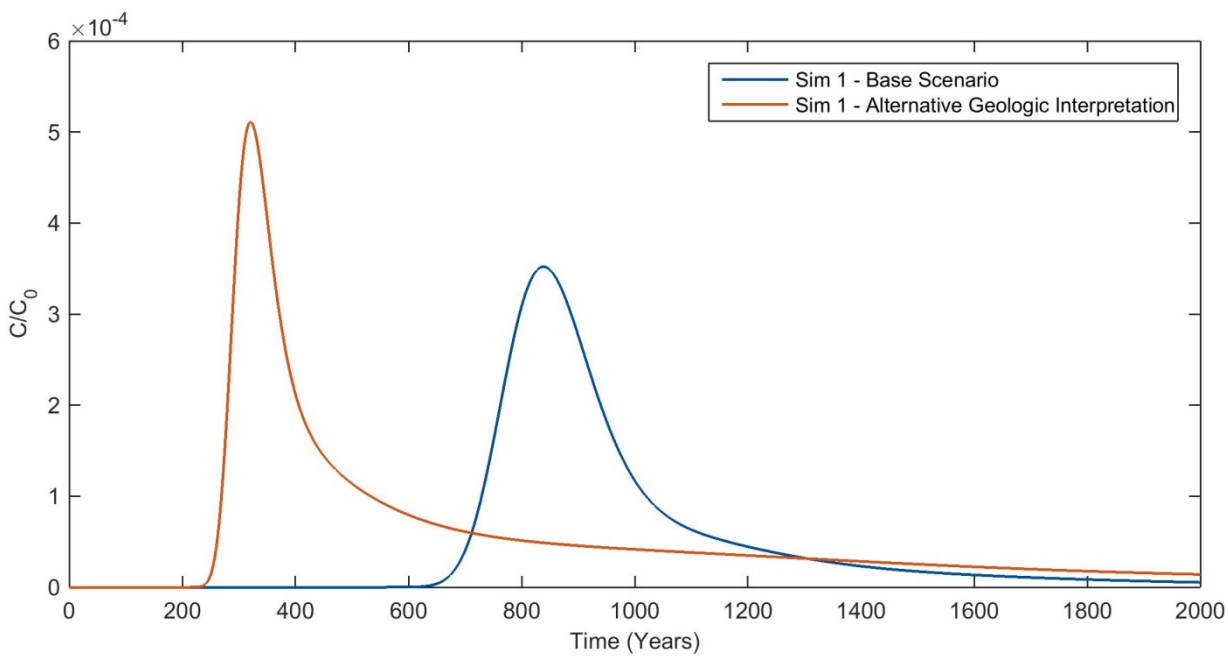

Figure B-14. Breakthrough curves generated by the cross-sectional regional model assuming instant migration from the Elko Formation to the carbonate unit (i.e., hydraulic fractures extend into carbonate unit) for Simulation 1 and the alternative geologic interpretation.

B.3 METHANE DEGASSING MODEL

B.3.1 Model Design

This scenario explores the potential for vertical transport of near-borehole gaseous methane along a density gradient. This process was simulated as a fully saturated 2-D vertical system using TOUGH2 (Pruess, 2012), a finite difference numerical simulator for nonisothermal flows of multiphase fluids. The TOUGH2 models the balance of mass and energy (i.e., heat) through the solution of equations that can be generally written as:

$$\frac{d}{dt}\int_{V_n} M^{\kappa} dV_n = \int_{\Gamma_n} \mathbf{F}^{\kappa} \bullet \mathbf{n} d\Gamma_n + \int_{V_n} q^{\kappa}\, dV_n \tag{B-8}$$

where V_n is an arbitrary subdomain of the flow system under study bounded by a closed surface Γ_n and n is a normal vector on that surface pointing into the subdomain. M is the mass or energy per volume where κ = 1,…, NK, labeling the mass components such that NK is the total number of mass components and κ = NK+1 designates the heat component. **F** is the sum of mass or heat flux over phases, defined by equation 6.10 in this document, and q is a source and sink term.

For multiphase flow, TOUGH2 governs the flux of an individual phase by the equation:

$$\mathbf{F}_{\beta} = \rho_{\beta}\mathbf{u}_{\beta} = -k\frac{k_{r\beta}\rho_{\beta}}{\mu_{\beta}}\left(\nabla P_{\beta} - \rho_{\beta}\mathbf{g}\right) \tag{B-9}$$

where $\boldsymbol{u}_{\beta}$ is the Darcy velocity for a phase β, k is absolute permeability, $k_{r\beta}$ is the relative permeability for that phase, ρ_{β} is the phase density, μ_{β} is the phase viscosity, $\boldsymbol{g}$ is the acceleration due to gravity, and P_{β} is the fluid pressure that phase. For the purposes of this model, the vertical migration of gaseous methane is the primary flux of interest, and therefore the model domain was designed as a column under hydrostatic conditions with no source or sink terms.

For multiphase flow, liquid and gas relative permeabilities were determined by the van Genuchten-Mualem model (Mualem, 1976; van Genuchten, 1980) such that:

$$k_{rl} = \begin{cases} \sqrt{S^*}\left\{1 - \left(1 - [S^*]^{1/\lambda}\right)^{\lambda}\right\}^2 \; if\; S_l < S_{ls} \\ 1 \;\; if\; S_l \geq S_{ls} \end{cases} \tag{B-10}$$

and

$$k_{rg} = \begin{cases} 1 - k_{rl}\; if\; S_{gr} = 0 \\ \left(1 - \hat{S}\right)^2\left(1 - \hat{S}^2\right)\; if\; S_{gr} > 0 \end{cases} \tag{B-11}$$

are subject to the restriction $0 \leq k_{rl}, k_{rg} \leq 1$, and where S^* and $\hat{S}$ are defined as:

$$S^* = (S_l - S_{lr})/(S_{ls} - S_{lr}) \tag{B-12}$$

$$\hat{S} = (S_l - S_{lr})/\left(1 - S_{lr} - S_{gr}\right) \tag{B-13}$$

Capillary pressure was determined by the corresponding van Genuchten function (van Genuchten, 1980), stated as:

$$P_{cap} = -P_0\left([S^*]^{-1/\lambda} - 1\right)^{1-\lambda} \quad \text{(B-14)}$$

subject to the restriction $-P_{max} \leq P_{cap} \leq 0$, and for which S^* is defined in Equation 6-13. For both the relative permeability and capillary pressure functions, S_l is liquid saturation, S_{lr} is residual liquid saturation, S_{ls} is the liquid saturation when k_{rl} is 1, S_{gr} is residual gas saturation, and λ is a fitting parameter defined by van Genuchten. P_0 is defined within TOUGH2 such that:

$$1/P_0 = \alpha/\rho_w g \quad \text{(B-15)}$$

where α is a water retention parameter proportional to hydraulic conductivity. For both the relative permeability and capillary pressure functions, values for S_{lr}, λ, and α were taken from values presented for a sand in Carsel and Parrish (1988). S_{gr} was set to 0.01, which was the lowest order of magnitude that resulted in a stable simulation.

Models in TOUGH2 were run using the EWASG (**WA**ter-**S**alt-**G**as) equation of state, which was designed for modeling geothermal reservoirs with saline fluids and noncondensable gas and was selected in this case because it allows for modeling of methane gas in particular. The primary variables incorporated by the EWASG module are pressure, salt mass fraction, noncondensable gas mass fraction or gas phase saturation, and temperature. For the purposes of this scenario, salinity was neglected and the salt mass fraction was considered to be zero for all models.

The model mesh created for this scenario is a simple 200 x 2530 meter grid composed of 10 x 10 meter grid cells over a 10 meter thickness, representative of a 200 meter wide column extending from the surface to the base of the Elko Formation at the M2C-M2-21B well. This mesh was subdivided based on the formation thicknesses found in the M2C-M2-21B well and appropriate porosities and hydraulic and thermal conductivities were assigned to each, as discussed in Section 6.2.2.1 (Table B-7). Grid cells representing the Elko formation were further subdivided to create a central section representative of the hydraulically fractured shale and cells on either side represent the unfractured shale (Figure B-15a). A second model mesh was created using the same design, but with the addition of a transmissive "fault zone," represented by a vertical column of cells with increased hydraulic conductivity extending from the contact between the Elko and Indian Well Formations to the upper boundary layer (Figure B-15b).

Table B-7. Parameters for methane degassing simulations.

Formation	Porosity	Hydraulic conductivity (m^2)	Thermal conductivity (W/m °C)
Tertiary sediments	0.35	1.18e-12	2.0
Indian Well Formation	0.20	1.18e-13	1.7
Elko Formation	0.20	5.90e-16	2.9
Elko Formation (fractured)	0.20	5.90e-13	2.9
Fault zone	0.20	5.00e-12	2.1

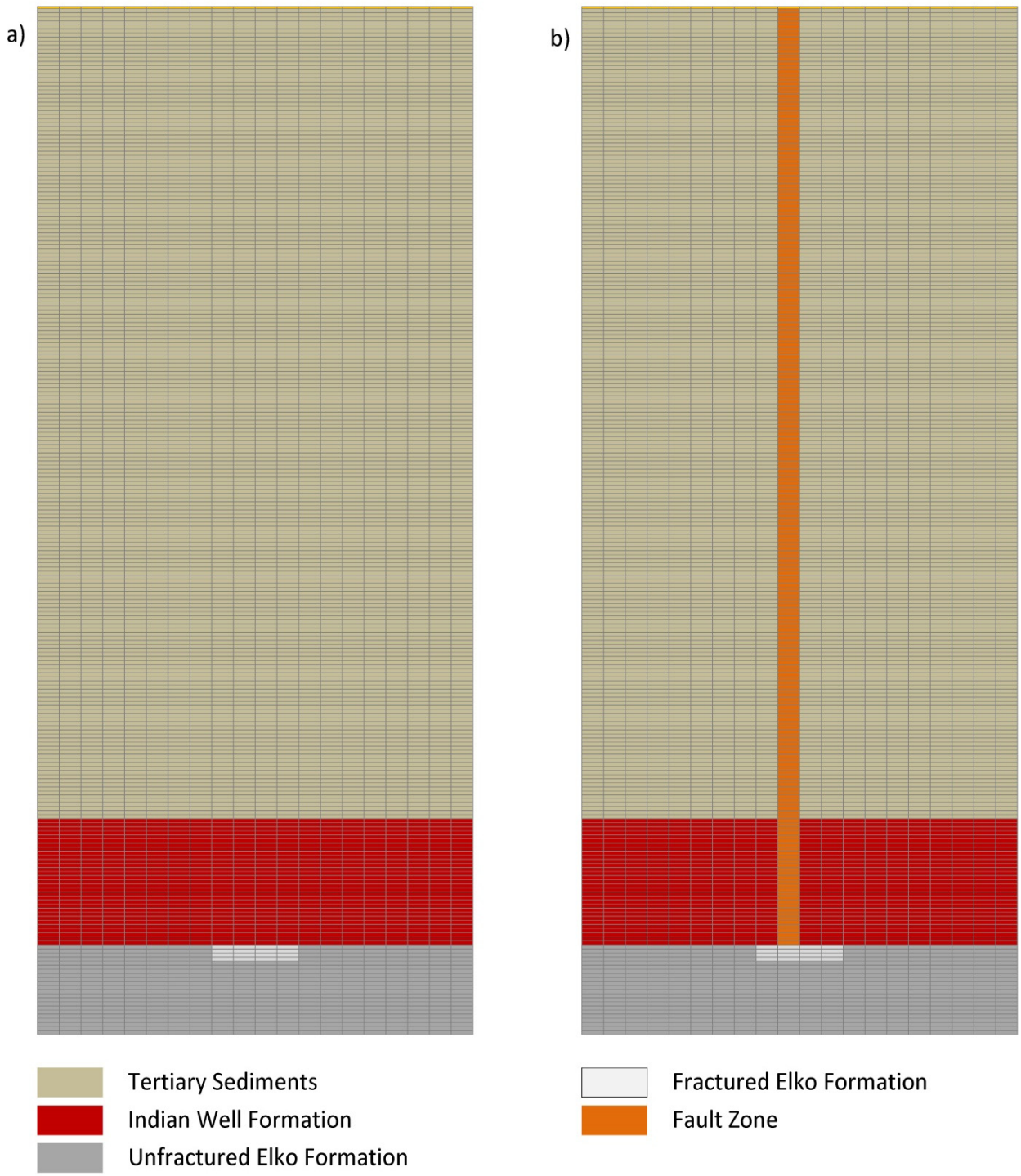

Figure B-15. Model domains for methane degassing scenario in TOUGH2, 0.25 vertical exaggeration.

Initial pressure and temperature conditions for the model were established by creating an upper boundary layer with a very small thickness but a very large volume and high specific heat, such that the temperature and pressure conditions prescribed for the cells in this layer would remain constant without being included in the balance equations for the model. The pressure within this layer was then set to atmospheric pressure (101.3 kPa) at a temperature of 15 °C and the model was run to steady state, creating a hydrostatic pressure gradient through the column. Using this pressure distribution as the initial conditions for a second run to steady state conditions, the temperature at the lower boundary was then set to 80 °C and the model was set to perform a semi-analytical heat exchange, allowing heat to propagate to the surface and resulting in temperatures approximating a typical geothermal gradient. These models were run to steady state under fully saturated conditions with no salinity and a ubiquitous mass fraction of dissolved methane of 1.0e-6.

The combination of these two model runs produced the pressure and temperature profile used in the initial conditions for the methane transport simulations. For both the fault and no-fault simulations, a 0.6 methane gas saturation was placed in all cells representing the fractured Elko Formation. Gas was then allowed to migrate and redissolve as dictated by pressure and temperature over a model period of 70 years.

B.3.2 Methane Degassing Results

In both simulations, methane gas migrates vertically along a density gradient and laterally under capillary pressures. As gas phase methane migrates to cells with low concentrations of dissolved methane, it enters the liquid phase where it is effectively immobilized by the no-flow boundary conditions imposed on the model domains. As the gas migrates, a small amount is also bound to cells by the residual gas saturation imposed on the model.

For the no-fault base simulation, methane gas migrates a total vertical distance of 760 meters in 70 years, with the majority of this distance (710 meters) reached within 30 years (Figures B-16 through B-19). Over the 70 year simulation period, 62.4 percent of the gas that was initially present dissolved and was immobilized, and although a very small amount of migration continues to occur, the remainder is effectively trapped.

For the fault zone simulation, methane gas migrates a total vertical distance of 1990 meters over a period of 70 years, with the majority of this distance (1900 meters) reached within 30 years (Figures B-20 through B-22). Over the 70 year simulation period, 66.9 percent of the gas initially present dissolved and was immobilized. Again, although migration has not completely ceased at the termination of the simulation, the remainder of the gas phase methane is effectively trapped and any remaining migration occurs at continuously declining velocities (Figure B-23).

For both simulations, the spatial distribution of cells containing dissolved methane follows the path of gaseous methane migration and concentrations decrease with depth according to the solubility of methane, which is determined by the pressure and temperature at that depth (Figure B-24). Although the presence of a fault drastically increases the distance of migration, neither simulation indicates migration of gaseous methane to the 600 foot (~180 meter) depth considered to be the base of the shallow water aquifer for these scenarios.

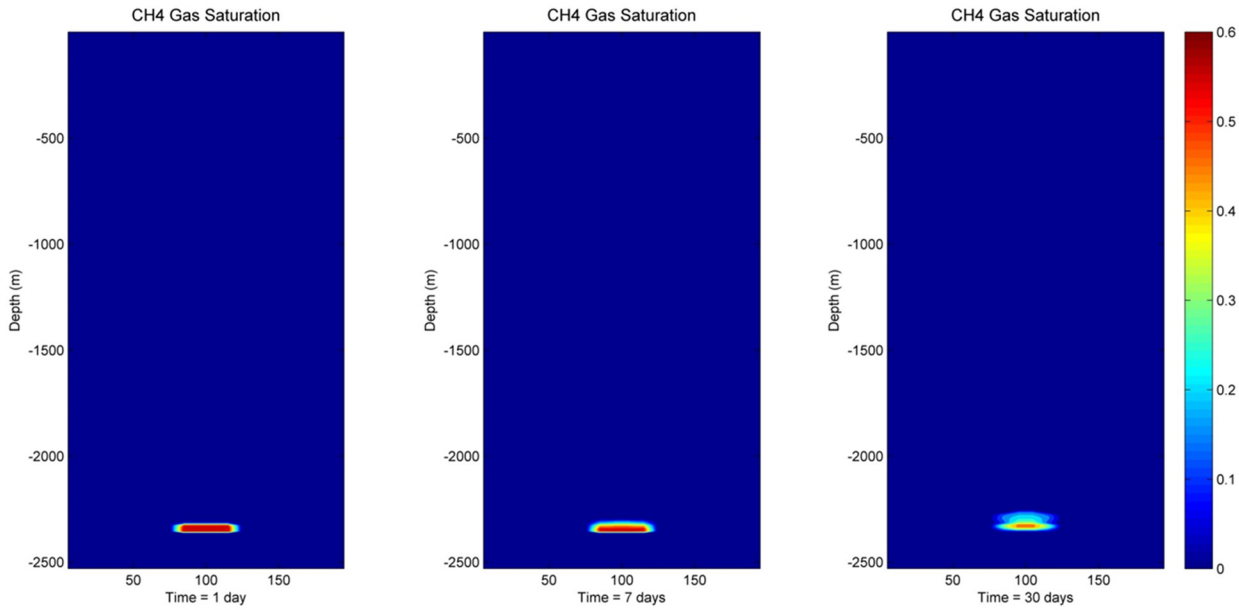

Figure B-16. No-fault simulation results, CH_4 gas saturation at 1 day, 7 days, and 30 days from beginning of simulation.

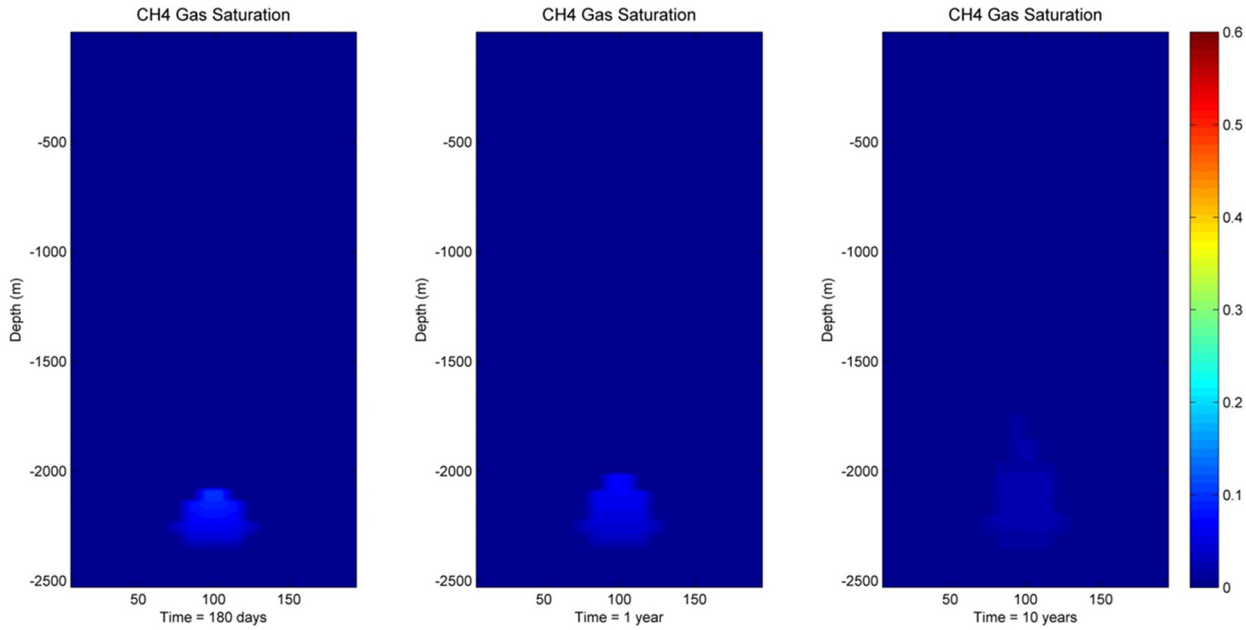

Figure B-17. No-fault simulation results, CH_4 gas saturation at 180 days, 1 year, and 10 years from beginning of simulation.

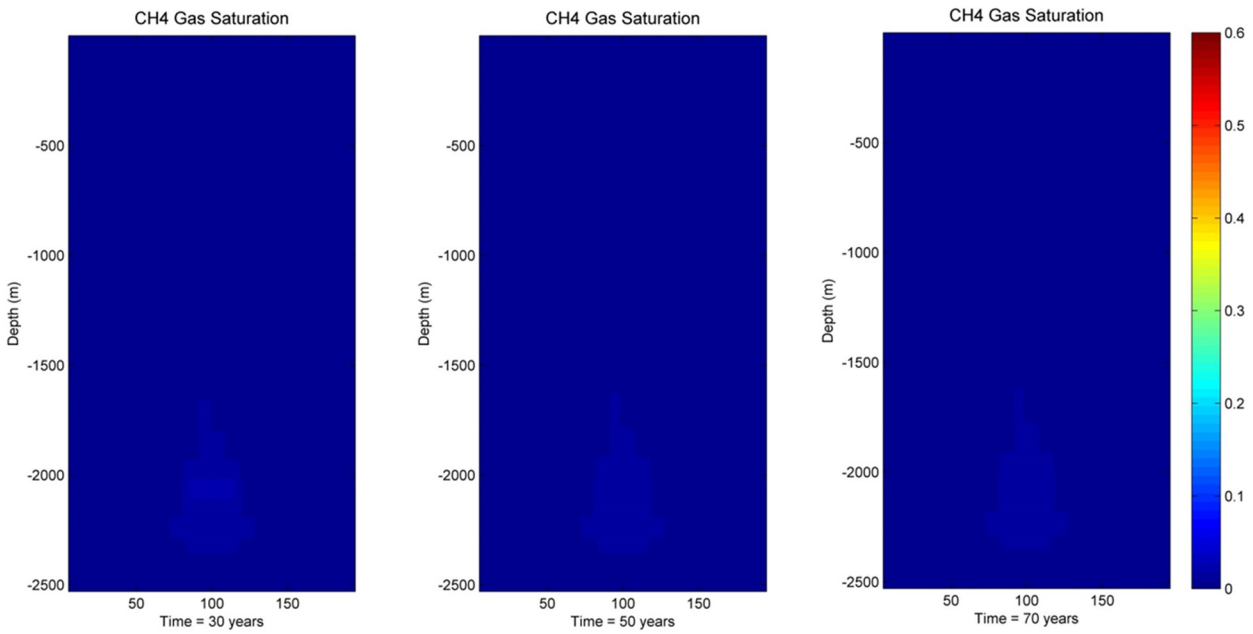

Figure B-18. No-fault simulation results, CH_4 gas saturation at 30 years, 50 years, and 70 years from beginning of simulation.

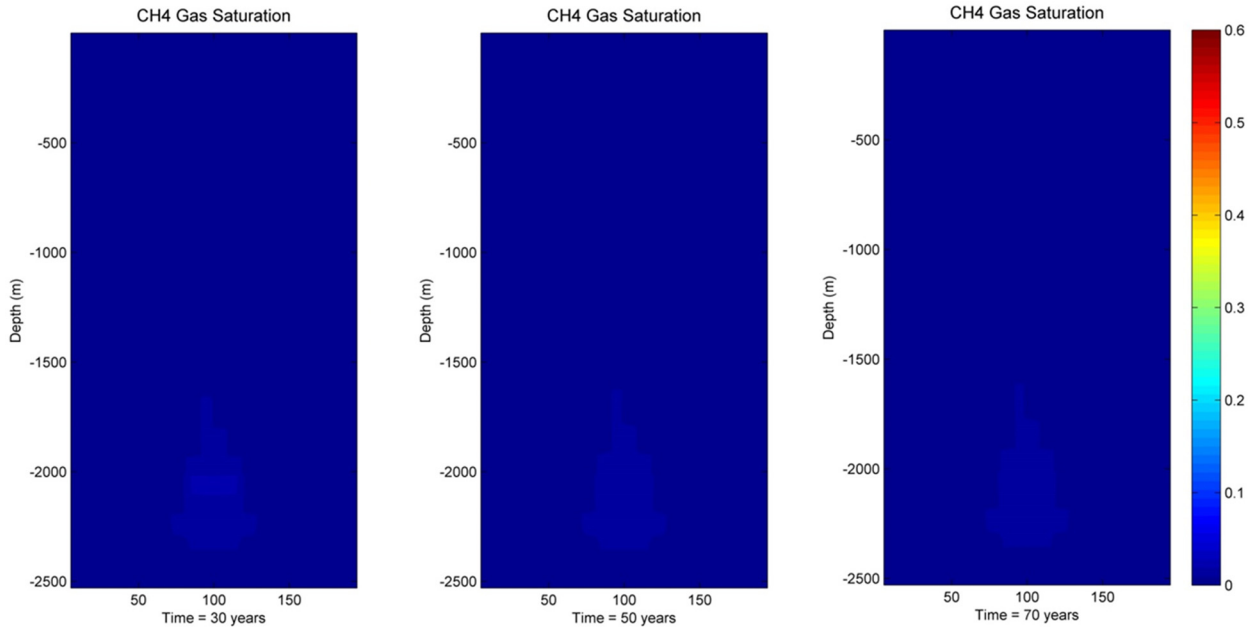

Figure B-19. No fault simulation results, CH_4 gas saturation at 30 years, 50 years, and 70 years from beginning of simulation.

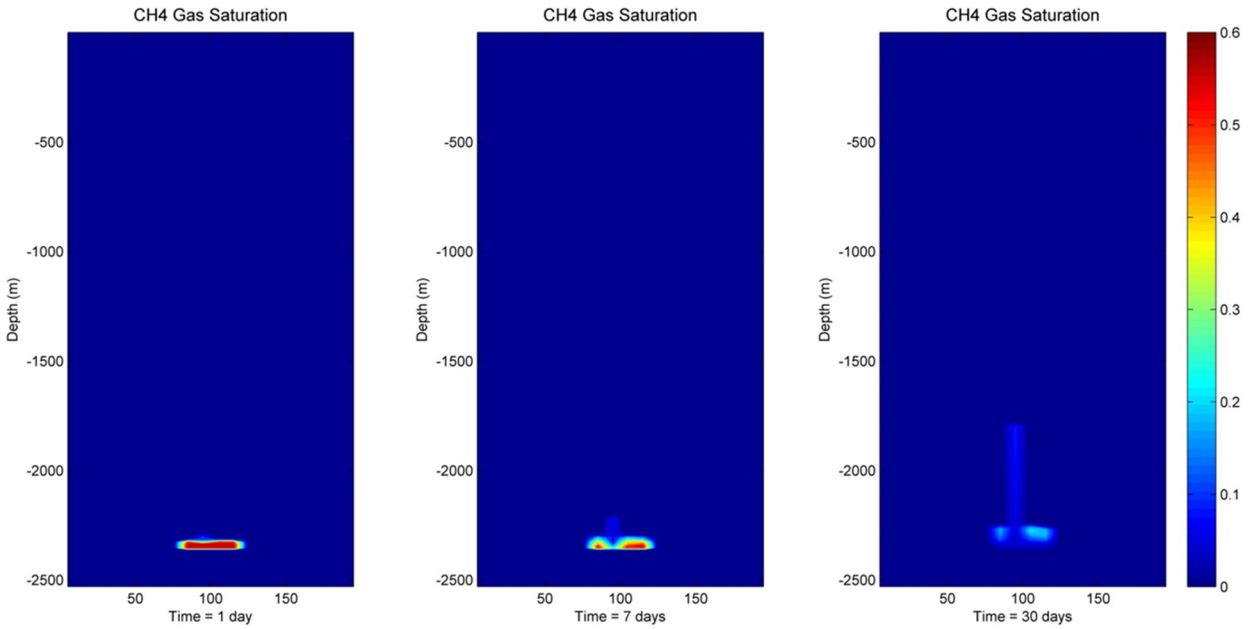

Figure B-20. Fault zone simulation results, CH_4 gas saturation at 1 day, 7 days, and 30 days from beginning of simulation.

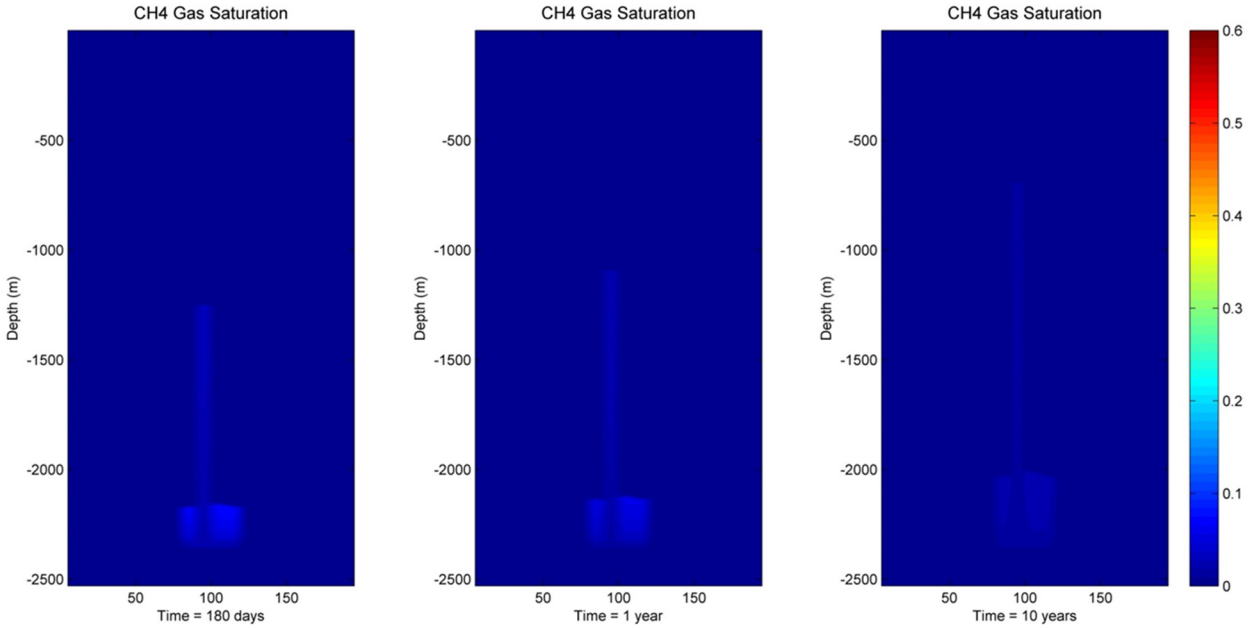

Figure B-21. Fault zone simulation results, CH_4 gas saturation at 180 days, 1 year, and 10 years from beginning of simulation.

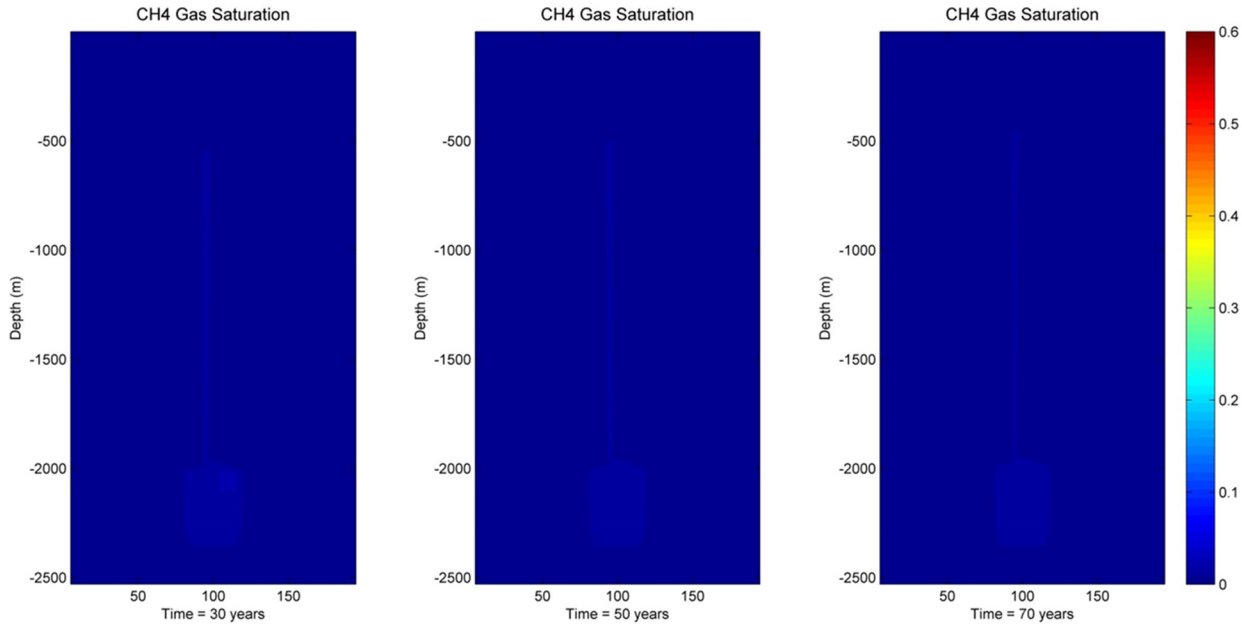

Figure B-22. Fault zone simulation results, CH_4 gas saturation at 30 years, 50 years, and 70 years from beginning of simulation.

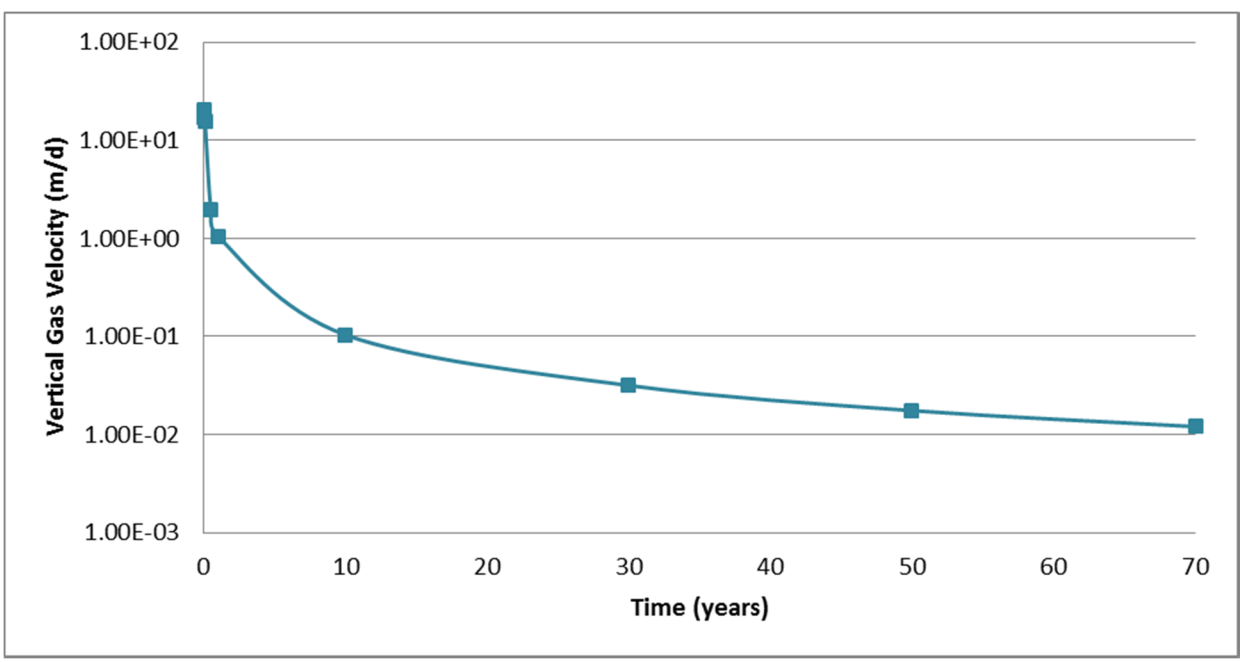

Figure B-23. Vertical gas velocities over time for fault zone scenario.

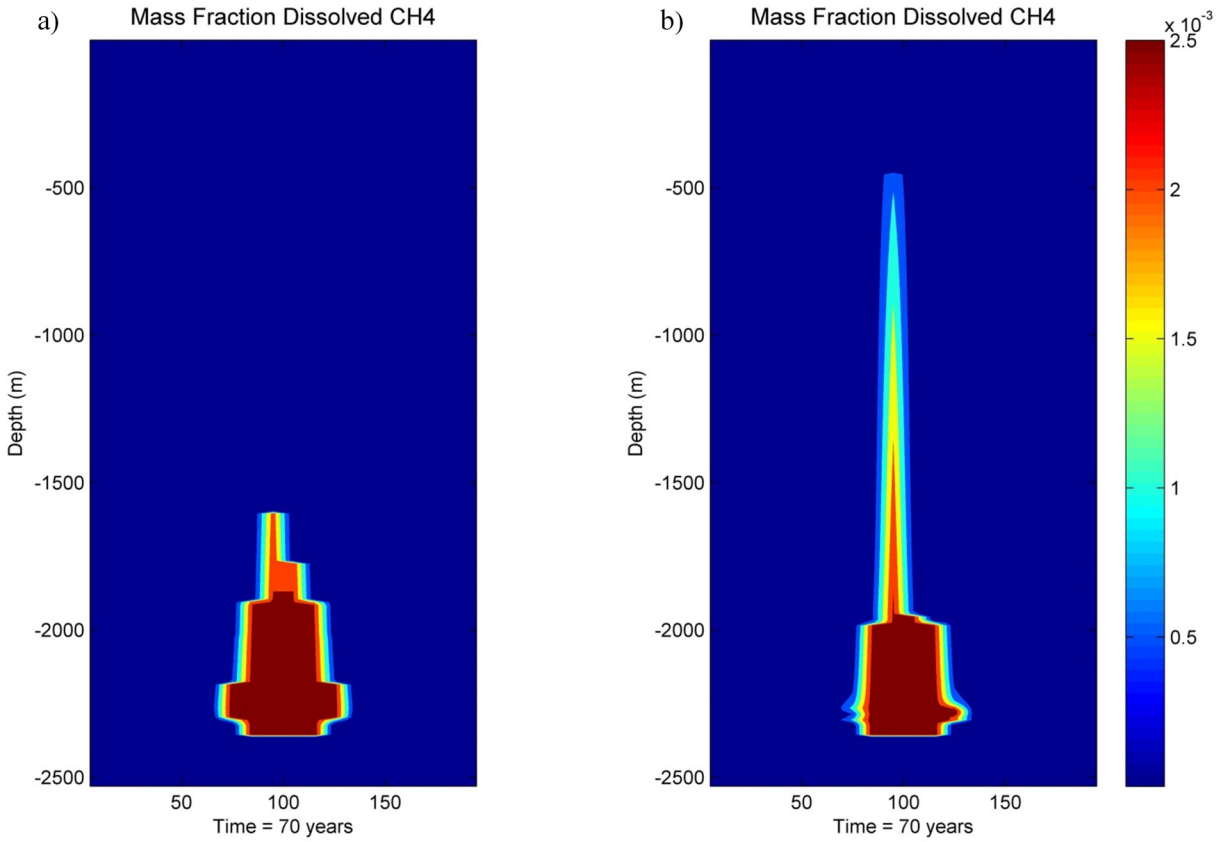

Figure B-24. Mass fraction of dissolved CH_4 at 70 years from beginning of simulation for a) no-fault simulation and b) Fault zone simulation.

B.4 References

Bear, J., 1972. Dynamics of Fluids in Porous Media. New York, NY: Elsevier Publishing Co.

Beardsmore, G.R., and J.P. Cull, 2002. Crustal heat flow: a guide to measurement and modeling. Cambridge University Press.

Buscheck, T. A., N.D. Rosenberg, J. Gansemer, and Y. Sun, 2002. Thermohydrologic behavior at an underground nuclear waste repository at Yucca Mountain, NV. *Water Resources Research*, 38 (3), 10, pp. 1-17.

Coolbaugh, M., R. Zehner, C. Creemer, D. Blackwell, G. Oppliger, D. Sawatzky, G. Blewitt, A. Pancha, M. Richards, L. Shevenell, G. Raines, G. Johnson, T. Minor, and T. Boyd, 2005. "Geothermal potential of the Great Basin region, Western United States." Nevada Bureau of Mining and Geology, Map 151.

DHI, 2012. DHI-WASY Software – FEFLOW 6.1, Finite Element Subsurface Flow and Transport Simulation System - User Manual, Berlin, Germany, p. 116.

Fetter, C.W., 2000. Applied Hydrogeology – 4th Edition, Prentice Hall, New Jersey.

Flewelling, S.A., M.P. Tymchak, and N. Warpinski, 2013. Hydraulic Fracture Height Limits and Fault Interactions in Tight Oil and Gas Formations. *Geophysical Research Letters*, 40(14), pp. 3602-3606, doi:10.1002/grl.50707.

Hao Y., Y. Sun, and J.J. Nitao, 2012. Overview of NUFT: A Versatile Numerical Model for Simulating Flow and Reactive Transport in Porous Media, in Groundwater Reactive Transport Models, F. Zhang, G.T. Yeh, and J.C. Parker eds. Oak Park, IL: Bentham Science Publishers.

LaBolle, E.M., and G.E. Fogg, 2001. Role of molecular diffusion in contaminant migration and recovery in an alluvial aquifer system. *Transport in Porous Media*, 42, pp.155-179.

LaBolle, E.M., G.E. Fogg, and A.F.B. Tompson, 1996. Random-walk simulation of transport in heterogeneous porous media: Local mass conservation problem and implementation methods. *Water Resources Research*, 32(3), pp. 583-593.

LaBolle, E.M., J. Quastel, G.E. Fogg, and J. Gravner, 2000. Diffusion processes in composite porous media and their numerical integration by random walks: Generalized stochastic differential equations with discontinuous coefficients. *Water Resources Research*, 36(3), pp. 651-662.

LaBolle, E.M., 2006. RWHet: Random walk particle model for simulating transport in heterogeneous media. Version 3.2 User's Manual and Program Documentation.

Liu, H.H., G.S. Bodvarsson, and L. Pan, 2000. Determination of particle transfer in random walk particle methods for fractured porous media. *Water Resources Research*, 36(3), pp.707-713.

Mualem, Y., 1976. A new model for predicting the hydraulic conductivity of unsaturated porous media. *Water Resources Research*, 12, pp. 513-522.

Newmark, R.L., W.D. Daily, K.R. Kyle and A.L. Ramirez, 1997. Monitoring DNAPL Pumping Using Integrated Geophysical Techniques, DOE report, Lawrence Livermore National Laboratory.

Nitao, J.J. 2000a. Reference Manual for the NUFT Flow and Transport Code, Version 3.0, UCRL-MA-130651-REV-1. Livermore, CA: Lawrence Livermore National Laboratory.

Nitao, J.J. 2000b. User's Manual for the USNT Module of the NUFT Code, Version 3.0, UCRL-MA-130643-REV-2. Livermore, CA: Lawrence Livermore National Laboratory.

Nitao, J.J., 2004. User's manual for the US1P module of the NUFT flow and transport code, Lawrence Livermore National Laboratory.

Pan, L. and G.S. Bodvarsson, 2002. Modeling transport in fractured porous media with the random-walk particle method: The transient activity range and the particle transfer probability. *Water Resources Research*, 38, p. 6, doi:10.1029/2001WR000901.

Pruess, K., C. Oldenburg, and G. Moridis, 2012. TOUGH2 User's Guide, Version 2.1, Report LBNL-43134, Lawrence Berkeley National Laboratory, Berkeley, CA.

Reeves, D.M., R. Parashar, K. Pohlmann, C. Russell, and J. Chapman, 2014. Development and calibration of dual-permeability flow models with discontinuous fault networks. *Vadose Zone Journal*, doi:10.2136/vzj2013.10.0183.

Romero, D.J., P.P. Valko, and M.J. Economides, 2002. The Optimization of the Productivity Index and the Fracture Geometry of a Stimulated Well with Fracture Face and Choke Skins. *Society of*

*Petroleum Engineers Inc. International Symposium and Exhibition on Formation Damage Contro*l, Lafayette, Louisiana, February, 20-21.

Tompson, A.F.B., G.B. Hudson, D.K. Smith, and J.R. Hunt, 2006. Analysis of Radionuclide Migration through a 200-m Vadose Zone following a 16-Year Infiltration Event. *Advances in Water Resources*, 29(2), pp. 281-292.

Van Genuchten, M.T., 1980. A closed form equation for predicting the hydraulic conductivity of unsatured soils. *Soil Society Science American Journal*, 44, pp. 892-898.

Zhang, Y., E.M. LaBolle, D.M. Reeves, and C. Russell, 2012. Development of RWHet to Simulate Contaminant Transport in Fractured Porous Media, DOE/NV/0000939-01, DRI Report No. 45244.

Zheng, C., and G.D. Bennett, 2002. Applied contaminant transport modeling (Vol. 2). New York: Wiley-Interscience.

THIS PAGE INTENTIONALLY LEFT BLANK

APPENDIX C: SUMMARY OF HYDRAULIC FRACTURING FLUID CHEMICALS AND PROPERTIES USED FOR HUNTINGTON K1L-1V, M10C-M10-11B, AND M2C-M2-21B

Table C-1. Summary of fracking fluid chemicals used for Humboldt M2C-M2-21B from FracFocus.org. RBCs, MCLs, and RSLs are from MSDSs and Jackson (2013). * Total water volume sources may include fresh water, produced water, and/or recycled water. ** Information is based on the maximum potential for concentration and thus the total may be over 100%.

Federal/Tribal Well:	NO
True Vertical Depth:	11,637
Total Base Water Volume (gal):	250,057
Total Base Non Water Volume:	0

Trade Name	Supplier	Purpose	Ingredients	Chemical Abstract Service Number (CAS #)	Maximum Ingredient Concentration in Additive (% by mass)**	Maximum Ingredient Concentration in HF Fluid (% by mass)**	Specific Gravity	Maximum Ingredient Concentration in HF Fluid (% by volume)**	log K_{oc}	log K_{ow}	Maximum Contaminant Level (MCL) / Risk Based Concentration (RBC) / Risk Screening Level (RSL) (mg/L)	Source of log K_{oc}
2% KCL Water	Operator	Base Fluid										
			2% KCL Water	7447-40-7	100.0	88.56148	1.013	87.42496				
PRC SAND PREMIUM	Halliburton	Proppant										
			Crystalline silica, quartz	14808-60-7	100.0	8.74261	2.650	3.29910				
			Phenol / formaldehyde resin	9003-35-4	5.0	0.43713	1.180	0.37045				
			Hexamethylenetetramine	100-97-0	2.0	0.17485	1.331	0.13137				
SAND - PREMIUM WHITE	Halliburton	Proppant										
			Crystalline silica, quartz	14808-60-7	100.0	0.65036	2.650	0.24542				
HYDROCHLORIC ACID 10-30%	Halliburton	Solvent										
			Hydrochloric acid	7647-01-0	30.0	0.33841	1.149	0.29445				
WG-18 GELLING AGENT	Halliburton	Gelling Agent										
			Guar gum derivative	Confidential	100.0	0.26270						

Table C-1. Summary of fracking fluid chemicals used for Humboldt M2C-M2-21B from FracFocus.org. RBCs, MCLs, and RSLs are from MSDSs and Jackson (2013). * Total water volume sources may include fresh water, produced water, and/or recycled water. ** Information is based on the maximum potential for concentration and thus the total may be over 100% (continued).

Federal/Tribal Well:	NO
True Vertical Depth:	11,637
Total Base Water Volume (gal):	250,057
Total Base Non Water Volume:	0

Trade Name	Supplier	Purpose	Ingredients	CAS #	Maximum Ingredient Concentration in Additive (% by mass)**	Maximum Ingredient Concentration in HF Fluid (% by mass)**	Specific Gravity	Maximum Ingredient Concentration in HF Fluid (% by volume)**	log K_{oc}	log K_{ow}	MCL / RBC / RSL (mg/L)	Source of log K_{oc}
LoSurf-300D	Halliburton	Non-ionic Surfactant										
			Ethanol	64-17-5	60.0	0.04644	0.787	0.05901	-0.14	-0.31		UNEP Publications
			Heavy aromatic petroleum naphtha	64742-94-5	30.0	0.02322	0.910	0.02552	2.96	3.30		EPA
			Naphthalene	91-20-3	5.0	0.00387	0.963	0.00402	3.30	3.36	200 (MCL)	EPA
			Poly(oxy-1,2-ethanediyl), alpha-(4-nonylphenyl)-omega-hydroxy-, branched	127087-87-0	5.0	0.00387	1.057	0.00366	0.8			Azichem www.azichem.com
VICON NF BREAKER	Halliburton	Breaker										
			Sodium chloride	7647-14-5	30.0	0.05125	2.170	0.02362				
			Chlorous acid, sodium salt	7758-19-2	10.0	0.01708	2.468	0.00692			1 (MCL)	
GEL-STA L STABILIZER	Halliburton	Stabilizer										
			Sodium thiosulfate	7772-98-7	60.0	0.05581	0.054	1.03778			500 (RBC)	
CL-37 CROSSLINKER	Halliburton	Crosslinker										
			Triethanolamine zirconate	101033-44-7	100.0	0.02368	0.018	1.31046				

Table C-1. Summary of fracking fluid chemicals used for Humboldt M2C-M2-21B from FracFocus.org. RBCs, MCLs, and RSLs are from MSDSs and Jackson (2013). * Total water volume sources may include fresh water, produced water, and/or recycled water. ** Information is based on the maximum potential for concentration and thus the total may be over 100% (continued).

Federal/Tribal Well:	NO
True Vertical Depth:	11,637
Total Base Water Volume (gal):	250,057
Total Base Non Water Volume:	0

Trade Name	Supplier	Purpose	Ingredients	CAS #	Maximum Ingredient Concentration in Additive (% by mass)**	Maximum Ingredient Concentration in HF Fluid (% by mass)**	Specific Gravity	Maximum Ingredient Concentration in HF Fluid (% by volume)**	log K_{oc}	log K_{ow}	MCL / RBC / RSL (mg/L)	Source of log K_{oc}
			Glycerin	56-81-5	30.0	0.0071	0.006	1.15707				
			Propanol	71-23-8	30.0	0.0071	0.010	0.72008				
FE-1A ACIDIZING COMPOSITION	Halliburton	Additive										
			Acetic anhydride	108-24-7	100.0	0.02259	1.080	0.02092				
			Acetic acid	64-19-7	60.0	0.01355	1.052	0.01288	0.00	(-0.15)-(-0.53)		
MUSOL A SOLVENT	Halliburton	Solvent										
			Ethylene glycol monobutyl ether	111-76-2	100.0	0.02379	0.900	0.02643			1.6 (RSL)	
			Oxylated alcohol	Confidential	30.0	0.00714						
CL-31 CROSSLINKER	Halliburton	Crosslinker										
			Potassium metaborate	13709-94-9	60.0	0.02063	2.300	0.00897				
			Potassium hydroxide	1310-58-3	5.0	0.00172	2.120	0.00081				
MO-67	Halliburton	pH Control Additive										
			Sodium hydroxide	1310-73-2	30.0	0.02182	2.130	0.01024				
FE-2A	Halliburton	Additive										
			Citric acid	77-92-9	60.0	0.01562	1.665	0.00938	-1.20	-1.64		

Table C-1. Summary of fracking fluid chemicals used for Humboldt M2C-M2-21B from FracFocus.org. RBCs, MCLs, and RSLs are from MSDSs and Jackson (2013). * Total water volume sources may include fresh water, produced water, and/or recycled water. ** Information is based on the maximum potential for concentration and thus the total may be over 100% (continued).

Federal/Tribal Well:	NO
True Vertical Depth:	11,637
Total Base Water Volume (gal):	250,057
Total Base Non Water Volume:	0

Trade Name	Supplier	Purpose	Ingredients	CAS #	Maximum Ingredient Concentration in Additive (% by mass)**	Maximum Ingredient Concentration in HF Fluid (% by mass)**	Specific Gravity	Maximum Ingredient Concentration in HF Fluid (% by volume)**	log K_{oc}	log K_{ow}	MCL / RBC / RSL (mg/L)	Source of log K_{oc}
BA-20 BUFFERING AGENT	Halliburton	Buffer										
			Ammonium acetate	631-61-8	100.0	0.01157	1.170	0.00989				
			Acetic acid	64-19-7	30.0	0.00347	1.052	0.00330	0.00	(-0.15)-(-0.53)		
BE-7™	Halliburton	Biocide										
			Sodium hypochlorite	7681-52-9	30.0	0.01361	1.110	0.01226				
			Sodium hydroxide	1310-73-2	2.0	0.00091	2.130	0.00043				
HAI-404M™	Halliburton	Corrosion Inhibitor										
			Methanol	67-56-1	30.0	0.00311	0.792	0.00393	0.44	(-0.81)-(-0.66)	7.8 (RSL)	
			Isopropanol	67-63-0	30.0	0.00311	0.786	0.00396	0.03			UNEP Publications
			Aldehyde	Confidential	30.0	0.00311						
			1-(Benzyl)quinolinium chloride	15619-48-4	10.0	0.00104	1.300	0.00080				
			Quaternary ammonium salt	Confidential	10.0	0.00104	1.527					
FR-66	Halliburton	Friction Reducer										
			Hydrotreated light petroleum distillate	64742-47-8	30.0	0.00868	0.800	0.01085				

Table C-1. Summary of fracking fluid chemicals used for Humboldt M2C-M2-21B from FracFocus.org. RBCs, MCLs, and RSLs are from MSDSs and Jackson (2013). * Total water volume sources may include fresh water, produced water, and/or recycled water. ** Information is based on the maximum potential for concentration and thus the total may be over 100% (continued).

Federal/Tribal Well:	NO
True Vertical Depth:	11,637
Total Base Water Volume (gal):	250,057
Total Base Non Water Volume:	0

Trade Name	Supplier	Purpose	Ingredients	CAS #	Maximum Ingredient Concentration in Additive (% by mass)**	Maximum Ingredient Concentration in HF Fluid (% by mass)**	Specific Gravity	Maximum Ingredient Concentration in HF Fluid (% by volume)**	log K_{oc}	log K_{ow}	MCL / RBC / RSL (mg/L)	Source of log K_{oc}
AS-10 ANTISLUDGING AGENT	Halliburton	Anti-sludging Agent										
			Dodecylbenzene sulfonic acid	27176-87-0	60.0	0.00341	0.992	0.00344				
BE-6 MICROBIOCIDE	Halliburton	Biocide										
			2-Bromo-2-nitro-1,3-propanediol	52-51-7	100.0	0.00202	1.100	0.00184			1.5 (RSL)	
CAT-3 ACTIVATOR	Halliburton	Activator										
			EDTA/Copper chelate	Confidential	30.0	0.00142						
CAT-4	Halliburton	Activator										
			Diethylenetriamine	111-40-0	60.0	0.00101	0.995	0.00102				
Ingredients shown above are subject to 29 CFR 1910.1200(i) and appear on Material Safety Data Sheets (MSDS). Ingredients shown below are Non-MSDS.												
		Other Ingredient(s)										
			Water	7732-18-5		1.57645	1.000	1.57645				
		Other Ingredient(s)										
			Oxyalkylated phenolic resin	Confidential		0.02322						
		Other Ingredient(s)										
			Sodium bicarbonate	144-55-8		0.01314	2.200	0.00597				

Table C-1. Summary of fracking fluid chemicals used for Humboldt M2C-M2-21B from FracFocus.org. RBCs, MCLs, and RSLs are from MSDSs and Jackson (2013). * Total water volume sources may include fresh water, produced water, and/or recycled water. ** Information is based on the maximum potential for concentration and thus the total may be over 100% (continued).

Federal/Tribal Well:	NO
True Vertical Depth:	11,637
Total Base Water Volume (gal):	250,057
Total Base Non Water Volume:	0

Trade Name	Supplier	Purpose	Ingredients	CAS #	Maximum Ingredient Concentration in Additive (% by mass)**	Maximum Ingredient Concentration in HF Fluid (% by mass)**	Specific Gravity	Maximum Ingredient Concentration in HF Fluid (% by volume)**	log K_{oc}	log K_{ow}	MCL / RBC / RSL (mg/L)	Source of log K_{oc}
		Other Ingredient(s)										
			Polyacrylamide copolymer	Confidential		0.00868					0.0	
		Other Ingredient(s)										
			Oxyalkylated phenolic resin	Confidential		0.00774						
		Other Ingredient(s)										
			Sodium sulfate	7757-82-6		0.00465	0.003	1.65610			500 (RBC)	
		Other Ingredient(s)										
			Dipropylene glycol	25265-71-8		0.00341	1.023	0.00333		-0.46		
		Other Ingredient(s)										
			Naphthenic acid ethoxylate	68410-62-8		0.00311	0.004	0.81516			0.5 (RBC)	
		Other Ingredient(s)										
			Silica, amorphous - fumed	7631-86-9		0.00263	1.300	0.00202				
		Other Ingredient(s)										
			Alcohols, C12-16, ethoxylated	68551-12-2		0.00248	0.900	0.00276			5.625 (RBC)	
		Other Ingredient(s)										
			Sodium chloride	7647-14-5		0.00217	2.170	0.00100				
		Other Ingredient(s)										
			Alkyl sulfonate	Confidential		0.00171						
		Other Ingredient(s)										

Table C-1. Summary of fracking fluid chemicals used for Humboldt M2C-M2-21B from FracFocus.org. RBCs, MCLs, and RSLs are from MSDSs and Jackson (2013). * Total water volume sources may include fresh water, produced water, and/or recycled water. ** Information is based on the maximum potential for concentration and thus the total may be over 100% (continued).

Federal/Tribal Well:	NO
True Vertical Depth:	11,637
Total Base Water Volume (gal):	250,057
Total Base Non Water Volume:	0

Trade Name	Supplier	Purpose	Ingredients	CAS #	Maximum Ingredient Concentration in Additive (% by mass)**	Maximum Ingredient Concentration in HF Fluid (% by mass)**	Specific Gravity	Maximum Ingredient Concentration in HF Fluid (% by volume)**	log K_{oc}	log K_{ow}	MCL / RBC / RSL (mg/L)	Source of log K_{oc}
			Fatty acid tall oil amide	Confidential		0.00145						
		Other Ingredient(s)										
			Ammonium chloride	12125-02-9		0.00145	1.530	0.00095				
		Other Ingredient(s)										
			Fatty acids, tall oil	Confidential		0.00104						
		Other Ingredient(s)										
			Polyethoxylated fatty amine salt	61791-26-2		0.00104	0.947	0.00110				
		Other Ingredient(s)										
			Sodium sulfite	7757-83-7		0.00093	2.630	0.00035				
		Other Ingredient(s)										
			Ethoxylated amine	Confidential		0.00052						
		Other Ingredient(s)										
			Hydrochloric acid	7647-01-0		0.00050	1.149	0.00044				
		Other Ingredient(s)										
			Sorbitan, mono-9-octadecenoate, (Z)	1338-43-8		0.00029	0.992	0.00029				
		Other Ingredient(s)										
			Sorbitan monooleate polyoxyethylene derivative	9005-65-6		0.00029	1.064	0.00027				

Table C-1. Summary of fracking fluid chemicals used for Humboldt M2C-M2-21B from FracFocus.org. RBCs, MCLs, and RSLs are from MSDSs and Jackson (2013). * Total water volume sources may include fresh water, produced water, and/or recycled water. ** Information is based on the maximum potential for concentration and thus the total may be over 100% (continued).

Federal/Tribal Well:	NO
True Vertical Depth:	11,637
Total Base Water Volume (gal):	250,057
Total Base Non Water Volume:	0

Trade Name	Supplier	Purpose	Ingredients	CAS #	Maximum Ingredient Concentration in Additive (% by mass)**	Maximum Ingredient Concentration in HF Fluid (% by mass)**	Specific Gravity	Maximum Ingredient Concentration in HF Fluid (% by volume)**	log K_{oc}	log K_{ow}	MCL / RBC / RSL (mg/L)	Source of log K_{oc}
		Other Ingredient(s)										
			Ammonium phosphate	7722-76-1		0.00010	1.803	0.00006				
		Other Ingredient(s)										
			Sodium iodide	7681-82-5		0.00010	3.670	0.00003			.16 (RSL)	

* Total Water Volume sources may include fresh water, produced water, and/or recycled water

** Information is based on the maximum potential for concentration and thus the total may be over 100%

Note: For Field Development Products (products that begin with FDP), MSDS level only information has been provided.

Ingredient information for chemicals subject to 29 CFR 1910.1200(i) and Appendix D are obtained from suppliers Material Safety Data Sheets (MSDS)

Table C-2. Summary of fracking fluid chemicals used for Humboldt M10C-M10-11B from FracFocus.org. RBCs, MCLs, and RSLs are from MSDSs and Jackson (2013). * Total water volume sources may include fresh water, produced water, and/or recycled water. ** Information is based on the maximum potential for concentration and thus the total may be over 100%.

Federal/Tribal Well:	NO
True Vertical Depth:	9,100
Total Base Water Volume (gal):	343,919
Total Base Non Water Volume:	0

Trade Name	Supplier	Purpose	Ingredients	Chemical Abstract Service Number (CAS #)	Maximum Ingredient Concentration in Additive (% by mass)**	Maximum Ingredient Concentration in HF Fluid (% by mass)**	Specific Gravity	Maximum Ingredient Concentration in HF Fluid (% by volume)**	log K_{oc}	log K_{ow}	MCL / RBC / RSL (mg/L)	Source of log K_{oc}
2% KCL Water	Operator	Base Fluid										
			2% KCL Water	7447-40-7	100.0	86.45119	1.013	85.34175				
PRC SAND	Halliburton	Proppant										
			Crystalline silica, quartz	14808-60-7	100.0	10.43356	2.650	3.93719				
			Phenol / formaldehyde resin	9003-35-4	5.0	0.52168	1.180	0.44210				
			Hexamethylenetetramine	100-97-0	2.0	0.20867	1.331	0.15678				
SAND - PREMIUM WHITE	Halliburton	Proppant										
			Crystalline silica, quartz	14808-60-7	100.0	0.59816	2.650	0.22572				
WG-36 GELLING AGENT	Halliburton	Gelling Agent										
			Guar gum	9000-30-0	100.0	0.34175	0.700	0.48821				
SSA-2	Halliburton	Proppant										
			Crystalline silica, quartz	14808-60-7	100.0	0.29878	2.650	0.11275				
Hydrochloric Acid 10-30%	Halliburton	Solvent										
			Hydrochloric Acid	7647-01-0	30.0	0.24019	1.149	0.20899				
VICON NF BREAKER	Halliburton	Breaker										

Table C-2. Summary of fracking fluid chemicals used for Humboldt M10C-M10-11B from FracFocus.org. RBCs, MCLs, and RSLs are from MSDSs and Jackson (2013).* Total water volume sources may include fresh water, produced water, and/or recycled water.
** Information is based on the maximum potential for concentration and thus the total may be over 100% (continued).

Federal/Tribal Well:	NO
True Vertical Depth:	9,100
Total Base Water Volume (gal):	343,919
Total Base Non Water Volume:	0

Trade Name	Supplier	Purpose	Ingredients	CAS #	Maximum Ingredient Concentration in Additive (% by mass)**	Maximum Ingredient Concentration in HF Fluid (% by mass)**	Specific Gravity	Maximum Ingredient Concentration in HF Fluid (% by volume)**	log K_{oc}	log K_{ow}	MCL / RBC / RSL (mg/L)	Source of log K_{oc}
			Sodium chloride	7647-14-5	30.0	0.14640	2.170	0.06747				
			Chlorous acid, sodium salt	7758-19-2	10.0	0.04880	2.468	0.01977			1 (MCL)	
GEL-STA L STABILIZER	Halliburton	Stabilizer										
			Sodium thiosulfate	7772-98-7	60.0	0.09275	1.670	0.05554			500 (RBC)	
LOSURF-300D	Halliburton	Non-ionic Surfactant										
			Ethanol	64-17-5	60.0	0.04574	0.787	0.05812	-0.14	-0.31		UNEP Publications
			Heavy aromatic petroleum naphtha	64742-94-5	30.0	0.02287	0.910	0.02513	2.96	3.30		EPA
			Naphthalene	91-20-3	5.0	0.00381	0.963	0.00396	3.30	3.36	200 (MCL)	EPA
			Poly(oxy-1,2-ethanediyl), alpha-(4-nonylphenyl)-omega-hydroxy-, branched	127087-87-0	5.0	0.00381	1.057	0.00360	0.79			Azichem www.azichem .com
			1,2,4 Trimethylbenzene	95-63-6	1.0	0.00076	0.876	0.00087	2.67	3.78	.015 (RSL)	EPA
CL-22UCw	Halliburton	Crosslinker										
			Modified alkane	Confidential	60.0	0.05483						
BA-20 BUFFERING AGENT	Halliburton	Buffer										
			Ammonium acetate	631-61-8	100.0	0.02600	1.170	0.02222				
			Acetic acid	64-19-7	30.0	0.00780	1.052	0.00741	0.00	(-0.15)-(-0.53)		
MO-67	Halliburton	pH Control Additive										

Table C-2. Summary of fracking fluid chemicals used for Humboldt M10C-M10-11B from FracFocus.org. RBCs, MCLs, and RSLs are from MSDSs and Jackson (2013).* Total water volume sources may include fresh water, produced water, and/or recycled water.
** Information is based on the maximum potential for concentration and thus the total may be over 100% (continued).

Federal/Tribal Well:	NO
True Vertical Depth:	9,100
Total Base Water Volume (gal):	343,919
Total Base Non Water Volume:	0

Trade Name	Supplier	Purpose	Ingredients	CAS #	Maximum Ingredient Concentration in Additive (% by mass)**	Maximum Ingredient Concentration in HF Fluid (% by mass)**	Specific Gravity	Maximum Ingredient Concentration in HF Fluid (% by volume)**	log K_{oc}	log K_{ow}	MCL / RBC / RSL (mg/L)	Source of log K_{oc}
			Sodium hydroxide	1310-73-2	30.0	0.02660	2.130	0.01249				
FE-1A ACIDIZING COMPOSITION	Halliburton	Additive										
			Acetic anhydride	108-24-7	100.0	0.01603	1.080	0.01484				
			Acetic acid	64-19-7	60.0	0.00962	1.052	0.00914	0.00	(-0.15)-(-0.53)		
MUSOL A SOLVENT	Halliburton	Solvent										
			Ethylene glycol monobutyl ether	111-76-2	100.0	0.01688	0.900	0.01876			1.6 (RSL)	
			Oxylated alcohol	Confidential	30.0	0.00507						
CL-31 CROSSLINKER	Halliburton	Crosslinker										
			Potassium metaborate	13709-94-9	60.0	0.01854	2.300	0.00806				
			Potassium hydroxide	1310-58-3	5.0	0.00155	2.120	0.00073				
FE-2A	Halliburton	Additive										
			Citric acid	77-92-9	60.0	0.01109	1.665	0.00666	-1.20	-1.64		
BE-7™	Halliburton	Biocide										
			Sodium hypochlorite	7681-52-9	30.0	0.01029	1.110	0.00927				
			Sodium hydroxide	1310-73-2	2.0	0.00069	2.130	0.00032				
HAI-404M™	Halliburton	Corrosion Inhibitor										

Table C-2. Summary of fracking fluid chemicals used for Humboldt M10C-M10-11B from FracFocus.org. RBCs, MCLs, and RSLs are from MSDSs and Jackson (2013).* Total water volume sources may include fresh water, produced water, and/or recycled water.
** Information is based on the maximum potential for concentration and thus the total may be over 100% (continued).

Federal/Tribal Well:	NO
True Vertical Depth:	9,100
Total Base Water Volume (gal):	343,919
Total Base Non Water Volume:	0

Trade Name	Supplier	Purpose	Ingredients	CAS #	Maximum Ingredient Concentration in Additive (% by mass)**	Maximum Ingredient Concentration in HF Fluid (% by mass)**	Specific Gravity	Maximum Ingredient Concentration in HF Fluid (% by volume)**	log K_{oc}	log K_{ow}	MCL / RBC / RSL (mg/L)	Source of log K_{oc}
			Isopropanol	67-63-0	30.0	0.00221	0.786	0.00281	0.03			UNEP Publications
			Aldehyde	Confidential	30.0	0.00221						
			Methanol	67-56-1	30.0	0.00221	0.792	0.00279	0.44	(-0.81)-(-0.66)	7.8 (RSL)	
			1-(Benzyl) quinolinium chloride	15619-48-4	10.0	0.00074	1.300	0.00057				
			Quaternary ammonium salt	Confidential	10.0	0.00074						
BE-6 MICROBIOCIDE	Halliburton	Biocide										
			2-Bromo-2-nitro-1,3-propanediol	52-51-7	100.0	0.00358	1.100	0.00325			1.5 (RSL)	
AS-10 ANTI-SLUDGING AGENT	Halliburton	Anti-sludging Agent										
			Dodecylbenzene sulfonic acid	27176-87-0	60.0	0.00242	0.992	0.00244				
CAT-3 ACTIVATOR	Halliburton	Activator										
			EDTA/Copper chelate	Confidential	30.0	0.00237						
FR-66	Halliburton	Friction Reducer										
			Hydrotreated light petroleum distillate	64742-47-8	30.0	0.00237	0.800	0.00296				
CAT-4	Halliburton	Activator										
			Diethylenetriamine	111-40-0	60.0	0.00168	0.995	0.00169				
Chemical FracTracer	Rotechnics	Diagnostics										

Table C-2. Summary of fracking fluid chemicals used for Humboldt M10C-M10-11B from FracFocus.org. RBCs, MCLs, and RSLs are from MSDSs and Jackson (2013).* Total water volume sources may include fresh water, produced water, and/or recycled water.
** Information is based on the maximum potential for concentration and thus the total may be over 100% (continued).

Federal/Tribal Well:	NO
True Vertical Depth:	9,100
Total Base Water Volume (gal):	343,919
Total Base Non Water Volume:	0

Trade Name	Supplier	Purpose	Ingredients	CAS #	Maximum Ingredient Concentration in Additive (% by mass)**	Maximum Ingredient Concentration in HF Fluid (% by mass)**	Specific Gravity	Maximum Ingredient Concentration in HF Fluid (% by volume)**	log K_{oc}	log K_{ow}	MCL / RBC / RSL (mg/L)	Source of log K_{oc}
			Water	7732-18-5	91.0	0.00060	1.000	0.00060				
			Sodium Salt	proprietary	10.0	0.00006	2.200	0.00003				
Zero Wash® Tracer	Pro Technics	Diagnostics										
			Water (major)	7732-18-5	70.0	0.00013	1.000	0.00013				
			Methanol (minor)	67-56-1	30.0	0.00005	0.792	0.00006	0.44	(-0.81)-(-0.66)	7.8 (RSL)	
			Ceramic Proppant	proprietary	14.0	0.00003						
			Dipropylene glycol methyl ether (minor)	34590-94-8	1.0	0.00000						
			Xanthan gum (minor)	11138-66-2	1.0		1.500					
Oil Frac Tracer	Pro Technics	Diagnostics										
			proprietary	proprietary	83.3							
			Water (major)	7732-18-5	15.3		1.000					
			Methanol (minor)	67-56-1	1.3		0.792		0.44	(-0.81)-(-0.66)	7.8 (RSL)	
Ingredients shown above are subject to 29 CFR 1910.1200(i) and appear on Material Safety Data Sheets (MSDS). Ingredients shown below are Non-MSDS.												
		Other Ingredient(s)										
			Water	7732-18-5		0.81819	1.000	0.81819				
		Other Ingredient(s)										
			Ulexite	1319-33-1		0.05483	1.430	0.03834			3.1 (RSL)	
		Other Ingredient(s)										
			Oxyalkylated phenolic resin	Confidential		0.02287						

Table C-2. Summary of fracking fluid chemicals used for Humboldt M10C-M10-11B from FracFocus.org. RBCs, MCLs, and RSLs are from MSDSs and Jackson (2013).* Total water volume sources may include fresh water, produced water, and/or recycled water.
** Information is based on the maximum potential for concentration and thus the total may be over 100% (continued).

Federal/Tribal Well:	NO
True Vertical Depth:	9,100
Total Base Water Volume (gal):	343,919
Total Base Non Water Volume:	0

Trade Name	Supplier	Purpose	Ingredients	CAS #	Maximum Ingredient Concentration in Additive (% by mass)**	Maximum Ingredient Concentration in HF Fluid (% by mass)**	Specific Gravity	Maximum Ingredient Concentration in HF Fluid (% by volume)**	log K_{oc}	log K_{ow}	MCL / RBC / RSL (mg/L)	Source of log K_{oc}
		Other Ingredient(s)										
			Bentonite, benzyl(hydrogenated tallow alkyl) dimethylammonium stearate complex	121888-68-4		0.01709	2.350	0.00727			5 (RBC)	
		Other Ingredient(s)										
			Sodium sulfate	7757-82-6		0.00773	2.664	0.00290			500 (RBC)	
		Other Ingredient(s)										
			Oxyalkylated phenolic resin	Confidential		0.00762						
		Other Ingredient(s)										
			Modified bentonite	Confidential		0.00457						
		Other Ingredient(s)										
			Surfactant mixture	Confidential		0.00342						
		Other Ingredient(s)										
			Surfactant mixture	Confidential		0.00342						
		Other Ingredient(s)										
			Silica gel	112926-00-8		0.00342	2.600	0.00132				
		Other Ingredient(s)										
			Dipropylene glycol	25265-71-8		0.00242	1.023	0.00237		-0.46		
		Other Ingredient(s)										
			Polyacrylamide copolymer	Confidential		0.00237						
		Other Ingredient(s)										

Table C-2. Summary of fracking fluid chemicals used for Humboldt M10C-M10-11B from FracFocus.org. RBCs, MCLs, and RSLs are from MSDSs and Jackson (2013).* Total water volume sources may include fresh water, produced water, and/or recycled water.
** Information is based on the maximum potential for concentration and thus the total may be over 100% (continued).

Federal/Tribal Well:	NO
True Vertical Depth:	9,100
Total Base Water Volume (gal):	343,919
Total Base Non Water Volume:	0

Trade Name	Supplier	Purpose	Ingredients	CAS #	Maximum Ingredient Concentration in Additive (% by mass)**	Maximum Ingredient Concentration in HF Fluid (% by mass)**	Specific Gravity	Maximum Ingredient Concentration in HF Fluid (% by volume)**	log K_{oc}	log K_{ow}	MCL / RBC / RSL (mg/L)	Source of log K_{oc}
			Naphthenic acid ethoxylate	68410-62-8		0.00221	0.920	0.00240			0.5 (RBC)	
		Other Ingredient(s)										
			Sodium sulfite	7757-83-7		0.00155	2.630	0.00059				
		Other Ingredient(s)										
			Sodium chloride	7647-14-5		0.00128	2.170	0.00059				
		Other Ingredient(s)										
			Alkyl sulfonate	Confidential		0.00121						
		Other Ingredient(s)										
			Propylene glycol	57-55-6		0.00091	1.036	0.00088			310 (RSL)	
		Other Ingredient(s)										
			Propylene carbonate	108-32-7		0.00091	1.189	0.00077	1.17	-0.41		EPA
		Other Ingredient(s)										
			Organic salt	Confidential		0.00091						
		Other Ingredient(s)										
			2-Ethylhexanol	104-76-7		0.00091	0.833	0.00109	1.42	2.90		Oltchim
		Other Ingredient(s)										
			Hydrochloric acid	7647-01-0		0.00084	1.149	0.00073				
		Other Ingredient(s)										
			Fatty acids, tall oil	Confidential		0.00074						
		Other Ingredient(s)										
			Alcohols, C12-16, ethoxylated	68551-12-2		0.00074	0.900	0.00082			5.625 (RBC)	
		Other Ingredient(s)										

Table C-2. Summary of fracking fluid chemicals used for Humboldt M10C-M10-11B from FracFocus.org. RBCs, MCLs, and RSLs are from MSDSs and Jackson (2013).* Total water volume sources may include fresh water, produced water, and/or recycled water.
** Information is based on the maximum potential for concentration and thus the total may be over 100% (continued).

Federal/Tribal Well:	NO
True Vertical Depth:	9,100
Total Base Water Volume (gal):	343,919
Total Base Non Water Volume:	0

Trade Name	Supplier	Purpose	Ingredients	CAS #	Maximum Ingredient Concentration in Additive (% by mass)**	Maximum Ingredient Concentration in HF Fluid (% by mass)**	Specific Gravity	Maximum Ingredient Concentration in HF Fluid (% by volume)**	log K_{oc}	log K_{ow}	MCL / RBC / RSL (mg/L)	Source of log K_{oc}
			Polyethoxylated fatty amine salt	61791-26-2		0.00074	0.947	0.00078				
		Other Ingredient(s)										
			Crystalline silica, quartz	14808-60-7		0.00043	2.650	0.00016				
		Other Ingredient(s)										
			Alcohols ethoxylated	Confidential		0.00039						
		Other Ingredient(s)										
			Amide	Confidential		0.00039						
		Other Ingredient(s)										
			Ammonium chloride	12125-02-9		0.00039	1.530	0.00025				
		Other Ingredient(s)										
			Ethoxylated amine	Confidential		0.00037						
		Other Ingredient(s)										
			Butyl alcohol	71-36-3		0.00009	0.810	0.00011			1.6 (RSL)	
		Other Ingredient(s)										
			Methanol	67-56-1		0.00009	0.792	0.00011			7.8 (RSL)	
		Other Ingredient(s)										
			Sorbitan monooleate polyoxyethylene derivative	9005-65-6		0.00008	1.064	0.00008				
		Other Ingredient(s)										
			Sorbitan, mono-9-octadecenoate, (Z)	1338-43-8		0.00008	0.992	0.00008				

Table C-2. Summary of fracking fluid chemicals used for Humboldt M10C-M10-11B from FracFocus.org. RBCs, MCLs, and RSLs are from MSDSs and Jackson (2013).* Total water volume sources may include fresh water, produced water, and/or recycled water.
** Information is based on the maximum potential for concentration and thus the total may be over 100% (continued).

Federal/Tribal Well:	NO
True Vertical Depth:	9,100
Total Base Water Volume (gal):	343,919
Total Base Non Water Volume:	0

Trade Name	Supplier	Purpose	Ingredients	CAS #	Maximum Ingredient Concentration in Additive (% by mass)**	Maximum Ingredient Concentration in HF Fluid (% by mass)**	Specific Gravity	Maximum Ingredient Concentration in HF Fluid (% by volume)**	log K_{oc}	log K_{ow}	MCL / RBC / RSL (mg/L)	Source of log K_{oc}
		Other Ingredient(s)										
			Ammonium phosphate	7722-76-1		0.00007	1.803	0.00004				
		Other Ingredient(s)										
			Sodium iodide	7681-82-5		0.00007	3.670	0.00002			.16 (RSL)	

* Total Water Volume sources may include fresh water, produced water, and/or recycled water

** Information is based on the maximum potential for concentration and thus the total may be over 100%

Note: For Field Development Products (products that begin with FDP), MSDS level only information has been provided.

Ingredient information for chemicals subject to 29 CFR 1910.1200(i) and Appendix D are obtained from suppliers Material Safety Data Sheets (MSDS)

Table C-3. Summary of fracking fluid chemicals used for Huntington K1L-1V from FracFocus.org. RBCs, MCLs, and RSLs are from MSDSs and Jackson (2013). * Total water volume sources may include fresh water, produced water, and/or recycled water. ** Information is based on the maximum potential for concentration and thus the total may be over 100%.

Trade Name	Supplier	Purpose	Ingredients	Chemical Abstract Service Number (CAS #)	Maximum Ingredient Concentration in Additive (% by mass)**	Maximum Ingredient Concentration in HF Fluid (% by mass)**	Specific Gravity	Maximum Ingredient Concentration in HF Fluid (% by volume)**	log K_{oc}	log K_{ow}	Maximum Contaminant Level (MCL) / Risk Based Concentration (RBC) / Regional Screening Level (RSL) (mg/L)	Source of log K_{oc}
Fresh Water	Operator	Base Fluid										
			Fresh Water	7732-18-5	100.0	88.96680	1.000	88.96680				
SAND - PREMIUM WHITE	Halliburton	Proppant										
			Crystalline silica, quartz	14808-60-7	100.0	7.08617	2.650	2.67403				
SSA-2	Halliburton	Proppant										
			Crystalline silica, quartz	14808-60-7	100.0	1.51319	2.650	0.57102				
Hydrochloric Acid 10-30%	Halliburton	Solvent										
			Hydrochloric acid	7647-01-0	30.0	0.38167	1.149	0.33209				
WG-18 GELLING AGENT	Halliburton	Gelling Agent										
			Guar gum derivative	Confidential	100.0	0.27694						
Oilperm FMM-1	Halliburton	Fluid Mobility Modifier										
			Ethanol	64-17-5	30.0	0.04074	0.787	0.05177	-0.14	-0.31		UNEP Publications
			Citrus Extract	94266-47-4	10.0	0.01358	0.840	0.01617				
			Isopropanol	67-63-0	10.0	0.01358	0.786	0.01728	0.03			UNEP Publications
			Terpenes and terpenoids, sweet orange oil	68647-72-3	10.0	0.01358	0.850	0.01598	3.10	4.47		EPA
			Heavy Aromatic Petroleum naphtha	64742-94-5	5.0	0.00679	0.910	0.00746	2.96	3.30		EPA

Table C-3. Summary of fracking fluid chemicals used for Huntington K1L-1V from FracFocus.org. RBCs, MCLs, and RSLs are from MSDSs and Jackson (2013). * Total water volume sources may include fresh water, produced water, and/or recycled water. ** Information is based on the maximum potential for concentration and thus the total may be over 100% (continued).

Trade Name	Supplier	Purpose	Ingredients	CAS #	Maximum Ingredient Concentration in Additive (% by mass)**	Maximum Ingredient Concentration in HF Fluid (% by mass)**	Specific Gravity	Maximum Ingredient Concentration in HF Fluid (% by volume)**	log K_{oc}	log K_{ow}	MCL / RBC / RSL (mg/L)	Source of log K_{oc}
			Poly(oxy-1, 2-ethanediyl), alpha-(4-nonylphenyl)-omega- hydroxy-, branched	127087-87-0	5.0	0.00679	1.057	0.00642	0.79			Azichem www.azichem .com
			Naphthalene	91-20-3	1.0	0.00136	1.150	0.00118	3.30	3.36	200 (MCL)	EPA
			1, 2, 4 Trimethylbenzene	95-63-6	1.0	0.00136	0.876	0.00155	2.67	3.78	.015 (RSL)	EPA
GEL-STA L STABILIZER	Halliburton	Stabilizer										
			Sodium thiosulfate	7772-98-7	60.0	0.08981	1.670	0.05378			500 (RBC)	
CLAYFIX 3	Halliburton	Additive										
			Sodium chloride	7647-14-5	30.0	0.07755	2.170	0.03574				
CL-37 CROSSLINK ER	Halliburton	Crosslinker										
			Triethanolamine zirconate	101033-44-7	100.0	0.02584	1.430	0.01807				
			Glycerin	56-81-5	30.0	0.00775	1.263	0.00614	0.00	-1.76		Schumer and Pohll, 2014
			Propanol	71-23-8	30.0	0.00775	0.786	0.00986				
FE-1A ACIDIZING COMPOSITI ON	Halliburton	Additive										
			Acetic anhydride	108-24-7	100.0	0.02548	1.080	0.02359				
			Acetic acid	64-19-7	60.0	0.01529	1.052	0.01453	0.00	(-0.15)-(-0.53)		
BA-20 BUFFERING AGENT	Halliburton	Buffer										
			Ammonium acetate	631-61-8	100.0	0.02773	1.170	0.02370				
			Acetic acid	64-19-7	30.0	0.00832	1.052	0.00791				

Table C-3. Summary of fracking fluid chemicals used for Huntington K1L-1V from FracFocus.org. RBCs, MCLs, and RSLs are from MSDSs and Jackson (2013). * Total water volume sources may include fresh water, produced water, and/or recycled water. ** Information is based on the maximum potential for concentration and thus the total may be over 100% (continued).

Trade Name	Supplier	Purpose	Ingredients	CAS #	Maximum Ingredient Concentration in Additive (% by mass)**	Maximum Ingredient Concentration in HF Fluid (% by mass)**	Specific Gravity	Maximum Ingredient Concentration in HF Fluid (% by volume)**	log K_{oc}	log K_{ow}	MCL / RBC / RSL (mg/L)	Source of log K_{oc}
VICON NF BREAKER	Halliburton	Breaker										
			Sodium chloride	7647-14-5	30.0	0.01713	2.170	0.00789				
			Chlorous acid, sodium salt	7758-19-2	10.0	0.00571	2.468	0.00231			1 (MCL)	
MO-67	Halliburton	pH Control Additive										
			Sodium hydroxide	1310-73-2	30.0	0.01812	2.130	0.00851				
FE-2A	Halliburton	Additive										
			Citric acid	77-92-9	60.0	0.01762	1.665	0.01058	-1.20	-1.64		Schumer and Pohll, 2014
BE-7™	Halliburton	Biocide										
			Sodium hypochlorite	7681-52-9	30.0	0.01493	1.110	0.01345				
			Sodium hydroxide	1310-73-2	2.0	0.001	2.130	0.00047				
CL-31 CROSSLINKER	Halliburton	Crosslinker										
			Potassium metaborate	13709-94-9	60.0	0.01279	2.300	0.00556			3.1 (RSL)	
			Potassium hydroxide	1310-58-3	5.0	0.00107	2.120	0.00050				
HAI-404M™	Halliburton	Corrosion Inhibitor										
			Methanol	67-56-1	30.0	0.00351	0.792	0.00443	0.44	(-0.81)-(-0.66)	7.8 (RSL)	
			Isopropanol	67-63-0	30.0	0.00351	0.786	0.00447				
			Aldehyde	Confidential	30.0	0.00351						
			1-(Benzyl)quinolinium chloride	15619-48-4	10.0	0.00117	1.300	0.00090				
			Quaternary ammonium salt	Confidential	10.0	0.00117						

Table C-3. Summary of fracking fluid chemicals used for Huntington K1L-1V from FracFocus.org. RBCs, MCLs, and RSLs are from MSDSs and Jackson (2013). * Total water volume sources may include fresh water, produced water, and/or recycled water. ** Information is based on the maximum potential for concentration and thus the total may be over 100% (continued).

Trade Name	Supplier	Purpose	Ingredients	CAS #	Maximum Ingredient Concentration in Additive (% by mass)**	Maximum Ingredient Concentration in HF Fluid (% by mass)**	Specific Gravity	Maximum Ingredient Concentration in HF Fluid (% by volume)**	log K_{oc}	log K_{ow}	MCL / RBC / RSL (mg/L)	Source of log K_{oc}
MUSOL A SOLVENT	Halliburton	Solvent										
			Ethylene glycol monobutyl ether	111-76-2	100.0	0.00537	0.900	0.00597			1.6 (RSL)	
			Oxylated alcohol	Confidential	30.0	0.00161						
FR-76	Halliburton	Friction Reducer										
			Hydrotreated light petroleum distillate	64742-47-8	30.0	0.00565	0.800	0.00706				
LOSURF-300D	Halliburton	Non-ionic Surfactant										
			Ethanol	64-17-5	60.0	0.00321	0.787	0.00408				
			Heavy aromatic petroleum naphtha	64742-94-5	30.0	0.00160	0.910	0.00176				
			Poly(oxy-1,2-ethanediyl), alpha-(4-nonylphenyl)-omega- hydroxy-, branched	127087-87-0	5.0	0.00027	1.057	0.00026				
			Naphthalene	91-20-3	5.0	0.00027	0.963	0.00028	3.30	3.36	200.0	EPA
			1,2,4 Trimethylbenzene	95-63-6	1.0	0.00005	0.876	0.00006	2.67	3.78	.015 (RSL)	EPA
BE-6 MICROBI OCIDE	Halliburton	Biocide										
			2-Bromo-2-nitro-1,3-propanediol	52-51-7	100.0	0.00213	1.100	0.00194			1.5 (RBC)	
Chemical Frac Tracer	Pro Technics	Diagnostics										
			Water	7732-18-5	91.0	0.00025	1.000	0.00025				
			Sodium Salt	proprietary	10.0	0.00003	2.200	0.00001				
ZeroWash Tracer	Pro Technics	Diagnostics										
			Water (major)	7732-18-5	70.0	0.00005	1.000	0.00005				

Table C-3. Summary of fracking fluid chemicals used for Huntington K1L-1V from FracFocus.org. RBCs, MCLs, and RSLs are from MSDSs and Jackson (2013). * Total water volume sources may include fresh water, produced water, and/or recycled water. ** Information is based on the maximum potential for concentration and thus the total may be over 100% (continued).

Trade Name	Supplier	Purpose	Ingredients	CAS #	Maximum Ingredient Concentration in Additive (% by mass)**	Maximum Ingredient Concentration in HF Fluid (% by mass)**	Specific Gravity	Maximum Ingredient Concentration in HF Fluid (% by volume)**	log K_{oc}	log K_{ow}	MCL / RBC / RSL (mg/L)	Source of log K_{oc}
			Methanol (major)	67-56-1	30.0	0.00002	0.792	0.00003	0.44	(-0.81)-(-0.66)	7.8 (RSL)	
			Ceramic Proppant	proprietary	14.0	0.00001						
			Xanthan gum (minor)	11138-66-2	1.0	0.00000	1.500	0.00000				
			Dipropylene glycol methyl ether (minor)	34590-94-8	1.0	0.00000						
Oil Frac Tracer	Pro Technics	Diagnostics										
			Proprietary	proprietary	83.3							
			Methanol (minor)	67-56-1	1.3		0.792		0.44	(-0.81)-(-0.66)	7.8 (RSL)	
			Water (major)	7732-18-5	15.3		1.000					
Ingredients shown above are subject to 29 CFR 1910.1200(i) and appear on Material Safety Data Sheets (MSDS). Ingredients shown below are Non-MSDS												
		.										
			Water	7732-18-5		0.61796	1.000	0.61796				
		Other Ingredient(s)										
			Sodium chloride	7647-14-5		0.01694	2.170	0.00781				
		Other Ingredient(s)										
			Sodium bicarbonate	144-55-8		0.01385	2.200	0.00630				
		Other Ingredient(s)										
			Inorganic salt	Confidential		0.01293						
		Other Ingredient(s)										
			Magnesium chloride hexahydrate	7791-18-6		0.01293	1.569	0.00824				
		Other Ingredient(s)										
			Sodium sulfate	7757-82-6		0.00748	2.664	0.00281			500 (RBC)	

Table C-3. Summary of fracking fluid chemicals used for Huntington K1L-1V from FracFocus.org. RBCs, MCLs, and RSLs are from MSDSs and Jackson (2013). * Total water volume sources may include fresh water, produced water, and/or recycled water. ** Information is based on the maximum potential for concentration and thus the total may be over 100% (continued).

Trade Name	Supplier	Purpose	Ingredients	CAS #	Maximum Ingredient Concentration in Additive (% by mass)**	Maximum Ingredient Concentration in HF Fluid (% by mass)**	Specific Gravity	Maximum Ingredient Concentration in HF Fluid (% by volume)**	log K_{oc}	log K_{ow}	MCL / RBC / RSL (mg/L)	Source of log K_{oc}
		Other Ingredient(s)										
			Acrylamide acrylate polymer	Confidential		0.00565					0.0	
		Other Ingredient(s)										
			Naphthenic acid ethoxylate	68410-62-8		0.00351	0.920	0.00382				
		Other Ingredient(s)										
			Silica, amorphous - fumed	7631-86-9		0.00277	2.648	0.00105				
		Other Ingredient(s)										
			Calcium chloride	10043-52-4		0.00259	2.150	0.00120				
		Other Ingredient(s)										
			Oxyalkylated phenolic resin	Confidential		0.00160						
		Other Ingredient(s)										
			Sodium sulfite	7757-83-7		0.00150	2.630	0.00057				
		Other Ingredient(s)										
			Fatty acids, tall oil	Confidential		0.00117						
		Other Ingredient(s)										
			Alcohols, C12-16, ethoxylated	68551-12-2		0.00117	0.900	0.00130			5.625 (RBC)	
		Other Ingredient(s)										
			Polyethoxylated fatty amine salt	61791-26-2		0.00117	0.947	0.00124				
		Other Ingredient(s)										
			Sodium chloride	7647-14-5		0.00060	2.170	0.00028				
		Other Ingredient(s)										
			Ethoxylated amine	Confidential		0.00058						

Table C-3. Summary of fracking fluid chemicals used for Huntington K1L-1V from FracFocus.org. RBCs, MCLs, and RSLs are from MSDSs and Jackson (2013). * Total water volume sources may include fresh water, produced water, and/or recycled water. ** Information is based on the maximum potential for concentration and thus the total may be over 100% (continued).

Trade Name	Supplier	Purpose	Ingredients	CAS #	Maximum Ingredient Concentration in Additive (% by mass)**	Maximum Ingredient Concentration in HF Fluid (% by mass)**	Specific Gravity	Maximum Ingredient Concentration in HF Fluid (% by volume)**	log K_{oc}	log K_{ow}	MCL / RBC / RSL (mg/L)	Source of log K_{oc}
		Other Ingredient(s)										
			Oxyalkylated phenolic resin	Confidential		0.00053						
		Other Ingredient(s)										
			Ammonium phosphate	7722-76-1		0.00012	1.600	0.00008				
		Other Ingredient(s)										
			Sodium iodide	7681-82-5		0.00012	3.670	0.00003			.16 (RSL)	
* Total Water Volume sources may include fresh water, produced water, and/or recycled water												
** Information is based on the maximum potential for concentration and thus the total may be over 100%												
Note: For Field Development Products (products that begin with FDP), MSDS level only information has been provided.												
Ingredient information for chemicals subject to 29 CFR 1910.1200(i) and Appendix D are obtained from suppliers Material Safety Data Sheets (MSDS)												

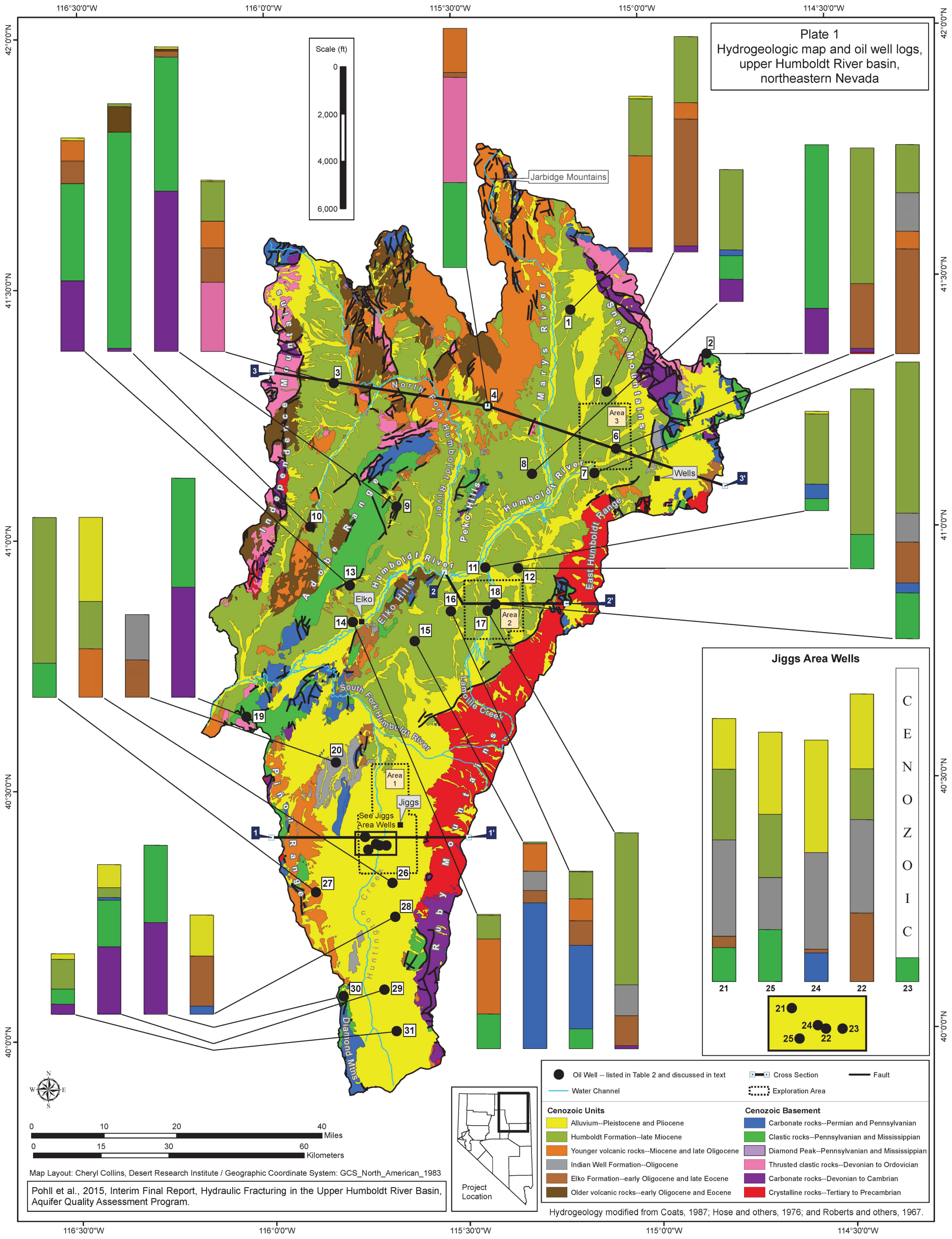
Plate 1
Hydrogeologic map and oil well logs, upper Humboldt River basin, northeastern Nevada
Scale (ft)
0
2,000
4,000
6,000
116°30'0"W
116°0'0"W
115°30'0"W
115°0'0"W
114°30'0"W
42°0'0"N
41°30'0"N
41°0'0"N
40°30'0"N
40°0'0"N
Jarbidge Mountains
Independence Mountains
Adobe Range
Pilot Range
Marys River
Snake Mountains
North Fork Humboldt River
Humboldt River
Pequop Hills
Elko Hills
South Fork Humboldt River
Lamoille Creek
East Humboldt Range
Ruby Mountains
Huntington Creek
Diamond Mtns
Elko
Jiggs
See Jiggs Area Wells
Wells
Area 1
Area 2
Area 3
Jiggs Area Wells
CENOZOIC
21
25
24
22
23
Oil Well -- listed in Table 2 and discussed in text
Cross Section
Fault
Water Channel
Exploration Area
Cenozoic Units
Alluvium--Pleistocene and Pliocene
Humboldt Formation--late Miocene
Younger volcanic rocks--Miocene and late Oligocene
Indian Well Formation--Oligocene
Elko Formation--early Oligocene and late Eocene
Older volcanic rocks--early Oligocene and Eocene
Cenozoic Basement
Carbonate rocks--Permian and Pennsylvanian
Clastic rocks--Pennsylvanian and Mississippian
Diamond Peak--Pennsylvanian and Mississippian
Thrusted clastic rocks--Devonian to Ordovician
Carbonate rocks--Devonian to Cambrian
Crystalline rocks--Tertiary to Precambrian
Project Location
0 10 20 40 Miles
0 15 30 60 Kilometers
Map Layout: Cheryl Collins, Desert Research Institute / Geographic Coordinate System: GCS_North_American_1983
Pohll et al., 2015, Interim Final Report, Hydraulic Fracturing in the Upper Humboldt River Basin, Aquifer Quality Assessment Program.
Hydrogeology modified from Coats, 1987; Hose and others, 1976; and Roberts and others, 1967.

Plate 2
Hydrogeologic sections, upper Humboldt River basin, northeastern Nevada

Vertical Exaggeration x4
(meters AMSL)

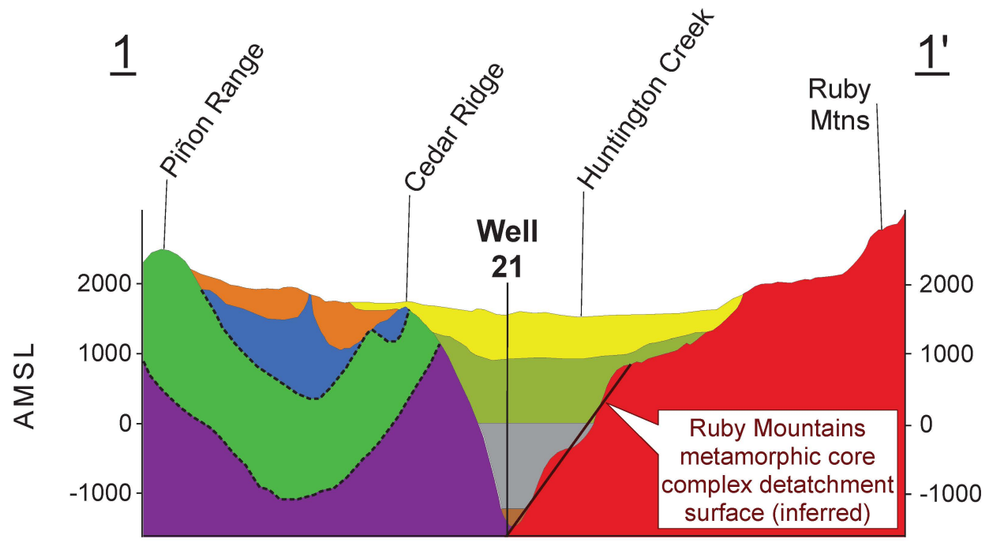

Geologic sources: Smith and Ketner, 1972, and Willden and Kistler, 1969.

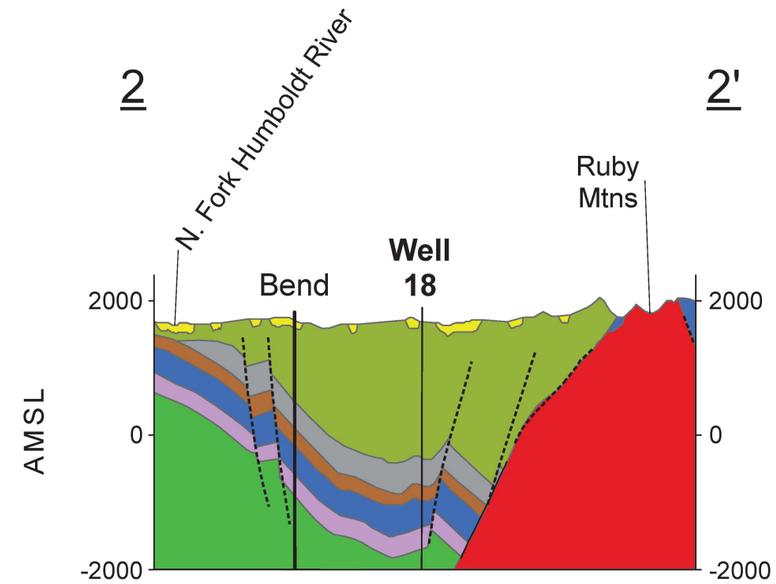

Geologic Sources: Coats, 1997; Hess and others, 2011; Howard and others, 1979; Ketner, 1990; and proprietary interpretation of seismic data from Noble Energy.

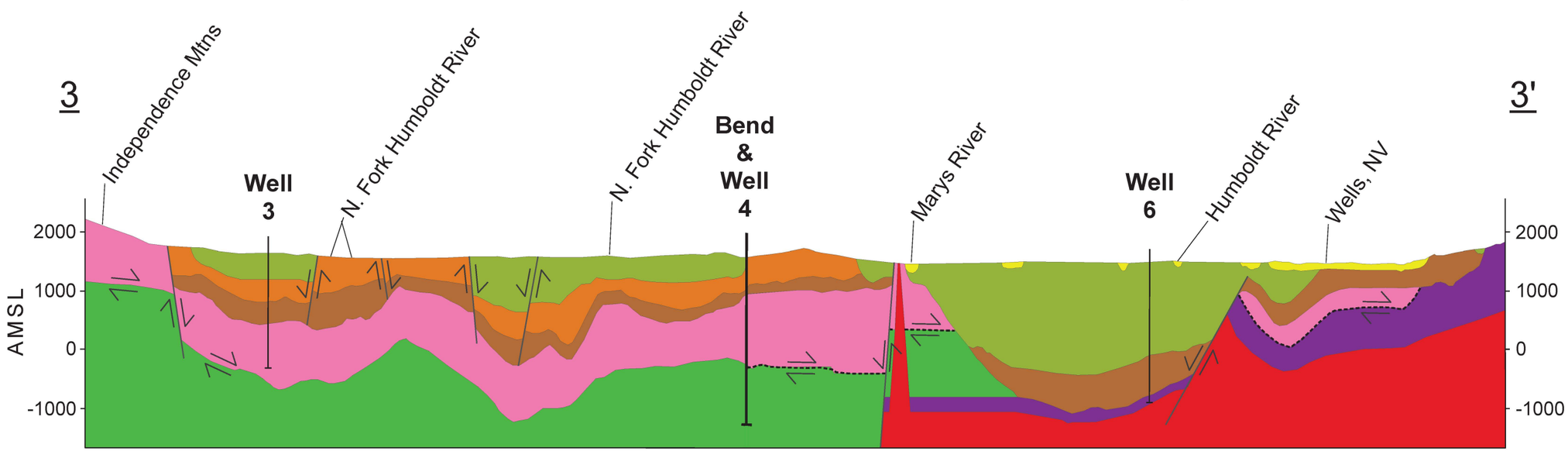

Geologic Source: Coats, 1987.

0 2.5 5 10 Kilometers

0 2.5 5 10 Miles

See Plate 1 for Geologic Unit Legend

Pohll et al., 2015, Interim Final Report, Hydraulic Fracturing in the Upper Humboldt River Basin, Aquifer Quality Assessment Program.

Layout: Cheryl Collins, Desert Research Institute